An investigation into BK Polyomavirus and host-virus interactions

Laura Grace Caller

**This dissertation is submitted for the degree Doctor of Philosophy
at the University of Cambridge**

An investigation into BK Polyomavirus and host-virus interactions

The potentially oncogenic human pathogen BK Polyomavirus (BKPyV) was first identified in 1971 and has since been associated with a number of diseases primarily in immunosuppressed patients.

Infection is established in early life and by adulthood up to 90% of populations show seroconversion for the major capsid protein VP1. Despite this infections are rarely cleared, maintaining a silent asymptomatic persistence punctuated with periods of viral shedding in the urine. The virus is non-enveloped and comprises a simple ~5.2 Kb dsDNA genome which expresses just seven known proteins, necessitating a heavy reliance on, and interactions with, host mechanisms in order to efficiently replicate and disseminate within a population.

The poorly understood lifelong persistence and failure to clear infection highlights our lack of understanding of the viral life cycle and viral interactions with host processes and responses to infection. Indeed, non-enveloped viruses are thought to spread solely through infected cell lysis but such large-scale lysis should trigger an acute inflammatory response, which is rarely seen in healthy immunocompetent individuals.

The research conducted for this thesis first investigates the egress of BKPyV in a non-lytic manner, presenting evidence for an active non-lytic method of viral egress that is dependent on cellular anion homeostasis. Moreover, data generated for this thesis suggests that virions egress via an unconventional secretion pathway which traffics directly from the endoplasmic reticulum (ER) to the plasma membrane in single-membraned vesicles.

Further research undertook a whole cell quantitative temporal viromic (QTV) approach, post-experimentally tagging whole cell lysate peptides with isobaric labels (Tandem Mass Tagging, TMT) to provide a greater understanding of host cell proteomic changes throughout BKPyV infection in two primary human cell types over 72 hours of infection. Such an approach identified ~9000 cellular proteins, of which a surprisingly small number changed significantly in abundance in response to BKPyV infection. Of those that were changed in abundance a large proportion were related to cell cycle, revealing that BKPyV infection induces a pseudo-G2 arrest, similar to the G2/M checkpoint. Validation of TMT results in both cell types provided confidence in this robust data set, and further studies highlighted the importance of not only cell cycle status, but the activity of CDK1 for efficient viral infection and replication. Additionally, TMT generated data emphasised the lack of innate immune induction in response to BKPyV infection, suggesting BKPyV exhibits a sophisticated evasion of pathogen recognition.

<div align="right">

Laura Grace Caller

</div>

This thesis is dedicated to my parents;

Lynne and David Caller,

and to my fiancé;

Michael Bodycomb

Table of Contents

Declaration

This dissertation is the result of my own work and includes nothing which is the outcome of work done in collaboration except where specifically indicated in the text.

It is not substantially the same as any that I have submitted, or, is being concurrently submitted for a degree or diploma or other qualification at the University of Cambridge or any other University or similar institution except as declared in the Preface and specified in the text. I further state that no substantial part of my dissertation has already been submitted, or, is being concurrently submitted for any such degree, diploma or other qualification at the University of Cambridge or any other University or similar institution except as declared in the Preface and specified in the text

This thesis contains approximately 45,000 words and 57 figures.

September 2018   Laura Grace Caller

Acknowledgements

Abstract

The potentially oncogenic human pathogen BK Polyomavirus (BKPyV) was first identified in 1971 and has since been associated with a number of diseases primarily in immunosuppressed patients.

Infection is established in early life and by adulthood up to 90% of populations show seroconversion for the major capsid protein VP1. Despite this infections are rarely cleared, maintaining a silent asymptomatic persistence punctuated with periods of viral shedding in the urine. The virus is non-enveloped and comprises a simple ~5.2 Kb dsDNA genome which expresses just seven known proteins, necessitating a heavy reliance on, and interactions with, host mechanisms in order to efficiently replicate and disseminate within a population.

The poorly understood lifelong persistence and failure to clear infection highlights our lack of understanding of the viral life cycle and viral interactions with host processes and responses to infection. Indeed, non-enveloped viruses are thought to spread solely through infected cell lysis but such large-scale lysis should trigger an acute inflammatory response, which is rarely seen in healthy immunocompetent individuals.

The research conducted for this thesis first investigates the egress of BKPyV in a non-lytic manner, presenting evidence for an active non-lytic method of viral egress that is dependent on cellular anion homeostasis. Moreover, data generated for this thesis suggests that virions egress via an unconventional secretion pathway which traffics directly from the endoplasmic reticulum (ER) to the plasma membrane in single-membraned vesicles.

Further research undertook a whole cell quantitative temporal viromic (QTV) approach, post-experimentally tagging whole cell lysate peptides with isobaric labels (Tandem Mass Tagging, TMT) to provide a greater understanding of host cell proteomic changes throughout BKPyV infection in two primary human cell types over 72 hours of infection. Such an approach identified ~9000 cellular proteins, of which a surprisingly small number changed significantly in abundance in response to BKPyV infection. Of those that were changed in abundance a large proportion were related to cell cycle, revealing that BKPyV infection induces a pseudo-G2 arrest, similar to the G2/M checkpoint. Validation of TMT results in both cell types provided confidence in this robust data set, and further studies highlighted the importance of not only cell cycle status, but the activity of CDK1 for efficient viral infection and replication. Additionally, TMT generated data emphasised the lack of innate immune induction in response to BKPyV infection, suggesting BKPyV exhibits a sophisticated evasion of pathogen recognition.

In summary, the research in this thesis has established a novel transmission pathway for BKPyV, along with providing a greater understanding of the interactions between virus and host throughout the course of infection.

Abbreviations

(q)PCR	(quantitative) Polymerase Chain Reaction
ADCC	Antibody Dependent Cellular Cytotoxicity
Agno	Agnoprotein
AIDS	Acquired Immunodeficiency Syndrome
AIPS	Autophagy Induced Protein Secretion
AML	Acute Myeloid Leukaemia
AMP	Adenosine Monophosphate
APC	Antigen Presenting Cell
ARF1	ADP-Ribosylation Factor 1
ATM	Ataxia Telengiectasia Mutated Kinase
ATR	Ataxia Telengiectasia and Rad3 Related Kinase
BFA	Brefeldin A
BHK-21	Baby Hamster Kidney 21
BKPyV	BK Polyomavirus
BST2	Bone marrow stromal antigen 2 (Tetherin)
CD	Cluster of Differentiation
CDK	Cyclin Dependent Kinase
CDT1	Chromatin Licensing and DNA Replication Factor 1
cFos	Cellular Fos
CFTR	Cystic Fibrosis Transmembrane Conductance Regulator
cGAS	cyclic GMP-AMP Synthase
CHX	Cycloheximide
ClC	Chloride Channel
COPI and II	Coat Protein I and II
CPE	Cytopathic Effects
CRISPR	Clustered Regularly Interspaced Short Palindromic Repeats
DAB	Diaminobenzidine
DAI	DNA-Dependent Activator of IFN-Regulatory Factors
DAPI	4',6-Diamidino-2-Phenylindole
DAVID	Database for Annotation, Visualisation and Integrated Discovery
DDR	DNA Damage Response
DENV	Dengue Virus
DIDS	4,4'-diisothiocyano-2,2'-stilbenedisulfonic acid
DMSO	Dimethyl Sulfoxide
DNA	Deoxyribonucleic Acid
DNAJC14	DnaJ Homolog Subfamily C Member 14
DNA-PK	DNA-dependent Protein Kinase
dpi	Days Post Infection
dsDNA	Double Stranded DNA
dsRNA	Double Stranded RNA
E2F1-5	Eukaryotic Transcrition Factors 1-5
EBV	Epstein Barr Virus
EdU	5-Ethynyl-2'-Deoxyuridine
EEA1	Endosome Antigen 1

eIF2α	Eukaryotic Initiation Factor 2 alpha
ER	Endoplasmic Reticulum
ERAD	ER Associated Protein Degradation
ERGIC	ER Golgi Intermediate Complex
ESCRT	Endosomal Sorting Complex Required for Transport
FAM111B	Homo sapiens Family with Sequence Similarity 111 Member B
FFU	Fluorescent Focus Unit
FGF2	Fibroblast Growth Factor 2
G0	No Growth
G1	First Growth
G2	Second Growth
GAP	GTPas Activating Protein
GDP	Guanosine Diphosphate
GEF	GDP/GTP Exchange Factor
GI	Gastro Intestinal
GMP	Guanosine Monophosphate
GPHR	Golgi-pH Regulator
GRASP/GORASP	Golgi-reassembly stacking protein
GTP	Guanosine Triphosphate
GTPase	Guanosine Triphosphatase
h	Hour
HAV	Hepatitis A Virus
HBV	Hepatitis B Virus
HC	Haemorrhagic Cystitis
HCMV	Human Cytomegalovirus
HCV	Hepatitis C Virus
HEPES	4-(2-Hydroxyethyl)-1-Piperazineethanesulfonic Acid
HERC5	HECT And RLD Domain Containing E3 Ubiquitin Protein Ligase 5
HHV-8	Human Herpes Virus 8
HIV	Human Immunodeficiency Virus
hpi	Hours Post Infection
HPV	Human Papillomavirus
HPyV6, 7, 9 and 12	Human Polyomavirus 6, 7, 9 and 12
HRP	Horseradish Peroxidase
HSCT	Haematopoietic Stem Cell Transplant
Hsp70	Heat Shock Protein 70
HSV-1	Herpes Simplex Virus 1
HU	Human Urothelial
HUV-EC	Human Umbilical Vein Endothelial Cells
ICP0	Infected Cell Protein 0
ICTV	International Committee on Taxonomy of Viruses
IFI16	Interferon Inducible Protein 16
IFIT1, 2 and 3	Interferon Induced Protein with Tetratricopeptide Repeats 1/2/3
IFN	Interferon
IL-1b, 2, 7 and 18	Interleukin-1b, 2, 7 and 18
IRF3 and 7	IFN Regulatory Factor 3 and 7

ISG	Interferon Stimulated Gene
ISG15	Interferon Stimulated Gene 15
IU/cell	Infectious Unit per Cell
IU/ml	Infectious Unit per Millilitre
JCPyV	JC Polyomavirus
kDa	KiloDalton
KIPyV	Karolinska Institute Polyomavirus
KSHV	Kaposi Sarcoma Herpes Virus
LAMP1	Lysosomal-Membrane Associated Protein 1
LIPyV	Lyon IARC Polyomavirus
LRR	Leucine Rich Repeat
M	Mitosis
MAVS	Mitochondrial Antiviral Signalling Protein
MCC	Merkel Cell Carcinoma
MCPyV	Merkel Cell Polyomavirus
MDA5	Melanoma Differentiation Protein 5
Mdm2	Mouse Double Minute Homolog 2
MEK/ERK	Mitogen-Activated Protein Kinase
MHC	Major Histocompatibility Complex
MQAE	N-Ethoxycarbonylmethyl-6-Methoxyquinolinium Bromide
MRE11	Meiotic Recombination 11
mRNA	Messenger RNA
MuPyV	Murine Polyomavirus
MVB	Multi Vesicular Bodies
MVM	Miute Virus of Mice
MWPyV	Malawi Polyomavirus
MX1	Interferon-induced GTP-binding protein Mx1
MyD88	Myeloid Differentiation Primary Reponse 88
NCCR	Non-Coding Control Region
NEMO	NK-κB Essential Modulator
NJPyV	New Jersey Polyomavirus
NK	Natural Killer
NK-κB	Nuclear Factor-Kappa B
NLS	Nuclear Localisation Sequence
OAS/L/3	Oligoadenylate Synthase /Ligand/3
Ori	Origin of Replication
PAMP	Pathogen Associated Molecular Pattern
PBS	Phosphate Buffered Saline
PCNA	Proliferating Cell Nuclear Antigen
PI	Propidium Iodide
PI(4,5)P2	Phosphatidylinositol 4,5-Biphosphate
PKR	Protein Kinase R
Plk1	Polo-like Kinase 1
PML	Progressive Multifocal Leukoenchephalopathy
PML-NB	Promyelocytic Leukaemia Nuclear Bodies
PMPF	Plasma Membrane Pore Formation

POL III	RNA Polymerase III
PP2A	Proteins Phosphatase 2A
pre-mRNA	Pre-messenger RNA
PROSAPIP1	proSAP Interacting Protein 1 (LZTS3)
PRR	Pattern Recognition Receptor
PVAN	Polyomavirus Associated Nephropathy
QTV	Quantitative Temporal Viromics
RacPyV	Raccoon Polyomavirus
Rb	Retinoblastoma
RIG-I	Retinoic Acid-Inducible Gene-I
RNA	Ribonucleic Acid
RNase L	Ribonuclease L
RNAseq	RNA Sequencing
RPTE	Renal Proximal Tubule Epithelial
S	Synthesis
shRNA	Short Hairpin RNA
SILAC	Stable Isotope Labelling with Amino Acids in Culture
siRNA	short interfering RNA
SITS	4-Acetamido-4'-Isothiocyanatostilbene-2,2'-Disulphonic Acid
ssRNA	Single Stranded RNA
STING	Stimulator of Interferon Genes
STLPyV	St Louis Polyomavirus
STRING	Search Tool for the Retrieval of Interacting Genes/Proteins
SV40	Simian Vacuolating Agent 40
TAg	Large Tumour (T) Antigen
tAg	Small Tumour (T) Antigen
TAP	Transport with Antigen Processing
TAT	Transactivator of Transcription
TCR	T Cell Receptor
TEM	Transmission Electron Microscopy
TGN	*trans*-Golgi Network
TIR	Toll/Interleukin-1 Receptor
TLR	Toll-Like Receptor
TMT	Tandem Mass Tagging
TNF	Tumour Necrosis Factor
TRIF	TIR-Domain-Containing Adaptor-Inducing Interferon-beta
truncTAg	Truncated Tumour Antigens
TSPyV	Trychodysplasia Spinulosa Polyomavirus
UV	Ultraviolet
v/t-SNARE	Vesicle/Tether-Soluble N-Ethylmaleimide Sensitive Factor Attachment Protein Receptor
VLP	Virus-Like Particle
VZV	Varicella Zoster Virus
WDR76	WD Repeat-Containing 76
WUPyV	Washington University Polyomavirus
α-SNAP	N-Ethylmaleimide-Sensitive Factor Attachment Protein Alpha

List of Figures

List of Tables

1. Introduction

1.1 An Introduction to *Polyomaviridae*

1.1.1 Classification and History

The family *Polyomaviridae* are a group of species-specific ubiquitous pathogens, known to cause cell-tropism dependant infection. Originally part of the family *Papovaviridae,* which contained both *Papillomavirus* and *Polyomavirus* genera, *Polyomaviridae* have been identified as a distinct virus family since 1999. In 2011 the single family was divided into three genera, the *Orthopolyomavirus* and *Wukipolyomavirus* genera containing mammalian viruses, while the *Avipolyomavirus* genera containing those viruses which infected birds (Johne et al., 2011, Schneider et al., 2014). This classification has been further updated by the International Committee on Taxonomy of Viruses (ICTV), and as of 2018 there are four distinct genera of polyomavirus based on their Large T Antigen (TAg) sequence similarity (Calvignac-Spencer et al., 2016).

The largest of these new genera containing more than 30 members, *Alphapolyomavirus*, encompasses a number which infect humans and other mammals, including the oncogenic Merkel Cell Polyomavirus (MCPyV), Murine Polyomavirus (MuPyV) and Raccoon Polyomavirus (RacPyV). With more than 20 species *Betapolyomavirus* is the next largest genus and, similar to *Alphapolyomavirus*, its members infect humans and other mammals. Both BK Polyomavirus (BKPyV) and JC Polyomavirus (JCPyV) are members of the *Betapolyomavirus* genus, as well as the primate polyomavirus Simian Vacuolating Agent 40 (SV40). *Gammapolyomavirus* includes fewer than 10 species, all of which infect only birds. While *Gammapolyomaviruses* are generally not thought to be oncogenic, disease presentations can be severe and at times fatal in various avian species. *Deltapolyomavirus* encompasses just four exclusively human tropic strains whose disease presentations are less apparent than either *Alphapolyomavirus* or *Betapolyomavirus* (Calvignac-Spencer et al., 2016, Moens et al., 2017).

The first polyomavirus to be identified was MuPyV in 1952, and this virus was shown to be the causative agent of tumours in newborn and immunocompromised mice (Gross, 1953). In 1960 SV40 was found to be a contaminating agent in several batches of the human oral poliovirus vaccine Sabin, which had been grown in monkey kidney cell cultures (Sweet and Hilleman, 1960). While SV40 has also been shown to cause tumours in mice, extensive cohort studies following large-scale exposure to humans in 1960 showed no increased risk of oncogenesis, thus SV40 shows inadequate evidence as the definitive causative agent of carcinoma in humans (Bouvard et al., 2012). It must be noted, however, SV40 viral gene products have been identified in a number of different tumours, suggesting a potential co-infectious association (Lowe et al., 2007), and most recently SV40 has been associated with malignant pleural mesothelioma (Thanh et al., 2016).

It was not until 1971 that the first human polyomaviruses were discovered. Named for the individual in which they were identified, BKPyV was isolated from a male Sudanese 39-year-old kidney transplant patient who had been suffering serious pyelonephritis and renal failure (Gardner et al., 1971), while JCPyV was isolated from the brain tissue of a patient that had suffered progressive multifocal leukoencephalopathy (PML) (Padgett et al., 1971). Since 2007 a further twelve human polyomaviruses have been discovered (Table 1.1), many of these have not yet been associated with disease and in a number of these a human host may not be the primary source of infection. One such example is Lyon IARC Polyomavirus (LIPyV), which shares 65% sequence similarity with RacPyV of raccoon origin (Gheit et al., 2017).

1.1.2 Human *Polyomaviridae* and Associated Disease

Table 1.1: An overview of all 14 human polyomaviruses discovered to date

Full Virus Name	Abbr.	Genus	Year of Discovery	Associated Disease	Isolation Source	Reference
BK Polyomavirus	BKPyV	Beta	1971	Haemorrhagic cystitis (HC); polyomavirus associated nephropathy (PVAN); Prostate cancer; Meningitis and encephalitis; Human Immunodeficiency Virus (HIV)-associated salivary gland disease; Retinitis; pneumonitis	Urine	(Erard et al., 2004, Hirsch et al., 2005, Keller et al., 2015, Chittick et al., 2013, Burger-Calderon et al., 2014, Reploeg et al., 2001, Hedquist et al., 1999)
JC Polyomavirus	JCPyV	Beta	1971	Progressive multifocal leukoencephalopathy (PML); Multiple sclerosis; Colon cancer	Urine	(Gheuens et al., 2013, Brew et al., 2010, Ramamoorthy et al., 2011)
Karolinska Institute Polyomavirus	KIPyV	Beta	2007	No clear disease correlation, may be involved in respiratory disease	Naso-pharynx	(Gaynor et al., 2007, Dehority et al., 2017)
Washington University Polyomavirus	WUPyV	Beta	2007	No clear disease correlation, may be involved in respiratory disease	Naso-pharynx	(Allander et al., 2007, Toptan et al., 2016)
Merkel Cell Polyomavirus	MCPyV	Alpha	2008	Merkel cell carcinoma	Skin lesion	(Feng et al., 2008)
Human Polyomavirus 6	HPyV6	Delta	2010	Pruritic dermatoses and dyskeratosis	Skin	(Nguyen et al., 2017)
Human Polyomavirus 7	HPyV7	Delta	2010	Pruritic dermatoses and dyskeratosis	Skin	(Nguyen et al., 2017)
Trychodysplasia Spinulosa Polyomavirus	TSPyV	Alpha	2010	Trychodysplasia Spinulosa	Hair follicle	(van der Meijden et al., 2010)
Human Polyomavirus 9	HPyV9	Alpha	2011	No clear disease correlation	Skin, blood and urine	(Scuda et al., 2011)

Malawi Polyomavirus	MWPyV	Delta	2012	No clear disease correlation	Stool	(Siebrasse et al., 2012)
St Louis Polyomavirus	STLPyV	Delta	2013	No clear disease correlation	Stool	(Lim et al., 2013)
Human Polyomavirus 12	HPyV12	Alpha	2013	No clear disease correlation	GI tract	(Korup et al., 2013)
New Jersey Polyomavirus	NJPyV	Alpha	2014	No clear disease correlation	Pancreatic epithelium	(Mishra et al., 2014)
Lyon IARC Polyomavirus	LIPyV	Alpha	2017	No clear disease correlation	Skin, oral gargle and hair follicle	(Gheit et al., 2017)

1.2 BKPyV

1.2.1 Seroprevalence, Disease and Treatment

BKPyV has been divided into four major subtypes, grouped by genetic heterogeneity. The worldwide distribution of subtype I means that it is also the most prevalent subtype, while subtype IV is found only in Europe and East Asia. Subtypes II and III are seldom isolated in any general population (Yogo et al., 2009). From these subtypes, five separate serotypes have been described; subtypes II, III, IV and the further subdivided subtype Ib1 and Ib2 (Pastrana et al., 2013). A high seroprevalence in a population is maintained throughout life. By the age of four 50% of children are thought to be infected, rising to more than 60% by the age of ten and continuing to rise into adulthood, by which time up to 90% of populations show seroconversion for at least one BKPyV serotype (Shah et al., 1973, Kean et al., 2009, Viscidi et al., 2011). Such high rates of seroconversion in a population must be treated with caution however because these studies have used seroconversion against the BKPyV major capsid protein VP1 as an indicator of prior infection, but there is known to be a high level of cross-reactivity between many polyomavirus VP1 motifs, notably between JCPyV and BPKyV VP1 which show 78% similarity (Moens et al., 2013).

Although the route of transmission of BKPyV is unclear, typically primary infection is thought to occur in the tonsils, through a respiratory or faecal-oral route, after which infected monocytes traffic the virus to various tissues and organs throughout the body (Hirsch and Steiger, 2003). This initial infection is largely asymptomatic and BKPyV maintains a silent persistence in the renourinary tract epithelium, where minimal episomal replication occurs. It has been suggested that this state represents a 'true latency' by BKPyV (Helle et al., 2017).

It is thought that once lifelong asymptomatic viral persistence is established in the renourinary tract the patient is unlikely to suffer any adverse clinical effects until such time that they may become immunosuppressed. Immune suppression, particularly by strong immunosuppressive therapies but

also clinical conditions such as Acquired Immuno-Deficiency Syndrome (AIDS), leads to a dramatic increase in BKPyV lytic replication. Viral loads over 10^4 copies/ml detected in patient urine by polymerase chain reaction (PCR) are indicative of 'reactivated infection' (Hirsch and Steiger, 2003). It is the large scale lysis of cells caused by virus replication from which many of the cytopathic effects (CPE) occur. Kidney transplant patients are particularly prone to polyomavirus associated nephropathy (PVAN), in which CPE are characterised by interstitial nephritis caused by breakdown of the infected epithelial layer of graft tubules, after which BKPyV gains access to the bloodstream. The resultant influx of inflammatory cells may lead to atrophy of the renal tubules and fibrosis. Up to 10% of transplant patients can be affected within the first two years post-transplant, of these up to 80% can result in graft failure (Egli et al., 2007). There is little treatment available for treatment of PVAN in patients. It is generally recommended that the immunosuppressive drug regimen is reduced to allow the host immune system to control viraemia levels as the currently available anti-viral drugs that show inhibitory effects on BKPyV replication, cidofovir and leflunomide, have very serious side effects including nephrotoxicity (Johnston et al., 2010). Graft failure, therefore, may be due to direct damage caused by viral replication and lysis or due to graft rejection caused by reduction of immunosuppression, or a combination of both.

In 10-25% of haematopoeitic stem cell transplant (HSCT) patients increased BKPyV-induced cell lysis due to immunosuppression can lead to haemorrhagic cystitis (HC) (Hingorani, 2016) Although not usually life threatening, HC can lead to greatly reduced rates of recovery from HSCT and in exceptional circumstances blood clots have been known to block the urinary tract, resulting in renal failure (Jiang et al., 2009a). It has also been noted that BKPyV has been found in the salivary glands of AIDS patients, causing Human Immunodeficiency Virus (HIV)-associated salivary gland disease (Burger-Calderon et al., 2014), the retina of AIDS patients with ophthalmological complications (Reploeg et al., 2001) and in the upper respiratory tract of children suffering interstitial pneumonitis (Hedquist et al., 1999), illustrating that BKPyV is an opportunistic pathogen with the potential to cause clinical disease at a number of sites in immunocompromised patients. While these disease presentations can be more effectively treated with anti-viral drugs they further demonstrate why a greater understanding of the interactions between virus and host is needed and may lead to a more effective treatment of BKPyV either pre- or post-transplant, with the potential to save lives and improve the clinical outcomes of many more.

BKPyV, like many polyomaviruses, has oncogenic potential and has been shown to transform Baby Hamster Kidney 21 (BHK-21) cells in vitro (Major and Dimayorc.G, 1973) and hamster kidneys in vivo (Takemoto and Martin, 1976). In humans however, while gene products have been found in a number of tumour tissues, most notably the prostate (Chittick et al., 2013), there is a great deal of variation

between studies as to levels of viral gene expression, or even the presence or absence of detectable virus in carcinomas, and there is currently little evidence of a causal of BKPyV infection with carcinogenesis; reviewed extensively in (Abend et al., 2009a). As such BKPyV is characterised as a group 2B carcinogenic biological agent, i.e. possibly carcinogenic to humans (Bouvard et al., 2012). The viral gene products TAg and small t antigen (tAg) have been shown to have oncogenic properties through their action of cell cycle deregulation and p53 induced apoptosis, which is discussed more extensively later.

1.2.2 Genome Organisation

BKPyV are small circular dsDNA viruses with a genome of ~5kb, whose bidirectional transcription is controlled by a non-coding control (NCCR) region of around 400bp. The principal early transcribed genes are TAg and tAg, which are splice variants of a single mRNA transcribed from the same genomic region and are named for the size of protein produced by said splicing (DeCaprio and Garcea, 2013). A truncated form of TAg has also been described (truncTAg) (Abend et al., 2009b), which initially goes through normal TAg splicing, but undergoes a secondary splicing event leading to a frameshift that introduces a stop codon in frame soon after the second splice acceptor site. The late region encodes for the structural capsid proteins, VP1, VP2 and VP3, and agnoprotein (Agno), a small multifunctional non-structural protein. VP3 is homologous to the C-terminus of VP2, originating from an alternative start site within the VP2 open reading frame.

While the transcribed portion of BKPyV is largely conserved throughout strains, the NCCR region is highly variable. Containing the origin of replication (Ori) with more than 30 transcription factor binding sites, the archetype strains contain 'blocks' of base pairs (designated as O, P, Q, R, S) that can be found to be rearranged, duplicated or lost in strains other than archetype, leading to differential effects on cell tropism, oncogenicity and preferential transcription of early or late genes (Bethge et al., 2015, Johnsen et al., 1995, Moens et al., 1995, Gosert et al., 2008). These rearrangements are often identified in patients with increased levels of viral replication, who frequently shed archetypal strain in urine while blood plasma virus is rearranged (Gosert et al., 2008). The reason for such variations in patients remains unclear, however such NCCR rearrangements may play a role in virus adaptation to different types of cell *in vitro.*
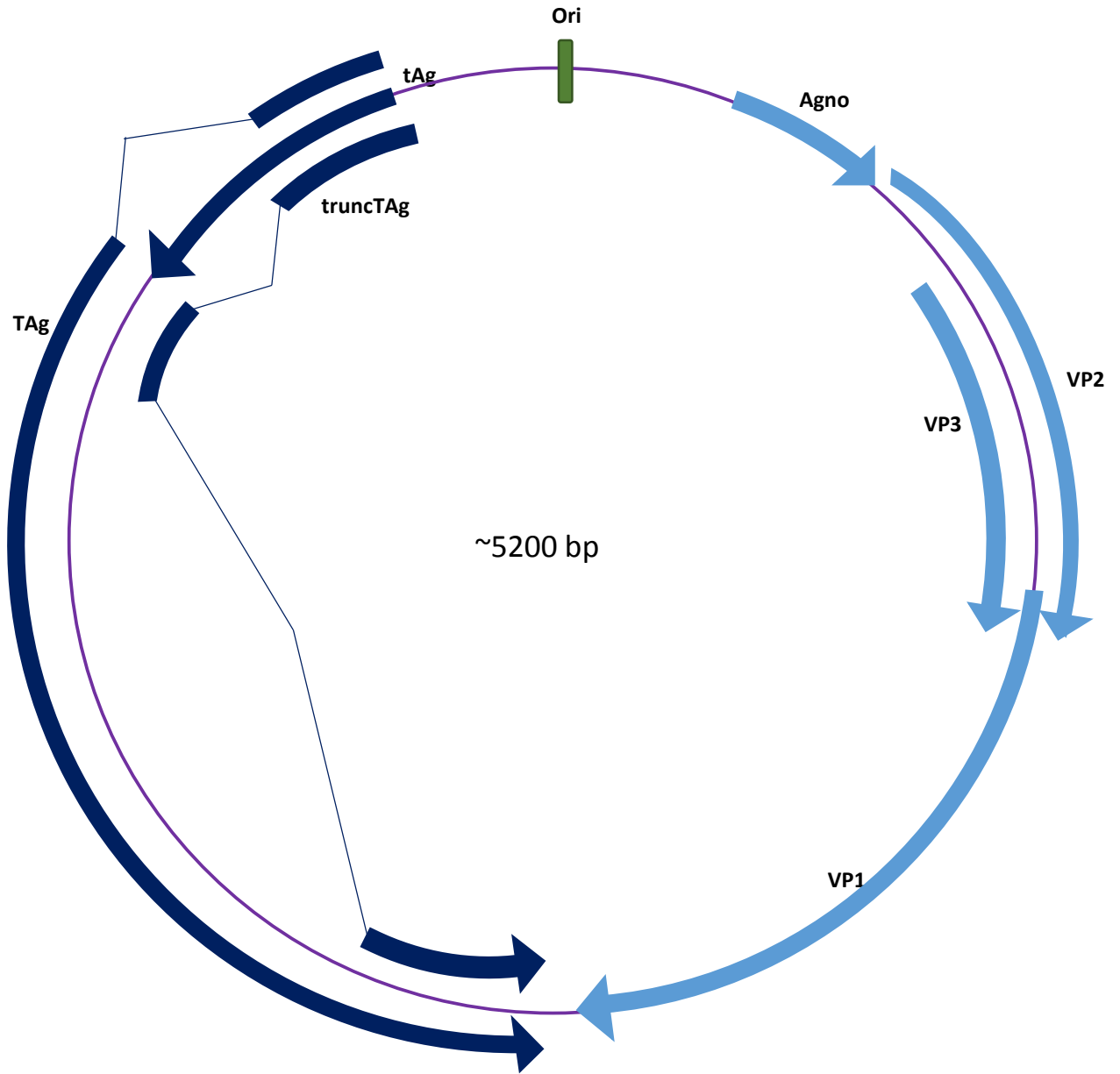
Figure 1.1: A schematic view of BKPyV circular dsDNA genome.
Dark blue regions represent early genes, while light blue regions represent late genes.

1.2.3 Virion Structure

Polyomaviruses such as BKPyV are small 45 nm non-enveloped virions comprising 72 VP1 pentamers, each associated with a single VP2 or VP3 on their inner cavity surface. The pentamers form a capsid with T = 7 icosahedral symmetry; sixty pentamers have six adjacent pentamers, while the remaining twelve have five adjacent pentamers. Each pentamer is stabilised by the C-terminal arms of VP1, while the capsomer as a whole is stabilised by both disulphide bonds and calcium ions. The N-terminal arm of VP1 is associated with the viral genome, condensed within the capsid by ~20 nucleosomes comprising the host-acquired histones H2A, H2B, H3 and H4 (Hurdiss et al., 2016, Fang et al., 2010).
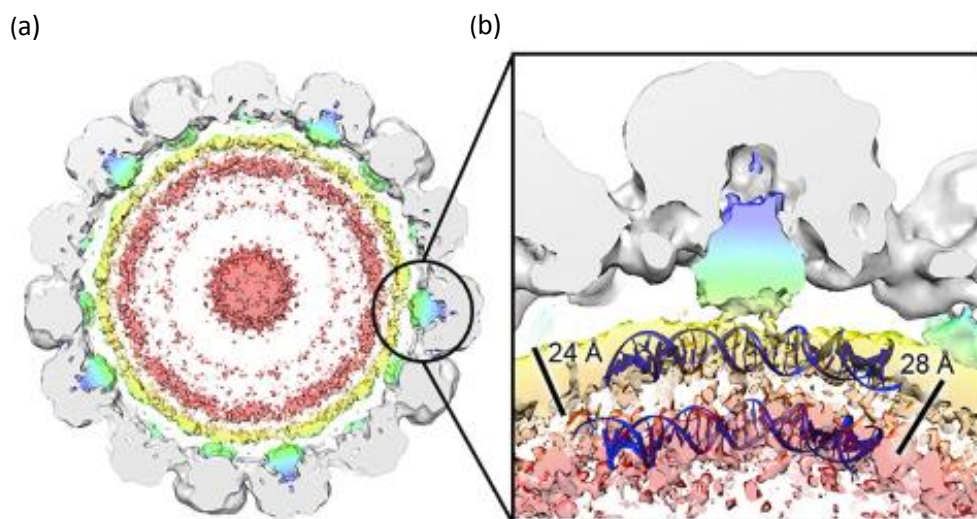
Figure 1.2: Cryo-EM structure of BKPyV virion.
A 40-Å-thick cross section of the virion highlights the VP2/3 attachment to the inner pentamer void, shown in blue/green, contour level 0.0032 (a). Under each VP1 pentamer a VP2/3 is associated. Condensed dsDNA can be seen in two layers of density (b). Image taken from (Hurdiss et al., 2016); used with permission.

1.2.4 Viral Proteins and Known Functions

Table 1.2: An overview of BKPyV viral proteins and their known functions

Viral Protein	Early/Late Expression	Size kDa	Functions and Features	Reference
Small T Antigen (tAg)	Early	20	The first protein, along with TAg and truncTAg to be expressed during infection through alternative splicing of the full length T-antigen mRNA. Modulates host replication processes to drive viral replication. tAg binds protein phosphatase 2A (PP2A), inhibiting it's enzymatic activity.	(Pallas et al., 1990)
Large T Antigen (TAg)	Early	80	The first protein, along with tAg and truncTAg to be expressed during infection through alternative splicing of the full length T-antigen mRNA. Contains an LXCXE motif allowing it to bind Rb, p107 and p130, stimulating cell cycle progression. TAg also functions as a helicase, forming a double hexamer to unwind viral DNA at the Ori, subsequently recruiting host DNA replication proteins. TAg can also bind p53, further modulating host cell cycle progression and apoptosis. Contains a nuclear localisation sequence (NLS).	(Stubdal et al., 1997, Sowd and Fanning, 2012, Lilyestrom et al., 2006, Doherty and Freund, 1997)
Truncated Large T Antigen (truncTAg)	Early	17	The first protein, along with TAg and tAg to be expressed during infection through alternative splicing of the full length T-antigen mRNA. Contains the LXCXE motif identified in TAg, allowing it to bind Rb, p107 and p130, stimulating cell cycle progression. Contains a nuclear localisation sequence (NLS).	(Abend et al., 2009b)
VP1	Late	42	A common feature of all polyomaviruses, the VP1 structural protein forms the main constituent protein of the virus capsid and comprises 5 surface exposed loops; BC, DE, EF, GH and HI. Five copies of VP1 form a pentamer stabilised by C-terminal arms of each VP1, while the N-terminal arms mediate DNA binding. 72 pentamers form each capsid, stabilised by Ca$^+$ cations and disulphide bonds.	(Liddington et al., 1991, Hurdiss et al., 2016)
VP2	Late	38	Minor capsid protein located on the internal side of the capsid. Structurally similar to VP3, sharing the C-terminus but has a longer N-terminus. One copy of VP2 or VP3 is associated with each VP1 pentamer via a hairpin loop inserted into the central pentamer cavity. May have a role in uncoating and targeting to the nucleus via an NLS.	(Chen et al., 1998, Hurdiss et al., 2016, Bennett et al., 2015)
VP3	Late	27	Minor capsid protein located on the internal side of the capsid. Structurally similar to VP2, sharing the C-terminus but has a truncated N-terminus in comparison. One copy of VP2 or VP3 is associated with each VP1 pentamer via a hairpin loop inserted into the central pentamer cavity. May have a role in uncoating and targeting to the nucleus via an NLS.	(Chen et al., 1998, Hurdiss et al., 2016, Bennett et al., 2015)
Agnoprotein (Agno)	Late	8	A small protein of 66 amino acids in length. Thought to colocalise with lipid droplets, and interact with PCNA in an inhibitory manner. Its exact function is unknown.	(Gerits et al., 2015, Unterstab et al., 2013)

1.3 Lifecycle of BKPyV

1.3.1 Attachment and Entry

The capacity to reduce infectivity of BKPyV after neuraminidase treatment along with the haemagglutination of erythrocytes after exposure to BKPyV lead to the discovery that virions, and specifically VP1, are able to bind sialic acid residues on the surface of target cells (Seganti et al., 1981, Sinibaldi et al., 1990). In culture BKPyV has been shown to bind a number of b-series gangliosides including GD3, GD2, GD1b and GT1b (Low et al., 2006, Neu et al., 2013). Those cells which do not express these gangliosides are resistant to BKPyV infection however these same cells, if induced to express GD3, GD2, GD1b or GT1b, become permissive to infection. It has been suggested that both the $\alpha(2,3)$-linkage of sialic acid to galactosyl residues and the $\alpha(2,8)$-linked sialic acid residues play an important role in the binding of BKPyV to the cell surface; enzymatic removal of these linkages was shown to reduce infection, whilst reinstatement of them once again caused cells to be permissive to infection (Dugan et al., 2005, Low et al., 2006).

Cell tropism differences have been noted for different BKPyV serotypes (Pastrana et al., 2013) and it is suspected that there may be more than just interaction with sialic acid residues required for infection. It has been shown for MCPyV that sialic acid binding is secondary to a potential glycosaminoglycan binding (Schowalter et al., 2012).

Once bound to a receptor, BKPyV has been shown to enters African Green Monkey Kidney (Vero) cells by caveolin-mediated endocytosis (Eash et al., 2004) although renal proximal epithelial tubule (RPTE) cells, a human primary cell type which better represents in vitro infection sites, show a cell entry mechanism which is both clathrin and caveolin independent (Zhao et al., 2016). Once endocytosed BKPyV are thought to remain within endocytic vesicles for up to four hours (Moriyama and Sorokin, 2008).
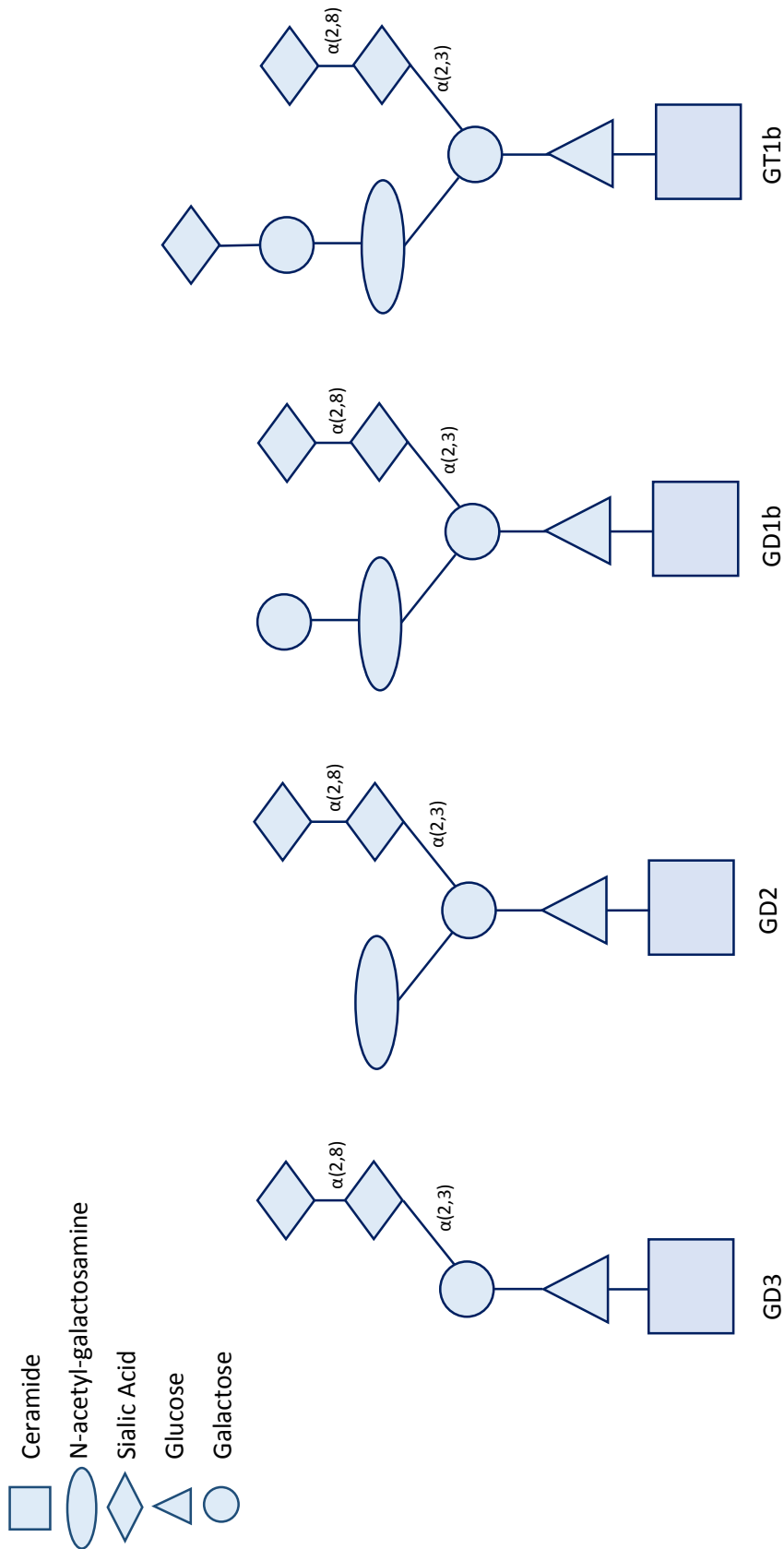
Figure 1.3: A schematic view of known host glycolipid receptors with sialic acid binding residues that bind BKPyV VP1 pentamers.

It is thought the two α(2,8)-linked sialic acid residues and the α(2,3)-linked galactose and sialic acid residues are key to modulating binding of BKPyV to host cells.

1.3.2 Transport to the Nucleus

Once internalised it has been shown that in RPTE cell vesicles containing BKPyV are trafficked along microtubules and as such, infection can be disrupted with the use of the microtubule depolymerising drug nocodazole. Vesicle bound BKPyV are targeted to the endoplasmic reticulum (ER), avoiding the Golgi apparatus, in a dynein independent manner (Moriyama et al., 2007, Moriyama and Sorokin, 2008). There is also compelling recent evidence that BKPyV entry involves Rab18 positive endosomes (Zhao and Imperiale, 2017). Delivery to the ER along this pathway is thought to take 8-12 hours (Moriyama and Sorokin, 2008). It is interesting to note that in Vero cells vesicle trafficking does not show the same dependency on microtubule dynamics (Eash and Atwood, 2005), further illustrating the importance of conducting experiments in cell types which most closely align with those of natural infection sites.

Upon reaching the ER BKPyV virions are deposited into the ER lumen through fusion of the host vesicle and ER membrane. It is thought that capsid disassembly begins in the ER through disassociation of VP1 disulfide bonds (Jiang et al., 2009b) exposing VP2 and VP3 hydrophobic residues that embed into the ER membrane. The ER associated protein degradation (ERAD) and proteasome pathways, both primarily used by cells to recycle misfolded proteins, are then hijacked to allow transport of the partially disassembled capsid out of the ER and to the nuclear pore via the targeting of the exposed NLS regions of VP2 and VP3 (Bennett et al., 2013). There is evidence that partially disassembled capsids are then imported into the nucleus by the α/β1 importin pathway (Bennett et al., 2015). It is generally considered to take 12-18 hours before the viral capsids reached the nucleus and the genome is fully uncoated.

1.3.3 Gene Expression and Genome Replication

BKPyV relies on host machinery for protein synthesis, regulated tightly by host transcription factors recruited to the bidirectional NCCR transcription factor binding sites, of which there are more than 30 (Moens et al., 1995, Johnsen et al., 1995). At around 12-24 hours after viral entry to the cell such transcription factors are recruited to the NCCR. The early genes are the first to be transcribed, which comprise primarily of TAg and tAg, as well as the lower abundance additionally spliced TAg transcript that encodes for truncTAg (Abend et al., 2009b). Each of the early proteins are translated from alternatively spliced T-antigen mRNA (DeCaprio and Garcea, 2013). The early proteins are essential for viral replication, working to promote cell growth, cell cycle checkpoint bypass, apoptotic resistance and thus stimulating a cellular environment favourable for viral DNA replication. Most studies into the effects of these early genes have been conducted in other human and primate polyomaviruses.,

however, due to extensive sequence homology between genomes one may tentatively extrapolate the data to encompass BKPyV. After its synthesis the NLS of TAg causes it to be quickly transported to the nucleus, where it plays a multifunctional role (Doherty and Freund, 1997). The binding of TAg to p53 has been shown to lead directly to apoptotic resistance, while also stimulating cell cycle progression through reduced checkpoint arrest signalling in response to any DNA damage in SV40 (Lilyestrom et al., 2006). In JCPyV, MCPyV and SV40, TAg has been shown to bind pRB family proteins, preventing early cell cycle arrest and stimulating progression from the early cell cycle growth phase (G1) to synthesis (S) phase, known as the G1/S checkpoint (Bollag et al., 2000, Borchert et al., 2014, White and Khalili, 2006). This is further enhanced in SV40 by TAg binding to Hsc70, an ATPase-containing chaperone protein which triggers the disassociation of pRb and E2F, allowing TAg to bind pRb directly (Sullivan et al., 2000). Cell growth in BKPyV infected cells has been shown to be stimulated by an activated MAP kinase pathway, stimulated by TAg (Seamone et al., 2010). The SV40 tAg, in contrast, has a more minor role in cell cycle progression. It binds and inhibits the enzymatic activity of protein phosphatase 2A (PP2A), a protein phosphatase which has more than 300 cell cycle regulatory targets (Skoczylas et al., 2004). BKPyV tAg also contains the Retinoblastoma (Rb) binding motif LXCXE suggesting it may, like TAg, also lead to bypass of the G1/S checkpoint, although this has yet to be formally demonstrated (Ehlers and Moens, 2014).

TAg also acts as a viral helicase, the only viral protein identified to be involved in viral genome replication. Forming a dimeric hexamer, TAg binds GAGGC motifs found at the Ori in the NCCR of the viral genome. Host replication factors are then recruited to the Ori, leading to viral replication at around 18-24 hours after infection (Bennett et al., 2012). During viral genome replication the host DNA damage response (DDR) pathway is activated, preventing BKPyV-induced damage to host DNA (Verhalen et al., 2015).

Late genes are transcribed and translated from around 24 hours after infection from a common pre-messenger RNA (pre-mRNA) which is alternatively spliced to form individual messenger RNA (mRNA) transcripts which are then transported from the nucleus (Huang and Carmichael, 1996). Transcribed from the complementary viral DNA strand, mRNA transcription is driven by both the increased copies of viral genomes and TAg induced changes in transcription factor binding in the NCCR (Moens et al., 1997). The late genes comprise the structural proteins VP1, VP2 and VP3 which make up the viral capsid, and also Agno, which may play a regulatory role in replication. Agno is known to bind proliferating cell nuclear antigen (PCNA) in an inhibitory manner, suggesting a role in reducing viral genome synthesis and promoting viral capsid assembly (Gerits et al., 2015). The roles of Agno are thought to extend beyond this, and it has also been shown to bind N-ethylmaleimide-sensitive factor Attachment Protein Alpha (α-SNAP), suggesting a role in trafficking (Panou et al., 2018).

However, point mutations of Agno in BKPyV genomes that prevent synthesis of Agno, have shown virus is still infectious in Vero cells (Johannessen et al., 2011). Furthermore, in RPTE cells infected with mutant BKPyV in which wild-type Agno expression is eliminated genome levels are comparable, and may even exceed, that of cells infected with wild type BKPyV (Panou et al., 2018).

1.3.4 Virion Assembly

Once synthesised in the cytoplasm VP1 forms pentamers, each associated with a single VP2 or VP3 on what will become the innermost surface (Lin et al., 1984). These are quickly transported into the nucleus due to NLS. Capsid assembly has been found to spontaneously occur with overexpression of VP1 alone, in this instance leading to virus-like particles (VLPs), although stability of VLPs is greatly increased in the presence of VP2 and VP3 (Teunissen et al., 2013).

Imported pentamers are transported to nuclear 'viral factories' which are located near promyelocytic leukaemia nuclear bodies (PML-NB), although these are not essential for viral replication and encapsidation (Erickson et al., 2012). For MuPyV the encapsidation of non-viral vector DNA was found to be dependent on total amount of vector DNA in the proximity of the virus factory and not sequence specific (Spanielova et al., 2014), however mutations in the N-terminus of SV40 TAg lead to less efficient viral assembly, suggesting a role for TAg in DNA encapsidation (Spence and Pipas, 1994a, Spence and Pipas, 1994b). Furthermore in JCPyV heat shock protein 70 (Hsp70), typically involved in protein folding and prevention of protein aggregation (Mayer, 2005), has been shown to mediate capsid DNA binding to TAg and VP2/3 (Saribas et al., 2014). Interestingly, Hsp70 is an essential viral replication factor recruited by not only *Polyomaviridae* but also *Adenoviridae*, *Poxviridae* and *Orthomyxoviridae* among others (Mayer, 2005).

In BKPyV the known DNA binding region of VP1 N-terminus is thought to stimulate encapsidation of viral genomes, ultimately leading to the completed synthesis of progeny virions in the nucleus (Hurdiss et al., 2016).

1.3.5 Lytic Virion Release

As a non-enveloped virus it has been commonly accepted that the primary method for viral release from an infected cell is through cellular lysis after rupturing the nuclear membrane. The swollen nuclei of infected cells are a distinctive infectious marker and tightly packed virions within the nucleus at late stages of infection in transplant patient derived renal tubular cells can be seen with transmission electron microscopy (TEM) (Drachenberg et al., 2003). In JCPyV it has been shown that neither VP1

nor Agno alone were capable of causing cell lysis, although Agno was found to act as a viroporin which may, in the context of late stage infection and swollen nuclei, contribute to nuclear membrane failure and rupture (Suzuki et al., 2010).

1.3.6 Non-Lytic Virion Release

There is little data that has been published on the mechanisms of polyomavirus release from infected cells. It has been postulated that a method of non-lytic release for polyomavirus may exist. The establishment of lifelong infections, coupled with minimal inflammatory responses to such an infection, suggests that cell lysis may not be occurring in this silent yet persistent stage of infection. Furthermore, evidence for non-lytic release of other non-enveloped viruses has been identified. The parvovirus Minute Virus of Mice (MVM) has been shown to be trafficked along cytoskeleton filaments, bound by vesicles, and that this process is necessary for effective viral release (Bar et al., 2008). Hepatitis A (HAV), a pathogenic picornavirus, appears to acquire host membranes prior to non-lytic release from an infected cell, cloaking the virus from recognition and neutralisation by host antibodies (Feng et al., 2013). Yet another non-enveloped virus, poliovirus, has been shown to require microtubules for extracellular release in a non-lytic manner (Taylor et al., 2009). Most notably the polyomavirus SV40 has been shown to be released from the apical surface of primate kidney epithelial cells without cell lysis, and that this release could be inhibited with monensin, a sodium ionophore which blocks the transport of secretory vesicles from the *trans*-Golgi network (Clayson et al., 1989).

In addition to evidence on non-lytic release in other non-enveloped viruses, it has been shown that JCPyV Agno mutant progeny are less able to egress the nucleus and release (Ellis et al., 2013). The role of BKPyV Agno interaction with α-SNAP has been suggested to play a role non-lytic egress, affecting the exocytosis pathway (Johannessen et al., 2011). Most recently BKPyV Agno has been shown to be an essential factor for nuclear egress in non-lytic infections (Panou et al., 2018). Our lab has also provided evidence for a non-lytic release mechanism for BKPyV (Evans et al., 2015), which will be discussed further as the basis of Chapter 2 of this thesis.
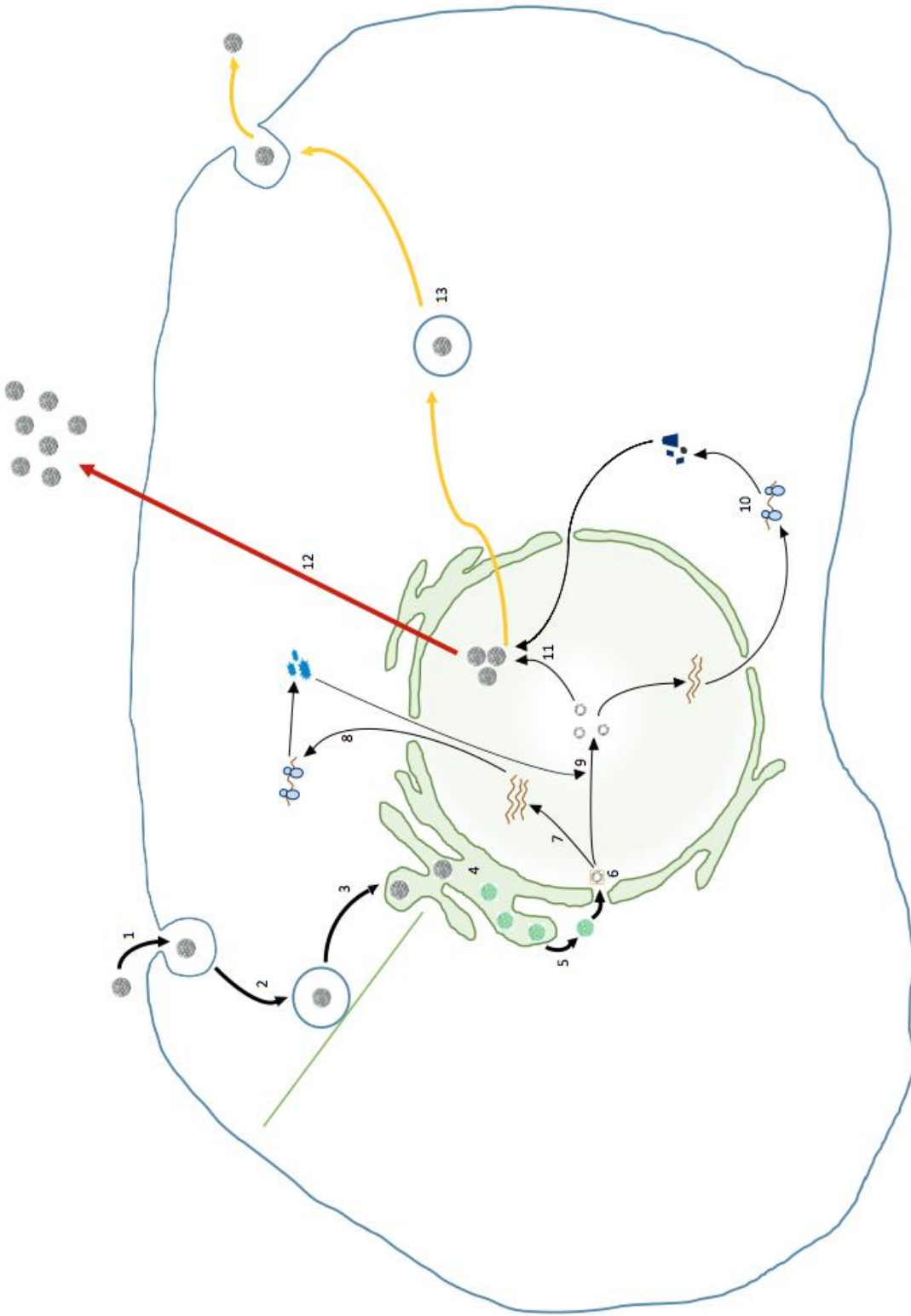
Figure 1.4: A model of the BKPyV lifecycle.

(1) Viral attachment is mediated by host glycolipid receptors with sialic acid residues that bind the virion, other unknown co-receptors may be involved in binding. Virions are internalised in a clathrin and caveolin independent manner. (2) Vesicle bound virions are trafficked via microtubules towards the ER bypassing the Golgi. (3) Vesicles fuse with the ER and deposit the virion into the ER lumen. (4) Virions undergo partial uncoating through the breaking of VP1 disulphide bonds, which is thought to partially expose VP2 and VP3 NLSs. (5) Partially uncoated virions exit the ER by the ERAD pathway and are targeted to the nucleus. (6) The BKPyV genome is deposited into the nucleus. (7) Early genes TAg, tAg and TruncTAg are transcribed. (8) Early genes are translated. TAg, TruncTAg and a proportion of tAg are trafficked into the nucleus. However, the vast majority of tAg remains cytoplasmic. (9) Newly synthesised TAg forms a viral helicase, allowing BKPyV genome to be replicated. (10) Late Genes, VP1, VP2, VP3 and Agno are transcribed, and then translated in the cytoplasm. Structural proteins are transported into the nucleus by NLSs, while a small proportion of Agno may be transported into the nucleus. (11) Structural proteins and newly synthesised genomes assemble to form progeny virions. (12) Exit from the cell has traditionally thought to occur exclusively by cellular lysis after nuclear membrane rupture. (13) Evidence is shown in this thesis for a non-lytic active secretion pathway of virus cellular exit and spread.

The work detailed in this thesis relates to a number of different host processes that appear to be involved in BKPyV release and/or modified during infection. The relevant host pathways are introduced below.

1.4 Eukaryotic Secretory Pathways

1.4.1 Conventional Secretion

Proteins that are secreted from cells, be they soluble extracellular proteins or residents of the cell surface membrane, can be transported via a number of routes. The same is also true for non-lytic release of viruses. The best understood and studied of these pathways is conventional vesicular egress, a pathway which traffics cargo from ER lumen through the Golgi and on to the cell surface, either by the constitutive secretory pathway or the regulated secretory pathway.

Constitutive secretion is the direct trafficking of vesicle bound proteins from the *trans*-Golgi network (TGN) directly to the cell surface, where the contents are released upon fusion of vesicle and cell surface membranes (Fig. 1.5). Cellular proteins known to traffic by the constitutive secretory pathway include serum proteins such as immunoglobulins and transferrin, and extracellular matrix proteins such as collagen and proteoglycans (Lodish et al., 1995). In contrast to this, upon vesicle budding from the TGN, regulated secretion pathways see proteins stored in immature secretory vesicles which mature and concentrate cargo until such time that a signal or cellular environmental change triggers release. Proteins known to release in this way may be peptide hormones, such as endorphins, digestive enzymes, such as ribonuclease or trypsin, or milk proteins such as casein or lactalbumin (Lodish et al., 1995). Another example of a regulated secretion protein is insulin. Within the pancreas reside β-cells which secrete insulin in response to high concentration of glucose which stimulate an action potential within the cell. Until such time as a high glucose concentration signal is received, insulin is stored and secretion regulated by inhibitory signals that control exocytosis (Rorsman and Braun, 2013).

The pathways for both constitutive and regulated conventional secretion begin in the same manner. The membrane-bound or soluble secreted proteins are translocated into the ER during synthesis, this is directed by the presence of a 5-16 amino acid signal peptide located towards the N-terminus of the nascent protein (Walter and Lingappa, 1986). If correctly folded by molecular chaperones found in the ER, the target protein will dock with membrane-bound receptors, which stimulate COPII vesicle formation. COPII coated vesicles are targeted to the endoplasmic reticulum Golgi intermediate complex (ERGIC) by Rab1, a small GTPase of the Ras superfamily, leading to fusion of vesicles with the ERGIC (Allan et al., 2000, Lodish et al., 1983).

The ERGIC organelle is situated between the ER and the Golgi, directing vesicles containing proteins between the two, thus any misfolded proteins may be transported back to the ER for re-folding in COPI coated vesicles. Correct folding in the ER may feature additional post-translational modifications such as disulphide bridge formation and N-linked glycosylation. Should refolding in the ER prove unsuccessful the misfolded protein will be retro-translocated from the ER back into the cytoplasm by the ERAD pathway, where they are ubiquitinated and targeted for proteasomal degradation (Kostova and Wolf, 2003). Correctly folded proteins are trafficked along microtubules from the ERGIC to the TGN in COPII coated vesicles, then on through the TGN in a targeted *cis* to *trans* manner in COPI vesicles. During transport through the TGN proteins may undergo further post-translational modification of glycans. Once protein synthesis and post-translational modification has been completed target proteins can be secreted (Munro, 2011).

In the constitutive secretory pathway cargo-containing vesicles that bud from the *trans*-Golgi can be trafficked directly to the plasma membrane, where upon docking they undergo membrane fusion resulting in the enclosed cargo being released directly into the extracellular space. Proteins that are transported via the constitutive secretory pathway are thought not to have specific secretory signals, instead large tethering complexes interact with the vesicle coat to target contents to the plasma membrane or other subcellular locations. Tethering complexes are Rab effectors/exchange factors, thus it is the interaction of specific tethering complexes and Rabs which direct intracellular trafficking (Cai et al., 2007). One example of tethering regulating vesicle targeting is the golgin tether GM130 which interacts with Golgi-reassembly stacking protein of 65kDa (GRASP65; also known as GORASP1), itself an effector of Rab1, leading to stacking of Golgi cisternae and regulation of COPII vesicle targeting to, and fusion with, the TGN (Barr et al., 1998).

There are ~70 human GTPases which form the well conserved family of Rab proteins. Membrane-bound through a covalently linked lipid-anchor, Rabs cycle between active guanosine triphosphate (GTP) and inactive guanosine diphosphate (GDP) states through the activity of GDP/GTP exchange factors (GEFs) and GTPase activating proteins (GAPs). Active Rabs facilitate membrane budding in response to cargo selection and tethering complex binding, followed by trafficking to target membranes. Once membranes fuse and cargo is released, Rabs become inactive and cycle back to their original cargo selection membrane. Each Rab shows a specific subcellular localisation and effector target membrane, for example Rab5 is found on the membranes of early endocytic cargo, but as the endosome matures it is replaced with Rab7 which targets vesicle contents to lysosomes (Rink et al., 2005). It must be noted however that there may be some overlap in function and/or partial redundancy that is not fully understood (Zhen and Stenmark, 2015).

Once brought into proximity with one another by tethering complexes and Rabs, soluble N-ethylmaleimide-sensitive factor attachment protein receptor (SNARE) proteins mediate fusion of membranes and release of vesicle contents (Sollner et al., 1993). SNARE proteins are present on both vesicle (v-SNARE) and target (t-SNARE) membranes, anchored to membranes by their N-terminus with a SNARE-specific 60-70 amino acid cytosolic region that forms coiled-coil helices through heptad repeats (Rothman and Warren, 1994). Further classification of SNAREs can be made by the key amino acid residues which form the centre of the helical bundle, R-SNAREs contain an arginine (R) in the helical bundle, while Q-SNAREs contain a glutamine (Q) (Fasshauer et al., 1998). Current understanding of SNARE complexes suggests that membrane fusion occurs entirely by mechanical force, once one v-SNARE and three t-SNAREs are brought into contact with one another the tightly formed four helix bundle draws opposing membranes together until the lipid bilayers merge and a fusion pore is made, spilling the vesicle contents through (Sudhof and Rothman, 2009).

In this way tethers, Rabs and SNAREs work in conjunction with one another to mediate complex and multifaceted trafficking pathways directing secretory cargo to their appropriate destination.
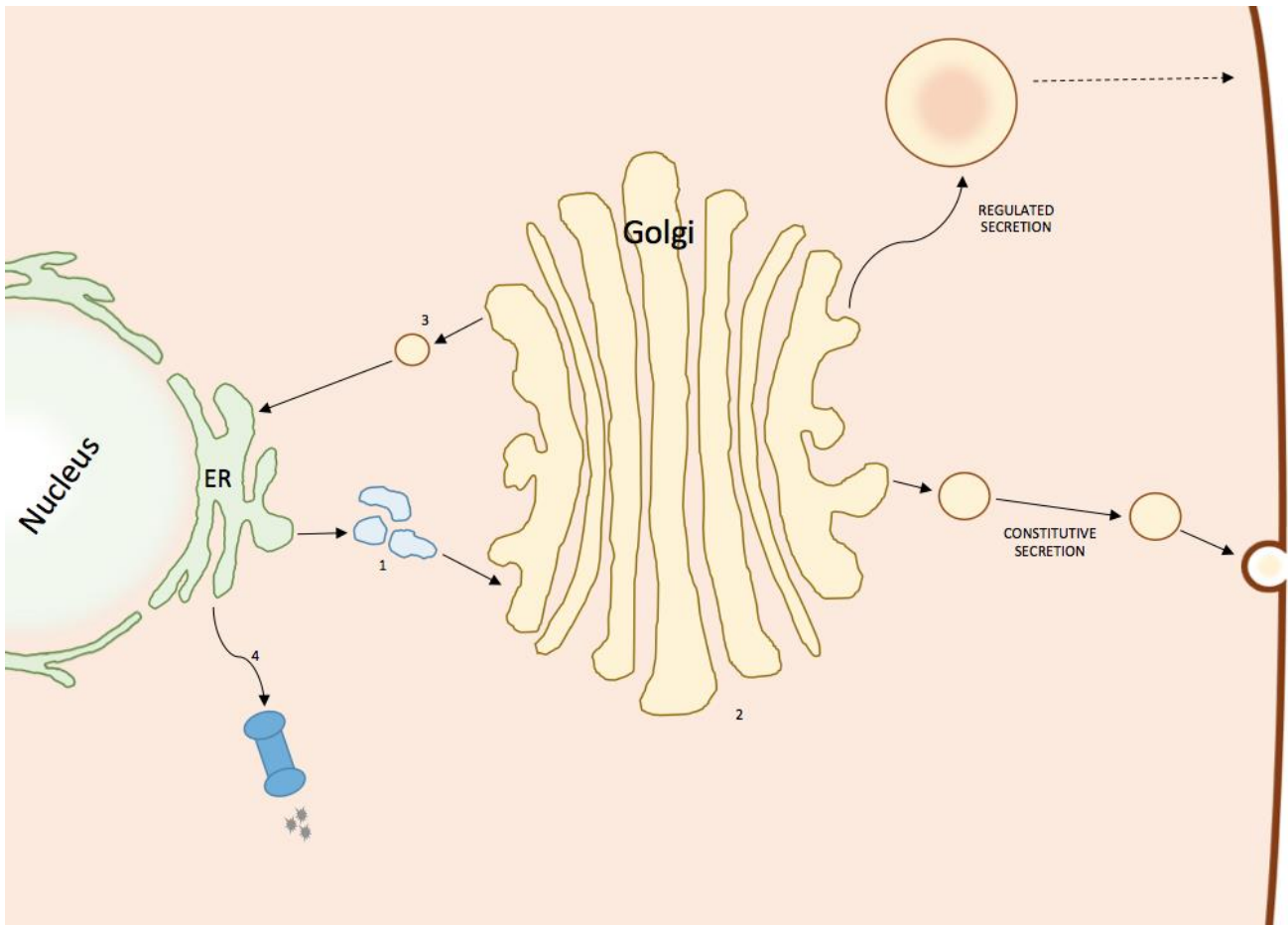
Figure 1.5: The ERGIC and ERAD both work as protein quality control pathways.
(1) The ERGIC directs proteins between the ER and Golgi, only allowing correctly folded and glycosylated to traffic onwards to the Golgi. Should proteins be incorrectly folded they are directed back towards the ER. (2) Further glycosylation occurs as proteins traffic from the *cis* to *trans* face of the Golgi, incorrectly glycosylated and processed proteins can still be trafficked back to the ER to allow correct processing. (4) Should folding and glycosylation fail repeatedly, proteins are trafficked out of the ER by the ERAD pathway, ubiquitinated and transported to the proteasome for degradation.

1.4.2 Unconventional Secretion

Unconventional secretory pathways are an umbrella term for those vesicular and non-vesicular secretory pathways which do not traffic from the ER to the Golgi, then via secretory vesicles to the plasma membrane, but utilise other methods to reach the extracellular space. First identified when Brefeldin A (BFA), an inhibitor of the small GTPase ADP-ribosylation factor 1 (ARF1), induced inhibition of Golgi trafficking yet still failed to prevent secretion for a number of cellular proteins (Nickel and Rabouille, 2009). At least four of pathways have thus far been described and it seems likely that there are others which are yet to be discovered.

The first of these suggested pathways, termed Plasma Membrane Pore Formation (PMPF), is the translocation of non-vesicular proteins into extracellular space through lipidic pores. These pores may either be constructed through oligomerisation of the protein being translocated, or of other cellular components which transiently form pores. In the first example certain fully-folded cytoplasmic proteins bind phosphatidylinositol 4,5-biphosphate (PI(4,5)P2) enriched in inner plasma membranes, forming a pore through self-oligomerisation. Once oligomerised they insert into the plasma membrane, then translocate to the extracellular membrane. They then dissociate and are able to able to enter the extracellular space (Rabouille, 2017). This pathway is not only identified in the secretion of cellular protein fibroblast growth factor 2 (FGF2) (Steringer et al., 2015), but also secretion of the viral HIV protein, transactivator of transcription (TAT) (Debaisieux et al., 2012), illustrating that viruses are able to subvert different secretory pathways.

Another example of PMPF is seen during inflammation, where inflammation itself drives pore formation. In macrophages it has been shown that IL-1b release can be triggered by the hyperpermeabilisation of the cell plasma membrane, suggested to utilise pores formed by gasdermin-N which is cleaved by caspase 1 in times of inflammation (Ding et al., 2012, Rabouille, 2017).

The second described pathway of unconventional protein secretion can occur for proteins targeted to late endosomal or lysosomal compartments forming Multi Vesicular Bodies (MVB). These endo-lysosomal compartments can be induced to fuse with the plasma membrane and their contents are released, allowing both organelle contents and any intraluminal vesicles, also known as exosomes, contained within to be released. Exosomes, small extracellular vesicles carrying various forms of cargo such as mRNA, proteins and even viruses, were once thought to bud directly from the plasma membrane. Exosome formation occurs through Endosomal Sorting Complex Required for Transport (ESCRT)-mediated budding events into the late endosomal or lysosomal compartments which go on to become MVBs (Kowal et al., 2014). This allows both free and membrane bound proteins to be released into the extracellular space. Both membrane bound and free IL-1b and Caspase 1 have been

shown to be released in this way in times of inflammation (Qu et al., 2007, Andrei et al., 2004). Targeting of MVBs to the plasma membrane has been shown to be mediated by Rab11, Rab27a, Rab27b and Rab35 (Zhen and Stenmark, 2015). Both HAV and the parvovirus MVM have evolved to hijack this secretory pathway to aid their release from cells, bound in exosomes such viral transmission likely reduces extracellular detection of viruses by both the innate and adaptive immune systems (Jackson et al., 2005, Feng et al., 2013). Norovirus and rotavirus, both non-enveloped enteric viruses appear to be released from cells in a non-lytic manner contained within large extracellular vesicles. Such vesicles, when shed in stool, were more infectious than free virus found within the same stool. These vesicles were proposed to be exosomal or potentially derived directly from plasma membrane budding, however a specific pathway remains to be elucidated (Santiana et al., 2018).

Times of stress may also lead to the third type of unconventional protein secretion, Autophagy Induced Protein Secretion (AIPS). In AIPS, autophagy derived membranes form vesicles termed 'secretory autophagosomes', comprising curved tubular double membranes which fuse with the plasma membrane, thus trafficking autophagic membrane bound proteins to the plasma membrane. In one such case, upon cellular starvation the Golgi-Associated Stacking and Reassembly (GRASP) family protein Grh1, a Rab1 interactor and yeast homolog of mammalian GRASP65 (also known as GORASP1), is relocated from the ER/Golgi to tubular membranes which are autophagy derived, although they may fail to form complete autophagic vesicles, these membranes go on to fuse with the plasma membrane (Bruns et al., 2011). One protein to be secreted by this pathway in *Dictyostelium* is Acb1, which is thought to be concentrated in the tubular membranes or within the lumen of the autophagosome itself and is released when the autophagic membrane fuses with the plasma membrane (Duran et al., 2010). Acquisition of these autophagic membrane and subversion of this unconventional secretion pathway has been described variously for varicella zoster virus (VZV), Epstein Barr virus (EBV) and poliovirus among others (Buckingham et al., 2014, Nowag et al., 2014, Jackson et al., 2005).

The fourth described pathway is termed Golgi-bypass and is the direct trafficking of proteins from the ER to the plasma membrane in small ER-derived vesicles. This is driven by ER stress and has been described in such circumstances where the ERAD pathway is unable to cause degradation of mis-folded proteins. In the case of F508-deleted Cystic Fibrosis Transmembrane Conductance Regulator (*CFTR) ER stress leads to S441 phosphorylation of GRASP55 (also known as GORASP2), causing it to monomerise and relocate to the ER where it interacts with the *CFTR cargo. Single membraned vesicles containing the membrane-bound *CFTR are formed, which traffic to the plasma membrane (Gee et al., 2011). A similar process has been described for H723R pendrin (*pendrin), whose over-abundance in the ER leads to increased expression of DnaJ homolog subfamily C member 14

(DNAJC14), and along with its co-chaperone Hsp70, traffics the membrane-bound protein directly to the plasma membrane (Jung et al., 2016).
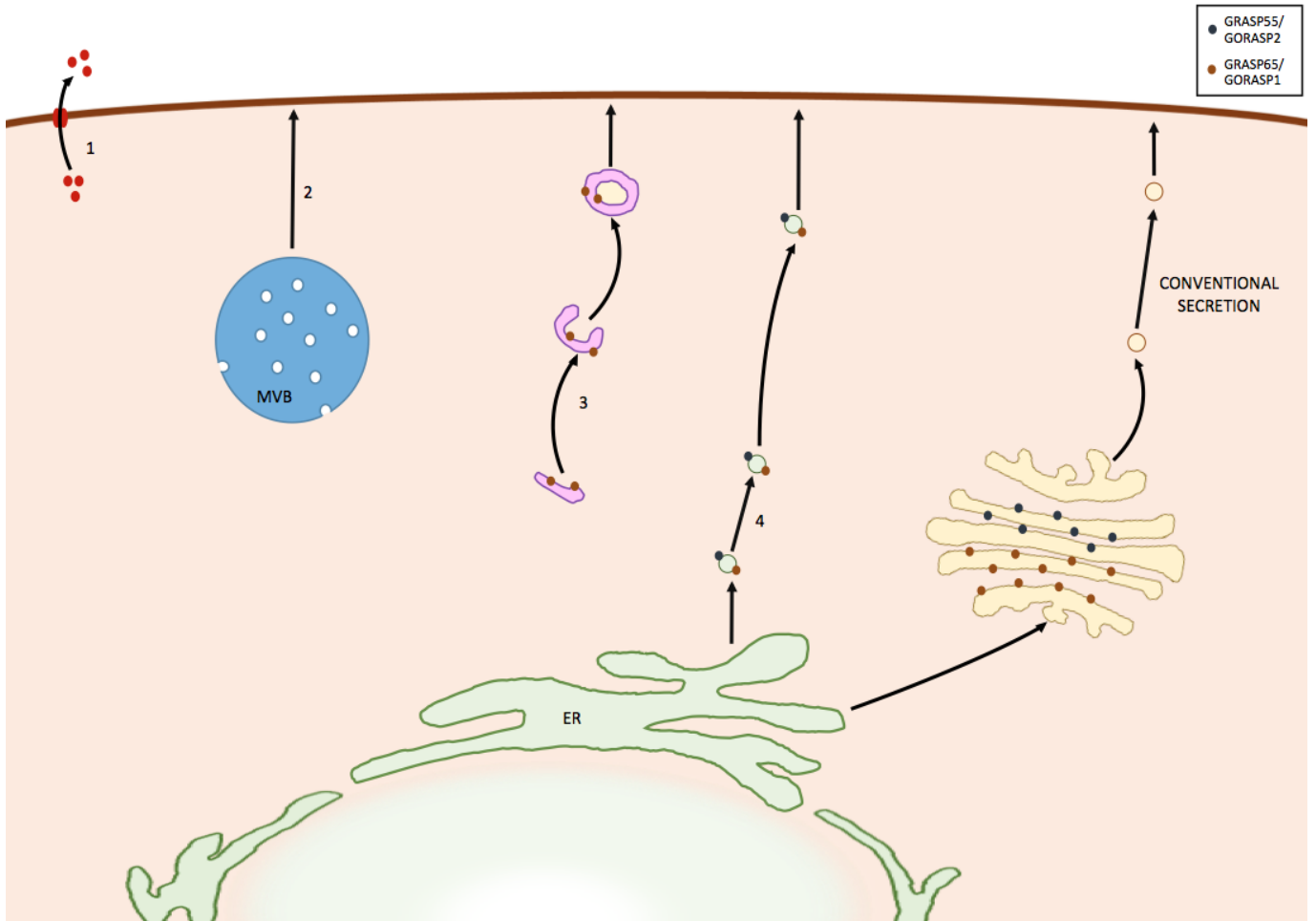
Figure 1.6: Unconventional secretion pathways.
Unconventional secretion pathways described so far include (1) direct translocation through pore formation, either by cellular stress or by the translocated proteins themselves. (2) MVBs of late endosomal or lysosomal origin fuse with the plasma membrane spilling the organelle contents, including exosomes, into the extracellular space. (3) Autophagy driven double membrane formation around cytoplasmic proteins lead to their delivery to the extracellular space. Autophagy membrane bound proteins are also secreted in this way. Grh1, a yeast homolog of mammalian GORASP1, is often translocated from the Golgi and found in these autophagy driven membranes. (4) Golgi bypass in times of ER stress leads to single membranes pinching off from the ER and trafficking directly to the plasma membrane; both GORASP1/2 and DNAJC14 have been found to be involved in Golgi-bypass trafficking.

1.5 Eukaryotic Cell Cycle Regulation

1.5.1 General Overview of Cell Cycle Regulation

Eukaryotic cell growth and division is universally represented as a cyclical process that is controlled by the organised accumulation, activation, deactivation and breakdown of the regulatory proteins, in particular cyclins and cyclin dependant kinases (CDKs). First identified in yeast in 1976 (Nurse et al., 1976) these regulatory proteins have been the subject of much research ever since. The cell cycle itself has four key distinct phases; G1, the first growth phase, is a cell which contains a single complement of chromosomes (2n), undergoing normal metabolic activity and growth. After G1 cells may enter S (synthesis) phase, in which a new complement of genomic material is synthesised. Once the genomic content of a cell reaches 4n cells enter G2, the second growth phase. During G2 cells continue to grow rapidly, duplicating organelles and preparing cell content to enable division, which occurs when cells enter M (mitosis) phase. M phase is the organisation and division of cell content into two distinct compartments which actively splits the cell into two daughter cells, whereby this process may begin again, or allow cells to exit the cell cycle, entering G0.

There are checkpoints within the cell cycle which are able to prevent a cell progressing through the cycle should insufficient growth signals or too many inhibitory signals be received (indicated with orange flashes in Fig. 1.7), and again it is through the activity of cyclins and CDKs that it is possible for these checkpoints to be implemented.

The first of these checkpoints is the G1 restriction checkpoint. Cells will only progress from G1 to S phase when the correct growth signals are received along with intracellular cues, such as the availability of sufficient cellular energy resources. Until the G1 checkpoint the transcriptional activators E2F1-3 are bound to and repressed by Rb protein, which prevents entry into S phase. This is further enhanced by the binding of p107 to E2F4 and p130 to E2F5 ensuring these transcriptional repressors located in the nucleus. As a cell progresses through G1 and upon receiving correct growth signals the levels of cyclin D increase and binds either CDK4 or CDK6. The cyclin D:CDK4/6 complex is active and phosphorylates Rb, p107 and p130. This phosphorylation releases the transcriptional activators E2F1-3, allowing them to translocate to the nucleus and drive transcription of S phase genes, while phosphorylated p107 and p130 release E2F4 and E2F5 which are transported to the cytoplasm where they can no longer repress transcription of the same family of genes (Bertoli et al., 2013).
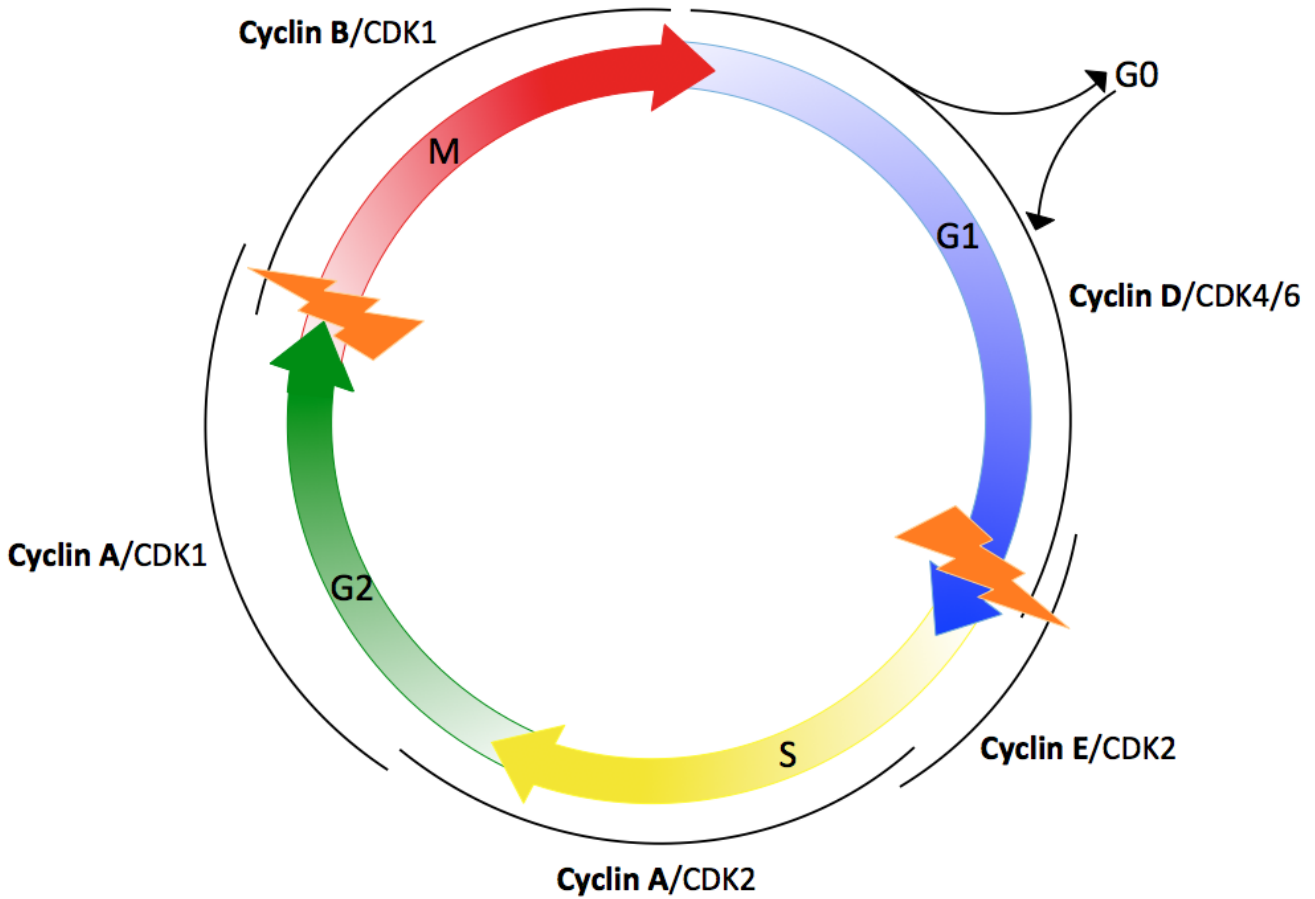
Figure 1.7: Cell cycle, cyclins and cyclin dependant kinases.
The cell cycle progresses from G1 through to S upon release of the transcription factors E2F1-3 (and associated removal of E2F4 and E2F5 repressors). Once DNA has been correctly synthesized in S phase cells can move into G2. Finally progressing onto M phase. The mitotic checkpoint ensures chromosomes are lined up on the mitotic spindle, sufficient organelles exist, and cells separate correctly. This process is completed through the cyclical synthesis, recruitment and degradation of cyclins and their binding partners, CDKs.

Among the genes transcribed by E2F1-3 is cyclin E that binds CDK2 and further enhances transition into S phase, forming a positive feedback loop. Later cyclin A, also transcribed by E1F1-3, preferentially binds CDK2, forming a complex that phosphorylates E2F1-3, preventing further transcription of S phase genes. E2F6-8, other transcriptional products of E2F1-3, also repress transcription of S phase genes, giving rise to an overall negative feedback loop, causing cells to exit S phase and enter G2 (Bertoli et al., 2013, Skotheim et al., 2008).

The second checkpoint occurs at the G2/M transition, where during the start of G2 phase cyclin A binds CDK1. During G2 the levels of cyclin B increase, but the protein remains inactive and cytoplasmic until it is phosphorylated by polo-like kinase 1 (Plk1) or CDK1, which allows cyclin B to translocate to the nucleus and act as a transcription factor for mitotic genes when in complex with CDK1, having displaced cyclin A. Upon displacement cyclin A is ubiquitin tagged for degradation (Hagting et al., 1999). CDK1 itself is held inactive throughout S phase through its phosphorylation by Wee1 kinase. Upon signalling to pass the G2/M checkpoint Wee1 is tagged for ubiquitination and degradation by phosphorylation by Plk1. Plk1 also phosphorylates cdc25, itself a phosphatase, and in doing so causes cdc25 to dephosphorylate CDK1, thereby activating CDK1 (Guardavaccaro and Pagano, 2006). Once cells have divided cyclin B is ubiquitinated and tagged for degradation by anaphase promoting complex (APC) allowing cells to exit M phase, returning to G1. Cell cycle de-regulation and inefficient checkpoint regulation can result in uninhibited proliferation of cells, this could be due to self-sufficiency in growth signals or insensitivity to anti-growth signals, both of these features are two of the key hallmarks of cancer. As such, it is easy to see how de-regulation of the cell cycle have wide ranging implications in the field of tumour growth and cancer development (Hanahan and Weinberg, 2000).

1.5.2 Polyomaviruses, BKPyV and Cell Cycle Deregulation

Members of the polyomavirus family have long been implicated in cell cycle manipulation and deregulation, indeed MCPyV is thought to be the primary causative agent of over 80% of Merkel Cell carcinoma (MCC) through clonal integration of the viral genome into the host, and the resultant effects of constitutive TAg and tAg expression on both the Rb-family and p53 proto-oncogenes. It has been shown that removing the effects of TAg and tAg by knocking down with short hairpin RNA (shRNA) can not only prevent MCC positive cells from replicating, they in fact go on to die, while those cells without viral clonal integration do not (Houben et al., 2010). As stated previously, SV40 TAg has been shown to carry a LXCXE motif which binds to Rb, p107 and p130, this has an effect similar to the phosphorylation of these proteins by the cyclin D:CDK4/6 complex, thus causing cells to bypass the G1/S restriction checkpoint even in the absence of the correct proliferation signals (Decaprio et al.,

1988, Stubdal et al., 1997). In addition to this, when TAg combines to its dimeric hexamer helicase form, the outer surface can bind p53. A tumour suppressor protein, p53 usually responds to ATM/ATR DNA damage signals by transcribing a number of genes which induce the cell cycle to be stalled at the G2/M phase checkpoint. Stalling of the cell cycle allows time for DNA repair to take place, should DNA repair not occur in a timely manner apoptosis is triggered. Inactivation of p53 therefore allows the cell cycle to progress through checkpoints, where it may normally be halted under such a circumstance (Lilyestrom et al., 2006). The overall effect of these interactions is to forcibly drive the cell cycle onward in the absence of the correct cues, and to override DNA damage signals which would cause the cell to exit the cycle and undergo apoptosis.

Furthermore, tAg is able to bind PP2A regulatory subunit A and catalytic subunit C. This causes the substrate adaptor subunit B to be substituted by tAg and so the activity and specificity of the whole PP2A holoenzyme is altered. The effect of this is wide ranging as PP2A has a large number of targets, however many of the effects are through proliferative signalling cascades such as the MAPK/ERK and AKT pathways, thus providing further cell cycle deregulation (Pallas et al., 1990).

It has further been shown that TAg must be phosphorylated to become active and able to form the dimeric hexamer helicase capable of unwinding viral DNA for replication. In SV40 this phosphorylation site has been shown to be T124, while in JCPyV it is T125 (McVey et al., 1996, Swenson and Frisque, 1995). Mutation of these residues prevents viral replication and these have been shown to be CDK recognition sites (Swenson et al., 1996, McVey et al., 1996). Furthermore it has been suggested that cyclin A:CDK2 and cyclin B:CDK1 complexes can efficiently phosphorylate TAg threonine residues (Li et al., 1997).

Unlike MCPyV, BKPyV and other non-integrating polyomaviruses have yet to be shown as the causative agent of any cancer. However BKPyV-induced cell cycle deregulation may contribute to its role as a suggested cofactor in a number of cancers induced by other oncoviruses such as Human Papilloma Virus (HPV), EBV and Human Herpes Virus 8 (HHV-8), having been isolated from tumours in tandem with these viruses (Moens et al., 2014).

BKPyV TAg and tAg carry the same motifs described for SV40 which would enable them to bind p53, Rb-family proteins and PP2A, thus indicating that they have the same activities; being able to de-regulate cell cycle check points (Moens et al., 2007, Harris et al., 1998). It has also been shown that increased MAPK/ERK signalling is able to increase levels of BKPyV replication in vivo (Seamone et al., 2010) suggesting that proliferative signalling is beneficial for BKPyV viral replication.

1.6 Innate Immunity

1.6.1 General Overview of Innate Antiviral Immunity

Viral infection can be detected by cells in a number of ways, triggering an antiviral immune response intended to reduce virus replication and reinfection rates. Cellular sensors may detect viral RNA, viral DNA or other pathogen associated molecular patterns (PAMPs), activating mitochondrial antiviral signalling protein (MAVS) and stimulator of interferon genes (STING) mediated pathways that culminate with the transcription of type I and III interferon (IFN), along with pro-inflammatory cytokines (Liu et al., 2015). In response viruses, due to their extensive co-evolution with hosts, have developed a variety of ways in which to evade activation of cellular antiviral responses.

Viral RNA can be sensed when it forms double strands (dsRNA), not normally found in host cells. Protein kinase R (PKR) upon sensing of dsRNA inhibits eukaryotic initiation factor 2α (eIF2α), preventing cap-dependant translation of both host and viral RNA, leading to reduced rates of replication. In addition, stimulated PKR can also induce autophagy and cause activation of inflammasomes, protein complexes which are able to recognise a variety of stressors and activate the pro-inflammatory IL-1β and IL-18, leading ultimately to pyroptotic cell death (Pindel and Sadler, 2011). Another sensor of dsRNA, oligoadenylate synthase (OAS), can directly bind dsRNA and activate RNase L, through production of 2'-5'-linked oligoadenylate. Ribonuclease L (RNase L) degrades both cellular and viral RNA, inhibiting viral replication. Furthermore the resultant RNA fragments are PAMPs, acting as ligands for retinoic acid-inducible gene-I (RIG-I) proteins, whose downstream signalling leads to the production of IFN (Chakrabarti et al., 2011).

Viral DNA is most often sensed in the cytoplasm, a subcellular location in which endogenous DNA is not usually found. The cytosolic DNA sensor, DNA-dependent activator of IFN-regulatory factors (DAI), senses poly dA:dT and induces the translocation of nuclear factor-κB (NF-κB) and IFN regulatory factor 3 (IRF3), which go on to transcribe type I IFNs (Takaoka et al., 2007). Both DNA-dependant protein kinase (DNA-PK) and meiotic recombination 11 homolog A (MRE11) can bind cytoplasmic DNA, triggering IRF3-mediated type I IFN transcription (Chu et al., 2000, Kondo et al., 2013). Cyclic GMP-AMP synthase (cGAS) directly binds the sugar-phosphate backbone of cytoplasmic dsDNA in a sequence independent manner, again causing the transcription of type I IFN, driven by IRF3 translocation (Sun et al., 2013). In the nucleus viral dsDNA, whose origins of replication tend to be AT-rich and serve as binding and recognition sites for TAg, are recognised and translated by RNA polymerase III (Pol III) into small RNA fragments, leading to the production of IFN through RIG-I activation as seen with RNA viruses (Chiu et al., 2009). Interferon-γ (IFNγ)-inducible protein 16 (IFI16)

can also sense nuclear viral DNA, leading to the activation of inflammasomes triggering inflammatory responses (Unterholzner et al., 2010).

PAMPs can also include 5'-triphophate or 5'-diphosphate RNA, not found in host cellular RNA, or poly-U/UC both recognised by RIG-I, while melanoma differentiation protein 5 (MDA5) recognises an improperly methylated 5'-cap of RNA along with high molecular weight dsRNA. These both lead to transcription of IFN (Kato et al., 2006).

In addition to these pattern recognition receptors (PRRs) another family of proteins, toll-like receptors (TLRs), mount an effective response to viral and other pathogens. TLRs are membrane bound dimeric receptors which recognise a number of PAMPs, leading to the expression of IFNs and proinflammatory cytokines via NF-κB, IRF3 or IRF7 mediated pathways. Most anti-viral TLRs are located within endosomal membranes, TLR3 can recognise endocytic dsRNA, TLR7/8 recognises ssRNA, while TLR9 recognises unmethylated CpG DNA often found in DNA viruses. TLR2 and TLR4 are found on the cell surface and can recognise viral haemagglutinin and envelope proteins (Akira and Hemmi, 2003). Leucine-rich repeats (LRRs) allow TLRs to recognise their specific substrates, going on to signal via the cytoplasmic Toll/interleukin-1 receptor (TIR) interactions with the cytoplasmic adaptor proteins MyD88 or TRIF (Yamamoto et al., 2003).

Coevolution of viruses with innate immune systems has resulted in the emergence of a plethora of evasion mechanisms. For example, many flaviviruses such as Hepatitis C (HCV) and Dengue Virus (DENV) replicate their RNA genomes in replication complexes located on and within ER membranes, shielding the nascent RNA from recognition by many of the PRRs primed to detect dsRNA in the cytoplasm. While HCV also synthesises a protease which is able to cleave MAVS, preventing many PRR signals from stimulating an antiviral response (Li et al., 2005). Furthermore, HCV NS4B and NS3 proteins prevent STING signalling and IRF3 activation by phosphorylation (Nitta et al., 2013). Evasion of detection by RNA viruses may be even more effective if conducted within intracellular organelles, such as Influenza whose replication takes place in the nucleus and incoming viral RNA is coated in nucleoprotein, once again shielding the viral RNA from detection in the cytoplasm by PRRs. Viral RNAs may also be processed from 5'-triphosphates to prevent activation of RIG-I, such as the 5' overhangs seen in Arenaviruses which are unable to activate RIG-I (Marq et al., 2011). If detection cannot be evaded PRRs or MAVS may be bound and modified, cleaved and degraded or even sequestered; one example is Hepatitis B virus (HBV) which encodes an X protein that interacts with MAVS and prevents signal transduction through stimulating its degradation (Wei et al., 2010).

DNA sensors may be degraded also, both Herpex Simplex Virus 1 (HSV-1) and human cytomegalovirus (HCMV) have been shown to degrade IFI16 through the activity of the encoded infected cell protein 0

(ICP0) and pUL83 protein respectively (Orzalli et al., 2012, Li et al., 2013b). Furthermore STING can be cleaved and inactivated, as is the case in DENV infection (Aguirre et al., 2012), while Kaposi Sarcoma Herpes Virus (KSHV) encodes a vIRF1 protein which can bind and inactivate STING (Ma et al., 2015).

In addition to these mechanisms to evade activation of interferon transcription, viruses may also evade the interferon stimulated genes (ISGs) themselves for example HCMV can antagonise PKR through preventing phosphorylation of eIF2α (Ziehr et al., 2016).

1.6.2 Polyomaviruses, BKPyV and Innate Antiviral Immunity

Little is known about the interactions of innate immunity and polyomaviruses. SV40 TAg was shown to stimulate ATR kinase, leading to an induction of ISGs such as IFIT3, IFIT1 and OASL, which resulted in an antiviral state (Forero et al., 2014). However, the same has not been shown for BKPyV. MCPyV tAg was observed to bind the NF-κB adaptor protein NEMO, preventing NF-κB activation and downstream interferon induction (Griffiths et al., 2013), while MCPyV TAg downregulates TLR9 (Shahzad et al., 2013); again these interactions appear to be specific for MCPyV and have not been shown for BKPyV.

Interestingly, expression of the early protein TAg, late protein VP1, and total viral replication is reduced significantly with IFN-γ treatment of cells from 3-6 hours post infection (hpi) in both BKPyV and JCPyV infections (Abend et al., 2007, De-Simone et al., 2015), suggesting that both these polyomaviruses are susceptible to IFN. However, while JCPyV replication was shown to be inhibited by an IFN-type I response stimulated during infection in Renal Proximal Tubule Epithelial (RPTE) cells, BKPyV infection of the same cell type sees no such attenuation of replication. Indeed, while IFN-β is generated by RPTE cells in both JCPyV and BKPyV infections, those cells infected with JCPyV showed much greater expression of ISGs than those infected with BKPyV, suggesting innate immune responses even between very closely related viruses may vary (Assetta et al., 2016).
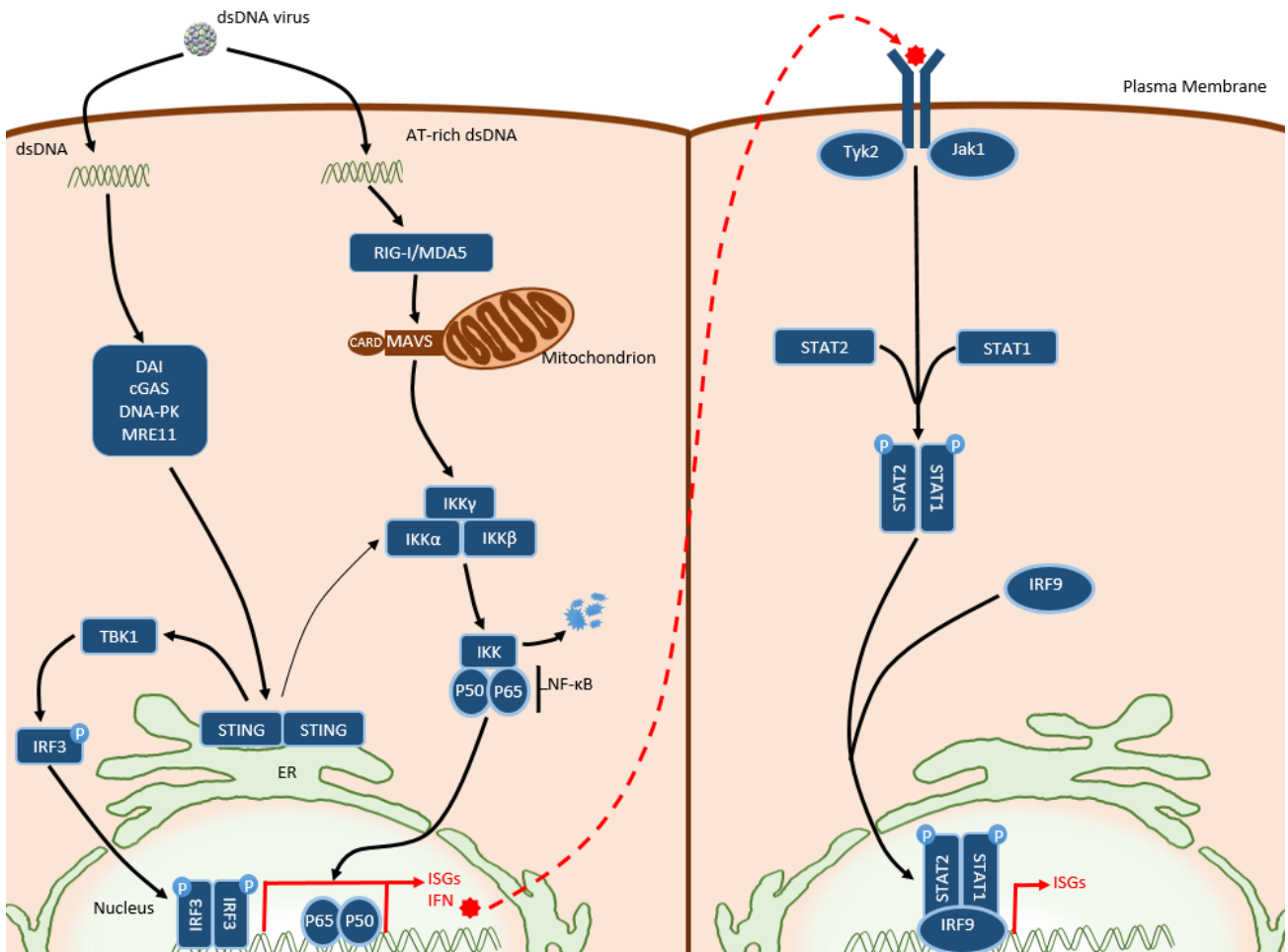
Figure 1.8: dsDNA viruses trigger transcription of ISGs and IFN.
Aberrant early uncoating of viral particles releases viral dsDNA into the cytoplasm, a compartment in which DNA is not usually located, triggering activation of DNA sensors of the STING and MAVS pathway. Pathway activation leads to translocation of phosphorylated IRF3 dimers or NF-κB (a p50/p65 dimer) that go on to transcribe an array of ISGs and IFN. Secreted IFN may then further activate surrounding cells by binding IFN receptors, a dimer of IFNAR-1 and IFNAR-2. The subsequent downstream signal leads to phosphorylation and dimerization of STAT1 and STAT2, which then binds to IRF9 and translocates to the nucleus and transcribes additional ISGs (Adapted from (Gale and Foy, 2005, Schneider et al., 2014))

1.7 Adaptive Immunity

1.7.1 General Overview of Adaptive Antiviral Immunity

Adaptive antiviral immunity relies on the processing of non-self viral proteins into peptides by antigen presenting calls (APCs) which are loaded onto major histocompatibility complexes (MHCs), presented to T cells and can lead to cytotoxic cellular killing by CD8+ T cells or B cell activation by CD4+ T cells.

Intracellular pathogens, such as viruses, are primarily tackled by MHC-I. Cytosolic viral peptides are cleaved by the proteasome and the resultant 8-10 amino acid peptides are transported to the ER where they are loaded into MHC-I binding groove by chaperones and transport associated with antigen processing (TAP) protein (Wieczorek et al., 2017). Once loaded the viral peptide and MHC-I is transported to the cell surface where it is presented to immature CD8+ T cells whose T cell receptors (TCRs) are rearranged and driven to become more specific for the antigen should the TCRs be repeatedly stimulated along with co-stimulation by CD80, CD86, or CD4+ T helper cells. Active CD8+ cells stimulated by IL-2 clonally expand to produce a population of CD8+ T cells which are able to recognise infected cells that are presenting MHC-I bound with the same stimulatory peptide. CD8+ T cells are cytotoxic and are able to effectively kill those infected cells by perforin and granzyme mediated lysis (Andersen et al., 2006).

Extracellular viral proteins that are taken up by antigen presenting cells (APCs) via endocytosis, or viral proteins which are contained within early endosome and lysosomes of APCs, are tackled by MHC-II. These viral proteins are cleaved by endosomal and lysosomal proteases in a subcellular antigen-processing compartment, generating 14-18 amino acid peptides that are then loaded into the binding groove of MHC-II found in the membranes of the same compartment (Wieczorek et al., 2017). MHC-II loaded with viral peptides are then transferred to the plasma membrane, where they are presented to naive CD4+ T cells in secondary lymphoid organs, activating them. Activated CD4+ T cells go on to activate naïve B cells which, with the help of T_{FH} cells, proliferate. Activated B cells are then able to produce antibodies as short-lived plasma cells, or undergo further affinity selection and clonal expansion, eventually generating highly specific antibody-secreting long-lived plasma cells and memory B cells (Damle et al., 1991).

The antibodies generated are able to challenge infection in a number of ways. Antibodies generated against capsid or envelope proteins can bind extracellular virions and either neutralise infectivity, opsonisation and phagocytosis, or induce complement-mediated lysis of membraned viruses. Alternatively antibodies may recognise infected cells that are presenting MHC loaded with viral peptides, leading to killing of infected cells by antibody dependant cellular cytotoxicity (ADCC) or complement-mediated lysis and phagocytosis (Forthal, 2014).

1.7.2 Polyomaviruses, BKPyV and Adaptive Antiviral Immunity

It is well established that polyomaviruses induce an adaptive immune response; indeed prior polyomavirus infection rates are measured by the presence of seroconverted antibody in patient serum (Shah et al., 1973, Kean et al., 2009, Viscidi et al., 2011). However, what remains unclear is why these responses often fail to clear polyomavirus infections entirely.

Studies of adaptive immune responses to polyomaviruses are largely limited to MuPyV due to the availability of a mouse model. These studies have determined that both CD4+ and CD8+ T cell responses are generated in response to infection, with CD4+ T cells going on to aid the establishment of long-term antibody-secreting B cells that mount an effective neutralising antibody response in the face of persistent infection from 3-4 weeks post infection (Guay et al., 2007). CD8+ T cells show the greatest response at around one week post infection, killing infected cells with perforin and granzyme mediated lysis (Kemball et al., 2005). Those mice lacking perforin show a much-increased viral load, emphasizing the importance of early CD8+ T cell responses (Byers et al., 2007). CD8+ T cells are also long lasting, but exhibit a switch from acute CD8+ T cells to chronic during the persistent infection, with acute CD8+ T cells possessing a lower activation threshold, higher levels of lymph node homing due to greater proportions expressing CD62L-selectin and CCR7 receptors, and a higher IL-7 Receptor-α expression, meaning greater response to cytokine expression (Kaech and Wherry, 2007). Even with these extensive adaptive immune responses MuPyV is rarely cleared but merely controlled, as MuPyV DNA is detected many weeks later in the presence of long-lived antibody-secreting B cells and chronic CD8+ T cells; without which increased critical levels of MuPyV replication is seen (Lee et al., 2006). In addition to the roles in viral clearance and management CD8+ T cells also play a role in the detection and prevention of MuPyV tumour development. β_2m -/- mice that cannot express MHC-I exhibit a higher occurrence of MuPyV related tumours, however B cells alone are unable to prevent such tumour development (Drake and Lukacher, 1998).

In relation to BKPyV similar observations have been made. BKPyV is rarely cleared but controlled by CD8+ T cells and antibody-secreting B cells, without which greatly increased levels of viral replication are seen, often leading to PVAN and renal failure (Binggeli et al., 2007, Comoli et al., 2008, Egli et al., 2009). Analogous to MuPyV differences in acute and chronic CD8+ T cell responses have also been observed in humans in response to BKPyV (Mueller et al., 2010), lending some weight to the use of MuPyV mouse models to understand BKPyV pathogenesis (Lee et al., 2006).

1.8 Aim of this Thesis

The broad aims of this thesis were to investigate BKPyV interactions with host proteins, pathways and processes throughout the viral lifecycle in order to better understand the ways in which such a simple virus is able to persist in the population. In investigating these interactions it was my specific intention to understand if BKPyV could be secreted from infected cells in a non-lytic manner, characterising any potential non-lytic secretory pathways discovered. Furthermore it was an objective to define changes to the host cell proteome during infection and study any pathways or processes which were dysregulated in infected cells compared with uninfected cells.

2. BKPyV can be released in an active and non-lytic manner

2.1 Introduction

The continued life cycle of BKPyV and other persistent polyomaviruses from primary infection in early childhood, through to lifelong persistence and propagation, is poorly understood. A predominantly lytic infection is observed in most BKPyV *in vitro* studies. However frequent rounds of lytic infection *in vivo* could lead to extensive cell lysis, tissue damage and inflammatory responses, such as those observed in patients suffering PVAN or HC (Rinaldo et al., 2013), which could induce a range of antiviral responses detrimental to virus persistence. A less destructive mechanism of virus spread that doesn't involve extensive cell lysis could therefore be advantageous for polyomaviruses *in vivo*. A better understanding of viral release from cells would be invaluable due to the growing need for new therapeutics to treat BKPyV related diseases in the ever increasing number of patients under immunosuppressive therapies (Hirsch et al., 2005).

While non-enveloped viruses are commonly thought to spread solely by cell lysis, either through expression of lytic viral proteins or passive cellular cytotoxic damage, it is now clear that a number of non-enveloped viruses can be released from cells in an active and non-lytic manner including the positive strand RNA viruses poliovirus and HAV. For poliovirus, evidence for non-lytic release was first identified when persistent poliovirus infection was observed *in vitro*, where release of virus into medium was detected without any appreciable cell death (Lloyd and Bovee, 1993). Moreover, in polarised Caco-2 cells poliovirus appeared to be trafficked along microtubules to the apical surface, where it was released from the vesicles in which it had aggregated (Tucker et al., 1993). These poliovirus secretory vesicles were observed to be autophagy induced, a method of viral release found to be common among a number of enteroviruses including Coxackievirus and rhinovirus (Mutsafi and Altan-Bonnet, 2018). Comparable observations about HAV have been made for some time. HAV is considered to be released primarily in a non-lytic manner from polarised cells, despite it being classed as a non-enveloped virus (Feng et al., 2013). During human infections with HAV it was noted that virus is excreted in stool, and livers are heavily infected before any immune-mediated responses or damage occur, indicating the virus spreads between cells without lysis (Cuthbert, 2001). Such release has been suggested to occur via the formation of exosomes within MVBs (Bird and Kirkegaard, 2015, Seggewiss et al., 2016).

Two non-enveloped dsDNA viruses also show evidence of non-lytic release from cells. The parvovirus Minute Virus of Mice (MVM) makes use of cellular gelsolin to mediate viral egress via lysosomal and late endosomal vesicles, exploiting an active secretory pathway (Bar et al., 2008). Particularly relevant to the work in this thesis, the primate polyomavirus SV40 was shown to be released from cells in an

active non-lytic manner that is inhibited by monensin (Clayson et al., 1989). Taking these discoveries of non-lytic release via both conventional and unconventional secretory pathways in other non-enveloped viruses, coupled with the lack of evidence for extensive cell lysis during *in vivo* BKPyV infections, investigations were begun into BKPyV secretion and the potential inhibition thereof. Some preliminary work had been commenced by Dr G Evans prior to my arrival in the lab (credited where applicable), which was continued and expanded upon in this thesis.

2.2 Results

2.2.1 Infectious BKPyV release from RPTE cells is inhibited by the anion channel inhibitor DIDS

The capacity for newly synthesised BKPyV virions to be trafficked and released from intact cells as a method of viral progeny release was investigated. Analysing the percentage of total infectious virions released into the supernatant of cells infected with BKPyV proved an efficient way to study the effect of a variety of trafficking inhibitors on BKPyV secretion. For these studies RPTE cells, a primary human cell type that is readily infected by BKPyV and in which the virus replicates efficiently, were used. RPTE cells currently represent the *in vitro* culture system that best mimics the natural site of BKPyV infection (Low et al., 2004). Prior to my arrival to the lab a number of preliminary investigations had been conducted by Dr G Evans. These studies demonstrated that the percentage of infectious BKPyV virions released into the supernatant at 48 hours post infection (hpi) from infected yet uninhibited cells was approximately 1% of total infectious BKPyV content (Fig. S1). Investigation into the effects of a number of trafficking inhibitors on the BKPyV secretion had also been conducted (Table S1). Just one inhibitor, 4,4'-diisothiocyano-2,2'-stilbenedisulfonic acid (DIDS), showed an appreciable reduction in percentage of BKPyV secretion while having little effect on total virus yields or cell viability, consequently this was chosen to be explored further and these subsequent studies form the basis of this chapter.

DIDS is a broadly acting anion channel inhibitor that blocks chloride channels (ClCs) with an approximate $IC_{50} = 40$ μM (Schulz et al., 2010). RPTE cells were infected at one infectious unit per cell (IU/cell) and at 24 hpi DIDS was added in a range of concentrations up to 100 μM. Dimethyl sulfoxide (DMSO) was the diluent for DIDS and so cells were treated with the highest amount of DMSO as an infection control. At 48 hpi the cell-associated and supernatant samples were harvested separately. Infectious virions reach the ER by 8 hpi (Moriyama and Sorokin, 2008), soon after which they enter the nucleus (Bennett et al., 2013). Consequently, addition of DIDS at 24 hpi should avoid any effects on initial viral infection and entry, whilst remaining effective throughout new virion synthesis and secretion. Viral titres of each supernatant and cell-associated harvest were ascertained using a fluorescent focus unit (FFU) assay (Fig. 2.1a). To remove any potential effect of DIDS on viral entry or replication in supernatant FFU titres, all DIDS was removed from supernatant samples by ultracentrifugation of virus. Supernatant virus pellets were then resuspended in PBS at twenty times the original concentration, allowing for dilution of virus into culture media when infecting for FFU.

A dose dependent reduction in supernatant virus titre was observed, reduced by three-and-a-half-fold at 25 μM to fifty-fold at 100 μM. Little effect was observed on cell-associated virus titre, reduced by no more than two-fold at the highest 100 μM DIDS concentration. The percentage of total infectious

virus that was released into the supernatant was calculated (Fig. 2.1b), demonstrating that DIDS caused a significant dose-dependent reduction in virus release by up to twenty-fold at the highest concentrations. Interestingly, more specific chloride channel inhibitors were tested in the initial inhibitor screens by Dr G Evans, but none showed an effect of BKPyV secretion (Table. S1).
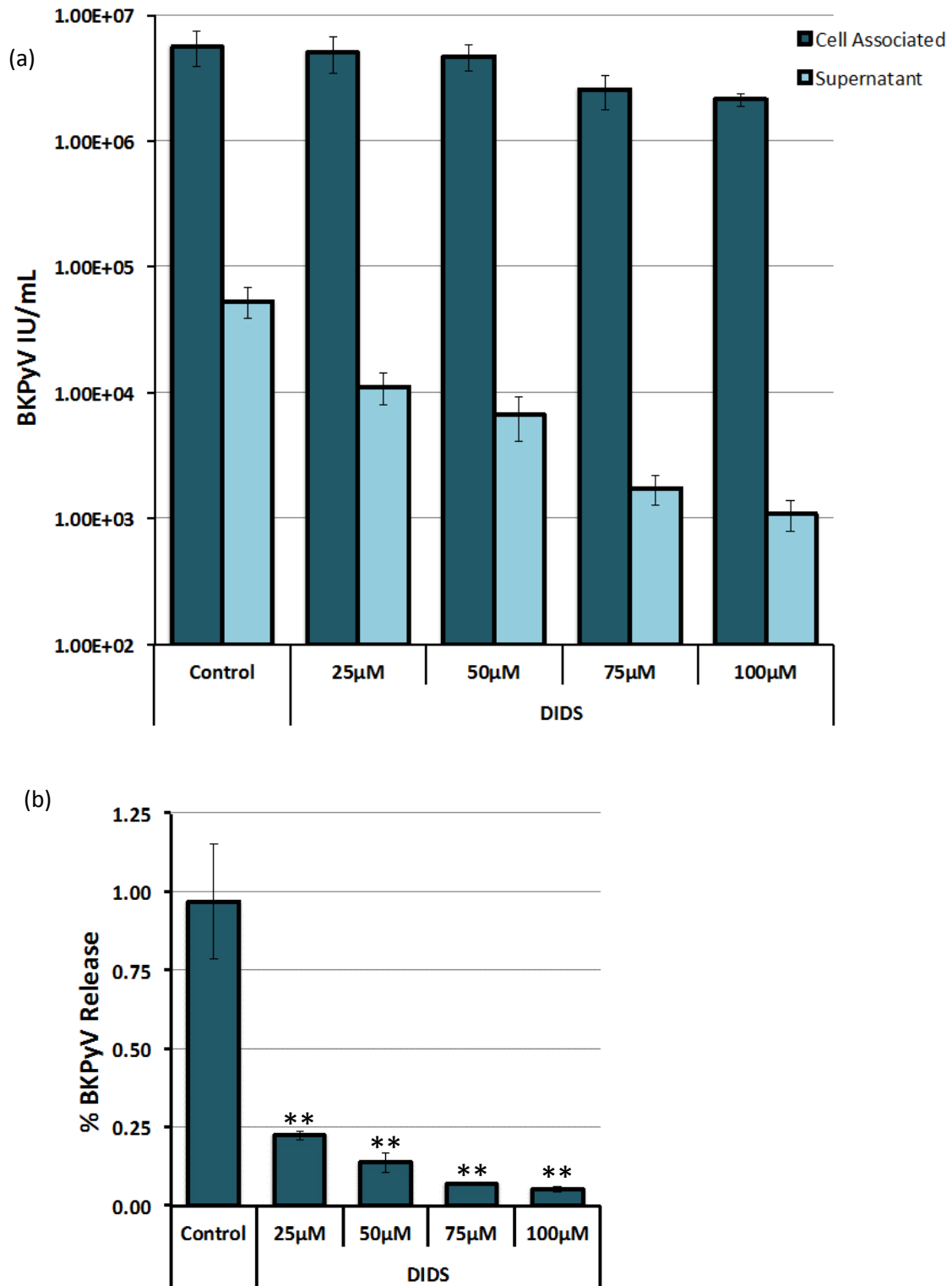
Figure 2.1: Infectious BKPyV release from RPTE cells is inhibited by the anion channel inhibitor DIDS.
RPTE cells were BKPyV infected at 1 IU/cell and treated with increasing concentration of DIDS, or DMSO as a control, at 24 hpi. At 48 hpi supernatant media and cells were harvested independently. Cell associated virus was freeze-thawed three times in fresh media to release the cell-associated virus, supernatant virus was pelleted by ultracentrifugation and resuspended in PBS at 20x the original volume. To determine the virus concentration in each harvest an FFU assay was conducted (a). The percentage of release for each condition was calculated (b). Graphs show the mean of 4 independent experiments, error bars show standard deviation. Students t-test against control, ** $p < 0.01$.

2.2.2 BKPyV capsid protein release from RPTE cells is inhibited by the anion channel inhibitor DIDS

To ascertain whether the reduction of infectious virus release was due to reduced numbers of BKPyV virions in the culture media, or rather if the infectivity of released virions was affected by the presence of DIDS, an immunoblot was conducted to detect the viral structural proteins in the supernatant and cell-associated fractions for each condition. RPTE cells were infected at 1 IU/cell and at 24 hpi DIDS was added in a range of concentrations up to 100 µM, or DMSO was added as a control, and mock infected cells were treated with 50 µM DIDS or DMSO. At 48 hpi the cell-associated and supernatant samples were harvested separately. Virions in the supernatant samples were pelleted by ultra centrifugation to ensure sufficient concentration of viral proteins to be observed by immunoblot. Immunoblots were conducted for the viral structural proteins VP1, VP2, VP3 and the early protein TAg on cell-associated harvests, using tubulin as a loading control (Fig. 2.2a), while an immunoblot for VP1, VP2, VP3 and tubulin was conducted on the supernatant harvests (Fig. 2.2b). The low levels of VP2 and VP3 in the supernatant harvest were at the limits of detection, this is due to the relatively low quantities of VP2 and VP3 incorporated into virions compared with an abundance of free VP2 and VP3 in cell-associated samples. TAg is an early viral gene which is not packaged into virions, as such TAg was not blotted in the supernatant. As a cellular protein tubulin was not clearly detected in the supernatant samples, strongly suggesting little cell lysis had occurred. The level of VP1 present in each sample was quantified using Li-Cor Odyssey software (Fig. 2.2c), which demonstrated that levels of released supernatant VP1 reduced to approximately 30% of control at 25 and 50 µM, and 20% of control at 100 µM. There was a small reduction in cell-associated levels of VP1 at 25-50 µM DIDS, although a greater effect of 100 µM DIDS was observed reducing cell-associated VP1 levels by up to approximately 50% in this experiment, although such drastic reductions were not always observed. Despite the reduction in cell-associated capsid protein levels, the greater reduction in the level of VP1 in supernatant fractions in the presence of DIDS further suggests that DIDS inhibits the release of BKPyV virions from RPTE cells in a dose dependant manner, rather than simply reducing the infectivity of released BKPyV virions. Independent experimental data produced by Dr G Evans showed these same observations and his further analysis by qPCR of BKPyV genomes released further validated the observed dose-dependent reduction of BKPyV release in the presence of DIDS (Fig. S2).
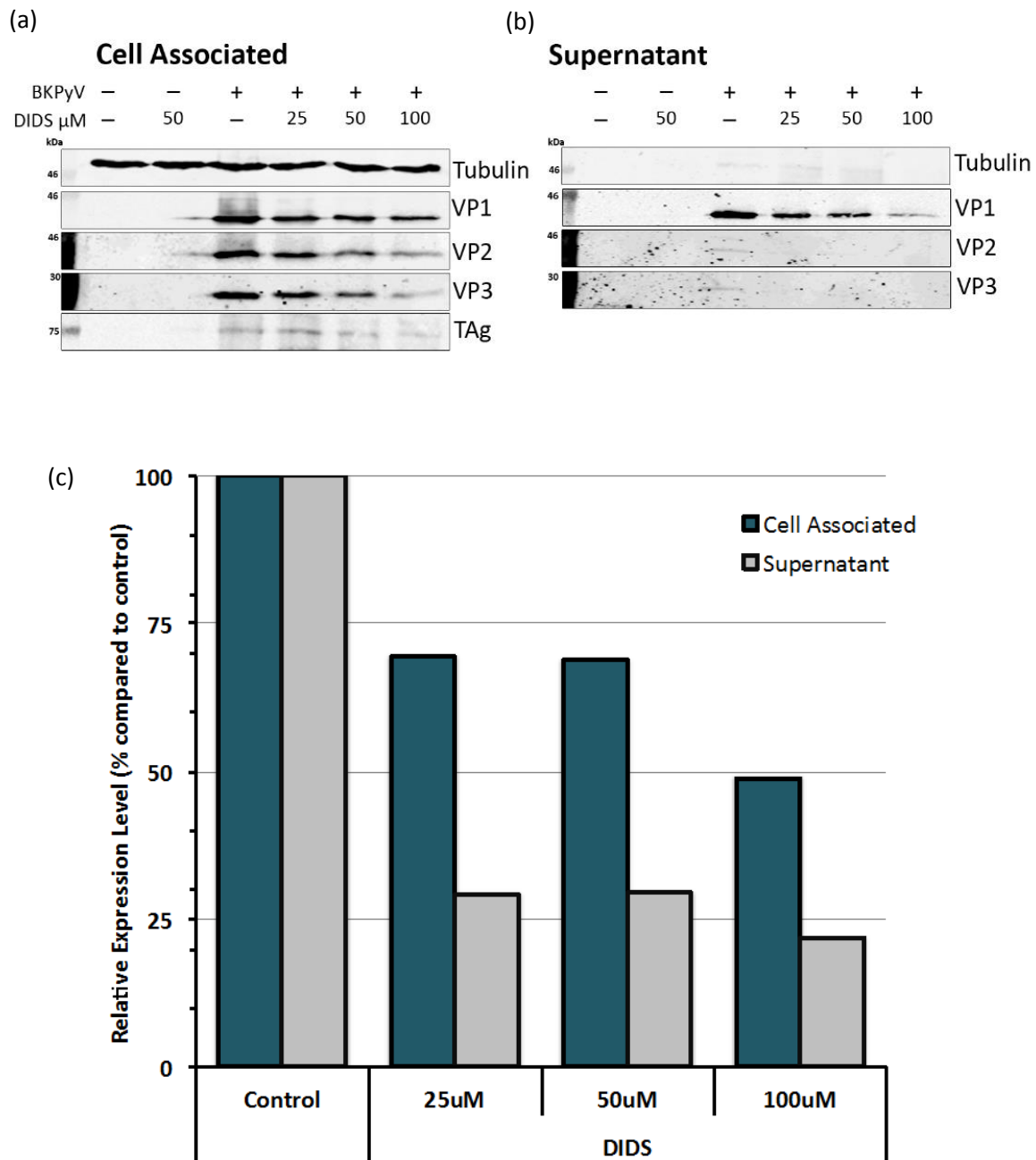
Figure 2.2: BKPyV major capsid protein release from RPTE cells is inhibited by DIDS.
RPTE cells were BKPyV infected at 1 IU/cell and treated with increasing concentration of DIDS, or DMSO as a control, at 24 phi. At 48 hpi supernatant media and cells were harvested independently. RPTE cellular control was mock infected and treated with DMSO, while DIDS control was mock infected and treated with 50 µM DIDS. To determine relative levels of capsid proteins in the cell-associated (a) and supernatant (b) samples immunoblots were conducted for the structural BKPyV proteins and the early protein TAg. To enable detection supernatant proteins were concentrated by ultracentrifugation and as such represent relative protein levels. Tubulin was used as a cellular loading control. Li-Cor Odyssey software was used to determine the density of VP1 bands of the cell-associated (corrected to tubulin) and the supernatant virus samples producing a graph showing relative VP1 levels in DIDS inhibited conditions, compared with control (arbitrarily set to 100%) (c). Data from one experiment shown.

2.2.3 DIDS does not affect RPTE cell viability or viral protein stability

Given the reduction in VP1 expression levels that were observed in the DIDS treated cells (~50% at 100 µM DIDS) there was some concern about whether DIDS was affecting cell viability or viral protein stability, which could impact the interpretation of the data described above. To address the concern that DIDS may be reducing viability of cells, a trypan blue exclusion assay was conducted on RPTE cells that had been incubated for 24 h in increasing concentrations of DIDS up to 100 µM, or DMSO as a control. Non-viable cells take up the trypan blue impermeable dye, whilst it is excluded from cells that are viable thus allowing quantitation of non-viable cells as a percentage of total cells. These data demonstrated that whilst the viability of RPTE cells was reduced slightly in the presence of DIDS, cell viability remained above 85% even at the highest concentration of DIDS (Fig. 2.3). This may partially explain the small decrease in cell-associated infectious virus shown in Fig 2.1a, but is unlikely to cause the large reduction in virus released into the supernatant observed throughout these experiments. For further experimental investigations a standard of 50 µM DIDS was adopted as more than 90% of cells remained viable at this concentration, yet virion secretion was reduced by almost eight-fold.

The stability of proteins can be assessed using a cycloheximide (CHX) chase assay. CHX is an inhibitor of protein synthesis in eukaryotes, interfering with ribosomal translocation and preventing elongation of nascent proteins (Ennis and Lubin, 1964). Addition of CHX to cells therefore inhibits new protein synthesis, and subsequent analysis of protein content over time after CHX addition by immunoblot allows the turnover rate of proteins to be determined in a number of conditions, as there is no new protein synthesis. The stability of major viral capsid protein VP1 was investigated in this manner. RPTE cells were infected with BKPyV at 1 IU/cell then treated at 24 hpi with either 50 µM DIDS, or DMSO as a control, with or without the inhibitor of protein synthesis CHX. Cells were harvested at 0, 12, 24 and 36 h after addition of DIDS +/- CHX and immunoblots for VP1 were then conducted, using tubulin as a cellular loading control (Fig. 2.4a). The levels of VP1, normalised to tubulin, were determined using Li-Cor Odyssey software and plotted (Fig. 2.4b). VP1 levels increased in the absence of CHX and decreased in the presence of CHX as expected, although VP1 levels decreased very little from 12-36 h after CHX addition suggesting that VP1 is a very stable protein with a long half-life. Importantly VP1 levels were comparable in the presence of DIDS or DMSO control, either when protein synthesis was inhibited by CHX or not, demonstrating that VP1 synthesis or stability is not affected by the presence of DIDS even after 36 h incubation with this inhibitor. Taken together these results suggest that DIDS does indeed inhibit the secretion of BKPyV virions, and that the reduction in BKPyV release is not due to changes in cell viability, viral protein expression or stability, or reduced virion infectivity in the presence of DIDS.
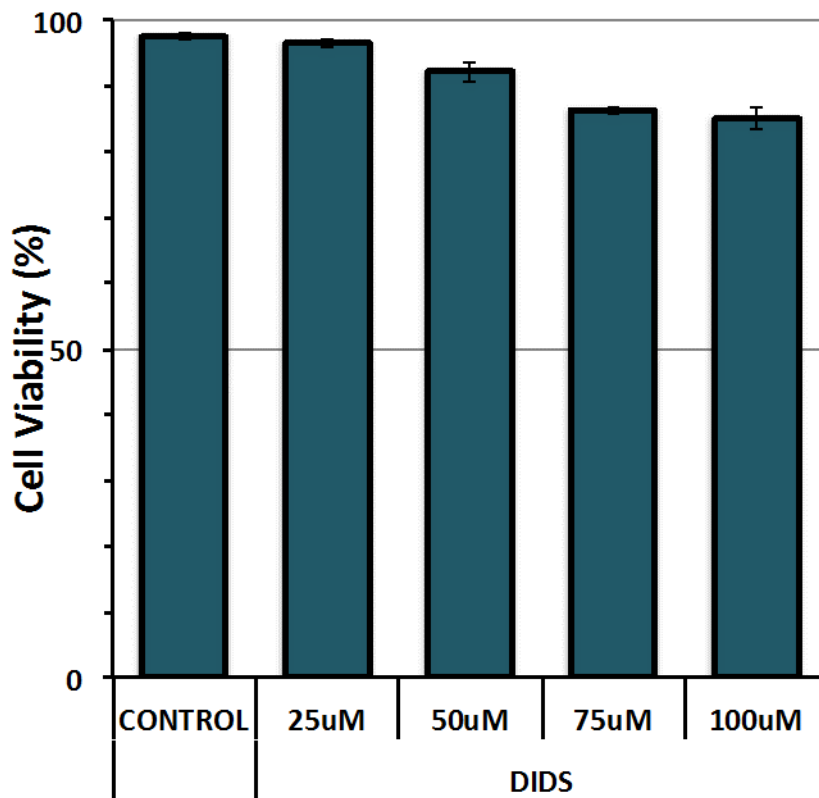
Figure 2.3: RPTE cell viability remains high in the presence of DIDS.
The effect of DIDS on RPTE cell viability was determined with a trypan blue exclusion assay. RPTE cells were treated with increasing concentrations of DIDS, or DMSO as a control, for 24 hours then harvested, incubated with trypan blue and cells scored as trypan blue positive or negative. Data represent mean percentage of cells that were trypan blue negative from three independent experiments. Error bars show standard deviation.

(a)
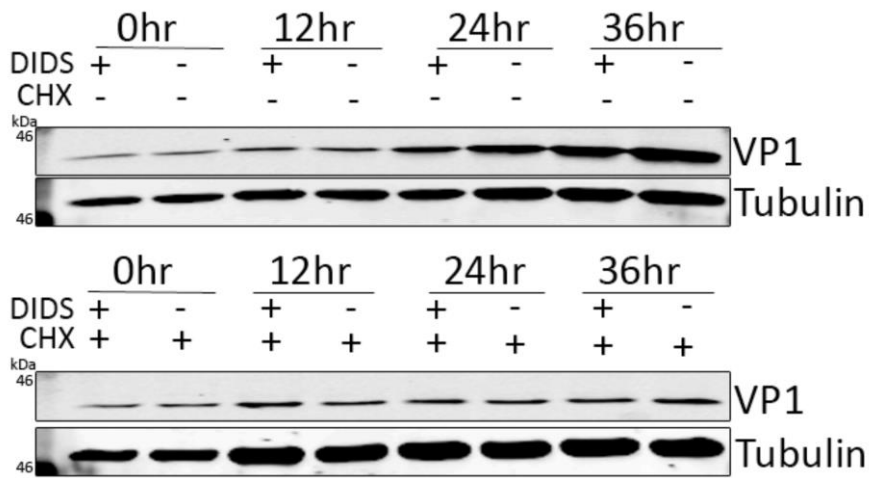
(b)
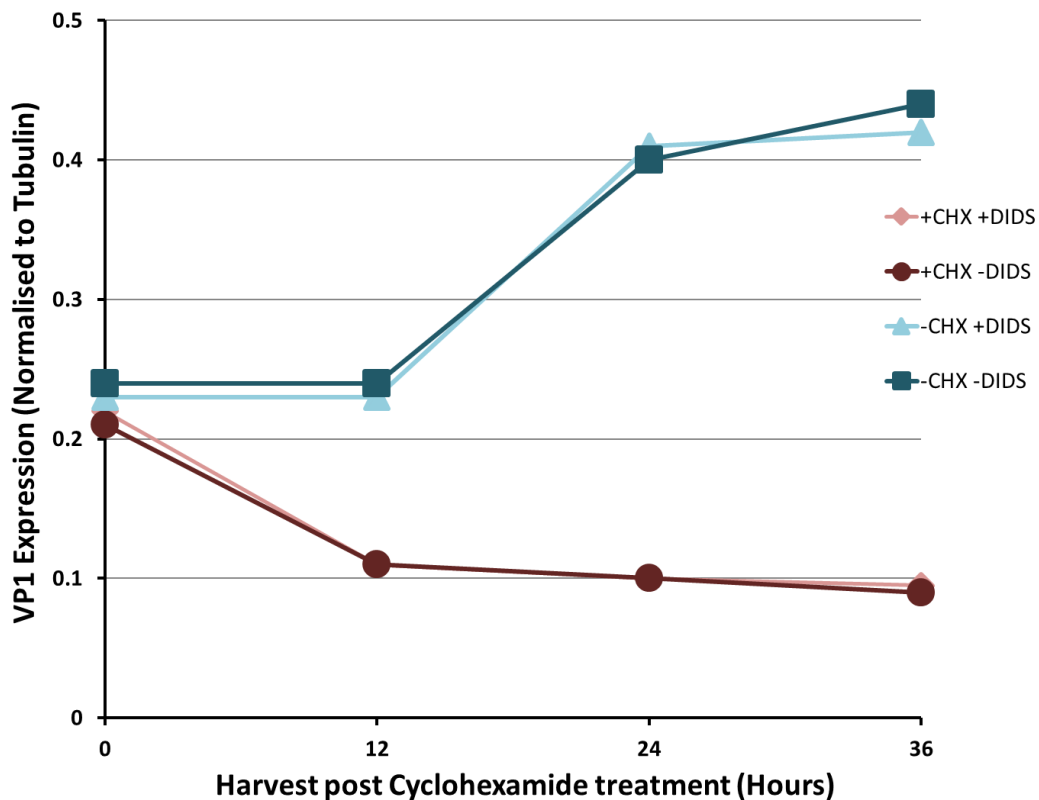
Figure 2.4: BKPyV capsid protein stability is not affected by the presence of DIDS.
RPTE cells were BKPyV infected at 1 IU/cell and were then treated with 50 µM DIDS, or DMSO as a control, with or without cycloheximide (CHX) at 24 hpi. Cells were harvested at 0, 12, 24 and 36 hours after addition of DIDS +/- CHX and analysed by immunoblot (a). Li-Cor Odyssey software was used to determine the density of VP1 bands (normalised to tubulin) and plotted on a graph (b); data from one experiment shown.

2.2.4 DIDS alters the subcellular localisation of BKPyV virions

Further consideration was then given to the intracellular location of BKPyV virions when virus secretion was inhibited by the addition of DIDS; namely whether virions remained nuclear or were cytoplasmic but restricted from reaching the supernatant though perturbation of trafficking. To address this question the subcellular localisation of BKPyV structural proteins in the presence or absence of DIDS was investigated by immunofluorescence microscopy. RPTE cells were infected with BKPyV at 1 IU/cell, or mock infected as a control, and treated with 50 µM DIDS or DMSO at 24 hpi. At 48 hpi cells were fixed and stained for either VP1 (antibody PAb597) (Fig. 2.5a) or VP2 and VP3 using an antibody which recognises both proteins due to their common C-terminal sequence (Fig. 2.5b). DIDS auto-fluoresces in the 415 nm channel (DAPI) and localises to cytoplasmic vesicle/vacuole structures which presumably contain DIDS-sensitive anion channels in their membrane. VP1 staining showed strong nuclear signals and a diffuse cytoplasmic signal that showed no change in the presence of DIDS. Staining for the minor capsid proteins VP2 and VP3 showed a clear accumulation in DIDS positive cytoplasmic vesicles. This suggested that virus particles may become trapped in these DIDS-containing vesicles. It was surprising that the major capsid protein VP1 wasn't detected in these vesicles and the minor capsid proteins were, even though VP2 and VP3 would be expected to be relatively inaccessible to antibodies in intact virions. The VP1 antibody used in these assays (PAb597) was originally generated to SV40 VP1 and likely recognises a linear epitope as it detects denatured VP1 by immunoblot (Broekema and Imperiale, 2012) and so may not recognise VP1 when folded into its native virion conformation. To determine whether the VP2/VP3 antibody or the VP1 PAb597 antibody can bind virions in their capsid conformation, immunofluorescence microscopy analysis of cells with surface attached BKPyV virus particles was conducted. RPTE cells were incubated with 1 IU/cell BKPyV on ice for 1 h, after which time cells were fixed and stained with either VP1 PAb597 or VP2/VP3 antibodies (Fig. 2.6a). Clear VP2/VP3 antibody staining was observed on cells with bound virions, while no signal could be detected for VP1 PAb597, supporting the notion that this VP1 antibody does not recognise intact virions but the VP2/3 antibody does. To further investigate VP1 localisation in the presence or absence of DIDS, a conformational-dependent VP1 monoclonal antibody (L5) that neutralises BKPyV infectivity and thus should bind mature virions was obtained (Randhawa et al., 2008). RPTE cells were infected with BKPyV, treated with or without DIDS at 24 hpi, and fixed at 48 hpi as before. Staining with VP1 L5 antibody showed clear accumulation of VP1 to DIDS positive vesicles (Fig. 2.6b), suggesting that DIDS treatment causes BKPyV virions to become trapped in intracellular vesicles.
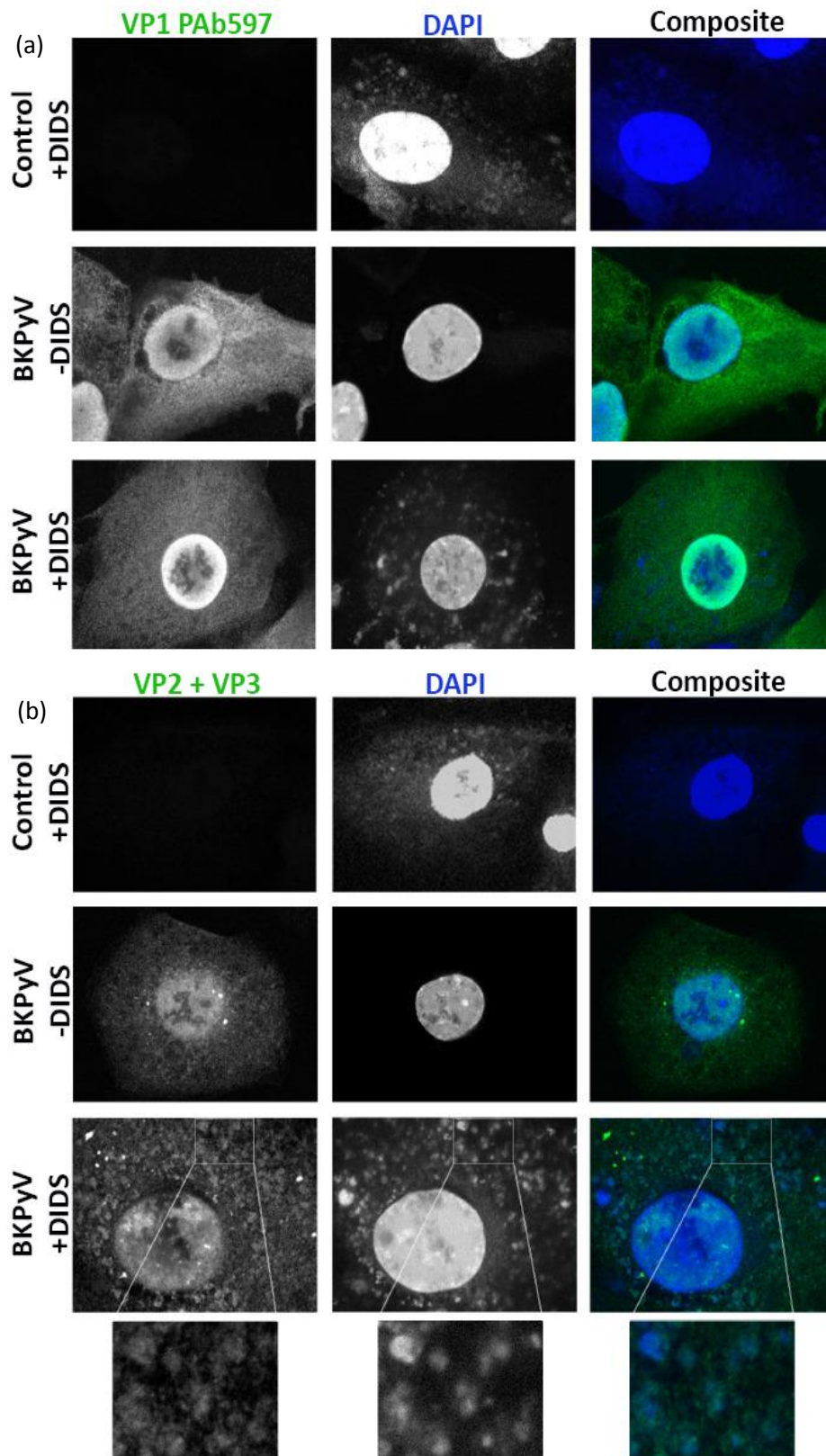
Figure 2.5: In BKPyV infected cells DIDS colocalises with VP2 and VP3.
RPTE cells were mock infected (control) or BKPyV infected at 1 IU/cell and treated with 50 µM DIDS, or DMSO as a drug treatment control, at 24 hpi. At 48 hpi cells were fixed and stained for VP1 (PAb597) or VP2/3 antibody (both shown in green). DAPI staining along with DIDS auto-fluorescence is shown in blue. VP1 (PAb597 staining is diffuse and does not localise with DIDS puncta (a), while VP2/3 staining showed clear coloalisation with DIDS positive puncta, shown in magnified images (b). Images produced from single z-slices from a Leica SP5 confocal microscope.
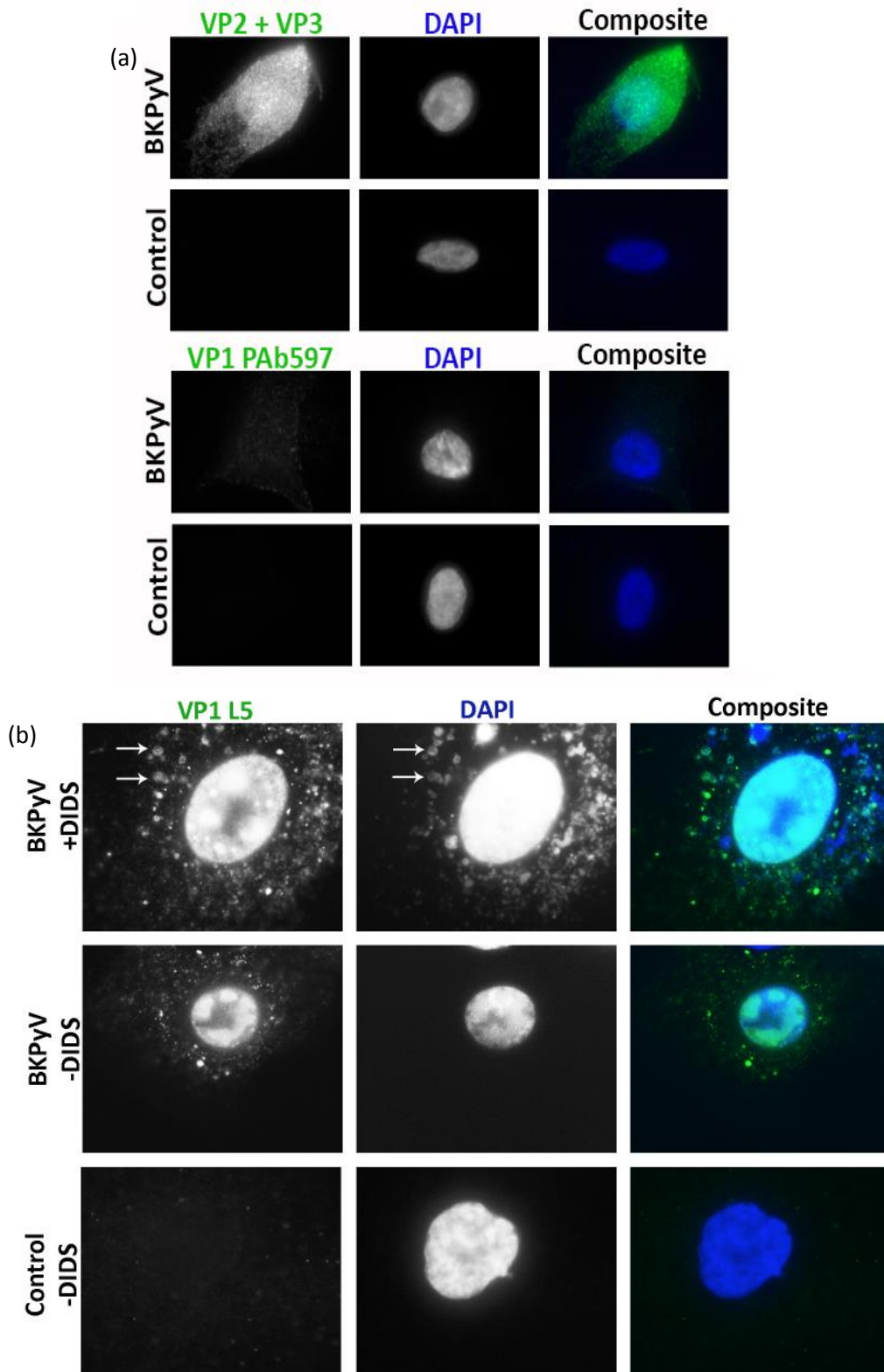
Figure 2.6: In BKPyV infected cells DIDS colocalises with VP2 and VP3, and conformational-dependent VP1 antibodies.
(a) RPTE cells were incubated with 1 IU/cell BKPyV, or mock media as a control, on ice for 1 hour and then fixed and stained with VP1 (PAb597) or VP2/3 antibodies (both shown in green). DAPI stain is shown in blue. VP1 (PAb597) does not bind to surface virions indicating the antibody does not recognise VP1 in virion conformation, while the VP2/3 antibody is able to bind surface epitopes available in virion conformation. (b) RPTE cells were BKPyV infected at 1 IU/cell or mock infected (control) and treated with 50 µM DIDS, or DMSO as a control, at 24 hpi. At 48 hpi cells were fixed and stained for VP1 (L5) (shown in green). DAPI staining and DIDS auto-fluorescence is shown in blue. The conformational VP1 (B5) antibody shows colocalisation with DIDS positive puncta. All images produced from single z-slices from a Leica SP5 confocal microscope.

2.2.5 VP2 and VP3 containing DIDS positive vesicles are LysoTracker and LAMP1 positive

The nature of the DIDS positive vesicles in which BKPyV particles appear to accumulate upon addition of DIDS was explored. Among other roles such as transport and membrane stabilisation ClCs can contribute to the acidification of intracellular vesicles. Acidic organelles such as endosomes and lysosomes contain a variety of import channels including ClC-3, ClC-5 and ClC-7 (Jentsch and Pusch, 2018), and so the BKPyV and DIDS-positive vesicles observed could be endosomal or lysosomal in nature. Immunofluorescence was used to examine this hypothesis. RPTE cells were infected at 1 IU/cell and 50 µM DIDS, or DMSO as a control, was added at 24 hpi. At 48 hpi cells were fixed and stained for VP2 and VP3, and either co-stained for lysosomal-membrane associated protein 1 (LAMP1) (Fig. 2.7b) or treated with LysoTracker 2 h before fixing (Fig. 2.7a). LysoTracker is a fluorescent marker of acidic cellular organelles, and will fluoresce in late endosomes and lysosomes, while LAMP1 is a lysosome associated membrane glycoprotein and is located primarily in lysosomal membranes. In infected cells treated with DIDS VP2/VP3, LysoTracker and DIDS were shown to colocalise in several large cytoplasmic vacuole-like structures (arrows Fig. 2.7a). This suggests that the compartments to which BKPyV particles are being relocalised in the presence of DIDS are acidic and thus may be late endosomal or lysosomal in nature. A number of vacuoles were positive for DIDS and LysoTracker which were not positive for VP2/3, this could be due to the varying types of acidic vesicles within the cell, for example lysosomal and endosomal vesicles may show differing levels of VP2/3 uptake or colocalisation. Similarly it must be noted that free VP2/3 within the cytoplasm of cells presents a somewhat diffuse background on which to observe these colocalisation puncta.

 VP2/3, LAMP1 and DIDS also showed some colocalisation in a few vacuole-like structures in infected cells (Fig. 2.7b arrows), however LAMP1 staining was relatively weak and diffuse. This was particularly evident in uninfected RPTE cells, where LAMP1 showed little concentration in any obvious cytoplasmic structures. To confirm that the LAMP1 antibody was effective the commonly used HeLa cell line was fixed and stained with this antibody in parallel with RPTE cells (Fig. 2.7c). Staining of HeLa cells showed the expected distribution of LAMP1 with several bright puncta observed in the cytoplasm, whereas RPTE cells showed a relatively diffuse somewhat ER-like pattern. This suggests the LAMP1 antibody is effective but that either this represents the normal distribution for these RPTE cells and there is little concentration of LAMP1 in the expected endosome/lysosome type compartments, or the antibody epitope is masked in these cells. Nevertheless, the detection of LAMP1 signals in DIDS and VP2/3 positive vacuoles, albeit relatively weak, further suggests that the compartments in which BKPyV particles becomes localised in the presence of DIDS are endo-lysosomal in nature.
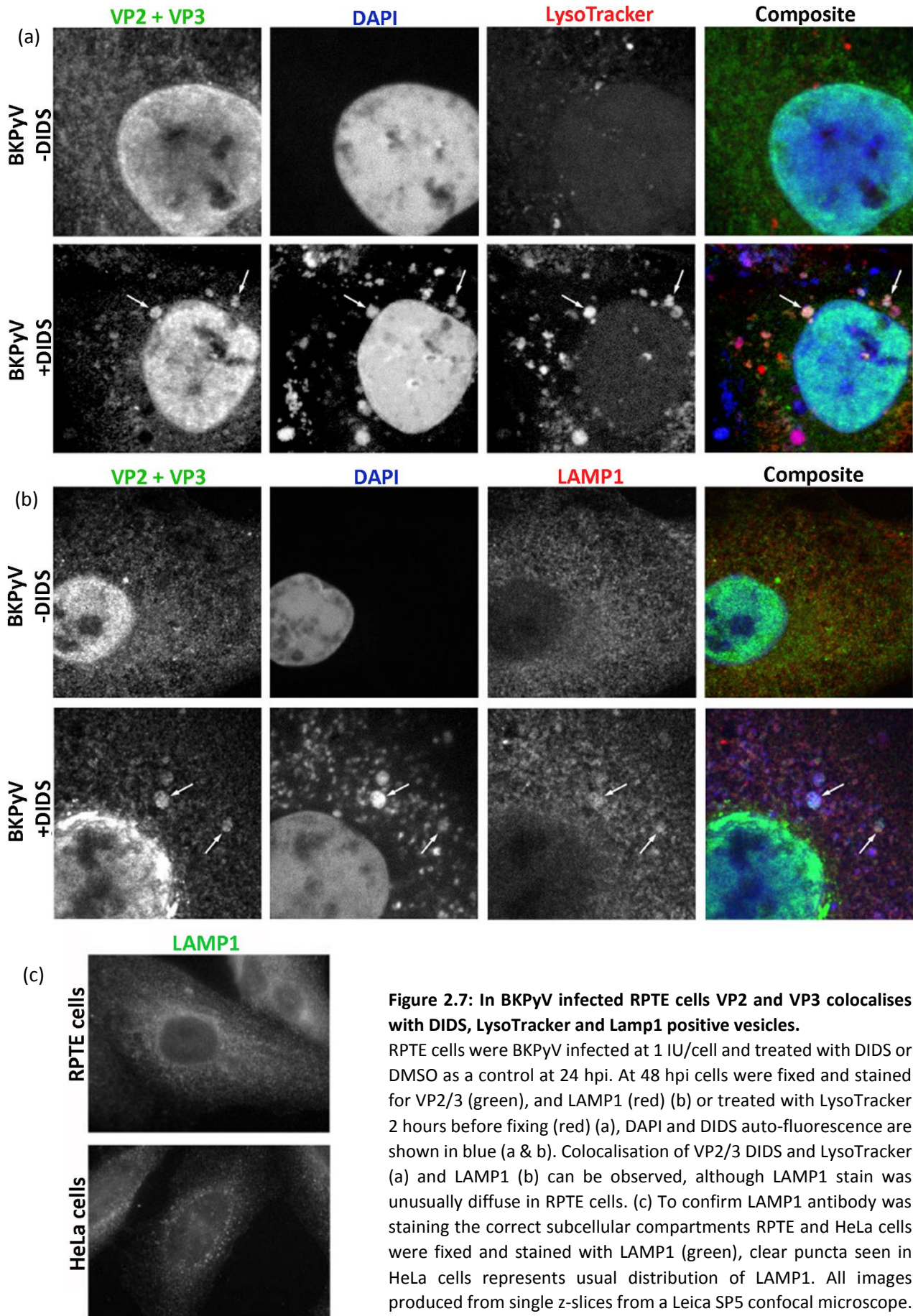
Figure 2.7: In BKPyV infected RPTE cells VP2 and VP3 colocalises with DIDS, LysoTracker and Lamp1 positive vesicles.
RPTE cells were BKPyV infected at 1 IU/cell and treated with DIDS or DMSO as a control at 24 hpi. At 48 hpi cells were fixed and stained for VP2/3 (green), and LAMP1 (red) (b) or treated with LysoTracker 2 hours before fixing (red) (a), DAPI and DIDS auto-fluorescence are shown in blue (a & b). Colocalisation of VP2/3 DIDS and LysoTracker (a) and LAMP1 (b) can be observed, although LAMP1 stain was unusually diffuse in RPTE cells. (c) To confirm LAMP1 antibody was staining the correct subcellular compartments RPTE and HeLa cells were fixed and stained with LAMP1 (green), clear puncta seen in HeLa cells represents usual distribution of LAMP1. All images produced from single z-slices from a Leica SP5 confocal microscope.

2.2.6 TAg localisation is unaffected by addition of DIDS

Thus far the effect of DIDS on the expression and location of late structural BKPyV proteins had been investigated, while only the total expression of the early protein TAg had been studied (Fig. 2.2a). To understand whether DIDS also affected the subcellular location of early BKPyV gene products immunofluorescence was conducted for BKPyV TAg expression in both the presence or absence of DIDS. RPTE cells were infected with BKPyV at 1 IU/cell and at 24 hpi 50 µM DIDS, or DMSO as a control, was added. At 48 hpi cells were fixed and stained for TAg and with DAPI (Fig. 2.8). The localisation of TAg in BKPyV infected cells showed no change upon addition of DIDS, demonstrating that the VP1 and VP2/3 positive vacuole-like structures observed in the presence of DIDS are unlikely to be blebs or fragments of nucleus.
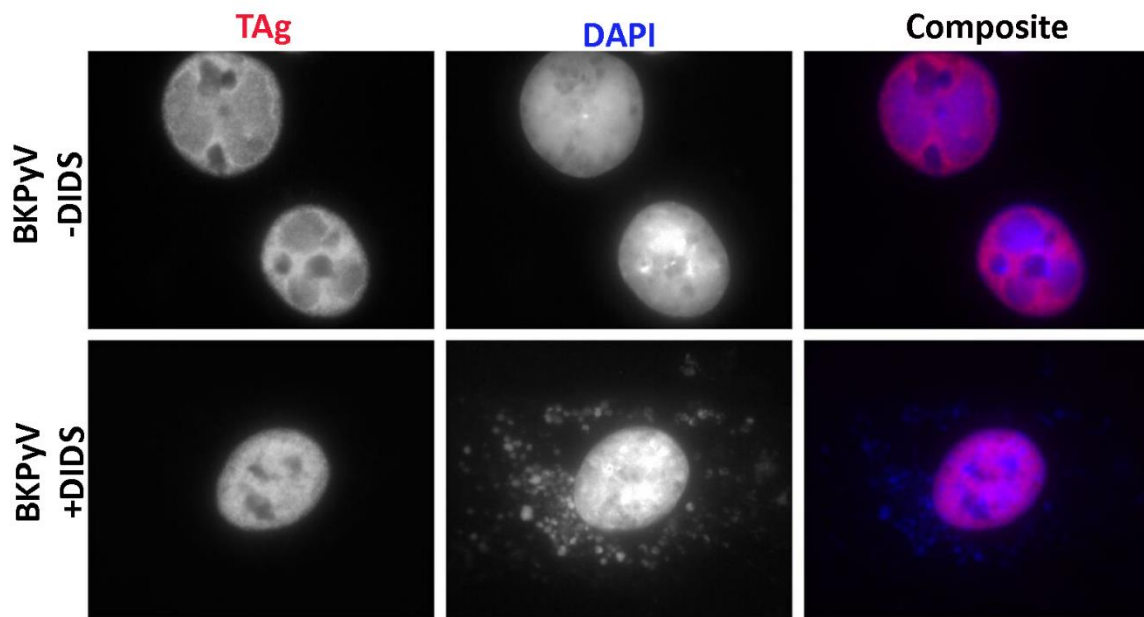
Figure 2.8: In BKPyV infected cells TAg localisation is unaffected by the presence of DIDS.
RPTE cells were BKPyV infected with 1 IU/cell and treated with 50 µM DIDS, or DMSO as a control, at 24 hpi. At 48 hpi cells were fixed and stained for TAg (red). DAPI and DIDS auto-fluorescence are shown in blue. Images produced from single z-slices from a Leica SP5 confocal microscope.

2.2.7 DIDS causes perturbation of chloride homeostasis and causes an increase in acidic vesicles.

DIDS is a broad-range inhibitor of ClCs but is also thought to inhibit the function of a wide variety of additional anion channels. Given the proposed importance of chloride ion transport for maintaining the acid environment in intracellular compartments the increase of acidic vesicles observed by immunofluorescence analysis of LysoTracker stained cells in the presence of this inhibitor may seem counter-intuitive. To ascertain whether the increase of LysoTracker positive acidic vesicles was driven by addition of DIDS alone, or whether BKPyV infection was also necessary to observe this effect, uninfected RPTE cells were treated with 50 µM DIDS, or DMSO as a control. LysoTracker was added 2 h prior to fixation, and after 24 h of treatment cells were fixed and stained with VP2/3 antibody, as a control for the absence of infection, and DAPI as a nuclear marker (Fig. 2.9a). A clear increase in LysoTracker positive vesicles was observed in the presence of DIDS treatment, suggesting that with the disruption of ClC activity, or other anion channels, does indeed increase the number of acidic vesicles within RPTE cells. DIDS blocks both chloride transporters and antiporters, although whether the observed the increase of vesicle acidification upon DIDS treatment is caused by inhibition of a specific channel or a combination of several is unclear.

To control for the effect of DIDS on chloride homeostasis in RPTE cells, staining with *N*-ethoxycarbonylmethyl-6-methoxyquinolinium bromide (MQAE) was used. MQAE is a fluorescent indicator that is quenched in the presence of intracellular Cl^-. RPTE cells were treated with 50 µM DIDS, or DMSO as a control, for 24 h, and MQAE was added for the last hour of incubation (Fig. 2.9b) and MQAE fluorescence was monitored in live cells by fluorescence microscopy (imaging performed by Dr G Evans). It can be seen that in untreated cells there is a strong signal MQAE signal, while in those cells treated with DIDS the signal is largely quenched, suggesting DIDS is effectively disrupting chloride transport, primarily the influx from the extracellular media.

(a)

(b)
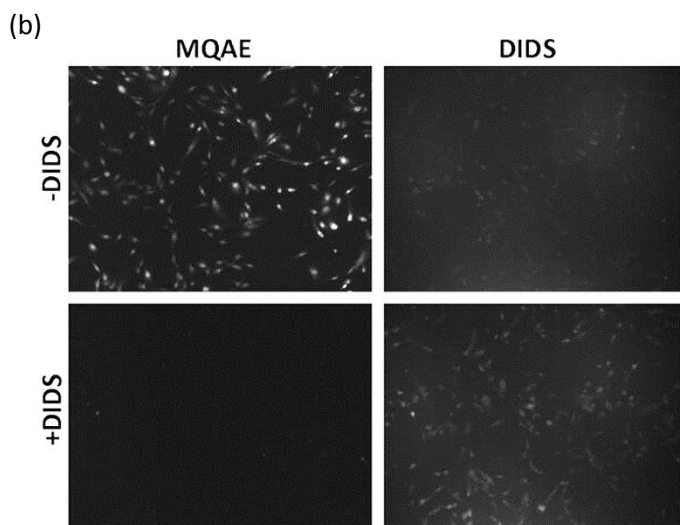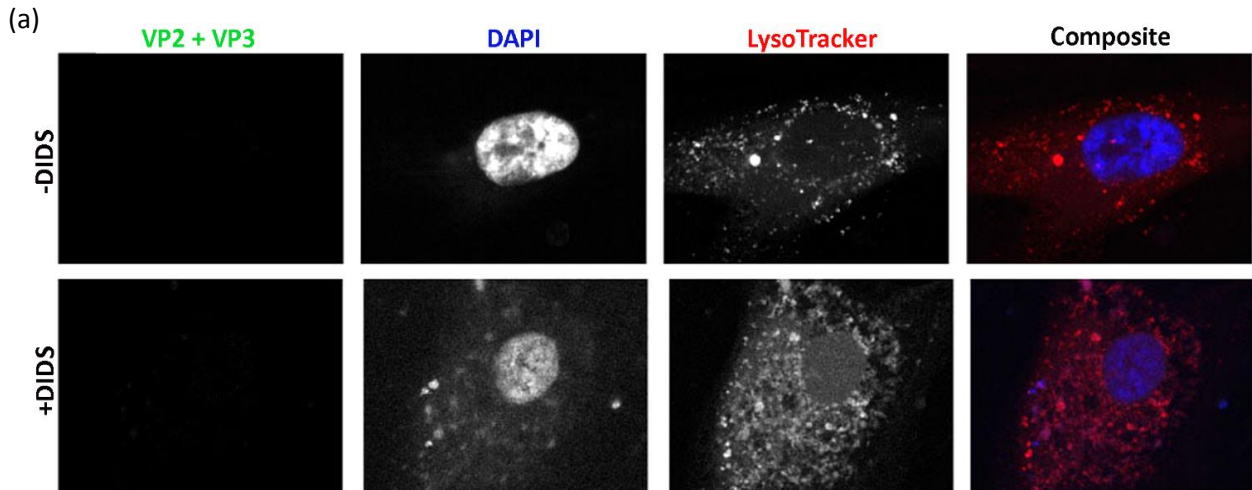
Figure 2.9: DIDS alone is sufficient to perturb chloride homeostasis and causes an increase in LysoTracker positive vesicles.

Uninfected cells were treated with 50 µM DIDS for 24 h. 2 h prior to fixing cells were treated with LysoTracker (red). DAPI and DIDS auto-fluorescence are shown in blue. Images produced from single z-slices from a Leica SP5 confocal microscope (a). RPTE cells were treated with DIDS, or DMSO as a control, for 24 h, and MQAE added for the last hour of incubation. Cells were washed with PBS and imaged using 10x lens of Olympus IX81 wide-field fluorescence microscope (b). MQAE experiment carried out in partnership with Dr G Evans.

2.2.8 DIDS inhibits BKPyV release in immortalised RPTEC/TERT1 cells

To confirm that the observed effects of BKPyV can be replicated in an alternative cell line RPTEC/TERT1 cells were used. These cells are a primary RPTE cell type that has been immortalised with the insertion of a human telomerase expression cassette (Wieser et al., 2008). RPTEC/TERT1 cells are not from the same patient that the RPTE cells used for these experiments were obtained from. They also display a different morphology yet can still be infected by BKPyV, representing a useful cell line in which to validate our results with DIDS, given that most other cell types do not support robust BKPyV replication. RPTEC/TERT1 and RPTE cells were infected with BKPyV at 1 IU/cell and treated with 50 µM DIDS, or DMSO as a control, at 24 hpi. At 48 hpi the cell-associated and supernatant samples were harvested separately. Viral titres of within supernatant and cell-associated fractions were determined using an FFU assay (Fig. 2.10). A greater than ten-fold reduction in supernatant virus titre was observed in DIDS treated cells compared with untreated, while the concentration of cell-associated virus titre remained relatively unaffected for both cell types. Both cell types showed equivalent reduction in BKPyV secretion in the presence of DIDS treatment demonstrating our data observations that DIDS inhibits BKPyV release reproducible in different renal epithelial cell lineages.
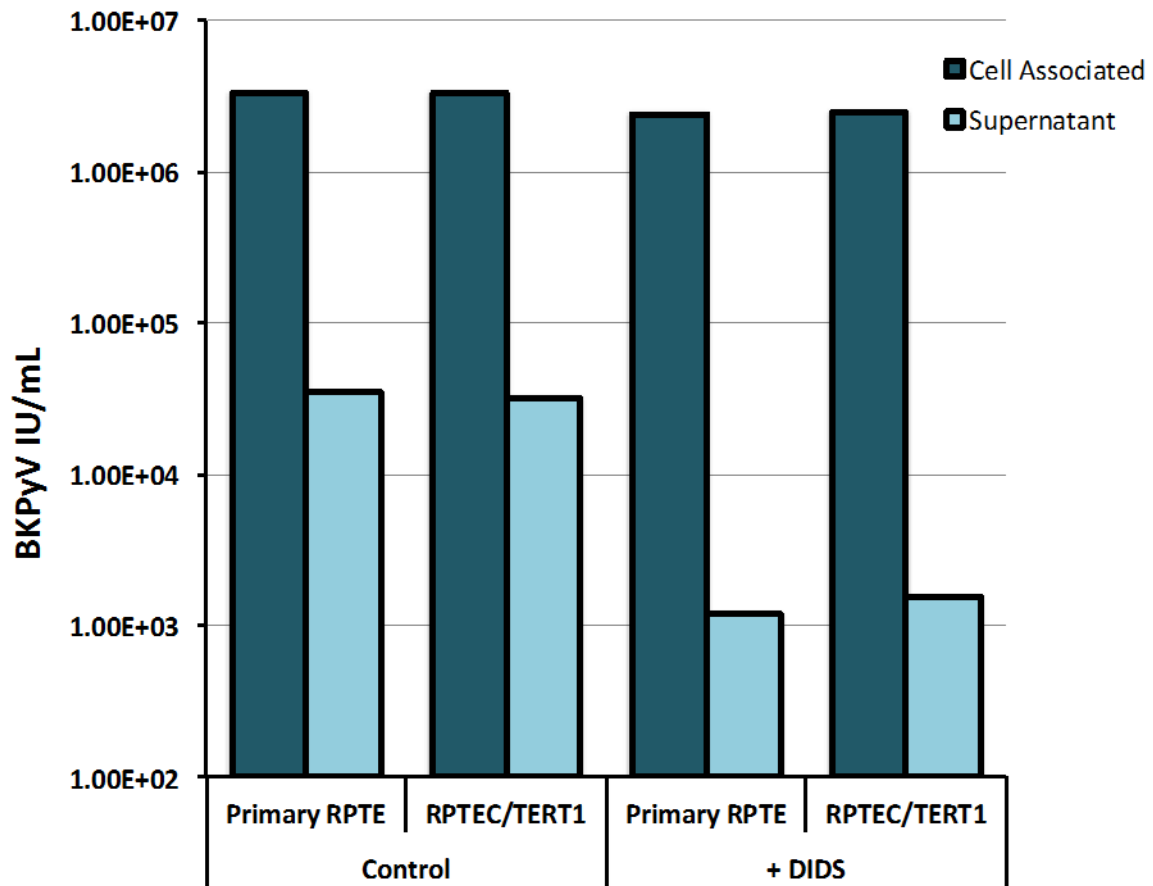
Figure 2.10: DIDS inhibition of BKPyV release is replicated in immortalised RPTEC/TERT1 cells.
RPTE or RPTEC/TERT1 cells were BKPyV infected at 1 IU/cell and treated with 50 µM of DIDS, or DMSO as a control, at 24 hpi. At 48 hpi supernatant media and cells were harvested independently. Cell associated virus was freeze-thawed three times in fresh media to release the cell-associated virus, supernatant virus was pelleted by ultracentrifugation and resuspended in PBS at 20x the original volume. To determine the virus concentration in each harvest an FFU assay was conducted; Data from one experiment shown.

2.3 Discussion

The observations made in this chapter provide compelling evidence that BKPyV secretes a proportion of progeny virions into the supernatant, and that this secretion is an active and non-lytic method of viral release, which can be inhibited by anion homeostasis disruption. Around 1% of total BKPyV is secreted into the supernatant in uninhibited conditions by 48 hpi, and the anion channel inhibitor DIDS inhibits this secretion of BKPyV by up to 20-fold, in a dose dependant manner. DIDS has a broad effect on a number ClCs, although ClC3-7 are potentially relevant targets of DIDS for this study. ClC3-7 are Cl^-/H^+ antiporters that are commonly expressed in mammalian cells and localised to intracellular organelles (Stauber and Jentsch, 2010). However DIDS also inhibits the activity of a number of other Cl^- channels including Golgi-pH regulator (GPHR) (Maeda et al., 2008). The use of more specific Cl^- inhibitors, such as 4-Acetamido-4'-isothiocyanatostilbene-2,2'-disulphonic acid (SITS) (Table S1), did not cause any clear reduction in BKPyV secretion, and thus it is impossible to conclude which specific ClCs may be responsible for these observed effects, and it may be that inhibition of several ClCs by the broad action of DIDS is necessary. Alternatively, the inhibition of BKPyV release could be due to some unknown off-target effect of DIDS.

These studies suggest that the reduction in secreted infectious BKPyV is not simply due to inhibition of secreted BKPyV particle infectivity. The fraction of the structural viral protein VP1 that was released into the supernatant was also reduced in the presence of DIDS in a dose dependant manner, and further work conducted by Dr G Evans showed that BKPyV genomes present in the supernatant were also reduced by DIDS in a dose dependant manner (Fig. S2). Taken together these data suggest DIDS is truly inhibiting the secretion of virions from infected cells and suggests BKPyV can be released by a non-lytic pathway as it seems highly unlikely that the effect of DIDS is to reduce cell lysis.

RPTE cell viability in the presence of 75-100 μM DIDS was reduced to around 85%. While this is considered an acceptable level of viability, taken in conjunction with the reduction in cell-associated virus titre observed in Fig. 2.1a and reduced viral protein load observed in Fig. 2.2a, it was decided that further experiments should be limited to 50 μM DIDS. The aim was to reduce any confounding effects that reduced cell viability may have as at 50 μM DIDS cell viability remained above 90% in all three replicates of the viability test. It is possible DIDS could affect extracellular virion stability, leading disruption of particle integrity and reducing the yield of virions harvested by ultracentrifugation. While this is formally possible, no effect on protein stability in cells was detected. At 50 μM DIDS viral proteins were no less stable than in the presence of DMSO control. This possibility could be addressed however by pre-treating purified virus with DIDS, then spinning out the virus to remove DIDS and comparing the infectivity of virus remaining.

Investigations into the localisation of cytoplasmic BKPyV in DIDS treated cells reveals that virions appear to be relocalised to acidic late endosomal or lysosomal organelles that presumably contain DIDS sensitive ClCs because of the accumulation of DIDS in these compartments. ClC-6 and ClC-7 are both localised to late endosomal and lysosomal compartments and are highly sensitive to DIDS inhibition (Verkman and Galietta, 2009), suggesting that these antiporters may play a role in BKPyV relocalisation in the presence of DIDS. There is no evidence at this stage, however, that these compartments form part of the normal pathway by which BKPyV is secreted and could be indicative of a dead-end pathway in which virions become trapped. Indeed, treatment with DIDS alone on uninfected cells also leads to an increase in acidic (LysoTracker positive) organelles, thus their increase is not driven by BKPyV infection.

The observed increase in acidic organelles in the presence of DIDS is somewhat surprising as ClCs have been shown to contribute to organelle acidification, and it therefore follows that their inhibition may lead to a reduction in acidic organelles (Hara-Chikuma et al., 2005, Gunther et al., 2003). The role of anion homeostasis and intracellular organelle pH, particularly lysosomal and late endosomal, is not well studied, and previous studies suggest lysosomal pH is not affected in ClC-6 or ClC-7 lacking mice (Kasper et al., 2005, Poet et al., 2006). Another rationalisation of this observed phenomena may be that the global effects on cellular anion homeostasis caused by DIDS may trigger a large number of secretory pathways to be disrupted. Such disruption would lead to an increase in autophagic vesicles taking up many cellular and viral products, including virions. Autophagic vesicles fuse with lysosomes and are of low pH, consistent with this hypothesis.

The observation that around 1% of BKPyV progeny can be actively secreted and that this secretion can be inhibited by addition of DIDS was replicated successfully in another cell line RPTEC/TERT1 cells. It should be noted that the effect of DIDS on BKPyV release was also observed, albeit less dramatic, when conducted in African Green Monkey Kidney (VERO) cells (completed by Dr G Evans, Table S1). However a number of studies have shown that VERO cells may traffic BKPyV during their entry in a different manner than RPTE cells (Eash et al., 2004, Zhao et al., 2016), suggesting viral trafficking pathways between the two cells lines are not directly comparable. Also VERO cells only support relatively low levels of BKPyV replication with low infectious titres produced from these cells compared to RPTE cells, furthermore while VERO cells are somewhat permissive to BKPyV they are not representative of a natural infection site *in vivo*.

In summary, the data in this chapter suggest BKPyV can be secreted via an active non-lytic pathway, which is sensitive to anion homeostasis. Much of the data in this chapter was included in a co-first

author paper published during the time of this thesis (Evans et al., 2015). Further work to investigate the pathway by which BKPyV is being non-lytically secreted is detailed in the following chapter.

3. Secretion of BKPyV virions is by an unconventional secretion pathway

3.1 Introduction

Having established that BKPyV can be released from cells by an active and non-lytic secretion mechanism, it was important to identify by which pathway secreted virions were being trafficked. Past studies have previously shown that non-enveloped viruses can be trafficked through conventional and unconventional secretory mechanisms. The well-studied primate polyomavirus SV40 was shown to secrete via a pathway that can be inhibited by monensin almost 30 years ago (Clayson et al., 1989), although no further characterisation of SV40 secretion was published. Monensin is a sodium ionophore which disrupts trafficking via the Golgi, part of the conventional secretion pathway.

Non-lytic spread of the non-enveloped picornavirus, poliovirus, has been observed after persistent infections in stable cell lines were described (Lloyd and Bovee, 1993). It is thought that poliovirus acquires LC3 positive autophagic double membranes, and subsequent trafficking via the unconventional autophagy induced secretory pathway leads to fusion of the outer vesicle membrane with the cell plasma membrane. This releases the inner single membraned vesicle, whose contents include viral progeny, into the extracellular space (Jackson et al., 2005, Bird and Kirkegaard, 2015). HAV is thought to release predominantly in an unconventional secretory manner, where it is incorporated into exosomes within MVBs which are released into the extracellular space upon MVB fusion with the plasma membrane (Feng et al., 2013). Further observations of norovirus and rotavirus, both non-enveloped enteric viruses, observed that virions were released from cells in a non-lytic manner contained within large extracellular vesicles and that these vesicles, when shed in stool, were more infectious than free virus found within the same stool. This pathway was found not to occur via LC3-positive autophagic membranes, but may be exosomal or derived directly from plasma membrane budding (Santiana et al., 2018).

Given the diverse range of pathways different non-enveloped viruses have been proposed to use to undergo non-lytic release, it was important to investigate a range of potential pathways of secretion for BKPyV using a variety of experimental methods including TEM, immunofluorescence and pharmacological inhibitors.

3.2 Results

3.2.1 Observation of BKPyV virion size and morphology by electron microscopy

Polyomaviruses are relatively small (~45nm) viruses and various cytoplasmic structures such as polysomes and glycogen granules can appear similar in size which can make it difficult to detect virions within infected cells. Therefore, the size and morphology of newly synthesized virions in the nucleus was observed in order to facilitate identification of cytoplasmic virions throughout future experiments. RPTE cells were infected at 3 IU/cell and cells were fixed for TEM sample processing and imaging at 72 hpi. At this late time point of infection large numbers of BKPyV progeny are expected to have been assembled in the nuclei of infected cells, becoming densely packed as their number increases. Indeed, upon imaging an infected nucleus (N) vast arrays of icosahedral 40-45 nm virions were clearly visible (Fig. 3.1a & b). Furthermore, in areas of nuclei where virions are particularly dense their icosahedral shape, combined with limited nuclear volume, cause virions to be arranged into a distinctive lattice-style structure (Fig. 3.1c & d).

These images allow clear identification of virions, and serve as a reference point for virion shape, size and electron density throughout further TEM imaging in this thesis.

(a)

N

C

2.5uM

(b)

500nM
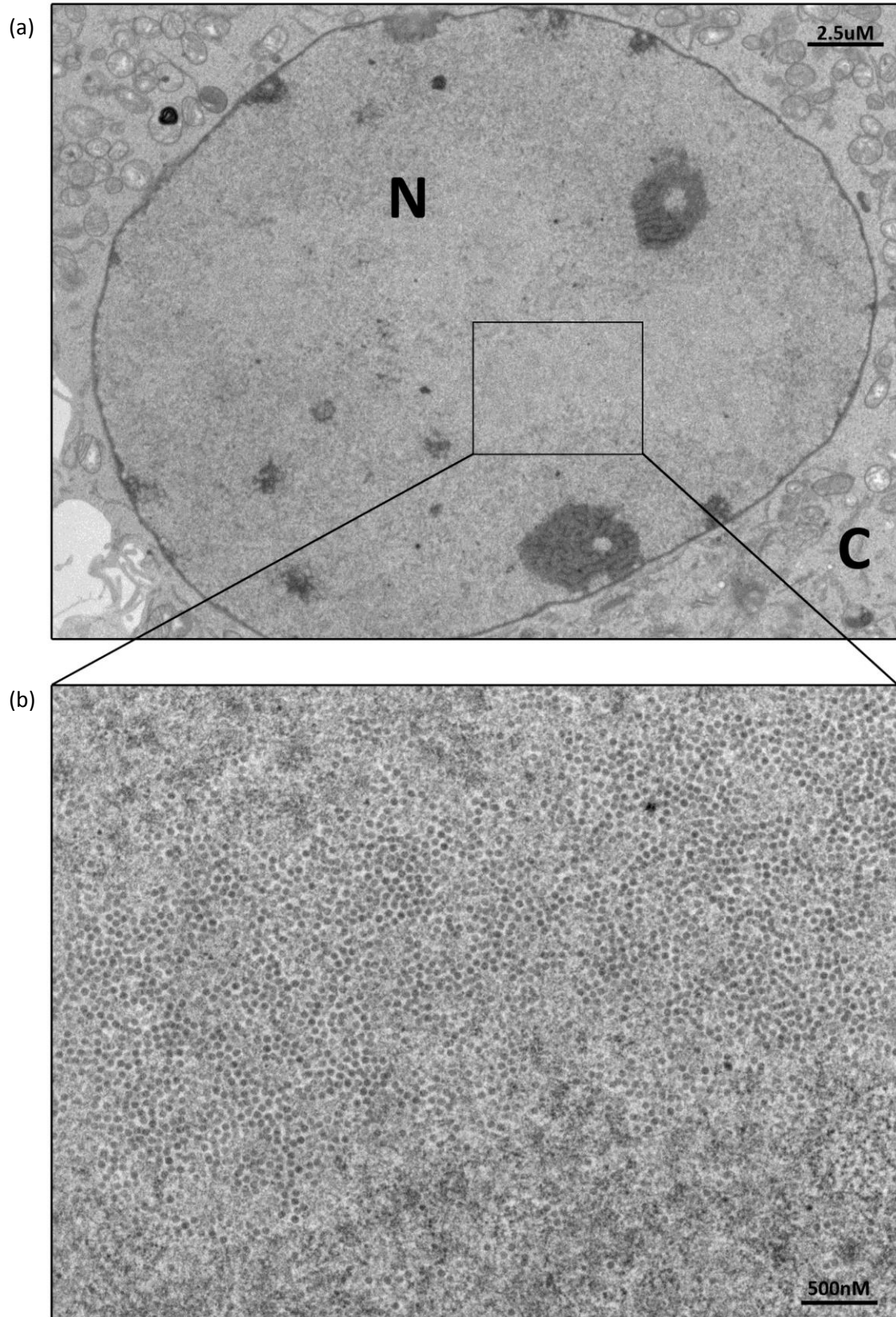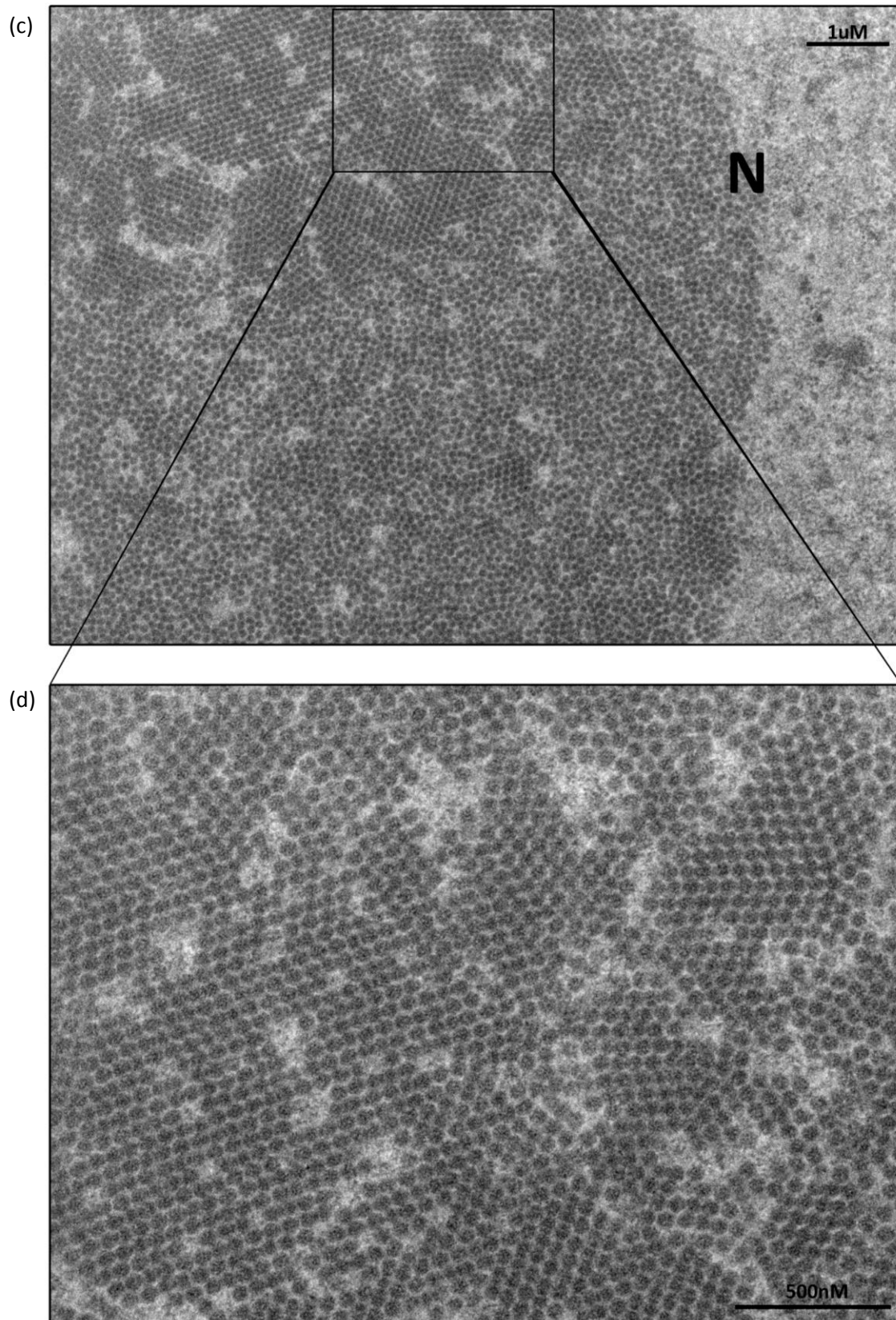
Figure 3.1: BKPyV virions are densely packed in the nuclei of infected cells.
RPTE cells were infected with BKPyV (3 IU/cell) and fixed for TEM at 72 hpi. Nuclear (N) and cytoplasmic (C) spaces are labelled. Virions are found in large numbers in the nucleus (a & b). In dense areas a distinctive lattice-style conformation of virions is observed (c & d). Images collected by M Hollinshead; Dept. of Pathology TEM facility.

3.2.2 BKPyV virions are in single membraned vesicles and ER-like membranes

To investigate the cellular location of virions at late time points of infection, which may be in the process of exiting the cell, RPTE cells were infected with BKPyV at 3 IU/cell. After one hour of inoculation the virus was removed and cells thoroughly washed 3 times with PBS to remove as much residual unattached virus as possible, before replacing with fresh media. At 72 hpi cells were fixed for TEM processing and images taken. 40-45 nM BKPyV virions were visible, not only tightly packed within the nucleus as seen previously (Fig. 3.3a, N) but also inside single membrane vesicles at the cell periphery (Fig. 3.2a & b) and in lumen of smooth convoluted membranes near the nucleus (Fig. 3.3a, b, c & d).

TEM images only allow observation of cellular ultrastructure at a fixed point in time and provides no information regarding directionality of, for example, transport vesicles. As such it is impossible to be certain about whether these observed virions within the lumen of cytoplasmic vesicles and membrane compartments are entering or exiting the cell, but some observations can be made in an attempt to address this question. During primary infection virions are thought to reach the ER by 8-12 hpi and BKPyV is known to enter cells in single membraned vesicles in a clathrin and caveolin independent manner (Eash et al., 2004, Zhao et al., 2016). Should endocytosed virions account for the single membraned virions we observe here in Fig. 3.2 they would be newly synthesised virions re-entering infected cells before 72 hpi. The observed titre of newly synthesised BKPyV virions that are secreted into the culture media by 72 hpi is approximately 5×10^5 IU in in the same experimental set up as the TEM sample preparation (Data taken from Fig. 3.5a). The number RPTE cells at full confluence after 72 h growth in this experimental set up is at least 6×10^5 cells, suggesting that there would be fewer than 1 newly synthesised infectious BKPyV virion for each cell to be re-infected with. Given that several single membraned virions were observed in the cytoplasm of cells (See Fig. 3.2a & b), only high particle:infectivity ratios could account for such numbers. Data on BKPyV particle:infectivity ratio is not known, however for SV40 ratios appear to be between 100-200 non-infectious virions for every one infectious virion (Black et al., 1964).

Similar interpretations can be made regarding the virions observed within smooth convoluted membranes (Fig. 3.3). These membranes have a morphology resembling smooth ER, and BKPyV is known to traffic via the ER during entry infectious entry into cells. During initial infection virions are thought to leave the ER and reach the nucleus by 12-18 hpi. The large number of virions observed in the smooth ER-like membranes at 72 hpi also suggests that they are unlikely to be virions re-infecting the cell, as the number of newly synthesized infectious virions released from cells at 72 hpi is fewer than 1 IU/cell (calculated above).
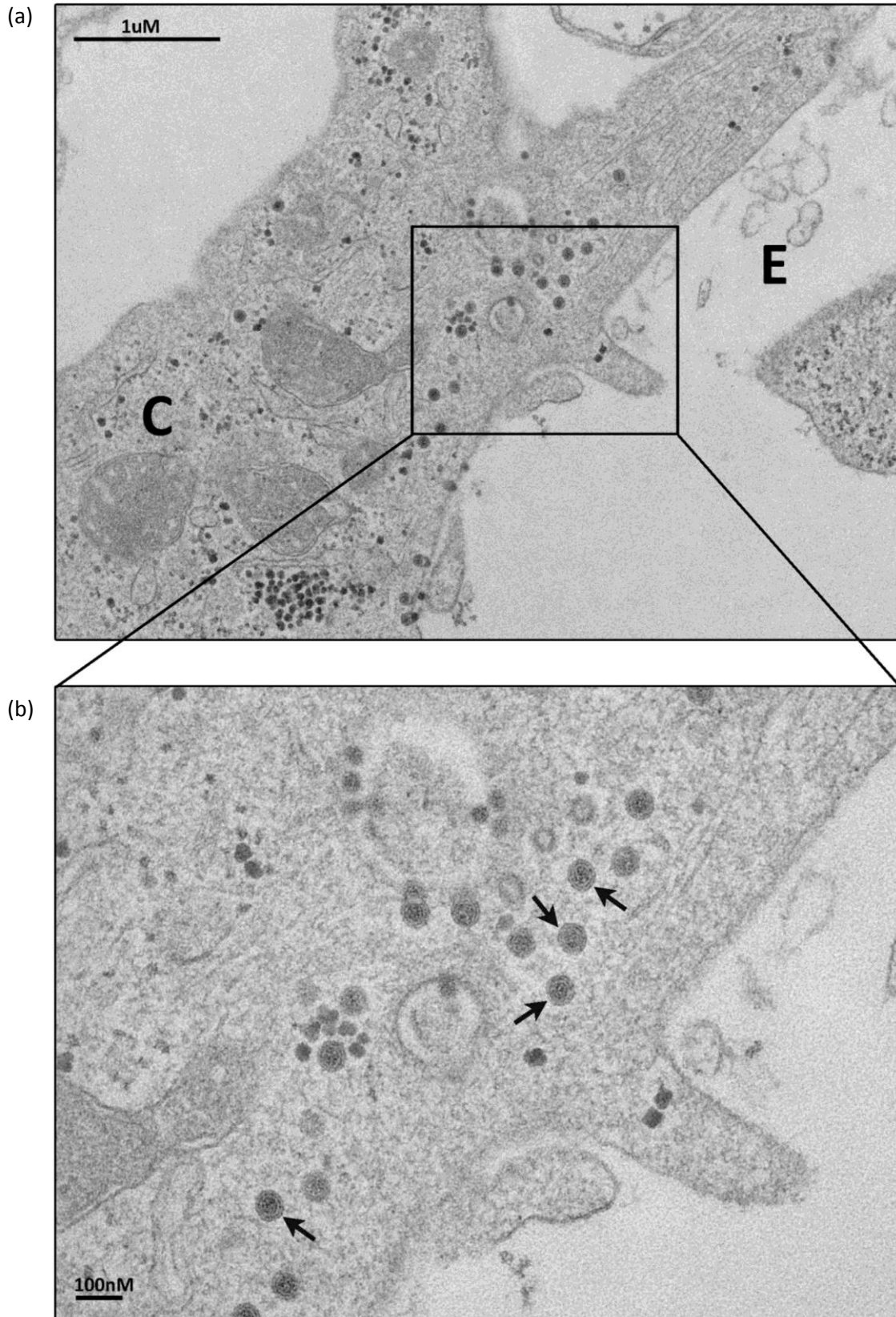
Figure 3.2: BKPyV virions are found within single membraned vesicles.
RPTE cells were infected with BKPyV (3 IU/cell) and fixed for TEM at 72 hpi. (a) Cytoplasmic (C) and extracellular (E) spaces are labelled, virions are found tightly wrapped within single membraned vesicles towards the cellular periphery. (b) Image of the same section in at higher magnification shows single membrane vesicles; highlighted with black arrows. Images collected by M Hollinshead; Dept. of Pathology TEM facility.
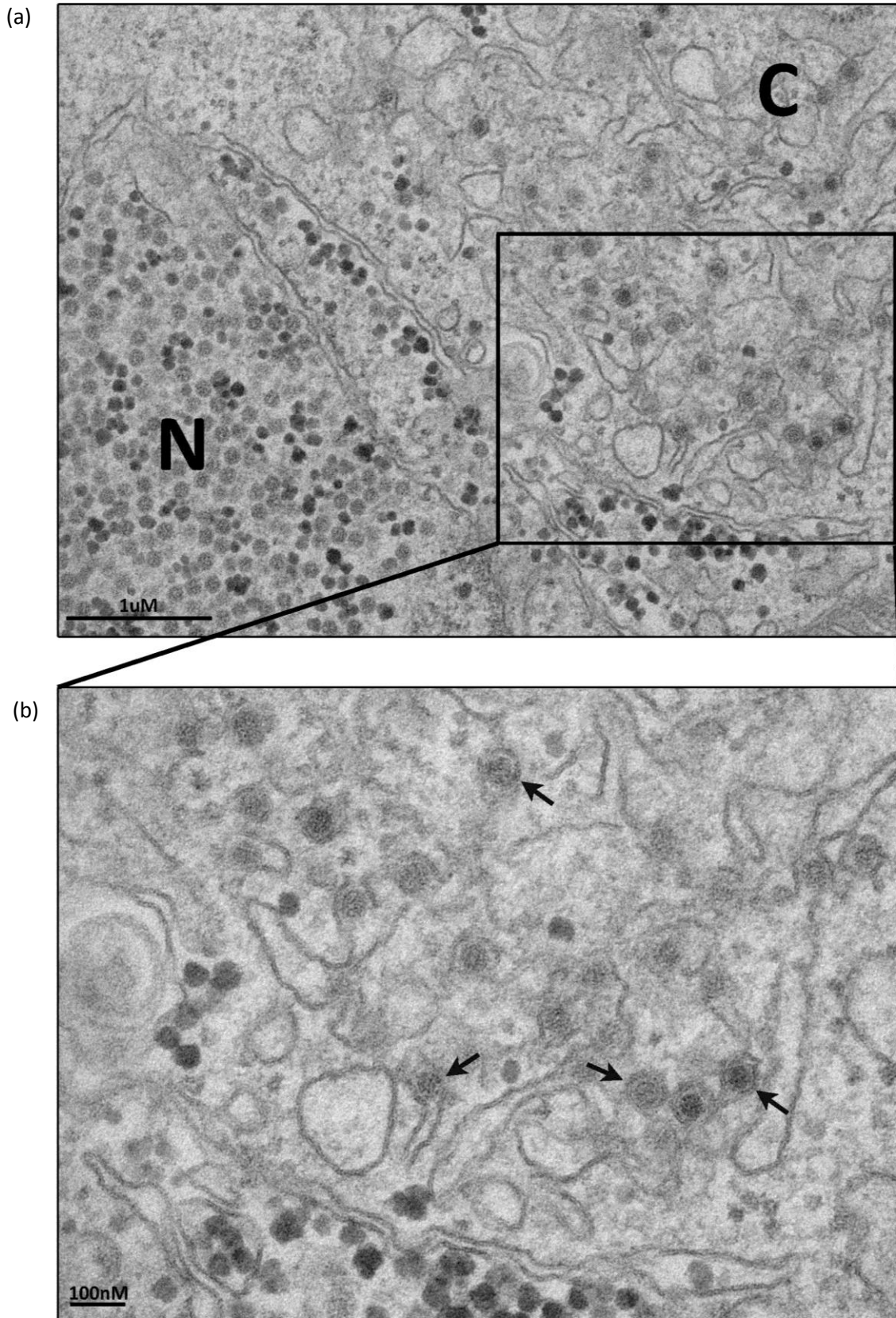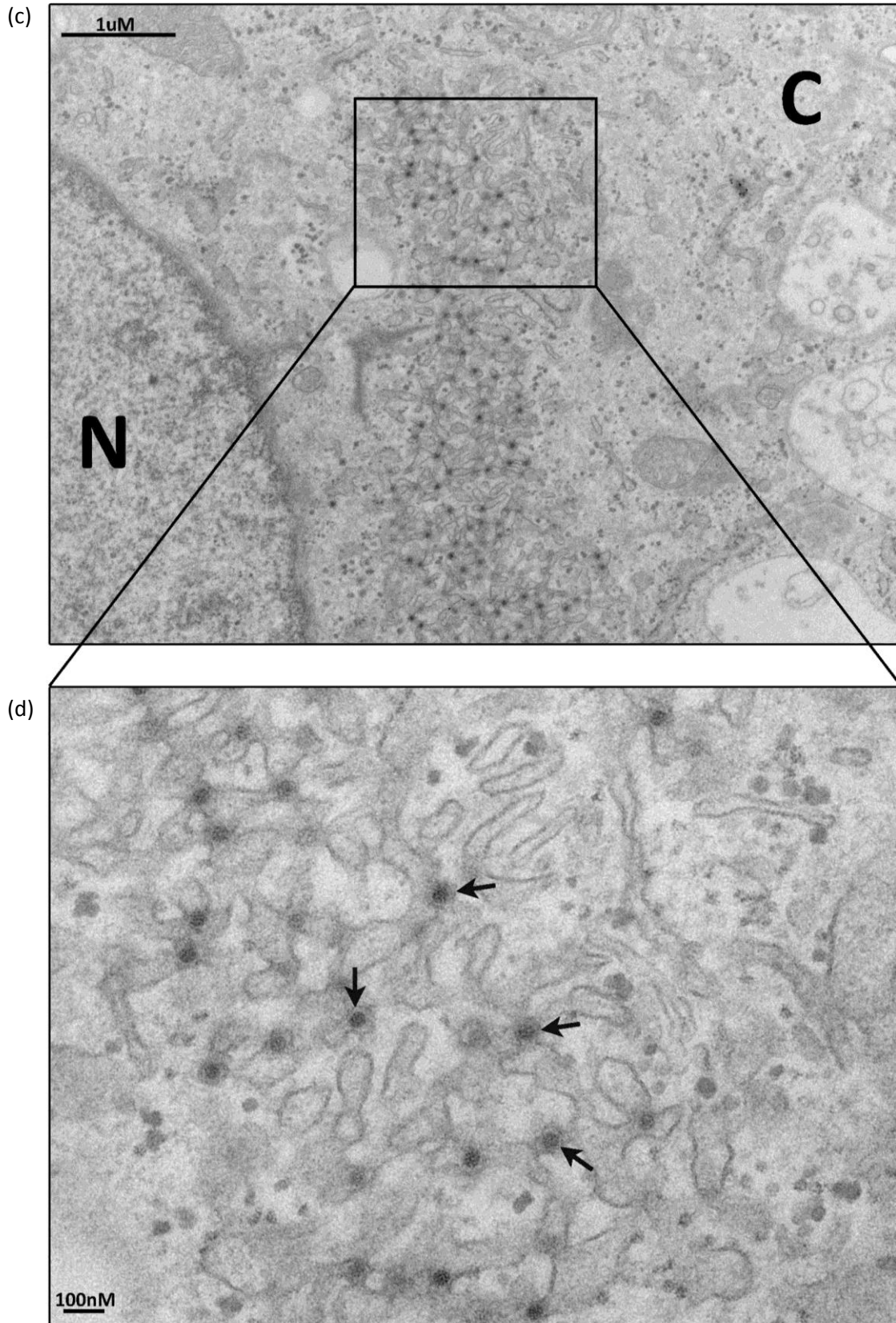
Figure 3.3: BKPyV virions are also located in convoluted membranes at the perinuclear space.
RPTE cells were infected with BKPyV (3 IU/cell) and fixed for TEM at 72 hpi. (a & c) Cytoplasmic (C) and nuclear (N) spaces are labelled, virions are found within smooth convoluted membranes at the perinuclear space. (b & d) At higher magnification of the same section virions can be clearly seen in smooth convoluted membranes, which resemble smooth ER; highlighted with black arrows. Images collected by M Holinshead; Dept. of Pathology TEM facility.

3.2.3 Convoluted membranes containing virions can be labelled with an ER marker

To identify the nature of the smooth ER-like membranes that were found to be laden with virions at 72 hpi, a unique property of ER sorting mechanisms was exploited. KDEL is an ER targeting sequence found at the C-terminus of proteins that need to be maintained within the lumen of the ER. KDEL-motif containing proteins that exit the ER are bound by the KDEL-receptor in subsequent compartments such as the *cis*-Golgi, which causes their recycling back to the ER by retrograde vesicle transport, and only upon cleavage of this sequence or saturation of the KDEL-receptor retrieval mechanism are such proteins able to leave the ER and continue along the secretory pathway (Pelham, 1990). Attaching a KDEL motif to a marker protein is therefore a useful method to label the ER. To this end a KDEL motif tagged to Horseradish Peroxidase (KDEL-HRP) containing plasmid was transfected into BKPyV infected cells at 48 hpi and the cells were fixed for TEM processing and imaging at 72 hpi. This transfection time point allowed ample time for expression of the KDEL-HRP but not to saturating levels, while being at a late time point post infection to avoid any potential effects on viral entry. The location of the HRP-KDEL marker was revealed by catalysis of a biotinylated tyramide solution to produce a diaminobenzidine (DAB) reaction product that could be detected as a darker stain by TEM.

The dark stain was seen exclusively in convoluted ER membranes (Fig. 3.4a & c), which once again contained numerous virions throughout (Fig. 3.4b & d; highlighted with black arrows). These data confirm that these observed virion containing organelles were indeed of ER origin, and likely smooth-ER given the lack of obvious ribosomes that decorate rough-ER. DAB can render such organelles less clear due to the dark nature of the stain, although the morphology of virions remained distinct.
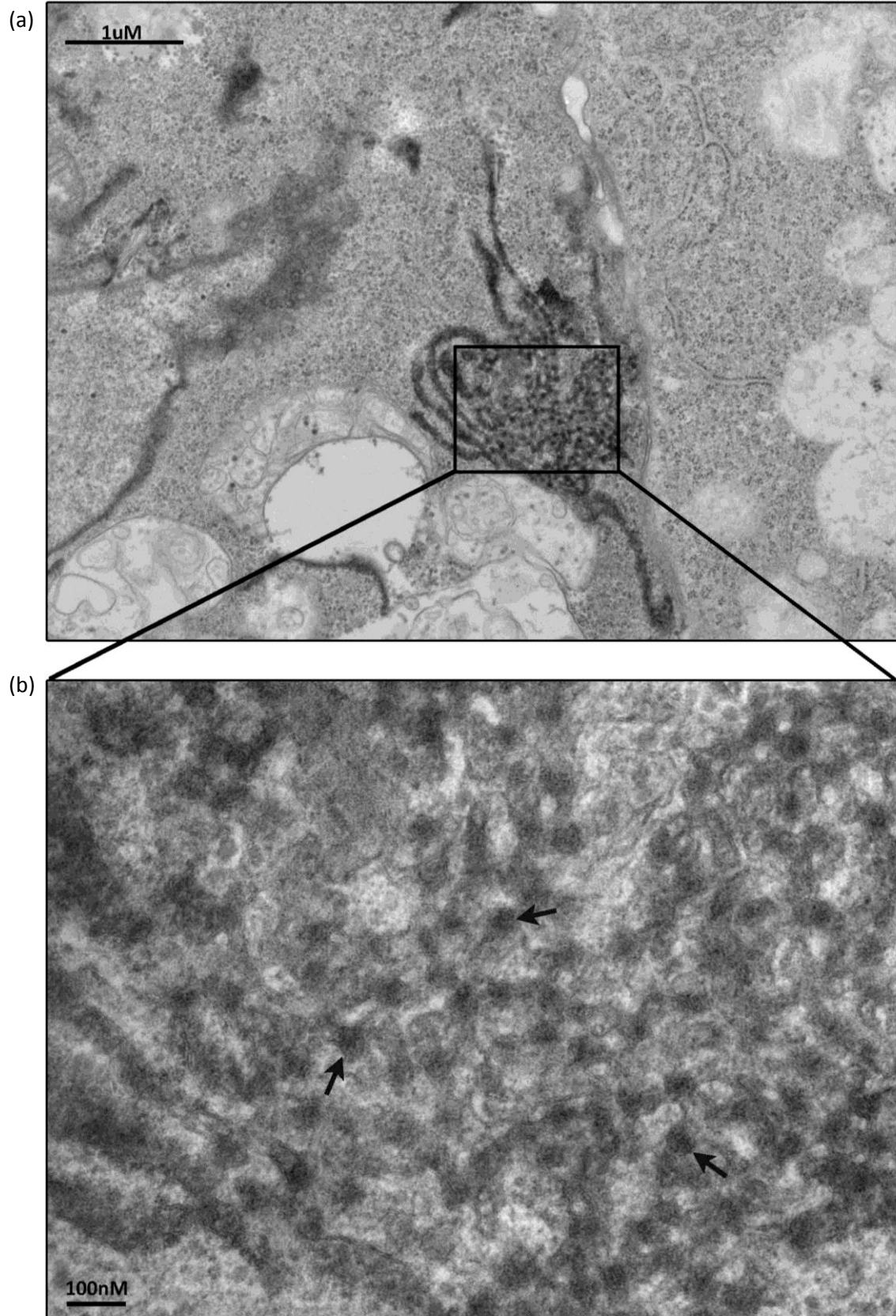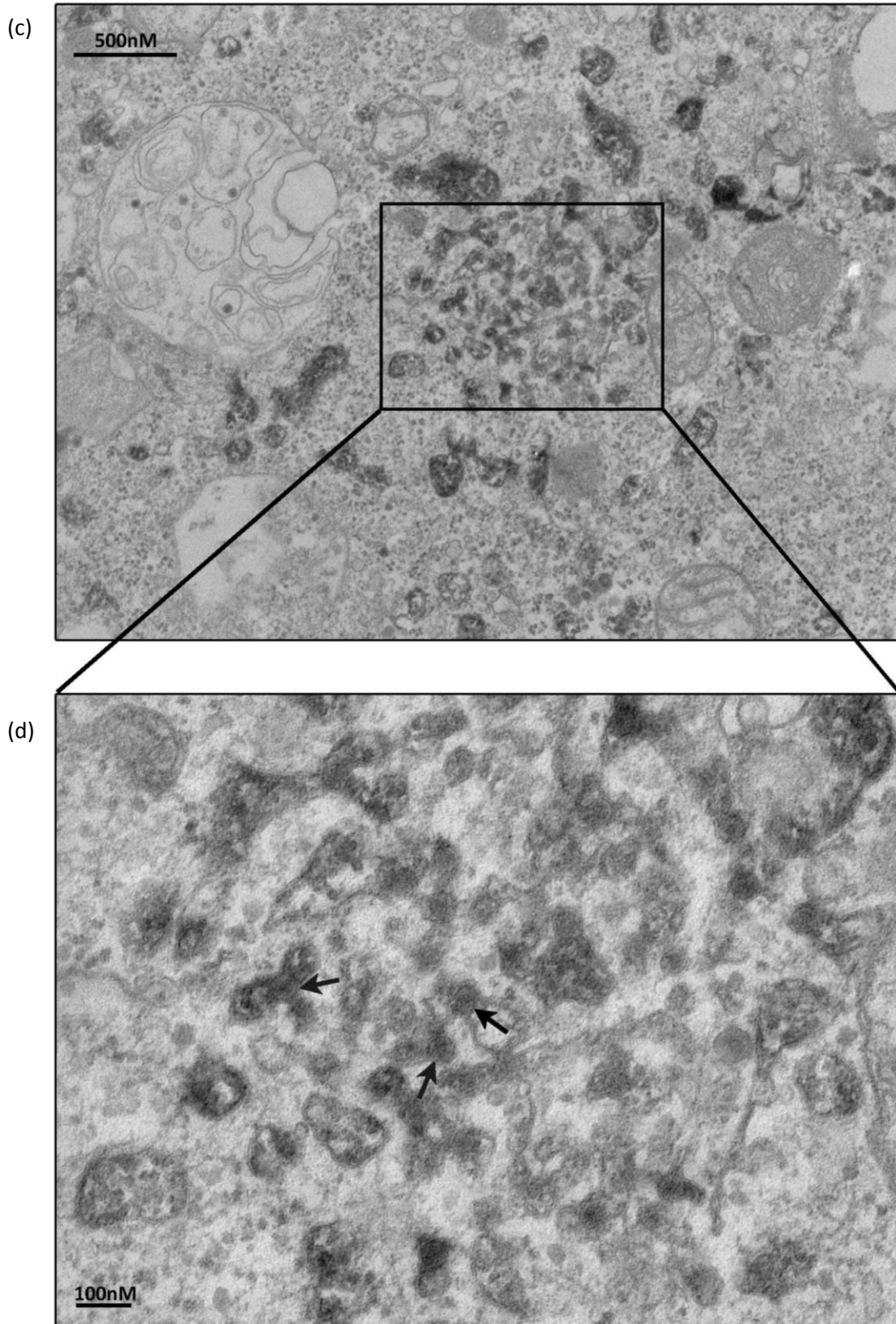
Figure 3.4: Convoluted membranes that contain virions are endoplasmic reticulum.
RPTE cells were infected with BKPyV (3 IU/cell), at 24 hpi cells were transfected with a KDEL-HRP plasmid. At 72 hpi cells were fixed for TEM and HRP developed for 5 minutes. The HRP, retained in the ER due to the KDEL motif, renders the ER darker than surrounding organelles. This darkened structure looks morphologically similar to the smooth convoluted membranes seen in Fig. 3.3 (a & c). Higher magnification reveals virions highly concentrated within this ER membrane (b & d), a number of which have been highlighted with black arrows. Images collected by M Hollinshead; Dept. of Pathology TEM facility.

3.2.4 Neutralising antibodies did not reduce the presence of virions within single membraned vesicles or smooth ER

In order to address whether virions observed with smooth-ER compartment and single membrane vesicles could be due to virions undergoing entry as opposed those that were egressing the cell, experiments were conducted in the presence of a neutralising antibody against BKPyV to neutralise the infectivity of virions that were secreted into the supernatant. Neutralised virions should then be prevented from re-infecting cells.

A conformation-dependent antibody to BKPyV VP1 (C1), previously shown to neutralise infection, was obtained (Randhawa et al., 2009). While published data provides evidence that pre-incubation with VP1 (C1) antibody can reduce BKPyV infectivity it was important to confirm this in our assay systems. RPTE cells were infected at 3 IU/cell and 40 µl VP1 (C1) antibody (kindly provided by Dr. Christensen) was added to the supernatant of cells at 24 hpi, at 48 hpi media was removed and retained for testing, cells were washed once gently with PBS and fresh media supplemented with 40 µl VP1 (C1) antibody was added. A mouse monoclonal antibody specific to HSV-1 glycoprotein D (LP2), which should have no effect on BKPyV, was used as an isotype control. Cells and supernatant virus were harvested at 72 hpi. Virus titres of supernatants and cells were then assessed by FFU, confirming that the neutralising antibody VP1 (C1) was able to reduce the infectivity of secreted BKPyV by 84%, compared to control (Fig. 3.5).

While these data demonstrate that the anti-VP1 (C1) antibody effectively neutralises released virus infectivity, it is possible that this could be through either inhibiting receptor binding and thus prevent virus internalisation, or by inhibiting a post-internalisation stage such genome release which is thought to require capsid conformational changes in the ER. In order to investigate this BKPyV (3 IU/cell), or mock media, were incubated in the presence or absence of anti-VP1 (C1) neutralising antibody or the anti-HSV-1 (LP2) isotype control for 1 h and then used to infect RPTE cells. Cells were fixed at 6 hpi to allow sufficient time for BKPyV binding and internalisation, and processed for immunofluorescence.

All fixed samples were then first incubated with the IgG2a anti-VP1 (C1) antibody, which had been used to neutralise the virions, and then anti-VP1 (B5, IgM). This was conducted to ensure that any potential failure to observe colocalisation or intracellular VP1 (B5) was not simply due to anti-VP1 (C1) obscuring the anti-VP1 (B5, IgM) epitope when bound to virions.

In samples that were not pre-treated with neutralising antibodies no specific signal was observed in mock infected cells, while in BKPyV infected samples numerous C1-positive puncta were observed in cells, many of which colocalised with the B5 antibody staining highlighted with white arrows (Fig. 3.6a). Overall, fewer B5-positive puncta were observed than C1-positive puncta, which could reflect

either more restricted epitope accessibility for the larger pentavalent IgM compared to the IgG, a better signal-to-noise ratio for the C1 antibody, and/or competition for binding between the two antibodies. Nevertheless, the detection of costained puncta within cells is indicative of virion internalisation. In samples pre-treated with anti-VP1 (C1) neutralising antibody relatively large blobs of signal were observed in mock infected cells, presumably due to aggregates of the C1 antibody binding to cells (Fig. 3.6b). While similar large aggregate-like anti-VP1 (C1) antibody stain was observed in BKPyV infected samples, the number of small C1-positive puncta observed in cells was greatly reduced and very few puncta showing C1 and B5 colocalisation could be seen. Samples pre-treated with the non-neutralising HSV-1 LP2 showed numerous small C1 positive puncta with many also positive for B5 staining, very similar to no antibody pre-treatment (Fig. 3.6c).

This data taken together suggests that the anti-VP1 (C1) antibody not only neutralises BKPyV infectivity, but also inhibits binding and/or internalisation of BKPyV into RPTE cells.
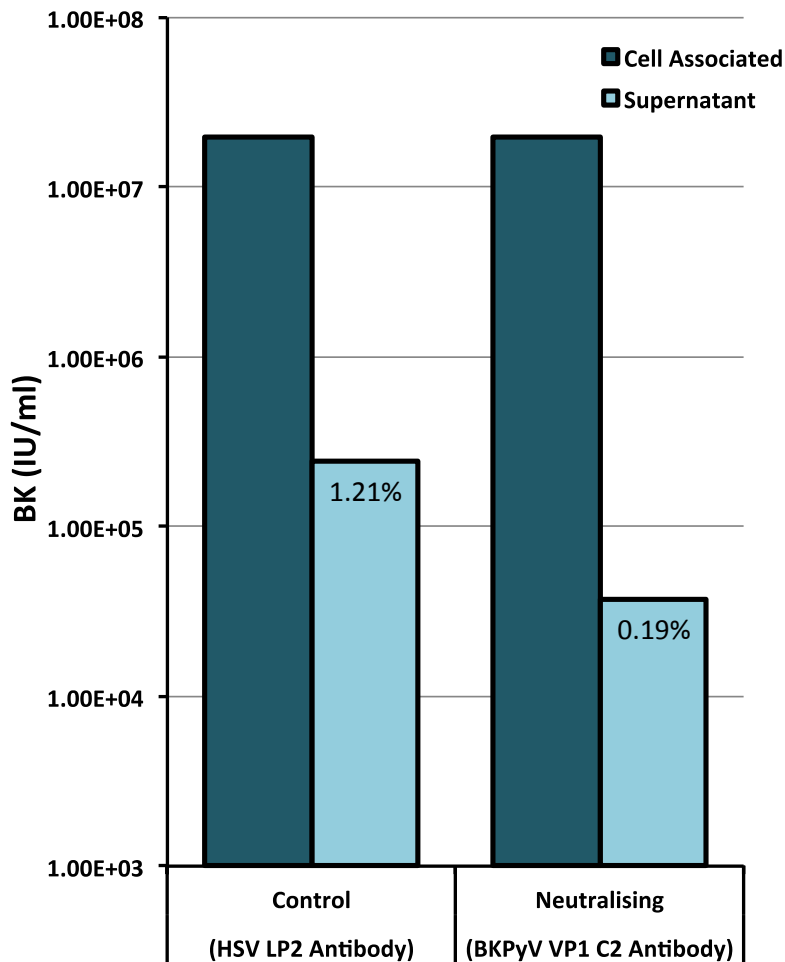
Figure 3.5: VP1 (C1) antibody can neutralise infection.
RPTE cells were infected (BKPyV 3 IU/cell), at 1 hpi cells were washed with PBS and fresh media added. At 24 hpi VP1 (C1) neutralising antibodies or non-neutralising HSV-1 LP2 antibodies were added to media to neutralise any virions released into the supernatant. At 48 hpi supernatant was removed and retained, cells washed with PBS and media supplemented with fresh antibody was added to cells. Cell-associated and supernatant virus was harvested at 72 hpi. Cell-associated samples were freeze/thawed three times to release virus, while the two supernatant virus harvests were combined, pelleted by ultracentrifugation and resuspended in 20x original volume. An FFU conducted was conducted to assess viral titres of each sample. Percentage of total infectious virus in the supernatant specified. Data from one experiment shown.

(a)
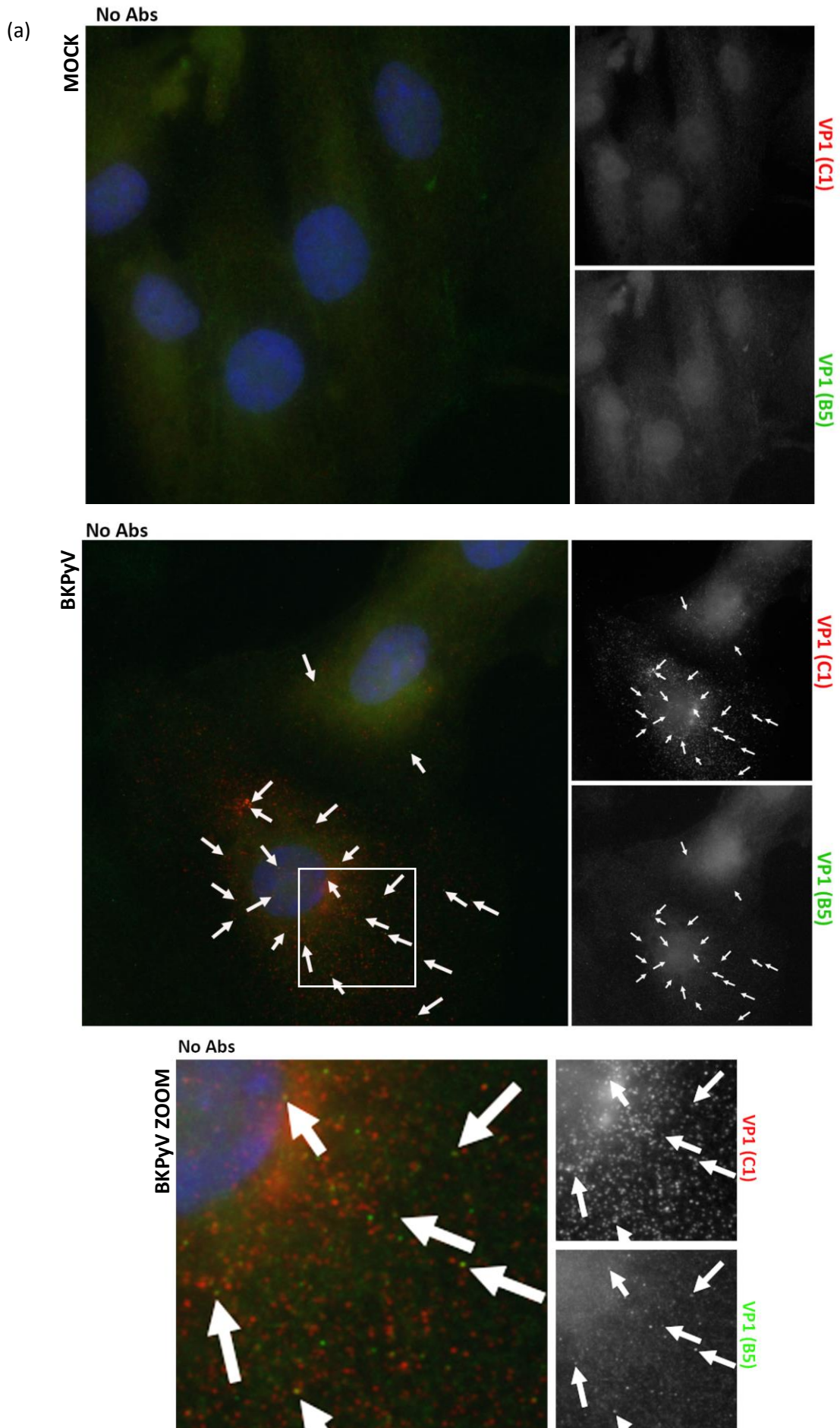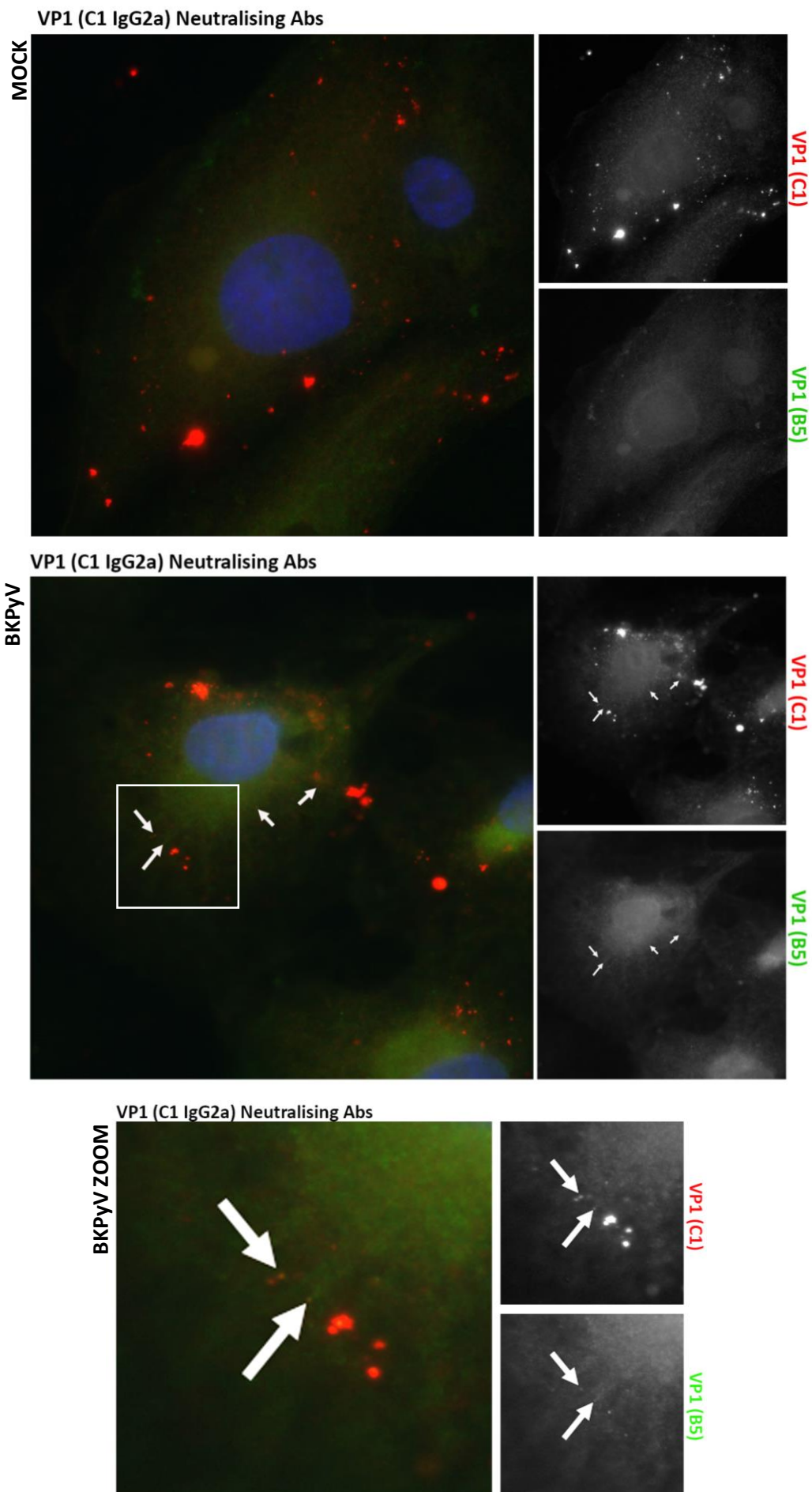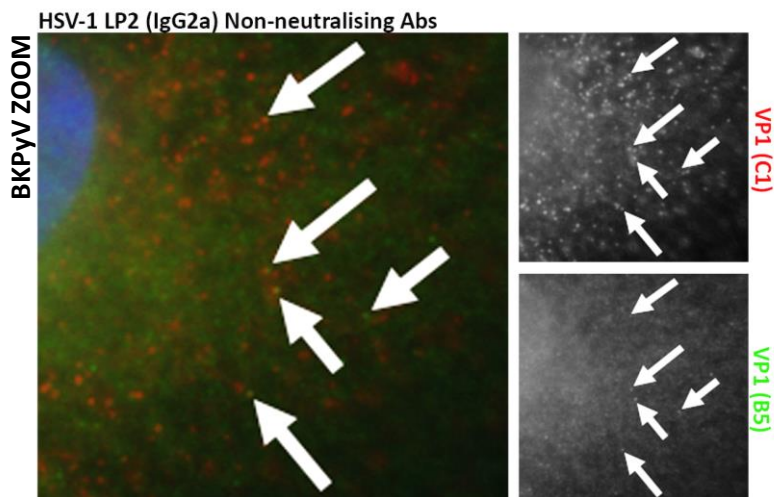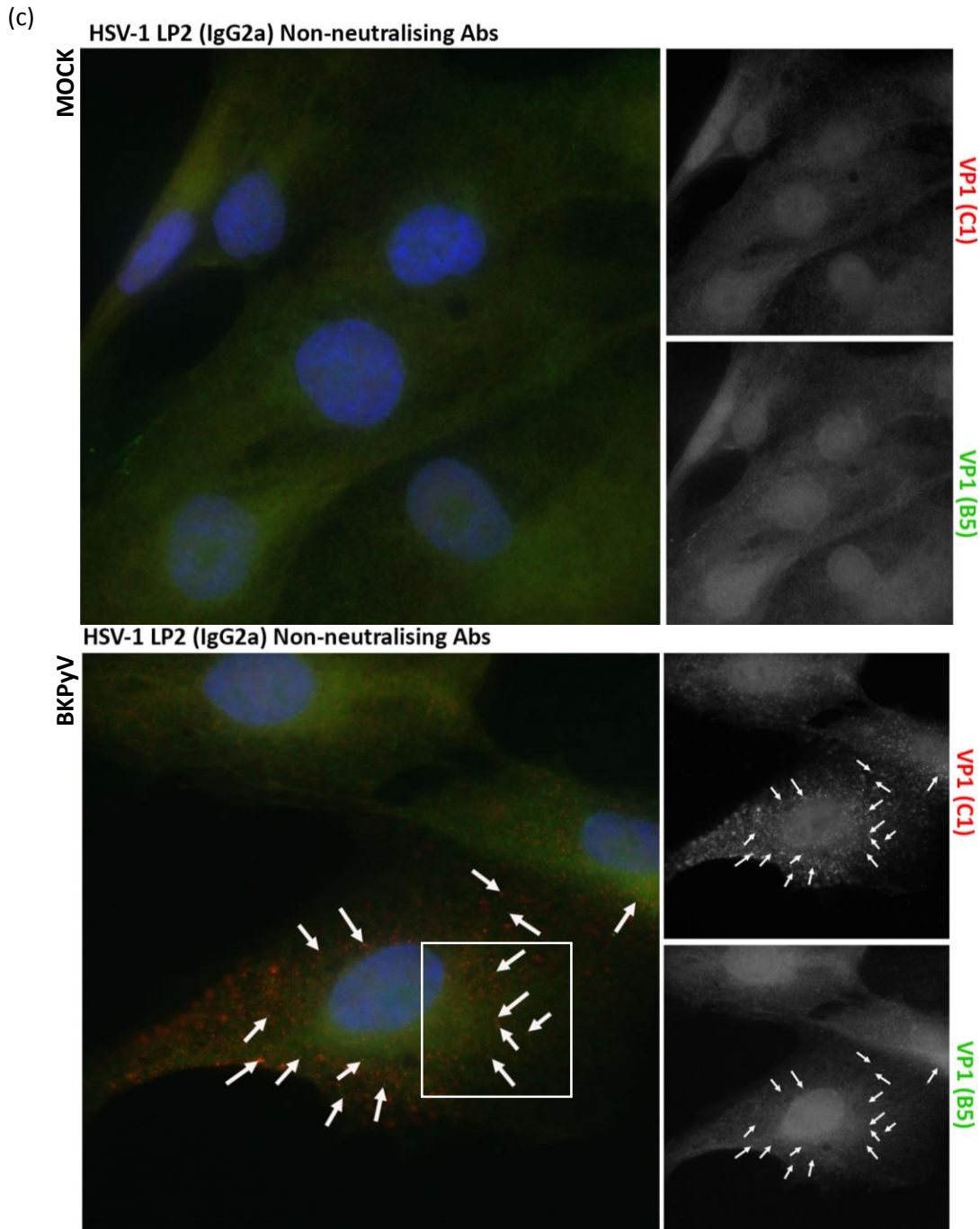
Figure 3.6: VP1 (C1) antibody reduces BKPyV entry into cells.

BKPyV (3 IU/cell) infectious media or mock media were incubated for 1 h with no antibodies (a), neutralising VP1 (C1) antibody (b), or non-neutralising HSV-1 LP2 antibody (c). RPTE cells were then infected with each incubation. At 48 hpi cells were fixed for immunofluorescence and stained. VP1 (C1) stain shown in red, VP1 (B5) shown in green, DAPI shown in blue.

White arrows are used to show points of colocalisation between VP1 (C1) and VP1 (B5) antibodies. Images taken on Olympus IX81 immunofluorescence microscope.

Given that VP1 (C1) can neutralise the infectivity and inhibit the entry of BKPyV, the TEM were repeated on RPTE cells that had been infected at 3 IU/cell followed by the addition of neutralising anti-VP1 (C1) antibody at 24 and 48 hpi to investigate whether this affected the observed BKPyV particles in the lumen of cytoplasmic vesicles or the ER lumen. Cells were fixed at 72 hpi and processed for TEM. In the presence of neutralising antibodies the same single membraned vesicles were observed as previously (Fig. 3.7a & b, arrowed), and were as numerous as observed previously. Similarly smooth-ER membranes were once again found to contain large quantities of virions (Fig. 3.7c & d).

These data, suggest that these observations are not due to the internalisation of virions into cells and support the hypothesis that BKPyV particles can undergo egress from cells via transport involving the smooth-ER and single membraned vesicles.
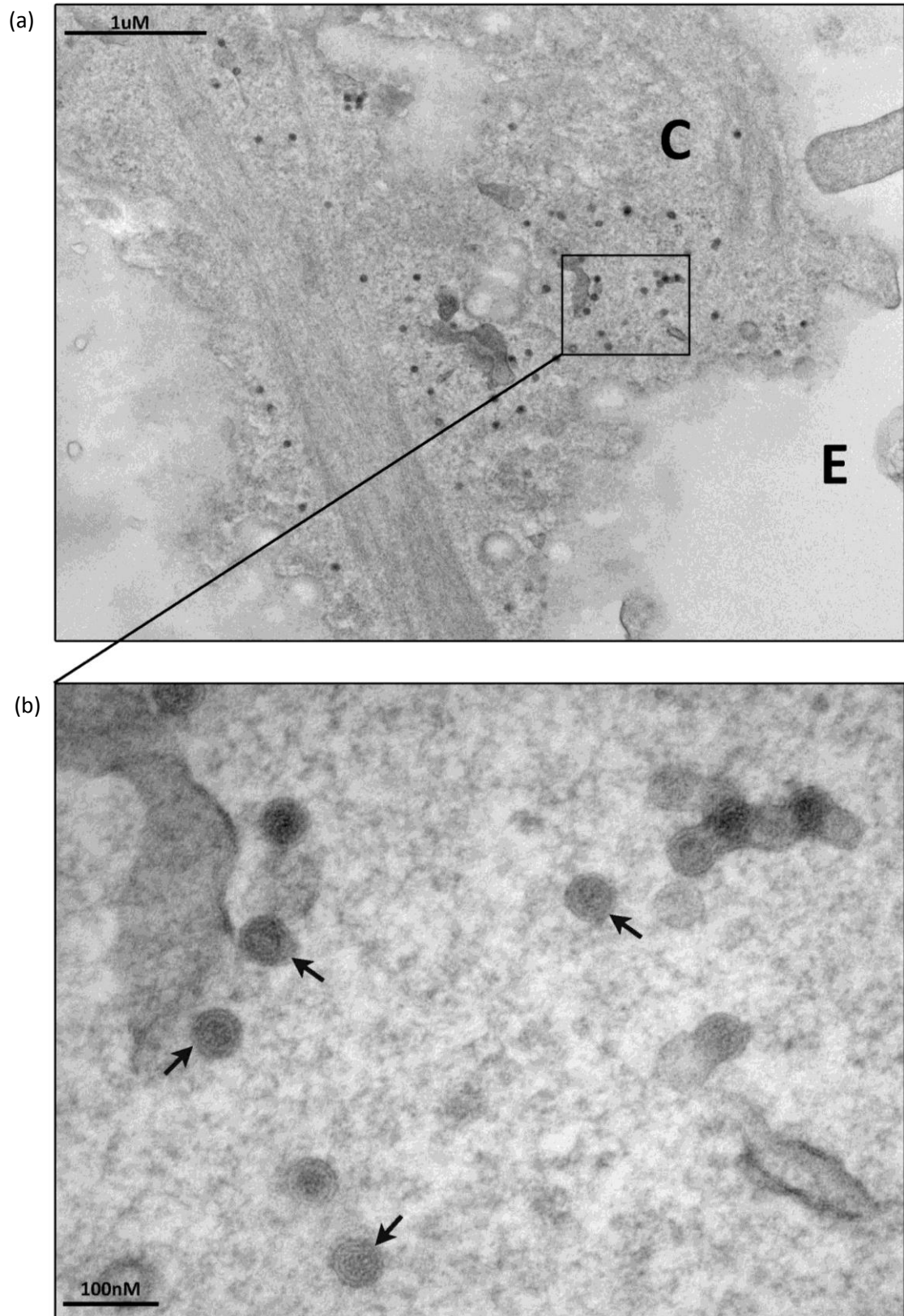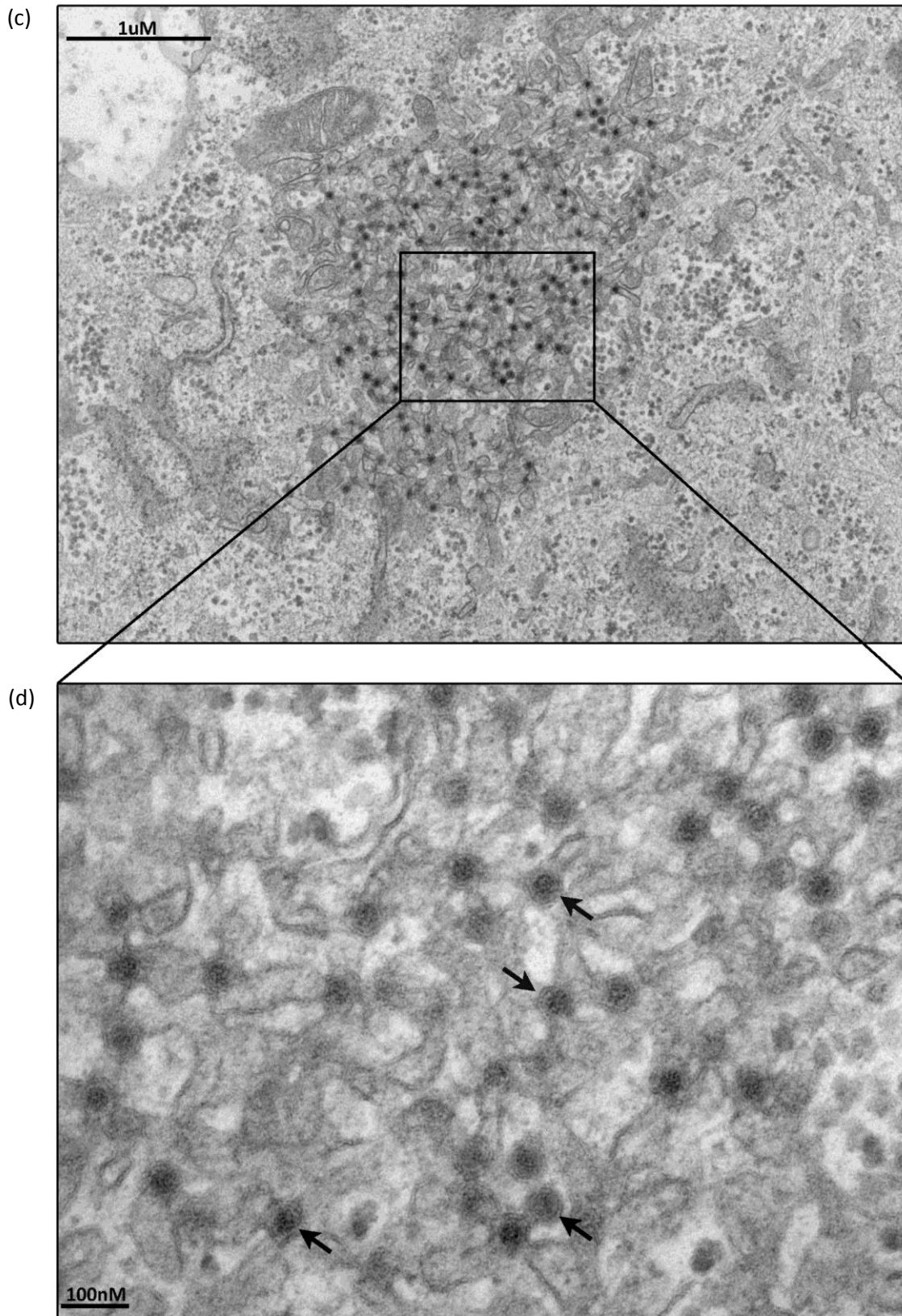
Figure 3.7: Single membraned vesicles and convoluted membranes containing BKPyV virions are seen in the presence of neutralising antibodies.
RPTE cells were infected (BKPyV 3 IU/cell), 1 hpi cells were washed with PBS and fresh media added along with VP1 (C1) neutralising antibodies. Neutralising antibodies were further replenished at 48 hpi.
(a & b) BKPyV virions were once again observed in the cytoplasm of cells towards the cellular periphery, highlighted with white arrows at higher magnification. (d & e) BKPyV virions were once again observed in convoluted smooth membranes in the cytoplasm of cells, highlighted with black arrows are higher magnification. Images collected by M Hollinshead; Dept. of Pathology TEM facility.

3.2.5 Disruption of Golgi transport does not affect BKPyV secretion

Conventional secretion involves transport from ER to *cis*-Golgi, through the Golgi stack and then *trans*-Golgi (outlined in Fig. 1.5). Golgi-dependent transport of proteins can be disrupted by monensin (Dinter and Berger, 1998), an ionophore that has previously been shown to inhibit secretion of SV40 from Vero cells (Clayson et al., 1989). To assess whether BKPyV virions are being secreted via Golgi mediated conventional secretion RPTE cells were subjected to monensin inhibition assays. RPTE cells were infected with BKPyV (1 IU/cell) and at 24 hpi were treated with monensin at ranges from 5nM to 5μM, or ethanol (the diluent) as a control. These concentrations were chosen based on concentrations used by Clayson et al. to inhibit SV40 without affecting viral protein synthesis (100 nM-10 μM), however concentrations 10 μM and above have been shown to have adverse effects in at least one cell type and as such concentrations were limited to 5 μM (Takemura et al., 1992).

Cells and supernatant were harvested separately at 48 hpi and infectious virus levels were titred by FFU (Fig. 3.8a). The proportion of virus secreted into the supernatant was unaffected by the addition of monensin, even at the highest concentrations, suggesting that BKPyV does not traffic via Golgi mediated conventional secretion. As a control for these assays it was important to ensure that monensin is active in RPTE cells. It is known that monensin treatment leads to an increase in early endosome antigen 1 (EEA1)-positive vesicles due to the disruption of endocytic pathway trafficking (Hellevik et al., 1998). RPTE cells were treated with 5μM monensin, or ethanol as a control, for 24h and fixed for immunostaining. EEA1 staining is much more abundant in those cells treated with monensin than in control conditions (Fig. 3.8b). In addition, Golgi transport is required for HSV-1 assembly, for the appropriate maturation and transport of HSV-1 envelope glycoproteins, as well as HSV-1 secretion after intracellular envelopment. To further validate the activity of the monensin stock replication and secretion of HSV-1 was assessed in the presence or absence of this inhibitor. Vero cells were infected with HSV-1 (3 PFU/cell) and treated with 5μM monensin from 6 hpi, or ethanol as a control. Cells and supernatant were harvested separately at 22 hpi and virus titres were assessed by plaque assay (Fig. 3.8c). Monensin treatment caused a reduction in the total production of infectious HSV-1 by approximately 90% and showed a greater reduction of virus release (approximately 60% reduction in proportion of total infectious virus that was released) demonstrating the expected inhibition of HSV-1 assembly and secretion by monensin. Taken together, these data suggest that BKPyV is secreted via a monensin-insensitive, Golgi-independent pathway.

(a)

(b)

(c)
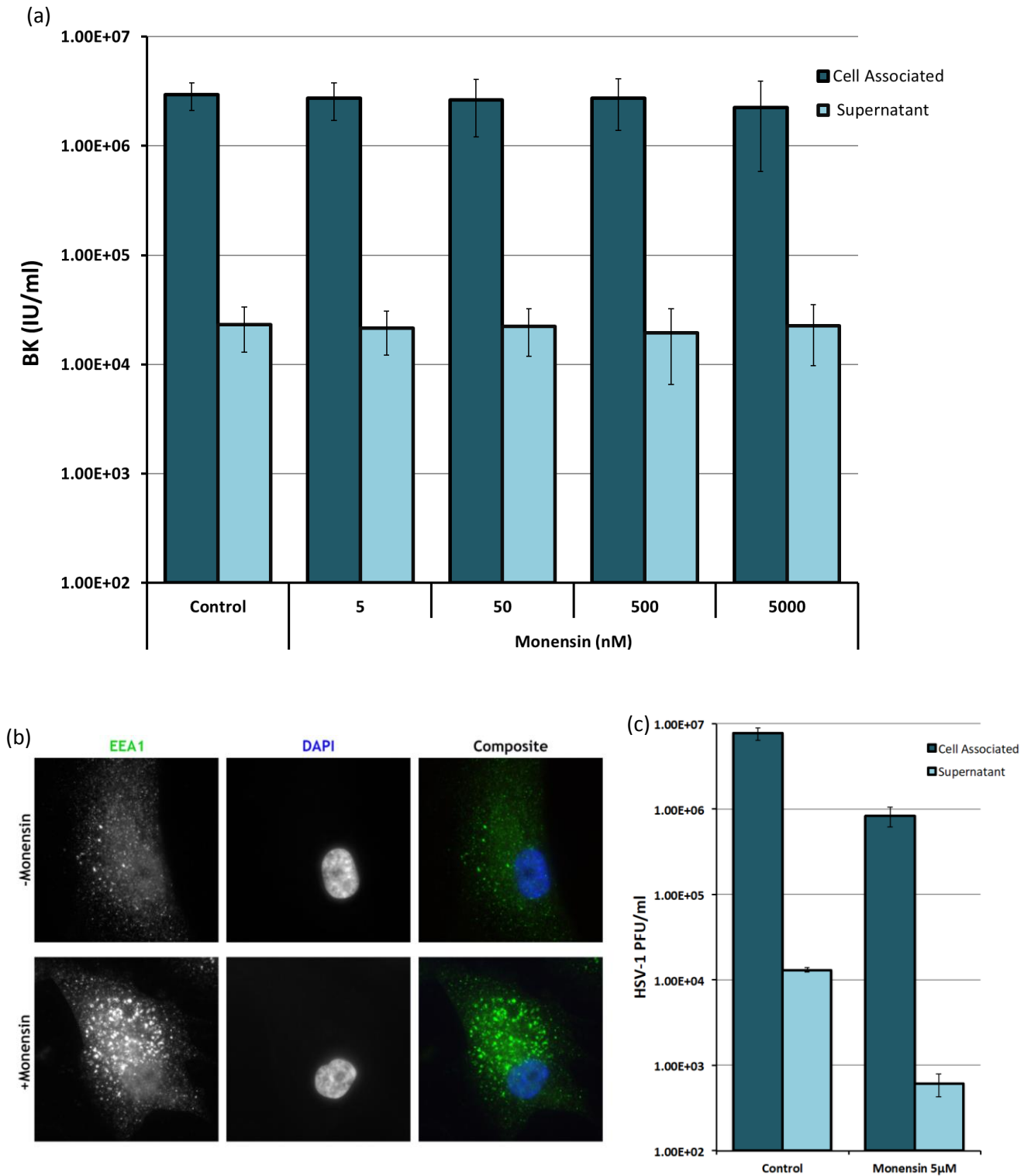
Figure 3.8: The inhibitor of Golgi transport, monensin, does not affect the release of BKPyV from cells.
(a) RPTE cells were BKPyV infected at 1 IU/cell and 24 hpi treated with increasing concentrations of monensin, or ethanol as a control. At 48 hpi cells and supernatant virus were harvested separately. Cell-associated samples were freeze/thawed three times to release virus, while supernatant virus was pelleted by ultracentrifugation and resuspended in 20x original volume. An FFU assay was then conducted. Mean data from two independent experiments, error bars show standard error. (b) Uninfected RPTE cells were treated for 24 h with 5μM monensin or ethanol as a control. Cells were then fixed for immunofluorescence and stained for EEA1 (green). DAPI is shown in blue. The abundance of EEA1 increases when Golgi transport is disrupted. Images taken on Olympus IX81 immunofluorescence microscope. (c) Vero cells were infected with HSV-1 at 3 IU/cell. At 6 hpi cells were treated with 5μM monensin or ethanol as a control. At 22 hpi cells and supernatant were harvested. Cell-associated samples were freeze/thawed three times to release virus. HSV-1 titres were determined by plaque assay on Vero cell monolayers. Mean data from two biological repeats, error bars show standard error.

3.2.6 Autophagic vesicles are not involved in BKPyV secretion for RPTE cells

Various unconventional secretion pathways that do not follow classical ER to Golgi routes have been described (Fig. 1.6). To date four distinct pathways have been described, while more may continue to be identified. As BKPyV does not appear to secrete via the Golgi, it was important to investigate which of the unconventional secretion pathways may be involved. The first pathway is one by which small proteins are able to translocate across the plasma membrane by pore formation (Nickel and Rabouille, 2009), a pathway which would seem highly unlikely for BKPyV due to its size (~45nm). MVBs serve as a conduit for the second type of unconventional secretion where cargo is incorporated into intraluminal vesicles of MVBs, which can be released as exosomes by fusion of the MVB with the plasma membrane (Qu et al., 2007, Andrei et al., 2004). If BKPyV were to use this pathway, this would result in the virus particles being inside intraluminal vesicles within MVBs and furthermore retaining a host derived lipid bilayer (the exosome) after they are released, as observed for HAV virus (Feng et al., 2013). No evidence of BKPyV particles within MVBs or being coated with a membrane in the extracellular matrix has been observed by TEM analysis of BKPyV infected cells, suggesting this MVB/exosome-based unconventional secretory pathway is unlikely to be exploited as a means of BKPyV release.

A third unconventional secretory pathway that has been described involves autophagy-derived membranes, which serve to envelop cytoplasmic components (Duran et al., 2010). This results in a double membrane autophagosome containing cytoplasmic contents, which has been shown to be a route of non-lytic egress for certain enteroviruses (Mutsafi and Altan-Bonnet, 2018). While the structures seen in TEM that contain BKPyV virions close to the cell periphery are single membraned vesicles thus unlikely to be autophagic in origin, it was nevertheless hypothesised that autophagy may regulate BKPyV secretion. To investigate this autophagy was induced or inhibited during the final stages of BKPyV infection to observe whether this increased or reduce levels of BKPyV secretion. RPTE cells were BKPyV infected (1 IU/cell) and treated with 3μg/ml Brefeldin A in serum-free OptiMEM to induce autophagy (Ding et al., 2007), 100nM wortmannin to inhibit autophagy, or DMSO as a control at 3, 6 and 12 h before harvesting at 48 hpi (Fig. 3.9a). Titres of cell-associated and supernatant virus showed that inducing autophagy lead to a small reduction in secreted virus, and by 12 h treatment intracellular viral loads were also vastly reduced. In addition to this, autophagy inhibition lead to a slight increase in BKPyV secretion. These data suggest that an autophagy-related pathway is not required for BKPyV secretion.

To confirm induction of autophagy by serum-starvation (OptiMEM) and Brefeldin A treatment an immunoblot was conducted on cell pellets taken from the same experiments and blotted for both LC3 and lipidated LC3 (Fig. 3.9b). When autophagy is induced LC3 becomes lipidated, as observed in the

Brefeldin A and OptiMEM treated cells. Low basal levels of lipidated LC3 in uninduced (control) RPTE cells meant validation of the autophagy inhibition activity of wortmannin was better validated by observing changes to the subcellular localisation of LC3 in RPTE cells, treated with or without wortmannin by immunofluorescence microscopy (Fig. 3.9c). Several LC3-positive puncta were observed in untreated RPTE cells indicating steady-state levels of autophagy, while in wortmannin treated cells no such puncta are present and LC3-staining displayed a diffuse signal indicating effected inhibition of autophagy by this inhibitor in RPTE cells. These data, in conjunction with the morphology of virion-containing ER-like compartments and single membrane vesicles strongly suggest that BKPyV does not exploit autophagy-related pathways for its secretion.

(a)

(b)

(c)
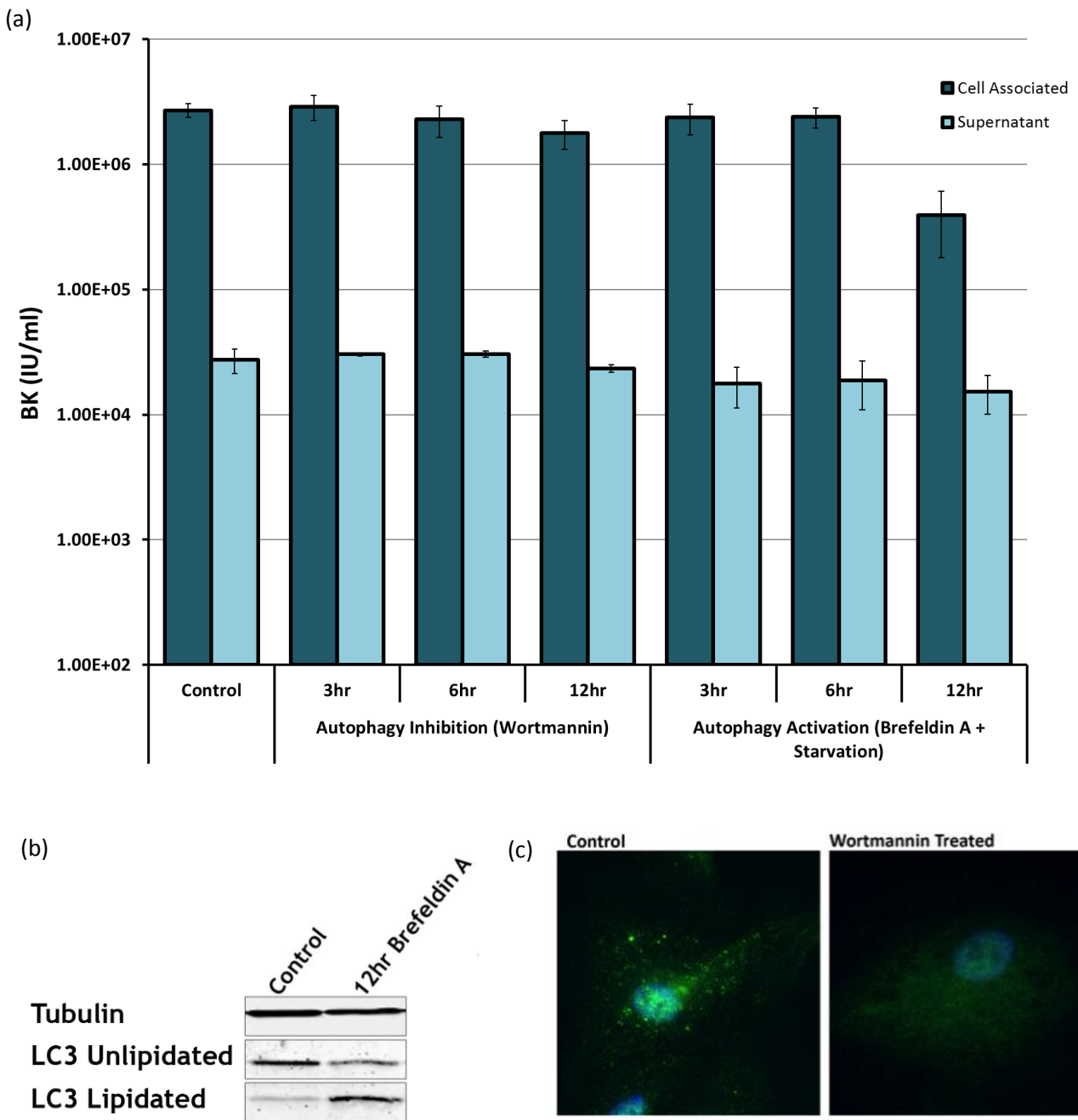
Figure 3.9: Autophagy modulation is not involved in BKPyV secretion.
(a) RPTE cells were infected with BKPyV (1 IU/cell). At 3, 6 and 12 hours prior to 48 hpi harvest cells were either treated to inhibit autophagy (10mM wortmannin), induce autophagy (3μg/ml Brefeldin A, in OptiMEM), or DMSO as a control. At 48 hpi cells were harvested for immunoblot analysis, and cellular and supernatant virus was harvested separately. Cell-associated samples were freeze/thawed three times to release virus, while supernatant virus was pelleted by ultracentrifugation and resuspended in 20x original volume. FFU titration was then conducted. Mean data from three independent experiments, error bars show standard deviation. (b) To validate the effectiveness of Brefeldin A plus starvation in inducing autophagy an immunoblot of lipidated and unlipidated LC3 in untreated (control) RPTE cells or in the presence of autophagy inducer Brefeldin A + optiMEM for 12h was conducted, LC3 becomes lipidated during autophagy. (c) To validate the effectiveness of wortmannin in inhibiting autophagy RPTE cells were untreated (control) or treated with the wortmannin and stained for LC3 and imaged by immunofluorescence, shown in green, DAPI is shown in blue. Images taken on Olympus IX81 immunofluorescence microscope.

3.2.7 VP1 conformational antibodies colocalise with GORASP1, GORASP2 and Calnexin, but not EEA1, TGN46, GM130 or LysoTracker

A fourth unconventional secretion pathway that has been described is termed 'Golgi bypass', and involves the trafficking of single membraned vesicles, pinched from the ER, directly to the cell surface (Rabouille et al., 2012). The Golgi-bypass associated single membraned vesicles have been shown to contain the Golgi Reassembly and Stacking Protein 1 (GORASP1) and Golgi Reassembly and Stacking Protein 2 (GORASP2), however this pathway has thus far only been described in mammals for transmembrane cellular proteins such as mis-folded CFTR (Gee et al., 2011). While we have seen clear localisation of virions to the ER by TEM, to further characterise the secretion pathway used by BKPyV it was important to investigate the localisation of BKPyV particles in subcellular organelles by immunofluorescence microscopy, particularly secretory and endocytic pathway compartments.

Having obtained a panel of conformation-dependent BKPyV VP1 antibodies (Randhawa et al., 2009), testing of these antibodies in immunofluorescence demonstrated that those of IgM subtype preferentially stained particles in the cytoplasm, while those of IgG subtypes stained both nuclear and cytoplasmic conformational VP1. This is presumably due to reduced accessibility for binding epitopes of the large IgM molecules within the densely packed nucleoplasm. As the majority of viral particles are contained within the nucleus, the ability to exclude this signal in colocalisation imaging is beneficial for the detection of viral particles in the cytoplasm; the relatively weak signals for virions in the cytoplasm can easily be obscured by the very bright signals in the nucleus when using IgG subtype anti-VP1. To confirm that cytoplasmic signals when using conformation-dependent anti-VP1 IgM antibody (B5) are virus particles RPTE cells were infected BKPyV (1 IU/cell) or mock infected, fixed at 48 hpi and then co-stained with an IgM subtype anti-VP1 (B5) and an IgG2a subtype anti-VP1 (D11), both of which are conformation-dependent VP1-specific antibodies that neutralise BKPyV infectivity (Fig. 3.10). Clear colocalisation was observed in the cytoplasm between both subtypes of conformational VP1 antibody in infected cells, while nuclear signal was lacking in VP1 (B5) staining. No signal was detected for either antibody in uninfected cells. All subsequent colocalisation studies with cellular compartment markers were conducted with the IgM anti-VP1 (B5) antibody.

To investigate localisation of BKPyV particles to sub-cellular compartments RPTE cells were infected with BKPyV (1 IU/cell), or mock infected, and fixed at 48 hpi and stained with anti-VP1 IgM (B5) together with a range of cellular markers. LysoTracker, a marker of acidic vesicles (Fig. 3.11a), GM130, a marker of the *cis*-Golgi (Fig. 3.11b), TGN46, a marker of the *trans*-Golgi network (Fig. 3.11c) or EEA1, an early endosomal marker (Fig. 3.11d) failed to show colocalisation with VP1 (B5), suggesting that BKPyV does not localise to these compartments during intracellular trafficking at late stages of infection. Interestingly, colocalisation between VP1 (B5) and GORASP1 (Fig. 3.11e), GORASP2 (Fig.

3.11f) and calnexin (Fig. 3.11g) was observed (highlighted with white arrows). Calnexin is an ER marker, and while staining is rather widespread in these cells, colocalisation can be seen, providing further evidence that virions are present in the ER at late times post infection. GORASP1 and GORASP2 are known to tether Golgi stacks together, but in times of cellular and ER stress a proportion can be relocalised to vesicles involved in 'Golgi-bypass' unconventional secretion, which involves direct vesicle transport from the ER to the cell surface. The observed colocalisation between GORASP1 or GORASP2 and VP1 suggests this pathway may be exploited during BKPyV secretion.
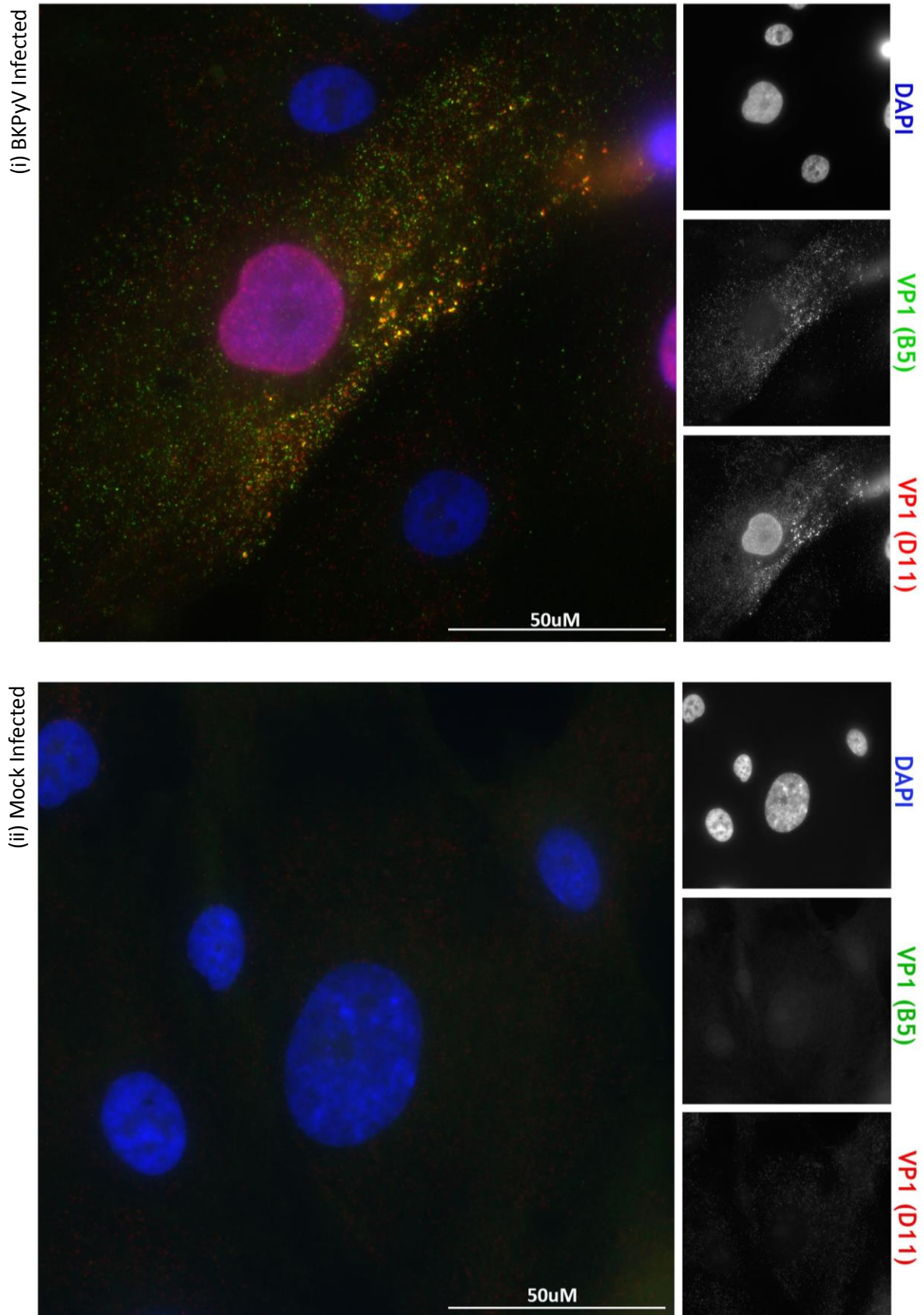
Figure 3.10: VP1 IgM conformational antibodies bind VP1 in the cytoplasm but not the nucleus.
RPTE cells were infected with BKPyV (1 IU/cell) or mock infected and fixed for immunofluorescence at 48 hpi. Cells were immunostained with VP1 (D11, IgG2a) (each shown in red), VP1 (B5, IgM) (green) and DAPI (blue). Images were acquired on Olympus IX81 (x60 magnification).

(e)

(f)
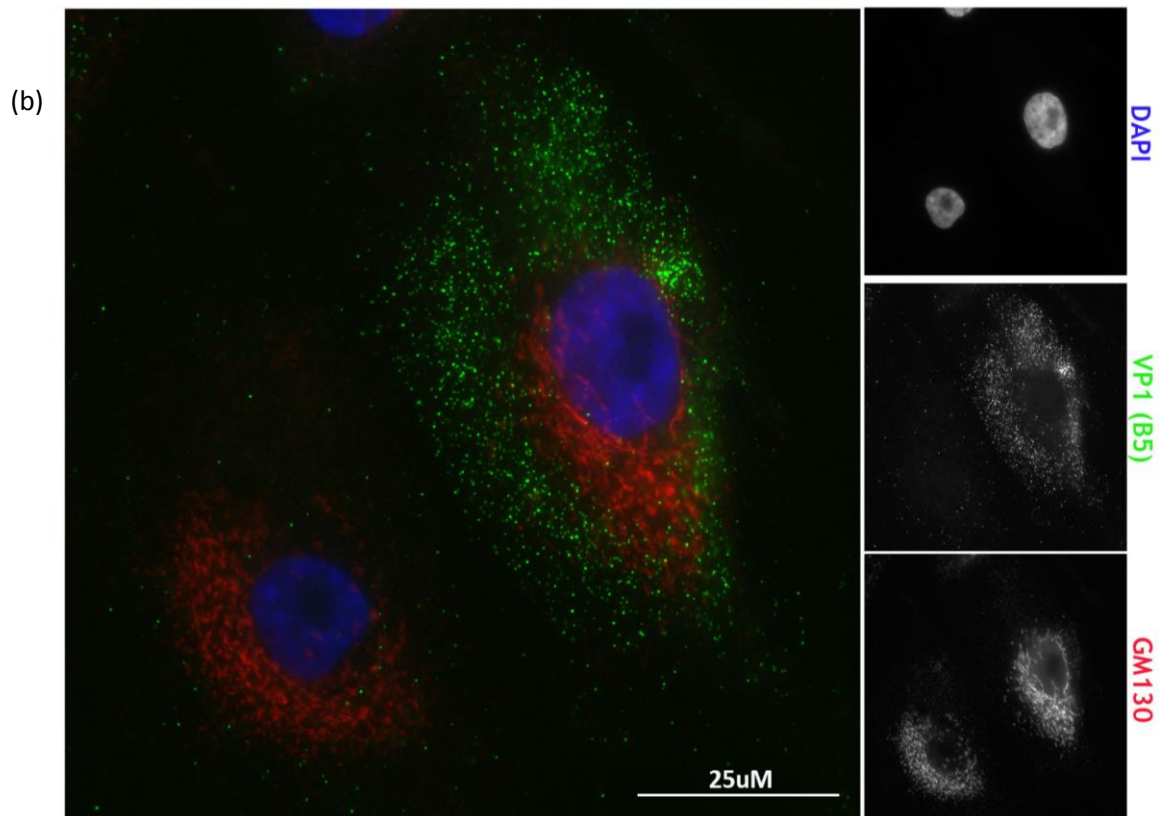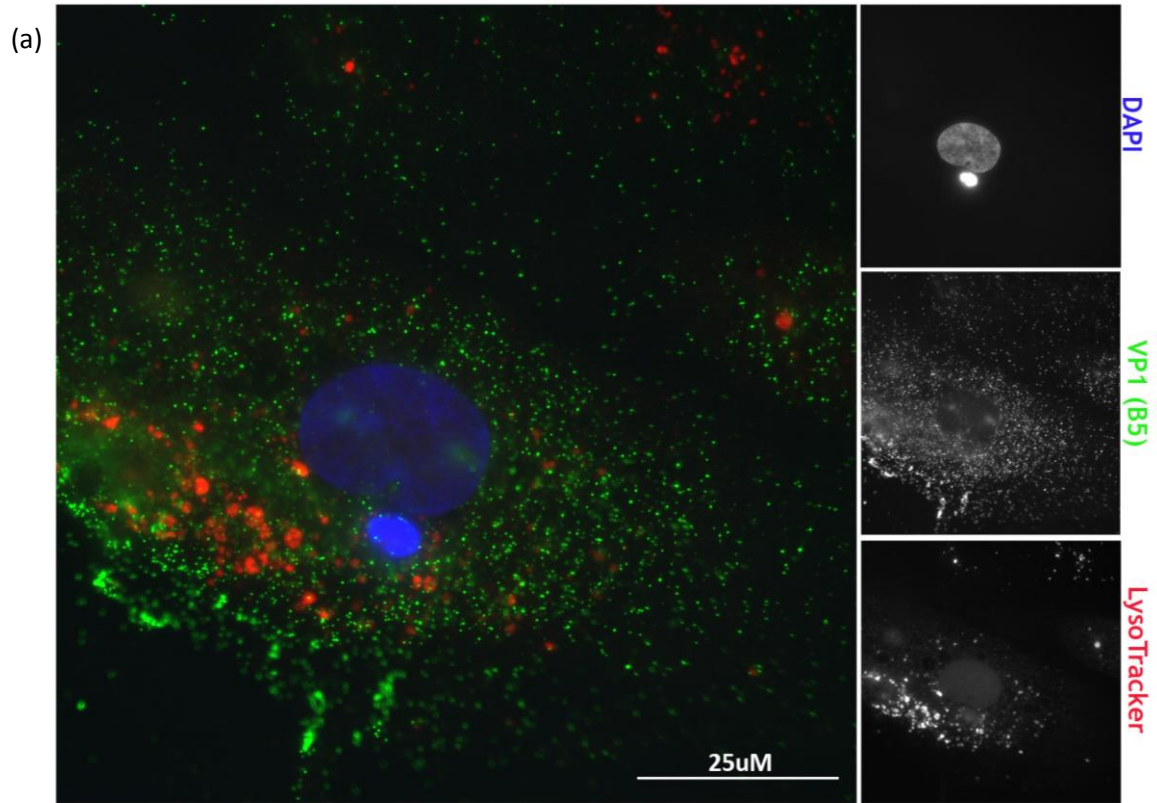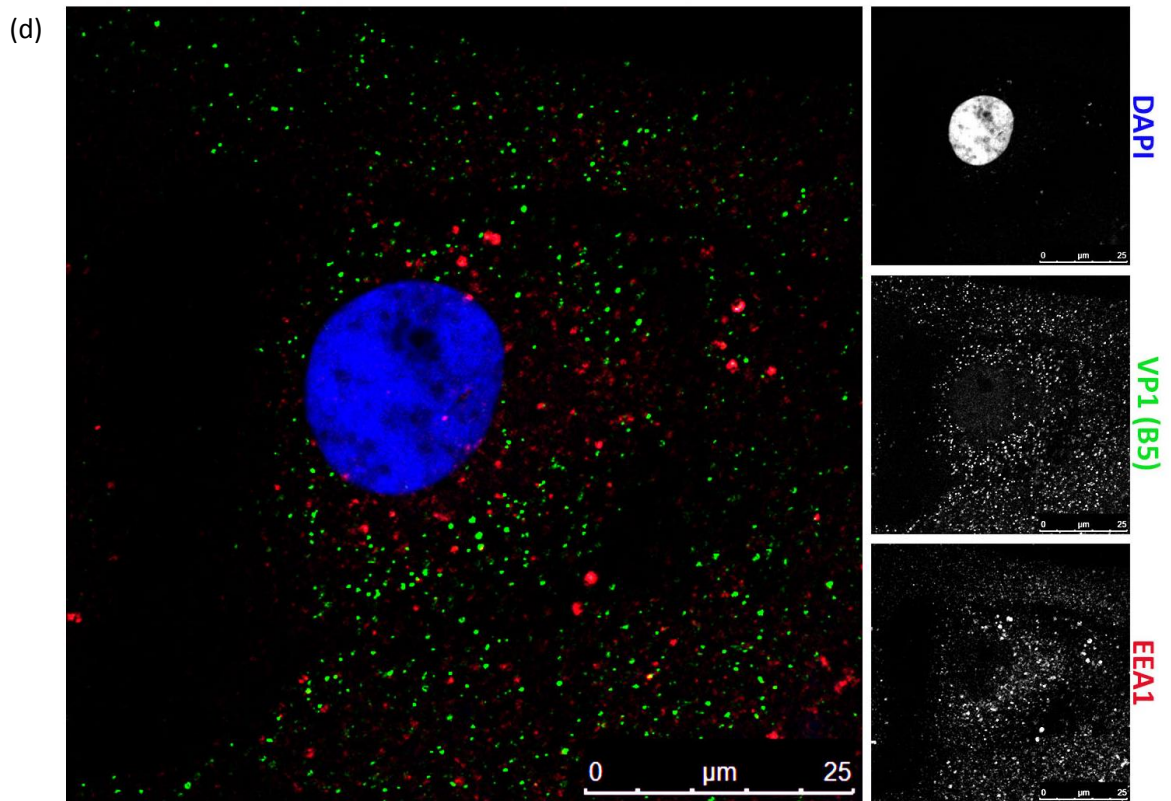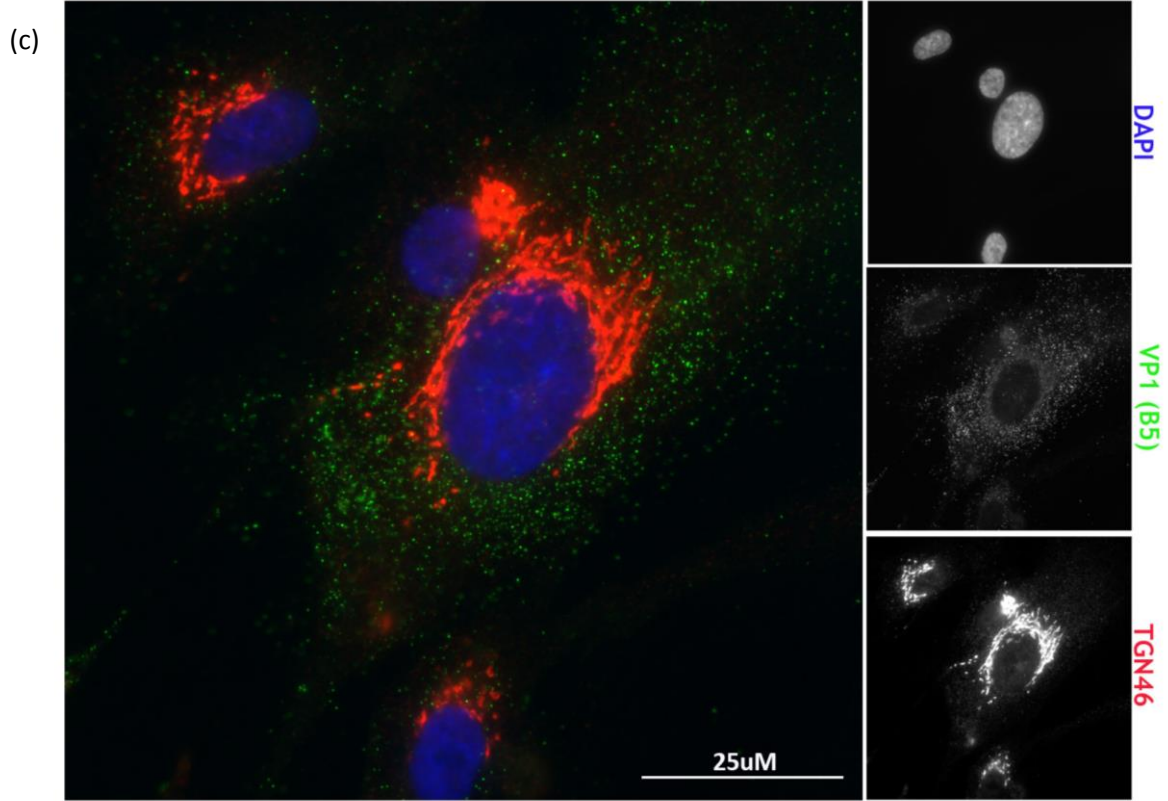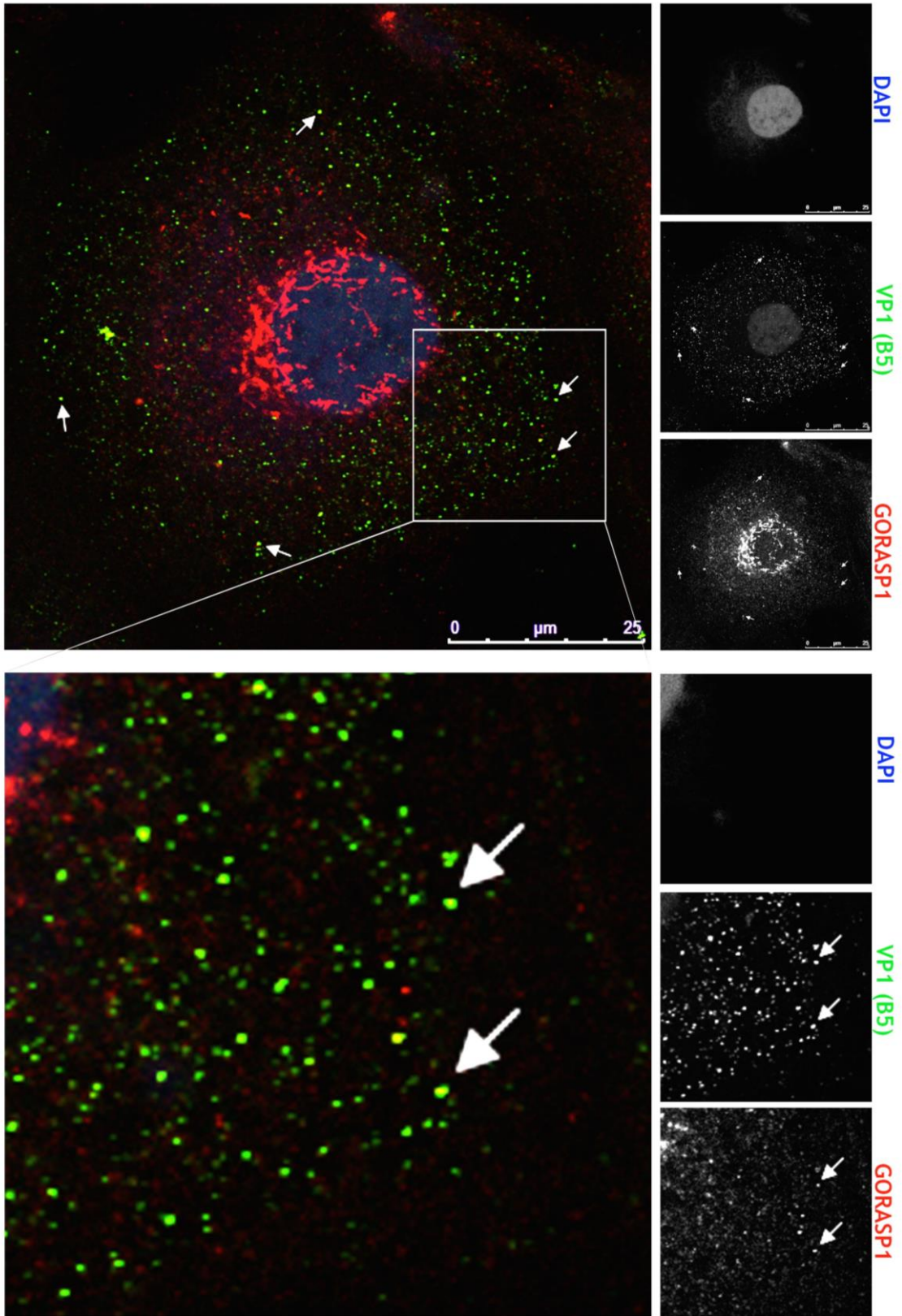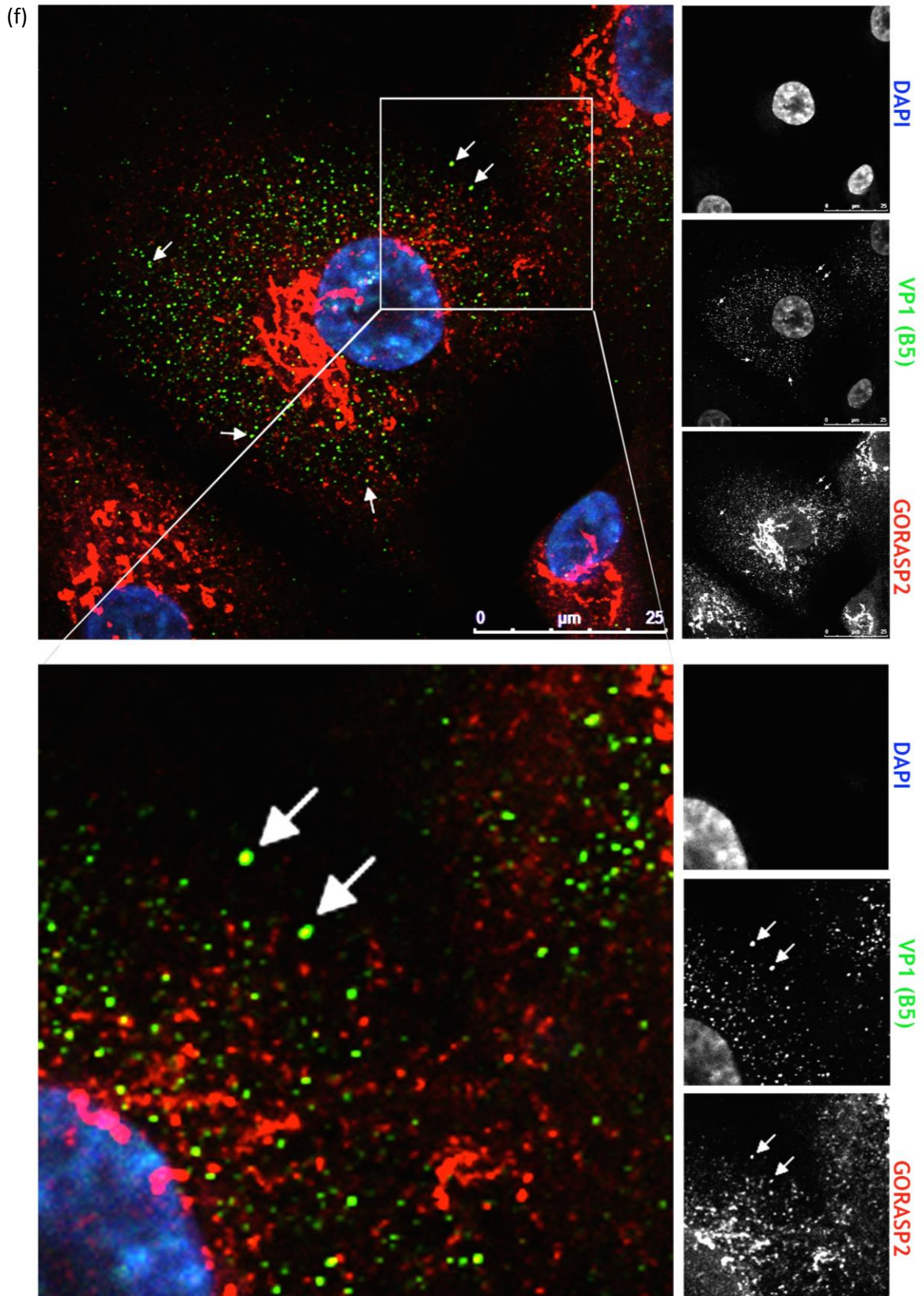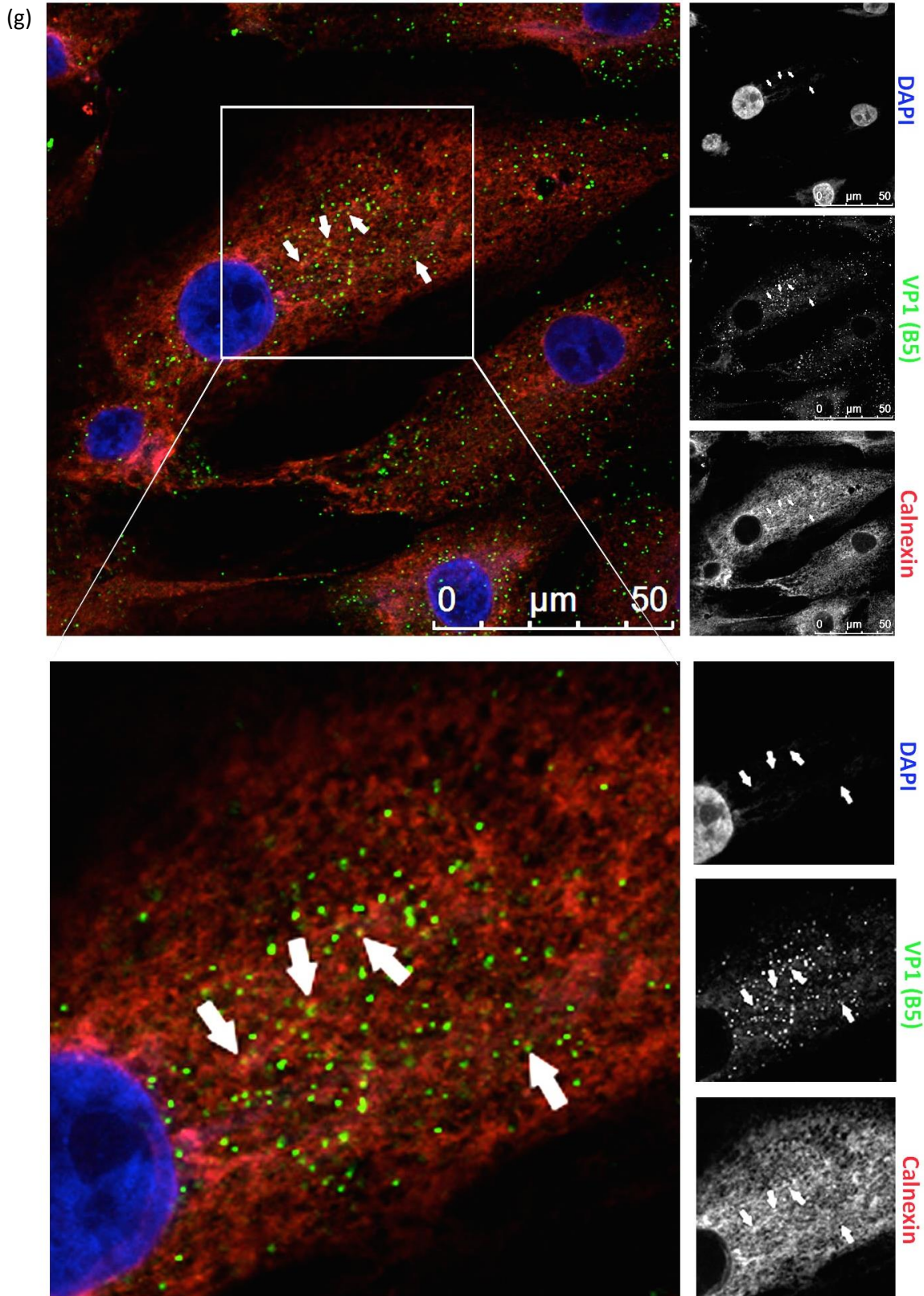
Figure 3.11: VP1 IgM conformational antibodies colocalise with GORASP1, GORASP2 and calnexin, but not EEA1, TGN46, GM130 or LysoTracker.

RPTE cells were infected with BKPyV (1 IU/cell) or mock infected and fixed for immunofluorescence at 48 hpi. Cells were immunostained with either LysoTracker (a), GM130 (b), TGN46 (c), EEA1 (d), GORASP1 (e), GORASP2 (f) or calnexin (g) (each shown in red), VP1 (B5) (green) and DAPI (blue). Colocalisation with VP1 (B5) seen with GORASP1 (f), GORASP2 (g) and calnexin is indicated with white arrows. Images a, b and c, were acquired on Olympus IX81 (x60 magnification). Images d, e, f and g were single z-slices acquired using confocal microscopy on Leica SP5 (x63 oil immersion magnification).

3.2.8 Optimisation of GORASP1 and GORASP2 siRNA knockdown

Further investigation into the role of GORASP1 and 2 during the egress of BKPyV was conducted by siRNA knock down of the expression of GORASPs 1 and 2. siRNA was chosen as the method of knockdown as primary RPTE cells are limited to approximately seven passages, which prohibits the possibility of creating CRISPR-Cas9 stable knockouts. GORASP1 and GORASP2 show >60% similarity and may be able to functionally compensate for one another (Bekier et al., 2017). Therefore, knockdown of both GORASP1 and 2 in combination may be necessary to understand their roles in the trafficking of BKPyV.

GORASP1 and 2 siRNA 4-plex pools were obtained from ThermoFisher. Each pool was reverse transfected into RPTE cells upon plating. Cells were fixed at 24, 48, 72 and 96 h after the first transfection and stained for GORASP1 or 2 and GM130 (Fig. 3.12a & b). The greatest level of depletion for either GORASP1 or GORASP2 was observed at 96 h, suggesting these proteins have relatively long half-lives and low levels of protein turnover in RPTE cells.

The activity of each individual siRNA construct for the 4-plex pools was then tested. The individual constructs of each pool were reverse transfected into RPTE cells when plating, followed by a further transfection at 52 h, cells were then fixed at 96 h and stained for either GORASP1 or GORASP2 (Fig. 3.12c & d). GORASP1 siRNA #2 and GORASP2 siRNA #3 yielded the greatest levels of depletion. These individual siRNAs were then used for all further knockdowns of GORASP1 or GORASP2.

(c)
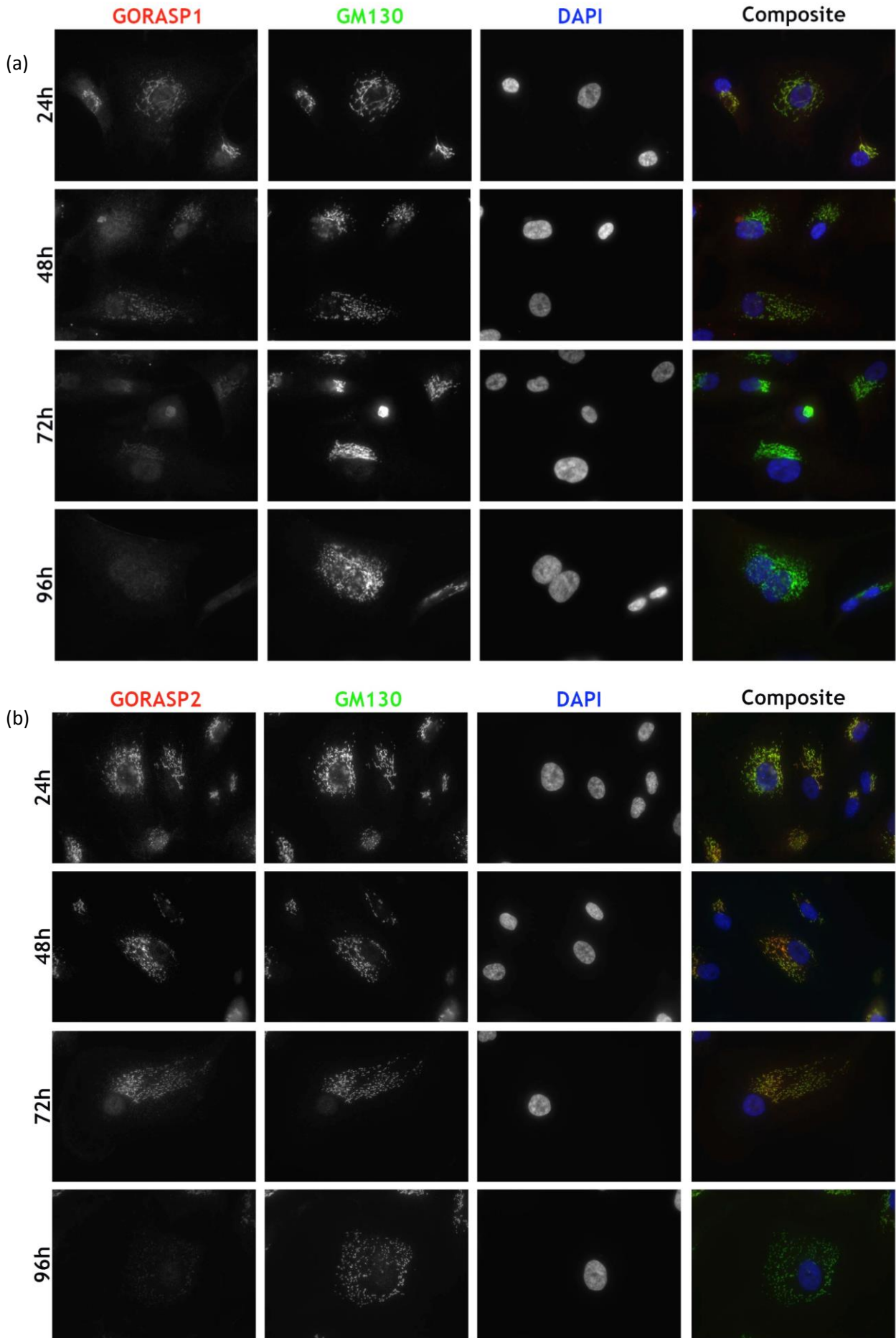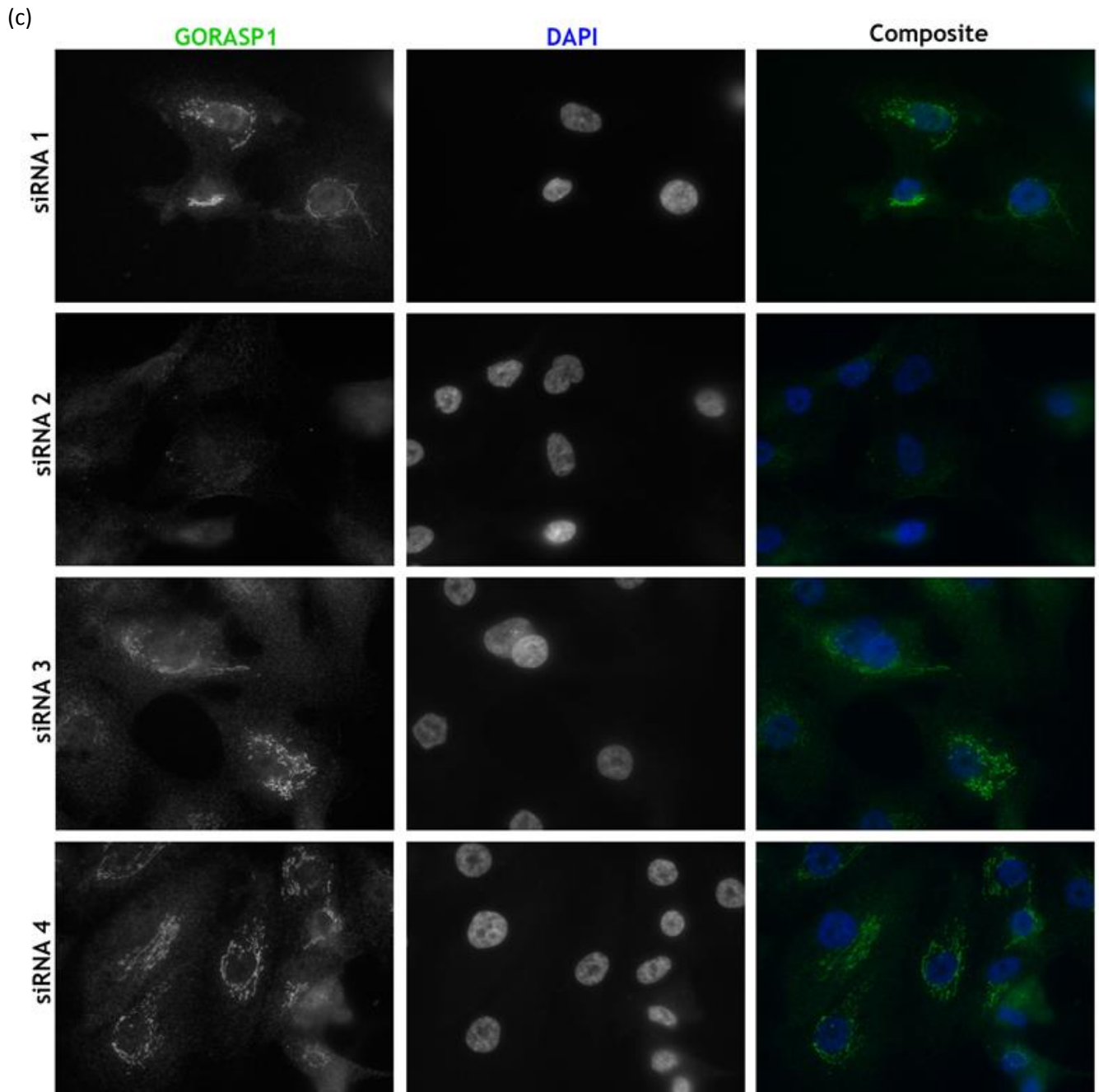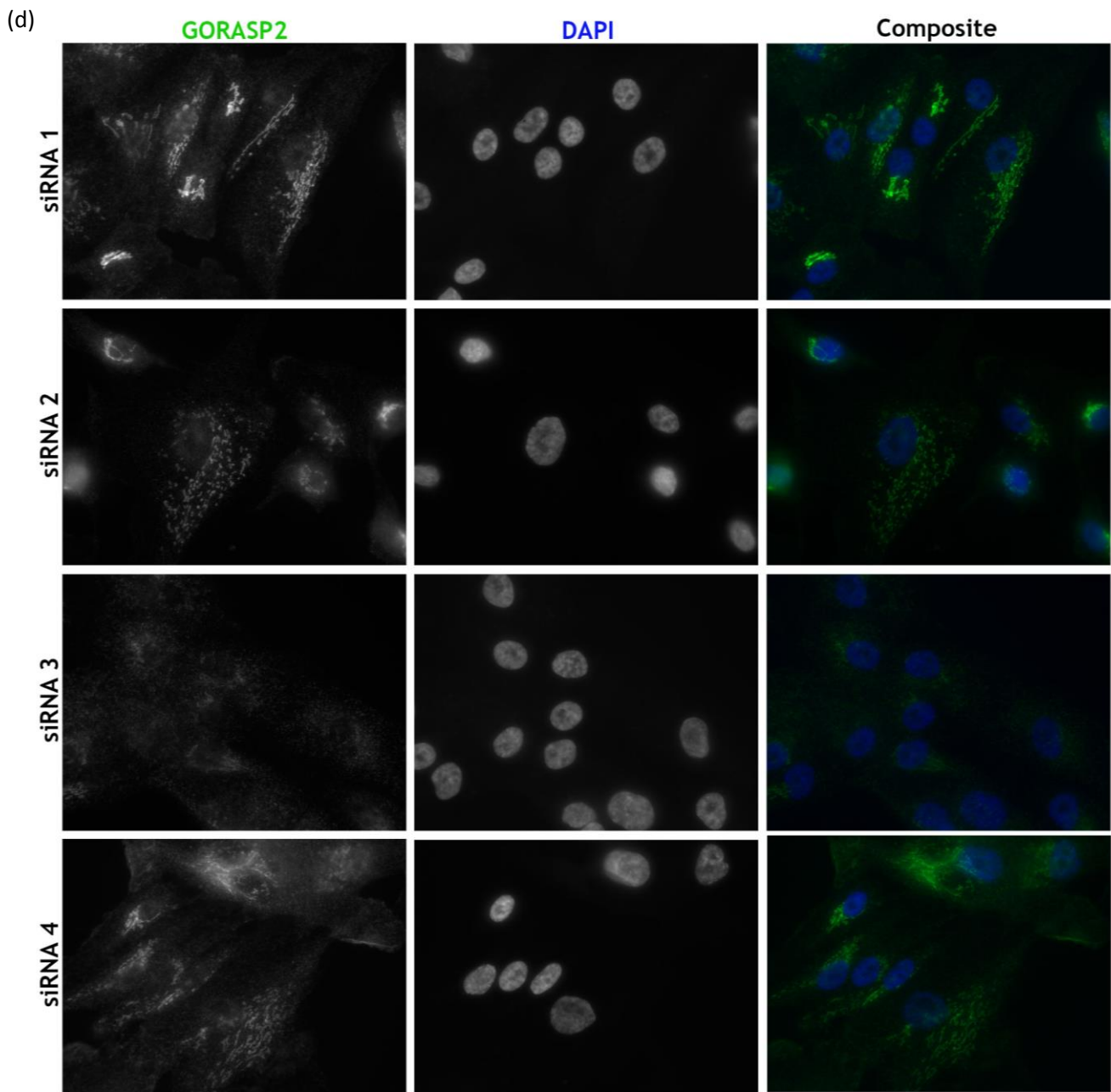
Figure 3.12: siRNA knockdown of GORASP1 and GORASP2 optimisation.
RPTE cells were reverse transfected with either siRNA pools (a & b) or individual constructs (c & d) when cells were plated. (a & b) Cells were fixed at 24, 48, 72 or 96 h and stained for GORASP1 (a) or GORASP2 (b) (red), GM130 (green) and DAPI (blue). (c & d) Cells were fixed at 96 h and stained for either GORASP1 (c) or GORASP2 (d) (green) and DAPI (blue). Construct 2 shows greatest depletion of GORASP1, while construct 3 shows greatest depletion of GORASP2. All images taken on Olympus IX81 immunofluorescence microscope.

3.2.9 Effects of siRNA knockdown of GORASP 1 and GORASP2 on BKPyV secretion

Knockdown of GORASP1 or GORASP2 individually, or combined knockdown of GORASP 1 and 2 from RPTE cells was then attempted using this protocol. Knocked down cells were also infected with BKPyV and the percentage of virus released into the supernatant after 48 h was determined by FFU.

RPTE cells were reverse transfected with GORASP1, GORASP2, GORASP1 and 2, or scrambled siRNA ConX as a control. 48 h after the first siRNA transfection cells were infected with BKPyV (1 IU/cell) for 1 h and then were washed with PBS and incubated in fresh media. At 6 hpi cells were transfected for a second time with the same siRNAs. At 48 hpi cells and supernatant were harvested separately and infectious titres determined for both by FFU assay and protein expression levels in cell samples determined by immunoblot. Knockdown was attempted in three separate experiments, with variable levels of depletion attained (Fig. 3.13c). Densitometry analysis of immunoblots, each normalised to tubulin control, were conducted. Knockdown of either GORASP1 or GORASP2 proved somewhat successful. When transfected alone GORASP2 siRNA caused GORASP2 protein depletion in all three experiments, showing a 61%, 55% and 36% reduction in experiments 1, 2 and 3 respectively. GORASP1 alone proved more difficult to deplete, showing a 13%, 49% and 24% reduction in experiments 1, 2 and 3 respectively. For both GORASP1 and GORASP2 knockdown, an increase in the expression levels of the other GORASP was observed. While this has not been previously noted during knockout experiments in mice *in vivo* (Veenendaal et al., 2014), it was observed for GORASP2 knockdown in the human cell line HEK293 and for GORASP1 knockdown in HeLa cells (Bekier et al., 2017). Combined knockdown of both GORASP1 and GORASP2 together was more inefficient. Whilst largely unsuccessful in experiments 1 and 2, appreciable levels of knockdown of both GORASP1 and 2 were obtained in experiment 3 (70% knockdown of GORASP1, 71% knockdown of GORASP2), however cells appeared unhealthy when examined by microscopy before harvest, as evidenced by reduced levels of tubulin (31% reduction in abundance compared to scrambled ConX siRNA control). Knockdown of both GORASP1 and GORASP2 has previously been shown to result in severe Golgi fragmentation (Bekier et al., 2017).

The effects GORASP1 and 2 depletions on the secretion of BKPyV at 48 hpi was determined by FFU assay (Fig. 3.13a). While these data must be treated with caution due to variable levels of knockdown by siRNA, a clear trend is evident. Scrambled control siRNA treated cells secreted 0.97% of total BKPyV into the supernatant, GORASP1 depletion alone reduced secretion to 0.54% of total BKPyV. GORASP2 depletion caused BKPyV secretion to be reduced to 0.72% of total BKPyV, although the low cell-associated titre in experiment 2 must be taken into account (Fig. S3). Interestingly, even though knockdown efficiencies were generally poorer in the combined GORASP1 and 2 siRNA transfected cells a greater reduction if the secretion of BKPyV was observed, to 0.37% (Fig. 3.13b).
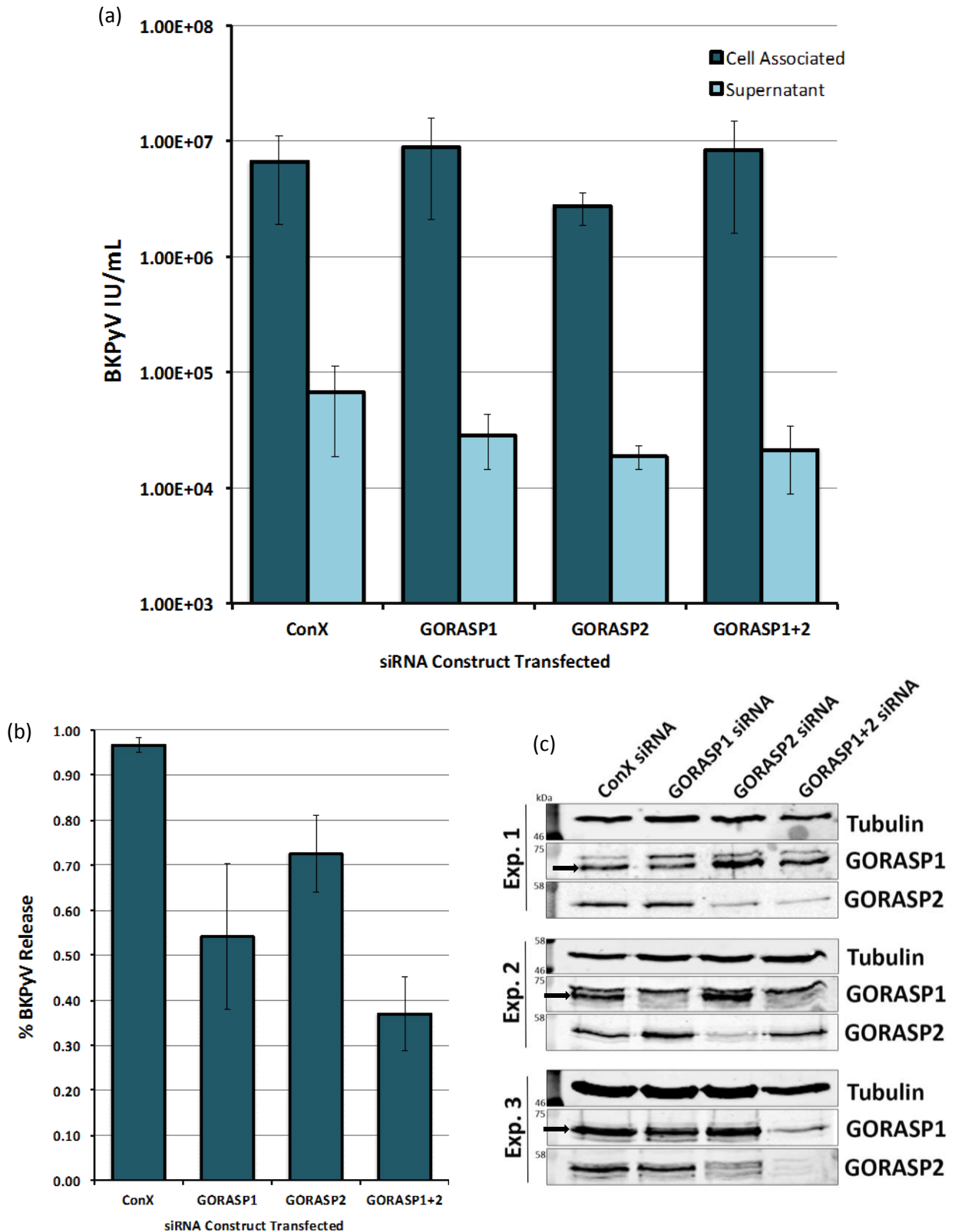
Figure 3.13: siRNA knockdown of GORASP1 and GORASP2 proteins suggests depletion may have an effect on BKPyV secretion.
RPTE cells were treated with double 100mM siRNA knockdowns of GORASP1, GORASP2, a combination of both GORASP1 and GORASP2, or ConX as a control. 48 h after siRNA treatment cells were infected with BKPyV (1 IU/cell). At 48 hpi cells and supernatant were harvested separately. Half of cell-associated samples were freeze/thawed three times to release virus and half kept for immunoblot, while supernatant virus was pelleted by ultracentrifugation and resuspended in 20x original volume. (a) Mean FFU titre of cell-associated and supernatant virus from three independent experiments. Error bars show standard error of mean. (b) Mean percentage level of secreted BKPyV taken from Fig. 3.12a; three independent experiments. Error bars show standard error of mean. (c) Immunoblot showing depletion levels of GORASP1 and GORASP2.

3.3 Discussion

TEM of infected RPTE cell nuclei allowed the morphology of BKPyV virions to be identified and described, which were then be used as reference when identifying virions in the cytoplasm of infected cells. While this proved useful it was not without limitations; identifying virions within ER-like convoluted membranes and single membraned vesicles relied exclusively on visual identification, and it is possible that individual virions could be mistaken for similar sized cellular structures, e.g. glycogen granules. Likewise, it is possible that virions in other cytoplasmic compartments could have been missed, particularly if they were sparse and individual particles. In order to limit errors of this nature the samples were extensively analysed by Dr M. Hollinshead, an extremely experienced electron microscopist, which provided confidence that we were indeed detecting BKPyV virions within these specific membrane compartments, although it is impossible to rule out rare examples of BKPyV particles in other compartments. The convoluted membranes in which virions were contained were confirmed to be ER through the retention of an ER retained HRP-KDEL marker. Furthermore, the accumulation of virions with the lumen of the ER and in single membrane vesicles near the cell periphery were observed even in the presence of neutralising antibodies, suggesting these particles are undergoing egress rather than entry. However, some caution must be given to the specific activity of neutralising antibodies. While the ability of the conformation-dependent VP1 (C1) antibody used in these studies to neutralise BKPyV infectivity has been well documented (Randhawa et al., 2009), it was not known whether the antibody completely blocks entry to cells. Some neutralising antibodies may inactivate virus not by preventing virion binding or endocytosis but may inhibit a post entry step such as ER-exit or genome uncoating. The data in this chapter suggests this antibody does reduce virus internalisation, providing more confidence that the virions detected in the ER and single membrane vesicles. It is worth noting that whilst BKPyV entry was reduced in the presence of neutralising VP1 (C1), it was not completely inhibited, so we cannot rule out a contribution of virion entry to the observed virus particles with cytoplasmic membrane compartments. However, in TEM experiments we conducted for a recent paper investigating the role of Agno demonstrated that in cells infected with an Agno deletion BKPyV virions are unable exit the nucleus and no virions were observed in the lumen of the ER or single membrane vesicles (Panou et al., 2018). These data demonstrate that the virus particles we detect in cytoplasmic ER compartments and vesicles are highly unlikely to be due to input virus from the initial infection of cells, although do not rule the possibility that they could be due to re-internalisation of newly synthesised virions that have been released from cells.

Active and non-lytic BKPyV secretion, which was perturbed by addition of DIDS, was not affected by the disruption of Golgi transport by monensin treatment, suggesting that an unconventional secretory pathway was responsible. Of those unconventional secretory pathways thus far described only

autophagy-derived membranes and exosome-related pathways have been shown to be used by other non-enveloped viruses as a means of virion secretion (Feng et al., 2013, Jackson et al., 2005). Both of these pathways would result in a double membrane structure around cytoplasmic virions and potentially host-derived membrane coating extracellular virions, neither of which were observed in extensive TEM analysis. The lack of observed viruses within double membraned vesicles along with data from this chapter showing that autophagy induction failed to increase secretion, while autophagy inhibition failed to reduce secretion, indicates that BKPyV does not secrete via such unconventional secretory pathways. The unconventional secretory pathway that best describes secretion which involves trafficking via the ER and single membraned vesicles, but not the Golgi, is the so-called 'Golgi-bypass' pathway. In times of ER stress Golgi-bypass enables vesicles to be pinched off from the ER and trafficking of membrane bound contents directly to the plasma membrane, upon which vesicle fusion occurs and contents are released into the extracellular space (Gee et al., 2011). Such Golgi-bypass transport vesicles have been described to contain GORASP proteins, which are usually responsible for holding Golgi ribbons together. Data in this chapter shows that while colocalisation of virions was not observed with any Golgi marker, clear colocalisation was seen between BKPyV particles and both GORASP1 and GORASP2. While only relatively few cytoplasmic VP1-positive puncta colocalised with GORASPs, this can be explained by only transient recruitment of GORASPs to virion-containing transport vesicles, or if many of the observed 'cytoplasmic' virus particles had actually already been released but were still attached to the extracellular surface of the cell. GORASPs have not been described to be involved in any internalisation of endocytic pathway, lending further weight to the argument that these BKPyV particles are undergoing egress rather than entry.

Attempts to define a functional role for GORASPs in BKPyV release were somewhat inconclusive, primarily because knockdown of GORASP1 and GORASP2 by siRNA proved difficult. While optimisation of individual siRNA constructs and protocol appeared successful, it was challenging to get knockdown results which could be replicated, particularly when attempting combined knockdown of both GORASP1 and 2. Indeed, in single knockdowns the alternative GORASP showed a slight increase in expression, possibly compensating for siRNA knockdown. It is also possible that depletion of both GORASPs simultaneously in deleterious to cells, published studies have shown that in cells where both GORASP1 and 2 have been deleted using CRISPR/Cas9 techniques Golgi stacking was impaired, the Golgi was fragmented and while protein secretion is increased, those secreted proteins were more likely to be incorrectly glycosylated (Bekier et al., 2017).

Even with these experimental limitations a trend was observed where GORASP knockdown resulted in a moderate reduction of BKPyV secretion, more so for the double knockdown and single GORASP1 knockdown than GORASP2 knockdown. To further investigate the role of GORASPs in BKPyV secretion,

gene knockout using CRISPR/Cas9 for one GORASP followed by transient siRNA depletion of the other, or gene knockout of both GORASP1 and 2 may be required.

4. Quantitative proteomics analysis of BKPyV infection

4.1 Introduction

Polyomaviruses such as BKPyV have small genomes with relatively little coding potential and express only a handful of proteins. As such these viruses are very reliant on host cell activities for their replication. In order to study virus-induced alteration of secretory pathways, which could facilitate non-lytic egress, in addition the more global effects on other cellular pathway modulations during BKPyV infection, a whole cell proteomic analysis approach was implemented.

While a number of studies have been conducted to investigate how BKPyV infection modulates the host cell environment during replicative infection, these have been primarily at the transcriptome level. Microarray studies of BKPyV infected primary RPTE and Human Umbilical Vein Endothelial (HUV-EC) cells demonstrated significant abundance increases of cell division, apoptotic, DNA damage/repair and DNA replication pathway associated RNA levels at 40 and 72 hours post infection (hpi) (Abend et al., 2010, Grinde et al., 2007). In HUV-EC cells signal transduction pathway RNA levels were down regulated from as early as 20 hpi. In RPTE cells the innate immunity-related transcripts PTX3 and MICB were up regulated at 72 hpi although few other immune response-related genes were induced in either cell type. While these studies have proved useful in understanding the effects of BKPyV infection on cellular mRNA levels, they do not provide information regarding virus-induced changes to cellular protein levels, as changes in mRNA levels do not necessarily correlate with protein abundance.

Similarly, an RNAseq study that included analysis of the effects of BKPyV infection on RPTE cells from 3 to 9 days post infection (dpi) has shown that infection can induce IFN-β production by RPTE cells by 3 dpi, but just four ISGs were found to be up regulated at 6 dpi (IFI6, IRF7, OAS3 and HERC5), and by 9 dpi just one ISG was up regulated at the transcript level (HERC5), suggesting BKPyV may actively block induction of ISG transcription. Similar to microarray studies, RNAseq only provides transcriptomic data and in this study failed to detect any changes to the host transcriptome during the first round of BKPyV infection and replication, which takes place before 3 dpi, likely because the experimental setup of this study used a low multiplicity of infection (Assetta et al., 2016).

To date there has only been one broad-scale analysis of the host cell proteome in BKPyV infection, where stable isotope labelling with amino acids in cell culture (SILAC) methods were used to determine protein abundance changes in nuclei isolated from primary RPTE cells at 3 days post infection. This study identified and quantified >2000 host proteins, of which 50 were shown to increase and 13 decrease in abundance to a significant level, including proteins involved in DNA damage response and apoptosis as well increased abundance of proteins which had not previously

been identified by RNA based analyses, such as p53. However, this study was restricted to a single time point of the viral replication cycle due to the limitations of using SILAC-techniques with passage-limited primary cells, and provided little information regarding host proteins not present in the nucleus. Indeed, in this study it is unclear whether the identified changes in protein abundance may truly reflect changes in the total amount of protein with the entire cell or is more due to effects on the nuclear import/export of proteins.

To gain a greater insight into host cell modification during BKPyV infect, a whole cell quantitative temporal viromic study of BKPyV infection comparing two independent BKPyV-permissive primary human cell types, RPTE and human urothelial (HU) cells, was conducted. This technique allows post-experimental tagging of up to 11 independent samples with isobaric labels (Tandem-Mass-Tagging, TMT) followed by MS^3 mass spectrometry, enabling the relative abundance of host proteins to be quantified throughout the time course of an infection in a highly multiplexed fashion (Weekes et al., 2014). The development of such high throughput techniques have enabled the extensive characterisation of whole cell proteomes, or indeed localised proteomes, and provided the opportunity to directly compare infected and mock infected cells at multiple time points, and/or multiple virus strains, in parallel. Analysing quantitative changes in host cell protein expression in infected cells facilitates the identification of those proteins which may be important for the viral lifecycle.

Once host proteins abundance changes during viral infection have been identified, these data can then be analysed using bioinformatic tools. In this way it has been possible to identify entire pathways or metabolic processes affected by viral infection to the point of being significant. Indeed, when used to study HCMV infection, TMT-based proteomics revealed the detailed temporal expression of cell surface signalling pathway proteins used to subvert cellular immune responses, and furthermore identified potential therapeutic targets for this virus (Weekes et al., 2014). These findings highlight the potential benefits of using TMT-based proteomics to elucidate the effects a BKPyV infection on the host cell proteome over the time course of an infection.

4.2 Results

4.2.1 Growth curves of two permissive cell types advises experimental design

Two human primary BKPyV-permissive cell types, RPTE and HU cells, were both chosen to be analysed by whole cell proteomic analysis. HU cells are one of the very few other cell types available that support BKPyV infection and are representative of a natural site of infection (Li et al., 2013a). Analysis of two independent cell types allows comparisons to be drawn between them, enabling identification of host pathways particularly important for the virus, and not simply cell type specific responses to infection. In order to determine the most appropriate time points of infection at which to perform proteomic analysis BKPyV growth curves were first conducted. RPTE and HU cells grow at different rates and may support replication of BKPyV to different levels, thus it was important to identify time points which were suitable for analysis in both lines. RPTE cells are known to support a full round of BKPyV replication by approximately 72 hpi, while HU cells are less well described. RPTE and HU cells were infected with BKPyV (3 IU/cell) and cells were harvested directly into media to collect total infectious virus every 12 hours from 12 hpi to 96 hpi. Once harvested the virus was released from cells by several freeze/thaw cycles, after which the virus titre of each sample was determined by FFU assay (Fig. 4.1a). BKPyV replicated efficiently in RPTE cells and infectious titres continued to increase until 84 hpi up to a maximum of 1.2×10^7 IU/mL, after which time virus levels began to plateau. HU cells supported BKPyV replication to a reduced extent to a maximum of 1.5×10^5 IU/mL by 48 hpi, after which infectious titres did not increase further. As such, the three time points chosen for infected cell analysis were 24 hpi, an early point of infection where early viral protein expression alone is expected to occur; 48 hpi, a middle point of infection for RPTE cells and a time at which HU cells should still be replicating virus; and 72 hpi, a late point in infection for RPTE cells, and a time at which BKPyV replication in HU cells has plateaued.

At the time of this experiment TMT-based proteomics were limited to a maximum of 10 isobaric tags, therefore whilst three infected time points were chosen for each cell type, just two mock-infected time points could be included for each cell type (Fig. 4.1b). The mock infected time points, against which the infected samples could be compared for levels of fold change, were chosen as 24 and 72 hpi. For data analysis these can be averaged allowing each infected time point to be compared against the average of the two mock time points for their cell type.

These TMT-based proteomics studies were conducted in collaboration with Dr Michael Weekes' laboratory. All infections, experimental conditions and harvesting were conducted in house, while tagging and mass-spectrometry analysis was conducted by members of the Weekes lab (credited where applicable).
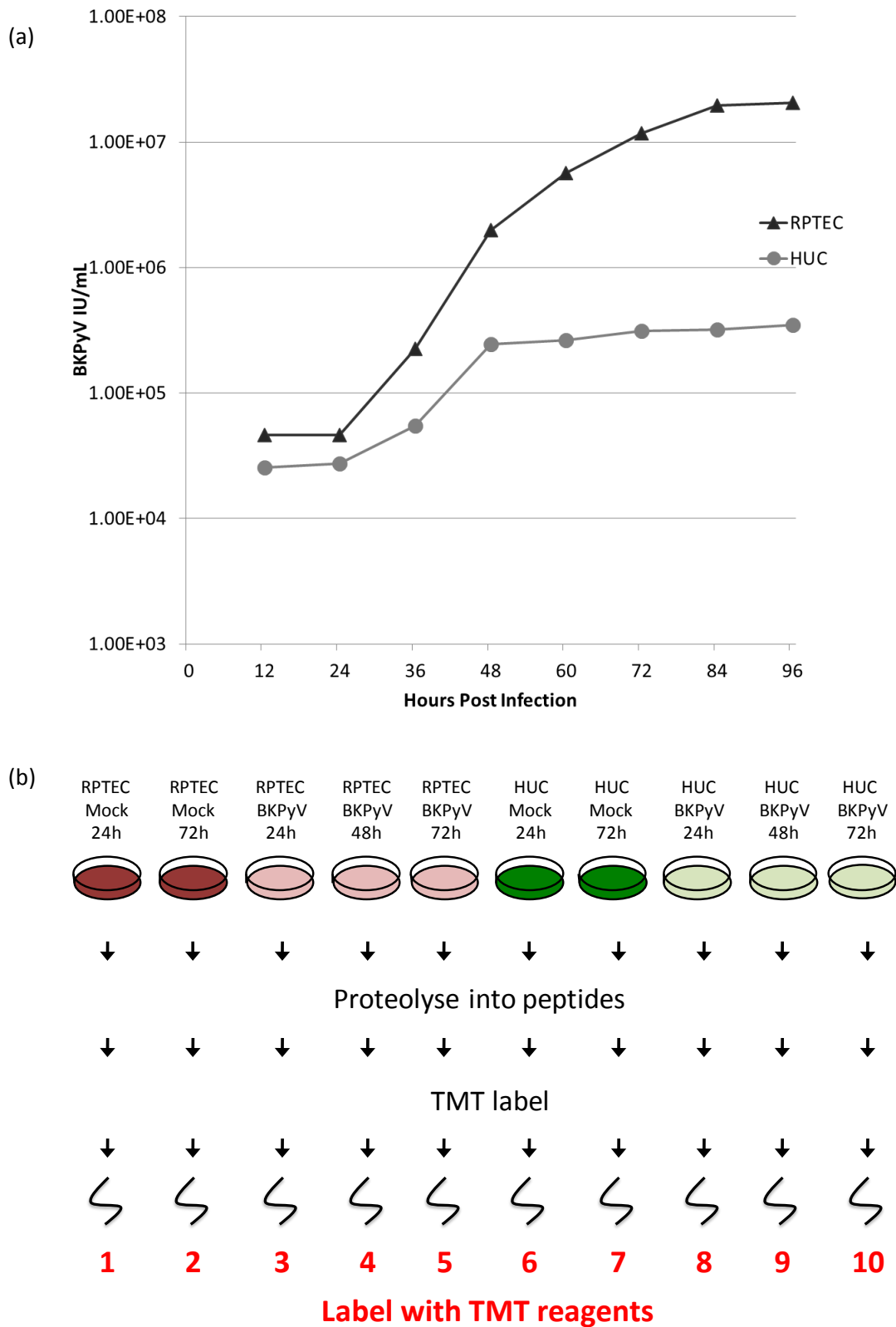
Figure 4.1: TMT experimental design.
(a) RPTE and HU cells were infected with BKPyV (3 IU/cell) and cell-associated and supernatant virus was harvested together every 12 h until 96 hpi. Infectious virus was released from cells by three rounds of freeze/thawing, then titred by FFU assay, producing a single-step growth curve for both cell types. (b) Three time points were the chosen to cover early (24 hpi), middle (48 hpi) and late (72 hpi) stages of infection, allowing an experimental workflow design to be produced.

4.2.2 Low numbers of cellular proteins were significantly changed in abundance throughout BKPyV infection.

RPTE and HU cells were infected with BKPyV and 10-plex TMT used to identify whole cell protein changes by LC-MS[3]. Cells were infected with BKPyV (5 IU/cell) or mock infected. BKPyV infected cells were harvested at 24, 48 and 72 hpi and mock infections were harvested at 24 and 72 hpi. When harvesting, cells were washed thoroughly with ice-cold proteomic grade PBS and 75 µl of TMT lysis buffer added, into which cells were scraped. Samples were transferred to an Eppendorf tube and then vortexed extensively. After 10 minutes at room temperature samples were sonicated and centrifuged to pellet DNA. Supernatants were transferred to a fresh tube, the centrifuge step was repeated and supernatants were then snap frozen in liquid nitrogen and passed to Dr Weekes' lab for processing. Digestion of samples in LysC protease in 200 mM HEPES (pH 8.5) and 1.5 M guanidine was conducted after cysteines were alkylated, a further digestion by trypsin in 200 mM HEPES (pH 8.5) and 0.5 M guanidine. After reactions were quenched digested peptides were subjected to solid phase extraction and vacuum-centrifuged. Samples were then labelled with TMT reagents and subjected to fractionation, vacuum centrifuge dried and resuspended in mass spectrometry solvent, ready for processing on the Orbitrap Lumos mass spectrometer. Parallel infections conducted at the same time as the initial infection in order to confirm cells were adequately infected. For this RPTE and HU cells were set up at the same confluency as TMT samples, infected with the same inoculum and fixed for immunofluorescence at 48 hpi. Cells were stained for TAg as a marker of infection and DAPI was used as a cellular marker. By calculating the number of cells expressing TAg it was confirmed 91.15% of RPTE cells and 91.3% of HU cells were infected.

In total 8992 cellular proteins and 6 viral proteins were identified, including a novel peptide from a previously undescribed variant of the TAg open reading frame (Table S2). Each protein detected was identified by at least a single unique peptide and the $\log_2$ fold change of individual proteins from each time point were established as a ratio of the averaged mocks for that cell type. The signal:noise ratio was determined (Du et al., 2008), in addition the p value was estimated using significance B (Cox and Mann, 2008). This allowed scatterplots to be compiled for either cell type at each time point, showing every protein identified either up regulated (to the right of scatterplots), or down regulated (to the left of scatter plots) (Fig. 4.2 and 4.3), with those proteins defined as highly significant ($p < 0.0005$) shown in red.

These scatterplots highlighted that very few cellular proteins are significantly changed in abundance in response to BKPyV infection. In RPTE cells at 24 hpi just 17 proteins are most significantly changed ($p < 0.0005$), 0.08% of all cellular proteins identified, at 48 hpi this number increases to 106 proteins although this remains just 1.2% of all proteins. At 72 hpi this number reduces to 85 proteins

significantly changed in abundance (0.9% of all cellular proteins). In HU cells similarly low numbers of proteins are most significantly modulated ($p < 0.0005$) in their expression. At 24 hpi 29 proteins are significantly changed in abundance (0.3% of total), and at 48 and 72 hpi this number remains low at 90 and 56 respectively (1% and 0.6% of total) (Tables S3-8). It was interesting to note that, in both RPTE and HU cells, at 72 hpi fewer proteins were most significantly changed in abundance than at 48 hpi. This might be attributable to the switch from early gene expression to late gene expression which occurs from 36-48h. The early proteins TAg and tAg are both multifunctional proteins which have large effects on cellular processes and cell cycle progression (Table 1.2), after early gene synthesis TAg is employed as a viral helicase and no further TAg is transcribed as late genes are then transcribed and translated. Such a switch might alter the effects of those early proteins on cellular processes, by 72 hpi seeing cell cycle processes less affected. However further investigation into this hypothesis would be necessary.

Also interesting to note were the numbers of most significantly down regulated proteins ($p < 0.0005$), which showed more changes in HU cells than RPTE cells at both 24 and 48 hpi. Whilst still a very small percentage to the total proteins identified, this suggests that there may be differences in how these two cell type respond to early infection, and may require further investigation.

Expression of BKPyV early viral proteins, TAg and tAg, were observed in both cell type from 24 hpi, along with a potential novel TAg variant predicted to expressed an alternatively spliced early gene transcript (NOVEL_ORF), based on the detection of a single unique peptide that was predicted from a 6 frame-translation of the entire BKPyV genome sequence. TruncTAg could not be identified due to its sequence being identical to the N-terminus of TAg, and the alternative C-terminus of TruncTAg would only result in the presence of only one very short (3 amino acid) peptide that is different to TAg being released after trypsin cleavage. VP1, VP2 and Agno were observed in both cell types from 48 hpi. VP3 was not be identified due to its 100% homology with the C terminus of VP2, and the peptide corresponding to the extreme N-terminus that would be unique to VP3 was not quantified.

Further analysis of proteins which were identified as significantly altered in abundance was undertaken, in order to identify specific host pathways that are modulated in response to BKPyV infection.
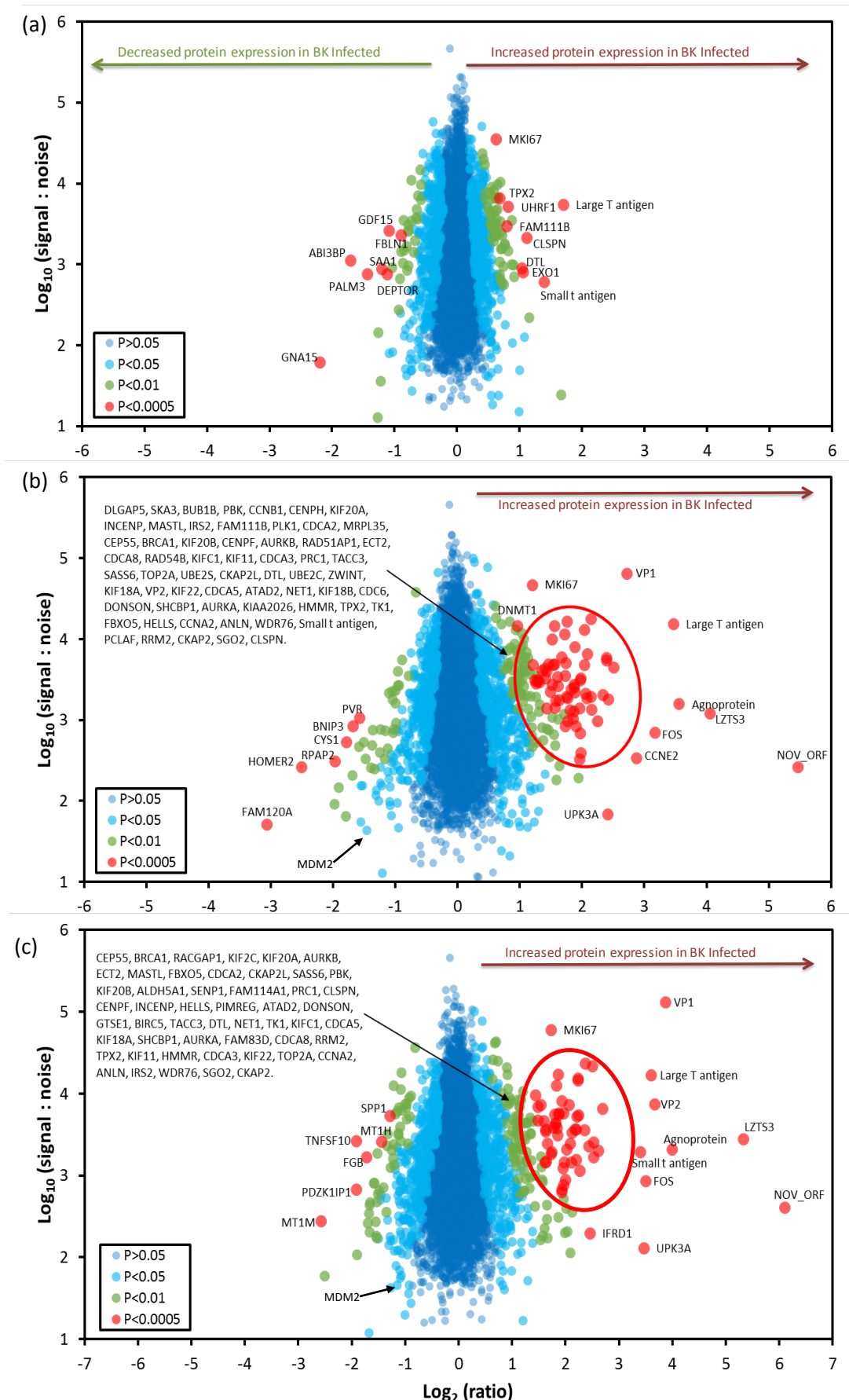
Figure 4.2: RPTE cell scatter plots of protein abundance change.

The abundance of proteins identified at each BKPyV-infected time point, 24 hpi (a), 48 hpi (b) and 72 hpi (c), was divided by the average of the mock-infected samples (24 and 72 hpi). Scatter plots show all proteins identified with unique peptides. Fold change (RPTE cell BKPyV-infected/RPTE cell mock-infected average) is shown as the $\log_2$ ratio on the x-axis, to the right increasing in abundance, and to the left decreasing in abundance. The signal:noise is shown on the y-axis as $\log_{10}$. Significance B was used to estimate p values (Cox and Mann, 2008). All scatter plots kindly produced by Dr C Davies.

Figure 4.3: HU cell scatter plots of protein abundance change.
The abundance of proteins identified at each BKPyV-infected time point, 24 hpi (a), 48 hpi (b) and 72 hpi (c), was divided by the average of the mock-infected samples (24 and 72 hpi). Scatter plots show all proteins identified with unique peptides. Fold change (HU cell BKPyV-infected/HU cell mock-infected average) is shown as the $\log_2$ ratio on the x-axis, to the right increasing in abundance, and to the left decreasing in abundance. The signal:noise is shown on the y-axis as $\log_{10}$. Significance B was used to estimate p values (Cox and Mann, 2008). All scatter plots kindly produced by Dr C Davies.

4.2.3 Cluster analysis of proteins significantly altered in abundance throughout infection

Those cellular proteins that were significantly altered in abundance ($p < 0.0005$) in each cell type and at each time point were assessed for correlation between cell types by venn diagram (Fig. 4.4). There was no overlap between cell types for down regulated proteins at any time point (Fig. 4.4a). When RPTE and HU cells down regulated proteins from any time point were analysed by the Search Tool for the Retrieval of Interacting Genes/Proteins (STRING) cluster analysis, an online bioinformatic tool which uses previously identified or predicted protein-protein interactions to link proteins, no clustering was found (Fig. S4). Further analysis using the functional Database for Annotation, Visualisation and Intergrated Discovery (DAVID) to predict enrichment of particular biological themes which link proteins and provides enrichment scores and p values that allow conclusions to be drawn on potential false discovery rates, shows no pathway enrichment for these down regulated groups of proteins (Fig. S5). For the purpose of this study a stringent cut off of $p < 0.0005$ was implemented, to further analyse these down regulated proteins it may be possible to amend this cut off to $p < 0.005$ and reanalyse, although there would be a concern that the possibility of identifying false positive hits in pathway analysis is then increased. It is not suggested that all the identified significantly down regulated proteins ($p < 0.0005$) are experimental noise, but some care must be taken when drawing conclusions of pathway analysis on such small protein numbers.

Significantly up regulated proteins showed somewhat more overlap between cell types (Fig. 4.4b). At 24 hpi 3 proteins were significantly up regulated in both RPTE and HU cells, while at 48 hpi 35 proteins were significantly up regulated in both RPTE and HU cells, and at 72 hpi 22 proteins were up regulated in both cell types (Table S9-11). The groups of proteins up regulated in both cell types were also analysed by STRING and DAVID bioinformatic tools (Fig. 4.5).

At 24 hpi two of the three proteins up regulated in both RPTE and HU cells are STRING linked (Fig. 4.5a), and the DAVID enrichment scores of the same three proteins suggest they are involved in acetylation and DNA damage responses and these pathways are up regulated at this time point. While these enriched pathways have p values of relatively low significance for DAVID analysis (>0.0005), these pathways have been shown to be up regulated in BKPyV infection in previous BKPyV studies (Verhalen et al., 2015, Justice et al., 2015). At 48 hpi the 35 proteins up regulated in both RPTE and HU cells are all linked in one large STRING cluster, with the exception of just 3 proteins (Fig. 4.5c). Furthermore, DAVID analysis of these same 35 proteins shows the top eight enriched processes are related to cell division (cell cycle, cell division, mitosis, cytoskeleton, microtubule) or protein modification (phosphoprotein, ubiquitin conjugation). Surprisingly we do not see enrichment of any intracellular trafficking or secretory pathways, which were expected to be altered due to non-lytic

unconventional secretion of virions, nor was any modulation of innate immune responses identified (Fig 4.5d).

Similar to 48 hpi, the analysis of the 22 proteins significantly up regulated in both cell types at 72 hpi shows STRING analysis is one large cluster, the same top eight enriched processes are identified by DAVID as was seen in 48 hpi (Fig. 4.5f). The three proteins which failed to cluster in up regulated 48 and 72 hpi conditions appear to have roles in either cell cycle regulation or DNA damage response, but have yet to be annotated in STRING due to limited understanding of their pathways or roles. WDR76, WD repeat-containing 76, is a DNA binding protein which rapidly responds to DNA damage signals (Gilmore et al., 2016). FAM111B, Homo sapiens family with sequence similarity 111 member B, is a cancer associated nucleoprotein whose mutation can lead to increased prostate cancer rates (Akamatsu et al., 2012), while PROSAPIP1, proSAP interacting protein 1 (identified in our screen by its alternative name LZTS3), is a tumour suppressor suggested to play a role in the regulation of non-small cell lung cancer cell proliferation and metastasis (He et al., 2018). This evidence suggests that these three STRING 'non-clustering' proteins may indeed be associated with the cell cycle pathways identified by DAVID once more evidence comes to light. Further scrutiny by STRING and DAVID pathway analysis of the most significantly ($p < 0.0005$) up and down regulated proteins at each time point for each cell type separately, rather than simply those which overlap between both cell types, revealed no clustering or pathways which were not previously identified in this described analysis (Fig. S4 & S5).

To observe no up regulation of specific secretory pathways was disappointing yet not entirely surprising as activity of secretory pathways may be altered by more subtle means, such as changes in protein phosphorylation or subcellular localisation, which would not be picked up by this screen. While we identified a large number of trafficking associated proteins including 45 Rabs, multiple Rab interacting proteins such as Rab GAPs and GEFs, and 12 vesicle trafficking Sec proteins, none were changed significantly in abundance (Table S11). GORASP2 was detected with 12 unique peptides, however it was not altered in abundance throughout the course of infection, suggesting it is not actively up regulated. GORASP1 was not detected in this experiment.

Figure 4.4: Correlation of significantly down regulated proteins between cells lines is low, while there is greater correlation between up regulated proteins of both cell types.
Those proteins identified as significantly changed in abundance at either 24, 48 or 72 hpi ($p < 0.0005$ taken from Fig. 4.3 scatterplots) for either RPTE or HU cells were analysed for overlap between the two cell types. Down regulated in abundance at any time point (a), or up regulated in abundance at each time point (b).

(a)

(b)

	Fold Enrichment
DNA damage	39.0
Acetylation	6.0

1.00E+00   1.00E-05

(c)

(d)

	Fold Enrichment
Cell cycle	18.7
Mitosis	35.7
Cell division	26.5
Cytoskeleton	9.9
Cytoplasm	3.7
Phosphoprotein	2.4
Ubl conjugation	6.0
Microtubule	20.0

1.00E+00   1.00E-05   1.00E-10   1.00E-15   1.00E-20

Log_{10} (P-value)

(e)

(f)
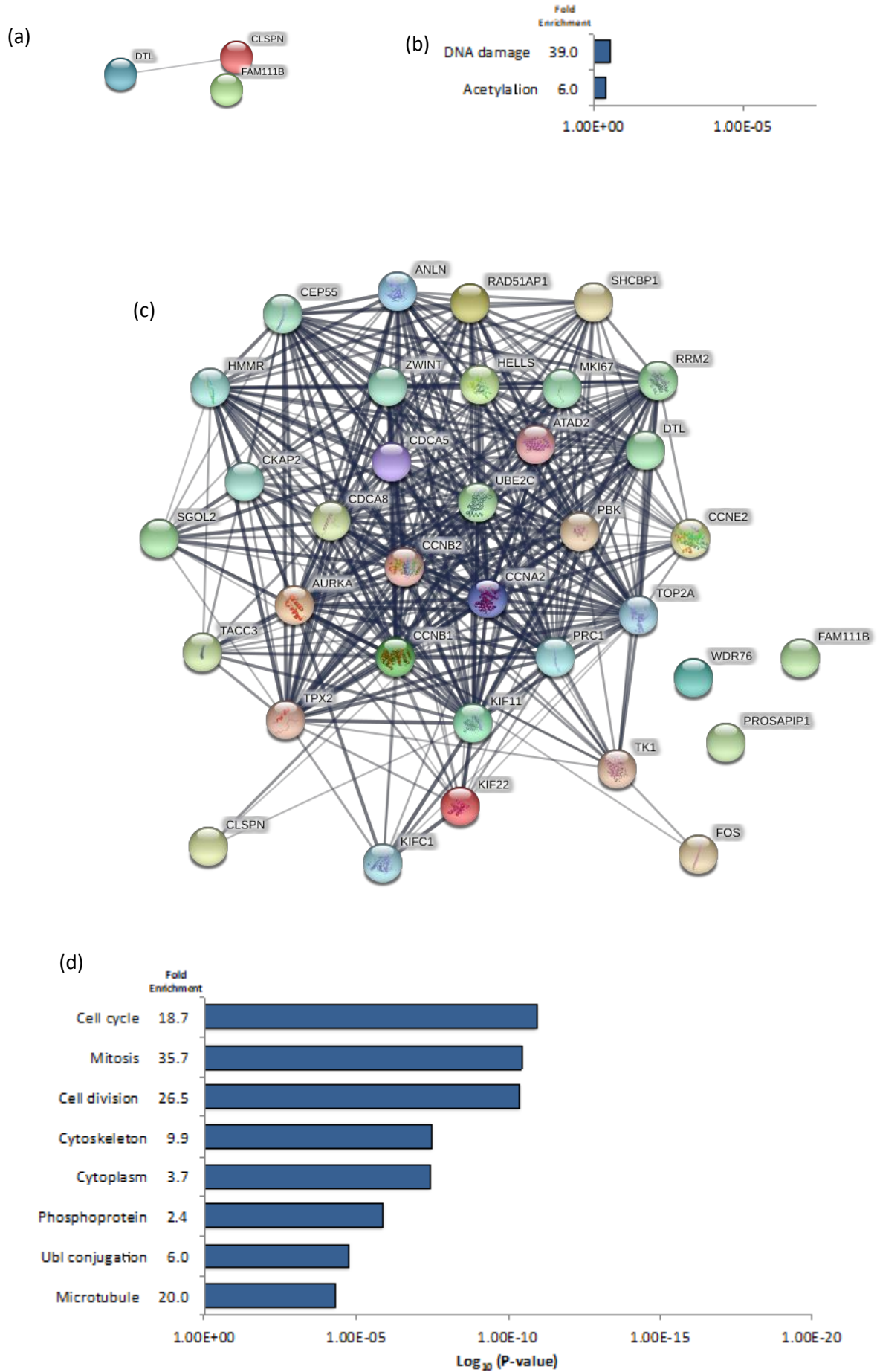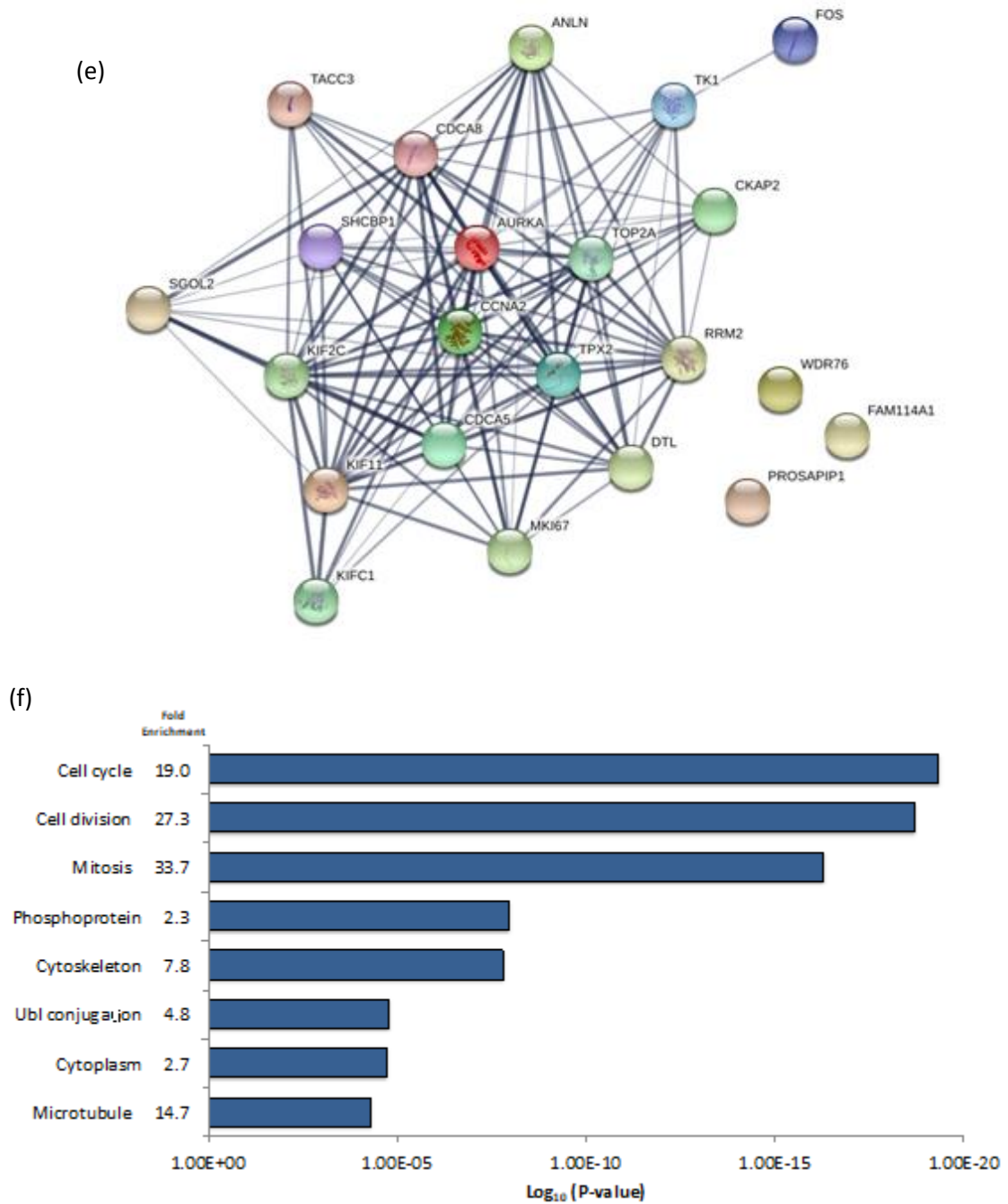
Figure 4.5: Cluster analysis of proteins significantly up regulated in both HU and RPTE cells.
Those proteins that were observed to be increased in abundance in both HU and RPTE cells at each time point (as shown in Fig. 4.4) were analysed using Search Tool for the Retrieval of Interacting Genes/Proteins (STRING) (a, c, & d) and the functional Database for Annotation, Visualisation and Integrate Discovery (DAVID) bioinformatic software (b, e, & f). STRING analysis shows each protein represented as a spot, with connections made between proteins representing known and predicted protein-protein interactions, the heavier the connecting line, the more confidence in the interaction based on experimental, co-expression, co-occurrence, gene fusion, textmining or neighbourhood evidence. DAVID analysis identifies functional pathways within groups of proteins, showing the fold enrichment of each pathway detected along with the significance of that pathway (compared to the background of the list of proteins submitted). The most significant eight pathways shown only for convenience.

4.2.4 Temporal profiles of BKPyV proteins throughout the course of infection

BKPyV proteins are known to be expressed in a clearly described order. Early genes are expressed 18-24 hpi, while late genes are expressed 36-48 hpi. The temporal expression of each protein found in the proteome can be plotted, showing time on the x-axis, while the fold change is shown on the y-axis, as can be seen with the viral proteins plotted (Fig. 4.6).

When plotting the temporal expression profiles of each detected viral protein a greater than two-fold increase in expression of TAg and tAg was observed by 24 hpi in both cell types, and while expression plateaus for TAg in both RPTE and HU cells at 48 hpi (11-fold and 7.7-fold increase respectively), tAg continues to increase in expression until 72 hpi, up to 10.9 and 10.5-fold in RPTE and HU cells respectively. TruncTAg was not identified due to its homology with the C-terminus of TAg, although a potential novel open reading frame predicted to be generated a splice variant of TAg, which has not yet been described, was observed to be expressed from 24 hpi in both RPTE and HU cells. This novel TAg variant was identified due to the detection of a single unique peptide that should not be generated by trypsin cleavage of canonical TAg due to the lack of an upstream arginine or lysine. The most likely explanation is the presence of a novel splice event that results in a lysine becoming immediately upstream of the detected peptide sequence. Such a potential splice site has been identified at base 4953 (Fig. 4.7).

The temporal profiles of the late viral proteins VP1, VP2 and Agno indicate that, as anticipated, these proteins are not widely expressed until after 36 hpi, in fact expression greater than two-fold was only recorded from 48 hpi, and the slight signal detected at 24 hpi for VP1 and VP2 could be due to input virions. VP1 and VP2 continue to increase in expression until 72 hpi, while Agno expression plateaus from 48 hpi.

These observed results are in agreement with previously published data on viral gene expression and BKPyV life cycle, giving confidence in these data.
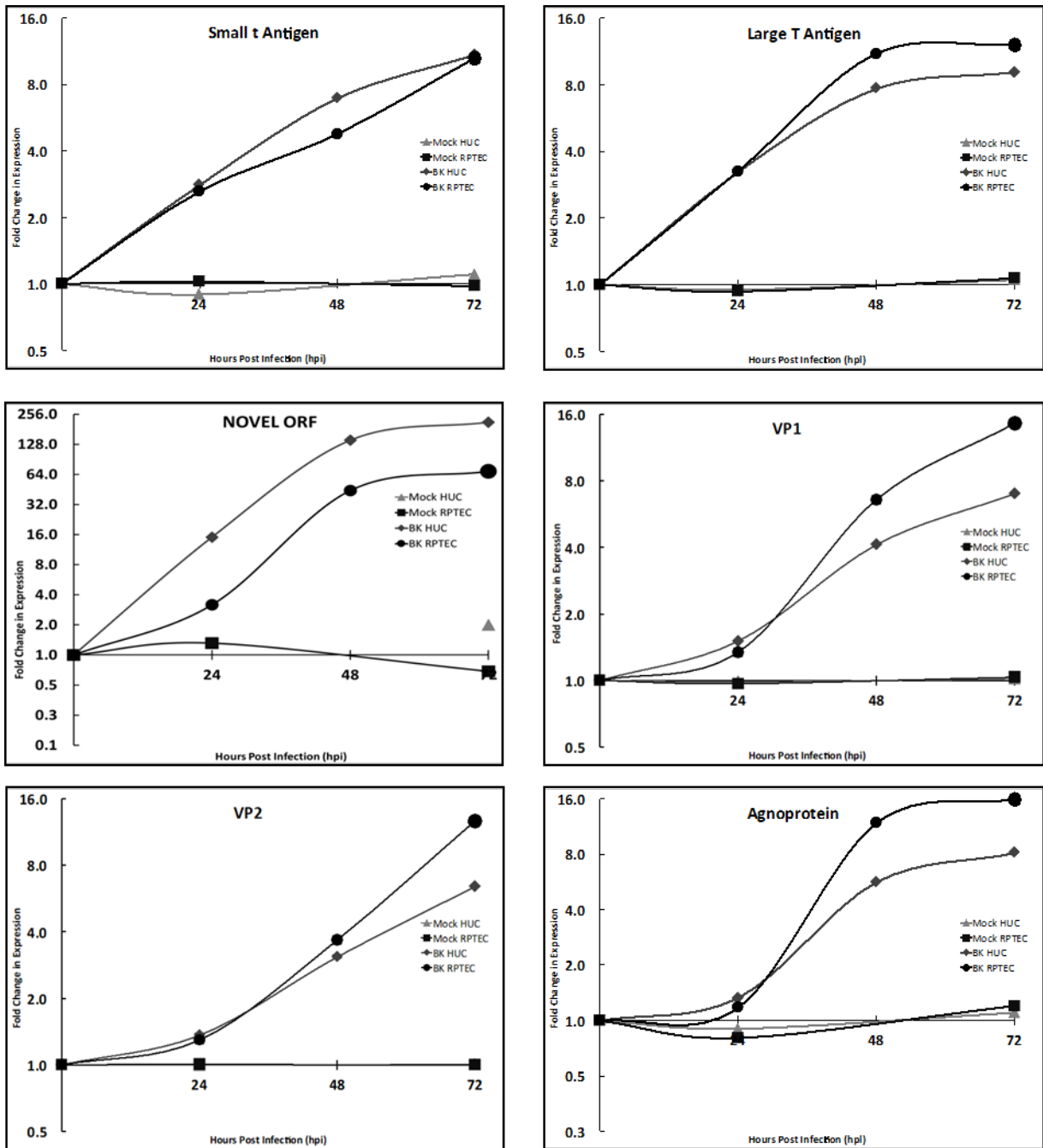
Figure 4.6: Temporal expression profiles of viral proteins identified.
Plots of relative peptide abundance changes over time for infected and uninfected RPTE and HU cells show expression of each viral protein as infection progresses. Time (hpi) is shown on the x-axis, fold change in expression shown on the y-axis. VP3 and TruncTAg could not be identified due to their homology with VP2 and TAg respectively. A potential novel open reading frame of the early viral protein TAg (NOVEL ORF) was identified in both HU and RPTE cells infected with BKPyV.
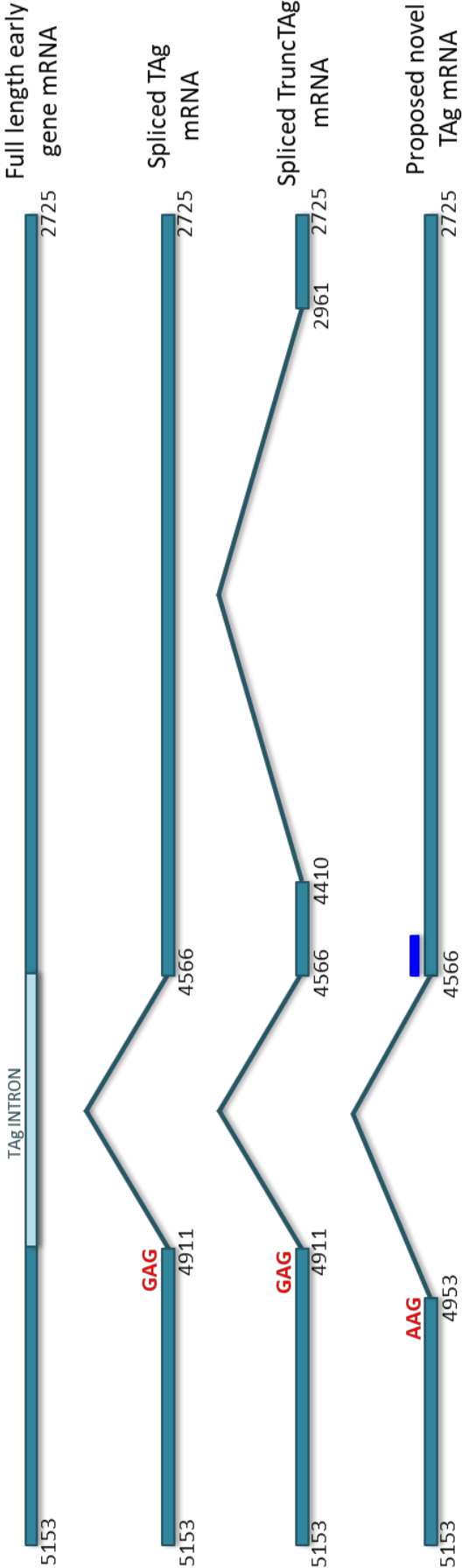
Figure 4.7: TAg, TruncTAg and proposed Novel TAg mRNA splicing.

A cartoon of the TAg mRNA transcript and splice variants of the BKPyV early gene region. Full length mRNA is transcribed from bases 5153 to 2725. The TAg intron is removed through a splicing event between mRNA of bases 4911 and 4566. This can lead to production of either TAg mRNA, or TruncTAg mRNA should a further splice event occur between mRNA of bases 4410 and 2961. Neither of these gene products will lead to generation the novel TAg peptide identified in this screen as a necessary upstream lysine to be cleaved is absent, both instead having an aspartic acid (GAG) upstream of the splice site.

An alternative splice donor site has been identified 42 bases upstream at 4953, which generates a peptide with a lysine (AAG) immediately upstream of the novel peptide identified (blue bar). Thus this is suggested to be the potential novel TAg splice site.

4.2.5 Temporal profiles and validation of key cellular proteins changed in abundance in BKPyV infection

A number of proteins were chosen for validation by immunoblot or immunofluorescence. Cyclin A2, cyclin B1 and cellular Fos (cFos) were chosen due to their significant up regulation in both RPTE and HU cells at either 48 or 72 hpi (Fig. 4.4b). Cyclin dependant kinase 1 (CDK1), p53, geminin, mouse double minute 2 homolog (Mdm2) and cyclin D2 were chosen due to their roles within the enriched functional pathways detected through DAVID analysis of the significantly up regulated proteins. Despite the fact that cyclin D2 and Mdm2 were observed to decrease in abundance during infection, they are both closely linked with the cell cycle. In choosing verify the expression of these eight, both up and down regulated proteins could be validated. The temporal profiles for each of these cellular proteins is shown in Fig. 4.8.

To validate changes in proteins abundance that were shown by TMT-based mass spectrometry, RPTE and HU whole cell lysates were harvested from BKPyV or mock infected cells at 24, 48 and 72 hpi and immunoblotted for cyclin A2, cyclin B1, cyclin D2, CDK1, p53, geminin, VP1 (infection marker) and tubulin (cellular loading control) (Fig.4.9). A substantial increase in the expression of cyclin A2, cyclin B1, CDK1, p53 and geminin was observed at 48 and 72 hpi, correlating with the observations made in the TMT data. Interestingly, by immunoblot CDK1 appeared to show a greater change in abundance at 48 and 72 hpi in RPTE cells than was observed in the TMT data. This could be due to failure to quantify some CDK1 peptides due to their being non-unique, or due to normalisation techniques used. In mock infected cells the abundance of cyclin A2, cyclin B1, CDK1, p53 and geminin was observed to decrease, this is likely due to mock infected cells reaching confluence at 72 hpi as both RPTE and HU cells are contact inhibited, exiting the cell cycle once they come into contact with one another (Aschauer et al., 2015, Ng et al., 2005). Cyclin D2 decreased in abundance by immunoblot in close correlation with TMT expression profile data. Geminin is a cellular regulator of DNA replication that inhibits the replication factor chromatin licensing and DNA replication factor 1 (CDT1), thus restricting assembly of the pre-replication complex (Ballabeni et al., 2013). In previous microarray studies geminin mRNA was observed to increase in expression in BKPyV infected cells (Abend et al., 2010), however this is the first time this increase in expression has been confirmed at the protein level, quantified by peptide abundance and validated by immunoblot.

To further validate these abundance changes and test additional proteins, immunofluorescence microscopy analysis was conducted on BKPyV or mock infected RPTE cells that were fixed at 72 hpi. Cells were immunostained for cyclin B1, cyclin D2, CDK1, p53, Mdm2, cFos, and VP1 (infection marker); Mdm2 and cFos could not be analysed as above because the available antibodies did not detect any protein in immunoblots. Signal levels for cyclin B1, CDK1, p53 and cFos were observed to increase in

infected cells, whereas Mdm2 and cyclin D2 levels decreased in infected cells, correlating with the TMT data. In addition to validating the increased abundance of these proteins, immunofluorescence microscopy enabled the relocalisation of proteins in response to BKPyV infection to be observed in tandem with expression level changes (Fig. 4.10). In BKPyV infected cells cyclin B1, although increased greatly in abundance, remains predominantly cytoplasmic unlike in control cells where low levels of total cyclin B1 expression is observed to be equally cytoplasmic and nuclear. Cyclin B1 is known to become nuclear as cells enter M phase (Pines and Hunter, 1991), suggesting that M phase has not been achieved in these BKPyV infected cells. CDK1 appears also to be distributed differently, observed in greater abundance in the cytoplasm of BKPyV infected cells compared to control. In contrast, in BKPyV infected and control cells p53 is observed as expressed in the cytoplasm at the same intensities, however in BKPyV infected cells nuclear stain in greatly increased, a subcellular location where p53 is usually active as a transcription factor (Milner and Cook, 1986). Cyclin D2 is an early cell cycle associated protein and decreases in abundance as BKPyV infection progresses, suggesting cells are accumulating in a later stage of the cell cycle. Mdm2 is an E3 ubiquitin ligase with the ability to bind and ubiquitinate p53 tagging it for degradation by the proteasome, thus Mdm2 is a negative regulator of p53. Mdm2 is also able to ubiquitinate itself, leading to its own degradation, while p53 acting as a transcription factor is able to drive expression of both Mdm2 and additional p53, dependent on signals received. In this way there exists both a positive and negative feedback loop controlling p53 activity in healthy uninfected cells (Barak et al., 1993). Mdm2 is reduced in infected cells compared to control, however expression remains largely nuclear, as observed in control cells. This data suggests that BKPyV infection may play a role in modulating the p53:Mdm2 functional interaction.

Taken together, the validation of abundance changes for all tested hits from the proteomics data, in HU and RPTE cells by immunoblot and in RPTE cells by immunofluorescence, suggests that our TMT proteomic analysis has yielded an extensive and robust data set.
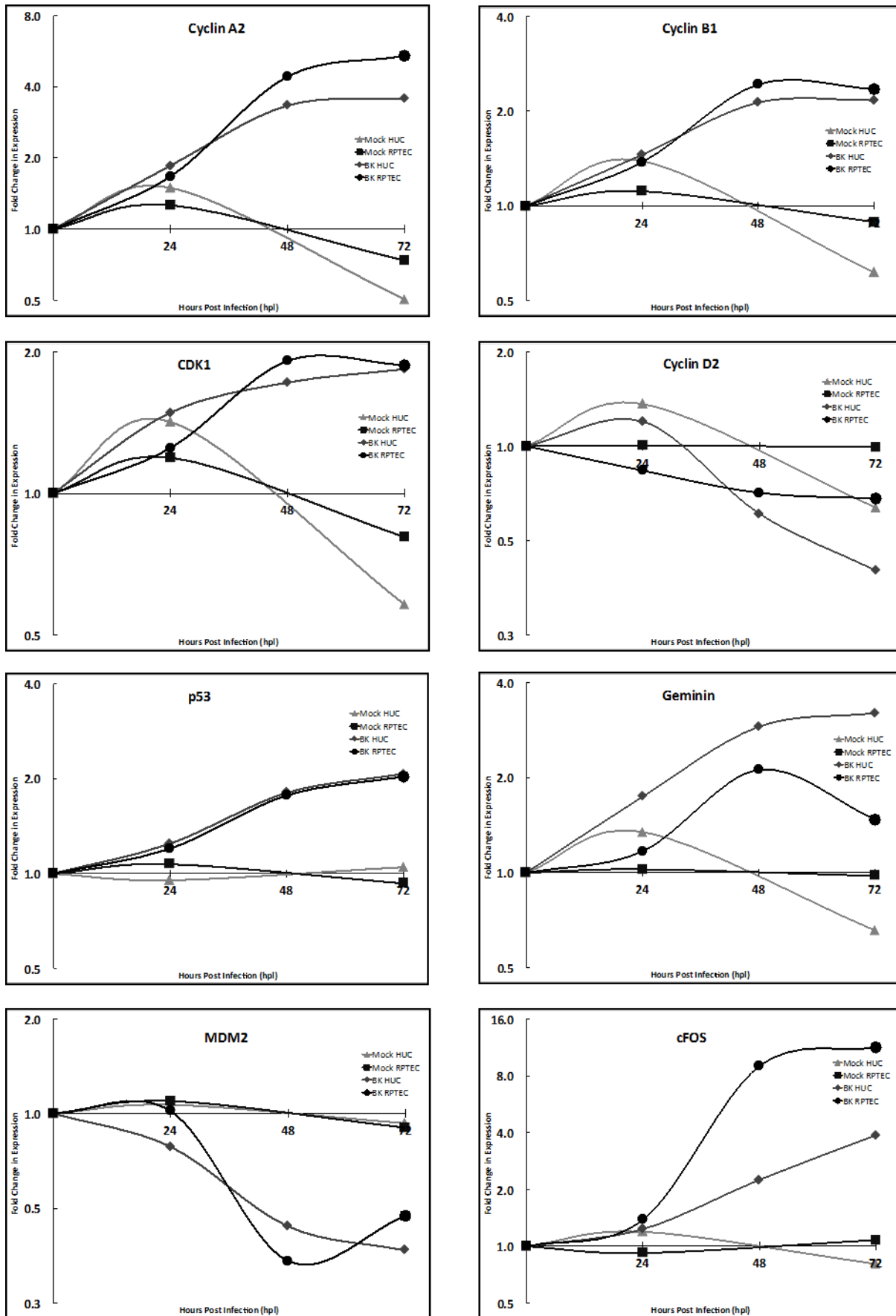
Figure 4.8: Temporal expression profiles of key cellular proteins whose abundances change.
Plots of relative protein abundance changes over time for infected and uninfected RPTE and HU cells show changes in expression of the host proteins chosen for validation by immunoblot and immunofluorescence. hpi is shown on the x-axis, fold change in expression shown on the y-axis. Fold change was calculated by normalising to an average of the mock samples, arbitrarily set to 1. A number of cell cycle associated proteins were chosen for validation, including not only those which were significantly changed in abundance, but also a number which showed less dramatic effects on expression.
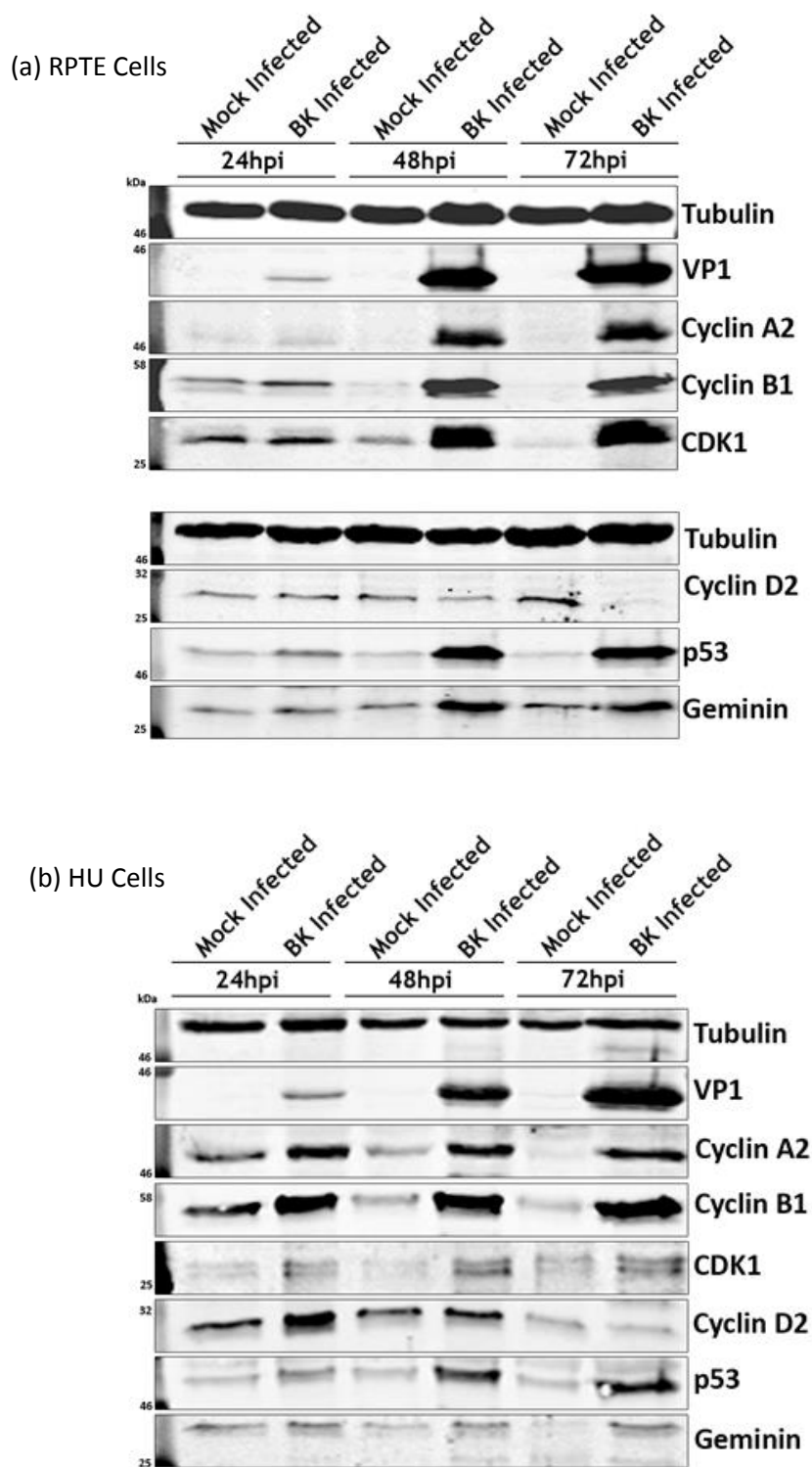
Figure 4.9: Validation by immunoblot of key cellular proteins whose abundances changed.
RPTE (a) and HU cells (b) were infected with BKPyV (5 IU/cell) or mock infected, then harvested at 24, 48 and 72 hpi. Immunoblots were then conducted blotting for the presence of cyclin A2, cyclin B1, cyclin D2, CDK1, p53 and geminin. VP1 was used as an infection control; tubulin was used for a cellular and loading control.
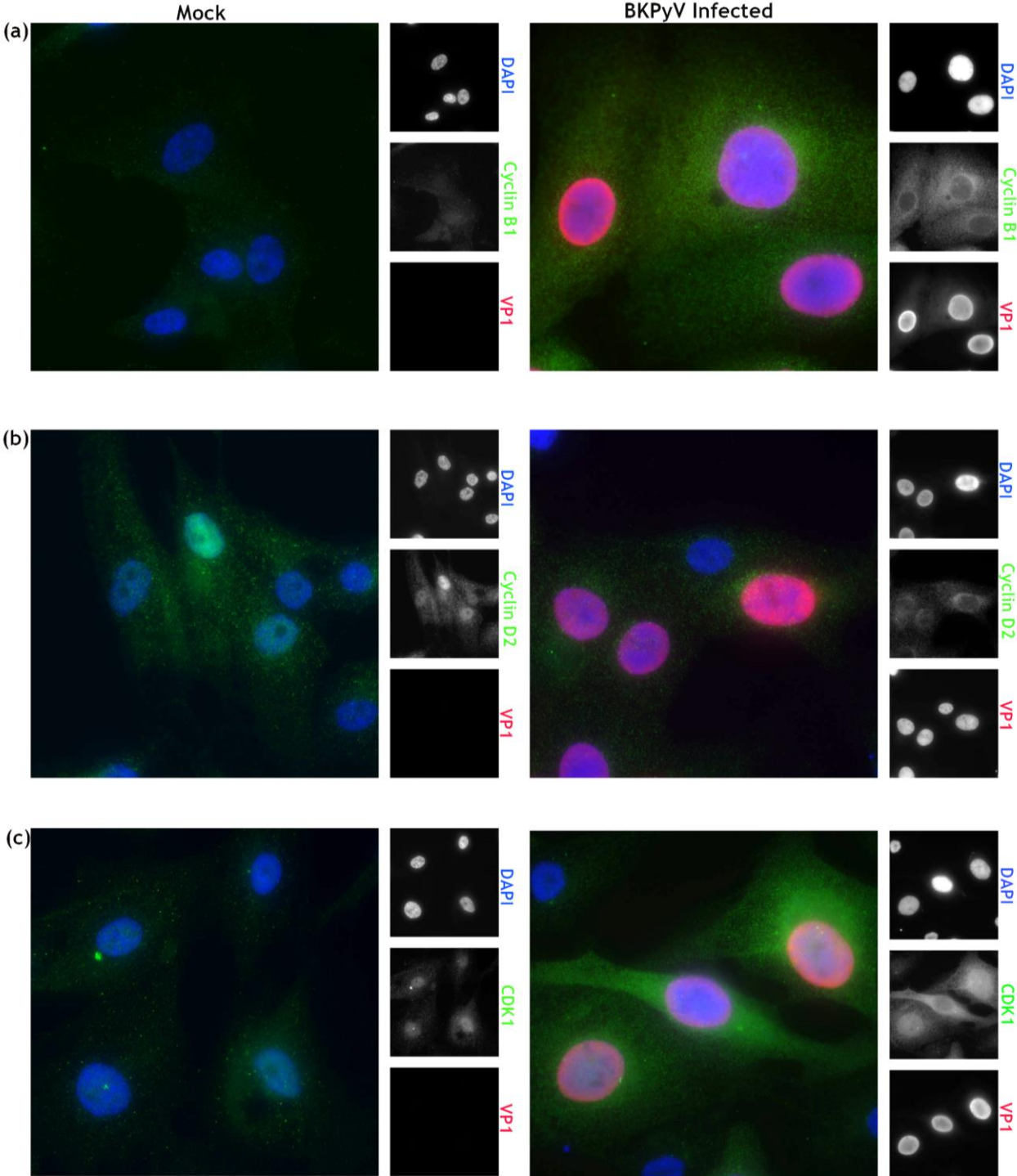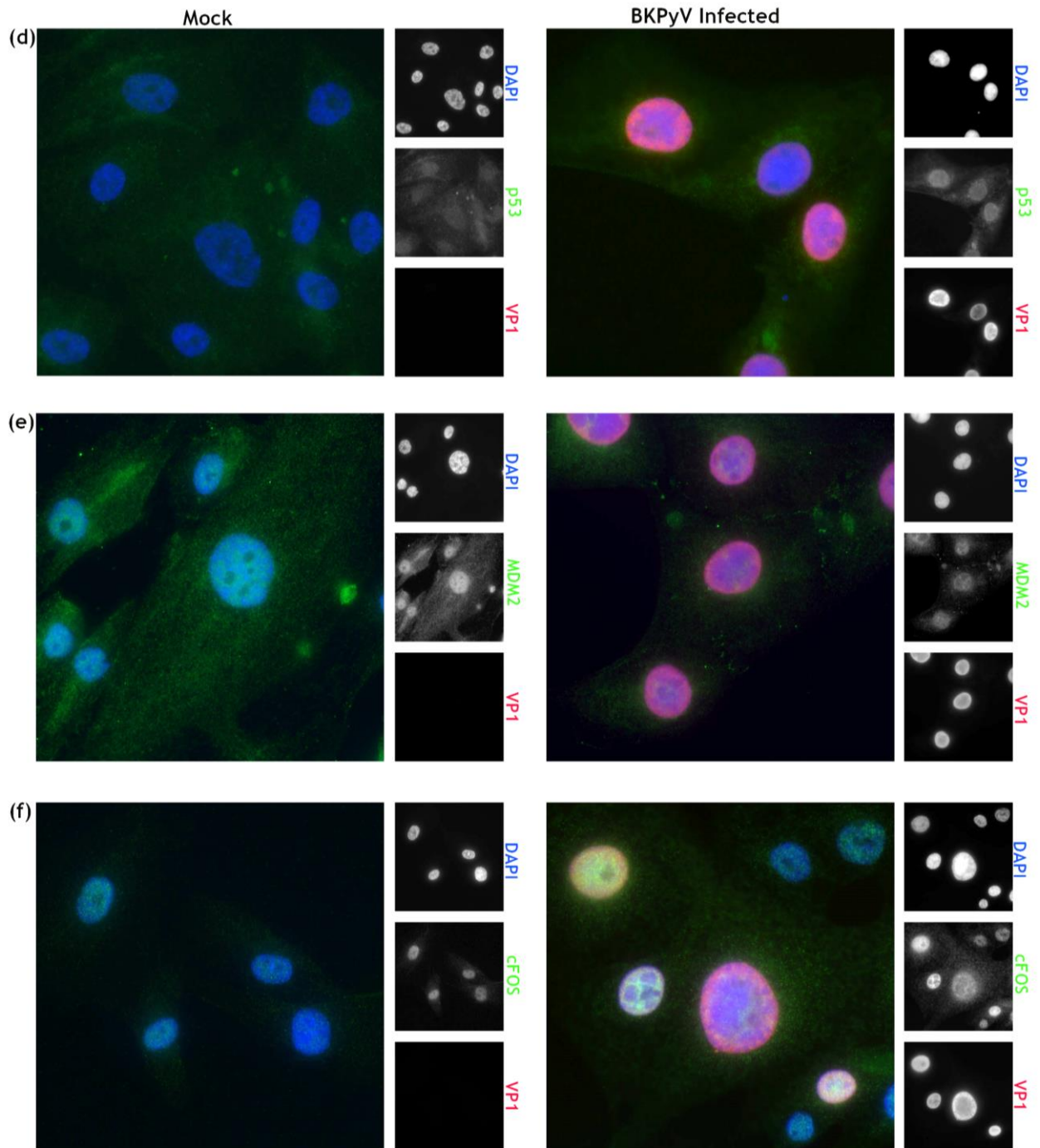
Figure 4.10: Validation by immunofluorescence of key cellular proteins whose abundances changed.
RPTE cells were infected with BKPyV (5 IU/cell) or mock infected, then fixed at 72 hpi. Immunofluorescence staining for cyclin B1 (a), cyclin D2 (b), CDK1 (c), p53 (d), Mdm2 (e) and cFos (f) (shown in green), VP1 (shown in red; an infection control) and DAPI (shown in blue; a nuclear marker) was then conducted. All images taken on Olympus IX81 wide-field immunofluorescence microscope.

4.2.6 Mdm2 and p53 levels are modulated by TAg and cell cycle arrest during BKPyV infection

To investigate the interplay between BKPyV infection, Mdm2 and p53, further investigations were made into their expression levels under different cellular conditions.

Mdm2 is an E3 ubiquitin ligase which regulates p53 activity through ubiquitination, tagging p53 for degradation by the proteasome (Brooks and Gu, 2006). Mdm2 also self-ubiquitinates regulating its own expression in the same way (Fang et al., 2000). Furthermore p53 is a transcription factor for both p53 and Mdm2 (Wei et al., 2006), this transcriptional activity is governed by the strength of p53 activity and signals which trigger initial p53 expression, such as cell cycle checkpoints, leading to the establishment of both positive and negative feedback loops (Boehme and Blattner, 2009). It has been established that TAg is able to bind, stabilise but also inhibit the activity of p53 (Sheppard et al., 1999), leading to increased p53 levels in infected cells. Our TMT data has shown for the first time that this is accompanied by a decrease in Mdm2 levels. It is hypothesised that this observed reduction in Mdm2 is due to its self-ubiquitinating activity, which does not appear to be affected by BKPyV infection or TAg expression. To study this the Mdm2 inhibitor Nutlin-3 was used on mock and BKPyV infected cells.

Nutlin-3 is an Mdm2 inhibitor which obstructs the interaction between p53 and Mdm2 by occupying the p53 binding pocket on Mdm2. When the ubiquitination activity of Mdm2 on p53 is inhibited by Nutlin-3 total Mdm2 levels in cells are known to increase. This is attributed to the inability of Mdm2 to regulate p53 by ubiquitination, leading to increased p53 activity and increased transcription of Mdm2 in attempt to initiate the negative feedback loop (Vassilev et al., 2004).

Mock or BKPyV infected RPTE cells, were treated with 5µM Nutlin-3 (or DMSO as a control) at 2 hpi and at 48 hpi cells were fixed for immunofluorescence. Cells were immunostained for expression of Mdm2, p53, TAg (an infection marker) and DAPI (a nuclear marker) (Fig. 4.11a).

Endogenous levels of both Mdm2 and p53 were observed in the nuclei of untreated mock infected cells. Upon BKPyV infection Mdm2 levels were observed to reduce, while p53 levels were substantially increased, correlating with the changes observed in the TMT quantification. In mock infected cells treated with Nutlin-3 the level of Mdm2 increased, accompanied by a slight increase in p53 levels, in accordance with published effects of Nutlin-3 (Vassilev et al., 2004). Interestingly, in BKPyV infected cells treated with Nutlin-3 levels of Mdm2 did not increase, in fact Mdm2 levels were seen to reduce, whilst p53 levels once again substantially increased. This suggests that during BKPyV infection Mdm2 may be able to self-ubiquitinate and be degraded by the proteasome in the presence of Nutlin-3, however transcription of Mdm2 by p53 is apparently inhibited, likely due to the published interaction of TAg and p53 (Sheppard et al., 1999).

To investigate whether TAg expression alone was sufficient to effect the observed Mdm2 decrease and p53 increase upon BKPyV infection, or if further stimuli such as G2/M phase cell cycle arrest was required, RPTE cells were transfected with TAg. At 2 h cells were treated with 5 μM Nutlin-3 (or DMSO as a control), in addition at 6 h cells were treated with 5 μM RO-3306 (or DMSO as a control). RO3306 is a CDK1 inhibitor which is used to arrest cells in G2/M phase. At 24 h cells were fixed for immunofluorescence and stained for Mdm2, p53, TAg and DAPI (a nuclear marker) (Fig. 4.11b).

Transfection of TAg alone was sufficient to induce a reduction in Mdm2 levels and slight increase in p53. However the increase in p53 levels observed was not comparable to p53 levels observed in BKPyV infected cells. This suggests there may be additional effects of BKPyV infection, other than TAg expression, on regulation of p53 and Mdm2 levels. Treatment of TAg transfected cells with Nutlin-3 did not lead to increased expression of Mdm2, but instead those cells expressing TAg had reduced Mdm2 levels and a slight increase in p53 levels, much like the results seen with BKPyV infected cells (Fig. 4.10a). Once again p53 levels were not equivalent to those seen in BKPyV infected cells. Treatment of TAg transfected cells with the CDK1 inhibitor RO-3306 at 6 h shows a marked increase in p53 levels, akin to those seen in BKPyV infected cells, suggesting that CDK1 inhibition leading to G2/M arrest induces p53 transcription. Mdm2 levels are decreased in those same TAg expressing cells, further suggesting that induced levels of p53 are not active or able to transcribe Mdm2. Nutlin-3 treatment on these RO-3306 inhibited TAg transfected cells further increased these observed changes.

The expression of TAg alone is sufficient to cause a reduction in Mdm2 levels, it is suggested that this is due to TAg activity on p53, binding and inactivating it, while Mdm2 remains able to self-ubiquitinate and be degraded. Further Mdm2 expression cannot be driven by inactive TAg bound p53, thus Mdm2 levels decrease. p53 levels increase only slightly as p53 is stabilised and not ubiquitinated by Mdm2, however the effects of BKPyV infection, in this instance G2/M arrest, appears to drive expression of p53. Both the cell cycle and mitosis were identified as enriched pathways in the significantly ($p <$ 0.0005) up regulated proteins (Fig. 4.5d & f). While it has been known for some time that p53 expression can drive cell cycle arrest (Kastan et al., 1991), it is more unusual to note that cell cycle arrest drives p53 expression itself. It has however been noted that RO-3306 can induce p53 in cell lines positive for acute myeloid leukaemia (AML) (Kojima et al., 2009).

This provides a potential mechanism by which p53 might be induced in BKPyV infected cells (Fig. 4.12).
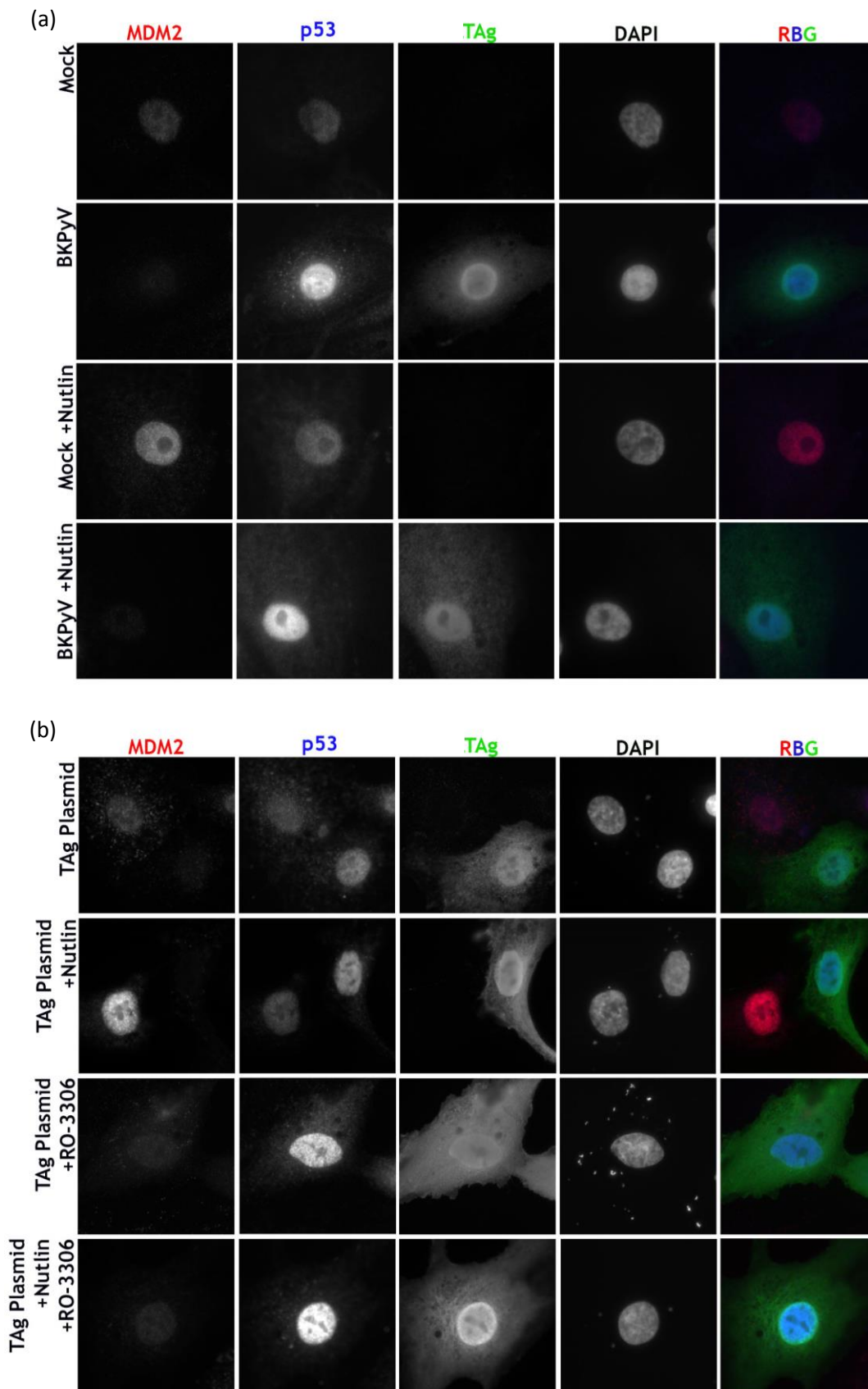
Figure 4.11: BKPyV infection, TAg expression, CDK1 inhibition and Nutlin-3 treatment modulate p53 and Mdm2 expression.

(a) RPTE cells were mock or BKPyV-infected (1 IU/cell) and either treated with 5µM Nutlin at 2 hpi or DMSO as a control. At 48 hpi cells were fixed for immunofluorescence and stained for Mdm2 (red), p53 (Blue), TAg (Green) and DAPI (used as a nuclear marker). (b) RPTE cells were transfected with TAg and at 2 h were treated with 5µM Nutlin (or DMSO as a control), and further treated at 6 h with 5µM RO3306 (or DMSO as a control). After 24 h cells were fixed for immunofluorescence and stained for Mdm2 (red), p53 (blue), TAg (Green) and DAPI as a nuclear marker.
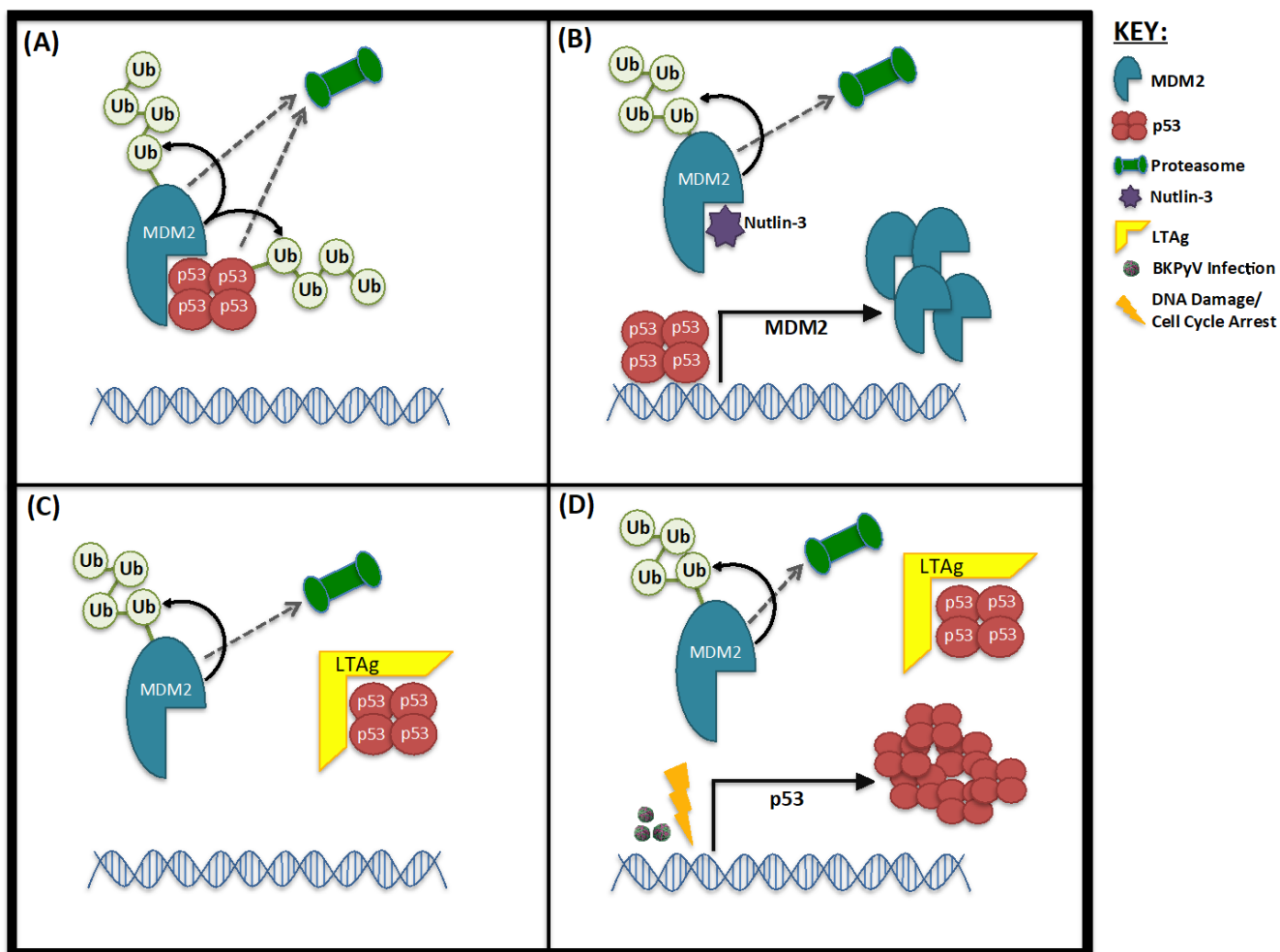
Figure 4.12: Proposed interaction mechanism of Mdm2, p53, TAg and Nutlin-3.
(A) Untreated cells undergo ubiquitination and proteasomal degradation of both p53 and Mdm2. (B) Nutlin-3 inbibits the interaction of MDM2 with p53, preventing p53 degradation. Mdm2 contibues to be ubiquitinated and degraded, causing p53 driven transcription of Mdm2 resulting in increased expression of Mdm2. (C) Cells expressing TAg in the absence of infection exhibit reduced Mdm2 expression as Mdm2 continues to be ubiquitinate and be proteasomally degraded, while TAg causes p53 to be inactive and unable to drive transcription of additional Mdm2. p53 levels remain stable, increased only slightly by prevention of degradation. (D) Cells which are BKPyV infected, or cells expressing TAg combined with cell cycle arrest/damage show reduced Mdm2 expression as seen in panel (C), however additional stimulation linked to infection, cell cycle arrest or DNA damage drive increased expression of p53.

4.2.7 Validation of innate immune response protein expression during BKPyV infection

One of the surprising findings from these whole cell proteomics, as highlighted in the DAVID analysis, was a lack of detectable induction of any anti-viral pathways such as an interferon response, despite the fact these are primary cells that should be competent to detect and respond to viral infection. Indeed, many components of PRR pathways and ISGs known to be involved in antiviral responses were identified in this screen. This was intriguing as it suggested that these cells are unable to detect or respond to BKPyV infection. To validate these findings RPTE cells were used, due to the difficulty in culturing HU cells.

To investigate the ability of these cells to mount an interferon response, RPTE cells were mock or BKPyV infected (5 IU/cell), or treated with IFNα2A (10^4 U/ml) as a positive control. Cells were then harvested at 24, 48 and 72 hpi. Immunoblots reveal that the expression of the well characterised ISGs MX1, ISG15, IFIT1, IFIT2, IFIT3, IRF3, IFI16, and BST2 do not appear to be changed greater than 2-fold in abundance upon BKPyV infection, throughout the time course (Fig. 4.13). This correlates somewhat to the temporal expression profiles of each protein throughout the course of infection (Fig. 4.14), with a few notable observations. By immunoblot MX1 appears to be extremely low in abundance in mock infected RPTE cells (Fig. 4.13), while the temporal expression profile shows a small decrease in abundance of MX1 when RPTE cells are infected with BKPyV (Fig. 4.14). It may not be possible to validate such changes by immunoblot due to the small nature of abundance changes (< two-fold) and the initial low abundance of the protein. Furthermore, there are small (< two-fold) increases in the abundance of IFIT1, IFIT2 and IFIT3 in HU cells and BST2 in both RPTE and HU cells which were not seen in the immunoblot validation in RPTE cells alone, suggesting it might be interesting to investigate HU cells further in future studies.

Stimulation with IFNα2A up regulated the expression of MX1, ISG15, IFIT1, IFIT2, IFIT3, IFI16, and BST2 upon stimulation, while IRF3 is not up regulated in response to stimulation. This was unsurprising as IRF3 may be phosphorylated in response to stimulation (Lin et al., 1998) but has not been shown to be induced in response to IFN. Further inspection of all 'innate immunity' or 'antiviral defence' related proteins (by UniProt key descriptors) that were identified in proteomics data shows there is little-to-no change in any of these proteins in response to BKPyV infection (Table S12), suggesting that RPTE cells do not appear to generate an innate immune response to BKPyV infection.
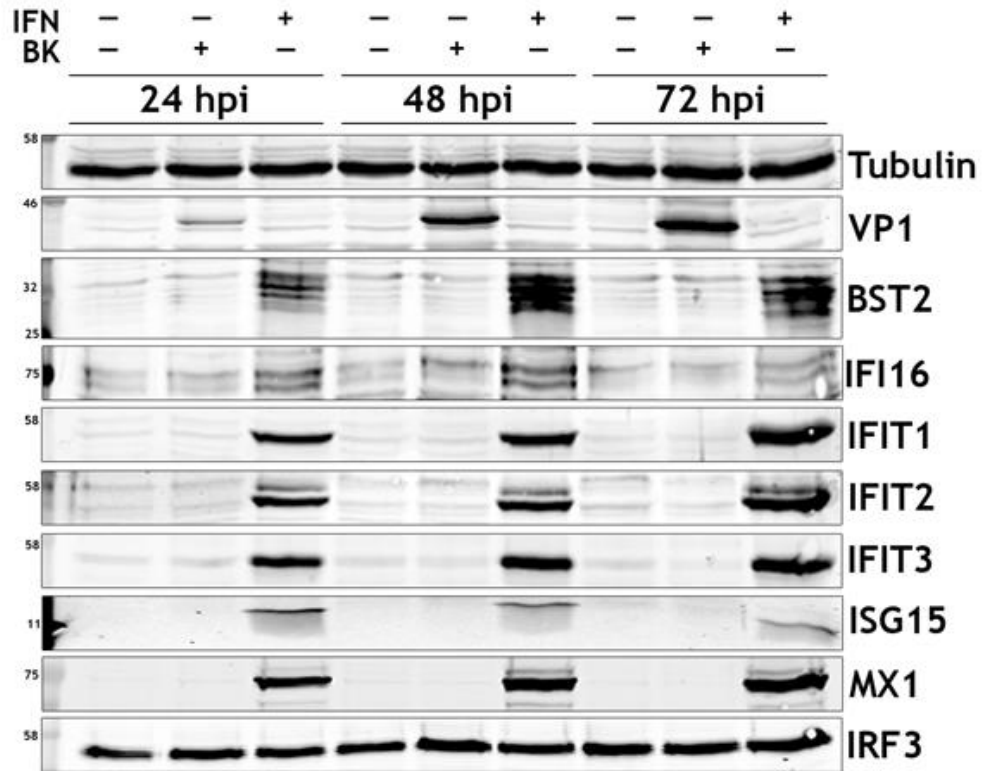
Figure 4.13: Validation by immunoblot of key innate immune proteins identified whose abundances did not change in BKPyV infection.
RPTE cells were infected with BKPyV (5 IU/cell), stimulated with IFNα2A (10^4 U/mL) or mock infected, then harvested at 24, 48 and 72 hpi or stimulation. Immunoblots were then conducted blotting for the presence of BST2, IFI16, IFIT1, IFIT2, IFIT3, ISG15, MX1 and IRF3. VP1 was used as an infection control; tubulin was used for a cellular and loading control. IFNα2A was used as a positive control to stimulate expression of interferon-induced genes.
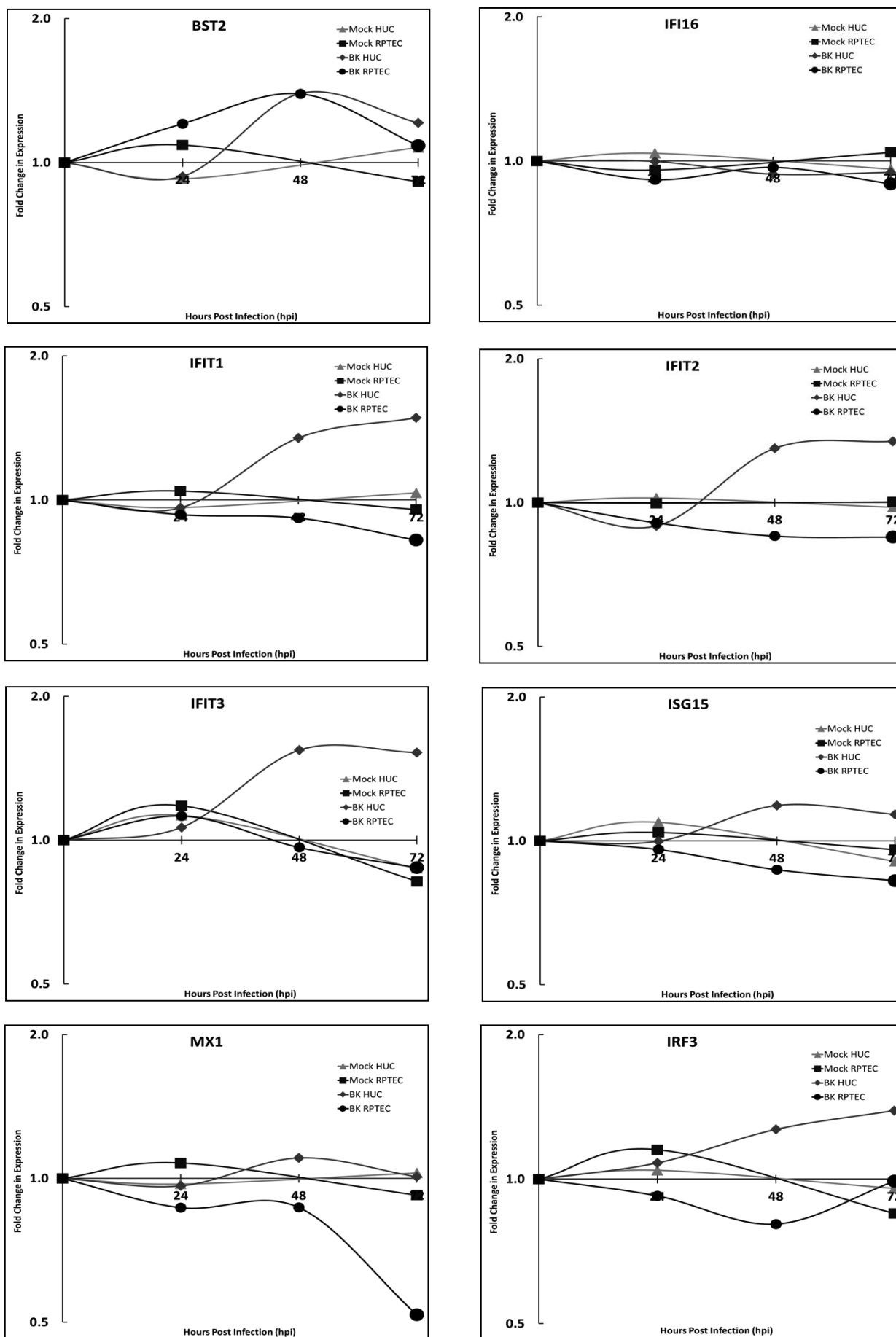
Figure 4.14: Temporal profiles of selected innate immune proteins.
Plots of relative protein abundance changes over time for infected and uninfected RPTE and HU cells showing minimal changes in expression a number of those innate immune host proteins that were quantified. hpi is shown on the x-axis, fold change in expression shown on the y-axis. A number of innate immune related host proteins were chosen for validation, particularly those that highly sensitive to IFN induction and are expected to change in abundance in response to viral infection.

129

4.2.8 RPTE cells are able to respond to stimulation by nucleic acids, but do not respond to BKPyV infection

The lack of ISG induction in BKPyV infected RPTE cells suggests that either the virus is not detected by these cells, or has potent mechanisms to block either interferon production or signalling. To investigate whether RPTE cells have active RNA and DNA sensing pathways, and whether these can be activated in response to BKPyV infection, the localisation of IRF3, a key transcription factor in antiviral responses, was analysed by immunofluorescence. Upon activation of RNA and DNA sensing pathways IRF3 is phosphorylated, allowing it to dimerise and translocate to the nucleus, leading to the transcription and expression of Type I and III interferons. As positive controls uninfected RPTE cells were stimulated with either poly(I:C), a double stranded RNA mimic which stimulates RIG-I and other RNA sensors, or a short mostly double stranded DNA molecule shown to be a potent inducer of cGAS then fixed after 6 hours (Herzner et al., 2015) (Fig. 4.15a). Translocation of IRF3 can be clearly seen in poly(I:C) stimulated cells, while in DNA stimulated cells IRF3 translocation can be seen in a number of cells, although to a lesser extent than in poly(I:C) stimulated cells. This confirms that RPTE cells are able to translocate IRF3 into the nucleus in response to either RNA or DNA stimulation. However, no nuclear translocation was observed in BKPyV infected RPTE cells at 48 hpi, and IRF3 remained wholly cytoplasmic, with infected cells being indistinguishable from mock infected cells.

This observation suggests that BKPyV infection does not activate IRF3 translocation, although whether this was by inhibition of translocation or prevention of phosphorylation was unclear. To address this question RPTE cells were mock or BKPyV infected (3 IU/cell) and harvested at 0, 6, 24, 48 and 72 hpi, while positive control samples treated with poly(I:C) or DNA were harvested at 6 hpi. An immunoblot was conducted to ascertain overall levels of IRF3 and of IRF3 phosphorylation (specific for phosphorylation at residue S386), with tubulin used as a loading control and VP1 as a marker of BKPyV infection (Fig. 4.15b). IRF3 remained unphosphorylated throughout the time course in both mock and BKPyV infected cells, while in poly(I:C) and DNA stimulated cells IRF3 was clearly phosphorylated, albeit differing in band size and density. This difference between IRF3 phosphorylation in poly(I:C) and DNA stimulated cells in intriguing, while it was initially hypothesised that the upper band could be dimerization of IRF3, often seen in DNA stimulated cells (Wu et al., 2013) it does not appear to be as large as an IRF3 dimer (94 kDa), being less than 75 kDa. It therefore suggested that the upper band is as a result of IRF3 hyperphosphorylation, a feature of highly stimulated IRF3 (Clement et al., 2008).

This suggests that rather than preventing the translocation of phosphorylated IRF3, IRF3 remains unphosphorylated in the presence of BKPyV infection.

(a)

(b)
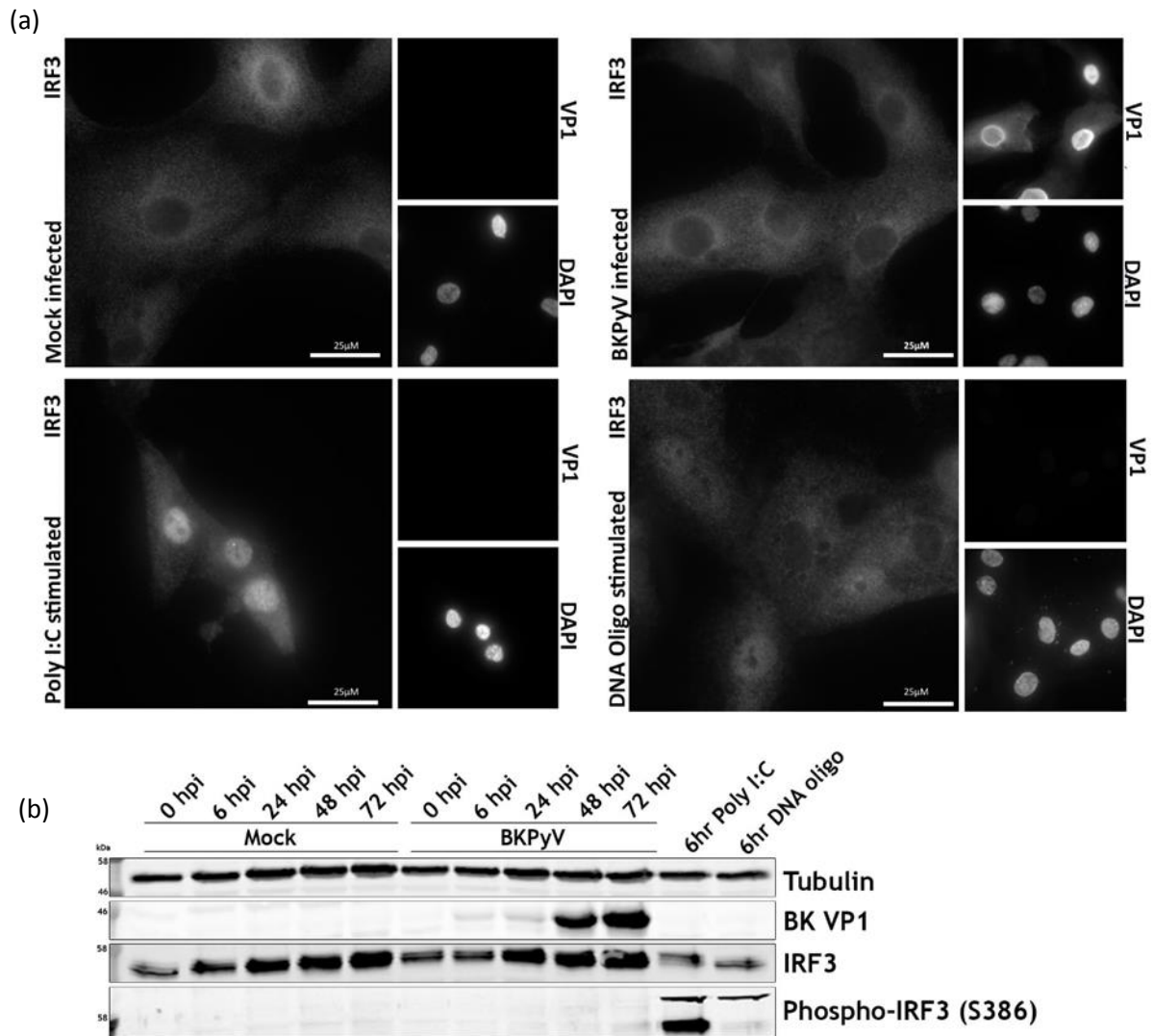
Figure 4.15: IRF3 is phosphorylated and translocated to the nuclei of cells when stimulated with synthetic RNA or DNA, but not in response to infection.
(a) RPTE cells were mock or BKPyV-infected (3 IU/cell) and fixed at 48 hpi, or stimulated with poly(I:C) (2 µg/ml) or annealed DNA oligonucleotides (2 µg/ml) and fixed at 6hpi. Cells were stained for IRF3, VP1 (infection control), DAPI (nuclear marker). Images were taken on Olympus IX81 wide-field immunofluorescence microscope. (b) To further validate RPTE cells were mock or BKPyV-infected (3 IU/cell) and harvested at 0, 6, 24, 48 and 72hpi, while poly(I:C) or annealed DNA oligonucleotides stimulated RPTE cells (2 µg/ml) were harvested at 6h. Samples were immunoblotted for IRF3 and phosphorylated IRF3 (S386), tubulin was used as a loading control, VP1 was used an infection control.

4.2.9 BKPyV infection does not inhibit synthetic RNA or DNA-induced IRF3 activation

The lack of observed IRF3 activation during BKPyV infection could be due to an active process of viral-mediated inhibition of RNA and DNA sensing pathways, such as through binding and inhibition of IRF3 as observed with HPV-16 E6 protein (Ronco et al., 1998), or by a more passive process of evading activation of these pathways. To address these questions, RPTE cells were mock or BKPyV infected (3 IU/cell) and subsequently stimulated with poly(I:C) or DNA at 42 hpi, followed by harvesting cells for immunoblot at 48 hpi. Immunoblots were stained for IRF3, phosphorylated IRF3 (S386), VP1 (as a marker of infection) and tubulin (as a loading control) (Fig. 4.16a). Phosphorylation of IRF3 occurred in poly(I:C) or DNA stimulated cells, whether infected with BKPyV or mock infected, and no differences were observed in the levels of IRF3 phosphorylation between infected and uninfected cells.

To confirm whether RNA/DNA-stimulated IRF3 translocation to the nucleus was affected by the presence of BKPyV , RPTE cells were infected with BKPyV (0.5 IU/cell) and at 42 hpi stimulated with poly(I:C) or DNA. Cells were subsequently fixed at 48 hpi for immunofluorescence and stained for IRF3 and TAg (Fig. 4.16b). IRF3 translocation to the nucleus was observed in response to both poly(I:C) or DNA stimulation irrespective of whether wells were infected (TAg positive) or not. As before, poly(I:C) gave a more robust stimulation of IRF3 nuclear translocation. These data confirm that BKPyV infection does not prevent the activation of IRF3 in response to synthetic RNA or DNA stimuli. These data taken together suggest that BKPyV does not actively down regulate the activation of IRF3, and so infected cells are fully competent to detect foreign nucleic acids and stimulate the transcription of type I and III interferons, and thus should be capable of mounting an effective antiviral innate immune response. This suggests BKPyV can efficiently evade detection by any PRRs in these kidney epithelial cells.
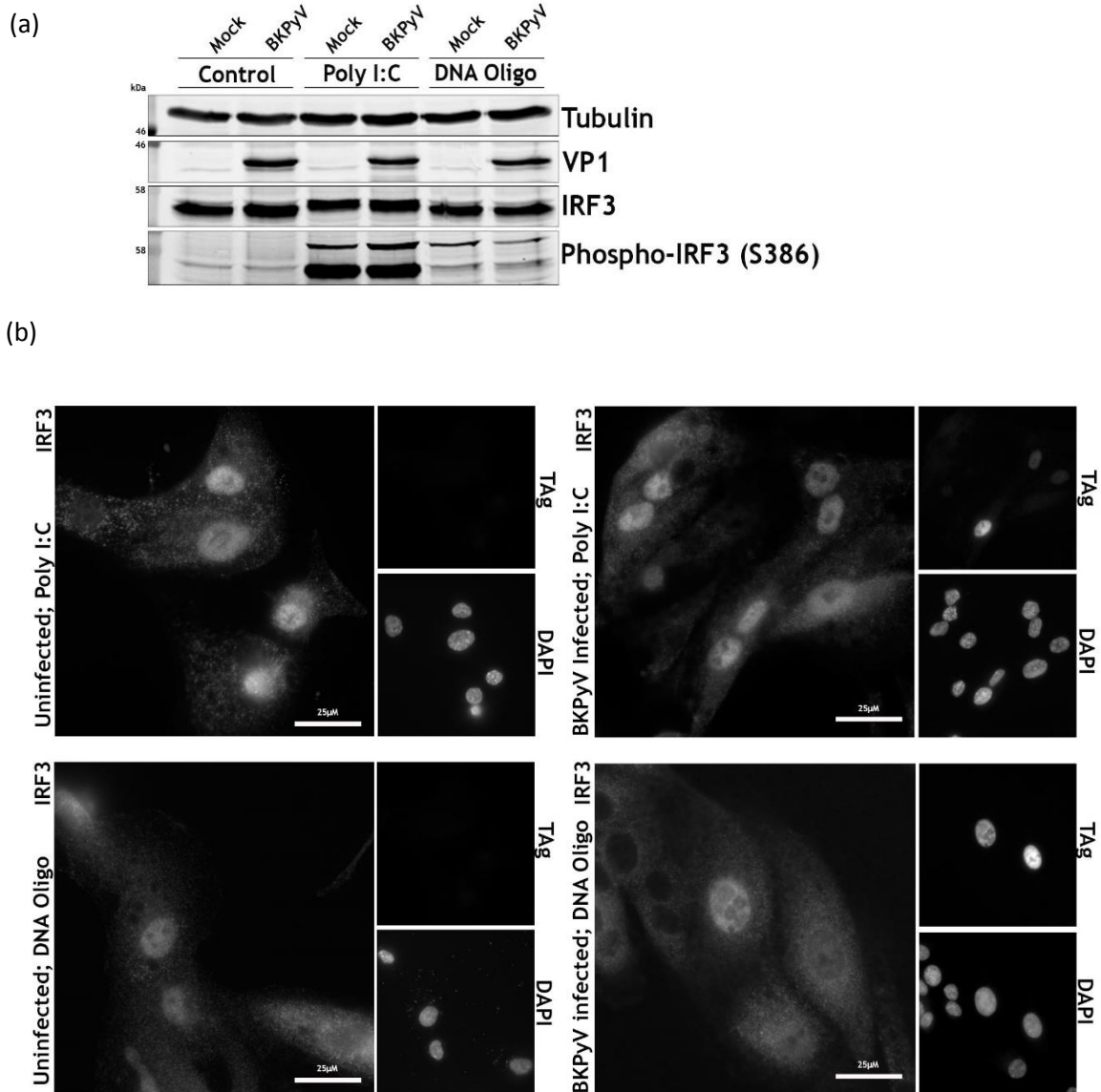
Figure 4.16: BKPyV and mock-infected RPTE cells do not differ in their responses to synthetic RNA and DNA stimulation.
(a) RPTE cells were mock or BKPyV-infected (3 IU/cell), stimulated at 42 hpi with poly(I:C) (2 µg/ml) or annealed DNA oligonucleotides (2 µg/ml), or unstimulated. Cells were then harvested for immunoblot at 48 hpi, tubulin was used as a loading control, VP1 was used as an infection control. (b) RPTE cells were mock or BKPyV-infected (0.5 IU/cell) and at 42 hpi stimulated with poly(I:C) (2 µg/ml) or annealed DNA oligonucleotides (2 µg/ml) and fixed at 48 hpi. Cells were stained for IRF3, TAg (infection control), DAPI (nuclear marker). Images were taken on Olympus IX81 wide-field immunofluorescence microscope.

4.2.10 Repeat TMT-based experiment reveals close correlations between data sets and no cellular effects of virion binding

The surprising lack of change in the host cell proteome at the earliest time point of 24 hpi suggested little or no effect of virus binding and penetration. To investigate this further a second TMT-based whole cell proteomics experiment was conducted at early time points, starting at just 12 hpi when little-to-no viral proteins are expressed.

As in the first TMT-based experiment RPTE cells were mock infected or infected with BKPyV (3 IU/cell), additionally RPTE cells were also infected with BKPyV (3 IU/cell) that had been inactivated with ultraviolet light. UV inactivation causes pyrimidine dimers which prevent DNA replication, effectively rendering the virus inert, while the capsid remains intact (Tseng and Li, 2007). As such any changes to the cellular proteome upon infection with UV inactivated BKPyV will be attributable to virion binding and viral entry.

Samples for mock, BKPyV and UV inactivated BKPyV were harvested at 12, 24 and 48 hpi for TMT processing and labelling as previously described (section 4.2.1), then subjected to MS^3 mass spectrometry. In this repeat 7703 cellular and 5 viral proteins were identified, 96% of which were identified in the first TMT-based data set.

Very few changes in protein abundance were observed at 12 or 24 hpi during BKPyV infection, while a similar set of cellular proteins observed in the first data set were upregulated at 48 hpi (Fig. 4.15a). UV-irradiated virus induced virtually no changes at any time point, suggesting that replicating virus was required to account for the effects observed (Fig. 4.17a). Correlation between the first experiment and the second showed a strong positive linear relationship (Fig. 4.17b), providing evidence that our dataset is strong and reproducible. Further analysis on this data has been limited due to the very small changes induced at this early additional time points.
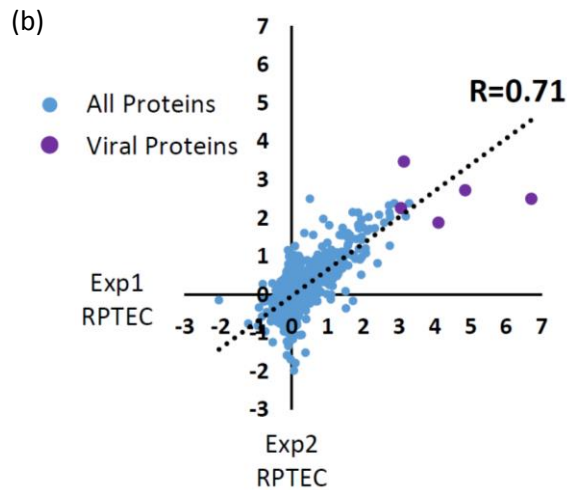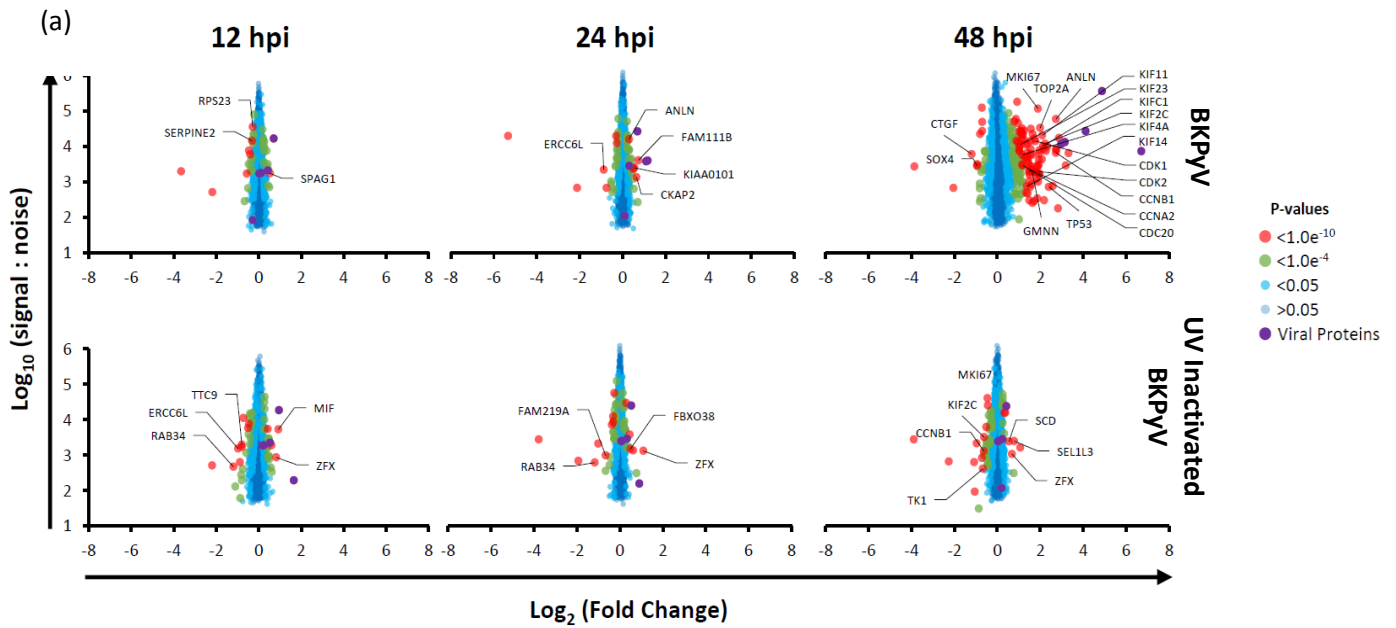
Figure 4.17: Correlation between repeat TMT-based analysis and first TMT-based analysis

(a) The abundance of proteins identified at each BKPyV-infected time point, 12, 24 and 48 hpi, was divided by the average of the mock-infected samples from each time point. Scatter plots show all proteins identified with unique peptides. Fold change (RPTE cell BKPyV-infected/RPTE cell mock-infected average) is shown as the $\log_2$ ratio on the x-axis, to the right increasing in abundance, and to the left decreasing in abundance. The signal:noise is shown on the y-axis as $\log_{10}$. Significance B was used to estimate *p* values (Cox and Mann, 2008). (b) Scatter plot showing the Pearson correlation between experiments 1 (first) and 2 (repeat) in RPTE cells, for proteins quantified by ≥2-peptides. All scatter plots kindly produced by Dr C Davies.

4.3 Discussion

The TMT-based proteomic analysis detailed in this chapter has established a comprehensive proteome resource for two primary human epithelial cell types from the reno-urinary system, RPTE and HU cells, and provided details of temporal changes in viral and host proteomes throughout the course of a productive BKPyV infection. Of the 8992 cellular proteins that were identified, surprisingly few changed significantly in abundance in response to BKPyV infection, taking into account fold-change and signal-to-noise corrections. In previous studies using the same proteome analysis technique to study a large dsDNA virus, HCMV, 56% of cellular proteins demonstrated abundance changes of more than two-fold in infected cells (Weekes et al., 2012). Here, with BKPyV infection, we see fewer than 5% of cellular proteins altered in abundance greater than two-fold.

Confidence that this data set is robust and reproducible was demonstrated by successful validation of a wide variety of cellular proteins that were up regulated, down regulated or unchanged during infection by immunoblot and/or immunofluorescence, in addition to a repeated TMT-based analysis at early time points. While experiments in HU cells were limited after initial validation due to these cells being more technically difficult to culture, there was considerable correlation in protein changes between RPTE and HU cells, providing confidence that data generated using RPTE cells reflects virus-host interactions in both cell types. The replication of BKPyV was overall less efficient in HU cells than RPTE cells, suggesting RPTE cells are a better model for BKPyV replication. All observed changes are unlikely to be as a result of virion binding and entry due to the limited observed effects of infection with UV inactivated BKPyV, thus the changes in cellular proteomes can be attributed to viral gene expression.

The viral protein data indicates that in RPTE cells the early proteins TAg and tAg were the first to be synthesized at 24 hpi, and relative abundance levels of the late proteins identified, VP1, VP2 and Agno, were much lower at this point. In HU cells the difference between early and late gene synthesis initiation is less marked, this may be due to the differences in cellular metabolisms and viral replication rates between these cell types (Li et al., 2013a). It was also observed that viral protein expression continued to increase throughout 72 h of infection, as the highest abundance of each is at the final 72 hpi in both RPTE and HU cells. Most interesting was the identification of a novel previously undescribed TAg variant, identified through a single unique peptide that could not be generated by trypsin cleavage due to the lack of arginine or lysine in the canonical TAg to cause such a peptide. An alternative splice donor site has been identified upstream of the canonical splice donor site which would place a lysine directly upstream of the splice site, such splicing could therefore explain the existence of the identified peptide after cleavage. Further investigations into this potential TAg variant

could include the generation of TAg splice donor site mutants in both virus and TAg expressing plasmids. This will allow study of phenotype, subcellular localisation of TAg variants and detect any changes in the number of TAg species by immunoblot.

Analysis of the virus-induced changes to the cellular proteomes of the two cell types demonstrated that BKPyV infection affects virtually no cellular processes other than those involved in cell cycle and DNA replication. These data support and expand upon evidence from previously published data indicating G2/M phase arrest is driven by polyomavirus infection (Harris et al., 1996, Lilyestrom et al., 2006, Stubdal et al., 1997, Rundell and Parakati, 2001). It is likely that infected cells are restricted from progressing through the G2/M check point, as indicated by cyclin B1 remaining primarily cytoplasmic in infected cells; nuclear translocation of cyclin B is a marker for M phase progression (Pines and Hunter, 1991). This M phase progression does not appear to occur in BKPyV infected cells, and G2-arrest has been previously observed in JC polyomavirus JCPyV TAg transfected cells (Orba et al., 2010).

Limitations of analysing these particular cell types have included the necessity to compare all proteome changes to an average of the mock samples (taken at 24 and 72 hpi). Whilst this is often done in immortalised cell lines that proliferate unimpeded, both HU and RPTE cells are contact inhibited (Aschauer et al., 2015, Ng et al., 2005). They exit the cell cycle as they come into contact with one another and form tight junctions. Such phenomena can mean that at 72 hpi mock infected cells have an altered protein expression profile (less proliferative, more senescent) than 24 hpi mock infected cells. The effect of averaging these samples to produce a 'base' against which to judge changes upon BKPyV infection might obscure more subtle changes. If given the opportunity to repeat this experiment I would suggest including a mock infected control for each time point being studied in order to directly compare against the appropriate mock time point.

An interesting observation from the proteomics data was the lack of any detectable changes that could be associated with an immune response upon infection. While we were able to identify a large number of well-established antiviral response-associated proteins, such as IFI16, TMEM173 (STING), NFκB, IRF3, and numerous ISGs, they showed very little change in abundance in response to BKPyV infection. Such a study was not, however, able to highlight any changes in subcellular locations of immunological proteins. For example, while MHC-I and NK receptors did not appear to change in abundance throughout infection, an altered expression at the plasma membrane might stimulate killing by NK cells *in vitro*. To address this question one could conduct plasma membrane profiling of BKPyV and mock infected cells.

What is true, however, is that BKPyV infection does not induce an IRF3-mediated immune response or expression of interferon stimulated genes. Furthermore, infection with BKPyV does not inhibit the

IRF3 response. This might be attributed to the stability of the BKPyV virion, maintaining very low levels of aberrant uncoating in the cytoplasm. In addition the BKPyV dsDNA genome is circular, thus not exhibiting any overhangs which are immunostimulatory (Herzner et al., 2015), and when condensed with host-derived histones, this might reduce sensing to negligible levels. It was interesting to note that stimulation of RPTE cells by DNA oligomer was much less pronounced than stimulation with poly(I:C), suggesting that recognition of DNA in the cytoplasm is sub-optimal, even when using a validated immunostimulatory DNA oligomer (Herzner et al., 2015).

The effect of BKPyV infection, compared with the roles individual viral proteins play, in the up and down regulation of cellular proteins is important to consider. While expression of TAg alone was sufficient to reduce overall levels of Mdm2 and increase levels of p53 slightly, likely through TAg binding and stabilising p53, the vastly increased levels of p53 observed in BKPyV infected cells was only replicated in TAg expressing cells when cell cycle was inhibited, specifically in G2/M phase. It seems likely that the DNA damage response (DDR), known to be activated in BKPyV infection (Verhalen et al., 2015), also contributes to induction of p53 levels.

Given the specific and extensive cell cycle deregulation and an apparent pseudo-G2 phase arrest caused by BKPyV infection, this may suggest that stalling cells in a G2-like state provides several advantages to the virus in addition to promoting viral DNA replication via stimulation of cells into S phase. Therefore further investigation into the role of BKPyV-regulated cell cycle status during viral replication was conducted.

5. Cell cycle status is important for productive BKPyV infection

5.1 Introduction

The predominance of cell cycle and cell cycle related pathways being induced throughout the observed TMT-based proteomic analysis of infected cells highlights the importance of cell cycle during BKPyV replication. Increased levels of G2 and M phase proteins during BKPyV infection, such as CDK1, cyclin B1, cyclin A2, geminin and p53, in conjunction with reduced early cell cycle proteins such as cyclin D2, suggests strongly that BKPyV induces a G2/M-like cell cycle arrest. Furthermore cyclin B1 was observed to remain cytoplasmic during BKPyV infection, signifying that these cells do not pass the G2/M checkpoint, at which time cyclin B1 would become nuclear. These observations suggest that BKPyV infection induces a pseudo-G2 arrest in both RPTE and HU cells, similar to that proposed for the closely related papillomavirus HPV-16 (Davy et al., 2002).

Cell cycle progression has been shown to be essential for a number of polyomaviruses including SV40 and JCPyV. Proliferating cell nuclear antigen (PCNA), only present in replicating cells, was revealed to be essential for SV40 replication *in vitro* (Prelich et al., 1987), while SV40 replication rates can be slowed by reducing cellular proliferation (Bettuzzi et al., 2002). Furthermore, inhibition of JCPyV with the CDK1/2 inhibitor Roscovitine, for in excess of 3 days, was able to drastically reduce infectivity, although this effect was largely attributed to Roscovitines inhibition of CDK1 and its activity on CDK2 was not considered (Orba et al., 2008). The phosphorylation of TAg is required for its viral helicase activity that is essential in viral replication (Moarefi et al., 1993). It has been proposed that phosphorylation of a number of TAg residues is effected by various protein kinases; primarily cyclin A:CDK2 and, to a lesser extent, cyclin B:CDK1 complexes (Li et al., 1997). However, just a single threonine residue is implicated in the formation of the TAg viral helicase, in SV40 this phosphorylation site has been shown to be T124, while in JCPyV it is T125 (McVey et al., 1996, Swenson and Frisque, 1995). Mutation of these threonine residues prevents viral replication (Swenson et al., 1996, McVey et al., 1996). For SV40 TAg, phosphorylation of T124 was shown to be primarily mediated by CDK1 (*cdc2*) (McVey et al., 1989). In BKPyV a threonine residue is present at TAg position 126, suggesting there may be a similar phosphorylation event required to form the viral helicase, although to date this has not been investigated.

The MAPK/ERK pathway, by stimulating cell cycle progression, has also been shown to be essential for BKPyV replication (Seamone et al., 2010). Moreover the activity of ATM/ATR kinases that are involved in DNA damage response pathways, which are key mediators of the G2 checkpoint, have been shown to be important for effective BKPyV replication (Verhalen et al., 2015, Jiang et al., 2012). While cell cycle progression during BKPyV infection is largely driven by the activity of both TAg and tAg on Rb

family proteins, PP2A and p53 among others (Harris et al., 1996, Pallas et al., 1990), the extent to which different stages of cell cycle inhibition can be overcome by BKPyV infection or effects on the replication of BKPyV is not well understood. To address this the effect of number of different cell cycle inhibitors on BKPyV replication was investigated.

5.2 Results

5.2.1 Cell cycle inhibition exhibits variable effects on BKPyV-induced cell cycle progression and pseudo-G2 arrest

In the first instance CDK inhibitors commonly used to inhibit the cell cycle were tested for toxicity in RPTE cells in a range of concentrations for 24 and 48 h (Fig. 5.1) with a trypan blue assay, allowing quantitation of cell death after inhibitor treatment. RPTE cells were treated with 250 nM, 500 nM and 1 μM concentrations of PD0332991, a CDK4/6 inhibitor that prevents cells from exiting G1 and entering S phase (Fig. 5.1a). More than 90% of RPTE cells remained viable even at the highest PD0332991 concentration for 48 h. Cells were also treated with 20 μM, 40 μM and 60 μM concentrations of Roscovitine, an inhibitor of both CDK1 and CDK2 that prevents cells from progressing through the G1/S checkpoint, S phase, G2 and M phase, thus it has a broad effect on general cell cycle progression (Fig. 5.1b). 60 μM Roscovitine treatment lead to a substantial reduction of cell viability after 24 h treatment (~70% of cells viable), while more than 95% of cells treated with 40 μM Roscovitine remained viable after 24 h of treatment, although viability was reduced to <85% by 48 h at this concentration. 20 μM Roscovitine treatment showed much less effect on cell viability, with ~92% of cells remaining viable after 48 h treatment. Finally cells were treated with 1 μM, 5 μM and 10 μM RO-3306, a CDK1 inhibitor that blocks cells in G2 and M phase (Fig. 5.1c). Treatment with RO-3306 reduced cell viability to below 90% by 48 h at any concentration, and at 10 μM RO-3306 by 24 h. However, little effect of treatment with 1 or 5 μM RO-3306 on cell viability was observed by 24 h. Conditions that resulted in >90% cell viability were deemed acceptable and so it was concluded that inhibitors should be used for no longer than 24 h, and at 1 μM for PD0332991, 20 μM for Roscovitine, and RO-3306 should be used at 5 μM.

(a)

(b)

(c)
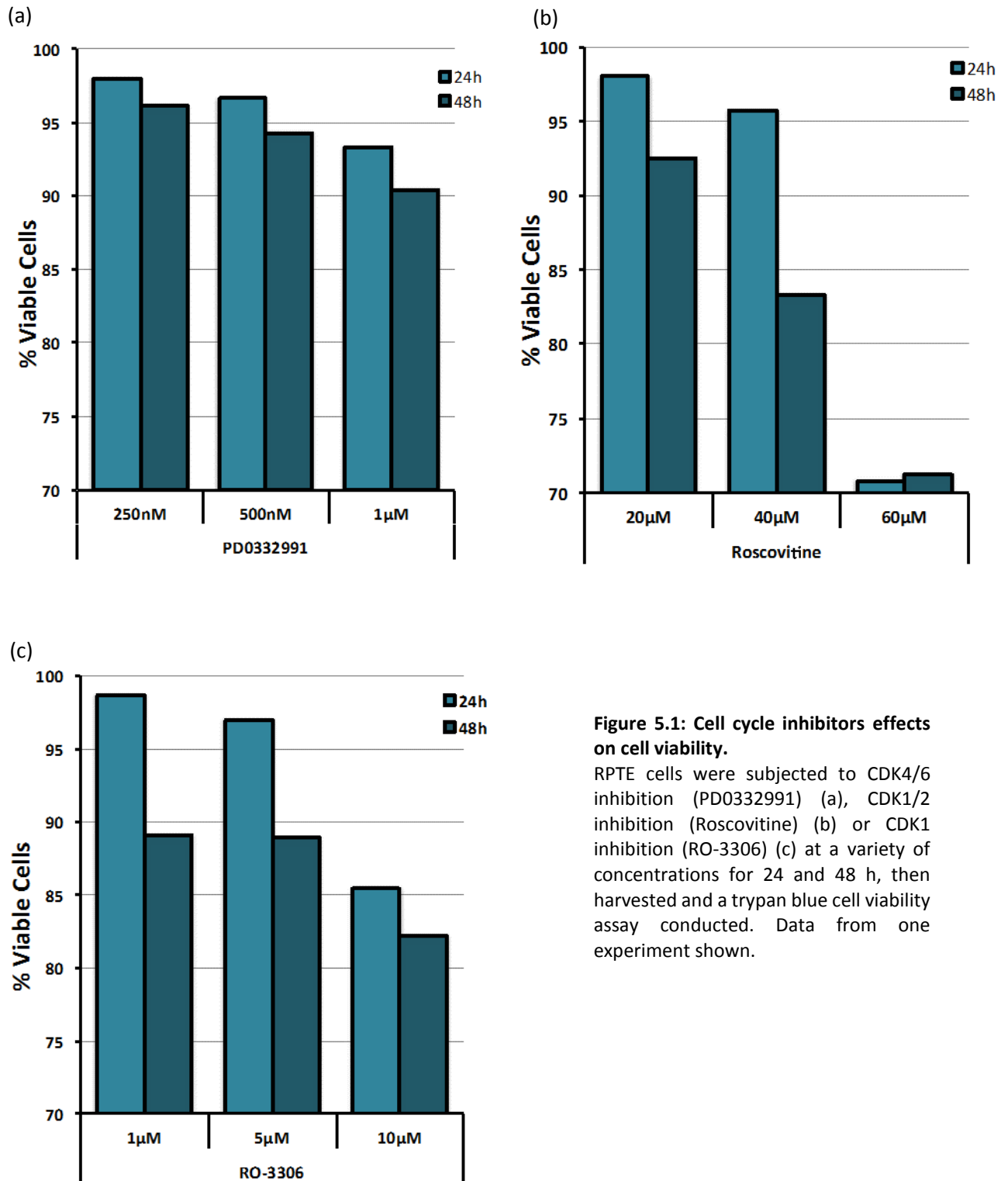
Figure 5.1: Cell cycle inhibitors effects on cell viability.
RPTE cells were subjected to CDK4/6 inhibition (PD0332991) (a), CDK1/2 inhibition (Roscovitine) (b) or CDK1 inhibition (RO-3306) (c) at a variety of concentrations for 24 and 48 h, then harvested and a trypan blue cell viability assay conducted. Data from one experiment shown.

These inhibitors were then tested in RPTE cells for their ability to perturb the cell cycle and induce various states of cell cycle arrest in both infected and uninfected cells. Cells were stained with propidium iodide (PI), a fluorescent DNA intercalator that is stoichiometric, binding DNA proportionally to the amount of DNA within each cell. Using this method those cells in G0 or G1, cells containing a single compliment of chromosomes (2n), will emit a base fluorescent signal, while double signal intensity indicates cells which have undergone genome synthesis but not yet undergone mitosis (4n). Any signal intensity between these two set values indicates a cell undergoing genome synthesis. In this way the cell cycle status of each cell can be determined by flow cytometry, using FlowJo cell cycle analysis software (v10.5). Thus, RPTE cells were mock or BKPyV infected (3 IU/cell), and at 24 hpi were either untreated, subjected to CDK4/6 inhibition (1 μM PD0332991), CDK1/2 inhibition (20 μM Roscovitine) or CDK1 inhibition (5 μM RO-3306) for a further 24 h, after which time cells were harvested and their DNA content stained with PI. Cells were then analysed by flow cytometry, and cell cycle status determined. Three independent experiments were conducted and the average proportion of cells in each cell cycle phase was calculated from the three independent datasets were calculated (Fig. 5.2a), flow cytometry histograms from a single experiment shown (Fig. 5.2b).

Mock infected cells responded as expected to inhibitor treatments. In mock infected untreated cells ~72% were in G1 or G0 phase, ~10% were in S phase and ~18% were in G2/M phase. RPTE cells are slow to replicate, taking up to 40 h to double in number (Lonza specifications), thus this relatively low number of cells in S, G2 or M phase was unsurprising. In mock infected cells the number of cells in G1 or G0 phase were increased to ~84% when inhibited with CDK4/6 inhibitor PD0332991, while those in S phase and G2/M phase reduced accordingly (~4.5% and ~11.5% respectively), indicating an increased number of cells in G0/G1 arrest. When inhibited with CDK1/2 inhibitor Roscovitine there was little difference to untreated cells with ~75% of mock infected cells were observed to be in G1 or G0 phase, ~9.5% were in S phase and ~14.5% were in G2/M phase. This was also expected because CDK1 and 2 activities are important not only throughout S, G2 and M phase, but also during late G1 where, in complex with cyclin E CDK2 orchestrates G1/S checkpoint progression, thus CDK1/2 inhibition should lock cells in the state in which they are in when the inhibitor is applied. Treatment of mock infected cells with CDK1 inhibitor RO-3306 resulted in an increased percentage of cells in G2/M (~23%), a similar percentage of cells in S phase as untreated cells (~12%) and a reduced percentage of cells in G1 or G0 (~65%). This was also as expected because suggests that the CDK1 inhibition should cause G2/M arrest and cells to accumulate in this phase. These results suggest the inhibitors are effective at the selected concentrations in RPTE cells.

In contrast to mock infected untreated samples, untreated BKPyV infected samples were observed to have just ~57% of cells in G1 or G0, ~12% were in S phase and ~31% were in G2/M phase. This agrees

with published data showing that TAg and tAg are able to promote cell cycle progression through the G1/S checkpoint in BKPyV infected cells, enhancing viral replication (Bollag et al., 2010, Hesbacher et al., 2016, Sheng et al., 1997). Furthermore, these data support the observations made in chapter 4 of this thesis that cell cycle arrest in a G2/M-like state is caused by BKPyV infection. BKPyV infected RPTE cells that were inhibited with CDK4/6 inhibitor PD0332991 showed little difference in their cell cycle status compared to untreated BKPyV infected cells, with a very small increase in the proportion of cells in G1 and S phases indicating a slight delayed in progression. The little-to-no effect of CDK4/6 inhibition on BKPyV infected cells can be explained by the ability of TAg to bind Rb-family members and release E2F, which can drive cells through the G1/S checkpoint independently of cyclin D:CDK4/6, and thus CDK4/6 inhibition is ineffective at preventing cell cycle progression in the face of BKPyV infection. CDK1 and 2 inhibition by Roscovitine had a much more dramatic effect on virus-induced cell cycle modulation leading to a profile more akin to uninfected untreated cells with ~73% of cells in G1 or G0 phase, 8% in S phase and ~19% in G2/M phase. This is best explained by an inhibition of virus-induced S phase progression because of CDK2 inhibition, which would prevent infected cells reaching and becoming stalled in G2. Finally, BKPyV infected cells which were inhibited with CDK1 inhibitor RO-3306 showed a similar proportion of cells in G2/M to untreated infected cells at ~30%, with more cells in S phase (~21%) and consequently fewer in G1 or G0 (~49%). This suggests that CDK1 inhibition does not prevent virus induced G2/M arrest, unsurprisingly as RO-3306 also causes G2/M arrest, but CDK1 inhibition either delays transition from S to G2 phase or increases G1 to S phase transition in infected cells. The increase in cells in S phase in infected cells caused by RO-3306 may have consequences for viral DNA synthesis. Overall, infection by BKPyV or inhibition of CDK1 by RO-3306 have very similar effects on cell cycle status, namely inducing cells to accumulate in G2/M. This might be explained by BKPyV inhibiting CDK1 activity, although it is likely to be more complicated as inhibition of CDK1 in infected cells appears to cause an additional increase in the proportion of cells in S phase in addition to G2 arrest. This leads to the question of whether CDK1 activity is required for BKPyV replication.

(a)

(b)
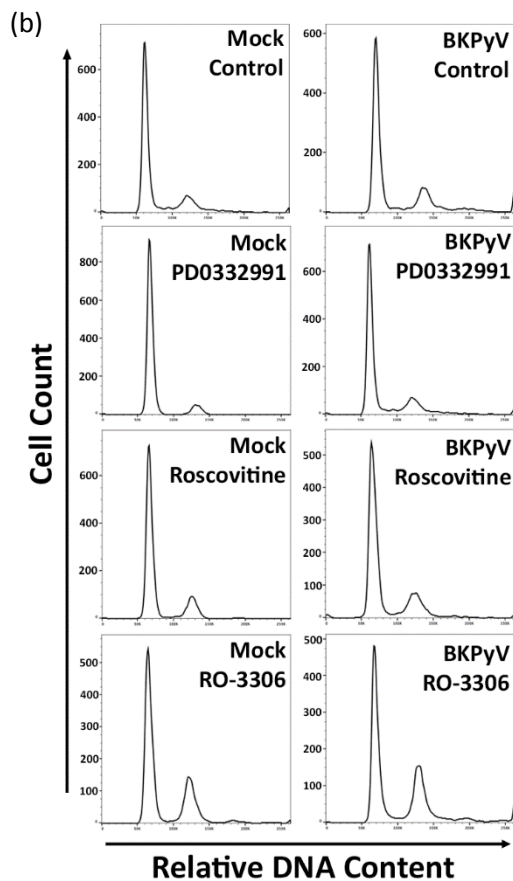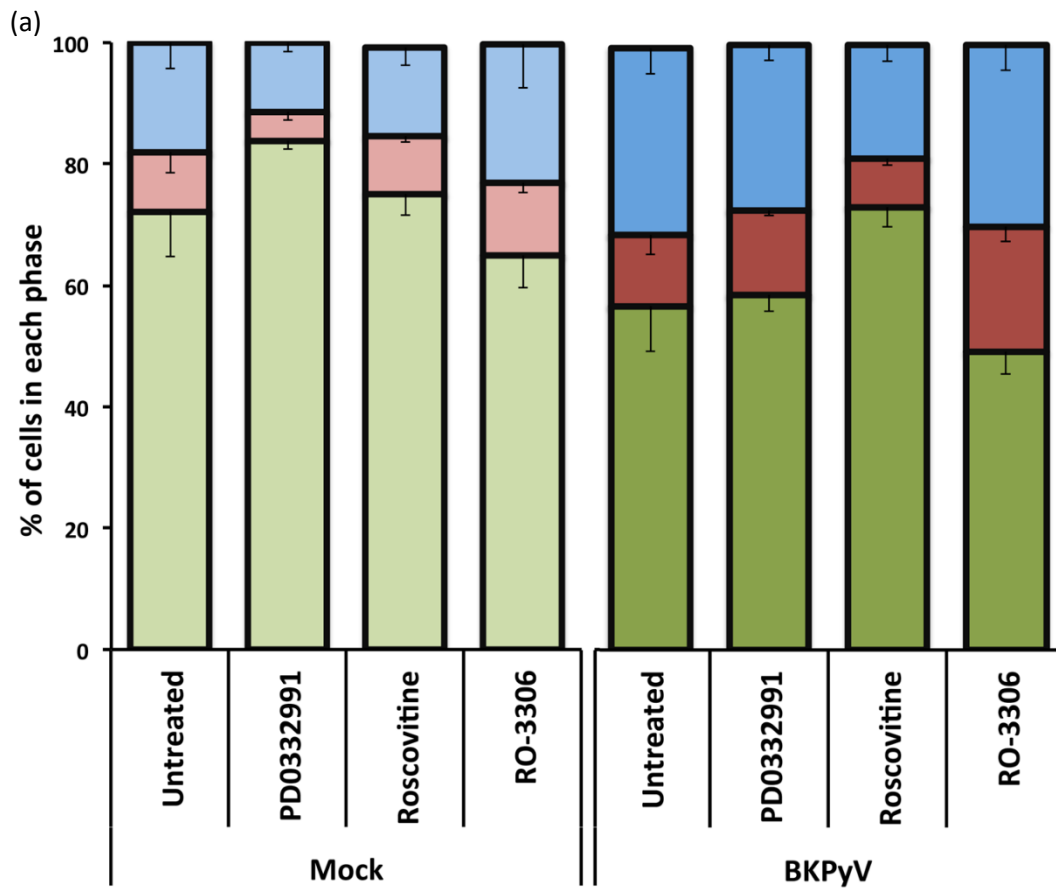
Figure 5.2: Cell cycle inhibitors modulate the RPTE cell cycle status of uninfected cells.

The cell cycle status of RPTE cells was determined for a number of different experimental conditions. RPTE cells were infected with BKPyV (3 IU/cell) or mock infected. At 24 hpi infected and mock infected cells were subjected to CDK4/6 inhibition (PD0332991 1 µM), CDK1/2 inhibition (Roscovitine 20 µM) or CDK1 inhibition (RO-3306 5 µM). At 48 hpi cells were harvested by trypsinisation. (a) Collected cells were stained with propidium iodide (PI) and analysed by flow cytometry. Data from three independent experiments show, error bars show standard deviation. (b) Histograms of PI stain intensity for each experimental condition of a single experiment shown.

5.2.2 Effects of cell cycle inhibition on BKPyV DNA synthesis gene expression and replication

To investigate the effects of cell cycle inhibitors on viral DNA replication RPTE cells were infected with BKPyV (3 IU/cell) and treated with PD0332991 (1 μM), Roscovitine (20 μM) or RO-3306 (5 μM) at 24 hpi. At 48 hpi cells were harvested and DNA extracted for analysis by qPCR for virus and host genome copy numbers. The number of BKPyV genome copies per sample were normalised to host DNA copy numbers (using primers to the TNFα gene) for each sample, to control for variations in samples such as DNA extraction efficiency. Data were normalised to uninhibited control samples (set arbitrarily to 1) for each experiment, and six independent experiments were conducted (Fig. 5.3a). Inhibition of CDK4/6 demonstrated no significant effect on BKPyV genome replication compared to control, which was anticipated because TAg can effectively bypass CDK4/6 regulated G1/S checkpoint and PD0332991 had virtually no effect on BKPyV-induced cell cycle progression. Inhibition of CDK1/2 exhibited a significant 86% reduction in BKPyV genome synthesis most likely due to inhibition of CDK2-dependent S phase progression which is important for viral DNA replication. Intriguingly, CDK1 inhibition caused a significant reduction in BKPyV genome replication by 56%, despite the fact RO-3306 had little effect on cell cycle progression in inhibited cells. This suggests that CDK1 activity is important for efficient viral DNA replication, which may be related to phosphorylation of TAg.

To examine viral genome synthesis occurs in the presence of Roscovitine, or whether the detected viral DNA is simply due to input virions, RPTE cells were infected with BKPyV (3 IU/cell) and at 2 h harvested, or at 24 hpi treated with Roscovitine (20 μM), the known inhibitor of viral DNA synthesis cidofovir (40 μg/mL), or untreated, then at 48 hpi harvested for DNA extraction and analysis by qPCR (Fig. 5.3b). Cidofovir is an effective antiviral against BKPyV through inhibiting incorporation of deoxycytidine triphosphate into nascent DNA, being incorporated into DNA in its place, leading to chain termination and prevention of genome replication (Bernhoff et al., 2008). BKPyV genome levels in the samples harvested at 2 hpi, a time point at which genomes will not have been replicated, were greater than ten-fold lower than those observed in cidofovir or Roscovitine treated samples, suggesting a limited amount of viral DNA synthesis occurs in the presence of these inhibitors, possibly during the first 24 h of infection before inhibitor addition, and the detected DNA is not simply from input virus. Roscovitine was almost as effective as cidofovir in inhibiting viral replication, and both caused a greater than ten-fold reduction in viral DNA levels.

(a)

(b)
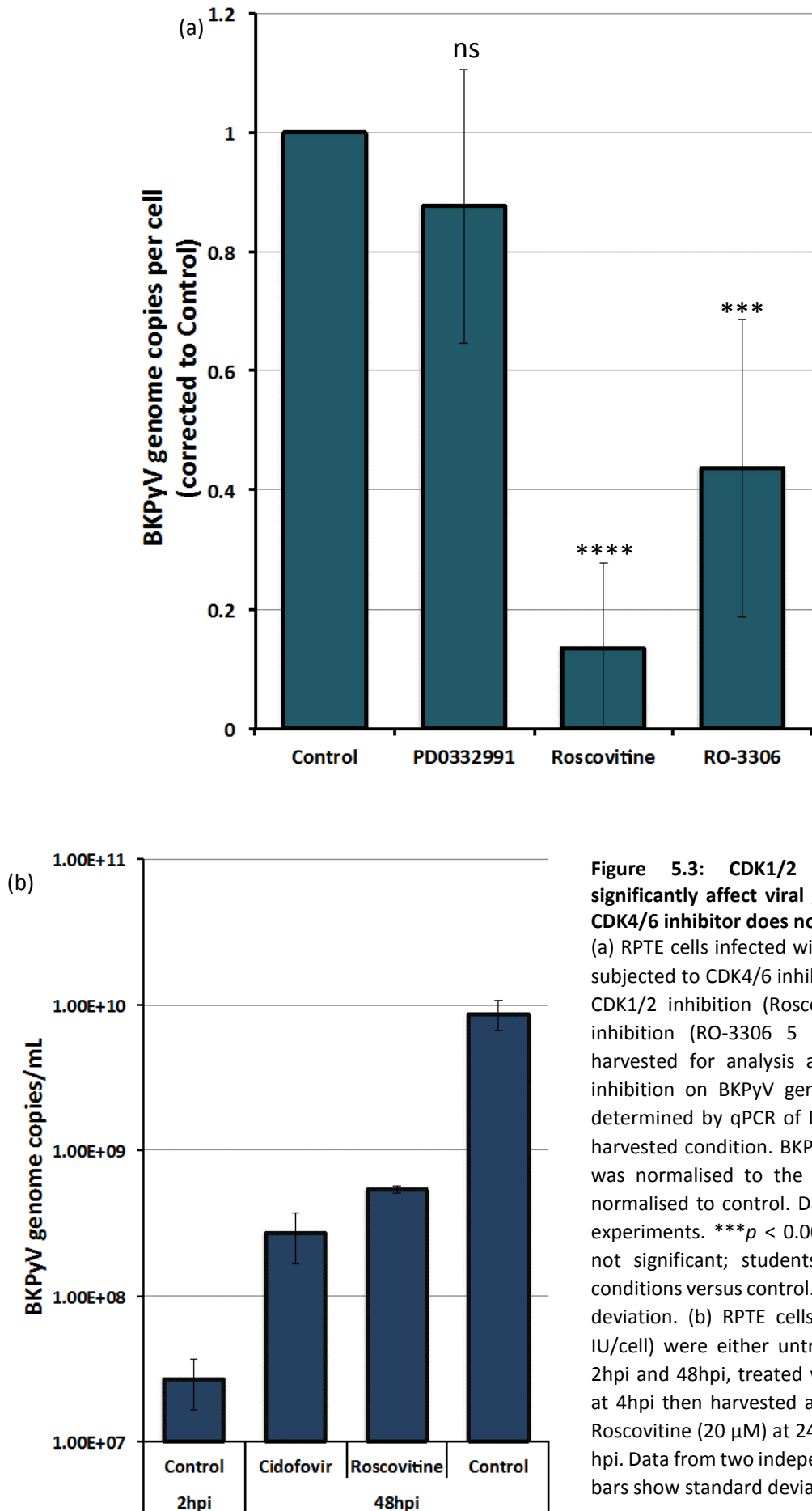
Figure 5.3: CDK1/2 and CDK1 inhibitors significantly affect viral genome synthesis, while CDK4/6 inhibitor does not.

(a) RPTE cells infected with BKPyV (3 IU/cell) were subjected to CDK4/6 inhibition (PD0332991 1 μM), CDK1/2 inhibition (Roscovitine 20 μM) or CDK1 inhibition (RO-3306 5 μM) from 24 hpi, and harvested for analysis at 48 hpi. The effect of inhibition on BKPyV genome copy number, was determined by qPCR of DNA extracted from each harvested condition. BKPyV genome copy number was normalised to the cellular gene TNFα, and normalised to control. Data from six independent experiments. ***$p < 0.001$; ****$p < 0.0001$; ns = not significant; students t-test of experimental conditions versus control. Error bars show standard deviation. (b) RPTE cells infected with BKPyV (3 IU/cell) were either untreated then harvested at 2hpi and 48hpi, treated with cidofovir (40 μg/mL) at 4hpi then harvested at 48 hpi, or treated with Roscovitine (20 μM) at 24 hpi then harvested at 48 hpi. Data from two independent experiments. Error bars show standard deviation.

The effects of cell cycle inhibition on viral protein expression levels were also examined. As before RPTE cells were infected, inhibitors added at 24 hpi and cells were harvested for immunoblot at 48 hpi (Fig. 5.4a), and protein expression levels quantified by densitometry (corrected to uninhibited control) (Fig. 5.4b). Blots were probed for the cellular loading control tubulin, VP1, VP2, VP3, Agno and TAg. CDK4/6 inhibition had no effect on viral protein levels whereas inhibition of CDK1 and 2 by Roscovitine caused a dramatic reduction in the amount of all viral protein. CDK1 inhibition by RO-3306 demonstrated little effect on the levels of viral capsid proteins (VP1, 2 and 3) although did cause a modest reduction in the levels of non-structural proteins TAg and Agno, although it is unknown whether this is due to effects on protein synthesis or turnover.

These effects of these cell cycle inhibitors on the production of infectious BKPyV was then determined. As before RPTE cells were infected, inhibitors added at 24 hpi and cells harvested at 48 hpi. Viral titres were then determined by FFU assay and the data was normalised to uninhibited control samples (arbitrarily set at 1) (Fig. 5.5). While CDK4/6 inhibition by PD0332991 had minimal effects on virus synthesis, Roscovitine caused a significant and dramatic reduction in infectious virus titres by ~99%. Interestingly CDK1 inhibition by RO-3306 also reduced infectious virus production by ~68%. This level of inhibition is similar to that observed for viral DNA synthesis, although there is presumably a large excess of viral DNA in cells compared to assembled virions. These data suggest that that the activity CDK1 is important for efficient production of infectious viruses.
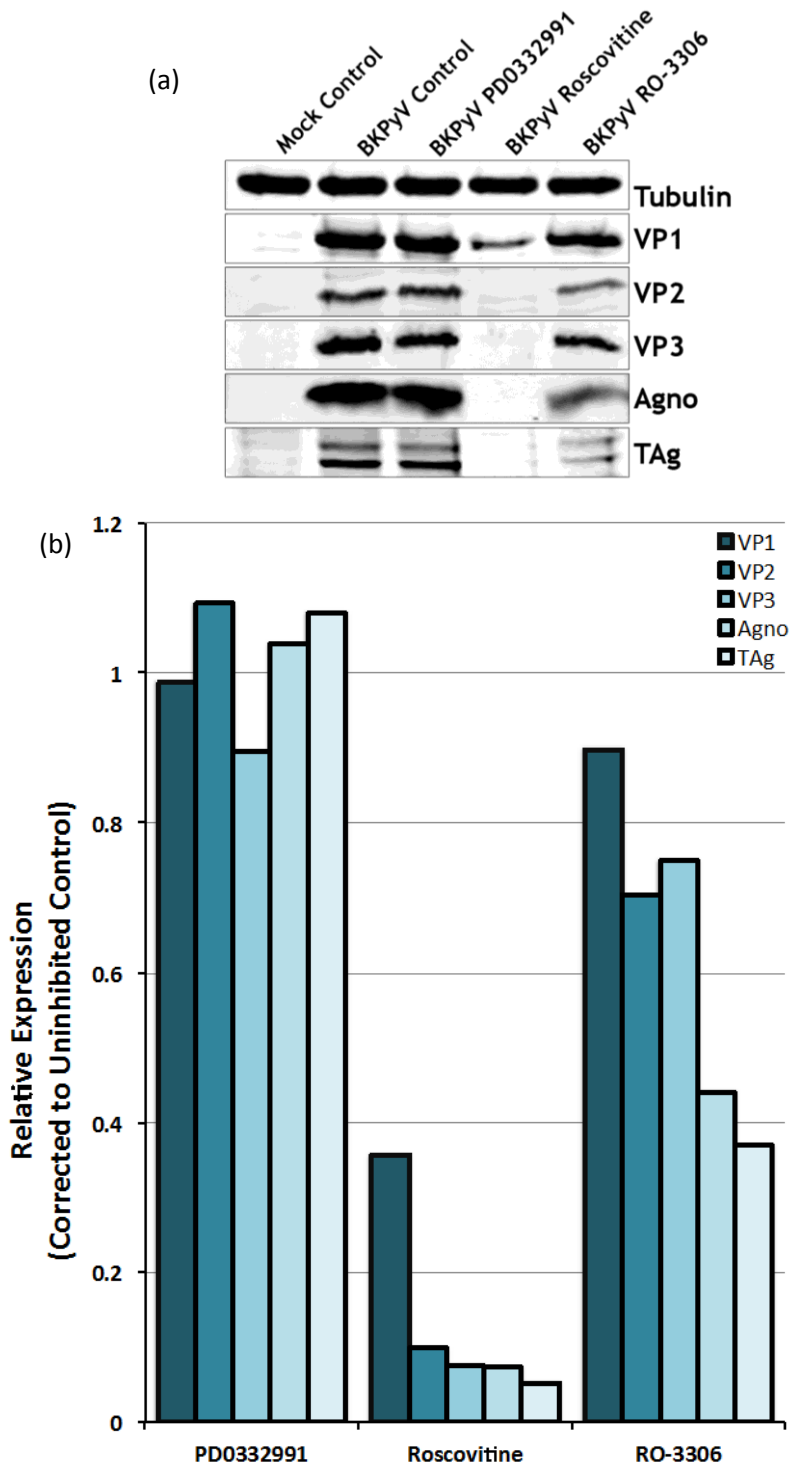
Figure 5.4: CDK1/2 inhibitor greatly affects viral protein synthesis, while CDK1 and CDK4/6 inhibitors do not.
RPTE cells mock infected or infected with BKPyV (3 IU/cell) were subjected to CDK4/6 inhibition (PD0332991 1 µM), CDK1/2 inhibition (Roscovitine 20 µM) or CDK1 inhibition (RO-3306 5 µM) from 24 hpi, and harvested for immunoblot analysis at 48 hpi. (a) Immunoblot showing the effect of inhibition on viral protein expression is shown, tubulin used as a loading control. (b) Band densities were determined using Li-Cor software, density blots show relative levels of VP1, VP2, VP3, Agno and TAg compared to uninhibited BKPyV infected control, corrected to tubulin.
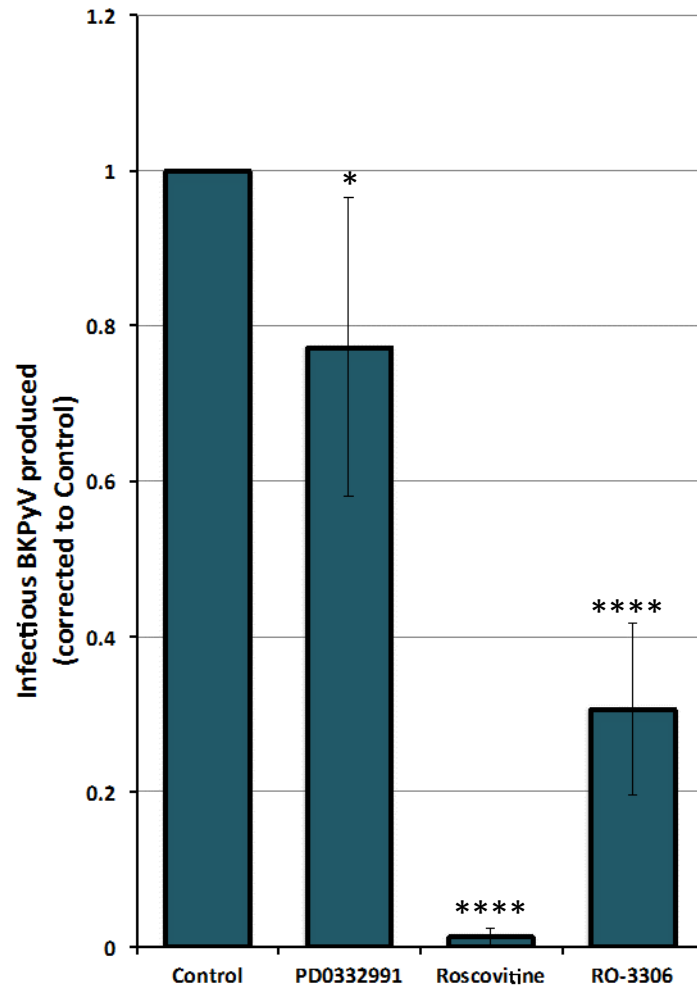
Figure 5.5: CDK1/2 and CDK1 inhibitors inhibit infectious virus production, while CDK4/6 inhibitor does not.
RPTE cells infected with BKPyV (3 IU/cell) were subjected to CDK4/6 inhibition (PD0332991 1 µM), CDK1/2 inhibition (Roscovitine 20 µM) or CDK1 inhibition (RO-3306 5 µM) from 24hpi, and harvested for analysis at 48hpi. Virus was released from cells by three rounds of freeze/thawing and infectious titres determined by fluorescent focus unit (FFU) assay, normalised to control. Data from seven independent experiments, error bars show standard deviation. *$p < 0.05$; **$p < 0.01$; ****$p < 0.0001$; ns = not significant; t-test experimental conditions versus control.

5.2.3 CDK1 inhibition impedes effective BKPyV secretion

After determining the effect of CDK1 inhibition on efficient BKPyV replication, consideration was then given to the effect CDK1 may have on non-lytic BKPyV secretion from cells. There is evidence that during mitosis GORASPs are phosphorylated, leading to fragmentation of the TGN and inhibition of conventional secretion (Preisinger et al., 2005, Colanzi and Sutterlin, 2013). RPTE cells were infected with BKPyV (1 IU/cell) and at 24 hpi inhibited with RO-3306 (5μM), or untreated, and at 48 hpi cell and supernatant virus samples were harvested separately for FFU (Fig. 5.6). For this experiment it was decided not to include inhibition with the CDK1/2 inhibitor Roscovitine as this inhibitor reduced infectious virus production so drastically (~99%) that assessing any secreted virus would be beyond the limits of detection in this instance.

After three replicates a ~70% reduction in the percentage of secreted virus was observed in RO-3306 inhibited samples in comparison to the uninhibited samples. This suggests that CDK1 activity may play a further role in viral dissemination above and beyond viral genome replication and virion assembly.
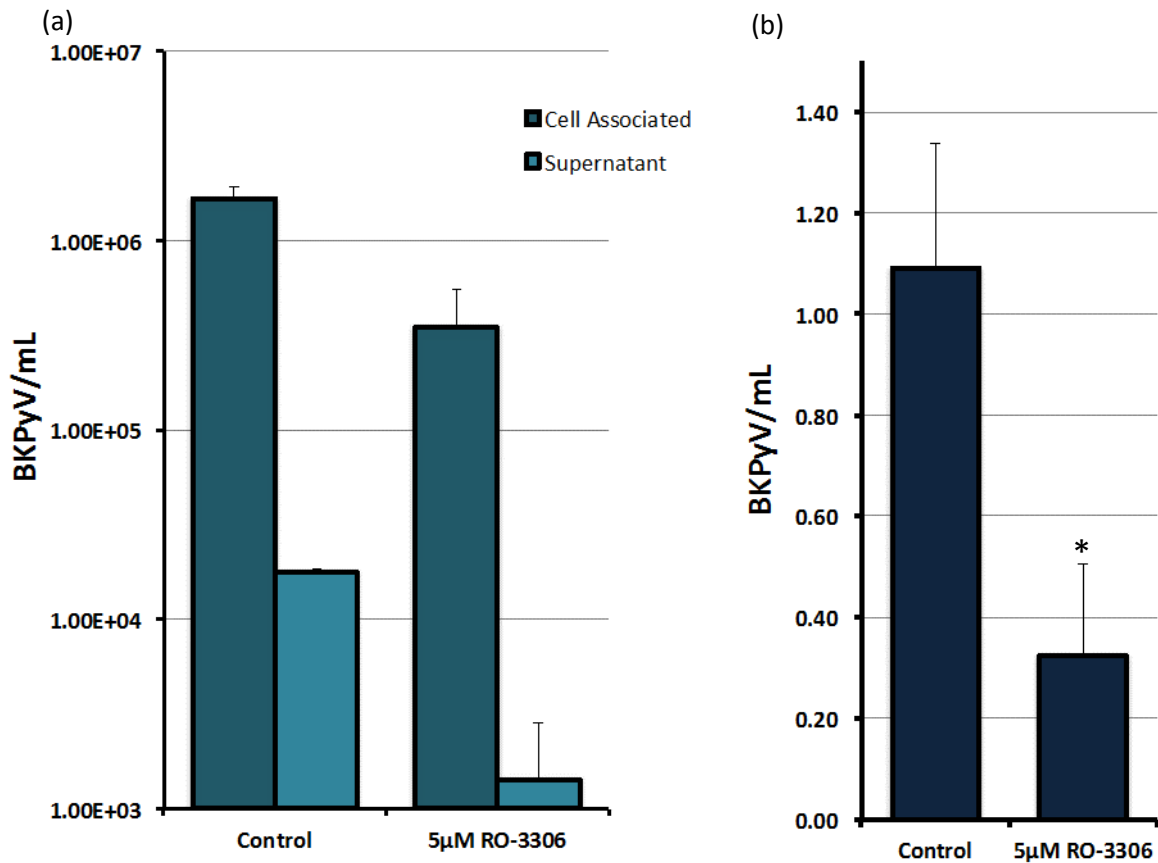
Figure 5.6: CDK1 inhibited cells show reduced levels of BKPyV secretion.
(a) RPTE cells infected with BKPyV (1 IU/cell) were either subjected CDK1 inhibition (RO-3306 5 µM) or uninhibited from 24hpi. At 48 hpi cell and supernatant virus was harvested separately, supernatant virus was pelleted by ultracentrifugation and resuspended in PBS in 1/20th of the original volume, and cell-associated virus was released from cells by three rounds of freeze/thawing. Infectious titres were determined by FFU assay. (b) The percentage of total virus released in each condition was then calculated. Data from three independent experiments, error bars show standard deviation. *$p < 0.05$ t-test inhibited conditions versus control.

5.2.4 RPTE cells of higher confluency are less able to be productively infected with BKPyV

Primary RPTE cells are contact inhibited, whereby upon approaching confluency their division rate decreases until they reach full confluence at which time they exit the cell cycle and enter G0, a state in which CDKs 4, 6, 2 and 1 are inactive. This property of primary cells can thus be exploited as another method by which to investigate the importance of cell cycle status for BKPyV infection. To investigate the effect cell confluency on the initiation of virus infection the expression of the early viral protein TAg in cells seeded at increasing densities, from subconfluent (1.25×10^4 cells per well in a 24 well plate), up to fully confluent (2×10^5 cells per well in a 24 well plate). Cells were infected the following day with 600,000 IU, equivalent of 3 IU/cell of the highest density condition and a maximum of 480 IU/cell at the lowest cell density. This should lead to 95-100% cells infected at the highest cell density. At 48 hpi cells were fixed and stained for TAg expression, along with DAPI to stain the nuclei. The percentage of cells which were expressing TAg was then calculated as a proportion of total DAPI positive cells (Fig.5.9).

These data clearly demonstrated that TAg was less readily expressed in cells which were of greater confluency, in a cell density-dependent manner. At the lowest cell density TAg was expressed in near 100% of cells, while at the highest density less than 10% were positive for TAg, far lower than the expected 95% for a multiplicity of infection of 3. This suggests cells which are contacted inhibited are less permissive to BKPyV infection, although whether TAg was unable to be expressed due to defects in BKPyV bind or entry into cells that are at high density, or whether cells had received genome but were less able to express TAg, was then investigated.
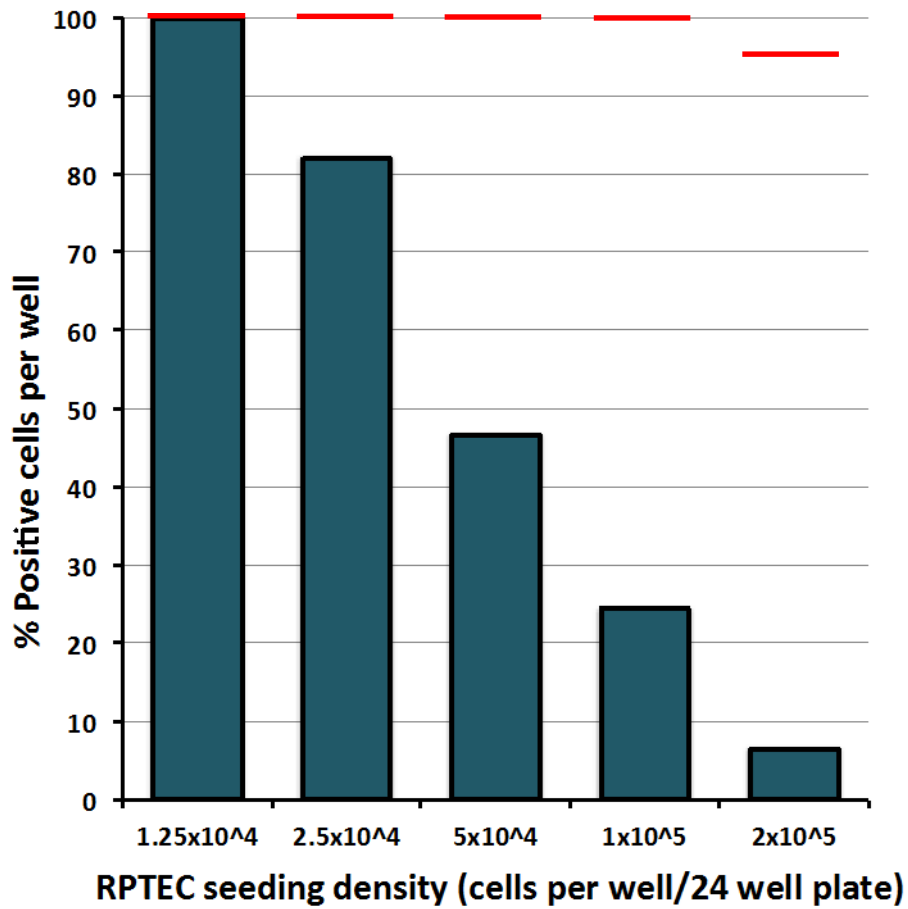
Figure 5.7: Cells at higher confluency are less permissive to BKPyV infection than expected.
RPTE cells were seeded on coverslips in 24 well plates at increasing densities, up to $2x10^5$ cells per well. 24 h later cells were BKPyV infected with 600,000 IU/well (3 IU/cell of highest density of seeding). At 48 hpi cells were fixed and stained with an antibody specific for the early gene TAg and DAPI, a nuclear marker. The number of TAg positive cells compared to DAPI-positive cells per well were then counted using images taken on an Olympus IX81 wide-field fluorescence microscope. Ten fields of view were counted per condition. Red lines representative of expected infection level determined by Poisson distribution for multiplicity of infection used in each condition.

5.2.5 BKPyV gene expression is affected by cell confluency, while genome delivery is not

To address the question as to whether BKPyV is less able to deliver viral genome to cells as they become confluent and contact inhibited, due to some physical restriction to virus binding for example, or whether BKPyV genomes are delivered to cells but viral gene expression is impaired due to changes in the intracellular environment caused by contact inhibition and exiting the cell cycle, a novel application of a classical scratch assay experiment was implemented. Scratch assays, where a section of a cell monolayer is damaged ('scratched'), are commonly used to investigate and measure cell migration. For investigating BKPyV infection, a scratch assay was employed to effectively generate two different zones within the same monolayer, one where cells are more actively replicating (the scratched zone) and one where cells are more contact inhibited (the unscratched zone), allowing direct comparison between the two zones in cells that have previously been treated equivalently (e.g infected with BKPyV). Cells were set up on coverslips at subconfluent (1.25×10^4 cells per well in a 24 well plate) or confluent (2×10^5 cells per well in a 24 well plate) densities, and the following day infected with BKPyV at 1 IU/cell, which would be expected to lead to ~63% of cells being infected. The coverslips were then either scratched immediately after infection or at 24 hpi, and then fixed for immunofluorescence at 48 hpi (Fig. 5.11a). Cells were stained with a TAg specific antibody and DAPI, while approximate boundary lines between the scratched and unscratched zones were drawn by eye due to obvious cell density differences. When drawing the boundary lines at scratch zones, the areas of each scratch were deliberately underestimated avoid include cells which may be at the scratch periphery, and so still potentially contact inhibited Example images of defined scratch zones are shown in Fig. 5.11b. All DAPI-positive and TAg positive cells were counted in ten fields of view per condition and the percentage of cells positive for TAg expression were calculated for four independent experiments (Fig.5.11c). Approximately 64% of subconfluent cells expressed TAg whether they were in unscratched or scratched zones at 0 hpi or at 24 hpi. This closely matched the expected proportion of infected cells at 1 IU/cell. However, in confluent cells it was only in the scratch zones that TAg was expressed at levels exceeding 60%, and it did not matter whether they were scratched immediately after infection or at 24 hpi. In the unscratched zones of confluent cells just 35% of cells were observed to express TAg, a significant reduction compared to the proportion of TAg positive cells in unscratched zones for subconfluent cells and the expected infection rate at 1 IU/cell.

These data suggest that BKPyV can enter and deliver its genome to a similar percentage of cells in confluent and subconfluent cells, but that expression of viral genes is substantially enhanced when cells are not contact inhibited and are actively cycling. The fact that the same effect was observed for scratch zones that were generated immediately after BKPyV infection (0 hpi) and at 24 hpi further suggests that intact BKPyV genomes can remain within cells and are not degraded for at least 24 hours

after delivery into contact inhibited cells. These data have interesting connotations for the mechanisms of BKPyV persistence in tissue, where the majority of cells would be expected to be in G0.

(a)

(b)

(c)
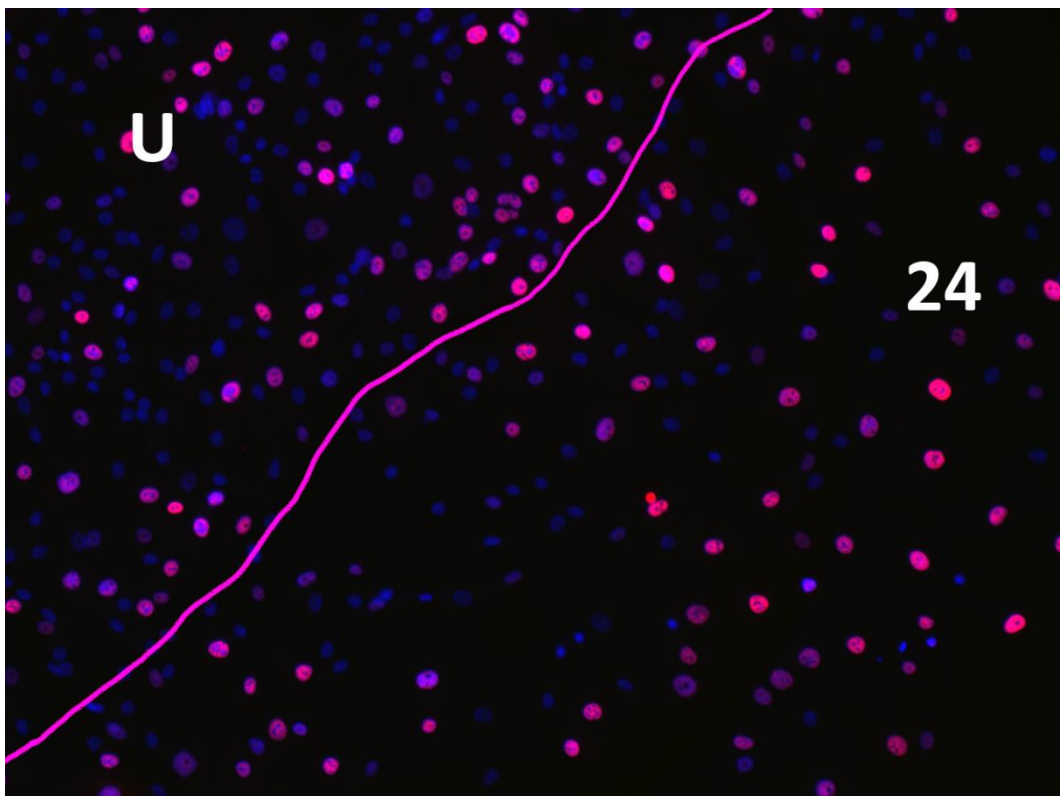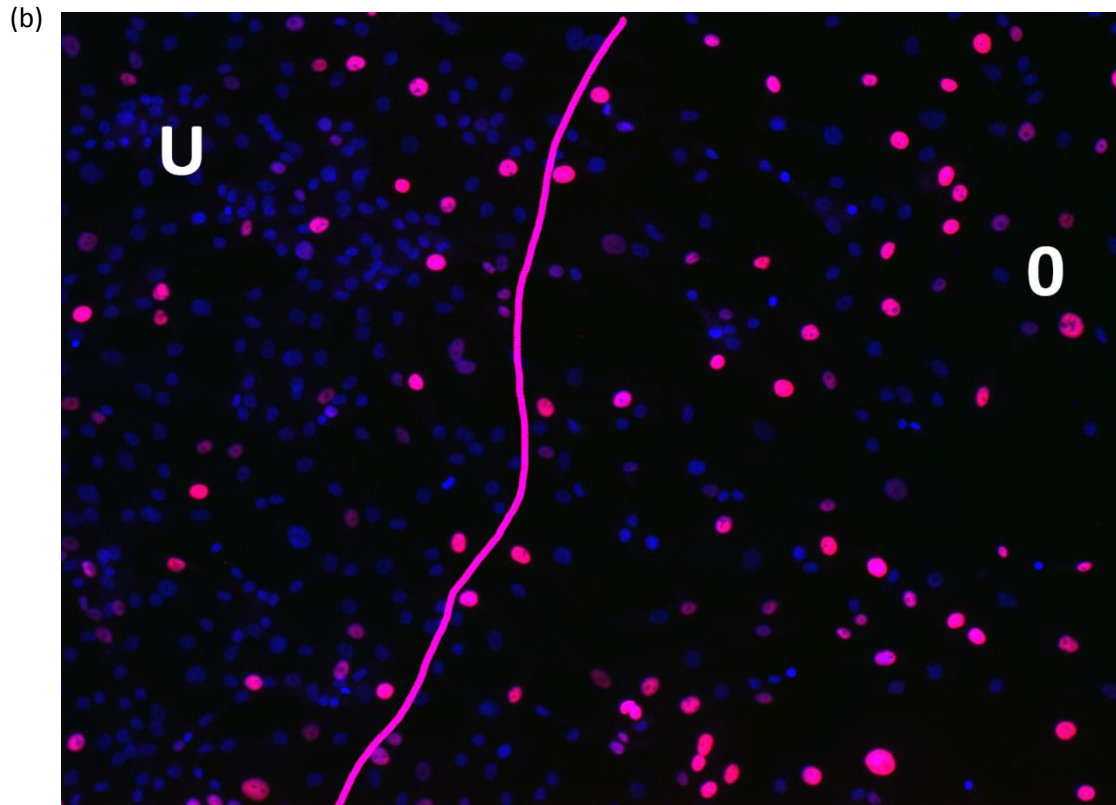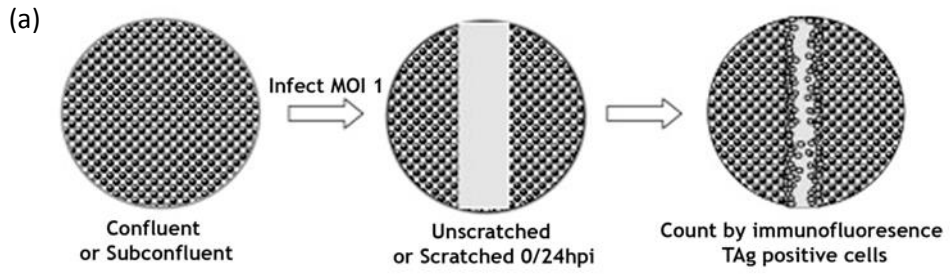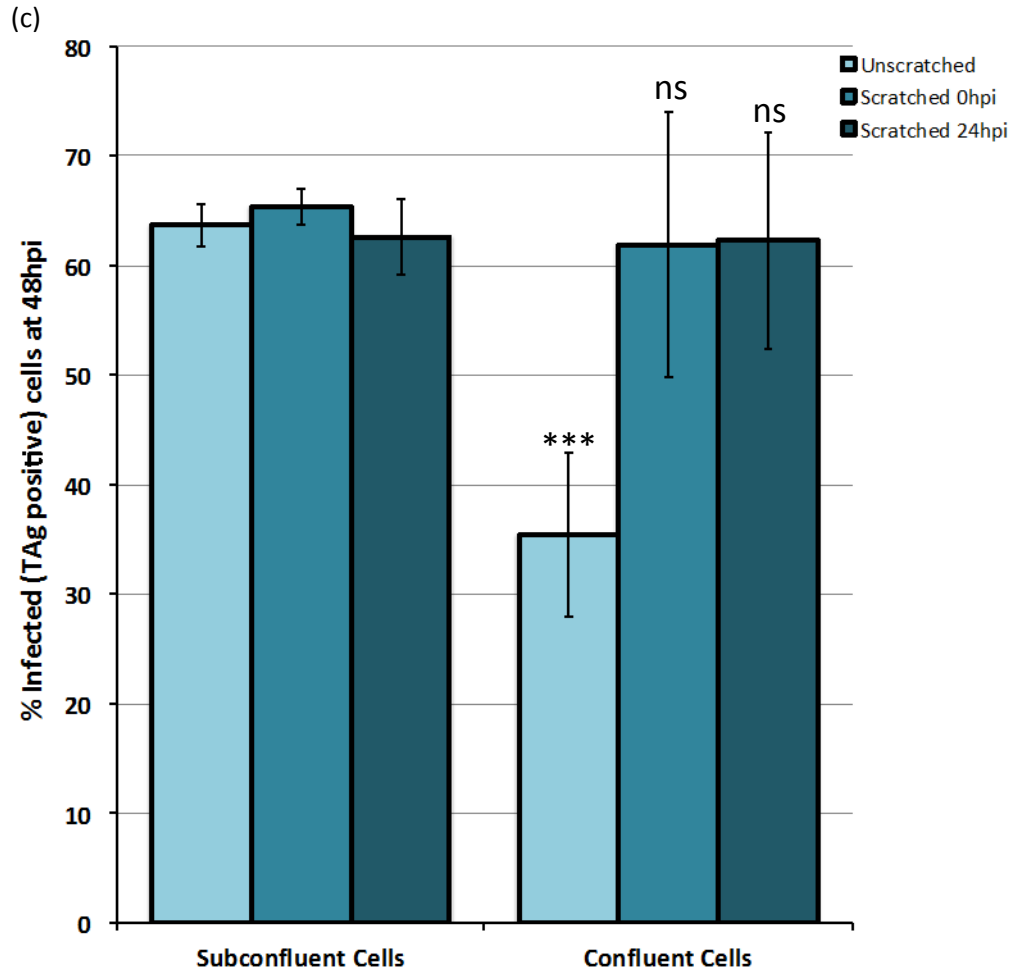
Figure 5.8: Scratch assays reveal BKPyV genome delivery appears to be unaffected by confluency, but gene expression is delayed in confluent cells.

Experimental design of the scratch assay (a). RPTE cells were seeded in 24 well plates at confluent (2x10^5 cells/well) or subconfluent (1.25x10^4 cells/well) densities. 24 h later cells were BKPyV infected at 1 IU/cell for each density. Coverslips were then either scratched at 0 hpi or 24 hpi. At 1 hpi cells were washed thoroughly with PBS and fresh media added. Cells were then fixed for immunostaining at 48 hpi. Cells were stained for TAg expression (red), and DAPI (blue) stained as a cellular marker, examples of scratch zones shown using images taken on an Olympus IX81 wide-field fluorescence microscope (b). Coverslips were counted for TAg expression, as a percentage total of cells in either the unscratched cell monolayer (U), the zone in the 0 hpi scratched monolayer (0), and the zone in the 24 hpi scratched monolayer (24), in both confluent and subconfluent conditions. Data from four independent experiments, error bars show standard deviation. ***$p < 0.001$; ns = not significant; t-test confluent cell conditions versus subconfluent conditions.

5.3 Discussion

The CDK inhibitors used in this chapter caused the expected cell cycle arrest effects in uninfected RPTE cells, although the magnitude of each cell cycle arrest was relatively small, presumably due to the slow cycling rate of RPTE cells (up to 40 hours to divide). This relatively slow rate of cell division likely prevents many cells reaching the stage of the cell cycle in which a particular CDK inhibitor is effective (G2/M for example with CDK1 inhibition) within the 24 h treatment timeframe. Unfortunately, inhibitor treatment could not be easily extended for longer than the 24 h to cause greater levels of cell cycle arrest because of cell toxicity issues, potential due to apoptosis that is induced by extended periods of cell cycle arrest. Another option to investigate cell cycle dependency of BKPyV replication would be to synchronise RPTE cell prior to these CDK inhibition experiments. However, serum starvation has little effect on RPTE cells, as the serum levels are already low in the media that is used to propagate these cells (0.5% FCS), while effective chemical synchronisation often uses CDK inhibitors such as RO-3306 and PD0332991, and using these inhibitors to synchronise cells prior to infection would confound investigation into the role of these inhibitors for virus replication.

The cell cycle status, and ability of BKPyV infection to overcome cell cycle arrest caused by chemical inhibitors, is important for BKPyV to replicate its genome, synthesise proteins, and ultimately produce infectious virions. BKPyV infection is not affected by CDK4/6 inhibition as TAg can bypass the G1/S checkpoint even in the absence of upstream cues that normally rely on CDK4/6 activity. Conversely, CDK1/2 inhibition showed a dramatic reduction in the ability of BKPyV to induce cell cycle progression through S phases and into a pseudo-G2 phase, and the synthesis of viral genomes, viral proteins and infectious virus were all significantly affected by CDK1/2 inhibition. This is likely to be due to inhibition of CDK2 primarily, as this kinase is necessary for S phase entry and progression. It must also be considered however, that Roscovitine appears to have off-target effects on CDK7 and CDK9. CDK7 and 9 are important for the initiation and completion of transcription by phosphorylating the C-terminal domain of RNA polymerase II, thus the widespread inhibition of BKPyV replication may also be somewhat attributed to an inhibition of protein synthesis (Holcakova et al., 2014). Without early viral protein synthesis there would be insufficient TAg to form a viral helicase, thus greatly reducing viral genome replication and eventually inhibiting infectious virus production. The effects of the CDK1 inhibitor RO-3306, on the other hand, are more likely to be due to reduced CDK1 activity as RO-3306 is more specific and is thought not to inhibit CDK7 or CDK9 (Kojima et al., 2009). RO-3306 had little effect on BKPyV-induced modulation of the cell cycle, and in fact RO-3306 and BKPyV infection independently lead to a similar amount of cells arrested in G2/M phase. Somewhat surprisingly CDK1 RO-3306 caused a decrease in the amount of viral genome and infectious virus production. These observations suggest that activity of CDK1, and not just cell cycle status, is important for effective

BKPyV replication, and conversely BKPyV-induced G2/M arrest cannot simply be due to virus inhibition of CDK1 activity. CDK1 activity also appeared to be important for effective BKPyV secretion, and it is tempting to speculate that BKPyV may promote CDK1 activity in the cytoplasm to enhance virus release, perhaps by phosphorylating mediators of Golgi-bypass type unconventional secretion such as GORASPs, but exclude active CDK1 from the nucleus where it would normally cause cell cycle progression into M phase and ultimately cell division. However, some caution must be exercised when interpreting the decreased proportion of virus secreted in RO-3306 treated cells because the total amount of infectious virus was also reduced by RO-3306 and it is currently unknown what effect reduced virus concentration within a cell may have on the release pathways used by the virus. Further experiments to specifically increase or inhibit cytoplasmic CDK1 activity or to analyse the effect of RO-3306 or other CDK1 inhibitors on cellular secretory pathways may shed more light on this.

The results in this chapter also demonstrate that the status of cells prior to infection is important to determine the outcome of virus genome entry. Cells which are contact inhibited, and so more likely to be in G0 and thus more refractory to virus induced cell cycle entry/progression, are less able to be infected, with a clear inverse correlation of the proportion of cells showing TAg expression with cell density. While this could be attributed to RPTE cells exiting the cell cycle once they become contact inhibited, this may equally be due to another intracellular metabolic change between subconfluent and confluent cells. However scratch tests of confluent and subconfluent cells suggests that genome is delivered to the same percentage of cells, whether subconfluent or confluent, however confluent cells are less able to initiate or support TAg expression.

In summary the data in this chapter suggests that BKPyV specifically alters the cell cycle to drive cells into S phase to enable efficient viral genome synthesis, but then to stall cells in a G2-type phase, which promotes the assembly and release of infectious virions. Furthermore, BKPyV can enter contact inhibited and actively cycling cells equivalently, but the initiation of viral gene expression only occurs when cells exit senescence and re-enter the cell cycle.

6: Concluding Remarks

6.1 Non-lytic BKPyV release from cells

The results in this thesis suggest there is an active pathway that secretes BKPyV from infected cells in a non-lytic manner. Around 1% of BKPyV progeny is released into the supernatant of cultured cells by 48 hpi without any appreciable cell death. Importantly, BKPyV secretion is specifically inhibited by the anion channel inhibitor DIDS, which perturbs anion homeostasis and leads to the formation of large intracellular vacuoles that are acidic and positive to BKPyV structural proteins. However, it is unclear why DIDS causes a specific inhibition of virus release, and whether anion homeostasis or acidic organelles are involved in the normal route of BKPyV non-lytic egress. It seems more likely that a widescale disruption of anion homeostasis by DIDS, which is active against many anion channels, may interfer with cellular secretion in a more general manner, rather than the drug specifically targeting the secretory pathway exploited by BKPyV. It is worth noting that other more specific anion channel inhibitors that were tested did not affect BKPyV secretion, and treatment with 50 µM DIDS, while not lethal to RPTE cells, is known to have off-target effects other than specific anion channels that could disrupt trafficking in a more general manner. One off target effect is the inhibition of GPHR by DIDS, as a regulator of Golgi pH it is plays an important role in acidification of the Golgi, mutations of which result in delayed proteins transport and incorrectly glycosylated proteins (Maeda et al., 2008). Furthermore DIDS appears to inhibit aquaporins at concentrations of just 10 µM (Endeward et al., 2006).

One possible explanation for the appearance of BKPyV structural proteins in large acidic vacuoles in response to DIDS could be autophagy of virion containing compartments (e.g. virus-containing ER-like membranes). Disruption of trafficking and ER stress has been shown to increase cellular autophagy (Ogata et al., 2006), and an inhibitor that disrupts trafficking of virus and causes its retention in the ER could increase such stress. These processes may account for the observed colocalisation between large DIDS positive vesicles, LysoTracker and VP2/3. Such structures were not detected with later TEM imaging of BKPyV infected cells that were not DIDS treated, suggesting they are induced by DIDS and may not be part of the BKPyV trafficking pathway. Moreover the acidic nature of these vesicles, determined by LysoTracker positive staining, suggests that they could be lysosomal. Virions autophagosytosed due to disrupted trafficking and cytoplasmic retention would then be exposed to lysosomal proteases, which could explain the exposure of VP2/3 epitopes enabling antibody binding and apparent colocalisation. LAMP1, a lysosomal and endosomal marker, was also found to colocalise with these vesicles, albeit against a more diffuse background. Caution must be exercised when interpreting intracellular VP2/3 staining as it is unclear whether this antibody would normally bind

fully intact virions, because VP2/3 is expected to be completely buried within the internal capsid structure and may be inaccessible to antibody binding. While it was demonstrated that the VP2/3 antibody binds surface virions, and non-conformational VP1 antibody (PAb597) does not, this may due to the presence of partially damaged virions causing VP2/3 exposure, and the binding epitope where the VP2/3 antibody binds remains undetermined. However, conformation-dependent VP1 antibodies also demonstrated colocalisation to these large acidic vacuoles suggesting intact virions are present in these structures. Taking these data together, the most logical explanation, is that BKPyV virions undergoing egress are mistakenly incorporated into acidic/degradative compartments, possibly via an autophagic process, leading to damage to a proportion of particles. Therefore, the presence of BKPyV virions within such acidic organelles after DIDS treatment may not actually reflect the secretion pathway normally used by this virus and acidic organelles may not be part of the route used by the virus to exit cells. However the striking conclusion remains; BKPyV is secreted from cells in a non-lytic manner which is inhibited by perturbation of anion homeostasis. This is the first time in almost 30 years that evidence for non-lytic release of polyomavirus has been established (Clayson et al., 1989, Evans et al., 2015). Such evidence is important for our understanding of the viral life cycle, in particular how BKPyV disseminates in healthy patients who appear not to experience inflammatory responses that would be expected from extensive lytic infections, but remain able to periodically shed virus (Urbano et al., 2016).

6.2 The pathway to non-lytic secretion

The observed path which newly synthesised BKPyV virions take on their route to exiting the cell appears to begin at the ER. Virions were easily observed in the lumen of smooth ER-like structures by TEM and the colocalisation of virions with the HRP-KDEL ER marker confirmed these observations. However, the mechanism by which virions can exit the nucleus and cross a membrane to gain access to the ER lumen without causing membrane damage is unclear It has been recently established that agnoprotein is important for nuclear egress of virions (Panou et al., 2018), furthermore agnoprotein is proposed to be a viroporin for some polyomaviruses (Suzuki et al., 2013). The ER is contiguous with the nuclear membrane (Hetzer, 2010), suggesting viral access to the ER could be achieved through breaching just the inner nuclear membrane, a process which could be facilitated by small pore formation. Many questions continue to remain regarding the physical process of membrane penetration of ~45nm diameter virions while keeping nuclear/ER integrity intact.

Immunofluorescence data showing of BKPyV with calnexin, an ER marker, supported the EM observations but calnexin staining was rather diffuse and made further interpretation difficult. It was

clear, however, that virions are not trafficked via the Golgi: no colocalisation by immunofluorescence was observed and disruption of Golgi trafficking by monensin did not alter the secretion of BKPyV. As such, BKPyV is appears to be secreted by an unconventional secretion pathway, potentially in a similar pathway to 'Golgi-bypass' secretion (Gee et al., 2011, Jung et al., 2016). Individual BKPyV virions were observed in small single-membraned vesicles, and canonical autophagy pathways do not appear to be involved in BKPyV secretion. The nature of these vesicles remains intriguing, they could be derived from ER but did not contain detectable HRP marker when imaged by TEM in KDEL-HRP expressing cells. This could be due to the efficiency of ER retention of the HRP-KDEL preventing this marker being incorporated into virion-containing vesicles, or could be due to tight apposition of the virion 'cargo' with the transport vesicle membrane excluding sufficient HRP so that it is below the detection sensitivity in such small tightly bound vesicles. The origin of these vesicles is evidently key to determining the pathway by which BKPyV is being secreted. Colocalisation observed through immunofluorescence of GORASP1 and GORASP2, both Golgi cisternae tethers whose tethering abilities are regulated via phosphorylation by CDK1 and other kinases (Lowe et al., 1998, Preisinger et al., 2005), with BKPyV conformation-dependent antibodies suggests that the transport of virus-containing vesicles could be mediated by these tethers. One note of caution regarding the observed virion containing vesicles near the cell periphery is the possibility of these vesicles representing incoming virus that have undergone endocytosis, although experiments with neutralising antibodies conducted for this thesis suggests this isn't the case. To further address this concern, TEM experiments could be conducted where the extracellular media and/or plasma membrane is labelled, with a HRP marker for example, from 24-48 hpi, to investigate whether these virion-containing vesicles are of plasma membrane origin. In addition, further understanding of the mechanism by which virions are neutralised by conformational-dependent VP1, whether they prevent BKPyV infection by inhibiting virion binding and entry, or simply inhibit uncoating, could address some of these concerns.

The discovery that BKPyV can be released from infected cells by non-lytic secretion via an unconventional secretion pathway adds further to the growing number of viruses which hijack novel cellular pathways to aid their dissemination (Bird and Kirkegaard, 2015).

6.3 The role of GORASPs in BKPyV secretion

While the role of GORASPs as tethers for the Golgi cisternae is well studied there has been limited understanding in their role as tethers during unconventional secretion (Ramirez and Lowe, 2009). Upon ER stress GORASPs have been shown to relocalise to the ER and become associated with vesicles trafficking directly to the cell surface (Gee et al., 2011, Jung et al., 2016). The hypothesis that BKPyV

might also be trafficked in such a way is the first description of this pathway being used for viruses, having been only described previously for membrane bound proteins (Gee et al., 2011, Jung et al., 2016). As such it is important to investigate the role which GORASPs might play during virus egress and unconventional secretion. siRNA knockdowns were complicated by the compensatory effect of alternative GORASPs in single knockdowns, where GORASP1 expression increased in GORAPS2 knockdown cells and vice versa, while simultaneous knockdown of both GORASP1 and 2 appeared to affect cell viability in these studies, which has also been observed by other labs (Bekier et al., 2017). While undoubtedly a difficult process to optimise, more success to identify the source of the single–membraned vesicles could be made through isolation and purification of them through fractionation experiments, followed by proteomic analysis to ascertain their composition. Another possibility would be immuno-isolation using GORASP1 and 2 antibodies to isolate those proteins and vesicles associated with GORASP1 and 2, comparing BKPyV infected and mock infected cells, as has been conducted previously with circulating exosomes (Caby et al., 2005).

It is interesting to note that CDK1, active during mitosis, phosphorylates GORASPs leading to fragmentation of the Golgi that is important for even distribution of this organelle into the daughter cells, and this study has shown CDK1 expression is induced during BKPyV infection. Furthermore, inhibition of CDK1 by RO-3306 caused a specific reduction in the proportion of infectious virus secretion, in addition to an overall reduction in total production of infectious virus. Therefore, one hypothesis is that CDK1 overexpression during BKPyV infection leads to phosphorylation of GORASPs and untethering from the Golgi followed by their relocalisation to the ER, which could also be stimulated by the ER stress due to the presence of virions within the ER lumen. If so this may be an effect on just a small population of total GORASPs because the Golgi complex appears to remain intact in infected cells. Such a process may promote the formation of vesicles containing single virions, and subsequent trafficking to the plasma membrane.

6.4 The proteomes of two primary cell types and BKPyV infection

By implementing TMT-based MS[3] mass spectrometry technology the proteomes of two primary epithelial human cell types have been revealed, highlighting changes induced by BKPyV infection in these two BKPyV permissive cells. Not only should this comprehensive study prove useful for the study of renourinary cell biology, but these data should also be invaluable as a resource for future BKPyV research. A wide variety of protein hits modified in infected cells were validated by immunoblot or immunofluorescence microscopy, giving confidence that our data set was robust and valid. Surprisingly few changes were identified, when taking $p < 0.0005$ significance as a cut off for proteins

of interest. Of course, with such a large data set generated there are different choices that can be made when considering significance of observed differences in protein abundance when analysing the data. Alternative thresholds for significance that could have been implemented, for example simply greater than 2-fold changes in abundance across all time points and both cells lines. This differs from the analysis in this thesis in that it would fail to take into account the signal:noise ratio for low abundance peptides. This might result in the inclusion of proteins which were identified as changing in abundance more than 2-fold, but in reality measured peptide abundance might change from 4 individual peptides identified, to 9 peptides. Whilst this represents a greater than 2-fold increase, it is unlikely to be of interest. However, if this greater than 2-fold change cut off were implemented for this study the number of proteins analysed for their changes in abundance would nevertheless remain less than 5% of the total proteomes identified.

Of more interest might be the experimental design, given the opportunity to repeat such an experiment further controls could be added. One example could be studying the two cell types independently of one another, allowing the inclusion of a greater range of time points and at later times. This could identify if, at very late times during BKPyV infection, cell responses to infection are reduced even further or new pathways are activated, such as apoptosis or other cell death pathways. Although the benefits of such a study might be limited, given our understanding of the limited responses made by these cell types even at 72 hpi.

The detection of a novel TAg peptide could be an important discovery which needs further investigation. The identified peptide should not be generated by trypsin cleavage of the canonical BKPyV large T antigen, or the published splice variant Trunc-TAg (Abend et al., 2009b), because there are no lysine or arginine residues immediately upstream of the N-terminus of this peptide in the amino acid sequences of these known TAg proteins. The most logical explanation is the presence of a further TAg splice variant that places the identified peptide downstream of a trypsin cleavage site, although this requires experimental validation. TAg has been described to play a number of roles, ranging from cell cycle stimulation and p53 binding, to its role as a viral helicase (Lilyestrom et al., 2006). Both Trunc-TAg and this potential novel splice variant of TAg may function in controlling these various TAg roles, with one or either of them modulating these activities due to alternative subcellular localisation or different binding affinities for cellular interactors. Generating recombinant viruses lacking these TAg splice variants will be important for investigating these possibilities.

6.5 BKPyV infection induces limited and specific proteome changes

Of those pathways identified as significantly altered by infection in both cell types, cell cycle and cell cycle related processes dominated, although the apparent lack of induction of innate immune responses was perhaps the most surprising. The apparent absence of any antiviral responses correlates with the lack of IRF3 phosphorylation and activation in BKPyV infected cells. Surprisingly, this does not appear to be due to any viral activity that directly antagonises the IRF3 activation because infection with BKPyV does not inhibit IRF3 phosphorylation in response to artificial DNA or RNA mimics. This suggests that BKPyV can completely hide itself from detection by pathogen recognition receptors that activate IRF3 despite causing cells to synthesise large amounts of foreign (viral) DNA, RNA and protein. This may reflect the extensive co-evolution of polyomaviruses with their hosts leading to these viruses developing a sophisticated mechanism to evade detection. Further investigation into NFκB activation in response to infection would be interesting to confirming whether lack of immune stimulation is true for other arms of innate immune response pathways. It is also worth noting that these experiments were conducted at high multiplicity of infections to ensure the majority of cells were infected for the proteomic analysis. Therefore, it is conceivable that a lower multiplicity of infection might lead to IFN signalling to neighbouring uninfected cells. However, the lack of any IRF3 phosphorylation or translocation to the nucleus suggests that IFN expression would not be stimulated in the infected cells, and previous data have suggested little-to-no activation of ISGs in cells infected with BKPyV at low multiplicity of infection. Furthermore, studies of global transcriptome changes in RPTE cells with low multiplicity (0.03) BKPyV infections show that even by 9 dpi few innate immune protein changes were observed (Assetta et al., 2016).

It is, however, clear that BKPyV is detected by the adaptive immune system, patients show seroconversion for VP1 epitopes (Kean et al., 2009, Viscidi et al., 2011) and infection is controlled by CD8+ T cells and antibody-secreting B cells, without which greatly increased levels of viral replication are seen, often leading to PVAN and renal failure (Binggeli et al., 2007, Comoli et al., 2008, Egli et al., 2009). This activity would rely heavily on APCs and associated peptide presentation and is clearly inefficient as BKPyV is rarely cleared by even healthy patients, as such it would be interesting to undertake plasma membrane profiling of BKPyV infected cells, compared with mock infected, to observe any effects on immune-related receptors such as MHC-I and NK receptors. Such localisation canges would not be detected by our whole cell proteome analysis. Indeed certain MHC mutations have been implicated in BKPyV reactivation in transplant patients suggesting that MHC play a role in viral restriction (Tonnerre et al., 2016).

One observation that could be worth investigating further is the small (< 2-fold) changes in the expression of IFIT proteins observed in HU cells, which may suggest a low level of IFN signalling in these cells. This was not studied further at the time, partly due to the difficulties in culturing HU cells, and also because relatively small changes in total peptide expression were observed which were only for IFIT proteins and not for other ISGs. It would be interesting to investigate activation of IRF3 and NFκB and IFN production in these cells response to BKPyV infection and sensing of exogenous nucleic acid.

Compared to the lack of any antiviral responses, the observed changes to cell cycle modulation causing a pseudo-G2/M-like arrest was less surprising. It has been well established that both TAg and tAg induce cell cycle progression through the G1/S checkpoint due to their actions on Rb and PP2A (Stubdal et al., 1997, Sowd and Fanning, 2012, Pallas et al., 1990), and further that members of the closely related *papillomaviridae* cause cells to undergo G2 arrested during infection (Davy et al., 2002). The benefit of G2 arrest for the virus is intriguing; arrest in S phase, a phase which favours DNA synthesis, would appear more beneficial for virus genome replication. However, G2 phase proteins where more highly upregulated than S-phase proteins. This suggest that certain properties of G2 phase proteins may play a role in efficient viral replication.

The data in this thesis has also shed more light on the mechanism of p53 regulation during BKPyV infection. While TAg has been suggested to be the main effector on p53 activity (Doherty and Freund, 1997), when validating observed proteomic changes on Mdm2 and p53 it became evident that TAg expression alone is insufficient to drive the increase in p53 expression that is observed during infection. Interestingly, TAg expression by transfection, combined with G2 arrest through CDK1 inhibition, increased p53 expression similar to that elicited by full BKPyV infection. This not only suggests that interaction of TAg with p53 to displace Mdm2 stabilises existing p53, but that another activity that is stimulated in G2 causes increased p53 synthesis which can also be stabilised by TAg. This may be related to ATM/ATR kinase activation as it is expected that a viral induced DNA damage response might also induce an equivalent response (Verhalen et al., 2015). Effects of ATM/ATR kinase activation by DNA damage on p53 levels in TAg expressing cells (by transfection) could be investigated; subjecting TAg transfected cells to DNA damage by ionising radiation would mimic the DDR induced during viral infection and may induce p53 levels to increase in cells much like CDK1 inhibition attained. This might help elucidate the various cellular states necessary for increased p53 synthesis during infection, as TAg expression alone is not sufficient to greatly increase p53 levels.

6.6 The importance of CDK1 activity in BKPyV infection

Inhibition of CDK1 and CDK2 by Roscovitine prevents cells from progressing through S phase blocking DNA synthesis, primarily due to CDK2 inhibition, and so it is unsurprising that BKPyV infected cells which were treated with Roscovitine showed a dramatic reduction in progeny virus synthesis. These effects may also be partly due to inhibition of viral protein synthesis because of the known "off-target" effects of Roscovitine on CDK7 and CDK9, which have important roles in protein transcription initiation and elongation (Holcakova et al., 2014).

CDK1 inhibition alone by RO-3306 afforded some interesting insights into the importance of BKPyV-induced G2 arrest. CDK1 inhibition causes cells to accumulate in G2/M, while BKPyV infection also induces G2 cell cycle arrest, so it was therefore surprising that inhibition of CDK1 was detrimental to viral replication, causing a significant reduction in genome replication and infectious virus production. It is possible that there may also be off-target effects of RO-3306 as yet undescribed, although this inhibitor is used regularly to induce cell synchronisation with no noted off-target complications (Ma and Poon, 2011). To understand better the effects of CDK1 inhibition on virus replication through TAg helicase regulation phosphorylation of TAg could be studied. Phosphorylation of TAg is known to be important for protein function as a helicase (Moarefi et al., 1993), thus mutation of the suspected CDK1 phosphorylation site, T126, could be conducted although similar experiments have already been undertaken with JCPyV and SV40 so may not further the field of study greatly (Swenson et al., 1996, McVey et al., 1996).

The data in this thesis also suggest that CDK1 activity may be important to enhance viral secretion. It is known that conventional secretion is reduced to a minimum as G2 phase ends and mitosis starts to occur (Farmaki et al., 1999), and that this is mediated by CDK1 phosphorylation of GORASPs and the GORASP1 binding protein GM130 (Lowe et al., 1998, Preisinger et al., 2005). The activity of unconventional secretion in G2/M has not been investigated and it is conceivable that some unconventional secretion pathways could be unaffected or even enhanced during this cell cycle phase, for example by releasing GORASPs from the Golgi enabling them to participate in Golgi-bypass-type secretion. This may provide another example of potential pro-viral effects of G2 arrest and increased CDK1 levels during BKPyV infection, enhancement of non-lytic egress of virions. We therefore hypothesise that not only is cell cycle modulation important for ensuring cells are in the correct state for efficient viral DNA synthesis, but G2 arrest and the activity of proteins such as CDK1 are important for efficient virus assembly and non-lytic exit from cells.

6.7 A proposed mechanism for viral latency

The observations that BKPyV genomes can remain in cells without viral gene expression, at least for 24 hours, might suggest a mechanism by which BKPyV can remain silently persistent within kidneys. One hypothesis is that after virus entry viral DNA can exist in differentiated cells in an inactive state, but when such a cell is induced by an exogenous signal to re-enter the cell cycle this stimulates early virus gene expression, promoting rapid progression of the cell into S phase and turning it into a virus-producing cell that becomes stalled in a G2 state. This could also help explain why high levels of BKPyV replication are associated with kidney transplantation, where the tubular epithelium is known to undergo extensive damage, which would lead to high levels of tubular epithelial cell division to repair this region of tissue, thus promoting BKPyV replication and shedding. Many questions remain, such as the nature of the stimulus that is required to initiate early viral gene expression when a cell re-enters the cell cycle and exits senescence, necessitating further investigation. Understanding this stimulus might provide novel drug targets in those patients who are seronegative but receiving a kidney from a seropositive donor. Furthermore, this may provide evidence for true viral latency during BKPyV infection (maintenance of silenced viral genome from which viral gene expression and can be reinitiated), rather than simply subclinical replication (continual low level virus gene expression and replication).

6.8 Future work

6.8.1 Viral trafficking

A variety of important questions remain regarding the mechanisms underlying the non-lytic secretion of BKPyV. The potential role of GORASPs could be addressed by gene knockout using CRISPR/Cas9 technology rather than depletion by siRNA, although this would inevitably require the use of an immortalised RPTE cell line because of the very low passage limit of primary RPTE cells. Cas9 expressing immortalised RPTE cells could be transduced with guide RNAs to each GORASP, creating a knockout cell type for each individual GORASP or a knockout of both proteins. If deletion of both GORASP1 and 2 is deleterious to cells, siRNA knock down could be used to suppress the remaining GORASP in each single knockout cell line. This may allow cells to survive long enough for any effect on secretion of virus to be observed before potential cytotoxic effects of lacking both GORASPs. In addition analysis of global protein secretion (the secretome) in mock and BKPyV-infected cells, may shed light on whether unconventional secretion pathways are upregulated and/or conventional secretion is down regulated. Given the possible effect of G2 arrest on secretion pathways extending these analyses to cells treated with RO-3306 and other cell cycle inhibitors would be interesting

comparison. Furthermore, the effects of DIDS on cellular secretion pathways in the presence or absence of BKPyV infection may shed more light on the disruption caused by this anion channel inhibitor.

6.8.2 Proteomic analysis of BKPyV infection

While the proteomic analysis presented here has given substantial information on global protein abundance, it hasn't provided information of phosphoproteome or compartment specific proteome changes. Such investigations might reveal subtler changes to infected cells such as activation of transporters or changes in catalytic activity of proteins. Furthermore, plasma membrane proteome profiling might also determine up or down regulated cell surface proteins affecting immune responses.

Also interesting would be further investigation into the newly discovered novel TAg splice variant. By using site directed mutagenesis to knock out known and suspected splice donor sites within TAg the properties and phenotypes of such splice mutants can be studied. These TAg variants might have differential effects on global TAg expression levels, subcellular localisation, Rb modulation, p53 binding ability and helicase activity, all of which should be investigated. Of particular interest is whether such splice variants are all phosphorylated, in doing so becoming the viral helicase, to the same extent.

6.8.3 Latency and the cell cycle

The importance of the role cell cycle status plays in the establishment of infection needs to be better understood. The employment of EdU labelled viruses could be applied. 5-Ethynyl-2'-deoxyuridine (EdU) is a thymidine analogue which is incorporated into newly synthesised DNA, when used during viral synthesis EdU is incorporated into the viral genome. These viruses can be used to infect fresh (non-EdU treated) cells. The presence of viral EdU can then be detected with click chemistry; a fluorescent azide will form a covalent bond with EdU allowing detection by immunofluorescence microscopy (Strang et al., 2012). Using this method non-replicating, non-viral protein expressing, input viral genomes could be detected in cells, detecting the presence of 'latent' input viral genomes in contact inhibited non-replicating cells would advise how long BKPyV is able to remain in fully confluent cells before any gene expression can be stimulated. In addition, the use of cell cycle stimulation by extracellular stimulus such as scratch assay, addition of growth factors or overexpression of CDK1, might inform the factors which drive initial early gene expression.

This thesis has uncovered details of BKPyV lifecycle in persistently infected individuals; the non-lytic unconventional secretion of BKPyV offers a method of transmission which would elicit minimal inflammatory responses, while the minimal detected innate immune responses of kidney epithelial cells suggests initial infection is unlikely to be recognised by cytosolic viral DNA sensors. In addition, a hypothesis for viral latency is proposed whereby viral proteins are not transcribed, and genome not replicated, in non-dividing cells.

7. Materials and Methods

7.1 Materials

7.1.1 General Reagents

Plasticware and tissue culture flasks were obtained from BD Biosciences, Gibco and Techno Plastic Products (TPP).

Biochemical reagents were obtained from the following companies; Amersham Bioscience, BDH Chemicals, Clontech, Invitrogen, New England Biolabs, Promega, Roche, Sigma-Aldrich, and Thermo Fisher Scientific, unless otherwise stated.

7.1.2 Solutions, Buffers and Media

Table 7.1 General solutions, buffers, and media used in this study.

Bacterial Culture	
2TY	1.6% (w/v) tryptone, 1% (w/v) yeast extract, 0.5% (w/v) NaCl. Prepared by Department of Pathology lab technicians, University of Cambridge.
2TY Agar	1.6% (w/v) tryptone, 1% (w/v) yeast extract, 0.5% (w/v) NaCl, 1.5% technical grade agar. Prepared by Department of Pathology lab technicians, University of Cambridge.
Kanamycin	Used to select for bacteria containing plasmids that code for kanamycin resistance. Used at 30µg/ml final concentration.
Mammalian Tissue Culture	
Freezing Medium	90% fetal calf serum (FCS), 10% dimethyl sulfoxide (DMSO).
Renal Epithelium General Medium (REGM)	Primary RPTEC tissue culture medium. Renal Epithelial Basal Medium (REBM) (Lonza), supplemented with SingleQuots Bulletkit containing 0.5ml rhEGF, 0.5ml insulin, 0.5ml hydrocortisone, 0.5ml GA-1000, 2.5ml FCS, 0.5ml epinephrine, 0.5ml T3, 0.5ml transferrin (Lonza).
Supplemented Dulbecco's Modified Eagle's Medium (DMEM)	HeLa and Vero cell tissue culture medium. DMEM (GE Healthcare), supplemented with 10% FCS, 2mM L-glutamine, 100 U/ml penicillin and 100µg/ml streptomycin.
Urothelial Cell Medium (UCM)	HUC tissue culture medium. UCM (ScienCell) supplemented with 5ml Urothelial Cell Growth Supplements (UCGS) (ScienCell), 100 U/ml penicillin and 100µg/ml streptomycin.
RPTEC/TERT1 Growth Medium (HRGM)	RPTEC/TERT1 tissue culture medium. 50% DMEM (GE Healthcare), 50% Ham's Nutrient Mixture F-12 with L-glutamine and sodium bicarbonate (Sigma), supplemented with SingleQuots Bulletkit containing 0.5ml rhEGF, 0.5ml insulin, 0.5ml hydrocortisone, 0.5ml GA-1000, 2.5ml FCS, 0.5ml epinephrine, 0.5ml T3, 0.5ml transferrin (Lonza).
Trypsin/EDTA	0.05% trypsin, 0.02% EDTA in PBS.
Trypsin/EDTA Neutralisation Solution (TNS)	Used to neutralise trypsin and EDTA in HUC tissue culture, supplied by ScienCell.
Poly-L-Lysine	10mg/ml stock used at 2µg/cm^2 in HUC tissue culture, supplied by ScienCell
Protein Manipulation	
5% Stacking Gel	0.67ml stock acrylamide solution, 0.5ml 1.0M Tris-HCl (pH 6.8), 40µl 10% SDS, 40µl 10% ammonium persulfate (APS), 4µl N,N,N',N'-tetramethylethylenediamene (TEMED), made up to 4ml with dH$_2$O.

8/10/12% Resolving Gel	2.7/3.3/4.0ml stock acrylamide solution, 2.5ml 1.5M Tris-HCl (pH 8.8), 100μl 10% SDS, 100μl 10% APS, 4μl TEMED, made up to 10ml with dH$_2$O.
Blocking Buffer	5% (w/v) non-fat powdered milk (Marvel Original) in PBS-T.
Loading Buffer (5X)	250mM Tris-HCl (pH 6.8), 10% SDS, 50% glycerol, 0.05% bromophenol blue, 3.5% β-mercaptoethanol.
Lysis Buffer (mRIPA)	50mM Tris (pH 7.5), 150mM NaCl, 1% Triton X-100, 1% sodium deoxycholate, Complete Protease Inhibitors without EDTA (Roche).
PBS-T	0.1% (v/v) Tween 20 in PBS.
Protein Marker	Broad range prestained protein markers (New England Biolabs).
SDS-PAGE Running Buffer	25mM Tris base, 200mM glycine, 0.1% SDS.
Stock Acrylamide Solution	30% (w/v) acrylamide/methylene bisacrylamide solution (ProtoGel).
Immunoblot Transfer Buffer	25mM Tris base, 200mM glycine, 10% methanol.
Virus Preparation	
Buffer A	10mM HEPES (pH 8.0), 1mM CaCl$_2$, 1mM MgCl$_2$, 5mM KCl.
20% Sucrose	200mg/ml sucrose in Buffer A.
CsCl Gradient Heavy	548.3mg/ml CsCl in Buffer A.
CsCl Gradient Light	277.3mg/ml CsCl in Buffer A.
Immunofluoresence Microscopy	
Blocking Solution	0.2% gelatin, 0.01% Triton X-100, 0.02% NaN$_3$ in PBS.
Fixative	3% formaldehyde (methanol free) in PBS.
Permeabilisation and Quench Solution	50mM NH$_4$Cl, 0.1% Triton X-100 in PBS.
Non-Permeabilising Quench	2% FCS in PBS.
Cover Slip Mount	ProLong Gold Antifade Reagent with DAPI (Invitrogen).
Transmission Electron Microscopy	
Fixative	0.5% glutaraldehyde in 200mM sodium cacodylate.
Buffer	200mM sodium cacodylate.
Flow Cytometry	
Fixative	100% ethanol.
Blocking Buffer	3% BSA, 0.05% NaN$_3$ in PBS.
DNA Stain	50μl/ml propidium iodide (PI).
RNA Protease	0.2mg/ml RNAse A.
Transfection	
siRNA Transfection Reagent	Santa Cruz siRNA transfection reagent (Santa Cruz).
Plasmid Transfection Reagent	TransIT LT1 (Mirus).
Serum Free Media	OptiMEM reduced serum media (Gibco).
Tandem Mass Tagging	
Lysis Buffer	6M guanidine HCl, 5mM HEPES in proteomic grade water (Bio-Rad).
DNA Extraction	
Lysis Buffer	4M guanidine thiocyanate, 25mM Tris pH 7, 134mM β-mercaptoethanol.
Wash Buffer 1	1M guanidine thiocyanate, 25mM Tris pH7, 10% ethanol.
Wash Buffer 2	25mM Tris pH 7, 70% ethanol.
Elution Buffer	Nuclease free water.
Miscellaneous	
PBS	138nM NaCl, 2.7mM KCl, 8mM Na$_2$HPO$_4$, 1.5mM KH$_2$PO$_4$ (pH 7.4). Prepared by Department of Pathology lab technicians, University of Cambridge.

7.1.3 Mammalian Cells

Table 7.2 Mammalian cell lines and types used in this study.

Cell Line/Type	Description
Renal Proximal Tubule Epithelial Cells (RPTEC)	Primary human kidney epithelium cell, used experimentally from passage 5-7. RPTECs are the closest model that is currently available for BKPyV primary infection site *ex vivo* (Li et al., 2013) (Lonza).
hTERT Immortalised Renal Proximal Tubule Epithelial Cells (RPTEC/TERT1)	Human telomerase reverse transcriptase (hTERT) immortalised RPTEC line, obtained from (American Type Culture Collection (ATCC)).
Human Urothelial Cells (HUC)	Primary human bladder epithelium cell, used experimentally from passage 4-10. HUCs are the only other natural host cell culture system other than RPTECs available for BKPyV infection *ex vivo*.
HeLa	Human cervical cancer epithelial cell line originally isolated from patient Henrietta Lacks in 1951 (kindly provided by Prof. Paul Lehner, CIMR).
Vero	African green monkey kidney epithelial cells.

7.1.4 Bacterial Cell Lines

Escherichia coli strain DH5α was used for propagating plasmids and cloning virus.

7.1.5 Viruses

Table 7.3 Viruses used in this study.

Virus	Description
BK Polyomavirus-Dunlop (BKPyV-D)	Lab adapted BKPyV virus shown by this group to grow most efficiently in RPTE cells due, in part, to an extremely strong early promoter activity (Barcena-Panero et al., 2012). This viral strain was very kindly donated by M. Imperiale (University of Michigan).
SC16 WT Herpes Simplex Virus-1 (HSV-1)	A clinical HSV-1 strain isolated from human oral lesions (Hill et al, 1975).

7.1.6 DNA Plasmids

Table 7.4 DNA plasmids used in this study.

Gene	Plasmid	Description	Source
BKPyV–D	pGEM-BKPyV-D	BKPYV-Dunlop in a pGEM vector.	MJI
KDEL-HRP	pGEM-KDEL-HRP	pGEM vector based plasmid containing horse radish peroxidase (HRP) conjugated to a KDEL endoplasmic reticulum (ER) retention motif.	MH
TAg	pcDNA3-TAg	Large T antigen in pcDNA3 vector.	GE

Plasmids were kindly donated by M. Imperiale, University of Michigan (MJI), Gareth Evans (GE) and M. Hollinshead, Dept. of Pathology (MH)

7.1.7 Antibodies

7.1.7.1 Primary Antibodies

Table 7.5 Primary antibodies used in immunofluoresence microscopy (IF), neutralisation assays (N) and Immunoblot (IB) analysis.

Antibody	Name	Species and Isotype	Applications and Dilution	Source
BST2	11721	Rabbit	IB 1:20,000	NIH
BK Agno	GB17043	Rabbit	IF purified 1:500, IB unpurified 1:500	EG
BK VP1	B5	Mouse IgM	IF 1:50	N.Ch
	C1	Mouse IgG2a	N 1:100	N.Ch
	D11	Mouse IgG2a	IF 1:50	N.Ch
	L5	Mouse IgM	IF 1:50	N.Ch
	P5G6	Mouse	IF 1:1000, IB 1:5000	D.Gall
	PAb597	Mouse	IF 1:10	W.At
Calnexin	MAB3126	Mouse IgG2a	IF 1:200	MP
CDK1	MA5-11472	Mouse IgG2a	IF 1:100, IB 1:200	TFS
cFos	ab190289	Rabbit	IF 1:100	AC
Cyclin A2 [Y193]	ab32386	Rabbit	IF 1:100, IB 1:1000	AC
Cyclin B1 [Y106]	ab32053	Rabbit	IF 1:100, IB 1:5000	AC
Cyclin D2	ab207604	Rabbit	IF 1:100, IB 1:1000	AC
EEA1	ab2900	Rabbit	IF 1:1000	AC
Geminin	GTX116125	Rabbit	IB 1:2000	GT
GM130	610882	Mouse IgG1	IF 1:1000	BDB
GORASP1 [Grasp65]	ab30315	Rabbit	IF 1:5000, IB 1:1000	AC
GORASP2 [Grasp55]	Ab204335	Rabbit	IF 1:150, IB 1:500	AC
HSV-1 gD	LP2	Mouse IgG2a	N 1:100	A.Min
IFIT1	PA3-848	Rabbit	IB 1:2000	TFS
IFIT2	12604-1-AP	Rabbit	IB 1:1000	PT
IFIT3	SAB1410691	Rabbit	IB 1:750	SA
IFI16	ac-8023	Mouse	IB 1:800	SC
IRF3	11904	Rabbit	IB 1:1000	CST
IRF3 (S386)	ab76493	Rabbit	IB 1:5000	AC
ISG15	2758	Rabbit	IB 1:1000	CST
LAMP1	H4A3	Mouse	IF 1:100	DSHB
LC3B	ab51520	Rabbit	IB 1:2000	AC
MDM2	ab16895	Mouse IgG2a	IF 1:100	AC
	86934	Rabbit	IF 1:400	CST
MX1	37849	Rabbit	IB 1:1000	CST
p53	ab1101	Mouse IgG2a	IF 1:500, IB 1:1000	AC
SV40 TAg	PAb416	Mouse IgG2a	IF 1:200, IB 1:1000. Cross reacts with BKPyV TAg	AC
SV40 VP2/3	ab53983	Rabbit	IF 1:1500, IB 1:5000. Cross reacts with BKPyV VP2/3	AC
TGN46	AHP500G	Sheep	IF 1:200	BR
Tubulin	ab6160	Rat	IB 1:2000	AC

All antibodies were purchased from AbCam (AC), BD Biosciences (BDB), Bio-Rad (BR), Cell Signalling Technologies (CST), Developmental Studies Hybridoma Bank (DSHB), Eurogentec (EG), Gene-Tex (GT), MilliPore (MP), National Institutes of Health, USA (NIH), Protein Tech (PT), Santa-Cruz (SC), Sigma-Aldrich (SA), Thermo Fisher Scientific (TFS) or kindly donated by N. Christensen, John Hopkins (N.Ch), W. Atwood, Brown University (W.At), D. Galloway, University of Washington (D.Gall) and A. Minson, University of Cambridge (A.Min).

7.1.7.2 Secondary Antibodies

Table 7.6 Secondary antibodies used in IF, IB and Immunoperoxidase assay (IPer).

Antibody	Name	Species and Isotype	Applications and Dilution	Source
Anti-Mouse 488	A21202	Donkey	IF 1:1000	LT
Anti-Mouse 568	A10037	Donkey	IF 1:1000	LT
Anti-Mouse 647	A21236	Goat	IF 1:1000	LT
Anti-Mouse IgG1 488	A21121	Goat	IF 1:1000	LT
Anti-Mouse IgG1 568	A21124	Goat	IF 1:1000	LT
Anti-Mouse IgG2a 488	A21131	Goat	IF 1:1000	LT
Anti-Mouse IgG2a 568	A21134	Goat	IF 1:1000	LT
Anti-Mouse IgG2a 647	A21241	Goat	IF 1:1000	LT
Anti-Mouse IgM 488	A21042	Goat	IF 1:1000	LT
Anti-Mouse IgM 568	A21043	Goat	IF 1:1000	LT
Anti-Rabbit 488	A21206	Donkey	IF 1:1000	LT
Anti-Rabbit 568	A11011	Goat	IF 1:1000	LT
Anti-Rabbit 647	A21245	Goat	IF 1:1000	LT
Anti-Sheep 568	A21099	Donkey	IF 1:1000	LT
Anti-Goat 800	925-32214	Donkey	IB 1:10000	LI-COR
Anti-Mouse 680	925-68020	Goat	IB 1:10000	LI-COR
Anti-Mouse 800	925-32350	Goat	IB 1:10000	LI-COR
Anti-Rabbit 680	925-68073	Donkey	IB 1:5000	LI-COR

Anti-Rabbit 800	925-32213	Donkey	IB 1:5000	LI-COR
Anti-Rat 680	925-68076	Goat	IB 1:10000	LI-COR
Anti-Mouse HRP	62-6520	Goat	IPer 1:1000	LT

Secondary antibodies were purchased from Life Technologies (LT) or LI-COR Biosciences (LI-COR).

7.1.8 siRNA

Table 7.7 siRNA oligonucleotide sequences.

Gene	Sequence/Description	Source
ConX (Control)	AUUCUAUCACUAGCGUGACUU	D
GORASP1 Quadruplex	ON-TARGETplus SMARTpool L-013510	D
GORASP1 (Construct 1)	GAUCUCUACCACAGAAUAAUU	D
GORASP1 (Construct 2)	GAGGACUUCUUUACGCUCAUU	D
GORASP1 (Construct 3)	GAACUGACCACCACAGCUGUU	D
GORASP1 (Construct 4)	CUGGAGGUGUUCAAUAUGAUU	D
GORASP2 Quadruplex	ON-TARGETplus SMARTpool L-019045	D
GORASP2 (Construct 1)	CCACACAGUGAUUAUAUAAUU	D
GORASP2 (Construct 2)	GCAGAUACAGUCAUGAAUGUU	D
GORASP2 (Construct 3)	CAUUGGAUAUGGUUAUUUGUU	D
GORASP2 (Construct 4)	GGAGUGAGCAUUCGUUUCUUU	D

siRNA oligonucelotides were sourced from Dharmacon (D).

7.1.9 Active Drugs and Inhibitors

Table 7.8 Drugs and inhibitors used.

Drug	Description	Source
4,4'-Diisothiocyano-2,2'-stilbenedisulfonic acid (DIDS)	A broadly specific anion channel inhibitor. Solubilised in DMSO.	LT
Brefeldin A (BFA)	Inhibits transport from ER to Golgi, induces retrograde transport from golgi to ER leading to apoptosis. Solubilised in DMSO.	ELS
Cidofovir	Selective inhibition of viral DNA polymerase, inhibiting viral DNA replication. Solubilised in dH$_2$O.	SA
Cycloheximide (CHX)	Inhibitor of protein synthesis. Solubilised in ethanol.	SA
Monensin	Sodium ionophore, secretion of proteins via disruption of the TGN. Solubilised in ethanol.	SA

N-(6-methoxyquinolyl)-acetoethyl ester (MQAE)	Fluorescent intracellular indicator for Cl$^-$ used to determine changes to chloride anion homeostasis. Solubilised in dH$_2$O.	TFS
Nutlin-3	Inhibitor of Mdm2:p53 interaction	SA
PD0133922	Inhibitor CDK4 and CDK6. Solubilised in dH$_2$O.	SA
Roscovitine	Inhibitor of CDK1, CDK2 and CDK5. Solubilised in DMSO.	SA
RO-3306	Inhibitor of CDK1. Solubilised in DMSO.	SA
Wortmannin	PI3K inhibitor. Inhibits autophagosome formation from 0.1-10µM. Solubilised in DMSO.	SA

Inhibitors were purchased from Enzo Life Sciences (ELS), Life Technologies (LT), Sigma-Aldrich (SA), Thermo Fisher Scientific (TFS).

7.1.10 Immune Stimulation

Table 7.9 Immune stimulation materials.

Stimulator	Description	Source
DNA Stimulation Oligo	GGGTATATATATGCATATATATAGGG dsDNA palindromic oligomer with GGG overhangs. Shown to strongly stimulate a cGAS/STING mediated innate immune response (Herzner et al., 2015).	GE
Poly I:C	Double-stranded polyribonucleotide poly(I):poly(C).	SA
IFNα2A	Human interferon alpha-2, Type I secreted interferon produced during viral infection.	GL

Materials supplied by GE Healthcare (GE), Sigma-Aldrich, and kindly donated by the Goodfellow Lab, University of Cambridge (GL).

7.1.11 qPCR

Table 7.10 Primer and probe sequences.

Primer or Probe	Sequence	Source
PolyF (BKPyV Forward)	TGTCACGWMARGCTTCWGTGAAAGTT	TM
BKR (BKPyV Reverse)	AGAGTCTTTTACAGCAGGTAAAGCAG	TM
BK Taqman FAM (BKPyV Probe)	6FAM-TTTTGCTGGAMTTTTGYASAGGTGAAGACAGTGT-BBQ	TM
Hu TNF Sense (TNFα Forward)	AGGAACAGCACAGGCCTTAGTG	TM
Hu TNF Antisense (TNFα Reverse)	AAGACCCCTCCCAGATAGATGG	TM
TNFα Cy5 Taqman (TNFα Probe)	CCAGGATGTGGAGAGTGAACCGACATG	TM

Primers and probes supplied by TIB-MOLBIOL (TM).

7.2 Methods

7.2.1 Eukaryotic Tissue Culture and Manipulation Techniques

7.2.1.1 Cell Culture Maintenance

RPTE cells were cultured for use from passage 5-7 only in Renal Epithelial Basal Medium (REBM) supplemented with Clonetics REGM SingleQuots containing 0.5ml rhEGF, 0.5ml insulin, 0.5ml hydrocortisone, 0.5ml GA-1000 (gentamycin and amphotericin), 2.5ml FCS, 0.5ml epinephrine, 0.5ml transferring, 0.5ml T3 (triiodothyronine) all supplied by Lonza. RPTEC/TERT1 cells were maintained in 50% DMEM (GE Healthcare), 50% Ham's Nutrient Mixture F-12 with L-glutamine and sodium bicarbonate (Sigma), supplemented with SingleQuots Bulletkit containing 0.5ml rhEGF, 0.5ml insulin, 0.5ml hydrocortisone, 0.5ml GA-1000, 2.5ml FCS, 0.5ml epinephrine, 0.5ml T3, 0.5ml transferrin (Lonza). HU cells were cultured for use from passage 4-10 in Urothelial Cell Medium (UCM) supplemented with 5ml Urothelial Cell Growth Supplements (UCGS), 100 U/ml penicillin and 100μg/ml streptomycin all supplied by ScienCell. HeLa and Vero cells were maintained in DMEM (GE Healthcare), supplemented with 10% FCS, 2mM L-glutamine, 100 U/ml penicillin and 100μg/ml streptomycin. In all HU cell culturing flasks and plates were coated with 5μg/cm^2 poly-$_L$-lysine (ScienCell). All cells were maintained in a humidified atmosphere at 37°C containing 5% CO_2.

7.2.1.2 Cell Freezing and Resuscitation

Cells were harvested, re-suspended in freezing medium and aliquotted to 1x10^6 cells per freezing vial. After slow freezing at -80°C vials were transferred to liquid nitrogen for long-term storage. Individual vials of cells were resuscitated at 37°C, and then transferred to a T150 tissue culture flask containing appropriate media pre-warmed to 37°C. 24h later any remaining DMSO was removed by replacing the medium with fresh culture medium.

7.2.1.3 Cell Culture Subculturing

RPTE, RPTEC and HU cells were passaged and subcultured on a weekly basis, HeLa and Vero cells were passaged and subcultured on a biweekly basis. For RPTE, RPTEC-TERT1, HeLa and Vero cells the culture medium was removed from the cell monolayer, which was washed gently with PBS. Trypsin/EDTA was then used to detach all cells from the culture flask, incubating for approximately 10 minutes at 37°C. The trypsin was then neutralised with 10ml of media and cells harvested then centrifuged (1,400rpm, 5 minutes at room temperature).

For HU cells the culture medium was removed from the cell monolayer, which was washed gently with PBS. 16ml PBS was added to the flask, along with 4ml Trypsin/EDTA and incubated at 37°C for 1-2 minutes or until the cells completely rounded up. The Trypsin/EDTA solution was transferred to 5ml

FCS, while the flask containing cells was incubated at 37°C for a further 1 minute with no solution. Cells were then detached with a sharp knock to the flask, and 5ml of trypsin neutralisation solution (ScienCell) added. This solution was added to the Trypsin/EDTA and FCS solution. Harvested cells were then centrifuged (1,000rpm, 5 minutes at room temperature).

All cells were resuspended in fresh media and $5x10^5$ cells used to reseed a new passage, or used for individual experiments by seeding at varying concentrations diluted further in fresh media.

7.2.1.4 Cell DNA Staining for Analysis by Flow Cytometry

In order to analyse cellular DNA content of RPTE cells set up in 6 well plates; all media was removed, cells were washed once in PBS and detached from wells by adding 1ml trypsin/EDTA, incubating at 37°C for approximately 15 minutes. After detachment, the cells were pelleted by centrifugation (5,000rpm, 5 minutes at room temperature) and the supernatant discarded. The cell pellet was resuspended in 1ml PBS, further pelleted by centrifugation (5,000rpm, 5 minutes at room temperature) and the supernatant discarded. Finally the cell pellet was resuspended in 300μl PBS, before 700μl ice cold 100% ethanol was added and the sample inverted several times to ensure thorough mixing. The sample was then stored at -20°C for at least 24hrs to ensure membrane permeabilisation.

The ethanol fixed and permeabilised samples were then centrifuged (5,000rpm, 5 minutes at 4°C) and the ethanol supernatant carefully removed. The remaining cell pellet was washed twice with ice cold PBS and resuspended in 1ml PBS containing 0.2mg RNAse A and 50μg/ml propidium iodide, then incubated at 37°C for 3 hours. The sample was then centrifuged (5,000rpm, 5 minutes at room temperature), the supernatant discarded and cell pellet resuspended in 500μl PBS.

7.2.1.5 Flow Cytometry

The BD FACSCalibur Flow Cytometry System (BD Biosciences) was used to collect a minimum of 10,000 cells per sample. Doublets and debris were discriminated against using forward and side light scatter gates. Fluorescence intensity corresponding to DNA content was collected in linear mode. FlowJo (v10.5.0) was used to analyse collected flow cytometry data, utilising the Cell Cycle analysis function.

7.2.1.6 siRNA Transfection

For each transfection two solutions were created, solution A contained 50nM of siRNA and 100μl OptiMEM, while solution B contained 6μl Santa Cruz siRNA Transfection Reagent and 100μl OptiMEM. The solutions were combined and gently mixed by pipetting. The final mixture was allowed to incubate at room temperature for 45 minutes, once incubated 800μl of appropriate media was added.

The media on the cells being transfected was removed and cells were washed gently with OptiMEM. All OptiMEM was fully aspirated before the prepared siRNA mixture was added to the cells and incubated at 37°C for 5-7 hours, after which time a further 1ml of media was added.

7.2.1.7 Plasmid Transfection

Prior to transfecting the cells media in wells was changed to include 10% FCS and antibiotics were removed. For each single well transfection of a 24 well plate 0.2μg of plasmid DNA was placed in an eppendorf tube, to which 0.6μl Trans-IT LT1 incubated with 20μl OptiMEM was added. After 20 minutes incubation plasmid transfection mix was added to each well and further incubated at 37°C.

7.2.1.8 Cell Viability Assay

Trypsinised cells were incubated in trypan blue (Sigma) for 5 to 15 mins and then counted using a haemocytometer. Those cells that were blue and could not exclude the dye were scored as non-viable, while those that excluded the dye were scored as viable.

7.2.1.9 MQAE Assay

In order to test for intracellular chloride cells were incubated with 5mM MQAE for 1 hour. Cells were then washed with PBS at least five times and immediately imaged by immunofluorescence with MQAE fluorescing in 488nM channel, unless quenched in the presence of chloride.

7.2.1.10 Immune Stimulation

RPTE cells were plated at 2x10^5 cells per will in a six well plate. To stimulate with synthetic RNA (Poly I:C) or synthetic DNA (DNA Oligo) 24 hours after plating cells were transfected with 2μg/ml of synthetic RNA/DNA, using 7μl Lipofectamine diluted in 240μl OptiMEM. To stimulate with IFNα2A 24 hours after plating 10^4 U/ml was added directly to cells.

7.2.2 Virus Techniques

7.2.2.1 Production of BKPyV Stocks

BKPyV working stocks were produced using BKPyV pcDNA transfection into RPTE cells, which were 60% confluent at the time of transfection. In a T150 flask, 16.6μg of BKPyV genome was added to 10μl TransIT LT-1 (Mirus) and 1600μl OptiMEM. The resulting transfection mixture was incubated at room temperature for 15 minutes. Fresh REGM media supplemented with 5% FCS was added to the RPTE cells and the transfection mixture added. The T150 flask was incubated in a humidified atmosphere at 37°C with 5% CO$_2$ for 1 week to allow cells to grow and propagate infection between cells. After 1

week the cells were scraped up into the media, frozen and thawed 3 times. The lysed cells and released virus was then transferred to 3 new T150 flasks containing 5% FCS REGM, seeded with 1x10^6 RPTE cells. These T150 were then incubated (37°C, 5% CO$_2$) for a further 3-5 weeks, after which time the cells were harvested by scraping up into the media. The media and cell harvest was then frozen to -80°C, then thawed at 37°C (freeze/thawed) 3 times to release virus.

7.2.2.2 Purification of BKPyV Stocks

Viral lysates were adjusted to pH 7.4 with HEPES pH 8.0 then centrifuged at 8,000 x g or 30 minutes at 4°C. Once centrifuged the supernatant was saved on ice and the remaining pellet resuspended in 10ml Buffer A. The resuspended pellets were then sonicated at 50-60A for 1 minute in a cup horn sonicator. The suspension was then centrifuged at 16,000 x g for 5 minutes at 4°C. Once again the supernatant was saved on ice and the remaining pellet resuspended in 10ml Buffer A and 0.1% sodium deoxycholate and then incubated at room temperature for 15 minutes. After incubation the suspension was centrifuged again at 16,000 x g for 5 minutes at 4°C. The supernatant was saved and the pellet discarded. The saved supernatants were then combined and centrifuged over a 20% sucrose cushion at 100,000 x g for 3 hrs at 4°C. Upon centrifugation supernatant and sucrose should be discarded and a milky pellet residue remain. The milky pellet should be resuspended in 1ml of Buffer A and layered over a heavy and light CsCl gradient. The CsCl gradient should be spun at 200,000 x g for at least 17 hours at 16°C.

The top band will contain empty capsids, while the bottom band is infectious virus (Fig. 7.1). This is harvested and dialysed against Buffer A for at least 24 hours. The virus stock was then aliquoted and stored at -80°C. The sample was subsequently assayed to determine the titre of infectious virus present in the stocks.
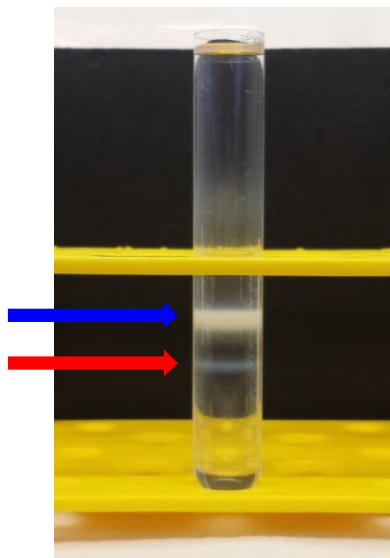
Figure 7.1: Typical CsCL gradient composition after centrifugation.
The top band (indicated with a blue arrow) contains empty capsids. The bottom band (indicated with a red arrow) contains infectious virus and must be harvested with a needle and dialysed to remove any CsCl from the virus preparation.

7.2.2.3 Fluorescent Focus Unit (FFU) Assay

In order to titre BKPyV virus in experimental samples RPTE cells were seeded at 5×10^4 cells per well in 24 well plates, and then infected with samples in a range of appropriate dilutions. At 48 hpi cells were fixed, permeabilised, quenched and blocked, then antibody stained for VP1 (PAb597 antibody). Infectious units (IU) were then calculated by counting infected cell numbers using immunofluoresence microscopy, multiplying by 341.9 fields of view at x10 magnification, thus giving an IU/ml value.

7.2.2.4 Immunoperoxidase Monolayer Assay

In order to titre HSV-1 virus in experimental samples RPTE cells were seeded at 5×10^4 cells per well in 24 well plates, and then infected with samples in a range of appropriate dilutions. Cells were fixed at 16 hpi in 4% formaldehyde in PBS for 10 minutes. Cells were then blocked with 5% FBS, 0.5% Tween 20 in PBS for 30 minutes. Cell monolayer was then incubated with HSV-1 LP2 primary antibody for 1 hour, washed thoroughly with blocking buffer and then incubated with anti-mouse HRP for a further hour. After final incubation cells were washed thoroughly with blocking buffer and then PBS. Cells were then developed with DAB peroxidase substrate (ImmPACT DAB HRP peroxidase substrate; Vector).

7.2.2.5 Infection of Cells for Fluorescence Microscopy

Cells were grown on 13mm glass coverslips in a 24 well plate, at 5×10^4 cells per well, and incubated at 37°C with 5% CO_2. The following day the cells were infected at 1 IU/cell. At varying time points post infection cells were fixed, permeabilised, quenched and blocked, preparing them for antibody staining and fluorescence microscopy. Slide were images

7.2.2.6 Infection of Cells for SDS-PAGE Analysis

Cells were seeded in a 6 well plate, at 2×10^5 cells per well, and incubated at 37°C with 5% CO_2. The following day the cells were infected at 1, 3 or 5 IU/cell. Cells were harvested at varying time points and processed for SDS-PAGE analysis.

7.2.2.7 Virus Growth Curves

To ascertain rate of viral replication in RPTE and HU cells a growth curve was conducted. Cells were seeded in a 6 well plate, at 2×10^5 cells per well, and incubated at 37°C with 5% CO_2. The following day the cells were infected at 1 IU/cell. Cells were harvested at 12, 24, 36, 48, 60, 72, 84 and 96 hpi and processed for titre analysis by FFU.

7.2.2.8 Virus Release Assay

Cells were seeded in a 6 well plate, at 2×10^5 cells per well, and incubated at 37°C with 5% CO_2. The following day the cells were infected at 1 IU/cell. Supernatant containing released virus was harvested and centrifuged (5,000rpm, 5 minutes at room temperature) to remove cell debris. Supernatant was then transferred to a new eppendorf, taking care not to disturb the pellet, and once again centrifuged (5,000rpm, 5 minutes at room temperature). The supernatant was then transferred to Microfuge Tubes TLA55 ultracentrifuge tubes (Beckman) and centrifuged in Beckman-Coulter Optima MAX-E Ultracentrifuge (100,000 x g, 2 hours at 4°C) using the TLA55 rotor. After centrifugation the supernatant was removed from the pelleted virus, and the pellet was resuspended in 70μl PBS. Cells were harvested by scraping up into in 1ml media and to release the cellular associated virus samples were freeze/thawed 3 times. FFU assays were conducted on prepared samples.

7.2.2.9 Virus Cell Surface Binding Assay

RPTE cells were grown on 13mm glass coverslips in a 24 well plate, at 5×10^4 cells per well, and incubated at 37°C with 5% CO_2. The following day cells were brought to 4°C and infected at 1 IU/cell and incubated for 1 hour at 4°C. 500μl of chilled media was then added to cells and incubated at 4°C for a further 2 hours. At 3 hpi cells were washed gently with PBS and then blocked in 2% FCS for 45 minutes. Cells were then stained with primary antibodies diluted in 2% FCS for 1 hour. Cells were then washed gently again in 2% FCS, then secondary antibodies in 2% FCS added. After a further one hour incubation cells were washed with 2% FCS and then fixed in 4% paraformaldehyde. Fixed slides were then attached to microscope slides.

7.2.2.10 Inhibitor Assays on Infected Cells

RPTE cells were seeded in a 6 well plate, at 2×10^5 cells per well, and incubated at 37°C with 5% CO_2. Cells were infected with 1 IU/cell the following day and at 1 hpi cells were washed gently with PBS and 2ml of REGM added 1 hpi cells were washed gently with PBS and 2ml of REGM added. Inhibitors were introduced at varying concentrations at 24 hpi. Cells were harvested at 48 h pi by scraping cells into the media and prepared for FFU assay, qPCR or immunoblot.

7.2.2.11 Autophagy Assays on Infected Cells

RPTE cells were seeded in a 6 well plate, at 2×10^5 cells per well, and incubated at 37°C with 5% CO_2. Cells were infected with 1 IU/cell the following day and at 1 hpi cells were washed gently with PBS and 2ml of REGM added 1 hpi cells were washed gently with PBS and 2ml of REGM added. 10nM of the autophagy inhibitor wortmannin, or 3μg/ml Brefeldin A in optiMEM to induce autophagy were

introduced at a range of times points prior to harvest. Cells and supernatant were harvested separately at 48 h pi and prepared for virus release assay or immunolot.

7.2.2.12 Virus Protein Stability Assay

RPTE cells were seeded in a 6 well plate, at $2x10^5$ cells per well, and incubated at 37°C with 5% CO_2. Cells were infected with 1 IU/cell the following day and at 1 hpi cells were washed gently with PBS and 2ml of REGM added 1 hpi cells were washed gently with PBS and 2ml of REGM added. 50ug/ml Cyclohexamide (CHX) was added at 0, 12, 24 and 36 hpi. Cells were harvested at 48 h pi by scraping cells into the media and prepared for immunoblot.

7.2.2.13 Sample Preparation for Transmission Electron Microscopy (TEM)

RPTE cells were seeded in a 35mm tissue culture dish at $4x10^5$ cells per well, and incubated at 37°C with 5% CO_2. Cells were infected at 3 IU/cell and at 72 hpi were fixed for TEM. To fix cells were brought to 4°C and washed twice with chilled PBS. Fixative was added for 30 minutes, over which time cells were slowly brought up to room temperature. Once fixed cells were washed twice with buffer, then incubated at 4°C for 4 hours. Where necessary cells were developed with DAB peroxidase substrate (ImmPACT DAB HRP peroxidase substrate; Vector). The cells were then secondarily fixed with 1% osmium tetroxide, 1.5% potassium ferricyanide for 1 hour, before being washed in dH_2O and treated with 0.5% magnesium uranyl acetate overnight at 4°C. After incubation the samples were rinsed again in dH_2O before being dehydrated in graded ethanol, the samples were then embedded in epoxy resin. Ultrathin 50-70nm sections were examined with a FEI Technai G2 Transmission electron microscope operated at 120Kv using AMT XR60B digital camera running Deben software. Samples were processed by M. Hollinshead of University of Cambridge, Pathology Department.

7.2.2.14 Scratch Assays

RPTE cells were grown on 13mm glass coverslips in a 24 well plate, at $5x10^4$ or $2x10^5$ cells per well, and incubated at 37°C with 5% CO_2. The following day cells were infected at 1 IU/cell and incubated for 1 hour at 37°C, after which time cells were thoroughly washed with PBS and fresh media added. Coverslips were then either left unscratched, scratched immediately or scratched at 24 hpi. At 48 hpi cells were fixed for immunofluorescence.

7.2.3 Protein Expression Analysis Techniques

7.2.3.1 Cell Lysate Preparation for SDS-PAGE Analysis

Cells were washed gently with PBS and then scraped into 1ml of fresh PBS. The cells were pelleted by centrifugation (5,000rpm, 5 minutes at room temperature) and the supernatant discarded. The cell pellets were lysed and resuspended in protease and phosphatase inhibitor supplemented mRIPA (lysis buffer) and incubated for 20 minutes on ice. Centrifugation (13,000rpm, 15minutes at 4°C) was used to remove cell debris and the supernatant protein samples were made up in 1x loading buffer. Each sample was then boiled for 5 minutes, or left unboiled if staining for TAg.

7.2.3.2 SDS-PAGE Electrophoresis

Once prepared the protein samples were resolved in SDS-polyacrylamide gels comprising resolving and stacking gels using the Bio-Rad Mini-PROTEAN System. In SDS-PAGE running buffer, gels were run at 170V for 1 hour. Broad range prestained protein markers (NEB) were used to identify molecular weight standards.

7.2.3.3 Immunoblot Analysis

After separation by SDS-PAGE electrophoresis proteins were transferred onto nitrocellulose membranes (0.45µm) via the 'wet transfer' method, using Mini Trans-Blot Electrophoretic Transfer Cells (Bio-Rad). These transfers were completed at 70V for 2 hours at room temperature, or overnight at 18V at 4°C. Once transferred, membranes were placed in immunoblot blocking buffer for at least 30 minutes at room temperature, followed by incubation in primary antibody for at least 1 hour at room temperature. Primary antibodies were diluted in blocking buffer. After primary antibody incubation 3x 5 minute washes with PBS-T were carried out before incubation with infrared-fluorescent conjugated secondary antibodies at room temperature for 1 hour. Secondary antibodies were diluted in PBS-T. Membranes were finally washed 6x in PBS-T for 5 minutes each, before scanning and visualization on the LI-COR Odyssey Infrared Imager. Densitometry analysis of visualised bands was conducted on LI-COR Image Studio Software (v5.2.5).

7.2.4 Fluorescence Microscopy Techniques

For standard fluorescence microscopy images were acquired using either a 60x oil immersion objective or 10x objective of an Olympus IX81 wide field microscope in conjunction with Image-Pro Plus software. Confocal fluorescence microscopy images were acquired using a 63x oil immersion objective of a Leica TCS SP5 II inverted confocal microscope in conjunction with Leica Application Suite software. Acquired images were processed using Adobe Photoshop.

7.2.5 Tandem Mass Tagging Spectrometry

7.2.5.1 Infection and Harvest of Cells for TMT Analysis

Either RPTE of HU cells set up at 3×10^5 cells per well in a 12 well plate. At 24 hpi cells were infected at 5 IU/cell. After 1 hour cells were washed with proteomic grade PBS thoroughly and fresh media added. Cells were harvested for TMT at 24, 48 and 72 hpi. To harvest cells were washed with ice-cold proteomic grade PBS, and 75µl of lysis buffer added. Cells were scraped up into an eppendorf and vortexed extensively. After 10 minutes at room temperature the lysates were sonicated on ice using the probe sonicator at 25W for 30 seconds. Lysates were then spun at 16,000 x g for 10 minutes, supernatant was carefully transferred to a fresh Eppendorf tube and centrifuged again at 16,000 x g for 10 minutes. Sample supernatants were then snap frozen in liquid nitrogen.

7.2.5.2 Whole cell lysate protein digestion

(Details provided by Weekes Lab, where this procedure was conducted)

Dithiothreitol (DTT) was added to a final concentration of 5 mM and samples were incubated for 20 mins. Cysteines were alkylated with 14 mM iodoacetamide and incubated 20 min at room temperature in the dark. Excess iodoacetamide was quenched with DTT for 15 mins. Samples were diluted with 200 mM HEPES pH 8.5 to 1.5 M guanidine followed by digestion at room temperature for 3 h with LysC protease at a 1:100 protease-to-protein ratio. Samples were further diluted with 200 mM HEPES pH 8.5 to 0.5 M guanidine. Trypsin was then added at a 1:100 protease-to-protein ratio followed by overnight incubation at 37°C. The reaction was quenched with 5% formic acid, then centrifuged at 21,000 g for 10 min to remove undigested protein. Peptides were subjected to C18 solid-phase extraction (SPE, Sep-Pak, Waters) and vacuum-centrifuged to near-dryness.

7.2.5.3 Peptide labelling with tandem mass tags and fractionation

(Details provided by Weekes Lab, where this procedure was conducted)

Desalted peptides were dissolved in 200 mM HEPES pH 8.5. Peptide concentration was measured by microBCA (Pierce), and 25 γ οφ πεπτιδε labeled with TMT reagent. TMT reagents (0.8 mg) were dissolved in 43 µl anhydrous acetonitrile and 3 µl added to peptide at a final acetonitrile concentration of 30% (v/v). Samples were labelled as follows;

126 – HU cells mock infection 24 hpi, 127N – HU cells mock infection 72 hpi, 127C – HU cells BKPyV infection 24 hpi, 128N – HU cells BKPyV infection 48 hpi, 128C – HU cells BKPyV infection 72 hpi, 129N – RPTE cells mock infection 24 hpi, 129C – RPTE cells mock infection 72 hpi, 130N – RPTE cells BKPyV infection 24 hpi, 130C – RPTE cells BKPyV infection 48 hpi, 131N – RPTE cells BKPyV infection 72 hpi.

Following incubation at room temperature for 1 h, the reaction was quenched with hydroxylamine to a final concentration of 0.3% (v/v). TMT-labelled samples were combined at a 1:1:1:1:1:1:1:1:1:1 ratio. The sample was vacuum-centrifuged to near dryness and subjected to C18 SPE (Sep-Pak, Waters). After an unfractionated singleshot quantities of each TMT labelled sample were adjusted prior to high pH reversed-phase (HpRP) so that normalisation factors were >0.25 and <1.5. TMT-labelled tryptic peptides were subjected to HpRP fractionation using an Ultimate 3000 RSLC UHPLC system (Thermo Fisher Scientific) equipped with a 2.1 mm internal diameter (ID) x 25 cm long, 1.7 µm particle Kinetix Evo C18 column (Phenomenex). This yielded combined fractions which were dried in a vacuum centrifuge and resuspended in 10 µl MS solvent (4% MeCN / 5% formic acid) prior to LC-MS3.

7.2.5.4 LC-MS^3

(Details provided by Dr. Robin Antrobus, who conducted the mass spectrometry)

Mass spectrometry data was acquired using an Orbitrap Lumos (Thermo Fisher Scientific, San Jose, CA). An Ultimate 3000 RSLC nano UHPLC equipped with a 300 µm ID x 5 mm Acclaim PepMap µ-Precolumn (Thermo Fisher Scientific) and a 75 µm ID x 50 cm 2.1 µm particle Acclaim PepMap RSLC analytical column was used.

Loading solvent was 0.1% FA, analytical solvent A: 0.1% FA and B: 80% MeCN + 0.1% FA. All separations were carried out at 55°C. Samples were loaded at 5 µL/minute for 5 minutes in loading solvent before beginning the analytical gradient. The following gradient was used: 3-7% B over 3 minutes, 7-37% B over 173 minutes, followed by a 4 minute wash at 95% B and equilibration at 3% B for 15 minutes. Each analysis used a MultiNotch MS3-based TMT method (McAlister et al., 2012, McAlister et al., 2014). The following settings were used Th, 120,000 Resolution, 2x10^5 automatic gain control (AGC) target, 50 ms maximum injection time. MS2: Quadrupole isolation at an isolation width of m/z 0.7, CID fragmentation (normalised collision energy (NCE) 35) with ion trap scanning in turbo mode from m/z 120, 1.5x10^4 AGC target, 120 ms maximum injection time. MS3: In Synchronous Precursor Selection mode the top 6 MS2 ions were selected for HCD fragmentation (NCE 65) and scanned in the Orbitrap at 60,000 resolution with an AGC target of 1x10^5 and a maximum accumulation time of 150 ms. Ions were not accumulated for all parallelisable time. The entire MS/MS/MS cycle had a target time of 3 s. Dynamic exclusion was set to +/- 10 ppm for 70 s. MS2 fragmentation was trigged on precursors 5x10^3 counts and above.

7.2.5.5 Data analysis

(Details provided by Weekes Lab, where this procedure was conducted)

Mass spectra were processed Sequest-based "MassPike" software pipeline for quantitative proteomics, through a collaborative arrangement with Professor Steve Gygi's laboratory at Harvard Medical School.

A combined database was constructed from (a) the human Uniprot database (4th February, 2014), (b) the BK polyomavirus database (6th October, 2014). The combined database was concatenated with a reverse database composed of all protein sequences in reversed order. Searches were performed using a 20 ppm precursor ion tolerance (Haas et al., 2006). Product ion tolerance was set to 0.03 Th. Peptide spectral matches (PSMs) were filtered to an initial peptide-level false discovery rate (FDR) of 1% with subsequent filtering to attain a final protein-level FDR of 1% (Kim et al., 2011, Wu et al., 2011).

Proteins were quantified by summing TMT reporter ion counts across all matching peptide-spectral matches using "MassPike", as described previously (McAlister et al., 2012, McAlister et al., 2014). Peptides meeting the criteria for reliable quantitation were then summed by parent protein, in effect weighting the contributions of individual peptides to the total protein signal based on their individual TMT reporter ion yields. Protein quantitation values were exported for further analysis in Excel.

7.2.6 DNA Manipulation Techniques

7.2.6.1 Transformation of DNA into competent *E. coli*

For the growth of pGEM-BKPyV plasmid volumes, heat shock was used to transform DH5α *E. coli.* 3μl of DNA was mixed with 50μl of competent *E. coli* and incubated on ice for 30 minutes, followed by heat shock at 42°C for 30 seconds. The transformed *E. coli* were then incubated on ice for a further 2 minutes. After incubation transformed cells were added to 200μl 2TY and shaken at 37°C for 1 hour. Samples could then be grown up to larger volumes overnight in 2TY at 37°C while shaken.

7.2.6.2 Plasmid Vector Removal

DNA plasmids were harvested from *E. coli* using the Plasmid DNA purification NucleoBond Xtra Midi kit (Macher-Nagel) as per the manufacturers instructions. BKPyV genome was cleaved from its pGEM vector backbone in 50μl reactions of 20μg DNA, 2μl BamH1 and 2μl BSA1 in BufferB incubated overnight at 37°C. After incubation pGEM vector was separated from BKPyV by 0.8% agarose gel (dissolved in TBE) with ethidium bromide, run at 100V for 2 hours in 1x TBE running buffer. 1kB plus DNA ladder (Invitrogen) was used to determine molecular weight standards. Bands were then visualised on the UV transilluminator and 5kB BKPyV bands were cut from agarose and purified using

QUAQuick Gel extraction kit (Qiagen) as per the manufacturers instructions. Genomes were then ligated in 20μl aliquots of T4 Ligase Buffer with 1μL T4 Ligase (NEB) and 17μl purified BKPyV.

7.2.6.3 Cellular DNA Harvest and Extraction

Cells were pelleted and 200μl lysis buffer added. Once incubated at 56°C for 10 minutes 200μl of 100% ethanol was added, then centrifuged through silica columns (Epoch Lifescience) at 13,000rom for 1 minute. The flow through was discarded and column washed with Wash Buffer 1 by centrifuging at 13,000rpm for 1 minute. Once again the flow through was discarded and the column washed with Wash Buffer 2 by centrifuging at 13,000rpm for 2 minutes. The column was then moved to a nuclease free eppendorf and 200μl of Elution Buffer added to the column. The DNA was then eluted by centrifuging at 13,000rpm for 1 minute. Samples were stored at -20°C.

7.2.6.4 qPCR

BKPyV genome and TNFα loads were measured by quantitative real-time PCR using HotStarTaq kits (Qiagen). Assays were performed in 20μl total reaction mixtures that contained 8μl extracted DNA sample and 12μl mastermix (Table 7.11).

Table 7.11: Mastermix total final concentrations made in MiiliQ water.

Optimised Ingredient	BKPyV	TNFα
PCR Buffer (Qiagen)	1x	1x
MgCl₂	2.5mM	10mM
DMSO	N/A	N/A
dNTPs	2.5mM	250μM
HotStartTaq DNA Polymerase (Qiagen)	0.04 U/μl	0.04 U/μl
Forward Primer	(Poly F) 300nM	(Hu TNF sense) 50nM
Reverse Primer	(BKR) 300nM	(Hu TNF antisense) 900nM
Probe	(BK Taqman Probe FAM) 50nM	(TNFα Cy5 Taqman) 50nM

Amplifications and detection were performed on a Rotor Gene RG-3000 (Corbett Research). Initial denaturation and polymerase activation was at 95°C for 15 minutes, followed by 45 cycles of denaturation at 95°C for 15 seconds, and elongation at 60°C for 1 minute. Each experiment was conducted in triplicate, with the threshold cycle value for each sample and copies per sample obtained using Rotor Gene Software v.6 (Corbett Research).

8. Appendix

8.1 Figures
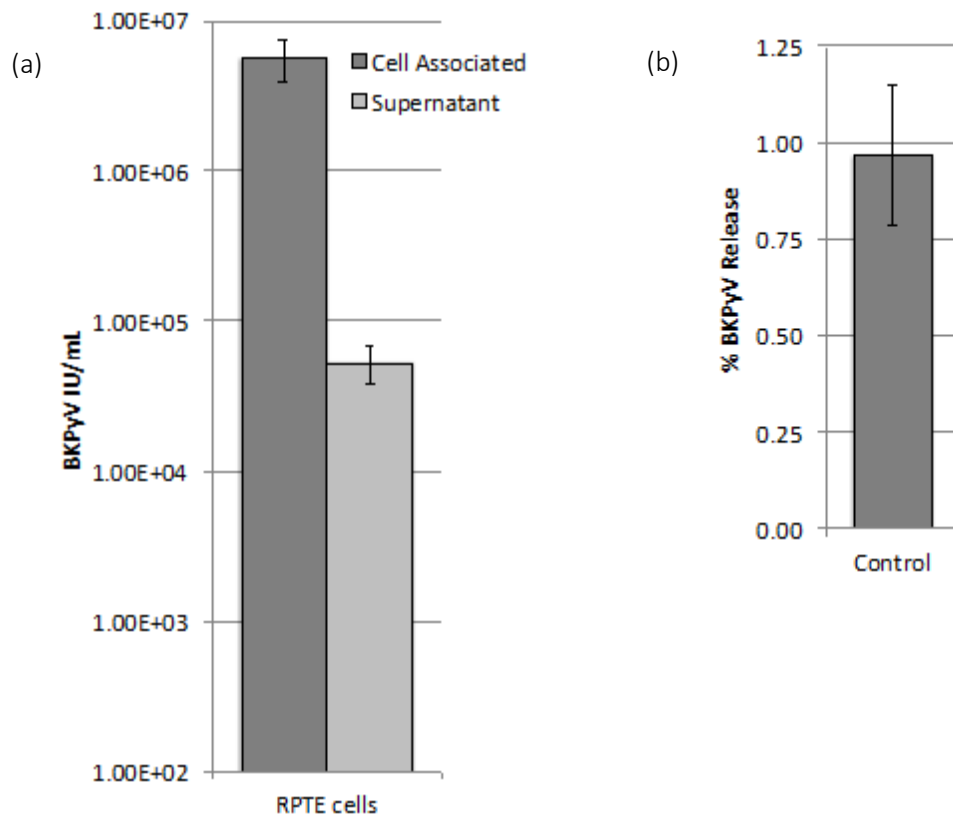
Figure S1: Infectious BKPyV release from RPTE cells conducted by Dr G Evans.
The levels of BKPyV secretion in uninhibited cells was determined prior to the start of this PhD. RPTE cells were BKPyV infected at 1 IU/cell. At 48 hpi supernatant media and cell associated virus were harvested independently. To determine the virus concentration in each harvest an FFU assay was conducted (a). The percentage of released BKPyV was determined (b). Error bars show standard deviation; 6 independent experiments.

(a)

(b)
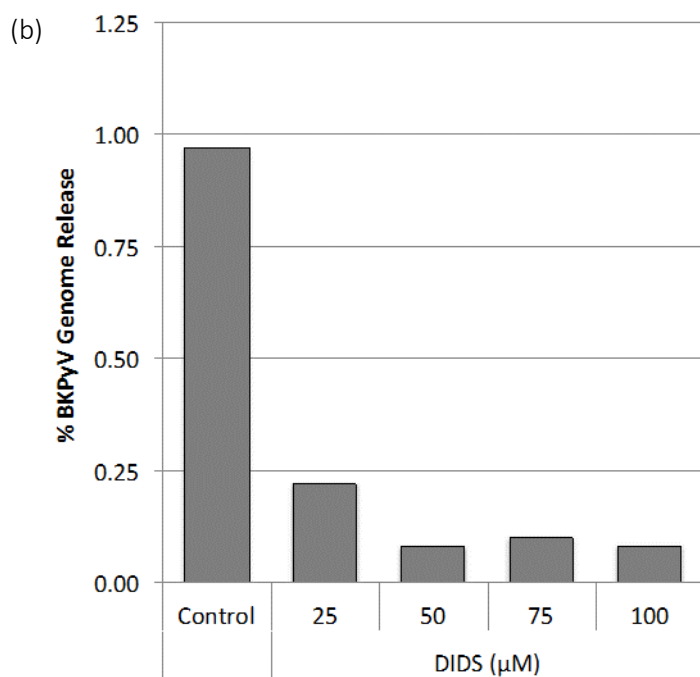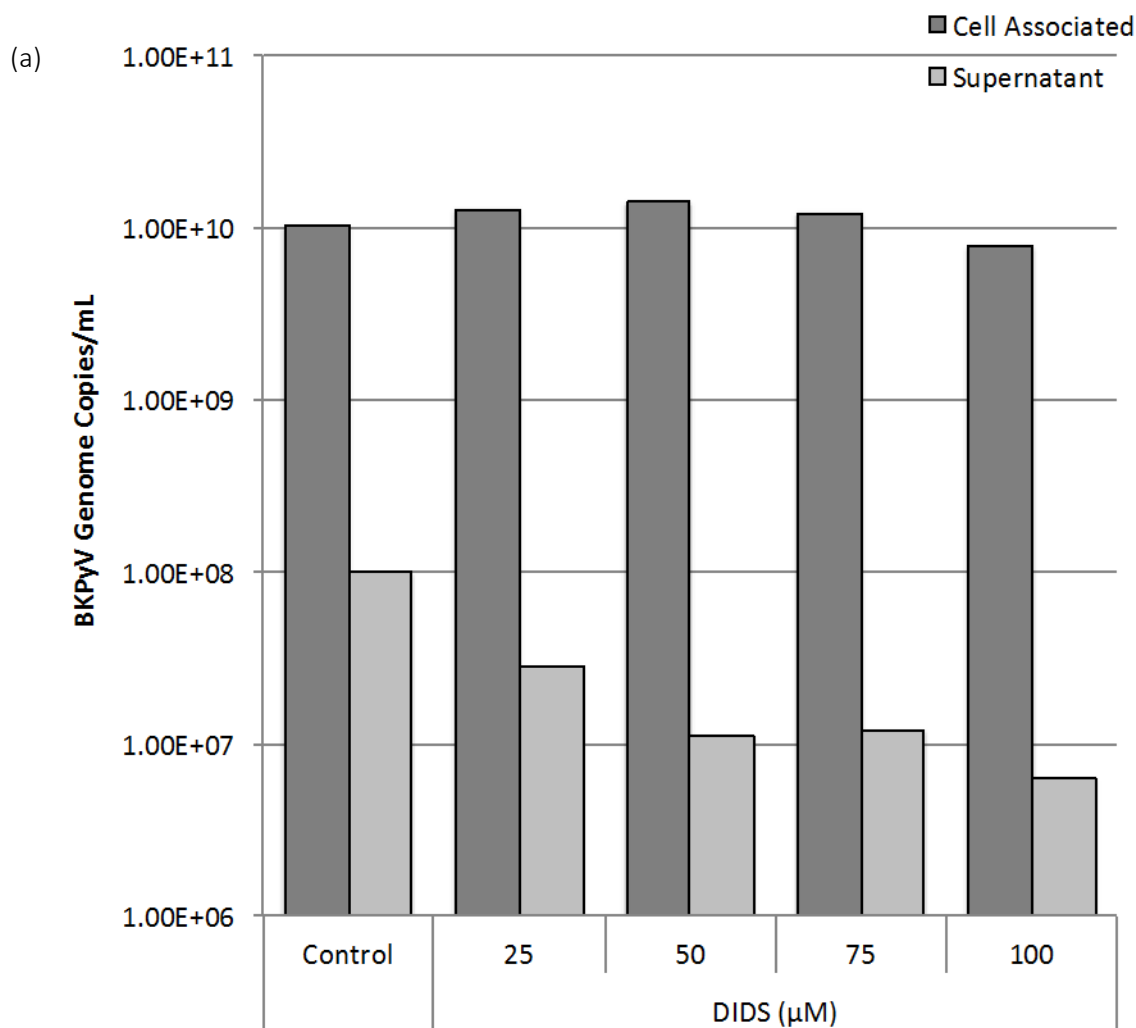
Figure S2: BKPyV genome release from RPTE cells conducted by Dr. G Evans.
The effect of DIDS on BKPyV genome secretion was determined prior to the start of this PhD. RPTE cells were BKPyV infected at 1 IU/cell and treated with DIDS at increasing concentrations, or DMSO as a control, at 24 hpi. At 48 hpi supernatant media and cells were harvested independently. Genome levels were detected from each sample using qPCR and analysed using Rotor-Gene (a). Percentage of BKPyV genomes released were then calculated (b).
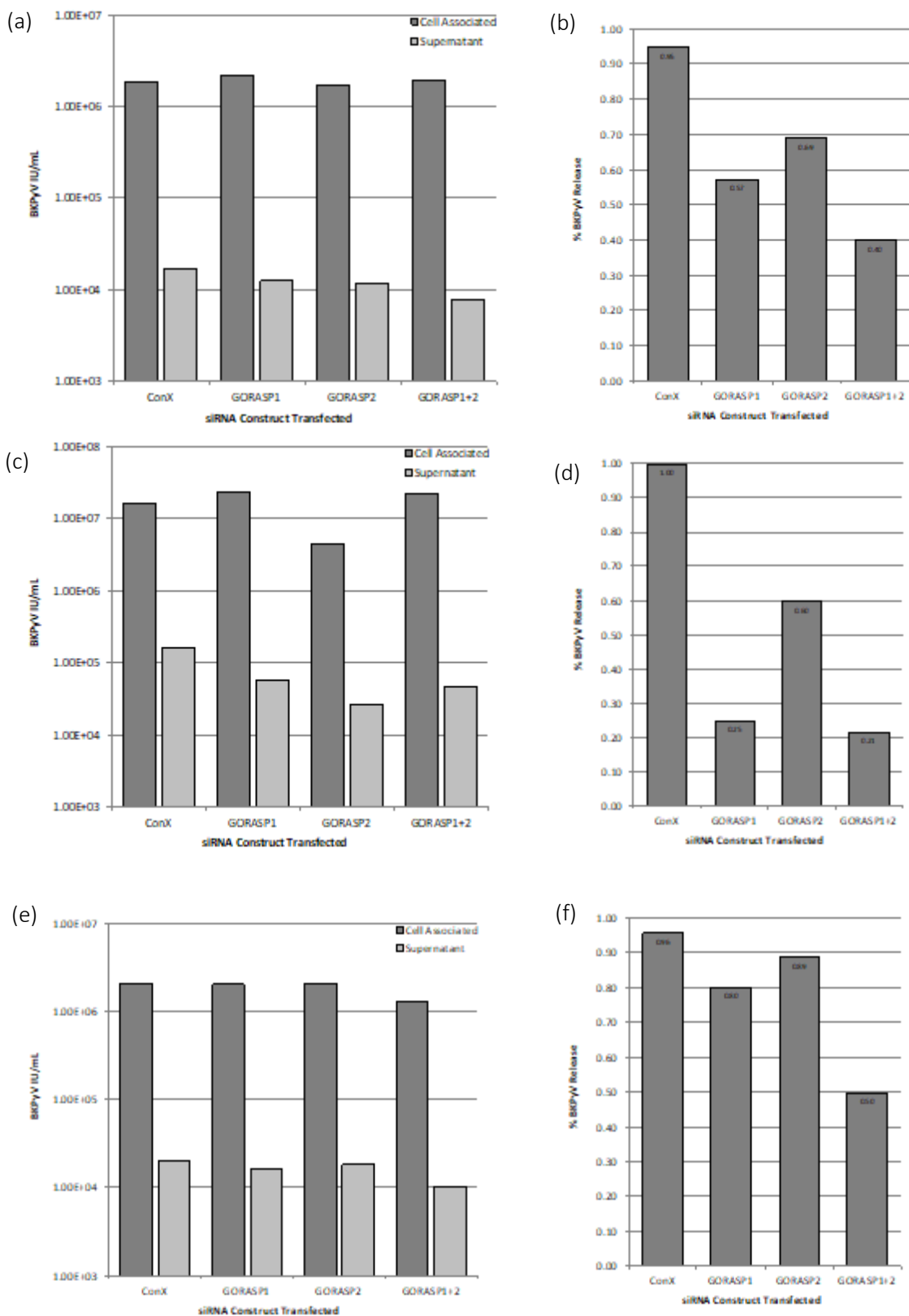
Figure S3: GORASP siRNA knockdown; individual experiment data.
RPTE cells were treated with double 100mM siRNA knockdowns of GORASP1, GORASP2, a combination of GORASP1 and 2, or ConX as a control for 96 h. Cells were infected with BKPyV (1 IU/cell) after 48 h of siRNA treatment and at 48 hpi cells and supernatant were harvested separately for FFU assay of viral titre. (a & b) Experiment 1; (c & d) Experiment 2; (e & f) Experiment 3. Combined summary data (Fig. 3.10).

(a) RPTE cells; 24 h.
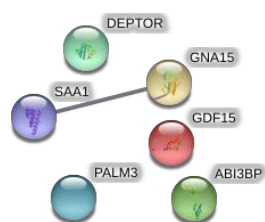
(d) HU cells; 24 h.
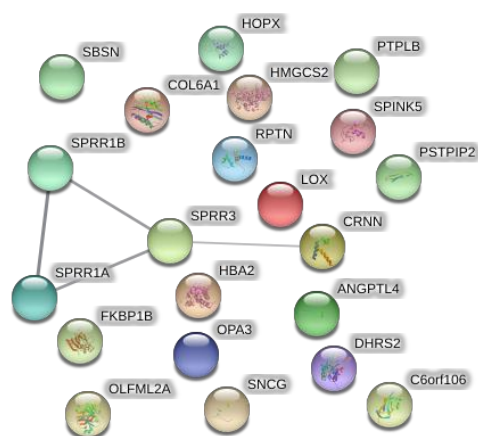
(b) RPTE cells; 48 h.
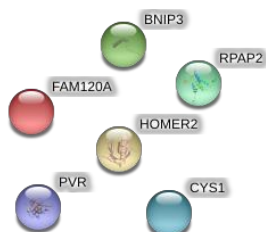
(e) HU cells; 48 h.
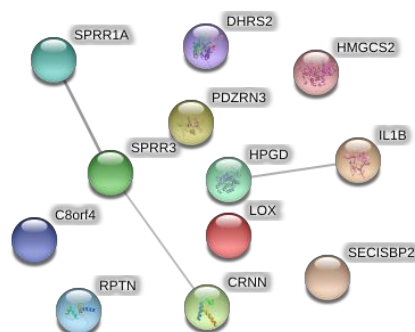
(c) RPTE cells; 72 h.
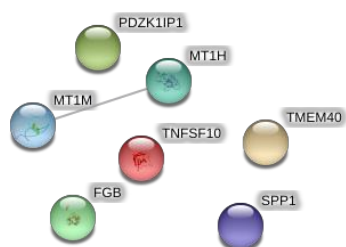
(f) HU cells; 72 h.
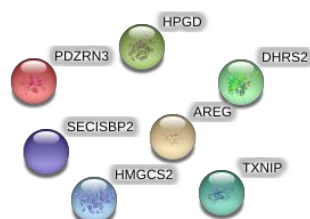
Figure S4: STRING analysis of most significantly (p < 0.0005) down regulated proteins in RPTE and HU cells.
Those proteins that were observed to be decreased in abundance RPTE (a, c & e) or HU (b, d & f) cells at each time point (as shown in Fig. 4.4) were analysed using Search Tool for the Retrieval of Interacting Genes/Proteins (STRING). STRING analysis shows each protein represented as a spot, with connections made between proteins representing known and predicted protein-protein interactions, the heavier the connecting line, the more confidence in the interaction based on experimental, co-expression, co-occurrence, gene fusion, textmining or neighbourhood evidence.

(a) RPTE cells; 24 h.
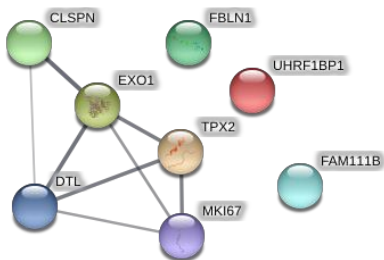
(b) RPTE cells; 48 h.
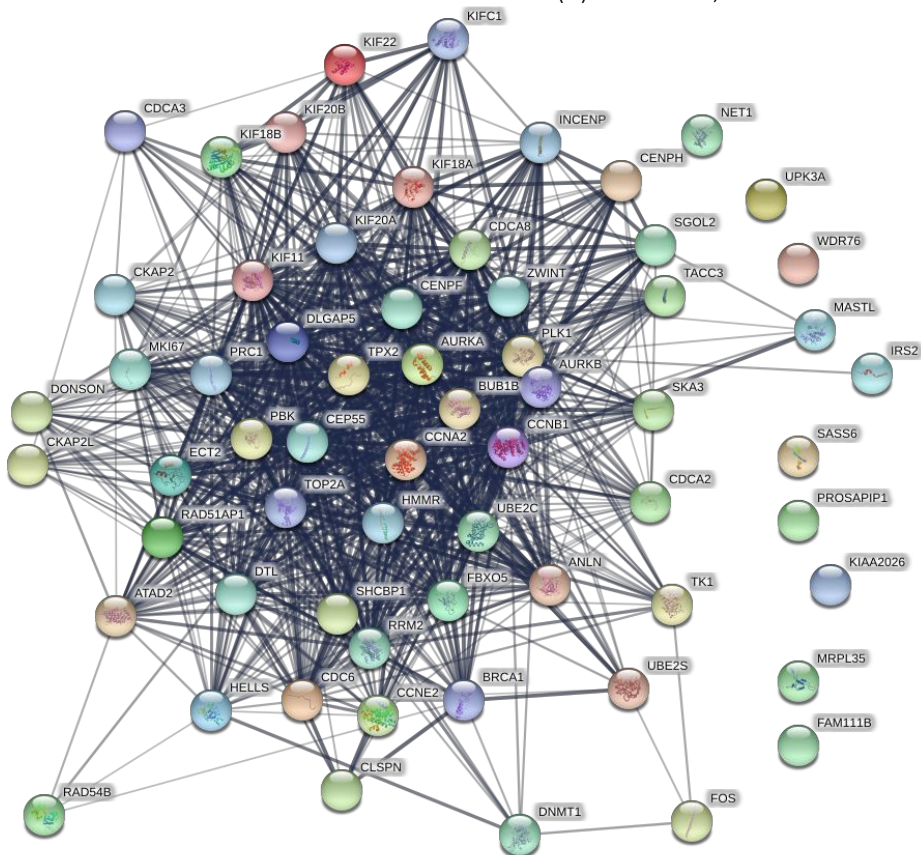
(c) RPTE cells; 72 h.
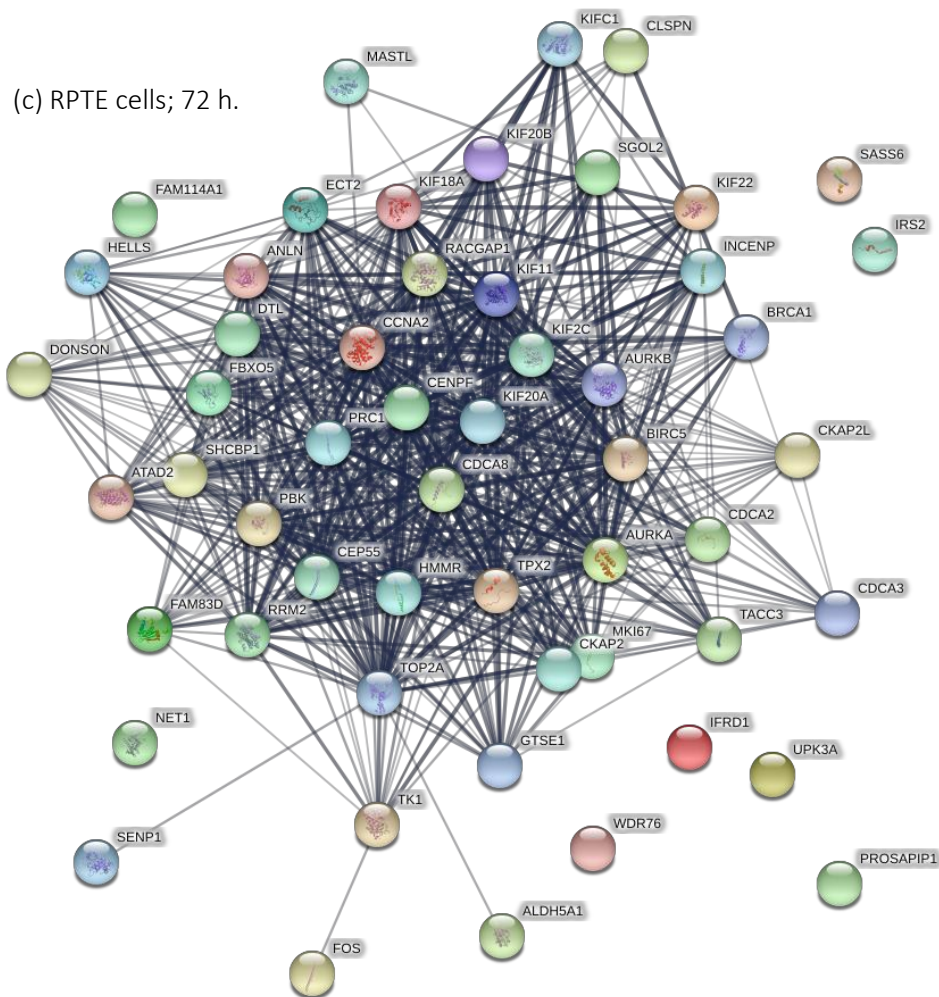
(d) HU cells; 24 h.
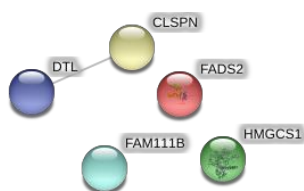
(e) HU cells; 48 h.
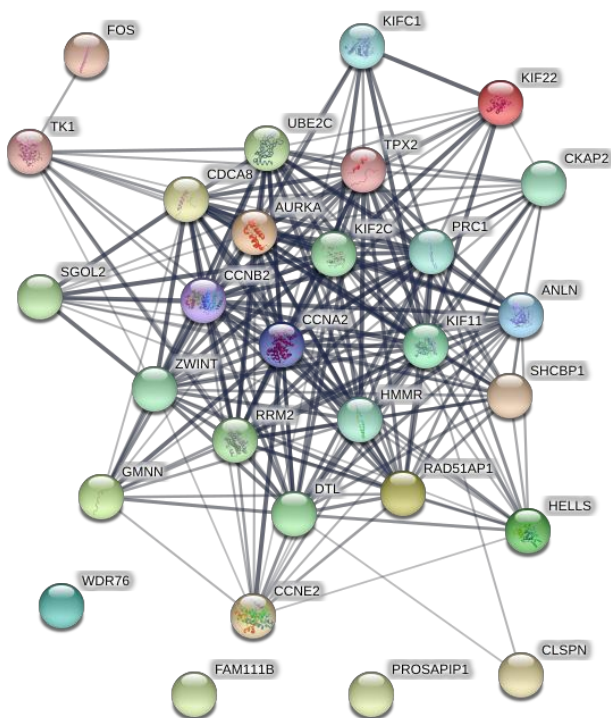
(f) HU cells; 72 h.
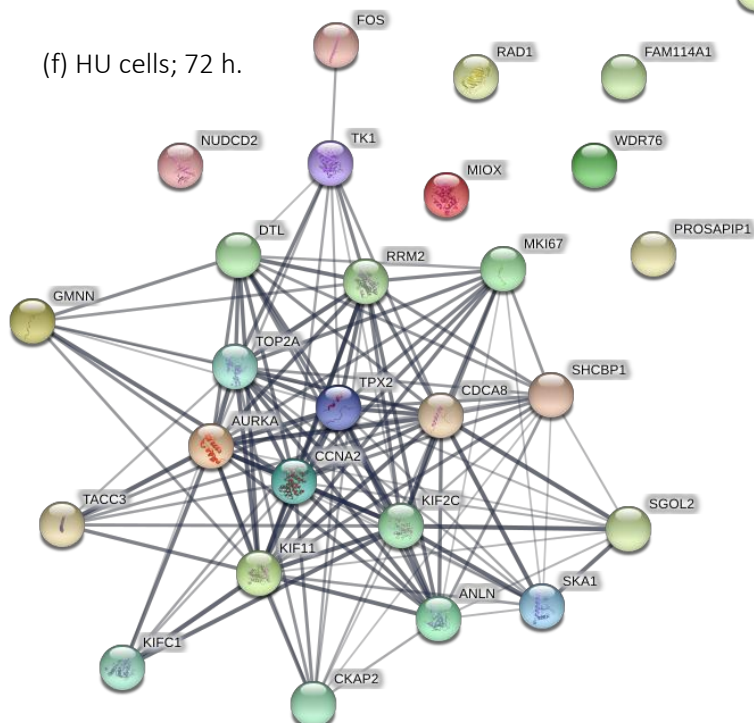
Figure S5: STRING analysis of most significantly (p < 0.0005) up regulated proteins in RPTE and HU cells.
Those proteins that were observed to be increased in abundance RPTE (a, b & c) or HU (d, e & f) cells at each time point
(as shown in Fig. 4.4) were analysed using Search Tool for the Retrieval of Interacting Genes/Proteins (STRING). STRING
analysis shows each protein represented as a spot, with connections made between proteins representing known and
predicted protein-protein interactions, the heavier the connecting line, the more confidence in the interaction based
on experimental, co-expression, co-occurrence, gene fusion, textmining or neighbourhood evidence.

8.2 Tables

Table S1: Inhibitor screen conducted by Dr G Evans.

The effects of various trafficking and ClC inhibitors on BKPyV secretion were determined prior to the start of this PhD. RPTE or VERO cells were BKPyV infected at 1 IU/cell and treated with inhibitors at a variety of concentrations, or DMSO as a control, at 24 hpi. At 48 hpi supernatant media and cells were harvested independently. To determine the virus concentration in each harvest an FFU assay was conducted. The proportion of released BKPyV was determined, normalised to the uninhibited controls for each experiment.

* = cell death was observed in these inhibitions; some caution must be given when analysing these data.

INHIBITOR	CELL LINE	0.05µM	0.1µM	0.5µM	1µM	5µM	10µM	20µM	25µM	30µM	40µM	50µM	75µM	100µM	200µM	500µM	750µM	1mM	1.5mM	2mM
DIDS	RPTE					0.85	0.68	0.58		0.38	0.35	0.18	0.09	0.05						
DIDS	VERO								0.79			0.62	0.46	0.41						
SITS	RPTE														2.39	1.73	1.89	1.75		
DNDS	RPTE															1.95		3.12	2.58	3.90*
NPPB	RPTE								1.00			0.89	2.28*							
Probecenid	RPTE		0.77	1.21	0.84	0.99														
Furosemide	RPTE	0.49	1.12	0.52	0.58															
Bafilomycin A	RPTE		1.97	4.84*	5.66*	16.87*														

Uniprot ID	Gene Name	Protein Name	Function	Peptide No.	HUC Mock 24h	HUC Mock 72h	HUC BK 24h	HUC BK 48h	HUC BK 72h	RPTEC Mock 24h	RPTEC Mock 72h	RPTEC BK 24h	RPTEC BK 48h	RPTEC BK 72h
Q9UBG3	CRNN	Cornulin	Survival factor that participates in the clonogenicity of squamous esophageal epithelium cell lines, attenuates deoxycholic acid (DCA)-induced apoptotic cell death and release of calcium.	15	0.2	1.8	0.2	0.3	0.9	1.1	0.9	0.9	1.1	1.0
Q6UWP8	SBSN	Suprabasin	Epidermal Differentiation Marker	2	0.3	1.7	0.3	0.5	0.7	1.0	1.0	0.9	0.9	0.8
Q9NQ38	SPINK5	Serine protease inhibitor Kazal-type 5	Serine protease inhibitor, probably important for the anti-inflammatory and/or antimicrobial protection of mucous epithelia	3	0.3	1.7	0.3	0.6	1.2	1.0	1.0	0.8	0.8	0.8
P28300	LOX	Protein-lysine 6-oxidase	Responsible for the post-translational oxidative deamination of peptidyl lysine residues in precursors to fibrous collagen and elastin. Regulator of Ras expression. May play a role in tumor suppression.	2	0.2	1.8	0.3	0.3	0.4	1.1	0.9	1.0	0.9	0.9
Q9H6K4	OPA3	Optic atrophy 3 protein	May play some role in mitochondrial processes	1	0.4	1.6	0.3	0.8	0.6	1.1	0.9	1.2	0.4	0.8
Q6XPR3	RPTN	Repetin	Involved in the cornified cell envelope formation. Multifunctional epidermal matrix protein. Reversibly binds calcium.	6	0.4	1.6	0.3	0.4	0.7	1.0	1.0	1.1	1.1	1.0
P54868	HMGCS2	Hydroxymethylglutaryl-CoA synthase	This enzyme condenses acetyl-CoA with acetoacetyl-CoA to form HMG-CoA, which is the substrate for HMG-CoA reductase	7	0.4	1.6	0.4	0.3	0.4	1.0	1.0	1.0	1.1	1.0
P35321	SPRR1A	Cornifin-A	Cross-linked envelope protein of keratinocytes	33	0.4	1.6	0.4	0.6	0.6	1.1	0.9	0.9	1.1	1.0
P12109	COL6A1	Collagen alpha-1(VI) chain	Collagen VI acts as a cell-binding protein	6	0.5	1.5	0.4	0.7	0.7	0.9	1.1	0.9	0.9	0.7
Q68BL7	OLFML2A	Olfactomedin-like protein 2A	Extracellular matrix binding and organisation	1	0.5	1.5	0.4	0.9	0.9	1.1	0.9	0.9	1.1	0.9
Q9H6K1	C6orf106	Uncharacterized protein C6orf106	May be ubiquitin binding and involved in macroautophagy	1	0.6	1.4	0.4	0.8	0.5	1.0	1.0	1.0	1.1	0.8
Q8BY76	ANGPTL4	Angiopoietin-related protein 4	Protein with hypoxia-induced expression in endothelial cells	14	0.7	1.3	0.4	1.0	0.9	1.4	0.6	1.1	0.8	0.5
Q6Y1H2	HACD2	Very-long-chain (3R)-3-hydroxyacyl-CoA dehydratase 2	Catalyzes the third of the four reactions of the long-chain fatty acids elongation cycle	1	0.5	1.5	0.4	0.9	0.6	1.2	0.8	1.1	1.5	1.4
P68106	FKBP1B	Peptidyl-prolyl cis-trans isomerase FKBP1B	Has the potential to contribute to the immunosuppressive and toxic effects of FK506 and rapamycin	1	0.3	1.7	0.4	0.7	0.6	1.0	1.0	1.1	1.0	1.1
Q9BPX8	HOPX	Isoform 3 of Homeodomain-only protein	Molecular chaperone implicated in a wide variety of cellular processes, including protection of the proteome from stress, folding and transport of newly synthesized polypeptides, activation of proteolysis of misfolded proteins and the formation and dissociation of protein complexes	4	0.4	1.6	0.5	0.6	1.0	0.9	1.1	0.9	1.0	0.9
P22528	SPRR1B	Cornifin-B	Cross-linked envelope protein of keratinocytes	10	0.5	1.5	0.5	0.6	0.8	1.1	0.9	0.9	1.0	1.1
Q13268	DHRS2	Dehydrogenase/reductase SDR family member 2, mitochondrial	Displays NADPH-dependent dicarbonyl reductase activity in vitro with 3,4-Hexanedione, 2,3-Heptanedione and 1-Phenyl-1,2-propanedione as substrates	12	0.6	1.4	0.5	0.5	0.4	1.0	1.0	0.9	0.9	0.9
P69905	HBA1	Hemoglobin subunit alpha	Involved in oxygen transport from the lung to the various peripheral tissues	21	0.7	1.3	0.5	0.8	0.8	1.0	1.0	1.3	0.7	0.8
O76070	SNCG	Gamma-synuclein	Plays a role in neurofilament network integrity. May be involved in modulating axonal architecture during development and in the adult	9	0.5	1.5	0.5	0.7	0.5	1.1	0.9	0.9	0.9	0.8
Q9UBC9	SPRR3	Small proline-rich protein 3	Cross-linked envelope protein of keratinocytes	23	0.5	1.5	0.5	0.5	0.7	1.0	1.0	0.9	0.9	0.9
Q9H939	PSTPIP2	Proline-serine-threonine phosphatase-interacting protein 2	Binds to F-actin. May be involved in regulation of the actin cytoskeleton	18	0.8	1.2	0.5	0.8	0.6	0.8	1.2	0.8	0.8	0.8
Q01581	HMGCS1	Hydroxymethylglutaryl-CoA synthase, cytoplasmic	This enzyme condenses acetyl-CoA with acetoacetyl-CoA to form HMG-CoA, which is the substrate for HMG-CoA reductase	26	1.5	0.5	1.7	1.3	0.8	0.8	1.2	2.1	2.1	1.6
O95864	FADS2	Fatty acid desaturase 2	Component of a lipid metabolic pathway that catalyzes biosynthesis of highly unsaturated fatty acids (HUFA) from precursor essential polyunsaturated fatty acids (PUFA) linoleic acid (LA) (18:2n-6) and alpha-linolenic acid (ALA) (18:3n-3)	15	1.6	0.4	1.7	1.6	0.8	0.9	1.1	2.6	1.6	0.9
Q6SJ93	FAM111B	Protein FAM111B	Cancer-associated nucleoprotein	12	1.5	0.5	2.0	2.4	2.0	1.3	0.7	1.7	2.7	2.1
Q9HAW4	CLSPN	Claspin	Required for checkpoint mediated cell cycle arrest in response to inhibition of DNA replication or to DNA damage induced by both ionizing and UV irradiation. Adapter protein which binds to BRCA1 and the checkpoint kinase CHEK1 and facilitates the ATR-dependent phosphorylation of both proteins	10	1.5	0.5	2.1	3.3	2.4	1.3	0.7	2.2	5.7	3.6
Q9NZJ0	DTL	Denticleless protein homolog	Substrate-specific adapter of a DCX (DDB1-CUL4-X-box) E3 ubiquitin-protein ligase complex required for cell cycle control, DNA damage response and translesion DNA synthesis	5	1.4	0.6	2.5	3.3	3.5	1.4	0.6	2.1	3.5	3.9
P03082	Small t antigen	Small t antigen	BKPyV VIRAL PROTEIN - Promotes efficient viral genome replication by accelerating both G1 and S phase progression of the cell cycle. Inhibits host PP2A by binding to the A subunit, thereby displacing lower affinity regulatory B subunit	6	0.9	1.1	2.8	6.9	10.9	1.0	1.0	2.6	4.8	10.5
P03071	Large T antigen	Large T antigen	BKPyV VIRAL PROTEIN - Large T antigen is a key early protein essential for both driving viral replication and inducing cellular transformation. Plays a role in viral genome replication by driving entry of quiescent cells into the cell cycle and by autoregulating the synthesis of viral early mRNA	37	0.9	1.1	3.2	7.7	9.1	0.9	1.1	3.2	11.0	12.1
NOVEL ORF	NOVEL ORF	NOVEL_ORF	BKPyV VIRAL PROTEIN - NOVEL Large T antigen transcript	1	0.0	2.0	15.1	140.5	212.9	1.3	0.7	3.2	44.1	68.7

Table S2: Significantly up and down regulated proteins at 24 hpi in HU cells ($p < 0.0005$).

Table of proteins observed to be significantly ($p < 0.0005$) up or down regulated in HU cells at 24 hpi, when compared to an average of the 24 and 72 h HU cell mock samples. Fold changes of every experimental condition shown for each protein (against an average of the 24 and 72 h mock samples for the corresponding cell type). Increasing red colour indicates greater up regulated fold changes, increasing green colour indicates greater down regulated fold changes).

Uniprot ID	Gene Name	Protein Name	Function	Peptide No.	HUC Mock 24h	HUC Mock 72h	HUC BK 24h	HUC BK 48h	HUC BK 72h	RPTEC Mock 24h	RPTEC Mock 72h	RPTEC BK 24h	RPTEC BK 48h	RPTEC BK 72h
Q9NR00	TCIM	Transcriptional and immune response regulator	c8orf4. Seems to be involved in the regulation of cell growth an differentiation, may play different and opposite roles depending on the tissue or cell type. Plays a role in the mitogen-activated MAPK2/3 signaling pathway, positively regulates G1-to-S-phase transition of the cell cycle. In endothelial cells, enhances key inflammatory mediators and inflammatory response through the modulation of NF-kappaB transcriptional regulatory activity	1	0.5	1.5	0.4	0.2	0.4	0.7	1.3	0.6	0.5	0.4
P28300	LOX	Protein-lysine 6-oxidase	Responsible for the post-translational oxidative deamination of peptidyl lysine residues in precursors to fibrous collagen and elastin. Regulator of Ras expression. May play a role in tumor suppression.	2	0.2	1.8	0.3	0.3	0.4	1.1	0.9	1.0	0.9	0.9
Q9UBG3	CRNN	Cornulin	Survival factor that participates in the clonogenicity of squamous esophageal epithelium cell lines, attenuates deoxycholic acid (DCA)-induced apoptotic cell death and release of calcium.	15	0.2	1.8	0.2	0.3	0.9	1.1	0.9	0.9	1.1	1.0
P54868	HMGCS2	Hydroxymethylglutaryl-CoA synthase, mitochondrial	This enzyme condenses acetyl-CoA with acetoacetyl-CoA to form HMG-CoA, which is the substrate for HMG-CoA reductase	7	0.4	1.6	0.4	0.3	0.4	1.0	1.0	1.0	1.1	1.0
P01584	IL1B	Interleukin-1 beta	Potent proinflammatory cytokine. Initially discovered as the major endogenous pyrogen, induces prostaglandin synthesis, neutrophil influx and activation, T-cell activation and cytokine production, B-cell activation and antibody production, and fibroblast proliferation and collagen production. Promotes Th17 differentiation of T-cells	4	1.2	0.8	1.1	0.4	0.4	1.0	1.0	0.9	0.9	0.8
P15428	HPGD	15-hydroxyprostaglandin dehydrogenase [NAD(+)]	Prostaglandin inactivation. Contributes to the regulation of events that are under the control of prostaglandin levels. Catalyzes the NAD-dependent dehydrogenation of lipoxin A4 to form 15-oxo-lipoxin A4. Inhibits in vivo proliferation of colon cancer cells	17	0.7	1.3	0.7	0.4	0.3	1.1	0.9	0.9	0.9	0.9
Q9UPQ7	PDZRN3	E3 ubiquitin-protein ligase PDZRN3	E3 ubiquitin-protein ligase. Plays an important role in regulating the surface level of MUSK on myotubes. Mediates the ubiquitination of MUSK, promoting its endocytosis and lysosomal degradation. Might contribute to terminal myogenic	2	0.7	1.3	0.6	0.4	0.4	1.1	0.9	0.9	0.9	0.8
B8A4K4	CYSRT1	Cysteine-rich tail protein 1	Secreted. Unknown function	1	0.6	1.4	0.7	0.4	0.4	1.2	0.8	0.9	0.7	0.7
Q6XPR3	RPTN	Repetin	Involved in the cornified cell envelope formation. Multifunctional epidermal matrix protein. Reversibly binds calcium.	6	0.4	1.6	0.3	0.4	0.7	1.0	1.0	1.1	1.1	1.0
Q96T21	SECISBP2	Selenocysteine insertion sequence-binding protein 2	Binds to the SECIS element in the 3'-UTR of some mRNAs encoding selenoproteins. Binding is stimulated by SELB	3	1.1	0.9	1.0	0.5	0.4	0.9	1.1	0.7	0.6	0.6
Q13268	DHRS2	Dehydrogenase/reductase SDR family member 2, mitochondrial	Displays NADPH-dependent dicarbonyl reductase activity in vitro with 3,4-Hexanedione, 2,3-Heptanedione and 1-Phenyl-1,2-propanedione as substrates	12	0.6	1.4	0.5	0.5	0.4	1.0	1.0	0.9	0.9	0.9
Q9UBC9	SPRR3	Small proline-rich protein 3	Cross-linked envelope protein of keratinocytes	23	0.5	1.5	0.5	0.5	0.7	1.0	1.0	0.9	0.9	0.9
P35321	SPRR1A	Cornifin-A	Cross-linked envelope protein of keratinocytes	33	0.4	1.6	0.4	0.6	0.6	1.1	0.9	0.9	1.1	1.0
P07996	THBS1	Thrombospondin-1	Adhesive glycoprotein that mediates cell-to-cell and cell-to-matrix interactions. Binds heparin. May play a role in dentinogenesis and/or maintenance of dentin and dental pulp (By similarity). Ligand for CD36 mediating antiangiogenic properties. Plays a role in ER stress response, via its interaction with the activating transcription factor 6 alpha (ATF6) which produces adaptive ER stress	78	1.5	0.5	1.3	0.6	0.5	1.2	0.8	1.2	0.9	0.7
Q9NSV4	DIAPH3	Protein diaphanous homolog 3	Binds to GTP-bound form of Rho and to profilin. Acts in a Rho-dependent manner to recruit profilin to the membrane, where it promotes actin polymerization. It is required for cytokinesis, stress fiber formation, and transcriptional activation of the serum	28	1.5	0.5	1.5	1.8	2.0	1.2	0.8	1.4	2.1	2.3
Q53EZ4	CEP55	Centrosomal protein of 55 kDa	Plays a role in mitotic exit and cytokinesis	18	1.5	0.5	1.5	1.8	1.8	1.3	0.7	1.6	2.9	2.7
O75717	WDHD1	WD repeat and HMG-box DNA-binding protein 1	Acts as a replication initiation factor that brings together the MCM2-7 helicase and the DNA polymerase alpha/primase complex in order to initiate DNA replication	30	1.4	0.6	1.5	1.9	2.0	1.3	0.7	1.4	2.0	2.2
P46013	MKI67	Proliferation marker protein Ki-67	Required to maintain individual mitotic chromosomes dispersed in the cytoplasm following nuclear envelope disassembly. Associates with the surface of the mitotic chromosome, the perichromosomal layer, and covers a substantial fraction of the	121	1.4	0.6	1.4	2.0	2.1	1.4	0.6	1.5	2.3	3.3
Q9Y6A5	TACC3	Transforming acidic coiled-coil-containing protein 3	Plays a role in the microtubule-dependent coupling of the nucleus and the centrosome. Involved in the processes that regulate centrosome-mediated interkinetic nuclear migration (INM) of neural progenitors (By similarity). Acts as component of the TACC3/ch-TOG/clathrin complex proposed to contribute to stabilization of kinetochore fibers of the mitotic spindle by acting as	20	1.2	0.8	1.3	2.1	2.5	1.2	0.8	1.5	3.3	3.9
P33981	TTK	Dual specificity protein kinase TTK	Phosphorylates proteins on serine, threonine, and tyrosine. Probably associated with cell proliferation. Essential for chromosome alignment by enhancing AURKB activity (via direct CDCA8 phosphorylation) at the centromere, and for the mitotic	10	1.5	0.5	1.5	2.1	2.0	1.3	0.7	1.5	1.6	1.9
Q96KB5	PBK	Lymphokine-activated killer T-cell-originated protein kinase	Phosphorylates MAP kinase p38. Seems to be active only in mitosis. May also play a role in the activation of lymphoid cells. When phosphorylated, forms a complex with TP53, leading to TP53 destabilization and attenuation of G2/M checkpoint during doxorubicin-induced DNA damage	15	1.4	0.6	1.6	2.1	2.7	1.4	0.6	1.5	2.4	3.4
P14635	CCNB1	G2/mitotic-specific cyclin-B1	Essential for the control of the cell cycle at the G2/M (mitosis) transition	13	1.4	0.6	1.5	2.1	2.2	1.1	0.9	1.4	2.4	2.4
P11388	TOP2A	Isoform 4 of DNA topoisomerase 2-alpha	Control of topological states of DNA by transient breakage and subsequent rejoining of DNA strands. Topoisomerase II makes double-strand breaks. Essential during mitosis and meiosis for proper segregation of daughter chromosomes, oscillation	61	1.4	0.6	1.4	2.2	2.7	1.3	0.7	1.6	3.4	5.1
Q6PL18	ATAD2	ATPase family AAA domain-containing protein 2	May be a transcriptional coactivator of the nuclear receptor ESR1 required to induce the expression of a subset of estradiol target genes, such as CCND1, MYC and E2F1. May play a role in the recruitment or occupancy of CREBBP at some ESR1 target gene promoters. May be required for histone hyperacetylation.	23	1.3	0.7	1.6	2.2	1.8	1.2	0.8	1.4	3.7	3.8

Accession	Gene	Protein name	Description											
Q9H0H5	RACGAP1	Rac GTPase-activating protein 1	Component of the centralspindlin complex that serves as a microtubule-dependent and Rho-mediated signaling required for the myosin contractile ring formation during the cell cycle cytokinesis. Required for proper attachment of the midbody to the cell membrane during cytokinesis.	17	1.4	0.6	1.6	2.2	2.2	1.4	0.6	1.5	2.2	2.8
O00762	UBE2C	Ubiquitin-conjugating enzyme E2 C	Accepts ubiquitin from the E1 complex and catalyzes its covalent attachment to other proteins. In vitro catalyzes 'Lys-11'- and 'Lys-48'-linked polyubiquitination. Acts as an essential factor of the anaphase promoting complex/cyclosome (APC/C), a cell cycle-regulated ubiquitin ligase that controls progression through mitosis.	4	1.9	0.1	2.0	2.2	1.7	1.4	0.6	1.8	3.5	1.8
Q53HL2	CDCA8	Borealin	Component of the chromosomal passenger complex (CPC), a complex that acts as a key regulator of mitosis.	7	1.4	0.6	1.5	2.2	3.0	1.3	0.7	1.4	3.0	4.5
O43663	PRC1	Protein regulator of cytokinesis 1	Key regulator of cytokinesis that cross-links antiparrallel microtubules at an average distance of 35 nM. Essential for controlling the spatiotemporal formation of the midzone and successful cytokinesis. Required for KIF14 localization to the central spindle and midbody. Required to recruit PLK1 to the spindle. Stimulates PLK1 phosphorylation of RACGAP1 to allow recruitment of ECT2	10	1.4	0.6	1.6	2.2	2.5	1.2	0.8	1.3	3.3	3.6
O75330	HMMR	Isoform 3 of Hyaluronan mediated motility receptor	Receptor for hyaluronic acid (HA) (By similarity). Involved in cell motility (By similarity). When hyaluronan binds to HMMR, the phosphorylation of a number of proteins, including PTK2/FAK1 occurs	16	1.4	0.6	1.6	2.2	2.2	1.2	0.8	1.4	4.1	4.7
P01100	FOS	Proto-oncogene c-Fos	Nuclear phosphoprotein which forms a tight but non-covalently linked complex with the JUN/AP-1 transcription factor. In the heterodimer, FOS and JUN/AP-1 basic regions each seems to interact with symmetrical DNA half sites. On TGF-beta activation, forms a multimeric SMAD3/SMAD4/JUN/FOS complex at the AP1/SMAD-binding site to regulate TGF-beta-mediated signaling	1	1.2	0.8	1.2	2.3	3.9	0.9	1.1	1.4	9.0	11.3
Q99661	KIF2C	Kinesin-like protein KIF2C	In complex with KIF18B, constitutes the major microtubule plus-end depolymerizing activity in mitotic cells	16	1.6	0.4	1.7	2.3	2.4	1.4	0.6	1.6	2.1	2.9
Q9NR29	HELLS	Lymphoid-specific helicase	Plays an essential role in normal development and survival. Involved in regulation of the expansion or survival of lymphoid cells. Required for de novo or maintenance DNA methylation	12	1.6	0.4	1.9	2.3	1.8	1.3	0.7	1.8	4.3	3.7
Q6SJ93	FAM111B	Protein FAM111B	Cancer-associated nucleoprotein	12	1.5	0.5	2.0	2.4	2.0	1.3	0.7	1.7	2.7	2.1
Q9BW19	KIFC1	Kinesin-like protein KIFC1	Minus end-directed microtubule-dependent motor required for bipolar spindle formation	19	1.4	0.6	1.5	2.4	2.9	1.2	0.8	1.5	3.2	4.2
P52732	KIF11	Kinesin-like protein KIF11	Motor protein required for establishing a bipolar spindle during mitosis. Required in non-mitotic cells for transport of secretory proteins from the Golgi complex to the cell surface	32	1.3	0.7	1.4	2.4	2.9	1.2	0.8	1.5	3.3	4.7
Q96801	RAD51AP1	RAD51-associated protein 1	May participate in a common DNA damage response pathway associated with the activation of homologous recombination and double-strand break repair. Functionally cooperates with PALB2 in promoting of D-loop formation by RAD51	4	1.2	0.8	1.3	2.4	2.3	1.2	0.8	1.4	3.0	2.9
O09067	CCNB2	G2/mitotic-specific cyclin-B2	Essential for the control of the cell cycle at the G2/M (mitosis) transition	6	1.3	0.7	1.4	2.4	2.2	1.1	0.9	1.3	2.5	2.4
Q9ULW0	TPX2	Targeting protein for Xklp2	Spindle assembly factor required for normal assembly of mitotic spindles. Required for normal assembly of microtubules during apoptosis. Required for chromatin and/or kinetochore dependent microtubule nucleation. Mediates AURKA localization to	30	1.5	0.5	1.5	2.5	2.7	1.3	0.7	1.6	4.1	4.7
Q8NEM2	SHCBP1	SHC SH2 domain-binding protein 1	May play a role in signaling pathways governing cellular proliferation, cell growth and differentiation. May be a component of a novel signaling pathway downstream of Shc. Acts as a positive regulator of FGF signaling in neural progenitor cells	10	1.6	0.4	1.8	2.5	3.3	1.4	0.6	1.7	3.9	4.4
B5MBX0	CDCA5	Sororin	Regulator of sister chromatid cohesion in mitosis stabilizing cohesin complex association with chromatin	6	1.4	0.6	1.7	2.6	3.1	1.1	0.9	1.5	3.7	4.2
Q14807	KIF22	Kinesin-like protein KIF22	Kinesin family member that is involved in spindle formation and the movements of chromosomes during mitosis and meiosis. Binds to microtubules and to DNA	9	1.5	0.5	1.7	2.6	2.6	1.3	0.7	1.6	3.7	5.1
P31350	RRM2	Isoform 2 of Ribonucleoside-diphosphate reductase subunit M2	Provides the precursors necessary for DNA synthesis. Catalyzes the biosynthesis of deoxyribonucleotides from the corresponding ribonucleotides. Inhibits Wnt signaling	25	1.3	0.7	1.7	2.7	2.9	1.2	0.8	1.6	5.2	4.5
Q9NQW6	ANLN	Anillin	Required for cytokinesis. Essential for the structural integrity of the cleavage furrow and for completion of cleavage furrow ingression. Plays a role in bleb assembly during metaphase and anaphase of mitosis	60	1.4	0.6	1.5	2.7	3.1	1.2	0.8	1.5	4.4	5.7
O14965	AURKA	Aurora kinase A	Mitotic serine/threonine kinase that contributes to the regulation of cell cycle progression. Associates with the centrosome and the spindle microtubules during mitosis and plays a critical role in various mitotic events including the establishment of mitotic spindle, centrosome duplication, centrosome separation as well as maturation, chromosomal alignment, spindle assembly checkpoint, and cytokinesis. Required for initial activation of CDK1 at centrosomes	9	1.7	0.3	1.9	2.7	2.9	1.3	0.7	1.7	3.9	4.5
O95229	ZWINT	ZW10 interactor	Part of the MIS12 complex, which is required for kinetochore formation and spindle checkpoint activity. Required to target ZW10 to the kinetochore at prometaphase	3	1.5	0.5	1.9	2.8	2.6	1.3	0.7	1.6	3.6	2.9

Accession	Gene	Protein	Description	#										
O75496	GMNN	Geminin	Inhibits DNA replication by preventing the incorporation of MCM complex into pre-replication complex (pre-RC). It is degraded during the mitotic phase of the cell cycle. Its destruction at the metaphase-anaphase transition permits replication in the succeeding cell cycle. Inhibits the transcriptional activity of a subset of Hox proteins, enrolling them in cell proliferative control	3	1.3	0.7	1.7	2.9	3.2	1.0	1.0	1.2	2.1	1.5
P03094	VP2	Minor capsid protein VP2	BKPyV VIRAL PROTEIN - VP2 is a structural protein that resides within the core of the capsid surrounded by 72 VP1 pentamers. Participates in host cell receptor binding together with VP1	18	1.0	1.0	1.4	3.1	6.4	1.0	1.0	1.3	3.7	12.7
P04183	TK1	Thymidine kinase, cytosolic	Two forms have been identified in animal cells, one in cytosol and one in mitochondria. Activity of the cytosolic enzyme is high in proliferating cells and peaks during the S-phase of the cell cycle; it is very low in resting cells	9	1.6	0.4	1.7	3.2	3.6	1.3	0.7	1.6	4.1	4.1
Q9H967	WDR76	WD repeat-containing protein 76	Specifically binds 5-hydroxymethylcytosine (5hmC), suggesting that it acts as a specific reader of 5hmC	5	1.5	0.5	1.9	3.2	4.1	1.3	0.7	1.9	4.4	5.8
Q9HAW4	CLSPN	Claspin	Required for checkpoint mediated cell cycle arrest in response to inhibition of DNA replication or to DNA damage induced by both ionizing and UV irradiation. Adapter protein which binds to BRCA1 and the checkpoint kinase CHEK1 and facilitates the ATR-dependent phosphorylation of both proteins	10	1.5	0.5	2.1	3.3	2.4	1.3	0.7	2.2	5.7	3.6
Q8WWK9	CKAP2	Isoform 3 of Cytoskeleton-associated protein 2	Possesses microtubule stabilizing properties. Involved in regulating aneuploidy, cell cycling, and cell death in a p53/TP53-dependent manner	18	1.5	0.5	1.6	3.3	4.7	1.2	0.8	1.6	5.2	6.5
P20248	CCNA2	Cyclin-A2	Cyclin which controls both the G1/S and the G2/M transition phases of the cell cycle. Functions through the formation of specific serine/threonine protein kinase holoenzyme complexes with the cyclin-dependent protein kinases CDK1 or CDK2	7	1.5	0.5	1.9	3.3	3.6	1.3	0.7	1.7	4.4	5.4
Q9NZI0	DTL	Denticleless protein homolog	Substrate-specific adapter of a DCX (DDB1-CUL4-X-box) E3 ubiquitin-protein ligase complex required for cell cycle control, DNA damage response and translesion DNA synthesis	5	1.4	0.6	2.5	3.3	3.5	1.4	0.6	2.1	3.5	3.9
O96020	CCNE2	G1/S-specific cyclin-E2	Essential for the control of the cell cycle at the late G1 and early S phase	1	1.3	0.7	2.2	3.9	3.2	1.1	0.9	2.1	7.3	4.1
Q562F6	SGO2	Shugoshin 2	Essential for recruiting KIF2C to the inner centromere and for correcting defective kinetochore attachments. Involved in centromeric enrichment of AUKRB in prometaphase	7	1.0	1.0	2.1	3.9	3.9	1.2	0.8	1.5	5.3	6.1
P03088	VP1	Major capsid protein VP1	BKPyV VIRAL PROTEIN - Forms an icosahedral capsid with a T=7 symmetry and a 50nm diameter. The capsid is composed of 72 pentamers linked to each other by disulfide bonds and associated with VP2 or VP3 proteins. Interacts with gangliosides GT1b and GD1b containing terminal alpha2-8-linked sialic acids on the cell surface to provide virion attachment to target cell	280	1.0	1.0	1.5	4.1	7.0	1.0	1.0	1.3	6.6	14.6
P03085	Agnoprotein	Agnoprotein	BKPyV VIRAL PROTEIN - Alters the structure of the nuclear envelope by interacting with host CBX5 and disrupting CBX5 association with LBR. Involved in the perinuclear-nuclear localization of the capsid protein VP1 during virion assembly and maturation. Plays an important role in the release of progeny virions from infected cells and in viral propagation	3	0.9	1.1	1.3	5.6	8.1	0.8	1.2	1.2	11.8	15.9
P03082	Small t antigen	Small t antigen	BKPyV VIRAL PROTEIN - Promotes efficient viral genome replication by accelerating both G1 and S phase progression of the cell cycle. Inhibits host PP2A by binding to the A subunit, thereby displacing lower affinity regulatory B subunit	37	0.9	1.1	3.2	7.7	9.1	0.9	1.1	3.2	11.0	12.1
P03071	Large T antigen	Large T antigen	BKPyV VIRAL PROTEIN - Large T antigen is a key early protein essential for both driving viral replication and inducing cellular transformation. Plays a role in viral genome replication by driving entry of quiescent cells into the cell cycle and by autoregulating the synthesis of viral early mRNA	6	0.9	1.1	2.8	6.9	10.9	1.0	1.0	2.6	4.8	10.5
O60299	LZTS3	Leucine zipper putative tumor suppressor 3	May be involved in promoting the maturation of dendritic spines, probably via regulating SIPA1L1 levels at the postsynaptic density of synapses	1	0.8	1.2	2.3	9.3	18.5	0.5	1.5	2.2	16.7	40.0
NOVEL ORF	NOVEL ORF	NOVEL_ORF	BKPyV VIRAL PROTEIN - NOVEL Large T antigen transcript	1	0.0	2.0	15.1	140.5	212.9	1.3	0.7	3.2	44.1	68.7

Table S3: Significantly up and down regulated proteins at 48 hpi in HU cells (*p* < 0.0005).
Table of proteins observed to be significantly (*p* < 0.0005) up or down regulated in HU cells at 48 hpi, when compared to an average of the 24 and 72 h HU cell mock samples. Fold changes of every experimental condition shown for each protein (against an average of the 24 and 72 h mock samples for the corresponding cell type). Increasing red colour indicates greater up regulated fold changes, increasing green colour indicates greater down regulated fold changes).

Uniprot ID	Gene Name	Protein Name	Function	Peptide No.	HUC Mock 24h	HUC Mock 72h	HUC BK 24h	HUC BK 48h	HUC BK 72h	RPTEC Mock 24h	RPTEC Mock 72h	RPTEC BK 24h	RPTEC BK 48h	RPTEC BK 72h
Q9H3M7	TXNIP	Thioredoxin-interacting protein	Functions as a transcriptional repressor, possibly by acting as a bridge molecule between transcription factors and corepressor complexes, and over-expression will induce G0/G1 cell cycle arrest	8	0.9	1.1	0.9	0.9	0.3	1.0	1.0	0.9	0.8	0.9
P15428	HPGD	15-hydroxyprostaglandin dehydrogenase [NAD(+)]	Prostaglandin inactivation. Contributes to the regulation of events that are under the control of prostaglandin levels. Catalyzes the NAD-dependent dehydrogenation of lipoxin A4 to form 15-oxo-lipoxin A4. Inhibits in vivo proliferation of colon cancer cells	17	0.7	1.3	0.7	0.4	0.3	1.1	0.9	0.9	0.9	0.9
P54868	HMGCS2	Hydroxymethylglutaryl-CoA synthase	This enzyme condenses acetyl-CoA with acetoacetyl-CoA to form HMG-CoA, which is the substrate for HMG-CoA reductase	7	0.4	1.6	0.4	0.3	0.4	1.0	1.0	1.0	1.1	1.0
Q13268	DHRS2	Dehydrogenase/reductase SDR family member 2, mitochondrial	Displays NADPH-dependent dicarbonyl reductase activity in vitro with 3,4-Hexanedione, 2,3-Heptanedione and 1-Phenyl-1,2-propanedione as substrates	12	0.6	1.4	0.5	0.5	0.4	1.0	1.0	0.9	0.9	0.9
Q9UPQ7	PDZRN3	E3 ubiquitin-protein ligase PDZRN3	E3 ubiquitin-protein ligase. Plays an important role in regulating the surface level of MUSK on myotubes. Mediates the ubiquitination of MUSK, promoting its endocytosis and lysosomal degradation. Might contribute to terminal myogenic differentiation	2	0.7	1.3	0.6	0.4	0.4	1.1	0.9	0.9	0.9	0.8
Q96T21	SECISBP2	Selenocysteine insertion sequence-binding protein 2	Binds to the SECIS element in the 3'-UTR of some mRNAs encoding selenoproteins. Binding is stimulated by SELB	3	1.1	0.9	1.0	0.5	0.4	0.9	1.1	0.7	0.6	0.6
D6RFX5	AREG	Amphiregulin	Ligand of the EGF receptor/EGFR. Autocrine growth factor as well as a mitogen for a broad range of target cells including astrocytes, Schwann cells and fibroblasts	7	1.2	0.8	1.0	0.6	0.4	1.2	0.8	1.0	0.9	0.8
Q8IWE2	FAM114A1	Protein NOXP20	May play a role in neuronal cell development	16	1.0	1.0	1.1	1.6	2.1	1.0	1.0	1.0	2.1	3.5
P46013	MKI67	Proliferation marker protein Ki-67	Required to maintain individual mitotic chromosomes dispersed in the cytoplasm following nuclear envelope disassembly. Associates with the surface of the mitotic chromosome, the perichromosomal layer, and covers a substantial fraction of the chromosome surface	121	1.4	0.6	1.4	2.0	2.1	1.4	0.6	1.5	2.3	3.3
Q99661	KIF2C	Kinesin-like protein KIF2C	In complex with KIF18B, constitutes the major microtubule plus-end depolymerizing activity in mitotic cells	16	1.6	0.4	1.7	2.3	2.4	1.4	0.6	1.6	2.1	2.9
Q9Y6A5	TACC3	Transforming acidic coiled-coil-containing protein 3	Plays a role in the microtubule-dependent coupling of the nucleus and the centrosome. Involved in the processes that regulate centrosome-mediated interkinetic nuclear migration (INM) of neural progenitors (By similarity). Acts as component of the TACC3/ch-TOG/clathrin complex proposed to contribute to stabilization of kinetochore fibers of the mitotic spindle by acting as inter-microtubule bridge	20	1.2	0.8	1.3	2.1	2.5	1.2	0.8	1.5	3.3	3.9
P11388	TOP2A	Isoform 4 of DNA topoisomerase 2-alpha	Control of topological states of DNA by transient breakage and subsequent rejoining of DNA strands. Topoisomerase II makes double-strand breaks. Essential during mitosis and meiosis for proper segregation of daughter chromosomes. oscillation	61	1.4	0.6	1.4	2.2	2.7	1.3	0.7	1.6	3.4	5.1
Q9ULW0	TPX2	Targeting protein for Xklp2	Spindle assembly factor required for normal assembly of mitotic spindles. Required for normal assembly of microtubules during apoptosis. Required for chromatin and/or kinetochore dependent microtubule nucleation. Mediates AURKA localization to spindle microtubules	30	1.5	0.5	1.5	2.5	2.7	1.3	0.7	1.6	4.1	4.7
Q96BD8	SKA1	Spindle and kinetochore-associated protein 1	Component of the SKA1 complex, a microtubule-binding subcomplex of the outer kinetochore that is essential for proper chromosome segregation. Required for timely anaphase onset during mitosis, when chromosomes undergo bipolar attachment on spindle microtubules leading to silencing of the spindle checkpoint	8	1.4	0.6	1.4	1.6	2.8	1.2	0.8	1.3	1.9	2.1
P31350	RRM2	Isoform 2 of Ribonucleoside-diphosphate reductase subunit M2	Provides the precursors necessary for DNA synthesis. Catalyzes the biosynthesis of deoxyribonucleotides from the corresponding ribonucleotides. Inhibits Wnt signaling	25	1.3	0.7	1.7	2.7	2.9	1.2	0.8	1.6	5.2	4.6
Q9BW19	KIFC1	Kinesin-like protein KIFC1	Minus end-directed microtubule-dependent motor required for bipolar spindle formation	19	1.4	0.6	1.5	2.4	2.9	1.2	0.8	1.5	3.2	4.2
O14965	AURKA	Aurora kinase A	Mitotic serine/threonine kinase that contributes to the regulation of cell cycle progression. Associates with the centrosome and the spindle microtubules during mitosis and plays a critical role in various mitotic events including the establishment of mitotic spindle, centrosome duplication, centrosome separation as well as maturation, chromosomal alignment, spindle assembly checkpoint, and cytokinesis. Required for initial activation of CDK1 at centrosomes	9	1.7	0.3	1.9	2.7	2.9	1.3	0.7	1.7	3.9	4.5
P52732	KIF11	Kinesin-like protein KIF11	Motor protein required for establishing a bipolar spindle during mitosis. Required in non-mitotic cells for transport of secretory proteins from the Golgi complex to the cell surface	32	1.3	0.7	1.4	2.4	2.9	1.2	0.8	1.5	3.3	4.7
Q53HL2	CDCA8	Borealin	Component of the chromosomal passenger complex (CPC), a complex that acts as a key regulator of mitosis	7	1.4	0.6	1.5	2.2	3.0	1.3	0.7	1.4	3.0	4.6
B5MBX0	CDCA5	Sororin	Regulator of sister chromatid cohesion in mitosis stabilizing cohesin complex association with chromatin	6	1.4	0.6	1.7	2.6	3.1	1.1	0.9	1.5	3.7	4.2

Accession	Gene	Protein name	Description	n										
Q8WVJ2	NUDCD2	NudC domain-containing protein 2	May regulate the LIS1/dynein pathway by stabilizing LIS1 with Hsp90 chaperone	6	1.2	0.8	1.0	1.2	3.1	1.0	1.0	0.9	1.2	1.2
Q9NQW6	ANLN	Anillin	Required for cytokinesis. Essential for the structural integrity of the cleavage furrow and for completion of cleavage furrow ingression. Plays a role in bleb assembly during metaphase and anaphase of mitosis	60	1.4	0.6	1.5	2.7	3.1	1.2	0.8	1.5	4.4	5.7
O75496	GMNN	Geminin	Inhibits DNA replication by preventing the incorporation of MCM complex into pre-replication complex (pre-RC). It is degraded during the mitotic phase of the cell cycle. Its destruction at the metaphase-anaphase transition permits replication in the succeeding cell cycle. Inhibits the transcriptional activity of a subset of Hox proteins, enrolling them in cell proliferative control	3	1.3	0.7	1.7	2.9	3.2	1.0	1.0	1.2	2.1	1.5
Q8NEM2	SHCBP1	SHC SH2 domain-binding protein 1	May play a role in signaling pathways governing cellular proliferation, cell growth and differentiation. May be a component of a novel signaling pathway downstream of Shc. Acts as a positive regulator of FGF signaling in neural progenitor cells	10	1.6	0.4	1.8	2.5	3.3	1.4	0.6	1.7	3.9	4.4
Q9NZJ0	DTL	Denticleless protein homolog	Substrate-specific adapter of a DCX (DDB1-CUL4-X-box) E3 ubiquitin-protein ligase complex required for cell cycle control, DNA damage response and translesion DNA synthesis	5	1.4	0.6	2.5	3.3	3.5	1.4	0.6	2.1	3.5	3.9
P20248	CCNA2	Cyclin-A2	Cyclin which controls both the G1/S and the G2/M transition phases of the cell cycle. Functions through the formation of specific serine/threonine protein kinase holoenzyme complexes with the cyclin-dependent protein kinases CDK1 or CDK2	7	1.5	0.5	1.9	3.3	3.6	1.3	0.7	1.7	4.4	5.4
P04183	TK1	Thymidine kinase, cytosolic	Two forms have been identified in animal cells, one in cytosol and one in mitochondria. Activity of the cytosolic enzyme is high in proliferating cells and peaks during the S-phase of the cell cycle; it is very low in resting cells	9	1.6	0.4	1.7	3.2	3.6	1.3	0.7	1.6	4.1	4.1
P01100	FOS	Proto-oncogene c-Fos	Nuclear phosphoprotein which forms a tight but non-covalently linked complex with the JUN/AP-1 transcription factor. In the heterodimer, FOS and JUN/AP-1 basic regions each seems to interact with symmetrical DNA half sites. On TGF-beta activation, forms a multimeric SMAD3/SMAD4/JUN/FOS complex at the AP1/SMAD-binding site to regulate TGF-beta-mediated signaling	1	1.2	0.8	1.2	2.3	3.9	0.9	1.1	1.4	9.0	11.3
Q562F6	SGO2	Shugoshin 2	Essential for recruiting KIF2C to the inner centromere and for correcting defective kinetochore attachments. Involved in centromeric enrichment of AUKRB in prometaphase	7	1.0	1.0	2.1	3.9	3.9	1.2	0.8	1.5	5.3	6.1
Q9H967	WDR76	WD repeat-containing protein 76	Specifically binds 5-hydroxymethylcytosine (5hmC), suggesting that it acts as a specific reader of 5hmC	5	1.5	0.5	1.9	3.2	4.1	1.3	0.7	1.9	4.4	5.8
Q8WWK9	CKAP2	Isoform 3 of Cytoskeleton-associated protein 2	Possesses microtubule stabilizing properties. Involved in regulating aneuploidy, cell cycling, and cell death in a p53/TP53-dependent manner	18	1.5	0.5	1.6	3.3	4.7	1.2	0.8	1.6	5.2	6.5
O60671	RAD1	Cell cycle checkpoint protein RAD1	Component of the 9-1-1 cell-cycle checkpoint response complex that plays a major role in DNA repair. The 9-1-1 complex is recruited to DNA lesion upon damage by the RAD17-replication factor C (RFC) clamp loader complex. Acts then as a sliding clamp platform on DNA for several proteins involved in long-patch base excision repair (LP-BER)	3	1.3	0.7	1.2	1.5	4.7	1.0	1.0	1.0	0.6	1.1
P03094	VP2	Minor capsid protein VP2	BKPyV VIRAL PROTEIN - VP2 is a structural protein that resides within the core of the capsid surrounded by 72 VP1 pentamers. Participates in host cell receptor binding together with VP1	18	1.0	1.0	1.4	3.1	6.4	1.0	1.0	1.3	3.7	12.7
P03088	VP1	Major capsid protein VP1	BKPyV VIRAL PROTEIN - Forms an icosahedral capsid with a T=7 symmetry and a 50 nm diameter. The capsid is composed of 72 pentamers linked to each other by disulfide bonds and associated with VP2 or VP3 proteins. Interacts with gangliosides GT1b and GD1b containing terminal alpha2-8-linked sialic acids on the cell surface to provide virion attachment to target cell	280	1.0	1.0	1.5	4.1	7.0	1.0	1.0	1.3	6.6	14.6
P03085	Agnoprotein	Agnoprotein	BKPyV VIRAL PROTEIN - Alters the structure of the nuclear envelope by interacting with host CBX5 and disrupting CBX5 association with LBR. Involved in the perinuclear-nuclear localization of the capsid protein VP1 during virion assembly and maturation. Plays an important role in the release of progeny virions from infected cells and in viral propagation	3	0.9	1.1	1.3	5.6	8.1	0.8	1.2	1.2	11.8	15.9
P03082	Small t antigen	Small t antigen	BKPyV VIRAL PROTEIN - Promotes efficient viral genome replication by accelerating both G1 and S phase progression of the cell cycle. Inhibits host PP2A by binding to the A subunit, thereby displacing lower affinity regulatory B subunit	37	0.9	1.1	3.2	7.7	9.1	0.9	1.1	3.2	11.0	12.1
P03071	Large T antigen	Large T antigen	BKPyV VIRAL PROTEIN - Large T antigen is a key early protein essential for both driving viral replication and inducing cellular transformation. Plays a role in viral genome replication by driving entry of quiescent cells into the cell cycle and by autoregulating the synthesis of viral early mRNA	6	0.9	1.1	2.8	6.9	10.9	1.0	1.0	2.6	4.8	10.5
Q9UG87	MIOX	Inositol oxygenase	This protein is involved in step 1 of the subpathway that synthesizes D-glucuronate from myo-inositol	1	2.0	0.0	0.0	1.3	14.3	0.7	1.3	0.7	0.8	0.7
O60299	LZTS3	Leucine zipper putative tumor suppressor 3	May be involved in promoting the maturation of dendritic spines, probably via regulating SIPA1L1 levels at the postsynaptic density of synapses	1	0.8	1.2	2.3	9.3	18.5	0.5	1.5	2.2	16.7	40.0
NOVEL ORF	NOVEL ORF	NOVEL_ORF	BKPyV VIRAL PROTEIN - NOVEL Large T antigen transcript	1	0.0	2.0	15.1	140.5	212.9	1.3	0.7	3.2	44.1	68.7

Table S4: Significantly up and down regulated proteins at 72 hpi in HU cells ($p < 0.0005$).
Table of proteins observed to be significantly ($p < 0.0005$) up or down regulated in HU cells at 72 hpi, when compared to an average of the 24 and 72 h HU cell mock samples. Fold changes of every experimental condition shown for each protein (against an average of the 24 and 72 h mock samples for the corresponding cell type). Increasing red colour indicates greater up regulated fold changes, increasing green colour indicates greater down regulated fold changes).

Uniprot ID	Gene Name	Protein Name	Function	Peptide No.	HUC Mock 24h	HUC Mock 72h	HUC BK 24h	HUC BK 48h	HUC BK 72h	RPTEC Mock 24h	RPTEC Mock 72h	RPTEC BK 24h	RPTEC BK 48h	RPTEC BK 72h
P30679	GNA15	Guanine nucleotide-binding protein subunit alpha-15	Guanine nucleotide-binding proteins (G proteins) are involved as modulators or transducers in various transmembrane signaling systems	2	1.0	1.0	1.1	1.0	1.0	1.4	0.6	0.2	0.3	0.2
D3YTG3	ABI3BP	Target of Nesh-SH3	Collagen and heparin binding protein	3	0.9	1.1	1.0	1.2	1.6	0.3	1.7	0.3	0.8	1.0
A6NDB9	PALM3	Paralemmin-3	ATP-binding protein, which may act as a adapter in the Toll-like receptor (TLR) signaling	2	0.9	1.1	1.0	1.1	1.2	0.4	1.6	0.4	0.6	0.8
E9PQD6	SAA1	Serum amyloid A-1 protein	Major acute phase protein	1	0.9	1.1	1.0	0.8	1.1	0.5	1.5	0.4	0.6	0.3
Q8TB45	DEPTOR	DEP domain-containing mTOR-interacting protein	Negative regulator of the mTORC1 and mTORC2 signaling pathways. Inhibits the kinase activity of both complexes	3	0.8	1.2	0.9	0.9	1.0	0.5	1.5	0.5	0.5	0.4
Q99988	GDF15	Growth/differentiation factor 15	Macrophage inhibitory cytokine involved in TGF-b receptor binding and cell-cell signalling	10	0.7	1.3	0.7	0.5	0.6	0.6	1.4	0.5	0.5	0.5
B1AHL2	FBLN1	Fibulin-1	Incorporated into fibronectin-containing matrix fibers. May play a role in cell adhesion and migration along protein fibers within the extracellular matrix (ECM)	13	1.1	0.9	1.1	1.9	1.6	0.6	1.4	0.5	1.0	1.2
P46013	MKI67	Proliferation marker protein Ki-67	Required to maintain individual mitotic chromosomes dispersed in the cytoplasm following nuclear envelope disassembly. Associates with the surface of the mitotic chromosome, the perichromosomal layer, and covers a substantial fraction of the chromosome surface	121	1.4	0.6	1.4	2.0	2.1	1.4	0.6	1.5	2.3	3.3
Q9ULW0	TPX2	Targeting protein for Xklp2	Spindle assembly factor required for normal assembly of mitotic spindles. Required for normal assembly of microtubules during apoptosis. Required for chromatin and/or kinetochore dependent microtubule nucleation. Mediates AURKA localization to spindle microtubules	30	1.5	0.5	1.5	2.5	2.7	1.3	0.7	1.6	4.1	4.7
Q6SJ93	FAM111B	Protein FAM111B	Cancer-associated nucleoprotein	12	1.5	0.5	2.0	2.4	2.0	1.3	0.7	1.7	2.7	2.1
Q96T88	UHRF1	Isoform 2 of E3 ubiquitin–protein ligase UHRF1	Multidomain protein that acts as a key epigenetic regulator by bridging DNA methylation and chromatin modification. Specifically recognizes and binds hemimethylated DNA at replication forks via its YDG domain and recruits DNMT1 methyltransferase to ensure faithful propagation of the DNA methylation patterns through DNA replication	19	1.5	0.5	1.7	1.5	1.2	1.4	0.6	1.8	1.8	1.4
Q9NZJ0	DTL	Denticleless protein homolog	Substrate-specific adapter of a DCX (DDB1-CUL4-X-box) E3 ubiquitin-protein ligase complex required for cell cycle control, DNA damage response and translesion DNA synthesis	5	1.4	0.6	2.5	3.3	3.5	1.4	0.6	2.1	3.5	3.9
Q9UQ84	EXO1	Exonuclease 1	5'->3' double-stranded DNA exonuclease which may also possess a cryptic 3'->5' double-stranded DNA exonuclease activity. Functions in DNA mismatch repair (MMR) to excise mismatch-containing DNA tracts directed by strand breaks located either 5' or 3' to the mismatch. Also exhibits endonuclease activity against 5'-overhanging flap structures similar to those generated by displacement synthesis when DNA polymerase encounters the 5'-end of a downstream Okazaki fragment	4	1.4	0.6	2.1	2.2	1.9	1.3	0.7	2.1	1.8	2.0
Q9HAW4	CLSPN	Claspin	Required for checkpoint mediated cell cycle arrest in response to inhibition of DNA replication or to DNA damage induced by both ionizing and UV irradiation. Adapter protein which binds to BRCA1 and the checkpoint kinase CHEK1 and facilitates the ATR-dependent phosphorylation of both proteins	10	1.5	0.5	2.1	3.3	2.4	1.3	0.7	2.2	5.7	3.6
P03082	Small t antigen	Small t antigen	BKPyV VIRAL PROTEIN - Promotes efficient viral genome replication by accelerating both G1 and S phase progression of the cell cycle. Inhibits host PP2A by binding to the A subunit, thereby displacing lower affinity regulatory B subunit	6	0.9	1.1	2.8	6.9	10.9	1.0	1.0	2.6	4.8	10.5
P03071	Large T antigen	Large T antigen	BKPyV VIRAL PROTEIN - Large T antigen is a key early protein essential for both driving viral replication and inducing cellular transformation. Plays a role in viral genome replication by driving entry of quiescent cells into the cell cycle and by autoregulating the synthesis of viral early mRNA	37	0.9	1.1	3.2	7.7	9.1	0.9	1.1	3.2	11.0	12.1

Table S5: Significantly up and down regulated proteins at 24 hpi in RPTE cells ($p < 0.0005$).
Table of proteins observed to be significantly ($p < 0.0005$) up or down regulated in RPTE cells at 24 hpi, when compared to an average of the 24 and 72 h HU cell mock samples. Fold changes of every experimental condition shown for each protein (against an average of the 24 and 72 h mock samples for the corresponding cell line). Increasing red colour indicates greater up regulated fold changes, increasing green colour indicates greater down regulated fold changes).

Uniprot ID	Gene Name	Protein Name	Function	Peptide No.	HUC Mock 24h	HUC Mock 72h	HUC BK 24h	HUC BK 48h	HUC BK 72h	RPTEC Mock 24h	RPTEC Mock 72h	RPTEC BK 24h	RPTEC BK 48h	RPTEC BK 72h
Q9NZB2	FAM120A	Constitutive coactivator of PPAR-gamma-like protein 1	May participate in mRNA transport in the cytoplasm (By similarity). Critical component of the oxidative stress-induced survival signaling. Activates src family kinases and acts as a scaffolding protein enabling src family kinases to phosphorylate and activate PI3-kinase. Binds RNA and promotes the secretion of IGF-II	1	1.1	0.9	1.4	1.5	1.3	1.0	1.0	1.1	0.1	0.8
Q9NSB8	HOMER2	Isoform 2 of Homer protein homolog 2	Postsynaptic density scaffolding protein. Binds and cross-links cytoplasmic regions of GRM1, GRM5, ITPR1, DNM3, RYR1, RYR2, SHANK1 and SHANK3. By physically linking GRM1 and GRM5 with ER-associated ITPR1 receptors, it aids the coupling of surface receptors to intracellular calcium release	1	1.0	1.0	1.1	1.2	1.2	1.0	1.0	1.1	0.2	0.9
Q8XWV5	RPAP2	Putative RNA polymerase II subunit B1 CTD phosphatase RPAP2	Protein phosphatase that displays CTD phosphatase activity and regulates transcription of snRNA genes. Recognizes and binds phosphorylated 'Ser-7' of the C-terminal heptapeptide repeat domain (CTD) of the largest RNA polymerase II subunit POLR2A	2	1.0	1.0	1.1	1.2	1.0	1.1	0.9	1.1	0.3	0.6
Q717R9	CYS1	Cystin-1	Cilia-associated protein, allows trafficking of myristoylated proteins to the cilium	2	1.0	1.0	1.1	1.4	1.8	0.8	1.2	0.9	0.3	0.6
Q12983	BNIP3	BCL2/adenovirus E1B 19 kDa protein-interacting protein 3	Apoptosis-inducing protein that can overcome BCL2 suppression	3	1.1	0.9	1.1	1.0	0.8	0.9	1.1	0.9	0.3	0.7
P15151	PVR	Poliovirus receptor	Mediates NK cell adhesion and triggers NK cell effector functions. Binds two different NK cell receptors: CD96 and CD226. These interactions accumulate at the cell-cell contact site, leading to the formation of a mature immunological synapse between NK cell and target cell	2	1.1	0.9	1.2	0.9	0.9	1.0	1.0	1.1	0.3	0.8
F5GX68	DNMT1	Cytosine-specific methyltransferase	Methylates CpG residues. Preferentially methylates hemimethylated DNA. Associates with DNA replication sites in S phase maintaining the methylation pattern in the newly synthesized strand, that is essential for epigenetic inheritance. Associates with chromatin during G2 and M phases to maintain DNA methylation independently of replication	2	1.5	0.5	1.5	1.7	1.3	1.4	0.6	1.7	2.1	2.0
P46013	MKI67	Proliferation marker protein Ki-67	Required to maintain individual mitotic chromosomes dispersed in the cytoplasm following nuclear envelope disassembly. Associates with the surface of the mitotic chromosome, the perichromosomal layer, and covers a substantial fraction of the chromosome surface	121	1.4	0.6	1.4	2.0	2.1	1.4	0.6	1.5	2.3	3.3
Q15398	DLGAP5	Disks large-associated protein 5	Potential cell cycle regulator that may play a role in carcinogenesis of cancer cells. Mitotic phosphoprotein regulated by the ubiquitin-proteasome pathway	19	1.4	0.6	1.4	1.9	2.1	1.3	0.7	1.4	2.3	2.5
Q8X90	SKA3	Spindle and kinetochore-associated protein 3	Component of the SKA1 complex, a microtubule-binding subcomplex of the outer kinetochore that is essential for proper chromosome segregation	13	1.5	0.5	1.6	1.9	2.1	1.3	0.7	1.5	2.4	2.5
O60566	BUB1B	Isoform 3 of Mitotic checkpoint serine/threonine-protein kinase BUB1 beta	Essential component of the mitotic checkpoint. Required for normal mitosis progression	13	1.4	0.6	1.4	1.8	1.8	1.2	0.8	1.4	2.4	2.4
Q96KB5	PBK	Lymphokine-activated killer T-cell-originated protein kinase	Phosphorylates MAP kinase p38. Seems to be active only in mitosis. May also play a role in the activation of lymphoid cells. When phosphorylated, forms a complex with TP53, leading to TP53 destabilization and attenuation of G2/M checkpoint during doxorubicin-induced DNA damage	15	1.4	0.6	1.6	2.1	2.7	1.4	0.6	1.5	2.4	3.4
P14635	CCNB1	G2/mitotic-specific cyclin-B1	Essential for the control of the cell cycle at the G2/M (mitosis) transition	13	1.4	0.6	1.5	2.1	2.2	1.1	0.9	1.4	2.4	2.4
Q9H3R5	CENPH	Centromere protein H	Component of the CENPA-NAC (nucleosome-associated) complex, a complex that plays a central role in assembly of kinetochore proteins, mitotic progression and chromosome segregation	5	1.4	0.6	1.5	2.0	2.2	1.3	0.7	1.2	2.5	2.2
O95235	KIF20A	Kinesin-like protein KIF20A	Mitotic kinesin required for chromosome passenger complex (CPC)-mediated cytokinesis. Following phosphorylation by PLK1, involved in recruitment of PLK1 to the central spindle	18	1.5	0.5	1.5	1.9	1.8	1.4	0.6	1.6	2.6	3.0
Q9NQS7	INCENP	Inner centromere protein	Component of the chromosomal passenger complex (CPC), a complex that acts as a key regulator of mitosis	17	1.2	0.8	1.3	1.9	2.3	1.1	0.9	1.3	2.6	3.7
Q96GX5	MASTL	Serine/threonine-protein kinase greatwall	Serine/threonine kinase that plays a key role in M phase by acting as a regulator of mitosis entry and maintenance. Acts by promoting the inactivation of protein phosphatase 2A (PP2A) during M phase	12	1.2	0.8	1.3	1.8	2.2	1.2	0.8	1.3	2.7	3.1
Q9Y4H2	IRS2	Insulin receptor substrate 2	May mediate the control of various cellular processes by insulin	7	0.8	1.2	0.9	1.1	1.5	1.1	0.9	1.3	2.7	5.7
Q6SJ93	FAM111B	Protein FAM111B	Cancer-associated nucleoprotein	12	1.5	0.5	2.0	2.4	2.0	1.3	0.7	1.7	2.7	2.1
P53350	PLK1	Serine/threonine-protein kinase PLK1	Serine/threonine-protein kinase that performs several important functions throughout M phase of the cell cycle, including the regulation of centrosome maturation and spindle assembly, the removal of cohesins from chromosome arms, the inactivation of anaphase-promoting complex/cyclosome (APC/C) inhibitors, and the regulation of mitotic exit and cytokinesis	13	1.5	0.5	1.6	1.6	1.4	1.4	0.6	1.6	2.7	2.4
Q69YH5	CDCA2	Cell division cycle-associated protein 2	Regulator of chromosome structure during mitosis required for condensin-depleted chromosomes to retain their compact architecture through anaphase. Acts by mediating the recruitment of phopsphatase PP1-gamma subunit (PPP1CC) to chromatin at anaphase and into the following interphase	12	1.5	0.5	1.6	2.0	2.2	1.2	0.8	1.4	2.8	3.2

Accession	Gene	Protein	Function	Count	R1	R2	R3	R4	R5	R6	R7	R8	R9	R10
Q9NZE8	MRPL35	39S ribosomal protein L35, mitochondrial	Structural constituent of ribosome	3	1.1	0.9	1.1	1.0	1.0	0.9	1.1	0.9	2.9	1.1
Q53E24	CEP55	Centrosomal protein of 55 kDa	Plays a role in mitotic exit and cytokinesis	18	1.5	0.5	1.5	1.8	1.8	1.3	0.7	1.6	2.9	2.7
E9PFC7	BRCA1	Breast cancer type 1 susceptibility protein	E3 ubiquitin-protein ligase that specifically mediates the formation of 'Lys-6'-linked polyubiquitin chains and plays a central role in DNA repair by facilitating cellular responses to DNA damage	11	1.4	0.6	1.5	1.9	2.0	1.2	0.8	1.4	2.9	2.8
Q96Q89	KIF20B	Isoform 2 of Kinesin-like protein KIF20B	Plus-end-directed motor enzyme that is required for completion of cytokinesis. Required for proper midbody organization and abscission in polarized cortical stem cells	15	1.2	0.8	1.4	1.9	1.6	1.3	0.7	1.5	2.9	3.5
P49454	CENPF	Centromere protein F	Required for kinetochore function and chromosome segregation in mitosis. Required for kinetochore localization of dynein, LIS1, NDE1 and NDEL1. Regulates recycling of the plasma membrane by acting as a link between recycling vesicles and the microtubule network though its association with STX4 and SNAP25	46	1.2	0.8	1.2	1.4	1.3	1.2	0.8	1.5	2.9	3.6
J9JID1	AURKB	Aurora kinase B	Serine/threonine-protein kinase component of the chromosomal passenger complex (CPC), a complex that acts as a key regulator of mitosis	6	1.4	0.6	1.6	1.9	2.1	1.2	0.8	1.4	3.0	3.1
Q96B01	RAD51AP1	RAD51-associated protein 1	May participate in a common DNA damage response pathway associated with the activation of homologous recombination and double-strand break repair. Functionally cooperates with PALB2 in promoting D-loop formation by RAD51	4	1.2	0.8	1.3	2.4	2.3	1.2	0.8	1.4	3.0	2.9
Q9H8V3	ECT2	Protein ECT2	Guanine nucleotide exchange factor (GEF) that catalyzes the exchange of GDP for GTP. Promotes guanine nucleotide exchange on the Rho family members of small GTPases, like RHOA, RHOC, RAC1 and CDC42. Required for signal transduction pathways involved in the regulation of cytokinesis	10	1.3	0.7	1.4	1.8	1.8	1.1	0.9	1.4	3.0	3.1
Q53HL2	CDCA8	Borealin	Component of the chromosomal passenger complex (CPC), a complex that acts as a key regulator of mitosis	7	1.4	0.6	1.5	2.2	3.0	1.3	0.7	1.4	3.0	4.6
Q9Y620	RAD54B	DNA repair and recombination protein RAD54B	Involved in DNA repair and mitotic recombination	4	1.1	0.9	1.5	1.7	1.7	1.3	0.7	1.4	3.1	2.4
Q9BW19	KIFC1	Kinesin-like protein KIFC1	Minus end-directed microtubule-dependent motor required for bipolar spindle formation	19	1.4	0.6	1.5	2.4	2.9	1.2	0.8	1.5	3.2	4.2
P52732	KIF11	Kinesin-like protein KIF11	Motor protein required for establishing a bipolar spindle during mitosis. Required in non-mitotic cells for transport of secretory proteins from the Golgi complex to the cell surface	32	1.3	0.7	1.4	2.4	2.9	1.2	0.8	1.5	3.3	4.7
Q99618	CDCA3	Cell division cycle-associated protein 3	F-box-like protein which is required for entry into mitosis. Acts by participating in E3 ligase complexes that mediate the ubiquitination and degradation of WEE1 kinase at G2/M phase	5	1.3	0.7	1.3	2.4	2.9	1.3	0.7	1.3	3.3	4.8
O43663	PRC1	Protein regulator of cytokinesis 1	Key regulator of cytokinesis that cross-links antiparallel microtubules at an average distance of 35 nM. Essential for controlling the spatiotemporal formation of the midzone and successful cytokinesis. Required for KIF14 localization to the central spindle and midbody. Required to recruit PLK1 to the spindle. Stimulates PLK1 phosphorylation of RACGAP1 to allow recruitment of ECT2 to the central spindle	10	1.4	0.6	1.6	2.2	2.5	1.2	0.8	1.3	3.3	3.6
Q9Y6A5	TACC3	Transforming acidic coiled-coil-containing protein 3	Plays a role in the microtubule-dependent coupling of the nucleus and the centrosome. Involved in the processes that regulate centrosome-mediated interkinetic nuclear migration (INM) of neural progenitors (By similarity). Acts as component of the TACC3/ch-TOG/clathrin complex proposed to contribute to stabilization of kinetochore fibers of the mitotic spindle by acting as inter-microtubule bridge	20										
Q6UVJ0	SASS6	Spindle assembly abnormal protein 6 homolog	Central scaffolding component of the centrioles ensuring their 9-fold symmetry. Required for centrosome biogenesis and duplication: required both for mother-centriole-dependent centriole duplication and deuterosome-dependent centriole amplification in multiciliated cells	6	1.2	0.8	1.3	2.1	2.5	1.2	0.8	1.5	3.3	3.9
P11388	TOP2A	Isoform 4 of DNA topoisomerase 2-alpha	Control of topological states of DNA by transient breakage and subsequent rejoining of DNA strands. Topoisomerase II makes double-strand breaks. Essential during mitosis and meiosis for proper segregation of daughter chromosomes. oscillation	61	1.4	0.6	1.3	2.2	2.6	1.1	0.9	1.4	3.4	3.3
Q16763	UBE2S	Ubiquitin-conjugating enzyme E2 S	Acts as an essential factor of the anaphase promoting complex/cyclosome (APC/C), a cell cycle-regulated ubiquitin ligase that controls progression through mitosis	3	1.6	0.4	1.8	2.2	2.7	1.3	0.7	1.6	3.4	5.1
Q8IYA6	CKAP2L	Cytoskeleton-associated protein 2-like	Microtubule-associated protein required for mitotic spindle formation and cell-cycle progression in neural progenitor cells	7	1.3	0.7	1.4	1.9	1.6	1.2	0.8	1.4	3.4	2.1
Q9NZJ0	DTL	Denticleless protein homolog	Substrate-specific adapter of a DCX (DDB1-CUL4-X-box) E3 ubiquitin-protein ligase complex required for cell cycle control, DNA damage response and translesion DNA synthesis	5	1.4	0.6	2.5	3.3	3.5	1.4	0.6	2.1	3.5	3.9
O00762	UBE2C	Ubiquitin-conjugating enzyme E2 C	Accepts ubiquitin from the E1 complex and catalyzes its covalent attachment to other proteins. In vitro catalyzes 'Lys-11'- and 'Lys-48'-linked polyubiquitination. Acts as an essential factor of the anaphase promoting complex/cyclosome (APC/C), a cell cycle-regulated ubiquitin ligase that controls progression through mitosis.	4	1.9	0.1	2.0	2.2	1.7	1.4	0.6	1.8	3.5	1.8
O95229	ZWINT	ZW10 interactor	Part of the MIS12 complex, which is required for kinetochore formation and spindle checkpoint activity. Required to target ZW10 to the kinetochore at prometaphase	3	1.5	0.5	1.9	2.8	2.6	1.3	0.7	1.6	3.6	2.9

UniProt	Gene	Protein name	Description	n										
Q8NI77	KIF18A	Kinesin-like protein KIF18A	Microtubule-depolymerizing kinesin which plays a role in chromosome congression by reducing the amplitude of preanaphase oscillations and slowing poleward movement during anaphase, thus suppressing chromosome movements. May stabilize the CENPE-BUB1B complex at the kinetochores during early mitosis and maintains CENPE levels at kinetochores during chromosome congression	4	1.5	0.5	1.8	2.2	2.0	1.2	0.8	1.6	3.6	4.3
P03094	VP2	Minor capsid protein VP2	BKPyV VIRAL PROTEIN - VP2 is a structural protein that resides within the core of the capsid surrounded by 72 VP1 pentamers. Participates in host cell receptor binding together with VP1	18	1.0	1.0	1.4	3.1	6.4	1.0	1.0	1.3	3.7	12.7
Q14807	KIF22	Kinesin-like protein KIF22	Kinesin family member that is involved in spindle formation and the movements of chromosomes during mitosis and meiosis. Binds to microtubules and to DNA	9	1.5	0.5	1.7	2.6	2.6	1.3	0.7	1.6	3.7	5.1
B5MBX0	CDCA5	Sororin	Regulator of sister chromatid cohesion in mitosis stabilizing cohesin complex association with chromatin	6	1.4	0.6	1.7	2.6	3.1	1.1	0.9	1.5	3.7	4.2
Q6PL18	ATAD2	ATPase family AAA domain-containing protein 2	May be a transcriptional coactivator of the nuclear receptor ESR1 required to induce the expression of a subset of estradiol target genes, such as CCND1, MYC and E2F1. May play a role in the recruitment or occupancy of CREBBP at some ESR1 target gene promoters. May be required for histone hyperacetylation.	23	1.3	0.7	1.6	2.2	1.8	1.2	0.8	1.4	3.7	3.8
Q7Z628	NET1	Neuroepithelial cell-transforming gene 1 protein	Acts as guanine nucleotide exchange factor (GEF) for RhoA GTPase	3	1.5	0.5	1.5	1.5	1.5	1.2	0.8	1.6	3.7	4.0
Q86Y91	KIF18B	Isoform 4 of Kinesin-like protein KIF18B	In complex with KIF2C, constitutes the major microtubule plus-end depolymerizing activity in mitotic cells	2	1.2	0.8	1.9	1.5	2.2	1.3	0.7	1.4	3.9	4.4
Q99741	CDC6	Cell division control protein 6 homolog	Involved in the initiation of DNA replication. Also participates in checkpoint controls that ensure DNA replication is completed before mitosis is initiated	4	1.1	0.9	1.6	1.9	1.4	1.1	0.9	1.6	3.9	2.2
Q9NYP3	DONSON	Protein downstream neighbor of Son	Replisome component that maintains genome stability by protecting stalled or damaged replication forks. After the induction of replication stress, required for the stabilization of stalled replication forks, the efficient activation of the intra-S-phase and G/2M cell-cycle checkpoints and the maintenance of genome stability	2	1.2	0.8	1.4	2.0	2.4	1.2	0.8	1.5	3.9	3.8
Q8NEM2	SHCBP1	SHC SH2 domain-binding protein 1	May play a role in signaling pathways governing cellular proliferation, cell growth and differentiation. May be a component of a novel signaling pathway downstream of Shc. Acts as a positive regulator of FGF signaling in neural progenitor cells	10	1.6	0.4	1.8	2.5	3.3	1.4	0.6	1.7	3.9	4.4
O14965	AURKA	Aurora kinase A	Spindle assembly factor required for normal assembly of mitotic spindles. Required for normal assembly of microtubules during apoptosis. Required for chromatin and/or kinetochore dependent microtubule nucleation. Mediates AURKA localization to spindle microtubules	9	1.7	0.3	1.9	2.7	2.9	1.3	0.7	1.7	3.9	4.5
Q5HYC2	KIAA2026	Uncharacterized protein KIAA2026	Unknown	1	0.4	1.6	1.8	0.4	2.1	1.0	1.0	1.0	3.9	4.0
O75330	HMMR	Isoform 3 of Hyaluronan mediated motility receptor	Receptor for hyaluronic acid (HA) (By similarity). Involved in cell motility (By similarity). When hyaluronan binds to HMMR, the phosphorylation of a number of proteins, including PTK2/FAK1 occurs	16	1.4	0.6	1.6	2.2	2.2	1.2	0.8	1.4	4.1	4.7
Q9ULW0	TPX2	Targeting protein for Xklp2	Spindle assembly factor required for normal assembly of mitotic spindles. Required for normal assembly of microtubules during apoptosis. Required for chromatin and/or kinetochore dependent microtubule nucleation. Mediates AURKA localization to spindle microtubules	30	1.5	0.5	1.5	2.5	2.7	1.3	0.7	1.6	4.1	4.7
P04183	TK1	Thymidine kinase, cytosolic	Two forms have been identified in animal cells, one in cytosol and one in mitochondria. Activity of the cytosolic enzyme is high in proliferating cells and peaks during the S-phase of the cell cycle; it is very low in resting cells	9	1.6	0.4	1.7	3.2	3.6	1.3	0.7	1.6	4.1	4.1
Q9UKT4	FBXO5	F-box only protein 5	Regulates progression through early mitosis by inhibiting the anaphase promoting complex/cyclosome (APC). Binds to the APC activators CDC20 and FZR1/CDH1 to prevent APC activation. Can also bind directly to the APC to inhibit substrate-binding	5	1.0	1.0	1.2	1.4	1.3	1.2	0.8	1.8	4.2	3.1
Q9NR29	HELLS	Lymphoid-specific helicase	Plays an essential role in normal development and survival. Involved in regulation of the expansion or survival of lymphoid cells. Required for de novo or maintenance DNA methylation	12	1.6	0.4	1.9	2.3	1.8	1.3	0.7	1.8	4.3	3.7
P20248	CCNA2	Cyclin-A2	Cyclin which controls both the G1/S and the G2/M transition phases of the cell cycle. Functions through the formation of specific serine/threonine protein kinase holoenzyme complexes with the cyclin-dependent protein kinases CDK1 or CDK2	7	1.5	0.5	1.9	3.3	3.6	1.3	0.7	1.7	4.4	5.4
Q9NQW6	ANLN	Anillin	Required for cytokinesis. Essential for the structural integrity of the cleavage furrow and for completion of cleavage furrow ingression. Plays a role in bleb assembly during metaphase and anaphase of mitosis	60	1.4	0.6	1.5	2.7	3.1	1.2	0.8	1.5	4.4	5.7
Q9H967	WDR76	WD repeat-containing protein 76	Specifically binds 5-hydroxymethylcytosine (5hmC), suggesting that it acts as a specific reader of 5hmC	5	1.5	0.5	1.9	3.2	4.1	1.3	0.7	1.9	4.4	5.8
P03082	Small t antigen	Small t antigen	BKPyV VIRAL PROTEIN - Promotes efficient viral genome replication by accelerating both G1 and S phase progression of the cell cycle. Inhibits host PP2A by binding to the A subunit, thereby displacing lower affinity regulatory B subunit	6	0.9	1.1	2.8	6.9	10.9	1.0	1.0	2.6	4.8	10.5
H0YMA4	PCLAF	HCG2039336, isoform CRA_b	Involved in cell cycle regulation and DNA damage response. Not widely characterised	4	1.4	0.6	1.8	2.2	1.7	1.3	0.7	1.9	5.0	2.3

ID	Gene	Protein	Description										
P31350	RRM2	Isoform 2 of Ribonucleoside-diphosphate reductase subunit M2	Provides the precursors necessary for DNA synthesis. Catalyzes the biosynthesis of deoxyribonucleotides from the corresponding ribonucleotides. Inhibits Wnt signaling	25	1.3	0.7	1.7	2.7	2.9	1.2	0.8	1.6	5.2	4.6
Q8WWK9	CKAP2	Isoform 3 of Cytoskeleton-associated protein 2	Possesses microtubule stabilizing properties. Involved in regulating aneuploidy, cell cycling, and cell death in a p53/TP53-dependent manner	18	1.5	0.5	1.6	3.3	4.7	1.2	0.8	1.6	5.2	6.5
O75631	UPK3A	Uroplakin-3a	Component of the asymmetric unit membrane (AUM); a highly specialized biomembrane elaborated by terminally differentiated urothelial cells. May play an important role in AUM-cytoskeleton interaction in terminally differentiated urothelial cells	1	0.6	1.4	0.6	0.5	0.5	1.3	0.7	0.9	5.3	11.0
Q562F6	SGO2	Shugoshin 2	Essential for recruiting KIF2C to the inner centromere and for correcting defective kinetochore attachments. Involved in centromeric enrichment of AUKRB in prometaphase	7	1.0	1.0	2.1	3.9	3.9	1.2	0.8	1.5	5.3	6.1
Q9HAW4	CLSPN	Claspin	Required for checkpoint mediated cell cycle arrest in response to inhibition of DNA replication or to DNA damage induced by both ionizing and UV irradiation. Adapter protein which binds to BRCA1 and the checkpoint kinase CHEK1 and facilitates the ATR-dependent phosphorylation of both proteins	10	1.5	0.5	2.1	3.3	2.4	1.3	0.7	2.2	5.7	3.6
P03088	VP1	Major capsid protein VP1	BKPyV VIRAL PROTEIN - Forms an icosahedral capsid with a T=7 symmetry and a 50 nm diameter. The capsid is composed of 72 pentamers linked to each other by disulfide bonds and associated with VP2 or VP3 proteins. Interacts with gangliosides GT1b and GD1b containing terminal alpha2-8-linked sialic acids on the cell surface to provide virion attachment to target cell	280	1.0	1.0	1.5	4.1	7.0	1.0	1.0	1.3	6.6	14.6
O96020	CCNE2	G1/S-specific cyclin-E2	Essential for the control of the cell cycle at the late G1 and early S phase	1	1.3	0.7	2.2	3.9	3.2	1.1	0.9	2.1	7.3	4.1
P01100	FOS	Proto-oncogene c-Fos	Nuclear phosphoprotein which forms a tight but non-covalently linked complex with the JUN/AP-1 transcription factor. In the heterodimer, FOS and JUN/AP-1 basic regions each seems to interact with symmetrical DNA half sites. On TGF-beta activation, forms a multimeric SMAD3/SMAD4/JUN/FOS complex at the AP1/SMAD-binding site to regulate TGF-beta-mediated signaling	1	1.2	0.8	1.2	2.3	3.9	0.9	1.1	1.4	9.0	11.3
P03071	Large T antigen	Large T antigen	BKPyV VIRAL PROTEIN - Large T antigen is a key early protein essential for both driving viral replication and inducing cellular transformation. Plays a role in viral genome replication by driving entry of quiescent cells into the cell cycle and by autoregulating the synthesis of viral early mRNA	37	0.9	1.1	3.2	7.7	9.1	0.9	1.1	3.2	11.0	12.1
P03085	Agnoprotein	Agnoprotein	BKPyV VIRAL PROTEIN - Alters the structure of the nuclear envelope by interacting with host CBX5 and disrupting CBX5 association with LBR. Involved in the perinuclear-nuclear localization of the capsid protein VP1 during virion assembly and maturation. Plays an important role in the release of progeny virions from infected cells and in viral propagation	3	0.9	1.1	1.3	5.6	8.1	0.8	1.2	1.2	11.8	15.9
O60299	LZTS3	Leucine zipper putative tumor suppressor 3	May be involved in promoting the maturation of dendritic spines, probably via regulating SIPA1L1 levels at the postsynaptic density of synapses	1	0.8	1.2	2.3	9.3	18.5	0.5	1.5	2.2	16.7	40.0
NOVEL ORF	NOVEL ORF	NOVEL_ORF	BKPyV VIRAL PROTEIN - NOVEL Large T antigen transcript	1	0.0	2.0	15.1	140.5	212.9	1.3	0.7	3.2	44.1	68.7

Table S6: Significantly up and down regulated proteins at 48 hpi in RPTE cells ($p < 0.0005$).
Table of proteins observed to be significantly ($p < 0.0005$) up or down regulated in RPTE cells at 48 hpi, when compared to an average of the 24 and 72 h HU cell mock samples. Fold changes of every experimental condition shown for each protein (against an average of the 24 and 72 h mock samples for the corresponding cell type). Increasing red colour indicates greater up regulated fold changes, increasing green colour indicates greater down regulated fold changes).

Uniprot ID	Gene Name	Protein Name	Function	Peptide No.	HUC Mock 24h	HUC Mock 72h	HUC BK 24h	HUC BK 48h	HUC BK 72h	RPTEC Mock 24h	RPTEC Mock 72h	RPTEC BK 24h	RPTEC BK 48h	RPTEC BK 72h
Q8WWA1	TMEM40	Isoform 2 of Transmembrane protein 40	Multipass membrane protein, function unclear	1	0.7	1.3	0.6	4.5	3.7	1.3	0.7	0.0	0.0	0.0
Q8N339	MT1M	Metallothionein-1M	Metallothioneins have a high content of cysteine residues that bind various heavy metals; these proteins are transcriptionally regulated by both heavy metals and glucocorticoids	1	1.0	1.0	1.0	0.9	1.6	1.1	0.9	1.1	0.8	0.2
P50591	TNFSF10	Tumor necrosis factor ligand superfamily member 10 - TRAIL	Cytokine that binds to TNFRSF10A/TRAILR1, TNFRSF10B/TRAILR2, TNFRSF10C/TRAILR3, TNFRSF10D/TRAILR4 (possibly also to TNFRSF11B/OPG) and induces apoptosis	8	0.8	1.2	0.8	0.8	0.8	1.0	1.0	0.9	0.6	0.3
Q13113	PDZK1IP1	PDZK1-interacting protein 1	May play an important role in tumor biology	2	0.9	1.1	0.8	1.0	1.0	0.6	1.4	0.6	0.4	0.3
P02675	FGB	Fibrinogen beta chain	Cleaved by the protease thrombin to yield monomers which, together with fibrinogen alpha (FGA) and fibrinogen gamma (FGG), polymerize to form an insoluble fibrin matrix	4	1.0	1.0	0.9	1.0	1.6	0.9	1.1	1.0	0.8	0.3
P80294	MT1H	Metallothionein-1H	Metallothioneins have a high content of cysteine residues that bind various heavy metals; these proteins are transcriptionally regulated by both heavy metals and glucocorticoids	4	1.2	0.8	1.1	0.9	0.9	1.0	1.0	1.0	1.0	0.4
P10451	SPP1	Osteopontin	Binds tightly to hydroxyapatite. Acts as a cytokine involved in enhancing production of interferon-gamma and interleukin-12 and reducing production of interleukin-10 and is essential in the pathway that leads to type I immunity	11	1.0	1.0	1.1	1.1	1.1	0.8	1.2	0.8	0.7	0.4
Q53EZ4	CEP55	Centrosomal protein of 55 kDa	Plays a role in mitotic exit and cytokinesis	18	1.5	0.5	1.5	1.8	1.8	1.3	0.7	1.6	2.9	2.7
E9PFC7	BRCA1	Breast cancer type 1 susceptibility protein	E3 ubiquitin-protein ligase that specifically mediates the formation of 'Lys-6'-linked polyubiquitin chains and plays a central role in DNA repair by facilitating cellular responses to DNA damage	11	1.4	0.6	1.5	1.9	2.0	1.2	0.8	1.4	2.9	2.8
Q9H0H5	RACGAP1	Rac GTPase-activating protein 1	Component of the centralspindlin complex that serves as a microtubule-dependent and Rho-mediated signaling required for the myosin contractile ring formation during the cell cycle cytokinesis. Required for proper attachment of the midbody to the cell membrane during cytokinesis.	17	1.4	0.6	1.6	2.2	2.2	1.4	0.6	1.5	2.2	2.8
Q99661	KIF2C	Kinesin-like protein KIF2C	In complex with KIF18B, constitutes the major microtubule plus-end depolymerizing activity in mitotic cells	16	1.6	0.4	1.7	2.3	2.4	1.4	0.6	1.6	2.1	2.9
O95235	KIF20A	Kinesin-like protein KIF20A	Mitotic kinesin required for chromosome passenger complex (CPC)-mediated cytokinesis. Following phosphorylation by PLK1, involved in recruitment of PLK1 to the central spindle	18	1.5	0.5	1.5	1.9	1.8	1.4	0.6	1.6	2.6	3.0
J9JID1	AURKB	Aurora kinase B	Serine/threonine-protein kinase component of the chromosomal passenger complex (CPC), a complex that acts as a key regulator of mitosis	6	1.4	0.6	1.6	1.9	2.1	1.2	0.8	1.4	3.0	3.1
Q9H8V3	ECT2	Protein ECT2	Guanine nucleotide exchange factor (GEF) that catalyzes the exchange of GDP for GTP. Promotes guanine nucleotide exchange on the Rho family members of small GTPases, like RHOA, RHOC, RAC1 and CDC42. Required for signal transduction pathways involved in the regulation of cytokinesis	10	1.3	0.7	1.4	1.8	1.8	1.1	0.9	1.4	3.0	3.1
Q96GX5	MASTL	Serine/threonine-protein kinase greatwall	Serine/threonine kinase that plays a key role in M phase by acting as a regulator of mitosis entry and maintenance. Acts by promoting the inactivation of protein phosphatase 2A (PP2A) during M phase	12	1.2	0.8	1.3	1.8	2.2	1.2	0.8	1.3	2.7	3.1
Q9UKT4	FBXO5	F-box only protein 5	Regulates progression through early mitosis by inhibiting the anaphase promoting complex/cyclosome (APC). Binds to the APC activators CDC20 and FZR1/CDH1 to prevent APC activation. Can also bind directly to the APC to inhibit substrate-binding	5	1.0	1.0	1.2	1.4	1.3	1.2	0.8	1.8	4.2	3.1
Q69YH5	CDCA2	Cell division cycle-associated protein 2	Regulator of chromosome structure during mitosis required for condensin-depleted chromosomes to retain their compact architecture through anaphase. Acts by mediating the recruitment of phopsphatase PP1-gamma subunit (PPP1CC) to chromatin at anaphase and into the following interphase	12	1.5	0.5	1.6	2.0	2.2	1.2	0.8	1.4	2.8	3.2
P46013	MKI67	Proliferation marker protein Ki-67	Required to maintain individual mitotic chromosomes dispersed in the cytoplasm following nuclear envelope disassembly. Associates with the surface of the mitotic chromosome, the perichromosomal layer, and covers a substantial fraction of the chromosome surface	121	1.4	0.6	1.4	2.0	2.1	1.4	0.6	1.5	2.3	3.3
Q8IYA6	CKAP2L	Cytoskeleton-associated protein 2-like	Microtubule-associated protein required for mitotic spindle formation and cell-cycle progression in neural progenitor cells	7	1.3	0.7	1.4	2.1	2.5	1.1	0.9	1.4	3.4	3.3
Q6UVJ0	SASS6	Spindle assembly abnormal protein 6 homolog	Central scaffolding component of the centrioles ensuring their 9-fold symmetry. Required for centrosome biogenesis and duplication; required both for mother-centriole-dependent centriole duplication and deuterosome-dependent centriole amplification in multiciliated cells	6	1.2	0.8	1.3	2.2	2.6	1.1	0.9	1.4	3.4	3.3

Accession	Gene	Protein name	Description											
Q96KB5	PBK	Lymphokine-activated killer T-cell-originated protein kinase	Phosphorylates MAP kinase p38. Seems to be active only in mitosis. May also play a role in the activation of lymphoid cells. When phosphorylated, forms a complex with TP53, leading to TP53 destabilization and attenuation of G2/M checkpoint during doxorubicin-induced DNA damage	15	1.4	0.6	1.6	2.1	2.7	1.4	0.6	1.5	2.4	3.4
Q9Q89	KIF20B	Isoform 2 of Kinesin-like protein KIF20B	Plus-end-directed motor enzyme that is required for completion of cytokinesis. Required for proper midbody organization and abscission in polarized cortical stem cells	15	1.2	0.8	1.4	1.9	1.6	1.3	0.7	1.5	2.9	3.5
P51649	ALDH5A1	Isoform 2 of Succinate-semialdehyde dehydrogenase, mitochondrial	Catalyzes one step in the degradation of the inhibitory neurotransmitter gamma-aminobutyric acid (GABA)	12	0.9	1.1	0.9	1.1	1.4	0.9	1.1	0.9	2.0	3.5
Q9P0U3	SENP1	Sentrin-specific protease 1	Protease that catalyzes two essential functions in the SUMO pathway	10	1.0	1.0	1.1	1.5	1.8	1.0	1.0	1.0	1.9	3.5
Q8IWE2	FAM114A1	Protein NOXP20	May play a role in neuronal cell development	16	1.0	1.0	1.1	1.6	2.1	1.0	1.0	1.0	2.1	3.5
O43663	PRC1	Protein regulator of cytokinesis 1	Key regulator of cytokinesis that cross-links antiparallel microtubules at an average distance of 35 nM. Essential for controlling the spatiotemporal formation of the midzone and successful cytokinesis. Required for KIF14 localization to the central spindle and midbody. Required to recruit PLK1 to the spindle. Stimulates PLK1 phosphorylation of RACGAP1 to allow recruitment of ECT2 to the central spindle	10	1.4	0.6	1.6	2.2	2.5	1.2	0.8	1.3	3.3	3.6
Q9HAW4	CLSPN	Claspin	Required for checkpoint mediated cell cycle arrest in response to inhibition of DNA replication or to DNA damage induced by both ionizing and UV irradiation. Adapter protein which binds to BRCA1 and the checkpoint kinase CHEK1 and facilitates the ATR-dependent phosphorylation of both proteins	10	1.5	0.5	2.1	3.3	2.4	1.3	0.7	2.2	5.7	3.6
P49454	CENPF	Centromere protein F	Required for kinetochore function and chromosome segregation in mitosis. Required for kinetochore localization of dynein, LIS1, NDE1 and NDEL1. Regulates recycling of the plasma membrane by acting as a link between recycling vesicles and the microtubule network though its association with STX4 and SNAP25	46	1.2	0.8	1.2	1.4	1.3	1.2	0.8	1.5	2.9	3.6
Q9NQS7	INCENP	Inner centromere protein	Component of the chromosomal passenger complex (CPC), a complex that acts as a key regulator of mitosis	17	1.2	0.8	1.3	1.9	2.3	1.1	0.9	1.3	2.6	3.7
Q9NRZ9	HELLS	Lymphoid-specific helicase	Plays an essential role in normal development and survival. Involved in regulation of the expansion or survival of lymphoid cells. Required for de novo or maintenance DNA methylation	12	1.6	0.4	1.9	2.3	1.8	1.3	0.7	1.8	4.3	3.7
I3L156	PIMREG	PIMREG	During mitosis, may play a role in the control of metaphase-to-anaphase transition	2	1.3	0.7	1.5	2.2	2.4	1.2	0.8	1.4	1.7	3.8
Q6PL18	ATAD2	ATPase family AAA domain-containing protein 2	May be a transcriptional coactivator of the nuclear receptor ESR1 required to induce the expression of a subset of estradiol target genes, such as CCND1, MYC and E2F1. May play a role in the recruitment or occupancy of CREBBP at some ESR1 target gene promoters. May be required for histone hyperacetylation.	23	1.3	0.7	1.6	2.2	1.8	1.2	0.8	1.4	3.7	3.8
Q9NYP3	DONSON	Protein downstream neighbor of Son	Replisome component that maintains genome stability by protecting stalled or damaged replication forks. After the induction of replication stress, required for the stabilization of stalled replication forks, the efficient activation of the intra-S-phase and G2/M cell-cycle checkpoints and the maintenance of genome stability	2	1.2	0.8	1.4	2.0	2.4	1.2	0.8	1.5	3.9	3.8
Q9NYZ3	GTSE1	G2 and S phase-expressed protein 1	May be involved in p53-induced cell cycle arrest in G2/M phase by interfering with microtubule rearrangements that are required to enter mitosis. Overexpression delays G2/M phase progression	5	1.3	0.7	1.4	2.0	1.9	1.3	0.7	1.5	3.1	3.9
O15392	BIRC5	Baculoviral IAP repeat-containing protein 5	Multitasking protein that has dual roles in promoting cell proliferation and preventing apoptosis	2	1.3	0.7	1.4	2.1	2.7	1.2	0.8	1.2	2.6	3.9
Q9Y6A5	TACC3	Transforming acidic coiled-coil-containing protein 3	Plays a role in the microtubule-dependent coupling of the nucleus and the centrosome. Involved in the processes that regulate centrosome-mediated interkinetic nuclear migration (INM) of neural progenitors (By similarity). Acts as component of the TACC3/ch-TOG/clathrin complex proposed to contribute to stabilization of kinetochore fibers of the mitotic spindle by acting as inter-microtubule bridge	20	1.2	0.8	1.3	2.1	2.5	1.2	0.8	1.5	3.3	3.9
Q9NZJ0	DTL	Denticleless protein homolog	Substrate-specific adapter of a DCX (DDB1-CUL4-X-box) E3 ubiquitin-protein ligase complex required for cell cycle control, DNA damage response and translesion DNA synthesis	5	1.4	0.6	2.5	3.3	3.5	1.4	0.6	2.1	3.5	3.9
Q7Z628	NET1	Neuroepithelial cell-transforming gene 1 protein	Acts as guanine nucleotide exchange factor (GEF) for RhoA GTPase	3	1.5	0.5	1.5	1.5	1.5	1.2	0.8	1.6	3.7	4.0

Accession	Gene	Protein	Description	Count										
P04183	TK1	Thymidine kinase, cytosolic	Two forms have been identified in animal cells, one in cytosol and one in mitochondria. Activity of the cytosolic enzyme is high in proliferating cells and peaks during the S-phase of the cell cycle; it is very low in resting cells	9	1.6	0.4	1.7	3.2	3.6	1.3	0.7	1.6	4.1	4.1
Q9BW19	KIFC1	Kinesin-like protein KIFC1	Minus end-directed microtubule-dependent motor required for bipolar spindle formation	19	1.4	0.6	1.5	2.4	2.9	1.2	0.8	1.5	3.2	4.2
B5MBX0	CDCA5	Sororin	Regulator of sister chromatid cohesion in mitosis stabilizing cohesin complex association with chromatin	6	1.4	0.6	1.7	2.6	3.1	1.1	0.9	1.5	3.7	4.2
Q8NI77	KIF18A	Kinesin-like protein KIF18A	Microtubule-depolymerizing kinesin which plays a role in chromosome congression by reducing the amplitude of preanaphase oscillations and slowing poleward movement during anaphase, thus suppressing chromosome movements. May stabilize the CENPE-BUB1B complex at the kinetochores during early mitosis and maintains CENPE levels at kinetochores during chromosome congression	4	1.5	0.5	1.8	2.2	2.0	1.2	0.8	1.6	3.6	4.3
Q8NEM2	SHCBP1	SHC SH2 domain-binding protein 1	May play a role in signaling pathways governing cellular proliferation, cell growth and differentiation. May be a component of a novel signaling pathway downstream of Shc. Acts as a positive regulator of FGF signaling in neural progenitor cells	10	1.6	0.4	1.8	2.5	3.3	1.4	0.6	1.7	3.9	4.4
O14965	AURKA	Aurora kinase A	Mitotic serine/threonine kinase that contributes to the regulation of cell cycle progression. Associates with the centrosome and the spindle microtubules during mitosis and plays a critical role in various mitotic events including the establishment of mitotic spindle, centrosome duplication, centrosome separation as well as maturation, chromosomal alignment, spindle assembly checkpoint, and cytokinesis. Required for initial activation of CDK1 at centrosomes	9	1.7	0.3	1.9	2.7	2.9	1.3	0.7	1.7	3.9	4.5
Q9H4I8	FAM83D	Protein FAM83D	Probable proto-oncogene that regulates cell proliferation, growth, migration and epithelial to mesenchymal transition. Through the degradation of FBXW7, may act indirectly on the expression and downstream signaling of MTOR, JUN and MYC	5	1.4	0.6	1.5	1.8	2.2	1.2	0.8	1.4	2.9	4.5
Q53HL2	CDCA8	Borealin	Component of the chromosomal passenger complex (CPC), a complex that acts as a key regulator of mitosis	7	1.4	0.6	1.5	2.2	3.0	1.3	0.7	1.4	3.0	4.6
P31350	RRM2	Isoform 2 of Ribonucleoside-diphosphate reductase subunit M2	Provides the precursors necessary for DNA synthesis. Catalyzes the biosynthesis of deoxyribonucleotides from the corresponding ribonucleotides. Inhibits Wnt signaling	25	1.3	0.7	1.7	2.7	2.9	1.2	0.8	1.6	5.2	4.6
Q9ULW0	TPX2	Targeting protein for Xklp2	Spindle assembly factor required for normal assembly of mitotic spindles. Required for normal assembly of microtubules during apoptosis. Required for chromatin and/or kinetochore dependent microtubule nucleation. Mediates AURKA localization to spindle microtubules	30	1.5	0.5	1.5	2.5	2.7	1.3	0.7	1.6	4.1	4.7
P52732	KIF11	Kinesin-like protein KIF11	Motor protein required for establishing a bipolar spindle during mitosis. Required in non-mitotic cells for transport of secretory proteins from the Golgi complex to the cell surface	32	1.3	0.7	1.4	2.4	2.9	1.2	0.8	1.5	3.3	4.7
O75330	HMMR	Isoform 3 of Hyaluronan mediated motility receptor	Receptor for hyaluronic acid (HA) (By similarity). Involved in cell motility (By similarity). When hyaluronan binds to HMMR, the phosphorylation of a number of proteins, including PTK2/FAK1 occurs	16	1.4	0.6	1.6	2.2	2.2	1.2	0.8	1.4	4.1	4.7
Q99618	CDCA3	Cell division cycle-associated protein 3	F-box-like protein which is required for entry into mitosis. Acts by participating in E3 ligase complexes that mediate the ubiquitination and degradation of WEE1 kinase at G2/M phase	5	1.3	0.7	1.3	2.4	2.9	1.3	0.7	1.3	3.3	4.8
Q14807	KIF22	Kinesin-like protein KIF22	Kinesin family member that is involved in spindle formation and the movements of chromosomes during mitosis and meiosis. Binds to microtubules and to DNA	9	1.5	0.5	1.7	2.6	2.6	1.3	0.7	1.6	3.7	5.1
P11388	TOP2A	Isoform 4 of DNA topoisomerase 2-alpha	Control of topological states of DNA by transient breakage and subsequent rejoining of DNA strands. Topoisomerase II makes double-strand breaks. Essential during mitosis and meiosis for proper segregation of daughter chromosomes. oscillation	61	1.4	0.6	1.4	2.2	2.7	1.3	0.7	1.6	3.4	5.1
P20248	CCNA2	Cyclin-A2	Cyclin which controls both the G1/S and the G2/M transition phases of the cell cycle. Functions through the formation of specific serine/threonine protein kinase holoenzyme complexes with the cyclin-dependent protein kinases CDK1 or CDK2	7	1.5	0.5	1.9	3.3	3.6	1.3	0.7	1.7	4.4	5.4
O00458	IFRD1	Interferon-related developmental regulator 1	Could play a role in regulating gene activity in the proliferative and/or differentiative pathways induced by NGF. May be an autocrine factor that attenuates or amplifies the initial ligand-induced signal	1	0.7	1.3	0.8	0.4	1.0	1.0	1.0	1.3	2.0	5.5
Q9NQW6	ANLN	Anillin	Required for cytokinesis. Essential for the structural integrity of the cleavage furrow and for completion of cleavage furrow ingression. Plays a role in bleb assembly during metaphase and anaphase of mitosis	60	1.4	0.6	1.5	2.7	3.1	1.2	0.8	1.5	4.4	5.7
Q9Y4H2	IRS2	Insulin receptor substrate 2	May mediate the control of various cellular processes by insulin	7	0.8	1.2	0.9	1.1	1.5	1.1	0.9	1.3	2.7	5.7
Q9H967	WDR76	WD repeat-containing protein 76	Specifically binds 5-hydroxymethylcytosine (5hmC), suggesting that it acts as a specific reader of 5hmC	5	1.5	0.5	1.9	3.2	4.1	1.3	0.7	1.9	4.4	5.8
Q562F6	SGO2	Shugoshin 2	Essential for recruiting KIF2C to the inner centromere and for correcting defective kinetochore attachments. Involved in centromeric enrichment of AUKRB in prometaphase	7	1.0	1.0	2.1	3.9	3.9	1.2	0.8	1.5	5.3	6.1

Accession	Gene	Protein name	#											Description
Q8WWK9	CKAP2	Isoform 3 of Cytoskeleton-associated protein 2	18	1.5	0.5	1.6	3.3	4.7	1.2	0.8	1.6	5.2	6.5	Possesses microtubule stabilizing properties. Involved in regulating aneuploidy, cell cycling, and cell death in a pS3/TP53-dependent manner
P03082	Small t antigen	Small t antigen	6	0.9	1.1	2.8	6.9	10.9	1.0	1.0	2.6	4.8	10.5	BKPyV VIRAL PROTEIN - Promotes efficient viral genome replication by accelerating both G1 and S phase progression of the cell cycle. Inhibits host PP2A by binding to the A subunit, thereby displacing lower affinity regulatory B subunit
O75631	UPK3A	Uroplakin-3a	1	0.6	1.4	0.6	0.5	0.5	1.3	0.7	0.9	5.3	11.0	Component of the asymmetric unit membrane (AUM); a highly specialized biomembrane elaborated by terminally differentiated urothelial cells. May play an important role in AUM-cytoskeleton interaction in terminally differentiated urothelial cells
P01100	FOS	Proto-oncogene c-Fos	1	1.2	0.8	1.2	2.3	3.9	0.9	1.1	1.4	9.0	11.3	Nuclear phosphoprotein which forms a tight but non-covalently linked complex with the JUN/AP-1 transcription factor. In the heterodimer, FOS and JUN/AP-1 basic regions each seems to interact with symmetrical DNA half sites. On TGF-beta activation, forms a multimeric SMAD3/SMAD4/JUN/FOS complex at the AP1/SMAD-binding site to regulate TGF-beta-mediated signaling
P03071	Large T antigen	Large T antigen	37	0.9	1.1	3.2	7.7	9.1	0.9	1.1	3.2	11.0	12.1	BKPyV VIRAL PROTEIN - Large T antigen is a key early protein essential for both driving viral replication and inducing cellular transformation. Plays a role in viral genome replication by driving entry of quiescent cells into the cell cycle and by autoregulating the synthesis of viral early mRNA
P03094	VP2	Minor capsid protein VP2	18	1.0	1.0	1.4	3.1	6.4	1.0	1.0	1.3	3.7	12.7	BKPyV VIRAL PROTEIN - VP2 is a structural protein that resides within the core of the capsid surrounded by 72 VP1 pentamers. Participates in host cell receptor binding together with VP1
P03088	VP1	Major capsid protein VP1	280	1.0	1.0	1.5	4.1	7.0	1.0	1.0	1.3	6.6	14.6	BKPyV VIRAL PROTEIN - Forms an icosahedral capsid with a T=7 symmetry and a 50 nm diameter. The capsid is composed of 72 pentamers linked to each other by disulfide bonds and associated with VP2 or VP3 proteins. Interacts with gangliosides GT1b and GD1b containing terminal alpha2-8-linked sialic acids on the cell surface to provide virion attachment to target cell
P03085	Agnoprotein	Agnoprotein	3	0.9	1.1	1.3	5.6	8.1	0.8	1.2	1.2	11.8	15.9	BKPyV VIRAL PROTEIN - Alters the structure of the nuclear envelope by interacting with host CBX5 and disrupting CBX5 association with LBR. Involved in the perinuclear-nuclear localization of the capsid protein VP1 during virion assembly and maturation. Plays an important role in the release of progeny virions from infected cells and in viral propagation
O60299	LZTS3	Leucine zipper putative tumor suppressor 3	1	0.8	1.2	2.3	9.3	18.5	0.5	1.5	2.2	16.7	40.0	May be involved in promoting the maturation of dendritic spines, probably via regulating SIPA1L1 levels at the postsynaptic density of synapses
NOVEL ORF	NOVEL_ORF	NOVEL_ORF	1	0.0	2.0	15.1	140.5	212.9	1.3	0.7	3.2	44.1	68.7	BKPyV VIRAL PROTEIN - NOVEL Large T antigen transcript

Table S7: Significantly up and down regulated proteins at 72 hpi in RPTE cells (*p* < 0.0005).

Table of proteins observed to be significantly (*p* < 0.0005) up or down regulated in RPTE cells at 72 hpi, when compared to an average of the 24 and 72 h HU cell mock samples. Fold changes of every experimental condition shown for each protein (against an average of the 24 and 72 h mock samples for the corresponding cell type). Increasing red colour indicates greater up regulated fold changes, increasing green colour indicates greater down regulated fold changes).

Uniprot ID	Gene Name	Protein Name	Function	Peptide No.	HUC Mock 24h	HUC Mock 72h	HUC BK 24h	HUC BK 48h	HUC BK 72h	RPTEC Mock 24h	RPTEC Mock 72h	RPTEC BK 24h	RPTEC BK 48h	RPTEC BK 72h
Q6SJ93	FAM111B	Protein FAM111B	Cancer-associated nucleoprotein	12	1.5	0.5	2.0	2.4	2.0	1.3	0.7	1.7	2.7	2.1
Q9HAW4	CLSPN	Claspin	Required for checkpoint mediated cell cycle arrest in response to inhibition of DNA replication or to DNA damage induced by both ionizing and UV irradiation. Adapter protein which binds to BRCA1 and the checkpoint kinase CHEK1 and facilitates the ATR-dependent phosphorylation of both proteins	10	1.5	0.5	2.1	3.3	2.4	1.3	0.7	2.2	5.7	3.6
Q9NZJ0	DTL	Denticleless protein homolog	Substrate-specific adapter of a DCX (DDB1-CUL4-X-box) E3 ubiquitin-protein ligase complex required for cell cycle control, DNA damage response and translesion DNA synthesis	5	1.4	0.6	2.5	3.3	3.5	1.4	0.6	2.1	3.5	3.9

Table S8: Significantly up and down regulated proteins at 24 hpi in both HU and RPTE cells ($p < 0.0005$).
Table of proteins observed to be significantly ($p < 0.0005$) up or down regulated in both HU and RPTE cells at 24 hpi, when compared to an average of the 24 and 72 h HU cell mock samples. Fold changes of every experimental condition shown for each protein (against an average of the 24 and 72 h mock samples for the corresponding cell type). Increasing red colour indicates greater up regulated fold changes, increasing green colour indicates greater down regulated fold changes).

Uniprot ID	Gene Name	Protein Name	Function	Peptide No.	HUC Mock 24h	HUC Mock 72h	HUC BK 24h	HUC BK 48h	HUC BK 72h	RPTEC Mock 24h	RPTEC Mock 72h	RPTEC BK 24h	RPTEC BK 48h	RPTEC BK 72h
Q53EZ4	CEP55	Centrosomal protein of 55kDa	Plays a role in mitotic exit and cytokinesis	18	1.5	0.5	1.5	1.8	1.8	1.3	0.7	1.6	2.9	2.7
P46013	MKI67	Proliferation marker protein Ki-67	Required to maintain individual mitotic chromosomes dispersed in the cytoplasm following nuclear envelope disassembly. Associates with the surface of the mitotic chromosome, the perichromosomal layer, and covers a substantial fraction of the chromosome surface	121	1.4	0.6	1.4	2.0	2.1	1.4	0.6	1.5	2.3	3.3
Q9Y6A5	TACC3	Transforming acidic coiled-coil-containing protein 3	Plays a role in the microtubule-dependent coupling of the nucleus and the centrosome. Involved in the processes that regulate centrosome-mediated interkinetic nuclear migration (INM) of neural progenitors (By similarity). Acts as component of the TACC3/ch-TOG/clathrin complex proposed to contribute to stabilization of kinetochore fibers of the mitotic spindle by acting as inter-microtubule bridge	20	1.2	0.8	1.3	2.1	2.5	1.2	0.8	1.5	3.3	3.9
Q96KB5	PBK	Lymphokine-activated killer T-cell-originated protein kinase	Phosphorylates MAP kinase p38. Seems to be active only in mitosis. May also play a role in the activation of lymphoid cells. When phosphorylated, forms a complex with TP53, leading to TP53 destabilization and attenuation of G2/M checkpoint during doxorubicin-induced DNA damage	15	1.4	0.6	1.6	2.1	2.7	1.4	0.6	1.5	2.4	3.4
P14635	CCNB1	G2/mitotic-specific cyclin-B1	Essential for the control of the cell cycle at the G2/M (mitosis) transition	13	1.4	0.6	1.5	2.1	2.2	1.1	0.9	1.4	2.4	2.4
P11388	TOP2A	Isoform 4 of DNA topoisomerase 2-alpha	Control of topological states of DNA by transient breakage and subsequent rejoining of DNA strands. Topoisomerase II makes double-strand breaks. Essential during mitosis and meiosis for proper segregation of daughter chromosomes. oscillation	61	1.4	0.6	1.4	2.2	2.7	1.3	0.7	1.6	3.4	5.1
Q6PL18	ATAD2	ATPase family AAA domain-containing protein 2	May be a transcriptional coactivator of the nuclear receptor ESR1 required to induce the expression of a subset of estradiol target genes, such as CCND1, MYC and E2F1. May play a role in the recruitment or occupancy of CREBBP at some ESR1 target gene promoters. May be required for histone hyperacetylation.	23	1.3	0.7	1.6	2.2	1.8	1.2	0.8	1.4	3.7	3.8
O00762	UBE2C	Ubiquitin-conjugating enzyme E2 C	Accepts ubiquitin from the E1 complex and catalyzes its covalent attachment to other proteins. In vitro catalyzes 'Lys-11'- and 'Lys-48'-linked polyubiquitination. Acts as an essential factor of the anaphase promoting complex/cyclosome (APC/C), a cell cycle-regulated ubiquitin ligase that controls progression through mitosis.	4	1.9	0.1	2.0	2.2	1.7	1.4	0.6	1.8	3.5	1.8
Q53HL2	CDCA8	Borealin	Component of the chromosomal passenger complex (CPC), a complex that acts as a key regulator of mitosis	7	1.4	0.6	1.5	2.2	3.0	1.3	0.7	1.4	3.0	4.6
O43663	PRC1	Protein regulator of cytokinesis 1	Key regulator of cytokinesis that cross-links antiparallel microtubules at an average distance of 35 nM. Essential for controlling the spatiotemporal formation of the midzone and successful cytokinesis. Required for KIF14 localization to the central spindle and midbody. Required to recruit PLK1 to the spindle. Stimulates PLK1 phosphorylation of RACGAP1 to allow recruitment of ECT2 to the central spindle	10	1.4	0.6	1.6	2.2	2.5	1.2	0.8	1.3	3.3	3.6
O75330	HMMR	Isoform 3 of Hyaluronan mediated motility receptor	Receptor for hyaluronic acid (HA) (By similarity). Involved in cell motility (By similarity). When hyaluronan binds to HMMR, the phosphorylation of a number of proteins, including PTK2/FAK1 occurs	16	1.4	0.6	1.6	2.2	2.2	1.2	0.8	1.4	4.1	4.7
P01100	FOS	Proto-oncogene c-Fos	Nuclear phosphoprotein which forms a tight but non-covalently linked complex with the JUN/AP-1 transcription factor. In the heterodimer, FOS and JUN/AP-1 basic regions each seems to interact with symmetrical DNA half sites. On TGF-beta activation, forms a multimeric SMAD3/SMAD4/JUN/FOS complex at the AP1/SMAD-binding site to regulate TGF-beta-mediated signaling	1	1.2	0.8	1.2	2.3	3.9	0.9	1.1	1.4	9.0	11.3
Q9NRZ9	HELLS	Lymphoid-specific helicase	Plays an essential role in normal development and survival. Involved in regulation of the expansion or survival of lymphoid cells. Required for de novo or maintenance DNA methylation	12	1.6	0.4	1.9	2.3	1.8	1.3	0.7	1.8	4.3	3.7
Q6SJ93	FAM111B	Protein FAM111B	Cancer-associated nucleoprotein	12	1.5	0.5	2.0	2.4	2.0	1.3	0.7	1.7	2.7	2.1
Q9BW19	KIFC1	Kinesin-like protein KIFC1	Minus end-directed microtubule-dependent motor required for bipolar spindle formation	19	1.4	0.6	1.5	2.4	2.9	1.2	0.8	1.5	3.2	4.2
P52732	KIF11	Kinesin-like protein KIF11	Motor protein required for establishing a bipolar spindle during mitosis. Required in non-mitotic cells for transport of secretory proteins from the Golgi complex to the cell surface	32	1.3	0.7	1.4	2.4	2.9	1.2	0.8	1.5	3.3	4.7
Q96801	RAD51AP1	RAD51-associated protein 1	May participate in a common DNA damage response pathway associated with the activation of homologous recombination and double-strand break repair. Functionally cooperates with PALB2 in promoting of D-loop formation by RAD51	4	1.2	0.8	1.3	2.4	2.3	1.2	0.8	1.4	3.0	2.9
O95067	CCNB2	G2/mitotic-specific cyclin-B2	Essential for the control of the cell cycle at the G2/M (mitosis) transition	6	1.3	0.7	1.4	2.4	2.2	1.1	0.9	1.3	2.5	2.4

Accession	Gene	Protein name	Function											
Q9ULW0	TPX2	Targeting protein for Xklp2	Spindle assembly factor required for normal assembly of mitotic spindles. Required for normal assembly of microtubules during apoptosis. Required for chromatin and/or kinetochore dependent microtubule nucleation. Mediates AURKA localization to spindle microtubules	30	1.5	0.5	1.5	2.5	2.7	1.3	0.7	1.6	4.1	4.7
Q8NEM2	SHCBP1	SHC SH2 domain-binding protein 1	May play a role in signaling pathways governing cellular proliferation, cell growth and differentiation. May be a component of a novel signaling pathway downstream of Shc. Acts as a positive regulator of FGF signaling in neural progenitor cells	10	1.6	0.4	1.8	2.5	3.3	1.4	0.6	1.7	3.9	4.4
B5MBX0	CDCA5	Sororin	Regulator of sister chromatid cohesion in mitosis stabilizing cohesin complex association with chromatin	6	1.4	0.6	1.7	2.6	3.1	1.1	0.9	1.5	3.7	4.2
Q14807	KIF22	Kinesin-like protein KIF22	Kinesin family member that is involved in spindle formation and the movements of chromosomes during mitosis and meiosis. Binds to microtubules and to DNA	9	1.5	0.5	1.7	2.6	2.6	1.3	0.7	1.6	3.7	5.1
P31350	RRM2	Isoform 2 of Ribonucleoside-diphosphate reductase subunit M2	Provides the precursors necessary for DNA synthesis. Catalyzes the biosynthesis of deoxyribonucleotides from the corresponding ribonucleotides. Inhibits Wnt signaling	25	1.3	0.7	1.7	2.7	2.9	1.2	0.8	1.6	5.2	4.6
Q9NQW6	ANLN	Anillin	Required for cytokinesis. Essential for the structural integrity of the cleavage furrow and for completion of cleavage furrow ingression. Plays a role in bleb assembly during metaphase and anaphase of mitosis	60	1.4	0.6	1.5	2.7	3.1	1.2	0.8	1.5	4.4	5.7
O14965	AURKA	Aurora kinase A	Mitotic serine/threonine kinase that contributes to the regulation of cell cycle progression. Associates with the centrosome and the spindle microtubules during mitosis and plays a critical role in various mitotic events including the establishment of mitotic spindle, centrosome duplication, centrosome separation as well as maturation, chromosomal alignment, spindle assembly checkpoint, and cytokinesis. Required for initial activation of CDK1 at centrosomes	9	1.7	0.3	1.9	2.7	2.9	1.3	0.7	1.7	3.9	4.5
O95229	ZWINT	ZW10 interactor	Part of the MIS12 complex, which is required for kinetochore formation and spindle checkpoint activity. Required to target ZW10 to the kinetochore at prometaphase	3	1.5	0.5	1.9	2.8	2.6	1.3	0.7	1.6	3.6	2.9
P04183	TK1	Thymidine kinase, cytosolic	Two forms have been identified in animal cells, one in cytosol and one in mitochondria. Activity of the cytosolic enzyme is high in proliferating cells and peaks during the S-phase of the cell cycle; it is very low in resting cells	9	1.6	0.4	1.7	3.2	3.6	1.3	0.7	1.6	4.1	4.1
Q9H967	WDR76	WD repeat-containing protein 76	Specifically binds 5-hydroxymethylcytosine (5hmC), suggesting that it acts as a specific reader of 5hmC	5	1.5	0.5	1.9	3.2	4.1	1.3	0.7	1.9	4.4	5.8
Q9HAW4	CLSPN	Claspin	Required for checkpoint mediated cell cycle arrest in response to inhibition of DNA replication or to DNA damage induced by both ionizing and UV irradiation. Adapter protein which binds to BRCA1 and the checkpoint kinase CHEK1 and facilitates the ATR-dependent phosphorylation of both proteins	10	1.5	0.5	2.1	3.3	2.4	1.3	0.7	2.2	5.7	3.6
Q8WWK9	CKAP2	Isoform 3 of Cytoskeleton-associated protein 2	Possesses microtubule stabilizing properties. Involved in regulating aneuploidy, cell cycling, and cell death in a p53/TP53-dependent manner	18	1.5	0.5	1.6	3.3	4.7	1.2	0.8	1.6	5.2	6.5
P20248	CCNA2	Cyclin-A2	Cyclin which controls both the G1/S and the G2/M transition phases of the cell cycle. Functions through the formation of specific serine/threonine protein kinase holoenzyme complexes with the cyclin-dependent protein kinases CDK1 or CDK2	7	1.5	0.5	1.9	3.3	3.6	1.3	0.7	1.7	4.4	5.4
Q9NZJ0	DTL	Denticleless protein homolog	Substrate-specific adapter of a DCX (DDB1-CUL4-X-box) E3 ubiquitin-protein ligase complex required for cell cycle control, DNA damage response and translesion DNA synthesis	5	1.4	0.6	2.5	3.3	3.5	1.4	0.6	2.1	3.5	3.9
O96020	CCNE2	G1/S-specific cyclin-E2	Essential for the control of the cell cycle at the late G1 and early S phase	1	1.3	0.7	2.2	3.9	3.2	1.1	0.9	2.1	7.3	4.1
Q56F26	SGO2	Shugoshin 2	Essential for recruiting KIF2C to the inner centromere and for correcting defective kinetochore attachments. Involved in centromeric enrichment of AUKRB in prometaphase	7	1.0	1.0	2.1	3.9	3.9	1.2	0.8	1.5	5.3	6.1
O60299	LZTS3	Leucine zipper putative tumor suppressor 3	May be involved in promoting the maturation of dendritic spines, probably via regulating SIPA1L1 levels at the postsynaptic density of synapses	1	0.8	1.2	2.3	9.3	18.5	0.5	1.5	2.2	16.7	40.0

Table S9: Significantly up and down regulated proteins at 48 hpi in both HU and RPTE cells (*p* < 0.0005).
Table of proteins observed to be significantly (*p* < 0.0005) up or down regulated in both HU and RPTE cells at 48 hpi, when compared to an average of the 24 and 72 h HU cell mock samples. Fold changes of every experimental condition shown for each protein (against an average of the 24 and 72 h mock samples for the corresponding cell type). Increasing red colour indicates greater up regulated fold changes, increasing green colour indicates greater down regulated fold changes).

Uniprot ID	Gene Name	Protein Name	Function	Peptide No.	HUC Mock 24h	HUC Mock 72h	HUC BK 24h	HUC BK 48h	HUC BK 72h	RPTEC Mock 24h	RPTEC Mock 72h	RPTEC BK 24h	RPTEC BK 48h	RPTEC BK 72h
Q8IWE2	FAM114A1	Protein NOXP20	May play a role in neuronal cell development	16	1.0	1.0	1.1	1.6	2.1	1.0	1.0	1.0	2.1	3.5
P46013	MKI67	Proliferation marker protein Ki-67	Required to maintain individual mitotic chromosomes dispersed in the cytoplasm following nuclear envelope disassembly. Associates with the surface of the mitotic chromosome, the perichromosomal layer, and covers a substantial fraction of the chromosome surface	121	1.4	0.6	1.4	2.0	2.1	1.4	0.6	1.5	2.3	3.3
Q99661	KIF2C	Kinesin-like protein KIF2C	In complex with KIF18B, constitutes the major microtubule plus-end depolymerizing activity in mitotic cells	16	1.6	0.4	1.7	2.3	2.4	1.4	0.6	1.6	2.1	2.9
Q9Y6A5	TACC3	Transforming acidic coiled-coil-containing protein 3	Plays a role in the microtubule-dependent coupling of the nucleus and the centrosome. Involved in the processes that regulate centrosome-mediated interkinetic nuclear migration (INM) of neural progenitors (By similarity). Acts as component of the TACC3/ch-TOG/clathrin complex proposed to contribute to stabilization of kinetochore fibers of the mitotic spindle by acting as inter-microtubule bridge	20	1.2	0.8	1.3	2.1	2.5	1.2	0.8	1.5	3.3	3.9
P11388	TOP2A	Isoform 4 of DNA topoisomerase 2-alpha	Control of topological states of DNA by transient breakage and subsequent rejoining of DNA strands. Topoisomerase II makes double-strand breaks. Essential during mitosis and meiosis for proper segregation of daughter chromosomes, oscillation	61	1.4	0.6	1.4	2.2	2.7	1.3	0.7	1.6	3.4	5.1
Q9ULW0	TPX2	Targeting protein for Xklp2	Spindle assembly factor required for normal assembly of mitotic spindles. Required for normal assembly of microtubules during apoptosis. Required for chromatin and/or kinetochore dependent microtubule nucleation. Mediates AURKA localization to spindle microtubules	30	1.5	0.5	1.5	2.5	2.7	1.3	0.7	1.6	4.1	4.7
P31350	RRM2	Isoform 2 of Ribonucleoside-diphosphate reductase subunit M2	Provides the precursors necessary for DNA synthesis. Catalyzes the biosynthesis of deoxyribonucleotides from the corresponding ribonucleotides. Inhibits Wnt signaling	25	1.3	0.7	1.7	2.7	2.9	1.2	0.8	1.6	5.2	4.6
Q98W19	KIFC1	Kinesin-like protein KIFC1	Minus end-directed microtubule-dependent motor required for bipolar spindle formation	19	1.4	0.6	1.5	2.4	2.9	1.2	0.8	1.5	3.2	4.2
O14965	AURKA	Aurora kinase A	Mitotic serine/threonine kinase that contributes to the regulation of cell cycle progression. Associates with the centrosome and the spindle microtubules during mitosis and plays a critical role in various mitotic events including the establishment of mitotic spindle, centrosome duplication, centrosome separation as well as maturation, chromosomal alignment, spindle assembly checkpoint, and cytokinesis. Required for initial activation of CDK1 at centrosomes	9	1.7	0.3	1.9	2.7	2.9	1.3	0.7	1.7	3.9	4.5
P52732	KIF11	Kinesin-like protein KIF11	Motor protein required for establishing a bipolar spindle during mitosis. Required in non-mitotic cells for transport of secretory proteins from the Golgi complex to the cell surface	32	1.3	0.7	1.4	2.4	2.9	1.2	0.8	1.5	3.3	4.7
Q53HL2	CDCA8	Borealin	Component of the chromosomal passenger complex (CPC), a complex that acts as a key regulator of mitosis	7	1.4	0.6	1.5	2.2	3.0	1.3	0.7	1.4	3.0	4.6
B5MBX0	CDCA5	Sororin	Regulator of sister chromatid cohesion in mitosis stabilizing cohesin complex association with chromatin	6	1.4	0.6	1.7	2.6	3.1	1.1	0.9	1.5	3.7	4.2
Q9NQW6	ANLN	Anillin	Required for cytokinesis. Essential for the structural integrity of the cleavage furrow and for completion of cleavage furrow ingression. Plays a role in bleb assembly during metaphase and anaphase of mitosis	60	1.4	0.6	1.5	2.7	3.1	1.2	0.8	1.5	4.4	5.7
Q8NEM2	SHCBP1	SHC SH2 domain-binding protein 1	May play a role in signaling pathways governing cellular proliferation, cell growth and differentiation. May be a component of a novel signaling pathway downstream of Shc. Acts as a positive regulator of FGF signaling in neural progenitor cells	10	1.6	0.4	1.8	2.5	3.3	1.4	0.6	1.7	3.9	4.4
Q9NZJ0	DTL	Denticleless protein homolog	Substrate-specific adapter of a DCX (DDB1-CUL4-X-box) E3 ubiquitin-protein ligase complex required for cell cycle control, DNA damage response and translesion DNA synthesis	5	1.4	0.6	2.5	3.3	3.5	1.4	0.6	2.1	3.5	3.9
P20248	CCNA2	Cyclin-A2	Cyclin which controls both the G1/S and the G2/M transition phases of the cell cycle. Functions through the formation of specific serine/threonine protein kinase holoenzyme complexes with the cyclin-dependent protein kinases CDK1 or CDK2	7	1.5	0.5	1.9	3.3	3.6	1.3	0.7	1.7	4.4	5.4
P04183	TK1	Thymidine kinase, cytosolic	Two forms have been identified in animal cells, one in cytosol and one in mitochondria. Activity of the cytosolic enzyme is high in proliferating cells and peaks during the S-phase of the cell cycle; it is very low in resting cells	9	1.6	0.4	1.7	3.2	3.6	1.3	0.7	1.6	4.1	4.1
P01100	FOS	Proto-oncogene c-Fos	Nuclear phosphoprotein which forms a tight but non-covalently linked complex with the JUN/AP-1 transcription factor. In the heterodimer, FOS and JUN/AP-1 basic regions each seems to interact with symmetrical DNA half sites. On TGF-beta activation, forms a multimeric SMAD3/SMAD4/JUN/FOS complex at the AP1/SMAD-binding site to regulate TGF-beta-mediated signaling	1	1.2	0.8	1.2	2.3	3.9	0.9	1.1	1.4	9.0	11.3
Q56ZF6	SGO2	Shugoshin 2	Essential for recruiting KIF2C to the inner centromere and for correcting defective kinetochore attachments. Involved in centromeric enrichment of AUKRB in prometaphase	7	1.0	1.0	2.1	3.9	3.9	1.2	0.8	1.5	5.3	6.1
Q9H967	WDR76	WD repeat-containing protein 76	Specifically binds 5-hydroxymethylcytosine (5hmC), suggesting that it acts as a specific reader of 5hmC	5	1.5	0.5	1.9	3.2	4.1	1.3	0.7	1.9	4.4	5.8
Q8WWK9	CKAP2	Isoform 3 of Cytoskeleton-associated protein 2	Possesses microtubule stabilizing properties. Involved in regulating aneuploidy, cell cycling, and cell death in a p53/TP53-dependent manner	18	1.5	0.5	1.6	3.3	4.7	1.2	0.8	1.6	5.2	6.5
O60299	LZTS3	Leucine zipper putative tumor suppressor 3	May be involved in promoting the maturation of dendritic spines, probably via regulating SIPA1L1 levels at the postsynaptic density of synapses	1	0.8	1.2	2.3	9.3	18.5	0.5	1.5	2.2	16.7	40.0

Table S10: Significantly up and down regulated proteins at 72 hpi in both HU and RPTE cells ($p < 0.0005$).

Table of proteins observed to be significantly ($p < 0.0005$) up or down regulated in both HU and RPTE cells at 72 hpi, when compared to an average of the 24 and 72 h HU cell mock samples. Fold changes of every experimental condition shown for each protein (against an average of the 24 and 72 h mock samples for the corresponding cell type). Increasing red colour indicates greater up regulated fold changes, increasing green colour indicates greater down regulated fold changes).

Uniprot-s	Gene Name	Description	HUC fold-change 24 hpi	HUC fold-change 48 hpi	HUC fold change 72 hpi	RPTEC fold-change 24 hpi	RPTEC fold-change 48 hpi	RPTEC fold-change 72 hpi
Q9ULU8	CADPS	Calcium-binding protein involved in exocytosis of vesicles filled with neurotransmitters and neuropeptides. P	0.71	0.89	0.94	0.98	1.13	1.07
Q86UW7	CADPS2	Calcium-binding protein involved in exocytosis of vesicles filled with neurotransmitters and neuropeptides. Isoform 2.	1.20	0.82	0.64	1.11	1.41	0.85
P24386	CHM	Substrate-binding subunit (component A1) of the Rab geranylgeranyltransferase (GGTase) complex.	1.07	1.02	0.94	1.05	1.08	1.04
P26374	CHML	Substrate-binding subunit (component A2) of the Rab geranylgeranyltransferase (GGTase) complex.	1.23	1.31	1.12	1.10	1.02	1.03
Q9HD42	CHMP1A	Peripherally associated component of the endosomal sorting required for transport complex III (ESCRT-III) which is involved in multivesicular bodies (MVBs) formation and sorting of endosomal cargo proteins into MVBs.	0.85	0.97	0.88	0.99	0.99	0.86
A6NG32	CHMP1A	Peripherally associated component of the endosomal sorting required for transport complex III (ESCRT-III) which is involved in multivesicular bodies (MVBs) formation and sorting of endosomal cargo proteins into MVBs.	1.21	0.89	1.03	1.12	1.02	0.95
Q7LBR1	CHMP1B	Peripherally associated component of the endosomal sorting required for transport complex III (ESCRT-III) which is involved in multivesicular bodies (MVBs) formation and sorting of endosomal cargo proteins into MVBs.	0.99	0.89	0.89	0.93	0.86	0.70
M0R1T5	CHMP2A	Core component of the endosomal sorting required for transport complex III (ESCRT-III) which is involved in multivesicular bodies (MVBs) formation and sorting of endosomal cargo proteins into MVBs.	0.89	1.05	1.04	0.97	1.04	0.99
Q9UQN3	CHMP2B	Core component of the endosomal sorting required for transport complex III (ESCRT-III) which is involved in multivesicular bodies (MVBs) formation and sorting of endosomal cargo proteins into MVBs.	0.99	1.01	0.99	0.91	1.11	0.95
Q9Y3E7	CHMP3	Core component of the endosomal sorting required for transport complex III (ESCRT-III) which is involved in multivesicular bodies (MVBs) formation and sorting of endosomal cargo proteins into MVBs.	0.84	0.91	0.81	1.12	1.03	1.01
Q14D22	CHMP4A	Core component of the endosomal sorting required for transport complex III (ESCRT-III) which is involved in multivesicular bodies (MVBs) formation and sorting of endosomal cargo proteins into MVBs.	1.01	1.07	0.98	0.99	0.81	0.88
Q9H444	CHMP4B	Core component of the endosomal sorting required for transport complex III (ESCRT-III) which is involved in multivesicular bodies (MVBs) formation and sorting of endosomal cargo proteins into MVBs.	0.87	0.95	0.79	1.05	0.91	0.87
Q96CF2	CHMP4C	Core component of the endosomal sorting required for transport complex III (ESCRT-III) which is involved in multivesicular bodies (MVBs) formation and sorting of endosomal cargo proteins into MVBs.	1.11	1.01	1.07	1.00	0.77	0.61
Q9NZ23	CHMP5	Peripherally associated component of the endosomal sorting required for transport complex III (ESCRT-III) which is involved in multivesicular bodies (MVBs) formation and sorting of endosomal cargo proteins into MVBs.	0.97	0.96	1.03	1.00	1.06	0.98
I3L4A1	CHMP6	Core component of the endosomal sorting required for transport complex III (ESCRT-III) which is involved in multivesicular bodies (MVBs) formation and sorting of endosomal cargo proteins into MVBs.	1.02	1.25	1.28	0.88	1.19	1.47
Q8WUX9	CHMP7	ESCRT-III-like protein required to recruit the ESCRT-III complex to the nuclear envelope during late anaphase.	1.01	1.15	1.07	1.05	1.00	1.07
Q9H0B8	CRISPLD2	Cysteine-rich secretory protein LCCL domain-containing 2, promotes matrix assembly.	0.79	1.29	1.30	1.19	0.81	0.74
P31150	GDI1	Rab GDP dissociation inhibitor alpha. Regulates the GDP/GTP exchange reaction of most Rab proteins by inhibiting the dissociation of GDP from them, and the subsequent binding of GTP to them.	0.98	0.96	1.07	0.94	0.95	0.97
E7EU23	GDI2	Rab GDP dissociation inhibitor beta. Regulates the GDP/GTP exchange reaction of most Rab proteins by inhibiting the dissociation of GDP from them, and the subsequent binding of GTP to them.	0.94	0.92	0.88	1.02	0.95	0.92
Q7LSD6	GET4	Golgi to ER traffic protein 4 homolog, part of a cytosolic protein quality control complex, the BAG6/BAT3 complex.	0.86	0.93	0.91	1.02	0.96	0.85
Q9Y3E0	GOLT1B	Vesicle transport protein that may be involved in fusion of ER-derived transport vesicles with the Golgi complex.	1.11	0.92	1.13	0.99	1.22	0.82
Q5T7V8	GORAB	RAB6-interacting golgin.	1.07	1.06	0.97	1.09	0.99	1.10
B4DKT0	GORASP2	Plays a role in the assembly and membrane stacking of the Golgi cisternae, and in the process by which Golgi stacks reform after mitotic breakdown. May regulate the intracellular transport and presentation of a defined set of transmembrane proteins, such as transmembrane TGFA.	0.98	1.04	1.07	0.96	1.02	1.08
G5E9T8	GOSR1	Involved in transport from the ER to the Golgi apparatus as well as in intra-Golgi transport. It belongs to a super-family of proteins called t-SNAREs or soluble NSF (N-ethylmaleimide-sensitive factor) attachment protein receptor.	1.13	1.20	1.26	1.06	1.07	1.13
E7EQ34	GOSR2	Involved in transport of proteins from the cis/medial-Golgi to the trans-Golgi network.	1.04	0.98	1.01	1.06	1.06	0.91

ID	Name	Description						
Q99698	LYST	Lysosomal-trafficking regulator equired for sorting endosomal resident proteins into late multivesicular endosomes by a mechanism involving microtubules.	0.87	0.94	0.98	0.90	0.91	0.85
P46459	NSF	Vesicle-fusing ATPase required for vesicle-mediated transport.	0.88	0.96	1.05	0.96	0.98	1.04
P61026	RAB10	Key regulator of membrane trafficking, Rab10 transports proteins from the Golgi to the plasma membrane including TLR4.	0.91	0.83	0.90	0.96	1.00	0.98
Q15907	RAB11B	Key regulator of membrane trafficking, Rab11b plays a role in endocytic recycling.	1.10	0.95	0.91	1.04	1.01	0.93
Q6WKZ4	RAB11FIP1	A Rab11 effector protein involved in the endosomal recycling process. Also involved in controlling membrane trafficking along the phagocytic pathway and in phagocytosis.	0.90	0.81	0.90	0.93	1.02	0.98
Q3I768	RAB11FIP2	A Rab11 effector binding preferentially phosphatidylinositol 3,4,5-trisphosphate (PtdInsP3) and phosphatidic acid (PA) and acting in the regulation of the transport of vesicles from the endosomal recycling compartment (ERC) to the plasma membrane.	1.13	1.09	1.08	0.93	0.97	0.90
Q9BXF6	RAB11FIP5	Rab effector involved in protein trafficking from apical recycling endosomes to the apical plasma membrane. Involved in insulin granule exocytosis.	1.00	1.00	0.91	1.01	0.80	0.86
Q6IQ22	RAB12	Key regulator of membrane trafficking, Rab12 plays a role in protein transport from recycling endosomes to lysosomes.	0.94	0.98	0.99	1.02	1.00	1.08
P51153	RAB13	Key regulator of membrane trafficking, Rab13 plays a role in endocytic recycling.	1.03	1.00	1.21	1.03	1.04	0.98
P61106	RAB14	Key regulator of membrane trafficking, Rab14 plays a role in Golgi to endosome transport of FGFR-containing vesicles in early development.	1.01	0.93	0.90	1.06	0.87	0.87
P59190	RAB15	Key regulator of membrane trafficking, Rab15 may act in concert with RAB3A in regulating aspects of synaptic vesicle membrane flow within the nerve terminal.	1.06	0.97	0.99	1.07	1.08	0.97
Q9NP72	RAB18	Key regulator of membrane trafficking, Rab18 plays a role in apical endocytosis/recycling.	1.14	1.02	1.06	1.04	1.17	1.24
P62820	RAB1A	Key regulator of membrane trafficking, Rab1A regulates vesicular protein transport from the endoplasmic reticulum (ER) to the Golgi compartment and on to the cell surface, and plays a role in IL-8 and growth hormone secretion.	0.99	1.00	0.95	1.01	0.99	1.02
Q9H0U4	RAB1B	Key regulator of membrane trafficking, Rab1B regulates vesicular transport between the endoplasmic reticulum and successive Golgi compartments.	0.96	1.04	1.13	0.98	0.96	0.93
Q9NX57	RAB20	Key regulator of membrane trafficking, Rab20 plays a role in apical endocytosis/recycling.	1.03	1.15	1.04	0.95	1.03	0.90
Q9UL25	RAB21	Key regulator of membrane trafficking, Rab21 regulates integrin internalization and recycling, but does not influence the traffic of endosomally translocated receptors in general.	0.99	1.05	1.20	1.01	1.09	1.11
Q9UL26	RAB22A	Key regulator of membrane trafficking, Rab22A plays a role in endocytosis and intracellular protein transport, mediating trafficking from early endosomes to recycling endosomes.	1.03	0.94	0.90	0.94	0.91	0.80
Q9ULC3	RAB23	Key regulator of membrane trafficking, Rab23 plays a role in autophagic vacuole assembly, and mediates defense against pathogens, such as S.aureus.	1.08	1.10	1.48	0.82	0.86	1.20
Q969Q5	RAB24	Key regulator of membrane trafficking, Rab24 may play a role in autophagy-related processes.	0.84	0.96	1.01	0.90	1.09	1.05
P57735	RAB25	Key regulator of membrane trafficking, Rab25 is involved in the regulation of cell survival. Promotes invasive migration of cells in which it functions to localize and maintain integrin alpha-V/beta-1 at the tips of extending pseudopodia.	0.89	0.81	0.89	0.88	1.16	0.93
P51159	RAB27A	Key regulator of membrane trafficking, Rab27A plays a role in cytotoxic granule exocytosis in lymphocytes. Required for both granule maturation and granule docking and priming at the immunologic synapse.	1.04	1.16	1.28	1.01	1.35	1.65
O00194	RAB27B	Key regulator of membrane trafficking, Rab27A may be involved in targeting uroplakins to urothelial apical membranes.	0.91	0.84	0.95	0.96	1.00	0.93
P51157	RAB28	Key regulator of membrane trafficking, Rab28 may be involved in intracellular trafficking.	1.06	1.24	1.30	0.97	1.06	1.13
O14966	RAB29	Key regulator of membrane trafficking, Rab29 plays a role in the retrograde trafficking pathway for recycling proteins between lysosomes and the Golgi apparatus in a retromer-dependent manner.	1.06	1.17	1.06	0.90	0.77	0.99
P61019	RAB2A	Key regulator of membrane trafficking, Rab2A is required for protein transport from the endoplasmic reticulum to the Golgi complex.	1.13	0.95	1.13	0.90	1.07	0.84
Q8WUD1	RAB2B	Key regulator of membrane trafficking, Rab2B is required for protein transport from the endoplasmic reticulum to the Golgi complex.	0.97	0.84	0.92	1.04	0.96	0.84
Q13636	RAB31	Key regulator of membrane trafficking, Rab31 is required for the integrity and for normal function of the Golgi apparatus and the trans-Golgi network.	1.05	1.09	1.12	0.95	0.85	1.02
Q13637	RAB32	Key regulator of membrane trafficking, Rab32 plays a role in the maturation of phagosomes that engulf pathogens, such as S.aureus and M.tuberculosis.	1.00	1.03	1.03	1.03	0.80	0.89
Q9H082	RAB33B	Key regulator of membrane trafficking, Rab33B acts, in coordination with RAB6A, to regulate intra-Golgi retrograde trafficking.	1.15	1.28	1.35	1.13	1.19	1.70
J3KQW8	RAB34	Key regulator of membrane trafficking, Rab34 plays a role in the fusion of phagosomes with lysosomes.	0.93	0.95	0.86	1.09	0.95	0.95
Q15286	RAB35	Key regulator of membrane trafficking, Rab35 is involved in the process of endocytosis and is an essential rate-limiting regulator of the fast recycling pathway back to the plasma membrane.	1.03	0.96	1.05	1.00	1.04	1.03

UniProt	Gene	Description						
O95755	RAB36	Key regulator of membrane trafficking, Rab36 is probably involved in intracellular transport.	0.41	0.62	0.38	0.77	0.79	0.67
P57729	RAB38	Key regulator of membrane trafficking, Rab38 is involved in melanosomal transport and docking.	0.95	1.05	1.27	0.76	0.97	1.03
P20336	RAB3A	Key regulator of membrane trafficking, Rab3A is involved in exocytosis by regulating a late step in synaptic vesicle fusion.	0.83	0.83	0.94	1.01	1.01	0.86
P20337	RAB3B	Key regulator of membrane trafficking, Rab3B is involved in exocytosis.	0.99	1.00	1.05	1.02	1.12	1.07
Q96E17	RAB3C	Key regulator of membrane trafficking, Rab3C is involved in exocytosis.	0.82	0.84	0.90	1.15	0.97	0.90
O95716	RAB3D	Key regulator of membrane trafficking, Rab3D is involved in exocytosis.	0.98	1.08	1.00	1.03	0.85	0.81
Q15042	RAB3GAP1	Catalytic subunit of a GTPase activating protein that has specificity for Rab3 subfamily (RAB3A, RAB3B, RAB3C and RAB3D).	1.00	0.85	0.75	1.00	0.85	0.77
Q9H2M9	RAB3GAP2	Catalytic subunit of a GTPase activating protein that has specificity for Rab3 subfamily (RAB3A, RAB3B, RAB3C and RAB3D).	1.06	0.94	0.83	1.00	0.94	0.86
Q96QF0	RAB3IP	Guanine nucleotide exchange factor (GEF) which may activate RAB8A and RAB8B.	0.96	1.14	1.16	0.89	0.97	1.02
Q86YS6	RAB43	Key regulator of membrane trafficking, Rab43 is involved in retrograde transport from the endocytic pathway to the Golgi apparatus.	1.35	1.20	1.21	1.06	1.10	1.04
P20338	RAB4A	Key regulator of membrane trafficking, Rab4A is probably involved in vesicular traffic.	0.89	0.82	0.94	1.00	0.63	0.82
P61018	RAB4B	Key regulator of membrane trafficking, Rab4B is probably involved in vesicular traffic.	0.97	0.94	0.94	1.08	0.96	0.90
P20339	RAB5A	Key regulator of membrane trafficking, Rab5A is required for the fusion of plasma membranes and early endosomes.	0.97	0.94	0.96	0.93	0.88	0.91
P61020	RAB5B	Key regulator of membrane trafficking, Rab5B is probably involved in vesicular traffic.	0.90	0.98	1.04	0.92	0.90	0.86
P51148	RAB5C	Key regulator of membrane trafficking, Rab5C is probably involved in vesicular traffic.	1.04	0.87	0.98	0.95	1.06	0.89
P20340	RAB6A	Key regulator of membrane trafficking, Rab6A is a regulator of membrane traffic from the Golgi apparatus towards the endoplasmic reticulum (ER).	0.91	1.10	1.03	1.03	0.86	0.99
Q9NRW1	RAB6B	Key regulator of membrane trafficking, Rab6B seems to have a role in retrograde membrane traffic at the level of the Golgi complex.	0.89	1.02	0.97	1.00	0.86	0.95
P51149	RAB7A	Key regulator of membrane trafficking, Rab7A is a key regulator in endo-lysosomal trafficking, governing early-to-late endosomal maturation.	1.07	0.95	0.96	0.95	0.95	0.87
Q96AH8	RAB7B	Key regulator of membrane trafficking, Rab7B controls vesicular trafficking from endosomes to the trans-Golgi network (TGN).	0.75	0.79	0.74	1.11	0.66	0.70
P61006	RAB8A	Key regulator of membrane trafficking, Rab8A is involved in polarized vesicular trafficking and neurotransmitter release.	1.07	1.01	1.06	1.01	1.04	1.09
Q92930	RAB8B	Key regulator of membrane trafficking, Rab8B ay be involved in polarized vesicular trafficking and neurotransmitter release.	0.88	0.92	0.85	0.94	0.74	0.96
P51151	RAB9A	Key regulator of membrane trafficking, Rab9A is involved in the transport of proteins between the endosomes and the trans Golgi network.	0.88	1.05	1.14	0.87	0.89	0.95
Q15276	RABEP1	Rab effector protein acting as linker between gamma-adaptin, RAB4A and RAB5A.	1.07	1.03	1.04	0.97	1.01	1.09
Q9H5N1	RABEP2	Plays a role in membrane trafficking and in homotypic early endosome fusion.	0.93	1.05	1.07	1.00	1.04	1.02
Q7Z6M1	RABEPK	Rab9 effector required for endosome to trans-Golgi network (TGN) transport.	1.02	1.00	1.00	1.01	1.04	1.04
Q9Y3P9	RABGAP1	May act as a GTPase-activating protein of RAB6A.	1.07	1.24	1.22	0.94	1.14	1.20
Q5R372	RABGAP1L	GTP-hydrolysis activating protein (GAP) for small GTPase RAB22A, converting active RAB22A-GTP to the inactive form RAB22A-GDP.	1.11	1.08	1.08	0.88	1.03	0.98
Q9UJ41	RABGEF1	Rab effector protein acting as linker between gamma-adaptin, RAB4A or RAB5A. Involved in endocytic membrane fusion and membrane trafficking of recycling endosomes.	1.05	1.02	1.06	0.95	1.09	0.98
Q92696	RABGGTA	Catalyzes the transfer of a geranylgeranyl moiety from geranylgeranyl diphosphate to both cysteines of Rab proteins with the C-terminal sequence -XXCC, -XCXC and -CCXX, such as RAB1A, RAB3A, RAB5A and RAB7A.	0.85	0.82	0.75	1.07	0.90	0.88
P53611	RABGGTB	Catalyzes the transfer of a geranylgeranyl moiety from geranylgeranyl diphosphate to both cysteines of Rab proteins with the C-terminal sequence -XXCC, -XCXC and -CCXX, such as RAB1A, RAB3A, RAB5A and RAB7A.	0.90	1.06	0.82	1.16	0.85	0.93
P47224	RABIF	Guanine-nucleotide-releasing protein that acts on members of the SEC4/YPT1/RAB subfamily.	1.12	1.10	1.08	1.24	1.23	1.08
Q9UBK7	RABL2A	Plays an essential role in male fertility, sperm intra-flagellar transport, and tail assembly.	1.07	0.99	0.85	1.15	0.87	0.76
Q5HYI8	RABL3	Rab-like protein, may be involved in intracellular transport.	0.95	1.06	1.14	1.02	1.05	1.06
Q3YEC7	RABL6	Rab-like protein, may enhance cellular proliferation. May reduce growth inhibitory activity of CDKN2A.	0.99	1.03	1.05	0.95	0.92	0.95
U3KQ30	SCAMP1	Secretory carrier-associated membrane protein 1, functions in post-Golgi recycling pathways. Acts as a recycling carrier to the cell surface.	0.94	1.07	1.08	0.93	0.69	0.92
O15127	SCAMP2	Secretory carrier-associated membrane protein 2, functions in post-Golgi recycling pathways. Acts as a recycling carrier to the cell surface.	1.10	1.06	1.15	0.99	1.07	0.94
O14828	SCAMP3	Secretory carrier-associated membrane protein 3, functions in post-Golgi recycling pathways. Acts as a recycling carrier to the cell surface.	1.09	0.97	1.08	0.91	1.04	0.94
Q969E2	SCAMP4	Secretory carrier-associated membrane protein 4, involved in membrane protein trafficking.	0.96	0.95	1.14	0.86	0.99	1.06
Q96IW7	SEC22A	May be involved in vesicle transport between the ER and the Golgi complex.	1.08	0.99	1.09	0.94	1.13	1.18

Accession	Gene	Description						
O75396	SEC22B	SNARE involved in targeting and fusion of ER-derived transport vesicles with the Golgi complex as well as Golgi-derived retrograde transport vesicles with the ER.	0.99	1.02	1.18	0.92	0.96	1.03
Q15436	SEC23A	Component of the coat protein complex II (COPII) which promotes the formation of transport vesicles from the endoplasmic reticulum (ER).	1.02	1.00	1.09	0.93	0.87	0.92
Q15437	SEC23B	Component of the coat protein complex II (COPII) which promotes the formation of transport vesicles from the endoplasmic reticulum (ER).	1.15	1.07	1.05	1.05	0.90	0.87
Q9Y6Y8	SEC23IP	Plays a role in the organization of endoplasmic reticulum exit sites. Specifically binds to phosphatidylinositol 3-phosphate (PI3P), phosphatidylinositol 4-phosphate (PI4P) and phosphatidylinositol 5-phosphate (PI5P).	0.99	1.00	0.96	1.01	0.94	0.95
O95486	SEC24A	Component of the coat protein complex II (COPII) which promotes the formation of transport vesicles from the endoplasmic reticulum (ER). Plays a central role in cargo selection.	1.03	0.94	1.00	0.98	1.05	1.01
B7ZKM8	SEC24B	Component of the coat protein complex II (COPII) which promotes the formation of transport vesicles from the endoplasmic reticulum (ER). Plays a central role in cargo selection.	0.93	0.99	1.04	1.00	0.90	0.94
P53992	SEC24C	Component of the coat protein complex II (COPII) which promotes the formation of transport vesicles from the endoplasmic reticulum (ER). Plays a central role in cargo selection.	0.98	1.00	0.97	1.03	0.89	0.85
O94855	SEC24D	Component of the coat protein complex II (COPII) which promotes the formation of transport vesicles from the endoplasmic reticulum (ER). Plays a central role in cargo selection.	1.06	0.99	0.97	1.03	0.88	0.82
D6REX3	SEC31A	Component of the coat protein complex II (COPII) which promotes the formation of transport vesicles from the endoplasmic reticulum (ER).	0.97	0.92	0.92	1.00	0.86	0.83
B4DR61	SEC61A1	Plays a crucial role in the insertion of secretory and membrane polypeptides into the ER.	0.98	1.00	0.99	1.05	0.87	0.86
P60468	SEC61B	Necessary for protein translocation in the endoplasmic reticulum, notably secretory proteins.	1.08	0.93	0.99	0.95	1.00	0.80
Q9UGK8	SERGEF	Probable guanine nucleotide exchange factor (GEF), which may be involved in the secretion process.	0.98	1.03	1.09	0.86	1.01	1.01
O00161	SNAP23	Essential component of the high affinity receptor for the general membrane fusion machinery and an important regulator of transport vesicle docking and fusion.	1.02	1.04	1.07	0.98	1.02	1.05
O95721	SNAP29	SNAP29 is a SNARE involved in autophagy through the direct control of autophagosome membrane fusion with the lysososome membrane.	1.06	1.16	1.19	1.02	1.19	1.10
O60641	SNAP91	SNARE adaptin, a component of the adapter complexes which link clathrin to receptors in coated vesicles.	0.92	0.75	0.71	1.02	0.81	0.75
O95295	SNAPIN	Plays a role in intracellular vesicle trafficking and synaptic vesicle recycling. May modulate a step between vesicle priming, fusion and calcium-dependent neurotransmitter release through its ability to potentiate the interaction of synaptotagmin with the SNAREs and the plasma-membrane-associated protein SNAP25.	0.80	0.78	0.87	0.84	0.83	0.70
O60499	STX10	SNARE involved in vesicular transport from the late endosomes to the trans-Golgi network.	1.17	1.28	1.20	0.95	1.20	1.09
Q86Y82	STX12	SNARE that acts to regulate protein transport between late endosomes and the trans-Golgi network.	0.96	1.02	1.07	0.92	0.95	0.98
H3BU86	STX16	SNARE involved in vesicular transport from the late endosomes to the trans-Golgi network.	0.99	1.08	1.07	0.96	0.86	0.89
P56962	STX17	SNARE of the autophagosome involved in autophagy through the direct control of autophagosome membrane fusion with the lysosome membrane.	1.11	1.06	1.22	0.89	1.02	0.94
Q9P2W9	STX18	Syntaxin that may be involved in targeting and fusion of Golgi-derived retrograde transport vesicles with the ER.	0.83	0.94	0.85	1.02	0.98	1.05
P32856	STX2	Essential for epithelial morphogenesis. May mediate Ca2+-regulation of exocytosis acrosomal reaction in sperm.	0.96	0.88	1.01	1.00	1.04	1.02
Q13277	STX3	Potentially involved in docking of synaptic vesides at presynaptic active zones.	0.99	1.03	1.15	0.91	0.84	0.82
Q12846	STX4	Plasma membrane t-SNARE that mediates docking of transport vesicles. Necessary for the translocation of SLC2A4 from intracellular vesicles to the plasma membrane.	1.01	1.05	1.09	0.92	0.92	0.95
Q13190	STX5	Mediates endoplasmic reticulum to Golgi transport.	1.00	1.01	1.04	0.98	0.97	1.01
O43752	STX6	Involved in intracellular vesicle trafficking.	1.03	1.15	1.30	0.83	1.00	1.05
O15400	STX7	Mediates the endocytic trafficking from early endosomes to late endosomes and lysosomes.	0.93	1.02	1.10	0.86	0.87	0.93
Q9UNK0	STX8	Vesicle trafficking protein that functions in the early secretory pathway, possibly by mediating retrograde transport from cis-Golgi membranes to the ER.	1.07	0.95	0.99	0.92	0.98	0.84
P61764	STXBP1	May participate in the regulation of synaptic vesicle docking and fusion, possibly through interaction with GTP-binding proteins. Can interact with syntaxins 1, 2, and 3 but not syntaxin 4, playing a role in determining the specificity of intracellular fusion reactions.	0.94	0.96	1.00	0.91	0.94	0.96
E7EQD5	STXBP2	Involved in intracellular vesicle trafficking and vesicle fusion with membranes.	1.01	0.98	1.02	0.89	0.91	0.90

Accession	Gene	Description						
O00186	STXBP3	Together with STX4 and VAMP2, may play a role in insulin-dependent movement of GLUT4 and in docking/fusion of intracellular GLUT4-containing vesicles with the cell surface in adipocytes.	0.95	0.99	1.02	0.93	0.88	0.87
Q6ZW11	STXBP4	Plays a role in the translocation of transport vesicles from the cytoplasm to the plasma membrane.	1.22	1.25	1.19	0.85	0.99	0.79
Q5T5C0	STXBP5	Plays a regulatory role in calcium-dependent exocytosis and neurotransmitter release. Inhibits membrane fusion between transport vesicles and the plasma membrane.	1.04	1.07	1.09	1.01	0.99	1.13
Q15836	VAMP3	SNARE involved in vesicular transport from the late endosomes to the trans-Golgi network.	0.97	0.99	1.04	0.98	0.97	0.91
O75379	VAMP4	Involved in the pathway that functions to remove an inhibitor (probably synaptotagmin-4) of calcium-triggered exocytosis during the maturation of secretory granules.	0.95	1.08	1.26	0.86	0.89	0.95
O95183	VAMP5	May participate in trafficking events that are associated with myogenesis, such as myoblast fusion and/or GLUT4 trafficking.	0.97	1.02	1.10	0.93	0.96	0.94
P51809	VAMP7	Involved in the targeting and/or fusion of transport vesicles to their target membrane during transport of proteins from the early endosome to the lysosome.	1.00	0.93	0.90	0.91	0.90	0.84
Q9BV40	VAMP8	NARE involved in autophagy through the direct control of autophagosome membrane fusion with the lysososome membrane via its interaction with the STX17-SNAP29 binary t-SNARE complex.	1.04	1.00	1.01	0.88	0.95	0.79
Q9P0L0	VAPA	May play a role in vesicle trafficking.	0.99	1.02	1.09	0.98	1.03	1.09
O95292	VAPB	Participates in the endoplasmic reticulum unfolded protein response (UPR) by inducing ERN1/IRE1 activity.	1.02	1.03	1.10	0.97	1.04	1.10
Q9NP79	VTA1	Involved in the endosomal multivesicular bodies (MVB) pathway.	0.93	0.99	0.96	1.09	0.98	1.10
Q96AJ9	VTI1A	V-SNARE that mediates vesicle transport pathways through interactions with t-SNAREs on the target membrane.	1.02	1.09	1.13	0.94	1.06	1.13
Q9UEU0	VTI1B	V-SNARE that mediates vesicle transport pathways through interactions with t-SNAREs on the target membrane.	0.91	0.99	0.92	1.02	0.90	0.87

Table S11: Vesicle targeting and fusion proteins identified in this screen.
Table of vesicle targeting and fusion proteins identified in the TMT-based proteomic screen in either cell type at any time point. Fold changes of experimental conditions shown (against an average of the 24 h and 72 h mock samples for the corresponding cell type).

Uniprot-s	Gene Name	Description	HUC fold-change 24 hpi	HUC fold-change 48 hpi	HUC fold-change 72 hpi	RPTEC fold-change 24 hpi	RPTEC fold-change 48 hpi	RPTEC fold-change 72 hpi
Q9NRW3	ABC3C	DNA dC->dU-editing enzyme APOBEC-3C (A3C) (EC 3.5.4.-) (APOBEC1-like) (Phorbolin I)	0.89	0.79	0.60	1.03	0.71	0.63
Q9HC16	ABC3G	DNA dC->dU-editing enzyme APOBEC-3G (EC 3.5.4.-) (APOBEC-related cytidine deaminase) (APOBEC-related protein) (ARCD) (APOBEC-related protein 9) (ARP-9) (CEM-15) (CEM15) (Deoxycytidine deaminase) (A3G)	0.95	0.89	0.79	1.00	1.09	1.09
Q9NUQ8	ABCF3	ATP-binding cassette sub-family F member 3	1.06	0.98	0.88	1.03	0.92	0.77
O43823	AKAP8	A-kinase anchor protein 8 (AKAP-8) (A-kinase anchor protein 95 kDa) (AKAP 95)	1.07	1.00	1.03	1.09	1.11	1.11
O75179	ANR17	Ankyrin repeat domain-containing protein 17 (Gene trap ankyrin repeat protein) (Serologically defined breast cancer antigen NY-BR-16)	1.15	1.05	0.92	1.03	1.06	1.02
P04083	ANXA1	Annexin A1 (Annexin I) (Annexin-1) (Calpactin II) (Calpactin-2) (Chromobindin-9) (Lipocortin I) (Phospholipase A2 inhibitory protein) (p35)	0.96	0.85	0.81	0.96	1.01	1.02
P78540	ARGI2	Arginase-2, mitochondrial (EC 3.5.3.1) (Arginase II) (Kidney-type arginase) (Non-hepatic arginase) (Type II arginase)	1.24	0.76	1.27	0.61	0.95	0.91
Q9ULZ3	ASC	Apoptosis-associated speck-like protein containing a CARD (hASC) (Caspase recruitment domain-containing protein 5) (PYD and CARD domain-containing protein) (Target of methylation-induced silencing 1)	0.99	1.10	1.03	1.01	0.97	0.81
Q92485	ASM3B	Acid sphingomyelinase-like phosphodiesterase 3b (ASM-like phosphodiesterase 3b) (EC 3.1.4.-)	0.85	0.87	1.30	0.79	0.83	0.84
Q14457	BECN1	Beclin-1 (Coiled-coil myosin-like BCL2-interacting protein) (Protein GT197) [Cleaved into: Beclin-1-C 35 kDa; Beclin-1-C 37 kDa]	1.04	1.05	0.99	0.96	0.96	0.90
Q10589	BST2	Bone marrow stromal antigen 2 (BST-2) (HM1.24 antigen) (Tetherin) (CD antigen CD317)	0.94	1.40	1.21	1.21	1.39	1.08
Q07021	C1QBP	Complement component 1 Q subcomponent-binding protein, mitochondrial (ASF/SF2-associated protein p32) (Glycoprotein gC1qBP) (C1qBP) (Hyaluronan-binding protein 1) (Mitochondrial matrix protein p32) (gC1q-R protein) (p33)	1.10	0.93	1.06	0.90	1.07	1.06
Q9NZP8	C1RL	Complement C1r subcomponent-like protein (C1r-LP) (C1r-like protein) (EC 3.4.21.-) (C1r-like serine protease analog protein) (CLSPa)	1.02	1.31	1.04	0.71	0.67	0.56
P49662	CASP4	Caspase-4 (CASP-4) (EC 3.4.22.57) (ICE and Ced-3 homolog 2) (ICH-2) (ICE(rel)-II) (Mih1) (Protease TX) [Cleaved into: Caspase-4 subunit 1; Caspase-4 subunit 2]	1.01	1.03	1.04	0.92	0.90	0.87
Q8WUQ7	CATIN	Cactin (Renal carcinoma antigen NY-REN-24)	1.12	1.09	1.07	1.01	1.08	1.01
P08571	CD14	Monocyte differentiation antigen CD14 (Myeloid cell-specific leucine-rich glycoprotein) (CD antigen CD14) [Cleaved into: Monocyte differentiation antigen CD14, urinary form; Monocyte differentiation antigen CD14, membrane-bound form]	1.22	1.23	0.94	0.85	0.99	1.03
P08603	CFAH	Complement factor H (H factor 1)	1.09	1.26	1.16	0.68	0.96	0.91
Q8N884	CGAS	Cyclic GMP-AMP synthase (cGAMP synthase) (cGAS) (h-cGAS) (EC 2.7.7.86) (2'3'-cGAMP synthase) (Mab-21 domain-containing protein 1)	1.22	1.07	1.23	1.25	1.37	1.54
P10909	CLUS	Clusterin (Aging-associated gene 4 protein) (Apolipoprotein J) (Apo-J) (Complement cytolysis inhibitor) (CLI) (Complement-associated protein SP-40,40) (Ku70-binding protein 1) (NA1/NA2) (Testosterone-repressed prostate message 2) (TRPM-2) [Cleaved into: Clusterin beta chain (Apolpalpha) (Complement cytolysis inhibitor a chain); Clusterin alpha chain (Apolbeta) (Complement cytolysis inhibitor b chain)]	0.93	1.00	1.09	0.55	0.70	0.69
Q9BT09	CNPY3	Protein canopy homolog 3 (CTG repeat protein 4a) (Expanded repeat-domain protein CAG/CTG 5) (Protein associated with TLR4) (Trinucleotide repeat-containing gene 5 protein)	1.06	1.09	1.17	0.98	0.92	0.96
P01024	CO3	Complement C3 (C3 and PZP-like alpha-2-macroglobulin domain-containing protein 1) [Cleaved into: Complement C3 beta chain; C3-beta-c (C3bc); Complement C3 alpha chain; C3a anaphylatoxin; Acylation stimulating protein (ASP) (C3adesArg); Complement C3b alpha' chain; Complement C3c alpha' chain fragment 1; Complement C3dg fragment; Complement C3g fragment; Complement C3d fragment; Complement C3f fragment; Complement C3c alpha' chain fragment 2]	0.86	0.82	0.91	0.65	0.60	0.48
P0C0L5	CO4B	Complement C4-B (Basic complement C4) (C3 and PZP-like alpha-2-macroglobulin domain-containing protein 3) [Cleaved into: Complement C4 beta chain; Complement C4-B alpha chain; C4a anaphylatoxin; C4b-B; C4d-B; Complement C4 gamma chain]	0.82	1.33	2.02	0.63	0.93	0.74
P13671	CO6	Complement component C6	1.16	1.31	1.34	1.28	1.18	2.13
Q5VWQ8	DAB2P	Disabled homolog 2-interacting protein (DAB2 interaction protein) (DAB2-interacting protein) (ASK-interacting protein 1) (AIP-1) (DOC-2/DAB-2 interactive protein)	0.94	0.97	0.86	1.00	0.95	0.96
P08174	DAF	Complement decay-accelerating factor (CD antigen CD55)	0.85	0.85	0.98	0.89	0.93	0.89

Accession	Gene	Description						
Q9NX09	DDIT4	DNA damage-inducible transcript 4 protein (HIF-1 responsive protein RTP801) (Protein regulated in development and DNA damage response 1) (REDD-1)	1.25	0.87	0.79	0.96	0.94	0.88
O00571	DDX3X	ATP-dependent RNA helicase DDX3X (EC 3.6.4.13) (DEAD box protein 3, X-chromosomal) (DEAD box, X isoform) (Helicase-like protein 2) (HLP2)	1.08	1.00	0.95	1.08	1.09	1.00
O95786	DDX58	Probable ATP-dependent RNA helicase DDX58 (EC 3.6.4.13) (DEAD box protein 58) (RIG-I-like receptor 1) (RLR-1) (Retinoic acid-inducible gene 1 protein) (RIG-1)	1.02	0.89	0.87	1.12	0.88	0.76
Q8IY21	DDX60	Probable ATP-dependent RNA helicase DDX60 (EC 3.6.4.13) (DEAD box protein 60)	1.10	1.18	1.33	0.96	1.04	0.92
Q08211	DHX9	ATP-dependent RNA helicase A (EC 3.6.4.13) (DEAH box protein 9) (DExH-box helicase 9) (Leukophysin) (LKP) (Nuclear DNA helicase II) (NDH II) (RNA helicase A)	1.08	0.96	0.98	1.02	1.10	0.99
Q13217	DNJC3	DnaJ homolog subfamily C member 3 (Endoplasmic reticulum DNA J domain-containing protein 6) (ER-resident protein ERdj6) (ERdj6) (Interferon-induced, double-stranded RNA-activated protein kinase inhibitor) (Protein kinase inhibitor of 58 kDa) (Protein kinase inhibitor p58)	1.01	1.04	1.02	1.05	0.97	1.00
Q8TDB6	DTX3L	E3 ubiquitin-protein ligase DTX3L (EC 2.3.2.27) (B-lymphoma- and BAL-associated protein) (Protein deltex-3-like) (RING-type E3 ubiquitin transferase DTX3L) (Rhysin-2) (Rhysin2)	1.07	1.11	1.12	0.98	0.98	0.88
P19525	E2AK2	Interferon-induced, double-stranded RNA-activated protein kinase (EC 2.7.11.1) (Eukaryotic translation initiation factor 2-alpha kinase 2) (eIF-2A protein kinase 2) (Interferon-inducible RNA-dependent protein kinase) (P1/eIF-2A protein kinase) (Protein kinase RNA-activated) (PKR) (Protein kinase R) (Tyrosine-protein kinase EIF2AK2) (EC 2.7.10.2) (p68 kinase)	1.07	1.17	1.22	1.05	1.11	1.13
Q9P2K8	E2AK4	eIF-2-alpha kinase GCN2 (EC 2.7.11.1) (Eukaryotic translation initiation factor 2-alpha kinase 4) (GCN2-like protein)	1.06	1.07	1.00	1.02	1.00	0.92
Q9BQ95	ECSIT	Evolutionarily conserved signaling intermediate in Toll pathway, mitochondrial (Protein SITPEC)	1.03	1.08	1.23	1.00	1.05	1.13
Q8IZ81	ELMD2	ELMO domain-containing protein 2	0.98	1.10	1.09	1.05	0.80	1.00
Q9NV70	EXOC1	Exocyst complex component 1 (Exocyst complex component Sec3)	0.97	0.94	0.89	0.99	0.83	0.79
Q96PZ2	F111A	Protein FAM111A	1.58	1.67	1.28	1.31	1.78	1.19
Q13158	FADD	FAS-associated death domain protein (FAS-associating death domain-containing protein) (Growth-inhibiting gene 3 protein) (Mediator of receptor induced toxicity) (Protein FADD)	1.16	1.09	1.09	1.06	1.06	1.03
P02675	FIBB	Fibrinogen beta chain [Cleaved into: Fibrinopeptide B; Fibrinogen beta chain]	0.89	0.98	1.57	0.95	0.81	0.30
P23771	GATA3	Trans-acting T-cell-specific transcription factor GATA-3 (GATA-binding factor 3)	1.12	1.04	1.04	1.16	1.14	0.96
P32455	GBP1	Guanylate-binding protein 1 (EC 3.6.5.-) (GTP-binding protein 1) (GBP-1) (HuGBP-1) (Guanine nucleotide-binding protein 1) (Interferon-induced guanylate-binding protein 1)	0.88	0.91	0.91	1.12	0.96	0.95
Q9H0R5	GBP3	Guanylate-binding protein 3 (EC 3.6.5.-) (GTP-binding protein 3) (GBP-3) (Guanine nucleotide-binding protein 3)	0.91	1.01	1.11	1.11	0.93	0.79
Q8TDQ0	HAVR2	Hepatitis A virus cellular receptor 2 (HAVcr-2) (T-cell immunoglobulin and mucin domain-containing protein 3) (TIMD-3) (T-cell immunoglobulin mucin receptor 3) (TIM-3) (T-cell membrane protein 3)	0.98	0.97	1.08	0.59	0.74	0.54
O94992	HEXI1	Protein HEXIM1 (Cardiac lineage protein 1) (Estrogen down-regulated gene 1 protein) (Hexamethylene bis-acetamide-inducible protein 1) (Menage a quatre protein 1)	1.15	1.07	1.08	1.09	1.03	1.14
P09429	HMGB1	High mobility group protein B1 (High mobility group protein 1) (HMG-1)	1.12	1.04	1.25	1.04	1.15	1.26
P26583	HMGB2	High mobility group protein B2 (High mobility group protein 2) (HMG-2)	1.14	1.26	1.58	1.09	1.03	1.47
O15347	HMGB3	High mobility group protein B3 (High mobility group protein 2a) (HMG-2a) (High mobility group protein 4) (HMG-4)	1.07	1.04	1.04	1.05	1.07	1.04
Q95460	HMR1	Major histocompatibility complex class I-related gene protein (MHC class I-related gene protein) (Class I histocompatibility antigen-like protein)	0.86	1.03	1.02	0.88	0.84	0.69
Q16666	IF16	Gamma-interferon-inducible protein 16 (Ifi-16) (Interferon-inducible myeloid differentiation transcriptional activator)	1.00	0.94	0.95	0.91	0.97	0.90
Q9BYX4	IFIH1	Interferon-induced helicase C domain-containing protein 1 (EC 3.6.4.13) (Clinically amyopathic dermatomyositis autoantigen 140 kDa) (CADM-140 autoantigen) (Helicase with 2 CARD domains) (Helicard) (Interferon-induced with helicase C domain protein 1) (Melanoma differentiation-associated protein 5) (MDA-5) (Murabutide down-regulated protein) (RIG-I-like receptor 2) (RLR-2) (RNA helicase-DEAD box protein 116)	1.16	1.16	1.05	0.92	0.97	0.82
P09914	IFIT1	Interferon-induced protein with tetratricopeptide repeats 1 (IFIT-1) (Interferon-induced 56 kDa protein) (IFI-56K) (P56)	0.96	1.35	1.49	0.93	0.92	0.82
P09913	IFIT2	Interferon-induced protein with tetratricopeptide repeats 2 (IFIT-2) (ISG-54 K) (Interferon-induced 54 kDa protein) (IFI-54K) (P54)	0.89	1.30	1.34	0.91	0.85	0.85
O14879	IFIT3	Interferon-induced protein with tetratricopeptide repeats 3 (IFIT-3) (CIG49) (ISG-60) (Interferon-induced 60 kDa protein) (IFI-60K) (P60) (RIG-G) (Interferon-induced protein with tetratricopeptide repeats 4) (IFIT-4) (Retinoic acid-induced gene G protein) (P60) (RIG-G)	1.06	1.54	1.53	1.12	0.97	0.88

Accession	Gene	Description						
Q13325	IFIT5	Interferon-induced protein with tetratricopeptide repeats 5 (IFIT-5) (Interferon-induced 58 kDa protein) (Retinoic acid- and interferon-inducible 58 kDa protein) (P58)	1.07	0.97	1.05	1.06	1.00	0.89
Q01628	IFM3	Interferon-induced transmembrane protein 3 (Dispanin subfamily A member 2b) (DSPA2b) (Interferon-inducible protein 1-8U)	1.17	0.95	1.24	0.79	0.78	0.75
Q9NPH3	IL1AP	Interleukin-1 receptor accessory protein (IL-1 receptor accessory protein) (IL-1RAcP) (Interleukin-1 receptor 3) (IL-1R-3) (IL-1R3)	1.20	1.01	0.94	1.05	1.09	1.17
Q12906	ILF3	Interleukin enhancer-binding factor 3 (Double-stranded RNA-binding protein 76) (DRBP76) (M-phase phosphoprotein 4) (MPP4) (Nuclear factor associated with dsRNA) (NFAR) (Nuclear factor of activated T-cells 90 kDa) (NF-AT-90) (Translational control protein 80) (TCP80)	1.16	1.20	1.19	0.90	1.08	1.10
Q3KP66	INAVA	Innate immunity activator protein	1.07	0.92	0.76	1.12	0.66	0.65
P51617	IRAK1	Interleukin-1 receptor-associated kinase 1 (IRAK-1) (EC 2.7.11.1)	0.94	0.90	0.89	0.99	0.95	0.76
Q9NWZ3	IRAK4	Interleukin-1 receptor-associated kinase 4 (IRAK-4) (EC 2.7.11.1) (Renal carcinoma antigen NY-REN-64)	0.94	1.03	0.93	0.98	0.95	0.96
Q14653	IRF3	Interferon regulatory factor 3 (IRF-3)	1.08	1.27	1.39	0.92	0.81	0.99
Q13568	IRF5	Interferon regulatory factor 5 (IRF-5)	0.92	0.97	0.93	0.80	0.95	0.94
Q00978	IRF9	Interferon regulatory factor 9 (IRF-9) (IFN-alpha-responsive transcription factor subunit) (ISGF3 p48 subunit) (Interferon-stimulated gene factor 3 gamma) (ISGF-3 gamma) (Transcriptional regulator ISGF3 subunit gamma)	0.96	1.10	1.05	0.83	0.80	0.75
P05161	ISG15	Ubiquitin-like protein ISG15 (Interferon-induced 15 kDa protein) (Interferon-induced 17 kDa protein) (IP17) (Ubiquitin cross-reactive protein) (hUCRP)	1.00	1.19	1.14	0.96	0.87	0.83
Q96J02	ITCH	E3 ubiquitin-protein ligase Itchy homolog (Itch) (EC 2.3.2.26) (Atrophin-1-interacting protein 4) (AIP4) (HECT-type E3 ubiquitin transferase Itchy homolog) (NFE2-associated polypeptide 1) (NAPP1)	1.22	1.03	1.04	1.00	1.05	0.90
O60674	JAK2	Tyrosine-protein kinase JAK2 (EC 2.7.10.2) (Janus kinase 2) (JAK-2)	1.14	1.19	1.26	1.18	1.12	0.92
Q15139	KPCD1	Serine/threonine-protein kinase D1 (EC 2.7.11.13) (Protein kinase C mu type) (Protein kinase D) (nPKC-D1) (nPKC-mu)	1.02	0.99	0.96	0.86	0.93	0.85
P43405	KSYK	Tyrosine-protein kinase SYK (EC 2.7.10.2) (Spleen tyrosine kinase) (p72-Syk)	1.03	1.02	1.03	1.01	1.03	0.98
P17931	LEG3	Galectin-3 (Gal-3) (35 kDa lectin) (Carbohydrate-binding protein 35) (CBP 35) (Galactose-specific lectin 3) (Galactoside-binding protein) (GALBP) (IgE-binding protein) (L-31) (Laminin-binding protein) (Lectin L-29) (Mac-2 antigen)	0.86	0.72	0.74	0.95	0.84	0.74
Q9BXB1	LGR4	Leucine-rich repeat-containing G-protein coupled receptor 4 (G-protein coupled receptor 48)	1.27	1.19	0.96	0.88	0.86	0.73
P07948	LYN	Tyrosine-protein kinase Lyn (EC 2.7.10.2) (Lck/Yes-related novel protein tyrosine kinase) (V-yes-1 Yamaguchi sarcoma viral related oncogene homolog) (p53Lyn) (p56Lyn)	1.08	0.92	1.15	0.92	1.11	0.74
Q99683	M3K5	Mitogen-activated protein kinase kinase kinase 5 (EC 2.7.11.25) (Apoptosis signal-regulating kinase 1) (ASK-1) (MAPK/ERK kinase kinase 5) (MEK kinase 5) (MEKK 5)	0.96	1.16	1.16	0.77	1.13	1.21
Q12851	M4K2	Mitogen-activated protein kinase kinase kinase kinase 2 (EC 2.7.11.1) (B lymphocyte serine/threonine-protein kinase) (Germinal center kinase) (GC kinase) (MAPK/ERK kinase kinase kinase 2) (MEK kinase kinase 2) (MEKKK 2) (Rab8-interacting protein)	1.11	1.11	1.26	0.95	1.07	1.17
Q7Z434	MAVS	Mitochondrial antiviral-signaling protein (MAVS) (CARD adapter inducing interferon beta) (Cardif) (Interferon beta promoter stimulator protein 1) (IPS-1) (Putative NF-kappa-B-activating protein 031N) (Virus-induced-signaling adapter) (VISA)	0.96	0.98	1.02	0.89	0.85	0.80
P15529	MCP	Membrane cofactor protein (TLX) (Trophoblast leukocyte common antigen) (CD antigen CD46)	1.10	1.05	1.28	0.93	1.16	0.97
P14174	MIF	Macrophage migration inhibitory factor (MIF) (EC 5.3.2.1) (Glycosylation-inhibiting factor) (GIF) (L-dopachrome isomerase) (L-dopachrome tautomerase) (EC 5.3.3.12) (Phenylpyruvate tautomerase)	0.98	1.02	1.09	0.94	1.00	1.02
P20591	MX1	Interferon-induced GTP-binding protein Mx1 (Interferon-induced protein p78) (IFI-78K) (Interferon-regulated resistance GTP-binding protein MxA) (Myxoma resistance protein 1) (Myxovirus resistance protein 1) [Cleaved into: Interferon-induced GTP-binding protein Mx1, N-terminally processed]	0.96	1.10	1.01	0.87	0.87	0.52
Q9NX02	NALP2	NACHT, LRR and PYD domains-containing protein 2 (Nucleotide-binding site protein 1) (PYRIN domain and NACHT domain-containing protein 1) (PYRIN-containing APAF1-like protein 2)	1.15	1.05	0.93	1.01	1.11	1.06
Q53F19	NCBP3	Nuclear cap-binding protein subunit 3 (Protein ELG)	1.06	1.08	1.11	1.03	1.03	0.96
Q9C000	NLRP1	NACHT, LRR and PYD domains-containing protein 1 (Caspase recruitment domain-containing protein 7) (Death effector filament-forming ced-4-like apoptosis protein) (Nucleotide-binding domain and caspase recruitment domain)	1.19	0.83	0.76	0.94	0.71	0.81
Q86UT6	NLRX1	NLR family member X1 (Caterpiller protein 11.3) (CLR11.3) (Nucleotide-binding oligomerization domain protein 26) (Nucleotide-binding oligomerization domain protein 5) (Nucleotide-binding oligomerization domain protein 9)	1.01	0.89	0.96	1.01	1.04	1.02

Accession	Gene	Description						
Q15233	NONO	Non-POU domain-containing octamer-binding protein (NonO protein) (54 kDa nuclear RNA- and DNA-binding protein) (55 kDa nuclear protein) (DNA-binding p52/p100 complex, 52 kDa subunit) (NMT55) (p54(nrb)) (p54nrb)	1.03	1.00	1.02	1.04	1.12	1.06
Q96RI1	NR1H4	Bile acid receptor (Farnesoid X-activated receptor) (Farnesol receptor HRR-1) (Nuclear receptor subfamily 1 group H member 4) (Retinoid X receptor-interacting protein 14) (RXR-interacting protein 14)	1.11	1.17	1.13	0.83	0.69	0.68
P00973	OAS1	2-5'-oligoadenylate synthase 1 ((2-5')oligo(A) synthase 1) (2-5A synthase 1) (EC 2.7.7.84) (E18/E16) (p46/p42 OAS)	1.09	1.16	1.13	0.82	1.07	1.00
P29728	OAS2	2-5'-oligoadenylate synthase 2 ((2-5')oligo(A) synthase 2) (2-5A synthase 2) (EC 2.7.7.84) (p69 OAS / p71 OAS) (p69OAS / p71OAS)	0.95	0.98	0.87	1.06	1.27	1.12
Q9Y6K5	OAS3	2-5'-oligoadenylate synthase 3 ((2-5')oligo(A) synthase 3) (2-5A synthase 3) (EC 2.7.7.84) (p100 OAS) (p100OAS)	1.04	1.09	1.17	1.07	1.11	1.07
Q96CV9	OPTN	Optineurin (E3-14.7K-interacting protein) (FIP-2) (Huntingtin yeast partner L) (Huntingtin-interacting protein 7) (HIP-7) (Huntingtin-interacting protein L) (NEMO-related protein) (Optic neuropathy-inducing protein) (Transcription factor IIIA-interacting protein) (TFIIIA-IntP)	1.00	1.03	1.02	0.95	0.89	0.80
Q96BN8	OTUL	Ubiquitin thioesterase otulin (EC 3.4.19.12) (Deubiquitinating enzyme otulin) (OTU domain-containing deubiquitinase with linear linkage specificity) (Ubiquitin thioesterase Gumby)	0.97	0.90	0.89	0.97	0.96	0.92
Q460N5	PAR14	Poly [ADP-ribose] polymerase 14 (PARP-14) (EC 2.4.2.30) (ADP-ribosyltransferase diphtheria toxin-like 8) (ARTD8) (B aggressive lymphoma protein 2)	1.03	1.21	1.19	1.04	0.99	0.89
P55085	PAR2	Proteinase-activated receptor 2 (PAR-2) (Coagulation factor II receptor-like 1) (G-protein coupled receptor 11) (Thrombin receptor-like 1) [Cleaved into: Proteinase-activated receptor 2, alternate cleaved 1; Proteinase-activated receptor 2, alternate cleaved 2]	1.15	1.01	0.92	0.81	0.75	0.79
Q8IXQ6	PARP9	Poly [ADP-ribose] polymerase 9 (PARP-9) (EC 2.4.2.30) (ADP-ribosyltransferase diphtheria toxin-like 9) (ARTD9) (B aggressive lymphoma protein)	1.01	1.15	1.23	0.93	0.99	0.94
Q15366	PCBP2	Poly(rC)-binding protein 2 (Alpha-CP2) (Heterogeneous nuclear ribonucleoprotein E2) (hnRNP E2)	1.03	1.03	0.99	1.07	1.05	0.96
O15162	PLS1	Phospholipid scramblase 1 (PL scramblase 1) (Ca(2+)-dependent phospholipid scramblase 1) (Erythrocyte phospholipid scramblase) (MmTRA1b)	1.05	0.84	1.15	0.85	1.08	1.14
P29590	PML	Protein PML (Promyelocytic leukemia protein) (RING finger protein 71) (Tripartite motif-containing protein 19)	0.95	0.98	0.83	0.97	0.77	0.75
O00743	PPP6	Serine/threonine-protein phosphatase 6 catalytic subunit (PP6C) (EC 3.1.3.16) [Cleaved into: Serine/threonine-protein phosphatase 6 catalytic subunit, N-terminally processed]	0.91	0.97	0.96	1.03	1.06	1.06
O60828	PQBP1	Polyglutamine-binding protein 1 (PQBP-1) (38 kDa nuclear protein containing a WW domain) (Npw38) (Polyglutamine tract-binding protein 1)	1.03	1.14	1.06	1.06	1.15	1.16
P78527	PRKDC	DNA-dependent protein kinase catalytic subunit (DNA-PK catalytic subunit) (DNA-PKcs) (EC 2.7.11.1) (DNPK1) (p460)	1.00	1.01	1.03	1.02	1.06	1.05
Q8WXF1	PSPC1	Paraspeckle component 1 (Paraspeckle protein 1)	0.96	0.99	0.96	1.01	1.03	1.05
Q96PK6	RBM14	RNA-binding protein 14 (Paraspeckle protein 2) (PSP2) (RNA-binding motif protein 14) (RRM-containing coactivator activator/modulator) (Synaptotagmin-interacting protein) (SYT-interacting protein)	1.03	0.99	1.02	1.04	1.06	1.04
P78563	RED1	Double-stranded RNA-specific editase 1 (EC 3.5.4.37) (RNA-editing deaminase 1) (RNA-editing enzyme 1) (dsRNA adenosine deaminase)	0.99	0.97	0.92	0.78	1.27	0.89
O14730	RIOK3	Serine/threonine-protein kinase RIO3 (EC 2.7.11.1) (RIO kinase 3) (sudD homolog)	0.93	0.76	0.85	1.05	0.72	0.95
O43353	RIPK2	Receptor-interacting serine/threonine-protein kinase 2 (EC 2.7.11.1) (CARD-containing interleukin-1 beta-converting enzyme-associated kinase) (CARD-containing IL-1 beta ICE-kinase) (RIP-like-interacting CLARP kinase) (Receptor-interacting protein 2) (RIP-2) (Tyrosine-protein kinase RIPK2) (EC 2.7.10.2)	1.10	0.95	0.92	1.02	1.00	0.92
Q8IUD6	RN135	E3 ubiquitin-protein ligase RNF135 (EC 2.3.2.27) (RIG-I E3 ubiquitin ligase) (REUL) (RING finger protein 135) (RING-type E3 ubiquitin transferase RNF135) (Riplet)	0.94	0.97	0.92	0.76	0.64	0.79
Q05823	RN5A	2-5A-dependent ribonuclease (2-5A-dependent RNase) (EC 3.1.26.-) (Ribonuclease 4) (Ribonuclease L) (RNase L)	0.85	1.11	0.93	1.07	0.84	1.09
Q04912	RON	Macrophage-stimulating protein receptor (MSP receptor) (EC 2.7.10.1) (CDw136) (Protein-tyrosine kinase 8) (p185-Ron) (CD antigen CD136) [Cleaved into: Macrophage-stimulating protein receptor alpha chain; Macrophage-stimulating protein receptor beta chain]	1.09	1.02	1.01	0.94	0.89	0.82
O14802	RPC1	DNA-directed RNA polymerase III subunit RPC1 (RNA polymerase III subunit C1) (EC 2.7.7.6) (DNA-directed RNA polymerase III largest subunit) (DNA-directed RNA polymerase III subunit A) (RNA polymerase III 155 kDa subunit) (RPC155) (RNA polymerase III subunit C160)	1.05	1.03	1.00	1.01	0.99	0.91

Accession	Gene	Description						
Q9Y2Y1	RPC10	DNA-directed RNA polymerase III subunit RPC10 (RNA polymerase III subunit C10) (DNA-directed RNA polymerase III subunit C11) (RNA polymerase III 12.5 kDa subunit) (RPC12.5) (RNA polymerase III subunit C11) (HsC11p) (RPC11) (hRPC11)	1.06	0.86	0.90	1.01	1.09	0.82
Q9NW08	RPC2	DNA-directed RNA polymerase III subunit RPC2 (RNA polymerase III subunit C2) (EC 2.7.7.6) (C128) (DNA-directed RNA polymerase III 127.6 kDa polypeptide) (DNA-directed RNA polymerase III subunit B)	1.04	1.01	0.94	1.03	0.99	0.94
Q9BUI4	RPC3	DNA-directed RNA polymerase III subunit RPC3 (RNA polymerase III subunit C3) (DNA-directed RNA polymerase III subunit C) (RNA polymerase III 62 kDa subunit) (RPC62)	1.14	1.10	1.04	1.15	1.22	1.14
P05423	RPC4	DNA-directed RNA polymerase III subunit RPC4 (RNA polymerase III subunit C4) (DNA-directed RNA polymerase III subunit D) (Protein BN51) (RNA polymerase III 47 kDa subunit) (RPC53 homolog)	1.13	1.03	0.99	0.99	1.06	0.94
Q9NVU0	RPC5	DNA-directed RNA polymerase III subunit RPC5 (RNA polymerase III subunit C5) (DNA-directed RNA polymerase III 80 kDa polypeptide)	1.03	0.96	0.92	1.00	1.13	0.90
Q9H1D9	RPC6	DNA-directed RNA polymerase III subunit RPC6 (RNA polymerase III subunit C6) (DNA-directed RNA polymerase III subunit F) (RNA polymerase III 39 kDa subunit) (RPC39)	1.14	1.04	1.03	1.02	1.15	1.01
O15318	RPC7	DNA-directed RNA polymerase III subunit RPC7 (RNA polymerase III subunit C7) (DNA-directed RNA polymerase III subunit G) (RNA polymerase III 32 kDa apha subunit) (RPC32-alpha) (RNA polymerase III 32 kDa subunit) (RPC32)	1.45	1.06	1.13	1.23	1.44	1.09
Q9Y535	RPC8	DNA-directed RNA polymerase III subunit RPC8 (RNA polymerase III subunit C8) (DNA-directed RNA polymerase III subunit H) (RNA polymerase III subunit 22.9 kDa subunit) (RPC22.9)	1.23	0.92	0.94	0.99	0.97	0.76
O75575	RPC9	DNA-directed RNA polymerase III subunit RPC9 (RNA polymerase III subunit C9) (Calcitonin gene-related peptide-receptor component protein) (CGRP-RCP) (CGRP-receptor component protein) (CGRPRCP) (HsC17)	1.12	1.41	1.07	0.79	0.97	0.72
Q9NUL5	RYDEN	Repressor of yield of DENV protein (RyDEN)	0.91	1.00	1.12	0.84	0.63	0.81
Q92503	S14L1	SEC14-like protein 1	1.03	0.84	0.84	1.10	0.86	0.61
Q9Y3Z3	SAMH1	Deoxynucleoside triphosphate triphosphohydrolase SAMHD1 (dNTPase) (EC 3.1.5.-) (Dendritic cell-derived IFNG-induced protein) (DCIP) (Monocyte protein 5) (MOP-5) (SAM domain and HD domain-containing protein 1)	0.96	1.01	1.23	0.98	0.99	1.08
Q9BYW2	SETD2	Histone-lysine N-methyltransferase SETD2 (EC 2.1.1.43) (HIF-1) (Huntingtin yeast partner B) (Huntingtin-interacting protein 1) (HIP-1) (Huntingtin-interacting protein B) (Lysine N-methyltransferase 3A) (Protein-lysine N-methyltransferase SETD2) (EC 2.1.1.-) (SET domain-containing protein 2) (hSET2) (p231HBP)	1.06	1.11	1.07	1.03	1.07	1.11
P23246	SFPQ	Splicing factor, proline- and glutamine-rich (100 kDa DNA-pairing protein) (hPOMp100) (DNA-binding p52/p100 complex, 100 kDa subunit) (Polypyrimidine tract-binding protein-associated-splicing factor) (PSF) (PTB-associated-splicing factor)	1.02	0.95	1.01	1.04	1.03	1.00
Q8IXJ6	SIR2	NAD-dependent protein deacetylase sirtuin-2 (EC 3.5.1.-) (Regulatory protein SIR2 homolog 2) (SIR2-like protein 2)	0.90	0.99	0.99	0.84	0.82	0.75
Q7Z7L1	SLN11	Schlafen family member 11	1.55	1.22	1.55	1.22	2.15	2.01
P03973	SLPI	Antileukoproteinase (ALP) (BLPI) (HUSI-1) (Mucus proteinase inhibitor) (MPI) (Protease inhibitor WAP4) (Secretory leukocyte protease inhibitor) (Seminal proteinase inhibitor) (WAP four-disulfide core domain protein 4)	0.79	0.69	0.62	0.77	0.72	0.76
P42224	STAT1	Signal transducer and activator of transcription 1-alpha/beta (Transcription factor ISGF-3 components p91/p84)	1.03	1.17	1.16	0.96	1.00	1.06
P52630	STAT2	Signal transducer and activator of transcription 2 (p113)	1.06	1.07	0.97	1.00	0.96	0.77
Q86WV6	STING	Stimulator of interferon genes protein (hSTING) (Endoplasmic reticulum interferon stimulator) (ERIS) (Mediator of IRF3 activation) (hMITA) (Transmembrane protein 173)	1.21	1.26	1.07	0.97	1.00	1.15
Q9UHD2	TBK1	Serine/threonine-protein kinase TBK1 (EC 2.7.11.1) (NF-kappa-B-activating kinase) (T2K) (TANK-binding kinase 1)	1.00	1.13	1.17	0.94	0.95	0.98
A7MCY6	TBKB1	TANK-binding kinase 1-binding protein 1 (TBK1-binding protein 1)	1.03	1.04	0.80	0.93	0.72	0.67
Q8IUC6	TCAM1	TIR domain-containing adapter molecule 1 (TICAM-1) (Proline-rich, vinculin and TIR domain-containing protein B) (Putative NF-kappa-B-activating protein 502H) (Toll-interleukin-1 receptor domain-containing adapter protein inducing interferon beta) (MyD88-3) (TIR domain-containing adapter protein inducing IFN-beta)	0.58	0.69	0.68	0.91	0.93	0.91

Accession	Gene	Description						
Q86XR7	TCAM2	TIR domain-containing adapter molecule 2 (TICAM-2) (Putative NF-kappa-B-activating protein 502) (TRIF-related adapter molecule) (Toll-like receptor adaptor protein 3) (Toll/interleukin-1 receptor domain-containing protein) (MyD88-4)	0.93	0.99	1.07	1.01	0.97	0.96
O15455	TLR3	Toll-like receptor 3 (CD antigen CD283)	0.90	0.97	1.05	0.90	0.81	0.88
Q9H0E2	TOLIP	Toll-interacting protein	0.88	0.90	0.94	0.89	1.03	0.91
Q96F44	TRI11	E3 ubiquitin-protein ligase TRIM11 (EC 2.3.2.27) (Protein BIA1) (RING finger protein 92) (RING-type E3 ubiquitin transferase TRIM11) (Tripartite motif-containing protein 11)	1.18	0.98	0.77	1.20	1.08	0.89
O60858	TRI13	E3 ubiquitin-protein ligase TRIM13 (EC 2.3.2.27) (B-cell chronic lymphocytic leukemia tumor suppressor Leu5) (Leukemia-associated protein 5) (Putative tumor suppressor RFP2) (RING finger protein 77) (RING-type E3 ubiquitin transferase TRIM13) (Ret finger protein 2) (Tripartite motif-containing protein 13)	0.95	0.85	0.81	0.86	0.85	0.77
Q8IYM9	TRI22	E3 ubiquitin-protein ligase TRIM22 (EC 2.3.2.27) (50 kDa-stimulated trans-acting factor) (RING finger protein 94) (RING-type E3 ubiquitin transferase TRIM22) (Staf-50) (Tripartite motif-containing protein 22)	1.03	0.86	0.89	0.95	0.86	0.68
Q14258	TRI25	E3 ubiquitin/ISG15 ligase TRIM25 (EC 6.3.2.n3) (Estrogen-responsive finger protein) (RING finger protein 147) (RING-type E3 ubiquitin transferase) (EC 2.3.2.27) (RING-type E3 ubiquitin transferase TRIM25) (Tripartite motif-containing protein 25) (Ubiquitin/ISG15-conjugating enzyme TRIM25) (Zinc finger protein 147)	1.00	0.94	0.95	1.04	0.79	0.86
Q12899	TRI26	Tripartite motif-containing protein 26 (EC 2.3.2.27) (Acid finger protein) (AFP) (RING finger protein 95) (Zinc finger protein 173)	1.16	0.92	0.93	1.11	1.23	0.91
Q14134	TRI29	Tripartite motif-containing protein 29 (Ataxia telangiectasia group D-associated protein)	0.79	0.84	0.83	0.97	0.93	0.92
O00635	TRI38	E3 ubiquitin-protein ligase TRIM38 (EC 2.3.2.27) (RING finger protein 15) (RING-type E3 ubiquitin transferase TRIM38) (Tripartite motif-containing protein 38) (Zinc finger protein RoRet)	0.85	0.94	1.02	0.88	0.78	0.75
Q9BRZ2	TRI56	E3 ubiquitin-protein ligase TRIM56 (EC 2.3.2.27) (RING finger protein 109) (RING-type E3 ubiquitin transferase TRIM56) (Tripartite motif-containing protein 56)	0.99	1.02	1.05	1.03	1.05	0.99
Q9C037	TRIM4	E3 ubiquitin-protein ligase TRIM4 (EC 2.3.2.27) (RING finger protein 87) (RING-type E3 ubiquitin transferase TRIM4) (Tripartite motif-containing protein 4)	0.91	0.97	0.93	0.85	0.88	0.78
P54578	UBP14	Ubiquitin carboxyl-terminal hydrolase 14 (EC 3.4.19.12) (Deubiquitinating enzyme 14) (Ubiquitin thioesterase 14) (Ubiquitin-specific-processing protease 14)	0.94	0.97	1.02	1.00	1.03	1.01
P30530	UFO	Tyrosine-protein kinase receptor UFO (EC 2.7.10.1) (AXL oncogene)	1.09	1.00	0.88	1.14	1.09	0.86
Q9H1C4	UN93B	Protein unc-93 homolog B1 (Unc-93B1) (hUNC93B1)	1.53	1.34	1.34	1.03	0.95	1.00
Q96S55	WRIP1	ATPase WRNIP1 (EC 3.6.1.3) (Werner helicase-interacting protein 1)	1.05	1.08	1.12	1.00	1.05	1.07
P13010	XRCC5	X-ray repair cross-complementing protein 5 (EC 3.6.4.-) (86 kDa subunit of Ku antigen) (ATP-dependent DNA helicase 2 subunit 2) (ATP-dependent DNA helicase II 80 kDa subunit) (CTC box-binding factor 85 kDa subunit) (CTC85) (CTCBF) (DNA repair protein XRCC5) (Ku80) (Ku86) (Lupus Ku autoantigen protein p86) (Nuclear factor IV) (Thyroid-lupus autoantigen) (TLAA) (X-ray repair complementing defective repair in Chinese hamster cells 5 (double-strand-break rejoining))	1.02	1.01	1.10	0.98	1.09	1.07
P12956	XRCC6	X-ray repair cross-complementing protein 6 (EC 3.6.4.-) (EC 4.2.99.-) (5'-deoxyribose-5-phosphate lyase Ku70) (5'-dRP lyase Ku70) (70 kDa subunit of Ku antigen) (ATP-dependent DNA helicase 2 subunit 1) (ATP-dependent DNA helicase II 70 kDa subunit) (CTC box-binding factor 75 kDa subunit) (CTC75) (CTCBF) (DNA repair protein XRCC6) (Lupus Ku autoantigen protein p70) (Ku70) (Thyroid-lupus autoantigen) (TLAA) (X-ray repair complementing defective repair in Chinese hamster cells 6)	1.05	1.02	1.06	0.98	1.08	1.04
Q9Y2K1	ZBTB1	Zinc finger and BTB domain-containing protein 1	1.18	1.24	1.04	0.94	1.10	0.90
Q5D1E8	ZC12A	Endoribonuclease ZC3H12A (EC 3.1.-.-) (Monocyte chemotactic protein-induced protein 1) (MCP-induced protein 1) (MCPIP-1) (Regnase-1) (Reg1) (Zinc finger CCCH domain-containing protein 12A)	0.89	0.92	0.86	0.78	0.54	0.80

Table S12: Innate immune and antiviral proteins identified in this screen (by GO term).
Table of innate immune and antiviral proteins identified in the TMT-based proteomic screen in either cell type at any time point. Fold changes of experimental conditions shown (against an average of the 24 h and 72 h mock samples for the corresponding

9. Bibliography

ABEND, J. R., JIANG, M. X. & IMPERIALE, M. J. 2009a. BK virus and human cancer: Innocent until proven guilty. Seminars in Cancer Biology, 19, 252-260.

ABEND, J. R., JOSEPH, A. E., DAS, D., CAMPBELL-CECEN, D. B. & IMPERIALE, M. J. 2009b. A truncated T antigen expressed from an alternatively spliced BK virus early mRNA. Journal of General Virology, 90, 1238-1245.

ABEND, J. R., LOW, J. A. & IMPERIALE, M. J. 2007. Inhibitory effect of gamma interferon on BK virus gene expression and replication. Journal of Virology, 81, 272-279.

ABEND, J. R., LOW, J. A. & IMPERIALE, M. J. 2010. Global effects of BKV infection on gene expression in human primary kidney epithelial cells. Virology, 397, 73-79.

AGUIRRE, S., MAESTRE, A. M., PAGNI, S., PATEL, J. R., SAVAGE, T., GUTMAN, D., MARINGER, K., BERNAL-RUBIO, D., SHABMAN, R. S., SIMON, V., RODRIGUEZ-MADOZ, J. R., MULDER, L. C. F., BARBER, G. N. & FERNANDEZ-SESMA, A. 2012. DENV Inhibits Type I IFN Production in Infected Cells by Cleaving Human STING. Plos Pathogens, 8.

AKAMATSU, S., TAKATA, R., HAIMAN, C. A., TAKAHASHI, A., INOUE, T., KUBO, M., FURIHATA, M., KAMATANI, N., INAZAWA, J., CHEN, G. K., LE MARCHAND, L., KOLONEL, L. N., KATOH, T., YAMANO, Y., YAMAKADO, M., TAKAHASHI, H., YAMADA, H., EGAWA, S., FUJIOKA, T., HENDERSON, B. E., HABUCHI, T., OGAWA, O., NAKAMURA, Y. & NAKAGAWA, H. 2012. Common variants at 11q12, 10q26 and 3p11.2 are associated with prostate cancer susceptibility in Japanese. Nature Genetics, 44, 426-U234.

AKIRA, S. & HEMMI, H. 2003. Recognition of pathogen-associated molecular patterns by TLR family. Immunology Letters, 85, 85-95.

ALLAN, B. B., MOYER, B. D. & BALCH, W. E. 2000. Rab1 recruitment of p115 into a cis-SNARE complex: Programming budding COPII vesicles for fusion. Science, 289, 444-448.

ALLANDER, T., ANDREASSON, K., GUPTA, S., BJERKNER, A., BOGDANOVIC, G., PERSSON, M. A. A., DALIANIS, T., RAMQVIST, T. & ANDERSSON, B. 2007. Identification of a third human polyomavirus. Journal of Virology, 81, 4130-4136.

ANDERSEN, M. H., SCHRAMA, D., STRATEN, P. T. & BECKER, J. C. 2006. Cytotoxic T cells. Journal of Investigative Dermatology, 126, 32-41.

ANDREI, C., MARGIOCCO, P., POGGI, A., LOTTI, L. V., TORRISI, M. R. & RUBARTELLI, A. 2004. Phospholipases C and A(2) control lysosome-mediated IL-1 beta secretion: Implications for inflammatory processes. Proceedings of the National Academy of Sciences of the United States of America, 101, 9745-9750.

ASCHAUER, L., CARTA, G., VOGELSANG, N., SCHLATTER, E. & JENNINGS, P. 2015. Expression of xenobiotic transporters in the human renal proximal tubule cell line RPTEC/TERT1. Toxicology in Vitro, 30, 95-105.

ASSETTA, B., DE CECCO, M., O'HARA, B. & ATWOOD, W. J. 2016. JC Polyomavirus Infection of Primary Human Renal Epithelial Cells Is Controlled by a Type I IFN-Induced Response. Mbio, 7.

BALLABENI, A., ZAMPONI, R., MOORE, J. K., HELIN, K. & KIRSCHNER, M. W. 2013. Geminin deploys multiple mechanisms to regulate Cdt1 before cell division thus ensuring the proper execution of DNA replication. Proceedings of the National Academy of Sciences of the United States of America, 110, E2848-E2853.

BAR, S., DAEFFLER, L., ROMMELAERE, J. & NUESCH, J. P. F. 2008. Vesicular egress of non-enveloped lytic parvoviruses depends on gelsolin functioning. Plos Pathogens, 4.

BARAK, Y., JUVEN, T., HAFFNER, R. & OREN, M. 1993. MDM2 EXPRESSION IS INDUCED BY WILD TYPE-P53 ACTIVITY. Embo Journal, 12, 461-468.

BARR, F. A., NAKAMURA, N. & WARREN, G. 1998. Mapping the interaction between GRASP65 and GM130, components of a protein complex involved in the stacking of Golgi cisternae. Embo Journal, 17, 3258-3268.

BEKIER, M. E., WANG, L. B., LI, J., HUANG, H. R., TANG, D. M., ZHANG, X. Y. & WANG, Y. Z. 2017. Knockout of the Golgi stacking proteins GRASP55 and GRASP65 impairs Golgi structure and function. Molecular Biology of the Cell, 28, 2833-2842.

BENNETT, S. M., BROEKEMA, N. M. & IMPERIALE, M. J. 2012. BK polyomavirus: emerging pathogen. Microbes and Infection, 14**,** 672-683.

BENNETT, S. M., JIANG, M. X. & IMPERIALE, M. J. 2013. Role of Cell-Type-Specific Endoplasmic Reticulum-Associated Degradation in Polyomavirus Trafficking. Journal of Virology, 87**,** 8843-8852.

BENNETT, S. M., ZHAO, L. B., BOSARD, C. & IMPERIALE, M. J. 2015. Role of a nuclear localization signal on the minor capsid Proteins VP2 and VP3 in BKPyV nuclear entry. Virology, 474**,** 110-116.

BERNHOFF, E., GUTTEBERG, T. J., SANDVIK, K., HIRSCH, H. H. & RINALDO, C. H. 2008. Cidofovir inhibits polyomavirus BK replication in human renal tubular cells downstream of viral early gene expression. American Journal of Transplantation, 8**,** 1413-1422.

BERTOLI, C., SKOTHEIM, J. M. & DE BRUIN, R. A. M. 2013. Control of cell cycle transcription during G1 and S phases. Nature Reviews Molecular Cell Biology, 14**,** 518-528.

BETHGE, T., HACHEMI, H. A., MANZETTI, J., GOSERT, R., SCHAFFNER, W. & HIRSCH, H. H. 2015. Sp1 Sites in the Noncoding Control Region of BK Polyomavirus Are Key Regulators of Bidirectional Viral Early and Late Gene Expression. Journal of Virology, 89**,** 3396-3411.

BETTUZZI, S., SCORCIONI, F., ASTANCOLLE, S., DAVALLI, P., SCALTRITI, M. & CORTI, A. 2002. Clusterin (SGP-2) transient overexpression decreases proliferation rate of SV40-immortalized human prostate epithelial cells by slowing down cell cycle progression. Oncogene, 21**,** 4328-4334.

BINGGELI, S., EGLI, A., SCHAUB, S., BINET, I., MAYR, M., STEIGER, J. & HIRSCH, H. H. 2007. Polyomavirus BK-specific cellular immune response to VP1 and large T-antigen in kidney transplant recipients. American Journal of Transplantation, 7**,** 1131-1139.

BIRD, S. W. & KIRKEGAARD, K. 2015. Escape of non-enveloped virus from intact cells. Virology, 479**,** 444-449.

BLACK, P. H., CRAWFORD, L. V. & CRAWFORD, E. M. 1964. Purificantion of Simian Virus 40. Virology, 24**,** 381-&.

BOEHME, K. A. & BLATTNER, C. 2009. Regulation of p53-insights into a complex process. Critical Reviews in Biochemistry and Molecular Biology, 44**,** 367-392.

BOLLAG, B., HOFSTETTER, C. A., REVIRIEGO-MENDOZA, M. M. & FRISQUE, R. J. 2010. JC Virus Small t Antigen Binds Phosphatase PP2A and Rb Family Proteins and Is Required for Efficient Viral DNA Replication Activity. Plos One, 5.

BOLLAG, B., PRINS, C., SNYDER, E. L. & FRISQUE, R. J. 2000. Purified JC virus T and T ' proteins differentially interact with the retinoblastoma family of tumor suppressor proteins. Virology, 274**,** 165-178.

BORCHERT, S., CZECH-SIOLI, M., NEUMANN, F., SCHMIDT, C., WIMMER, P., DOBNER, T., GRUNDHOFF, A. & FISCHER, N. 2014. High-Affinity Rb Binding, p53 Inhibition, Subcellular Localization, and Transformation by Wild-Type or Tumor-Derived Shortened Merkel Cell Polyomavirus Large T Antigens. Journal of Virology, 88**,** 3144-3160.

BOUVARD, V., BAAN, R. A., GROSSE, Y., LAUBY-SECRETAN, B., EL GHISSASSI, F., BENBRAHIM-TALLAA, L., GUHA, N., STRAIF, K. & CANC, W. H. O. I. A. R. 2012. Carcinogenicity of malaria and of some polyomaviruses. Lancet Oncology, 13**,** 339-340.

BREW, B. J., DAVIES, N. W. S., CINQUE, P., CLIFFORD, D. B. & NATH, A. 2010. Progressive multifocal leukoencephalopathy and other forms of JC virus disease. Nature Reviews Neurology, 6**,** 667-679.

BROEKEMA, N. M. & IMPERIALE, M. J. 2012. Efficient propagation of archetype BK and JC polyomaviruses. Virology, 422**,** 235-241.

BROOKS, C. L. & GU, W. 2006. p53 ubiquitination: Mdm2 and beyond. Molecular Cell, 21**,** 307-315.

BRUNS, C., MCCAFFERY, J. M., CURWIN, A. J., DURAN, J. M. & MALHOTRA, V. 2011. Biogenesis of a novel compartment for autophagosome-mediated unconventional protein secretion. Journal of Cell Biology, 195**,** 979-992.

BUCKINGHAM, E. M., CARPENTER, J. E., JACKSON, W. & GROSE, C. 2014. Autophagy and the Effects of Its Inhibition on Varicella-Zoster Virus Glycoprotein Biosynthesis and Infectivity. Journal of Virology, 88**,** 890-902.

BURGER-CALDERON, R., MADDEN, V., HALLETT, R. A., GINGERICH, A. D., NICKELEIT, V. & WEBSTER-CYRIAQUE, J. 2014. Replication of Oral BK Virus in Human Salivary Gland Cells. Journal of Virology, 88**,** 559-573.

BYERS, A. M., HADLEY, A. & LUKACHER, A. E. 2007. Protection against polyoma virus-induced tumors is perforin-independent. Virology, 358**,** 485-492.

CABY, M. P., LANKAR, D., VINCENDEAU-SCHERRER, C., RAPOSO, G. & BONNEROT, C. 2005. Exosomal-like vesicles are present in human blood plasma. International Immunology, 17**,** 879-887.

CAI, H. Q., REINISCH, K. & FERRO-NOVICK, S. 2007. Coats, tethers, Rabs, and SNAREs work together to mediate the intracellular destination of a transport vesicle. Developmental Cell, 12**,** 671-682.

CALVIGNAC-SPENCER, S., FELTKAMP, M. C. W., DAUGHERTY, M. D., MOENS, U., RAMQVIST, T., JOHNE, R., EHLERS, B. & INT COMM TAXONOMY, V. 2016. A taxonomy update for the family Polyomaviridae. Archives of Virology, 161**,** 1739-1750.

CHAKRABARTI, A., JHA, B. K. & SILVERMAN, R. H. 2011. New Insights into the Role of RNase L in Innate Immunity. Journal of Interferon and Cytokine Research, 31**,** 49-57.

CHEN, X. J. S., STEHLE, T. & HARRISON, S. C. 1998. Interaction of polyomavirus internal protein VP2 with the major capsid protein VP1 and implications for participation of VP2 in viral entry. Embo Journal, 17**,** 3233-3240.

CHITTICK, P., WILLIAMSON, J. C. & OHL, C. A. 2013. BK Virus Encephalitis: Case Report, Review of the Literature, and Description of a Novel Treatment Modality. Annals of Pharmacotherapy, 47**,** 1229-1233.

CHIU, Y. H., MACMILLAN, J. B. & CHEN, Z. J. J. 2009. RNA Polymerase III Detects Cytosolic DNA and Induces Type I Interferons through the RIG-I Pathway. Cell, 138**,** 576-591.

CHU, W. M., GONG, X., LI, Z. W., TAKABAYASHI, K., OUYANG, H. H., CHEN, Y., LOIS, A., CHEN, D. J., LI, G. C., KARIN, M. & RAZ, E. 2000. DNA-PKcs is required for activation of innate immunity by immunostimulatory DNA. Cell, 103**,** 909-918.

CLAYSON, E. T., BRANDO, L. V. J. & COMPANS, R. W. 1989. Rlease of Simian Virus-40 virions from epithelial cells is polarized and occurs without cell lysis. Journal of Virology, 63**,** 2278-2288.

CLEMENT, J. F., BIBEAU-POIRIER, A., GRAVEL, S. P., GRANDVAUX, N., BONNEIL, E., THIBAULT, P., MELOCHE, S. & SERVANT, M. J. 2008. Phosphorylation of IRF-3 on Ser 339 generates a hyperactive form of IRF-3 through regulation of dimerization and CBP association. Journal of Virology, 82**,** 3984-3996.

COLANZI, A. & SUTTERLIN, C. 2013. Signaling at the Golgi During Mitosis. Methods for Analysis of Golgi Complex Function, 118**,** 383-400.

COMOLI, P., HIRSCH, H. H. & GINEVRI, F. 2008. Cellular immune responses to BK virus. Current Opinion in Organ Transplantation, 13**,** 569-574.

COX, J. & MANN, M. 2008. MaxQuant enables high peptide identification rates, individualized p.p.b.-range mass accuracies and proteome-wide protein quantification. Nature Biotechnology, 26**,** 1367-1372.

CUTHBERT, J. A. 2001. Hepatitis A: Old and new. Clinical Microbiology Reviews, 14**,** 38-+.

DAMLE, N. K., LINSLEY, P. S. & LEDBETTER, J. A. 1991. Direct helper T-cell induced B-cell differentiation involves interaction between T-cell antigen-CD28 and B-cell activation antigen-B7. European Journal of Immunology, 21**,** 1277-1282.

DAVY, C. E., JACKSON, D. J., WANG, Q., RAJ, K., MASTERSON, P. J., FENNER, N. F., SOUTHERN, S., CUTHILL, S., MILLAR, J. B. A. & DOORBAR, J. 2002. Identification of a G(2) arrest domain in the E1 boolean AND E4 protein of human papillomavirus type 16. Journal of Virology, 76**,** 9806-9818.

DE-SIMONE, F. I., SARIYER, R., OTALORA, Y. L., YARANDI, S., CRAIGIE, M., GORDON, J. & SARIYER, I. K. 2015. IFN-Gamma Inhibits JC Virus Replication in Glial Cells by Suppressing T-Antigen Expression. Plos One, 10.

DEBAISIEUX, S., RAYNE, F., YEZID, H. & BEAUMELLE, B. 2012. The Ins and Outs of HIV-1 Tat. Traffic, 13, 355-363.

DECAPRIO, J. A. & GARCEA, R. L. 2013. A cornucopia of human polyomaviruses. Nature Reviews Microbiology, 11, 264-276.

DECAPRIO, J. A., LUDLOW, J. W., FIGGE, J., SHEW, J. Y., HUANG, C. M., LEE, W. H., MARSILIO, E., PAUCHA, E. & LIVINGSTON, D. M. 1988. SV40 Large tumour-antigen froms a specific complex with the product of the retinoblastoma susceptibility gene. Cell, 54, 275-283.

DEHORITY, W. N., EICKMAN, M. M., SCHWALM, K. C., GROSS, S. M., SCHROTH, G. P., YOUNG, S. A. & DINWIDDIE, D. L. 2017. Complete Genome Sequence of a KI Polyomavirus Isolated From an Otherwise Healthy Child With Severe Lower Respiratory Tract Infection. Journal of Medical Virology, 89, 926-930.

DING, W. X., NI, H. M., GAO, W. T., HOU, Y. F., MELAN, M. A., CHEN, X. Y., STOLZ, D. B., SHAO, Z. M. & YIN, X. M. 2007. Differential effects of endoplasmic reticulum stress-induced autophagy on cell survival. Journal of Biological Chemistry, 282, 4702-4710.

DING, Y., WANG, J., WANG, J. Q., STIERHOF, Y. D., ROBINSON, D. G. & JIANG, L. W. 2012. Unconventional protein secretion. Trends in Plant Science, 17, 606-615.

DINTER, A. & BERGER, E. G. 1998. Golgi-disturbing agents. Histochemistry and Cell Biology, 109, 571-590.

DOHERTY, J. & FREUND, R. 1997. Polyomavirus large T antigen overcomes p53 dependent growth arrest. Oncogene, 14, 1923-1931.

DRACHENBERG, C. B., PAPADIMITRIOU, J. C., WALI, R., CUBITT, C. L. & RAMOS, E. 2003. BK polyoma virus allograft nephropathy: Ultrastructural features from viral cell entry to lysis. American Journal of Transplantation, 3, 1383-1392.

DRAKE, D. R. & LUKACHER, A. E. 1998. beta(2)-microglobulin knockout mice are highly susceptible to polyoma virus tumorigenesis. Virology, 252, 275-284.

DU, P. C., STOLOVITZKY, G., HORVATOVICH, P., BISCHOFF, R., LIM, J. & SUITS, F. 2008. A noise model for mass spectrometry based proteomics. Bioinformatics, 24, 1070-1077.

DUGAN, A. S., EASH, S. & ATWOOD, W. J. 2005. An N-linked glycoprotein with alpha-(2,3)-linked sialic acid is a receptor for BK virus. Journal of Virology, 79, 14442-14445.

DURAN, J. M., ANJARD, C., STEFAN, C., LOOMIS, W. F. & MALHOTRA, V. 2010. Unconventional secretion of Acb1 is mediated by autophagosomes. Journal of Cell Biology, 188, 527-536.

EASH, S. & ATWOOD, W. J. 2005. Involvement of cytoskeletal components in BK virus infectious entry. Journal of Virology, 79, 11734-11741.

EASH, S., QUERBES, W. & ATWOOD, W. J. 2004. Infection of Vero cells by BK virus is dependent on Caveolae. Journal of Virology, 78, 11583-11590.

EGLI, A., BINGGELI, S., BODAGHI, S., DUMOULIN, A., FUNK, G. A., KHANNA, N., LEUENBERGER, D., GOSERT, R. & HIRSCH, H. H. 2007. Cytomegalovirus and polyomavirus BK posttransplant. Nephrology Dialysis Transplantation, 22, 72-82.

EGLI, A., KOHLI, S., DICKENMANN, M. & HIRSCH, H. H. 2009. Inhibition of Polyomavirus BK-Specific T-Cell Responses by Immunosuppressive Drugs. Transplantation, 88, 1161-1168.

EHLERS, B. & MOENS, U. 2014. Genome analysis of non-human primate polyomaviruses. Infection Genetics and Evolution, 26, 283-294.

ELLIS, L. C., NORTON, E., DANG, X. & KORALNIK, I. J. 2013. Agnogene Deletion in a Novel Pathogenic JC Virus Isolate Impairs VP1 Expression and Virion Production. Plos One, 8.

ENDEWARD, V., CARTRON, J. P., RIPOCHE, P. & GROS, G. 2006. Red cell membrane CO2 permeability in normal human blood and in blood deficient in various blood groups, and effect of DIDS. Transfusion Clinique Et Biologique, 13, 123-127.

ENNIS, H. L. & LUBIN, M. 1964. Cycloheximide - Aspects of inhbition of protein synthesis in mammalian cells. Science, 146, 1474-&.

ERARD, V., STORER, B., COREY, L., NOLLKAMPER, J., HUANG, M. L., LIMAYE, A. & BOECKH, M. 2004. BK virus infection in hematopoietic stem cell transplant recipients: Frequency, risk factors, and association with postengraftment hemorrhagic cystitis. Clinical Infectious Diseases, 39, 1861-1865.

ERICKSON, K. D., BOUCHET-MARQUIS, C., HEISER, K., SZOMOLANYI-TSUDA, E., MISHRA, R., LAMOTHE, B., HOENGER, A. & GARCEA, R. L. 2012. Virion Assembly Factories in the Nucleus of Polyomavirus-Infected Cells. Plos Pathogens, 8.

EVANS, G. L., CALLER, L. G., FOSTER, V. & CRUMP, C. M. 2015. Anion homeostasis is important for non-lytic release of BK polyomavirus from infected cells. Open Biology, 5.

FANG, C. Y., CHEN, H. Y., WANG, M. L., CHEN, P. L., CHANG, C. F., CHEN, L. S., SHEN, C. H., OU, W. C., TSAI, M. D., HSU, P. H. & CHANG, D. C. 2010. Global analysis of modifications of the human BK virus structural proteins by LC-MS/MS. Virology, 402, 164-176.

FANG, S. Y., JENSEN, J. P., LUDWIG, R. L., VOUSDEN, K. H. & WEISSMAN, A. M. 2000. Mdm2 is a RING finger-dependent ubiquitin protein ligase for itself and p53. Journal of Biological Chemistry, 275, 8945-8951.

FARMAKI, T., PONNAMBALAM, S., PRESCOTT, A. R., CLAUSEN, H., TANG, B. L., HONG, W. J. & LUCOCQ, J. M. 1999. Forward and retrograde trafficking in mitotic animal cells - ER-Golgi transport arrest restricts protein export from the ER into COPII-coated structures. Journal of Cell Science, 112, 589-600.

FASSHAUER, D., SUTTON, R. B., BRUNGER, A. T. & JAHN, R. 1998. Conserved structural features of the synaptic fusion complex: SNARE proteins reclassified as Q- and R-SNAREs. Proceedings of the National Academy of Sciences of the United States of America, 95, 15781-15786.

FENG, H. C., SHUDA, M., CHANG, Y. & MOORE, P. S. 2008. Clonal integration of a polyomavirus in human Merkel cell carcinoma. Science, 319, 1096-1100.

FENG, Z. D., HENSLEY, L., MCKNIGHT, K. L., HU, F. Y., MADDEN, V., PING, L. F., JEONG, S. H., WALKER, C., LANFORD, R. E. & LEMON, S. M. 2013. A pathogenic picornavirus acquires an envelope by hijacking cellular membranes. Nature, 496, 367-+.

FORERO, A., GIACOBBI, N. S., MCCORMICK, K. D., GJOERUP, O. V., BAKKENIST, C. J., PIPAS, J. M. & SARKAR, S. N. 2014. Simian Virus 40 Large T Antigen Induces IFN-Stimulated Genes through ATR Kinase. Journal of Immunology, 192, 5933-5942.

FORTHAL, D. N. 2014. Functions of Antibodies. Microbiology spectrum, 2, AID-0019-2014.

GALE, M. & FOY, E. M. 2005. Evasion of intracellular host defence by hepatitis C virus. Nature, 436, 939-945.

GARDNER, S. D., FIELD, A. M., COLEMAN, D. V. & HULME, B. 1971. New human papovavirus (BK) isolated from urine after renal transplantation. Lancet, 1, 1253-&.

GAYNOR, A. M., NISSEN, M. D., WHILEY, D. M., MACKAY, I. M., LAMBERT, S. B., WU, G., BRENNAN, D. C., STORCH, G. A., SLOOTS, T. P. & WANG, D. 2007. Identification of a novel polyomavirus from patients with acute respiratory tract infections. Plos Pathogens, 3, 595-604.

GEE, H. Y., NOH, S. H., TANG, B. L., KIM, K. H. & LEE, M. G. 2011. Rescue of Delta F508-CFTR Trafficking via a GRASP-Dependent Unconventional Secretion Pathway. Cell, 146, 746-760.

GERITS, N., JOHANNESSEN, M., TUMMLER, C., WALQUIST, M., KOSTENKO, S., SNAPKOV, I., VAN LOON, B., FERRARI, E., HUBSCHER, U. & MOENS, U. 2015. Agnoprotein of polyomavirus BK interacts with proliferating cell nuclear antigen and inhibits DNA replication. Virology Journal, 12.

GHEIT, T., DUTTA, S., OLIVER, J., ROBITAILLE, A., HAMPRAS, S., COMBES, J. D., MCKAY-CHOPIN, S., LE CALVEZ-KELM, F., FENSKE, N., CHERPELIS, B., GIULIANO, A. R., FRANCESCHI, S., MCKAY, J., ROLLISON, D. E. & TOMMASINO, M. 2017. Isolation and characterization of a novel putative human polyomavirus. Virology, 506, 45-54.

GHEUENS, S., WUTHRICH, C. & KORALNIK, I. J. 2013. Progressive Multifocal Leukoencephalopathy: Why Gray and White Matter. Annual Review of Pathology: Mechanisms of Disease, Vol 8, 8, 189-215.

GILMORE, J. M., SARDIU, M. E., GROPPE, B. D., THORNTON, J. L., LIU, X. Y., DAYEBGADOH, G., BANKS, C. A., SLAUGHTER, B. D., UNRUH, J. R., WORKMAN, J. L., FLORENS, L. & WASHBURN, M. P. 2016. WDR76 Co-Localizes with Heterochromatin Related Proteins and Rapidly Responds to DNA Damage. Plos One, 11.

GOSERT, R., RINALDO, C. H., FUNK, G. A., EGLI, A., RAMOS, E., DRACHENBERG, C. B. & HIRSCH, H. H. 2008. Polyomavirus BK with rearranged noncoding control region emerge in vivo in renal transplant patients and increase viral replication and cytopathology. Journal of Experimental Medicine, 205, 841-852.

GRIFFITHS, D. A., ABDUL-SADA, H., KNIGHT, L. M., JACKSON, B. R., RICHARDS, K., PRESCOTT, E. L., PEACH, A. H. S., BLAIR, G. E., MACDONALD, A. & WHITEHOUSE, A. 2013. Merkel Cell Polyomavirus Small T Antigen Targets the NEMO Adaptor Protein To Disrupt Inflammatory Signaling. Journal of Virology, 87, 13853-13867.

GRINDE, B., GAYORFAR, M. & RINALDO, C. H. 2007. Impact of a polyomavirus (BKV) infection on mRNA expression in human endothelial cells. Virus Research, 123, 86-94.

GROSS, L. 1953. Biological properties of the mouse leukaemia agent. Cancer, 6, 153-158.

GUARDAVACCARO, D. & PAGANO, M. 2006. Stabilizers and destabilizers controlling cell cycle oscillators. Molecular Cell, 22, 1-4.

GUAY, H. M., ANDREYEVA, T. A., GARCEA, R. L., WELSH, R. M. & SZOMOLANYI-TSUDA, E. 2007. MyD88 is required for the formation of long-term humoral immunity to virus infection. Journal of Immunology, 178, 5124-5131.

GUNTHER, W., PIWON, N. & JENTSCH, T. J. 2003. The ClC-5 chloride channel knock-out mouse - an animal model for Dent's disease. Pflugers Archiv-European Journal of Physiology, 445, 456-462.

HAAS, W., FAHERTY, B. K., GERBER, S. A., ELIAS, J. E., BEAUSOLEIL, S. A., BAKALARSKI, C. E., LI, X., VILLEN, J. & GYGI, S. P. 2006. Optimization and use of peptide mass measurement accuracy in shotgun proteomics. Molecular & Cellular Proteomics, 5, 1326-1337.

HAGTING, A., JACKMAN, M., SIMPSON, K. & PINES, J. 1999. Translocation of cyclin B1 to the nucleus at prophase requires a phosphorylation-dependent nuclear import signal. Current Biology, 9, 680-689.

HANAHAN, D. & WEINBERG, R. A. 2000. The hallmarks of cancer. Cell, 100, 57-70.

HARA-CHIKUMA, M., YANG, B. X., SONAWANE, N. D., SASAKI, S., UCHIDA, S. & VERKMAN, A. S. 2005. ClC-3 chloride channels facilitate endosomal acidification and chloride accumulation. Journal of Biological Chemistry, 280, 1241-1247.

HARRIS, K. F., CHRISTENSEN, J. B. & IMPERIALE, M. J. 1996. BK virus large T antigen: Interactions with the retinoblastoma family of tumor suppressor proteins and on cellular growth control. Journal of Virology, 70, 2378-2386.

HARRIS, K. F., CHRISTENSEN, J. B., RADANY, E. H. & IMPERIALE, M. J. 1998. Novel mechanisms of E2F induction by BK virus large-T antigen: Requirement of both the pRb-binding and the J domains. Molecular and Cellular Biology, 18, 1746-1756.

HE, J., YU, L., WANG, C. M. & ZHOU, X. F. 2018. MiR-1275 promotes non-small cell lung cancer cell proliferation and metastasis by regulating LZTS3 expression. European Review for Medical and Pharmacological Sciences, 22, 2680-2687.

HEDQUIST, B. G., BRATT, G., HAMMARIN, A. L., GRANDIEN, M., NENNESMO, I., SUNDELIN, B. & SEREGARD, S. 1999. Identification of BK virus in a patient with Acquired Immune Deficiency Syndrome and bilateral atypical retinitis. Ophthalmology, 106, 129-132.

HELLE, F., BROCHOT, E., HANDALA, L., MARTIN, E., CASTELAIN, S., FRANCOIS, C. & DUVERLIE, G. 2017. Biology of the BKPyV: An Update. Viruses-Basel, 9.

HELLEVIK, T., MARTINEZ, I., OLSEN, R., TOH, B. H., WEBSTER, P. & SMEDSROD, B. 1998. Transport of residual endocytosed products into terminal lysosomes occurs slowly in rat liver endothelial cells. Hepatology, 28**,** 1378-1389.

HERZNER, A. M., HAGMANN, C. A., GOLDECK, M., WOLTER, S., KUBLER, K., WITTMANN, S., GRAMBERG, T., ANDREEVA, L., HOPFNER, K. P., MERTENS, C., ZILLINGER, T., JIN, T., XIAO, T. S., BARTOK, E., COCH, C., ACKERMANN, D., HORNUNG, V., LUDWIG, J., BARCHET, W., HARTMANN, G. & SCHLEE, M. 2015. Sequence-specific activation of the DNA sensor cGAS by Y-form DNA structures as found in primary HIV-1 cDNA. Nature Immunology, 16**,** 1025-+.

HESBACHER, S., PFITZER, L., WIEDORFER, K., ANGERMEYER, S., BORST, A., HAFERKAMP, S., SCHOLZ, C. J., WOBSER, M., SCHRAMA, D. & HOUBEN, R. 2016. RB1 is the crucial target of the Merkel cell polyomavirus Large T antigen in Merkel cell carcinoma cells. Oncotarget, 7**,** 32956-32968.

HETZER, M. W. 2010. The Nuclear Envelope. Cold Spring Harbor Perspectives in Biology, 2.

HINGORANI, S. 2016. Renal Complications of Hematopoietic-Cell Transplantation. New England Journal of Medicine, 374**,** 2256-2267.

HIRSCH, H. H., BRENNAN, D. C., DRACHENBERG, C. B., GINEVRI, F., GORDON, J., LIMAYE, A. P., MIHATSCH, M. J., NICKELEIT, V., RAMOS, E., RANDHAWA, P., SHAPIRO, R., STEIGER, J., SUTHANTHIRAN, M. & TROFE, J. 2005. Polyomavirus-associated nephropathy in renal transplantation: Interdisciplinary analyses and recommendations. Transplantation, 79**,** 1277-1286.

HIRSCH, H. H. & STEIGER, J. 2003. Polyomavirus BK. Lancet Infectious Diseases, 3**,** 611-623.

HOLCAKOVA, J., MULLER, P., TOMASEC, P., HRSTKA, R., NEKULOVA, M., KRYSTOF, V., STRNAD, M., WILKINSON, G. W. G. & VOJTESEK, B. 2014. Inhibition of Post-Transcriptional RNA Processing by CDK Inhibitors and Its Implication in Anti-Viral Therapy. Plos One, 9.

HOUBEN, R., SHUDA, M., WEINKAM, R., SCHRAMA, D., FENG, H. C., CHANG, Y. A., MOORE, P. S. & BECKER, J. C. 2010. Merkel Cell Polyomavirus-Infected Merkel Cell Carcinoma Cells Require Expression of Viral T Antigens. Journal of Virology, 84**,** 7064-7072.

HUANG, Y. Q. & CARMICHAEL, G. G. 1996. A suboptimal 5' splice site is a cis-acting determinant of nuclear export of polyomavirus late mRNAs. Molecular and Cellular Biology, 16**,** 6046-6054.

HURDISS, D. L., MORGAN, E. L., THOMPSON, R. F., PRESCOTT, E. L., PANOU, M. M., MACDONALD, A. & RANSON, N. A. 2016. New Structural Insights into the Genome and Minor Capsid Proteins of BK Polyomavirus using Cryo-Electron Microscopy. Structure, 24**,** 528-536.

JACKSON, W. T., GIDDINGS, T. H., TAYLOR, M. P., MULINYAWE, S., RABINOVITCH, M., KOPITO, R. R. & KIRKEGAARD, K. 2005. Subversion of cellular autophagosomal machinery by RNA viruses. Plos Biology, 3**,** 861-871.

JENTSCH, T. J. & PUSCH, M. 2018. ClC chloride channels and transporters: Structure, function, physiology, and disease. Physiological Reviews, 98**,** 1493-1590.

JIANG, M. X., ABEND, J. R., JOHNSON, S. F. & IMPERIALE, M. J. 2009a. The role of polyomaviruses in human disease. Virology, 384**,** 266-273.

JIANG, M. X., ABEND, J. R., TSAI, B. & IMPERIALE, M. J. 2009b. Early Events during BK Virus Entry and Disassembly. Journal of Virology, 83**,** 1350-1358.

JIANG, M. X., ZHAO, L. B., GAMEZ, M. & IMPERIALE, M. J. 2012. Roles of ATM and ATR-Mediated DNA Damage Responses during Lytic BK Polyomavirus Infection. Plos Pathogens, 8.

JOHANNESSEN, M., WALQUIST, M., GERITS, N., DRAGSET, M., SPANG, A. & MOENS, U. 2011. BKV Agnoprotein Interacts with alpha-Soluble N-Ethylmaleimide-Sensitive Fusion Attachment Protein, and Negatively Influences Transport of VSVG-EGFP. Plos One, 6.

JOHNE, R., BUCK, C. B., ALLANDER, T., ATWOOD, W. J., GARCEA, R. L., IMPERIALE, M. J., MAJOR, E. O., RAMQVIST, T. & NORKIN, L. C. 2011. Taxonomical developments in the family Polyomaviridae. Archives of Virology, 156**,** 1627-1634.

JOHNSEN, J. I., SETERNES, O. M., JOHANSEN, T., MOENS, U., MANTYJARVI, R. & TRAAVIK, T. 1995. Subpopulations of noncoding control regionvariants within a cell culture-passaged stock of BK

virus - sequence comparisions and biological characteristics. Journal of General Virology, 76, 1571-1581.

JOHNSTON, O., JASWAL, D., GILL, J. S., DOUCETTE, S., FERGUSSON, D. A. & KNOLL, G. A. 2010. Treatment of Polyomavirus Infection in Kidney Transplant Recipients: A Systematic Review. Transplantation, 89, 1057-1070.

JUNG, J., KIM, J., ROH, S. H., JUN, I., SAMPSON, R. D., GEE, H. Y., CHOI, J. Y. & LEE, M. G. 2016. The HSP70 co-chaperone DNAJC14 targets misfolded pendrin for unconventional protein secretion. Nature Communications, 7.

JUSTICE, J. L., VERHALEN, B., KUMAR, R., LEFKOWITZ, E. J., IMPERIALE, M. J. & JIANG, M. X. 2015. Quantitative Proteomic Analysis of Enriched Nuclear Fractions from BK Polyomavirus-Infected Primary Renal Proximal Tubule Epithelial Cells. Journal of Proteome Research, 14, 4413-4424.

KAECH, S. M. & WHERRY, E. J. 2007. Heterogeneity and cell-fate decisions in effector and memory CD8(+) T cell differentiation during viral infection. Immunity, 27, 393-405.

KASPER, D., PLANELLS-CASES, R., FUHRMANN, J. C., SCHEEL, O., ZEITZ, O., RUETHER, K., SCHMITT, A., POET, M., STEINFELD, R., SCHWEIZER, M., KORNAK, U. & JENTSCH, T. J. 2005. Loss of the chloride channel ClC-7 leads to lysosomal storage disease and neurodegeneration. Embo Journal, 24, 1079-1091.

KASTAN, M. B., ONYEKWERE, O., SIDRANSKY, D., VOGELSTEIN, B. & CRAIG, R. W. 1991. Participation of p53 protein in the cellular-response to DNA damage. Cancer Research, 51, 6304-6311.

KATO, H., TAKEUCHI, O., SATO, S., YONEYAMA, M., YAMAMOTO, M., MATSUI, K., UEMATSU, S., JUNG, A., KAWAI, T., ISHII, K. J., YAMAGUCHI, O., OTSU, K., TSUJIMURA, T., KOH, C. S., SOUSA, C. R. E., MATSUURA, Y., FUJITA, T. & AKIRA, S. 2006. Differential roles of MDA5 and RIG-I helicases in the recognition of RNA viruses. Nature, 441, 101-105.

KEAN, J. M., RAO, S., WANG, M. & GARCEA, R. L. 2009. Seroepidemiology of Human Polyomaviruses. Plos Pathogens, 5.

KELLER, E. X., DELBUE, S., TOGNON, M. & PROVENZANO, M. 2015. Polyomavirus BK and prostate cancer: a complex interaction of potential clinical relevance. Reviews in Medical Virology, 25, 366-378.

KEMBALL, C. C., LEE, E. D. H., SZOMOLANYI-TSUDA, E., PEARSON, T. C., LARSEN, C. P. & LUKACHER, A. E. 2005. Costimulation requirements for polyomavirus-specific CD8+T cells differ between acute and persistent phases of infection. Journal of Neurovirology, 14, 45-45.

KIM, W., BENNETT, E. J., HUTTLIN, E. L., GUO, A., LI, J., POSSEMATO, A., SOWA, M. E., RAD, R., RUSH, J., COMB, M. J., HARPER, J. W. & GYGI, S. P. 2011. Systematic and Quantitative Assessment of the Ubiquitin-Modified Proteome. Molecular Cell, 44, 325-340.

KOJIMA, K., SHIMANUKI, M., SHIKAMI, M., ANDREEFF, M. & NAKAKUMA, H. 2009. Cyclin-dependent kinase 1 inhibitor RO-3306 enhances p53-mediated Bax activation and mitochondrial apoptosis in AML. Cancer Science, 100, 1128-1136.

KONDO, T., KOBAYASHI, J., SAITOH, T., MARUYAMA, K., ISHII, K. J., BARBER, G. N., KOMATSU, K., AKIRA, S. & KAWAI, T. 2013. DNA damage sensor MRE11 recognizes cytosolic double-stranded DNA and induces type I interferon by regulating STING trafficking. Proceedings of the National Academy of Sciences of the United States of America, 110, 2969-2974.

KORUP, S., RIETSCHER, J., CALVIGNAC-SPENCER, S., TRUSCH, F., HOFMANN, J., MOENS, U., SAUER, I., VOIGT, S., SCHMUCK, R. & EHLERS, B. 2013. Identification of a Novel Human Polyomavirus in Organs of the Gastrointestinal Tract. Plos One, 8.

KOSTOVA, Z. & WOLF, D. H. 2003. For whom the bell tolls: protein quality control of the endoplasmic reticulum and the ubiquitin-proteasome connection. Embo Journal, 22, 2309-2317.

KOWAL, J., TKACH, M. & THERY, C. 2014. Biogenesis and secretion of exosomes. Current Opinion in Cell Biology, 29, 116-125.

LEE, E. D. H., KEMBALL, C. C., WANG, J., DONG, Y., STAPLER, D. C., HAMBY, K. M., GANGAPPA, S., NEWELL, K. A., PEARSON, T. C., LUKACHER, A. E. & LARSEN, C. P. 2006. A mouse model for

polyomavirus-associated nephropathy of kidney transplants. American Journal of Transplantation, 6, 913-922.

LI, H. Y., BHATTACHARYYA, S. & PRIVES, C. 1997. Cyclin-dependent kinase regulation of the replication functions of polyomavirus large T antigen. Journal of Virology, 71, 6479-6485.

LI, R. M., SHARMA, B. N., LINDER, S., GUTTEBERG, T. J., HIRSCH, H. H. & RINALDO, C. H. 2013a. Characteristics of polyomavirus BK (BKPyV) infection in primary human urothelial cells. Virology, 440, 41-50.

LI, T., CHEN, J. & CRISTEA, I. M. 2013b. Human Cytomegalovirus Tegument Protein pUL83 Inhibits IFI16-Mediated DNA Sensing for Immune Evasion. Cell Host & Microbe, 14, 591-599.

LI, X. D., SUN, L. J., SETH, R. B., PINEDA, G. & CHEN, Z. J. J. 2005. Hepatitis C virus protease NS3/4A cleaves mitochondrial antiviral signaling protein off the mitochondria to evade innate immunity. Proceedings of the National Academy of Sciences of the United States of America, 102, 17717-17722.

LIDDINGTON, R. C., YAN, Y., MOULAI, J., SAHLI, R., BENJAMIN, T. L. & HARRISON, S. C. 1991. Structure of Simian Virus-40 at 3.8-A resolution. Nature, 354, 278-284.

LILYESTROM, W., KLEIN, M. G., ZHANG, R. G., JOACHIMIAK, A. & CHEN, X. J. S. 2006. Crystal structure of SV40 large T-antigen bound to p53: interplay between a viral oncoprotein and a cellular tumor suppressor. Genes & Development, 20, 2373-2382.

LIM, E. S., REYES, A., ANTONIO, M., SAHA, D., IKUMAPAYI, U. N., ADEYEMI, M., STINE, O. C., SKELTON, R., BRENNAN, D. C., MKAKOSYA, R. S., MANARY, M. J., GORDON, J. I. & WANG, D. 2013. Discovery of STL polyomavirus, a polyomavirus of ancestral recombinant origin that encodes a unique T antigen by alternative splicing. Virology, 436, 295-303.

LIN, R. T., HEYLBROECK, C., PITHA, P. M. & HISCOTT, J. 1998. Virus-dependent phosphorylation of the IRF-3 transcription factor regulates nuclear translocation, transactivation potential, and proteasome-mediated degradation. Molecular and Cellular Biology, 18, 2986-2996.

LIN, W., HATA, T. & KASAMATSU, H. 1984. Subcellular-distribution of viral structural proteins during Simian Virus-40 infection. Journal of Virology, 50, 363-371.

LIU, S. Q., CAI, X., WU, J. X., CONG, Q., CHEN, X., LI, T., DU, F. H., REN, J. Y., WU, Y. T., GRISHIN, N. V. & CHEN, Z. J. J. 2015. Phosphorylation of innate immune adaptor proteins MAVS, STING, and TRIF induces IRF3 activation. Science, 347, 1217-U17.

LLOYD, R. E. & BOVEE, M. 1993. Persistent infection of human erythroblastoid cells by poliovirus. Virology, 194, 200-209.

LODISH, H., BALTIMORE, D., BERK, A., ZIPURSKY, S. L., MATSUDAIRA, P. & DARNELL, J. 1995. Molecular cell biology; Third edition. Molecular cell biology, Third edition, l+1344p-l+1344p.

LODISH, H. F., KONG, N., SNIDER, M. & STROUS, G. 1983. Hepatoma secretory proteins migrate from rough endoplasmic-reticulum to Golgi at characteristic rates. Nature, 304, 80-83.

LOW, J., HUMES, H. D., SZCZYPKA, M. & IMPERIALE, M. 2004. BKV and SV40 infection of human kidney tubular epithelial cells in vitro. Virology, 323, 182-188.

LOW, J. A., MAGNUSON, B., TSAI, B. & IMPERIALE, M. J. 2006. Identification of gangliosides GD1b and GT1b as receptors for BK virus. Journal of Virology, 80, 1361-1366.

LOWE, D. B., SHEARER, M. H., JUMPER, C. A. & KENNEDY, R. C. 2007. SV40 association with human malignancies and mechanisms of tumor immunity by large tumor antigen. Cellular and Molecular Life Sciences, 64, 803-814.

LOWE, M., RABOUILLE, C., NAKAMURA, N., WATSON, R., JACKMAN, M., JAMSA, E., RAHMAN, D., PAPPIN, D. J. C. & WARREN, G. 1998. Cdc2 kinase directly phosphorylates the cis-Golgi matrix protein GM130 and is required for Golgi fragmentation in mitosis. Cell, 94, 783-793.

MA, H. T. & POON, R. Y. C. 2011. Synchronization of HeLa Cells. Cell Cycle Synchronization: Methods and Protocols, 761, 151-161.

MA, Z., JACOBS, S. R., WEST, J. A., STOPFORD, C., ZHANG, Z., DAVIS, Z., BARBER, G. N., GLAUNSINGER, B. A., DITTMER, D. P. & DAMANIA, B. 2015. Modulation of the cGAS-STING DNA sensing

pathway by gammaherpesviruses. Proceedings of the National Academy of Sciences of the United States of America, 112, E4306-E4315.

MAEDA, Y., IDE, T., KOIKE, M., UCHIYAMA, Y. & KINOSHITA, T. 2008. GPHR is a novel anion channel critical for acidification and functions of the Golgi apparatus. Nature Cell Biology, 10, 1135-1145.

MAJOR, E. O. & DIMAYORC.G 1973. Malignant transformation of BHK21 clone 13 cells by BK virus - Human papovavirus. Proceedings of the National Academy of Sciences of the United States of America, 70, 3210-3212.

MARQ, J. B., HAUSMANN, S., VEILLARD, N., KOLAKOFSKY, D. & GARCIN, D. 2011. Short Double-stranded RNAs with an Overhanging 5 ' ppp-Nucleotide, as Found in Arenavirus Genomes, Act as RIG-I Decoys. Journal of Biological Chemistry, 286, 6108-6116.

MAYER, M. P. 2005. Recruitment of Hsp70 chaperones: a crucial part of viral survival strategies. Reviews of Physiology Biochemistry and Pharmacology, 153, 1-46.

MCALISTER, G. C., HUTTLIN, E. L., HAAS, W., TING, L., JEDRYCHOWSKI, M. P., ROGERS, J. C., KUHN, K., PIKE, I., GROTHE, R. A., BLETHROW, J. D. & GYGI, S. P. 2012. Increasing the Multiplexing Capacity of TMTs Using Reporter Ion Isotopologues with Isobaric Masses. Analytical Chemistry, 84, 7469-7478.

MCALISTER, G. C., NUSINOW, D. P., JEDRYCHOWSKI, M. P., WUEHR, M., HUTTLIN, E. L., ERICKSON, B. K., RAD, R., HAAS, W. & GYGI, S. P. 2014. MultiNotch MS3 Enables Accurate, Sensitive, and Multiplexed Detection of Differential Expression across Cancer Cell Line Proteomes. Analytical Chemistry, 86, 7150-7158.

MCVEY, D., BRIZUELA, L., MOHR, I., MARSHAK, D. R., GLUZMAN, Y. & BEACH, D. 1989. Phosphorylation of large tumor-antigen by CDC2 stimulates SV40 DNA-replication. Nature, 341, 503-507.

MCVEY, D., WOELKER, B. & TEGTMEYER, P. 1996. Mechanisms of simian virus 40 T-antigen activation by phosphorylation of threonine 124. Journal of Virology, 70, 3887-3893.

MILNER, J. & COOK, A. 1986. The localisation of p53, a transformed-related protein, is cell-cycle dependent in normal and in transformed cells. European Journal of Cell Biology, 40, 13-13.

MISHRA, N., PEREIRA, M., RHODES, R. H., AN, P., PIPAS, J. M., JAIN, K., KAPOOR, A., BRIESE, T., FAUST, P. L. & LIPKIN, W. I. 2014. Identification of a Novel Polyomavirus in a Pancreatic Transplant Recipient With Retinal Blindness and Vasculitic Myopathy. Journal of Infectious Diseases, 210, 1595-1599.

MOAREFI, I. F., SMALL, D., GILBERT, I., HOPFNER, M., RANDALL, S. K., SCHNEIDER, C., RUSSO, A. A. R., RAMSPERGER, U., ARTHUR, A. K., STAHL, H., KELLY, T. J. & FANNING, E. 1993. Mutation of the cyclin-dependent kinase phosphorylation site in Simian-Virus 40 (SV40) Large T-Antigen specifically blocks SV40 origin DNA unwinding. Journal of Virology, 67, 4992-5002.

MOENS, U., CALVIGNAC-SPENCER, S., LAUBER, C., RAMGVIST, T., FELTKAMP, M. C. W., DAUGHERTY, M. D., VERSCHOOR, E. J., EHLERS, B. & CONSORTIUM, I. R. 2017. ICTV Virus Taxonomy Profile: Polyomaviridae. Journal of General Virology, 98, 1159-1160.

MOENS, U., JOHANSEN, T., JOHNSEN, J. I., SETERNES, O. M. & TRAAVIK, T. 1995. Noncoding control region of naturally-occurrng BK virus variants - Sequence comparison and functional analysis. Virus Genes, 10, 261-275.

MOENS, U., SETERNES, O. M., JOHANSEN, B. & REKVIG, O. P. 1997. Mechanisms of transcriptional regulation of cellular genes by SV40 large T- and small T-antigens. Virus Genes, 15, 135-154.

MOENS, U., VAN GHELUE, M. & EHLERS, B. 2014. Are human polyomaviruses co-factors for cancers induced by other oncoviruses? Reviews in Medical Virology, 24, 343-360.

MOENS, U., VAN GHELUE, M. & JOHANNESSEN, M. 2007. Oncogenic potentials of the human polyomavirus regulatory proteins. Cellular and Molecular Life Sciences, 64, 1656-1678.

MOENS, U., VAN GHELUE, M., SONG, X. B. & EHLERS, B. 2013. Serological cross-reactivity between human polyomaviruses. Reviews in Medical Virology, 23, 250-264.

MORIYAMA, T., MARQUEZ, J. P., WAKATSUKI, T. & SOROKIN, A. 2007. Caveolar endocytosis is critical for BK virus infection of human renal proximal tubular epithelial cells. Journal of Virology, 81, 8552-8562.

MORIYAMA, T. & SOROKIN, A. 2008. Intracellular trafficking pathway of BK Virus in human renal proximal tubular epithelial cells. Virology, 371, 336-349.

MUELLER, K., SCHACHTNER, T., NOVOTNA, E., HINRICHS, C., NICKEL, P., REINKE, P. & BABEL, N. 2010. BKV-Specific Polyfunctional and Single IFN gamma-Producing T Cells Might Determine the Clinical Course of BKV Infection in Renal Transplant Patients. American Journal of Transplantation, 10, 450-450.

MUNRO, S. 2011. Q&A: What is the Golgi apparatus, and why are we asking? Bmc Biology, 9.

MUTSAFI, Y. & ALTAN-BONNET, N. 2018. Enterovirus Transmission by Secretory Autophagy. Viruses-Basel, 10.

NEU, U., ALLEN, S. A. A., BLAUM, B. S., LIU, Y., FRANK, M., PALMA, A. S., STROH, L. J., FEIZI, T., PETERS, T., ATWOOD, W. J. & STEHLE, T. 2013. A Structure-Guided Mutation in the Major Capsid Protein Retargets BK Polyomavirus. Plos Pathogens, 9.

NG, K. W., LEONG, D. T. W. & HUTMACHER, D. W. 2005. The challenge to measure cell proliferation in two and three dimensions. Tissue Engineering, 11, 182-191.

NGUYEN, K. D., LEE, E. E., YUE, Y. B., STORK, J., POCK, L., NORTH, J. P., VANDERGRIFF, T., COCKERELL, C., HOSLER, G. A., PASTRANA, D. V., BUCK, C. B. & WANG, R. C. 2017. Human polyomavirus 6 and 7 are associated with pruritic and dyskeratotic dermatoses. Journal of the American Academy of Dermatology, 76, 932-+.

NICKEL, W. & RABOUILLE, C. 2009. Mechanisms of regulated unconventional protein secretion. Nature Reviews Molecular Cell Biology, 10, 148-155.

NITTA, S., SAKAMOTO, N., NAKAGAWA, M., KAKINUMA, S., MISHIMA, K., KUSANO-KITAZUME, A., KIYOHASHI, K., MURAKAWA, M., NISHIMURA-SAKURAI, Y., AZUMA, S., TASAKA-FUJITA, M., ASAHINA, Y., YONEYAMA, M., FUJITA, T. & WATANABE, M. 2013. Hepatitis C virus NS4B protein targets STING and abrogates RIG-I-mediated type I interferon-dependent innate immunity. Hepatology, 57, 46-58.

NOWAG, H., GUHL, B., THRIENE, K., ROMAO, S., ZIEGLER, U., DENGJEL, J. & MUNZ, C. 2014. Macroautophagy Proteins Assist Epstein Barr Virus Production and Get Incorporated Into the Virus Particles. Ebiomedicine, 1, 116-125.

NURSE, P., THURIAUX, P. & NASMYTH, K. 1976. Genetic control of cell-division cycle in fission yeast schizosaccharomyces-pombe. Molecular & General Genetics, 146, 167-178.

OGATA, M., HINO, S. I., SAITO, A., MORIKAWA, K., KONDO, S., KANEMOTO, S., MURAKAMI, T., TANIGUCHI, M., TANII, I., YOSHINAGA, K., SHIOSAKA, S., HAMMARBACK, J. A., URANO, F. & IMAIZUMI, K. 2006. Autophagy is activated for cell survival after endoplasmic reticulum stress. Molecular and Cellular Biology, 26, 9220-9231.

ORBA, Y., SUNDEN, Y., SUZUKI, T., NAGASHIMA, K., KIMURA, T., TANAKA, S. & SAWA, H. 2008. Pharmacological cdk inhibitor R-Roscovitine suppresses JC virus proliferation. Virology, 370, 173-183.

ORBA, Y., SUZUKI, T., MAKINO, Y., KUBOTA, K., TANAKA, S., KIMURA, T. & SAWA, H. 2010. Large T Antigen Promotes JC Virus Replication in G(2)-arrested Cells by Inducing ATM- and ATR-mediated G(2) Checkpoint Signaling. Journal of Biological Chemistry, 285, 1544-1554.

ORZALLI, M. H., DELUCA, N. A. & KNIPE, D. M. 2012. Nuclear IFI16 induction of IRF-3 signaling during herpesviral infection and degradation of IFI16 by the viral ICP0 protein. Proceedings of the National Academy of Sciences of the United States of America, 109, E3008-E3017.

PADGETT, B. L., WALKER, D. L., ZURHEIN, G. M., ECKROADE, R. J. & DESSEL, B. H. 1971. Cultivation of a papova-like virus from human brain with progressive multifocal leukoenchephalopathy. Lancet, 1, 1257-&.

PALLAS, D. C., SHAHRIK, L. K., MARTIN, B. L., JASPERS, S., MILLER, T. B., BRAUTIGAN, D. L. & ROBERTS, T. M. 1990. Polyoma small and middle T-antigens and SV40 small T-antigen from stable complexes with protein phosphatase-2A. Cell, 60**,** 167-176.

PANOU, M.-M., PRESCOTT, E. L., HURDISS, D. L., SWINSCOE, G., HOLLINSHEAD, M., CALLER, L. G., MORGAN, E. L., CARLISLE, L., MUELLER, M., ANTONI, M., KEALY, D., RANSON, N. A., CRUMP, C. M. & MACDONALD, A. 2018. Agnoprotein Is an Essential Egress Factor during BK Polyomavirus Infection. International Journal of Molecular Sciences, 19.

PASTRANA, D. V., RAY, U., MAGALDI, T. G., SCHOWALTER, R. M., CUBURU, N. & BUCK, C. B. 2013. BK Polyomavirus Genotypes Represent Distinct Serotypes with Distinct Entry Tropism. Journal of Virology, 87**,** 10105-10113.

PELHAM, H. R. B. 1990. THE RETENTION SIGNAL FOR SOLUBLE-PROTEINS OF THE ENDOPLASMIC-RETICULUM. Trends in Biochemical Sciences, 15**,** 483-486.

PINDEL, A. & SADLER, A. 2011. The Role of Protein Kinase R in the Interferon Response. Journal of Interferon and Cytokine Research, 31**,** 59-70.

PINES, J. & HUNTER, T. 1991. Human cyclin-A and cyclin-B1 are differentially located in the cell and undergo cell-cycle dependent nuclear transport. Journal of Cell Biology, 115**,** 1-17.

POET, M., KORNAK, U., SCHWEIZER, M., ZDEBIK, A. A., SCHEEL, O., HOELTER, S., WURST, W., SCHMITT, A., FUHRMANN, J. C., PLANELLS-CASES, R., MOLE, S. E., HUBNER, C. A. & JENTSCH, T. J. 2006. Lysosomal storage disease upon disruption of the neuronal chloride transport protein CIC-6. Proceedings of the National Academy of Sciences of the United States of America, 103**,** 13854-13859.

PREISINGER, C., KORNER, R., WIND, M., LEHMANN, W. D., KOPAJTICH, R. & BARR, F. A. 2005. Plk1 docking to GRASP65 phosphorylated by Cdk1 suggests a mechanism for Golgi checkpoint signalling. Embo Journal, 24**,** 753-765.

PRELICH, G., KOSTURA, M., MARSHAK, D. R., MATHEWS, M. B. & STILLMAN, B. 1987. The cell-cycle regulated proliferating cell nuclear antigen is required for SV40-DNA replication invitro. Nature, 326**,** 471-475.

QU, Y., FRANCHI, L., NUNEZ, G. & DUBYAK, G. R. 2007. Nonclassical IL-1 beta secretion stimulated by P2X7 receptors is dependent on inflammasome activation and correlated with exosome release in murine macrophages. Journal of Immunology, 179**,** 1913-1925.

RABOUILLE, C. 2017. Pathways of Unconventional Protein Secretion. Trends in Cell Biology, 27**,** 230-240.

RABOUILLE, C., MALHOTRA, V. & NICKEL, W. 2012. Diversity in unconventional protein secretion. Journal of Cell Science, 125**,** 5251-5255.

RAMAMOORTHY, S., DEVARAJ, B., MIYAI, K., LUO, L., LIU, Y. T., BOLAND, C. R., GOEL, A. & CARETHERS, J. M. 2011. John Cunningham Virus T-Antigen Expression in Anal Carcinoma. Cancer, 117**,** 2379-2385.

RAMIREZ, I. B. R. & LOWE, M. 2009. Golgins and GRASPs: Holding the Golgi together. Seminars in Cell & Developmental Biology, 20**,** 770-779.

RANDHAWA, P., VISCIDI, R., CARTER, J. J., GALLOWAY, D. A., CULP, T. D., HUANG, C., RAMASWAMI, B. & CHRISTENSEN, N. D. 2009. Identification of species-specific and cross-reactive epitopes in human polyomavirus capsids using monoclonal antibodies. Journal of General Virology, 90**,** 634-639.

REPLOEG, M. D., STORCH, G. A. & CLIFFORD, D. B. 2001. BK virus: A clinical review. Clinical Infectious Diseases, 33**,** 191-202.

RINALDO, C. H., TYLDEN, G. D. & SHARMA, B. N. 2013. The human polyomavirus BK (BKPyV): virological background and clinical implications. Apmis, 121**,** 728-745.

RINK, J., GHIGO, E., KALAIDZIDIS, Y. & ZERIAL, M. 2005. Rab conversion as a mechanism of progression from early to late endosomes. Cell, 122**,** 735-749.

RONCO, L. V., KARPOVA, A. Y., VIDAL, M. & HOWLEY, P. M. 1998. Human papillomavirus 16 E6 oncoprotein binds to interferon regulatory factor-3 and inhibits its transcriptional activity. Genes & Development, 12**,** 2061-2072.

RORSMAN, P. & BRAUN, M. 2013. Regulation of Insulin Secretion in Human Pancreatic Islets. Annual Review of Physiology, Vol 75, 75**,** 155-179.

ROTHMAN, J. E. & WARREN, G. 1994. Implications of the SNARE hypothesis for intracellular membrane topology and dynamics. Current Biology, 4**,** 220-233.

RUNDELL, K. & PARAKATI, R. 2001. The role of the SV40ST antigen in cell growth promotion and transformation. Seminars in Cancer Biology, 11**,** 5-13.

SANTIANA, M., GHOSH, S., HO, B. A., RAJASEKARAN, V., DU, W. L., MUTSAFI, Y., DE JESUS-DIAZ, D. A., SOSNOVTSEV, S. V., LEVENSON, E. A., PARRA, G. I., TAKVORIAN, P. M., CALI, A., BLECK, C., VLASOVA, A. N., SAIF, L. J., PATTON, J. T., LOPALCO, P., CORCELLI, A., GREEN, K. Y. & ALTAN-BONNET, N. 2018. Vesicle-Cloaked Virus Clusters Are Optimal Units for Inter-organismal Viral Transmission. Cell Host & Microbe, 24**,** 208-+.

SARIBAS, A. S., MUN, S., JOHNSON, J., EL-HAJMOUSSA, M., WHITE, M. K. & SAFAK, M. 2014. Human polyoma JC virus minor capsid proteins, VP2 and VP3, enhance large T antigen binding to the origin of viral DNA replication: Evidence for their involvement in regulation of the viral DNA replication. Virology, 449**,** 1-16.

SCHNEIDER, W. M., CHEVILLOTTE, M. D. & RICE, C. M. 2014. Interferon-Stimulated Genes: A Complex Web of Host Defenses. Annual Review of Immunology, Vol 32, 32**,** 513-545.

SCHOWALTER, R. M., REINHOLD, W. C. & BUCK, C. B. 2012. Entry Tropism of BK and Merkel Cell Polyomaviruses in Cell Culture. Plos One, 7.

SCHULZ, P., WERNER, J., STAUBER, T., HENRIKSEN, K. & FENDLER, K. 2010. The G215R Mutation in the Cl-/H+-Antiporter ClC-7 Found in ADO II Osteopetrosis Does Not Abolish Function but Causes a Severe Trafficking Defect. Plos One, 5.

SCUDA, N., HOFMANN, J., CALVIGNAC-SPENCER, S., RUPRECHT, K., LIMAN, P., KUEHN, J., HENGEL, H. & EHLERS, B. 2011. A Novel Human Polyomavirus Closely Related to the African Green Monkey-Derived Lymphotropic Polyomavirus. Journal of Virology, 85**,** 4586-4590.

SEAMONE, M. E., WANG, W. J., ACOTT, P., BECK, P. L., TIBBLES, L. A. & MURUVE, D. A. 2010. MAP kinase activation increases BK polyomavirus replication and facilitates viral propagation in vitro. Journal of Virological Methods, 170**,** 21-29.

SEGANTI, L., MASTROMARINO, P., SUPERTI, F., SINIBALDI, L. & ORSI, N. 1981. Receptors for BK virus on human erythrocytes. Acta Virologica, 25**,** 177-181.

SEGGEWISS, N., PAULMANN, D. & DOTZAUER, A. 2016. Lysosomes serve as a platform for hepatitis A virus particle maturation and nonlytic release. Archives of Virology, 161**,** 43-52.

SHAH, K. V., DANIEL, R. W. & WARSZAWS.RM 1973. High prevalence of antibodies to BK-virus, and SV40-related papovavirus, in residents of Maryland. Journal of Infectious Diseases, 128**,** 784-787.

SHAHZAD, N., SHUDA, M., GHEIT, T., KWUN, H. J., CORNET, I., SAIDJ, D., ZANNETTI, C., HASAN, U., CHANG, Y., MOORE, P. S., ACCARDI, R. & TOMMASINO, M. 2013. The T Antigen Locus of Merkel Cell Polyomavirus Downregulates Human Toll-Like Receptor 9 Expression. Journal of Virology, 87**,** 13009-13019.

SHENG, Q., DENIS, D., RATNOFSKY, M., ROBERTS, T. M., DECAPRIO, J. A. & SCHAFFHAUSEN, B. 1997. The DnaJ domain of polyomavirus large T antigen is required to regulate Rb family tumor suppressor function. Journal of Virology, 71**,** 9410-9416.

SHEPPARD, H. M., CORNEILLIE, S. I., ESPIRITU, C., GATTI, A. & LIU, X. A. 1999. New insights into the mechanism of inhibition of p53 by simian virus 40 large T antigen. Molecular and Cellular Biology, 19**,** 2746-2753.

SIEBRASSE, E. A., REYES, A., LIM, E. S., ZHAO, G. Y., MKAKOSYA, R. S., MANARY, M. J., GORDON, J. I. & WANG, D. 2012. Identification of MW Polyomavirus, a Novel Polyomavirus in Human Stool. Journal of Virology, 86**,** 10321-10326.

SINIBALDI, L., GOLDONI, P., PIETROPAOLO, V., LONGHI, C. & ORSI, N. 1990. Involvement of gangliosides in the interaction between BK virus and Vero cells. Archives of Virology, 113**,** 291-296.

SKOCZYLAS, C., FAHRBACH, K. M. & RUNDELL, K. 2004. Cellular targets of the SV40 small-t antigen in human cell transformation. Cell Cycle, 3**,** 606-610.

SKOTHEIM, J. M., DI TALIA, S., SIGGIA, E. D. & CROSS, F. R. 2008. Positive feedback of G1 cyclins ensures coherent cell cycle entry. Nature, 454**,** 291-U12.

SOLLNER, T., WHITEHART, S. W., BRUNNER, M., ERDJUMENTBROMAGE, H., GEROMANOS, S., TEMPST, P. & ROTHMAN, J. E. 1993. SNAP receptors implicated in vesicle targetting and fusion. Nature, 362**,** 318-324.

SOWD, G. A. & FANNING, E. 2012. A Wolf in Sheep's Clothing: SV40 Co-opts Host Genome Maintenance Proteins to Replicate Viral DNA. Plos Pathogens, 8.

SPANIELOVA, H., FRAIBERK, M., SUCHANOVA, J., SOUKUP, J. & FORSTOVA, J. 2014. The encapsidation of polyomavirus is not defined by a sequence-specific encapsidation signal. Virology, 450**,** 122-131.

SPENCE, S. L. & PIPAS, J. M. 1994a. Simian-virus 40 large-T-antigen host-range domain functions in virion assembly. Journal of Virology, 68**,** 4227-4240.

SPENCE, S. L. & PIPAS, J. M. 1994b. SV40 Lareg T-antigen functions at 2 distinct steps in virion assembly. Virology, 204**,** 200-209.

STAUBER, T. & JENTSCH, T. J. 2010. Sorting Motifs of the Endosomal/Lysosomal CLC Chloride Transporters. Journal of Biological Chemistry, 285**,** 34537-34548.

STERINGER, J. P., MULLER, H. M. & NICKEL, W. 2015. Unconventional Secretion of Fibroblast Growth Factor 2-A Novel Type of Protein Trans location across Membranes? Journal of Molecular Biology, 427**,** 1202-1210.

STRANG, B. L., BOULANT, S., CHANG, L., KNIPE, D. M., KIRCHHAUSEN, T. & COEN, D. M. 2012. Human Cytomegalovirus UL44 Concentrates at the Periphery of Replication Compartments, the Site of Viral DNA Synthesis. Journal of Virology, 86**,** 2089-2095.

STUBDAL, H., ZALVIDE, J., CAMPBELL, K. S., SCHWEITZER, C., ROBERTS, T. M. & DECAPRIO, J. A. 1997. Inactivation of pRB-related proteins p130 and p107 mediated by the J domain of simian virus 40 large T antigen. Molecular and Cellular Biology, 17**,** 4979-4990.

SUDHOF, T. C. & ROTHMAN, J. E. 2009. Membrane Fusion: Grappling with SNARE and SM Proteins. Science, 323**,** 474-477.

SULLIVAN, C. S., CANTALUPO, P. & PIPAS, J. M. 2000. The molecular chaperone activity of simian virus 40 large T antigen is required to disrupt Rb-E2F family complexes by an ATP-dependent mechanism. Molecular and Cellular Biology, 20**,** 6233-6243.

SUN, L. J., WU, J. X., DU, F. H., CHEN, X. & CHEN, Z. J. J. 2013. Cyclic GMP-AMP Synthase Is a Cytosolic DNA Sensor That Activates the Type I Interferon Pathway. Science, 339**,** 786-791.

SUZUKI, T., ORBA, Y., MAKINO, Y., OKADA, Y., SUNDEN, Y., HASEGAWA, H., HALL, W. W. & SAWA, H. 2013. Viroporin activity of the JC polyomavirus is regulated by interactions with the adaptor protein complex 3. Proceedings of the National Academy of Sciences of the United States of America, 110**,** 18668-18673.

SUZUKI, T., ORBA, Y., OKADA, Y., SUNDEN, Y., KIMURA, T., TANAKA, S., NAGASHIMA, K., HALL, W. W. & SAWA, H. 2010. The Human Polyoma JC Virus Agnoprotein Acts as a Viroporin. Plos Pathogens, 6.

SWEET, B. H. & HILLEMAN, M. R. 1960. THE VACUOLATING VIRUS, SV40. Proceedings of the Society for Experimental Biology and Medicine, 105**,** 420-427.

SWENSON, J. J. & FRISQUE, R. J. 1995. Biochemical-characterization domains of JC large-T-antigen phosphorylation domains. Virology, 212**,** 295-308.

SWENSON, J. J., TROWBRIDGE, P. W. & FRISQUE, R. J. 1996. Replication activity of JC virus large T antigen phosphorylation and zinc finger domain mutants. Journal of Neurovirology, 2**,** 78-86.

TAKAOKA, A., WANG, Z., CHOI, M. K., YANAI, H., NEGISHI, H., BAN, T., LU, Y., MIYAGISHI, M., KODAMA, T., HONDA, K., OHBA, Y. & TANIGUCHI, T. 2007. DAI (DLM-1/ZBP1) is a cytosolic DNA sensor and an activator of innate immune response. Nature, 448**,** 501-U14.

TAKEMOTO, K. K. & MARTIN, M. A. 1976. Transformation of hamster kidney cells by BK papovavirus DNA. Journal of Virology, 17**,** 247-253.

TAKEMURA, H., LI, Z. & OHSHIKA, H. 1992. Practical usage concentrations of monensin have nonspecific actions other than as a sodium ionophore at rat paratoid acinar-cells. Biochemical Pharmacology, 44**,** 1395-1400.

TAYLOR, M. P., BURGON, T. B., KIRKEGAARD, K. & JACKSON, W. T. 2009. Role of Microtubules in Extracellular Release of Poliovirus. Journal of Virology, 83**,** 6599-6609.

TEUNISSEN, E. A., DE RAAD, M. & MASTROBATTISTA, E. 2013. Production and biomedical applications of virus-like particles derived from polyomaviruses. Journal of Controlled Release, 172**,** 305-321.

THANH, T. D., THO, N. V., LAM, N. S., DUNG, N. H., TABATA, C. & NAKANO, Y. 2016. Simian virus 40 may be associated with developing malignant pleural mesothelioma. Oncology Letters, 11**,** 2051-2056.

TONNERRE, P., GERARD, N., GAVLOVSKY, P. J., MAZALREY, S., HOURMANT, M., CHENEAU, M. L., CESBRON-GAUTIER, A., RENAUDIN, K., BRESSOLLETTE-BODIN, C. & CHARREAU, B. 2016. MICA Mutant A5.1 Influences BK Polyomavirus Reactivation and Associated Nephropathy After Kidney Transplantation. Journal of Infectious Diseases, 214**,** 807-816.

TOPTAN, T., YOUSEM, S. A., HO, J., MATSUSHIMA, Y., STABILE, L. P., FERNANDEZ-FIGUERAS, M. T., BHARGAVA, R., RYO, A., MOORE, P. S. & CHANG, Y. 2016. Survey for human polyomaviruses in cancer. Jci Insight, 1.

TSENG, C. C. & LI, C. S. 2007. Inactivation of viruses on surfaces by ultraviolet germicidal irradiation. Journal of Occupational and Environmental Hygiene, 4**,** 400-405.

TUCKER, S. P., THORNTON, C. L., WIMMER, E. & COMPANS, R. W. 1993. Vectorial release of poliovirus from polarized human intestinal epithelial cells. Journal of Virology, 67**,** 4274-4282.

UNTERHOLZNER, L., KEATING, S. E., BARAN, M., HORAN, K. A., JENSEN, S. B., SHARMA, S., SIROIS, C. M., JIN, T. C., LATZ, E., XIAO, T. S., FITZGERALD, K. A., PALUDAN, S. R. & BOWIE, A. G. 2010. IFI16 is an innate immune sensor for intracellular DNA. Nature Immunology, 11**,** 997-U42.

UNTERSTAB, G., MANZETTI, J. & HIRSCH, H. H. 2013. The polyomavirus BK agnoprotein co-localizes with lipid droplets (vol 399, pg 322, 2010). Virology, 441**,** 197-199.

URBANO, P. R. P., OLIVEIRA, R. R., ROMANO, C. M., PANNUTI, C. S. & FINK, M. 2016. Occurrence, genotypic characterization, and patterns of shedding of human polyomavirus JCPyV and BKPyV in urine samples of healthy individuals in SAo Paulo, Brazil. Journal of Medical Virology, 88**,** 153-158.

VAN DER MEIJDEN, E., JANSSENS, R. W. A., LAUBER, C., BAVINCK, J. N. B., GORBALENYA, A. E. & FELTKAMP, M. C. W. 2010. Discovery of a New Human Polyomavirus Associated with Trichodysplasia Spinulosa in an Immunocompromized Patient. Plos Pathogens, 6.

VASSILEV, L. T., VU, B. T., GRAVES, B., CARVAJAL, D., PODLASKI, F., FILIPOVIC, Z., KONG, N., KAMMLOTT, U., LUKACS, C., KLEIN, C., FOTOUHI, N. & LIU, E. A. 2004. In vivo activation of the p53 pathway by small-molecule antagonists of MDM2. Science, 303**,** 844-848.

VEENENDAAL, T., JARVELA, T., GRIEVE, A. G., VAN ES, J. H., LINSTEDT, A. D. & RABOUILLE, C. 2014. GRASP65 controls the cis Golgi integrity in vivo. Biology Open, 3**,** 431-443.

VERHALEN, B., JUSTICE, J. L., IMPERIALE, M. J. & JIANG, M. X. 2015. Viral DNA Replication-Dependent DNA Damage Response Activation during BK Polyomavirus Infection. Journal of Virology, 89**,** 5032-5039.

VERKMAN, A. S. & GALIETTA, L. J. V. 2009. Chloride channels as drug targets. Nature Reviews Drug Discovery, 8**,** 153-171.

VISCIDI, R. P., ROLLISON, D. E., SONDAK, V. K., SILVER, B., MESSINA, J. L., GIULIANO, A. R., FULP, W., AJIDAHUN, A. & RIVANERA, D. 2011. Age-Specific Seroprevalence of Merkel Cell Polyomavirus, BK Virus, and JC Virus. Clinical and Vaccine Immunology, 18**,** 1737-1743.

WALTER, P. & LINGAPPA, V. R. 1986. MECHANISM OF PROTEIN TRANSLOCATION ACROSS THE ENDOPLASMIC-RETICULUM MEMBRANE. Annual Review of Cell Biology, 2**,** 499-516.

WEEKES, M. P., ANTROBUS, R., TALBOT, S., HOR, S., SIMECEK, N., SMITH, D. L., BLOOR, S., RANDOW, F. & LEHNER, P. J. 2012. Proteomic Plasma Membrane Profiling Reveals an Essential Role for gp96 in the Cell Surface Expression of LDLR Family Members, Including the LDL Receptor and LRP6. Journal of Proteome Research, 11**,** 1475-1484.

WEEKES, M. P., TOMASEC, P., HUTTLIN, E. L., FIELDING, C. A., NUSINOW, D., STANTON, R. J., WANG, E. C. Y., AICHELER, R., MURRELL, I., WILKINSON, G. W. G., LEHNER, P. J. & GYGI, S. P. 2014. Quantitative Temporal Viromics: An Approach to Investigate Host-Pathogen Interaction. Cell, 157**,** 1460-1472.

WEI, C. L., WU, Q., VEGA, V. B., CHIU, K. P., NG, P., ZHANG, T., SHAHAB, A., YONG, H. C., FU, Y. T., WENG, Z. P., LIU, J. J., ZHAO, X. D., CHEW, J. L., LEE, Y. L., KUZNETSOV, V. A., SUNG, W. K., MILLER, L. D., LIM, B., LIU, E. T., YU, Q., NG, H. H. & RUAN, Y. J. 2006. A global map of p53 transcription-factor binding sites in the human genome. Cell, 124**,** 207-219.

WEI, C. W., NI, C. F., SONG, T., LIU, Y., YANG, X. L., ZHENG, Z. R., JIA, Y. X., YUAN, Y. A., GUAN, K., XU, Y., CHENG, X. Z., ZHANG, Y. H., YANG, X. A., WANG, Y. L., WEN, C. Y., WU, Q., SHI, W. & ZHONG, H. 2010. The Hepatitis B Virus X Protein Disrupts Innate Immunity by Downregulating Mitochondrial Antiviral Signaling Protein. Journal of Immunology, 185**,** 1158-1168.

WHITE, M. K. & KHALILI, K. 2006. Interaction of retinoblastoma protein family members with large T-antigen of primate polyomaviruses. Oncogene, 25**,** 5286-5293.

WIECZOREK, M., ABUALROUS, E. T., STICHT, J., ALVARO-BENITO, M., STOLZENBERG, S., NOE, F. & FREUND, C. 2017. Major Histocompatibility Complex (MHC) Class I and MHC Class II Proteins: Conformational Plasticity in Antigen Presentation. Frontiers in Immunology, 8.

WIESER, M., STADLER, G., JENNINGS, P., STREUBEL, B., PFALLER, W., AMBROS, P., RIEDL, C., KATINGER, H., GRILLARI, J. & GRILLARI-VOGLAUER, R. 2008. hTERT alone immortalizes epithelial cells of renal proximal tubules without changing their functional characteristics. American Journal of Physiology-Renal Physiology, 295**,** F1365-F1375.

WU, J. X., SUN, L. J., CHEN, X., DU, F. H., SHI, H. P., CHEN, C. & CHEN, Z. J. J. 2013. Cyclic GMP-AMP Is an Endogenous Second Messenger in Innate Immune Signaling by Cytosolic DNA. Science, 339**,** 826-830.

WU, R., DEPHOURE, N., HAAS, W., HUTTLIN, E. L., ZHAI, B., SOWA, M. E. & GYGI, S. P. 2011. Correct Interpretation of Comprehensive Phosphorylation Dynamics Requires Normalization by Protein Expression Changes. Molecular & Cellular Proteomics, 10.

YAMAMOTO, M., SATO, S., HEMMI, H., HOSHINO, K., KAISHO, T., SANJO, H., TAKEUCHI, O., SUGIYAMA, M., OKABE, M., TAKEDA, K. & AKIRA, S. 2003. Role of adaptor TRIF in the MyD88-independent toll-like receptor signaling pathway. Science, 301**,** 640-643.

YOGO, Y., SUGIMOTO, C., ZHONG, S. & HOMMA, Y. 2009. Evolution of the BK polyomavirus: epidemiological, anthropological and clinical implications. Reviews in Medical Virology, 19**,** 185-199.

ZHAO, L. B. & IMPERIALE, M. J. 2017. Identification of Rab18 as an Essential Host Factor for BK Polyomavirus Infection Using a Whole-Genome RNA Interference Screen. Msphere, 2.

ZHAO, L. B., MARCIANO, A. T., RIVET, C. R. & IMPERIALE, M. J. 2016. Caveolin- and clathrin-independent entry of BKPyV into primary human proximal tubule epithelial cells. Virology, 492**,** 66-72.

ZHEN, Y. & STENMARK, H. 2015. Cellular functions of Rab GTPases at a glance. Journal of Cell Science, 128**,** 3171-3176.

ZIEHR, B., VINCENT, H. A. & MOORMAN, N. J. 2016. Human Cytomegalovirus pTRS1 and pIRS1 Antagonize Protein Kinase R To Facilitate Virus Replication. Journal of Virology, 90**,** 3839-3848.